Nickel Catalyzed Coupling Reactions and Studies on Pyranopyrazole Heterocyclic Molecules

THESIS

Submitted in partial fulfillment of the requirements for the degree

of

DOCTOR OF PHILOSOPHY

by

Ashok Sharma

Under the supervision of

Dr. Paritosh Shukla

BIRLA INSTITUTE OF TECHNOLOGY AND SCIENCE

PILANI (RAJASTHAN) INDIA

2016

Dedicated to

My Parents and My

Supervisor

BIRLA INSTITUTE OF TECHNOLOGY AND SCIENCE

PILANI (RAJASTHAN)

CERTIFICATE

This is to certify that the thesis entitled **"Nickel Catalyzed Coupling Reactions and Studies on Pyranopyrazole Heterocyclic Molecules."** submitted by **Mr. Ashok Sharma** ID No **2010PHXF009P** for the award of Ph.D Degree of the Institute embodies the original work done by him under our supervision.

Signature in full of the Supervisors:

Name in capital block letters: **Dr. PARITOSH SHUKLA**

Designation: Assistant Professor

Date:

ACKNOWLEDGEMENT

ABSTRACT

Nitrogen containing heterocyclic compounds and coupling reactions have been known to have a tremendous potential in multidisciplinary fields. The thesis entitled "**Nickel Catalyzed Coupling Reactions and Studies on Pyranopyrazole Heterocyclic Molecules.**" deals with designing and the synthesis of some selected *N*-fused heterocycles by employing the multi-bond forming procedures like tandem sequences, multicomponent reactions, and also utilizing transition metal catalyzed alkene-alkyl reductive coupling reactions. The thesis is divided into six chapters.

The first chapter of thesis describes the brief literature overview on recent progress in the alkene-alkyl reductive coupling reactions and this strategy was further extended to couple oxabenzonorbornadiene with the alkyl halides resulting in ring opening to give rise to bicyclic alcohol products. The mechanism for both the reactions appears to be the usual oxidative-addition driven alkene insertion reaction where the water appears to act as the protonating agent. The brief literature overview on recent progress in the construction of pyranopyrazole scaffolds and a detailed mechanisms for multi-component reactions, tandem processes, Knoevenegeal Condensation followed by Michael addition have been discussed for the selected transformations. The brief idea about the molecular docking has been discussed to understand the protein ligand interaction and to know about the protein stability in the system as well as the stability of the designed molecules in the binding pocket of the protein. The brief overviews of the copper metal corrosion inhibitors designed and synthesized by the researchers were discussed in detail.

The second chapter describes the Ni/Co catalyzed coupling of alkyl halide with various alkenes. Although transition metal catalysed reactions have come long way, still some areas remain virtually unexplored. Our interest in nickel and cobalt-catalyzed reactions prompted us to explore the coupling of alkyl halides with alkenes. Herein, we describe an efficient nickel and cobalt-catalyzed C-C bond forming process via the reductive coupling of $1^{°}$, $2^{°}$ and $3^{°}$ alkyl halides with electron withdrawing alkenes under mild conditions. The catalytic mechanism appears to be different from that proposed previously involving the addition of alkyl radical to C-C double bond. The fact that our strategy can work equally well with nickel as well cobalt catalysts makes the protocol all the more attractive. An efficient Nickel and cobalt-catalyzed reductive coupling reaction of alkyl halides with electron-withdrawing alkenes ($CH_2=CR^1EWG$, EWG is electron-withdrawing group) in the presence of water and zinc powder in acetonitrile to give the corresponding Michael-type addition product (RCH_2CR^1EWG) was described. For the alkyl halides used in the reaction, the iodides generally gave better yields compared to those of the corresponding bromides. It is a unique method employing $NiCl_2(PPh_3)_2$, $NiBr_2(PPh_3)_2$ and CoI_2dppe, zinc, and alkyl halides, affording conjugate addition products in high yields. Mechanistically, the reaction appears to follow an oxidative addition driven route rather than the previously reported radical route.

The third chapter demonstrates about the synthesis of pyranopyrazole by various methodologies and their biological application. The chapter is divided into three parts as:

Part A: In this part a series of compounds having the pyrazolopyran pharmacophore were synthesized by the traditional method and then by an unreported rapid four-component microwave assisted method. The prepared molecules were tested *in-vitro* for their cytotoxic activity against the Hep3B cancer cell lines. The activity results were subsequently rationalized for a quick structure-activity relationship leading to the conclusion that the presence of certain heteroatom substituent's at a given position of the pharmacophore may be crucial for anticancer potency. The X-ray crystallographic analysis of 6-amino-1,4-dihydro-3-methyl-4-phenylpyrano[2,3-*c*]pyrazole-5-carbonitrile crystallizes in the triclinic crystal system with space group P–1. The crystal structure as elucidated by X-ray diffraction methods shows the presence of different intermolecular interactions, and the nature and energetics associated with these interactions have been characterized using PIXEL software.

Part B: The spiro and non-spiro pyranopyrazole heterocyclic molecules were synthesized by conventional method and the synthesized compounds were tested *in-vitro* for their cytotoxic activity against the Hep3B cancer cell lines and their binding study on the calf thymus DNA. The binding of the molecules with DNA has been confirmed by UV-visible spectroscopy. A quick SAR (Structure-activity relationship) study of all the synthesized molecules and their activity results has been subsequently streamlined which lead to the idea that presence of certain heteroatom substituent's at a given position of the pharmacophore may be decisive for anticancer potency. Finally, the molecule with the best activity was docked against CDK-2 receptor to get an insight into the mode of interaction. The results showed that these pyranopyrazoles could act as potential cytotoxic agents.

Part C: In this part all the pyranopyrazole compounds were synthesized by novel grinding methodology and were evaluated for their *in-vitro* antibacterial activity against three different bacterial and three different fungal strains. The highlight of this work is that the synthesis was activity-driven. The brief SAR correlation found that the tested compounds showed better activity against fungal strains. Another interesting observation was that the new chemical entities exhibited complementary activity such that most molecules that were active against bacteria were inactive against fungi and vice-versa. Also, the presence of H-bond donors at a particular position of the pharmacophore seemed to enhance antibacterial potency. Later on, the 7 best selected anticancer compounds from the previous part A and B of Chapter-3 were evaluated for their *in-vitro* and *in-vivo* oxidative stress activities. The results obtained showed that compounds AK-62 and AK-50 possessed significant *in-vitro* as well as in-vivo antioxidant properties.

The fourth chapter of the thesis describes the designing of pyranopyrazole molecules as CDK-2 inhibitors. The chapter is divided into two parts.

Part-A: In this part we have designed 69 novel pyrazolopyran analogues as Cyclin Dependent Kinase-2 (CDK-2) inhibitors in three consecutive series-I, II & III (23 molecules in each series). Docking studies of the designed analogs were performed by molecular modeling software autodock 4.2 using CDK-2 (PDB ID: 1HCK) which is the class of aurora kinase protein, a small family of serine/threonine kinase receptors. Lipinski's rule of five parameters and toxicity parameters were derived through online servers like Molinspiration and Osiris property explorer. Docking parameters such as binding free energy and

predicted inhibitory constant (K_i) values of the designed analogues were compared with standard drug olomoucine. Among the designed analogues, AK-26, AK-72K and AK-60E from series-I, II and III respectively showed significant and comparable binding free energy and predicted inhibitory constant values as that of standard drug. These results indicate that the designed analogs adopt a similar orientation and share the same binding mode as that of some of the classical CDK-2 inhibitors within the active site of 1HCK inhibitory binding pocket of Aurora kinase.

Part-B: In this part we have designed 62 Coumarin derivatives as CDK-2 inhibitors (PDB ID: 1HCK). The idea behind the designing was to check out the effect of variation of different molecules at position no. R^1, R^2, R^3, and R^4 on binding energy and inhibitory constant value. All the designed analogues were CDK-2 inhibitors and were docked by using autodock 4.2 using CDK-2 (PDB ID: 1HCK) which is the class of aurora kinase, a small family of serine/threonine kinase receptors. Very well known online software's like Molinspiration and Osiris property explorer were used to derive the molecular properties like toxicity and Lipinski's rule of five. A close observation reveals out that the substitution at R^1 and R^4 enhances the binding energy and inhibitory constant values from nanomolar to picomolar range. Among the designed analogues THC-42, THC-43, THC-58 and THC-59 showed the significant binding energy and inhibiotory constant values as that of the standard drug. Most of the designed analogues showed similar binding mode and orientation inside the active site of the protein as that of the standard drug which give us hope that the molecules should be potent in the inhibition of 1HCK protein.

The fifth chapter describes the inhibitory corrosion effect of five substituted pyranopyrazole on Cu metal surface. Five substituted pyranopyrazole (ppz) derivatives were selected from the chapter-3 (Part: C). The differential scanning calorimetry (DSC), thermogravimetric analysis (TGA) analyses and the corrosion inhibitor properties on mild copper in 1 M HCl were investigated using open circuit potential (OCP) and impedance measurements. Scanning electron microscopy (SEM), energy dispersive spectroscopy (EDS), and X-ray diffraction (XRD) analysis showed good anti-corrosion behavior as did the conductivity study and mechanical property investigations. Finally, the inhibition action was evaluated by quantum chemical parameters. All the experimental results pointed that the ppz molecules acted as excellent anti-corrosion surface active agents.

The sixth chapter of the thesis demonstrates the overall conclusions of the thesis work and is summarized here. The future scopes of the research work have also been highlighted in this chapter.

Anticancer Agents

LIST OF TABLES

LIST OF FIGURES

LIST OF ABBREVIATIONS / SYMBOLS

Abbreviation/Symbol	Description
α	Alpha
β	Beta
Δ	Delta
°C	Degree centigrade
Å	Angstrom
A	Ampere
acac	Acetylacetone
AIDS	Acquired immune deficiency syndrome
ASTM	American society for testing and materials
Ac	Acetyl
ACN	Acetonitrile
Ar	Aryl
ATA	3-amino-1, 2, 4-triazole
AMTA	3-amino-5-mercapto-1, 2, 4-triazole
Aβ	Amyloid beta
AC	Alternating current
BTA	Benzotriazole
Bu	Butyl
BBB	Blood brain barrier
BE	Binding energy
t-BuOK	Potassium $tert$-butoxide
Calcd.	Calculated
^{13}C	Carbon-13
Cat.	Catalyst
CAN	Ceric ammonium nitrate
CMA	Copper manganese- aluminium
COD	Cyclooctadiene
$CDCl_3$	Deuterated chloroform
Conc.	Concentration
CLP	Couloumb- London- Pauli
CCDC	Cambridge crystallographic data centre
CHK-1	Checkpoint kinase

CT-DNA	Calf thymus deoxyribonucleic acid
CDK	Cyclin dependent kinase
CPE	Constant phase element
C_{inh}	Corrosion inhibitor
C_{dl}	Double layer capacitance at the material/solution interface
d	Doublet
dd	Doublet of doublet
dppm	Diphenyl phosphino methane
dppe	Diphenyl phosphino ethane
DCE	Dichloroethane
DCM	Dichloromethane
DMF	*N,N*-Dimethylformamide
DMSO-d_6	Deuterated dimethylsulfoxide
DNA	Deoxyribonucleic acid
DFT	Density function theory
DTNB	5,5′-dithiobis-(2-nitrobenzoic acid)
DC	Direct current
ETDA	5-Ethyl-1,3,4-thiadiazol-2-amine
EtOAc	Ethyl acetate
Equiv	Equivalent
ELISA	Enzyme-linked immune-sorbent assay
EDS	Energy dispersive spectroscopy
EIS	Electrochemical impedance spectroscopy
FBS	Fetal bovine serum
GSH	Glutathione
GHz	Giga hertz
GB	Giga byte
GROMACS	Groningen machine for chemical simulations
GCE	Glassy carbon electrode
HRMS	High resolution mass spectrometry
h	Hours
HIV	Human immune deficiency virus
Hep3B	Hepatocellular carcinoma cell line
HBA	Hydrogen bond acceptor

HBD	Hydrogen bond donor
1HCK	Human cyclin dependent kinase
HOMO	Highest occupied molecular orbital
IC_{50}	Inhibitory concentration
ICV	Intracerebroventricular
IRRI	Irritant
Hz	Hertz
HF	Higher frequency
J	Coupling constant
K_I	Inhibitory constant
LUMO	Lowest unoccupied molecular orbital
LF	Lower frequency
LGA	Lamarckian genetic algorithm
MCR	Multi component reaction
Me	Methyl
M.P	Melting point
m	Multiplet
mg	Milligram
MHz	Mega hertz
min	Minutes
mL	Milliliter
mmol	Millimole
MWA	Microwave assisted
MEM	Minimum essential medium
MIC	Minimum inhibitory concentration
MDA	Malondialdehyde
MD	Molecular Docking
MUT	Mutogenic
M4PPs	Microscopic four-point probes
MPa	Megapascal
MMI	2-Mercapto-1-methylimidazole
MBT	2-mercaptobenzothiazole
MAP	2-mercapto-4-amino-5-nitroso-6-hydroxy pyrimidine
N_2	Nitrogen gas

NBS	*N*-bromosuccinimide
NCCS	National centre for cell science
NFT	Neurofibrillary tangles
ns	Nanosecond
η%	Inhibition efficiency
O_2	Oxygen gas
OCP	Open circuit potential
OD	Optical density
Ω	Ohm
PEG	Polyethylene glycol
Ph	Phenyl
PPh_3	Triphenylphosphine
Ppm	Parts per million
PBS	Phosphate-buffered saline
PDB	Potato dextrose broth
PDB	Protein data bank
PME	Particle mesh Ewald
PPZ	Pyranopyrazole
%	Percentage
R	Hydrocarbon
ROS	Reactive oxygen species
RNS	Reactive nitrogen species
rt	Room temperature
RAM	Random access memory
RMSD	Root mean square deviation
REP	Reproductive
RMSF	Root mean square fluctuation
R_g	Radius of gyration
R_{ct}	Charge transfer resistance
R_s	Material/solution resistance
s	Singlet
SAR	Structure-Activity Relationship
STZ	Streptozotocin
SPC216	Space point charge216

SEM	Scanning electron microscopy
t	Triplet
θ	Surface coverage
THF	Tetrahydrofuran
TLC	Thin layer chromatography
Tris-EDTA	Trisaminomethane- Ethylenediaminetetraacetic acid
TUMO	Tumorigenic
THC	Tetrahydroxy coumarin
δ	Parts per million
ω	Angular frequency
V	Voltmeter
XRD	X-ray Diffractometer

Chapter I

A Brief Overview on Chemistry of Reductive Heck Coupling Reactions, Heterocyclic Molecules, Drug Designing and Corrosion Inhibitors Study

Section A: Transition metal catalyzed Heck and Reductive Heck reactions

1.1 Introduction: Transition metal catalyzed reactions represents a recognized area of continuous effort from last few decades and shows significant new and often unexpected developments in organometallic chemistry area. Remarkably, till now three Nobel Prizes (2001, 2005, and 2010) have been awarded in the area of organometallic chemistry, shared among nine scientists for their outstanding contributions. It would not be surprising if another Nobel Prize is awarded in the same area because transition metal catalyzed reactions platforms are experiencing rapidly increasing application. The most fundamental operation in organic chemistry is the formation of Carbon-Carbon (C-C) bonds and the development of new bond forming technique is one of the most challenging and significant task in organic synthesis. Furthermore, the construction of various C-C bonds including open chain, carbocyclic, and heterocyclic compounds[1] has been undertaken by very powerful tools like transition metal-catalyzed couplings, carbocyclizations, and heterocyclizations. Even though, the transition metal catalyzed reactions have come long way, but some areas still remain practically unexplored. That may be because of the relative inertness of some types of substrates towards customary organic reagents in general and transition metal reagents in particular. Among such substrates, we may include unreactive C-H bonds, C-C bonds etc.

Now a days, transition metal mediated C-H activation is much in vogue[2-3] and quite at the forefront of such research. The Heck reaction[4] has long been the beacon of activation of alkenic C-H bonds in the presence of palladium catalyst, wherein vinylic or arylic halides react with alkenes to form coupled products **(Figure 1.1)** and is one of the most influential methods for the construction of C-C bonds.

where X= Br, I
R_1= COOCH$_3$, COOC$_2$H$_5$,

Heck coupling product
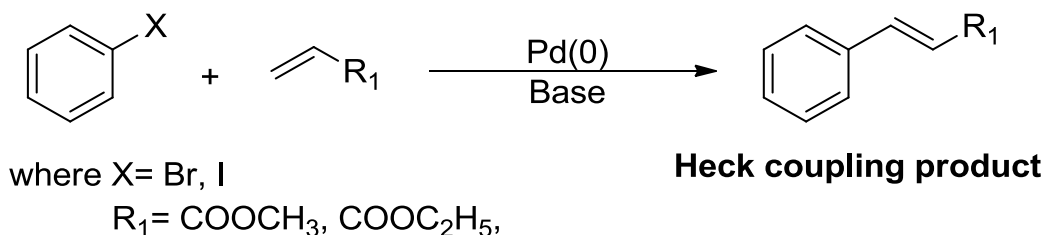
Figure 1.1 The Heck coupling reaction among alkyl halide and alkene.

1.2 Mechanism of Heck Reaction: The Heck reaction is catalyzed by Pd(0) species and the catalyst is stabilized by two phosphine ligands. The reaction mechanism **(Figure 1.2)** includes four steps: (1) Oxidative addition involving the formation of a σ-aryl-Pd(II) or σ-alkenyl-Pd(II) complex (2) Either one of the phosphine ligands or the halide anion dissociates from the complex, leaving behind a vacant co-ordination site that is occupied by the olefin substrate. Insertion of the olefin at the aryl-Pd or alkenyl-Pd bond takes place consequently (3) The coupling product is given by an intramolecular β-hydride

elimination (4) PdL$_2$ catalyst is regenerated after the removal of HX from the complex mediated by the base.
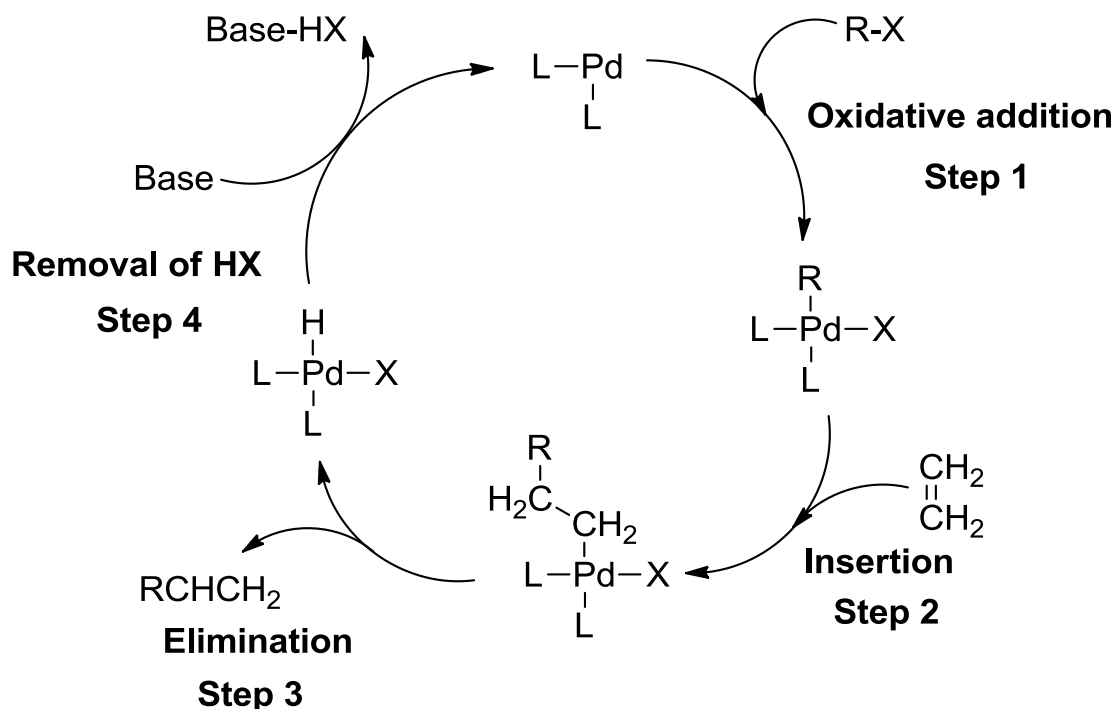
Figure 1.2 Mechanism for Heck coupling reaction.

The Heck reaction is one of the significant tool in organic synthesis and its scope and limitations have been extensively investigated since last few decades.[5] However, the major limitation of the Heck reaction is that one can not use alkyl halide having β-hydrogen, because of β-hydride elimination problem[6] by such type of substrates. Therefore, if a strategy could be developed for Heck coupling which encompassed the successful use of sp^3 alkyl halides, it would go a long way in satisfying the requirement of modern day transition metal mediated synthesis. After close observation, we find that the C=C (from the alkene moiety) is still intact in Heck product **(Figure 1.3a)**. The presence of the intact double bond may be more attractive synthetically, but when the double bond be desired in the product. If, however, there is desire of saturated product as in the preparation of saturated esters, then the Heck product needs further reduction to convert it to a saturated product **(Figure 1.3b)**. Hence, to obtain reductively coupled product, through one step route, from an alkene and alkyl halide makes an interesting challenge worth taking up.
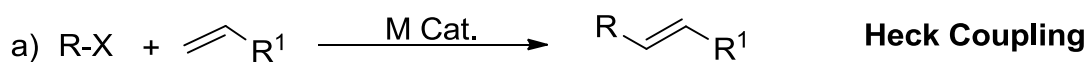
a) R-X + ⟋R¹ —— M Cat. ——→ R⟋⟍R¹ **Heck Coupling**

where R= Alkyl/ aryl group

X= Br, I

R^1= CO-OCH$_3$, CO-OC$_2$H$_5$, CO-OC$_3$H$_7$

M= Ni

- -

b) R-X + ⟋R¹ —— M Cat. ——→ R⟍⟋⟍R¹ **Reductive Coupling**

where R= Alkyl/ aryl group

X= Br, I

R^1= CO-OCH$_3$, CO-OC$_2$H$_5$, CO-OC$_3$H$_7$

M= Ni

Figure 1.3 Shows the (a) Heck coupling and, (b) Reductive Heck coupling reaction.

Generally, the transition metal mediated construction of C-C bonds can be divided into two main types as: (1) The first one involves catalytic or stoichiometric coupling of saturated alkyl halides with alkenes in the presence of transition metal complexes (2) The second approach is the cross coupling reaction of alkyl electrophiles (halide, sulfonate, etc.) with main group metal alkyls mediated by transition metal complexes of palladium, nickel, iron, etc. However, to bring about the desired C-C bond formation most previous available reports pertaining to such couplings have used stoichiometric amounts of the metal complexes. The latter strategy suffers from a major drawback because of the use of large amounts of metallic species. It is undesirable not only from the standpoint of economic viability but also from the standpoint of chemistry as well as environment.

1.3 First Approach of Coupling Reactions

1.3.1 Zinc-copper coupled organometallic reaction: Fourrey and coworkers[7] reported a zinc-copper couple induced addition of carbohydrate or amino acid residues derived from their primary iodides to various activated olefins brought about by vibromixing. The reaction of methyl 5-deoxy-5-iodo-2,3-O-isopropylidineribofuranoside (**1**) with methyl acrylate (**2**) in the presence of zinc/cuprous iodide in a stirred vibromixer, the chain extended compound 5-(6-methoxy-2,2-dimethyltetrahydrofuro[3,4 *d*][1,3]dioxol-4-yl)pentanoate **3** was obtained in a moderate yield of 50% **(Scheme 1.1)**. Later on, a modified version of the above reaction was reported by the same author,[8] wherein other electron sources in Zn/MCl$_n$ [where M = Ni (n = 2), Co (n = 2), and Fe (n = 3)] were examined.
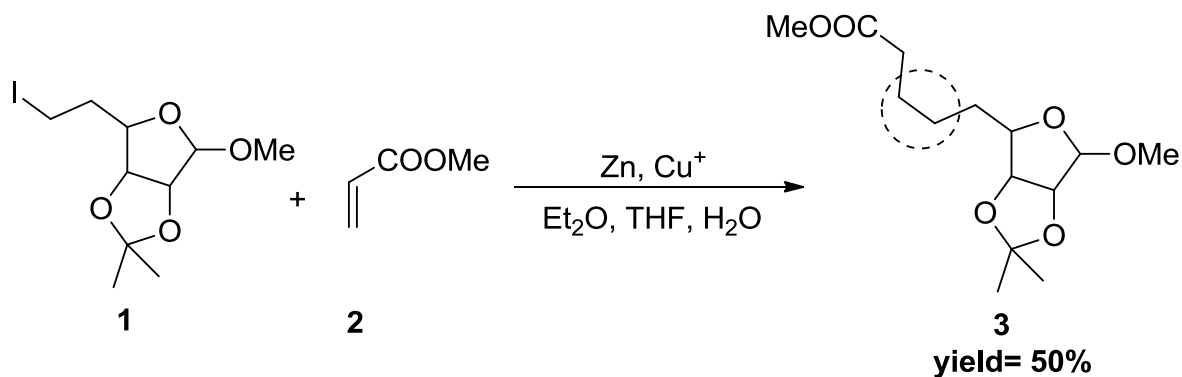
Scheme 1.1 Shows the synthesis of methyl 5-(6-methoxy-2,2-dimethyltetrahydrofuro[3,4-*d*][1,3]dioxol-4-yl)pentanoate.

1.3.2 Reactions of Iodotriflate with Olefins: Maurino *et al.* reported[9] conjugate addition of iodo triflate derivatives to electron deficient olefins by ultrasonic induced method. They prepared the upper fragment of vitamin D_3 by ultrasonic methodology **(Scheme 1.2)** and reported the preparation of side chain of the hormone 1α, 25-dihydroxyvitamin D_3. Treatment of the triflate **4** with methyl acrylate **5** under sonochemical aqueous conditions, gave the reduced product methyl 5-(((1R,7aR)-7a-methyl-4-((((trifluoromethyl)sulfonyl)oxy)-2,3,3a,6,7,7a-hexahydro-1*H*-inden-1-yl)hexanoate **6** in 73% yield.
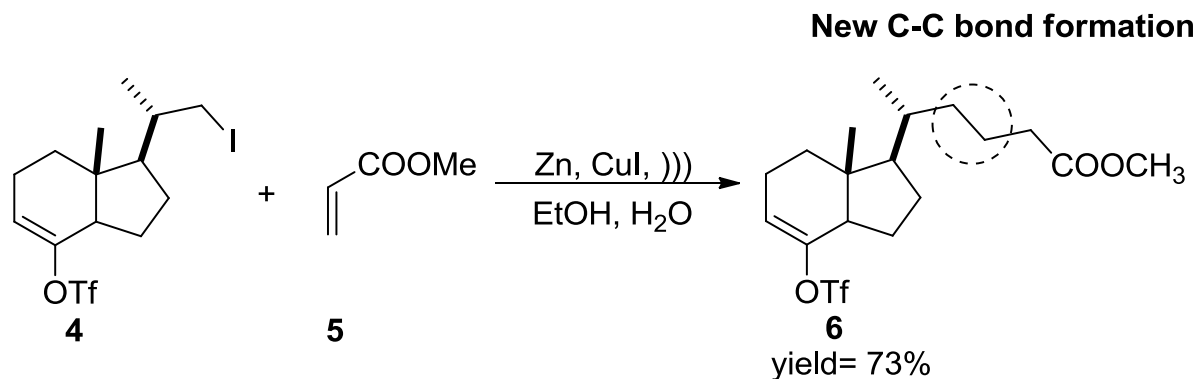
Scheme 1.2 Shows the synthesis of methyl 5-(((1R,7aR)-7a-methyl-4-((((trifluoromethyl)sulfonyl)oxy)-2,3,3a,6,7,7a-hexahydro-1*H*-inden-1-yl)hexanoate.

1.3.3 Nickel catalyzed organometallic reaction: Manchand[10] and his group reported the coupling of sp^3 iodides **7** with ethyl acrylate **8** in presence of nickel(0) catalyst to give esters **9** in good yields **(Scheme 1.3)** with **10** as side product and also reported that how to introduce side chain of hormone calcitriol.
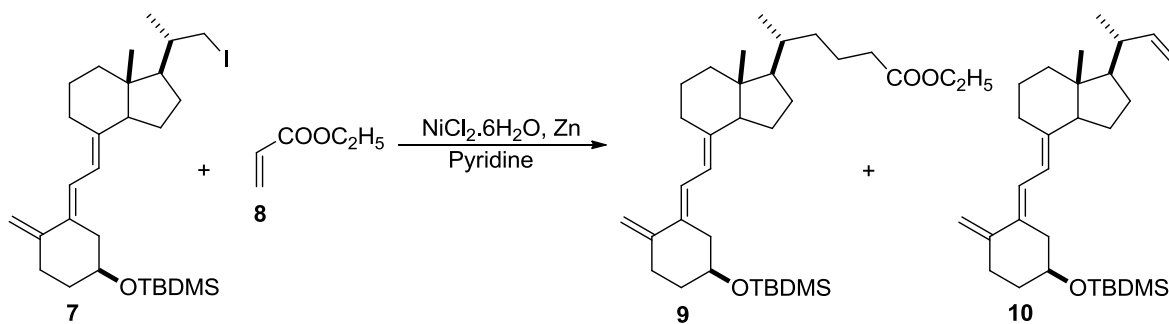
Scheme 1.3 Shows the synthesis of ester and calcitriol hormone.

1.3.4 Fe or Mn radical catalyzed reaction: Giese *et al.*[11] reported the radical C-C bond formation by using dimeric metal complexes as mediators. They used the complexes of Fe **(11)** or Mn **(12)** as radical electron initiators in the presence of irradiations**.** Treatment of alkyl halide **13** with alkene **14** in presence of radiation gives both saturated **15** as well as unsaturated product **16 (Scheme 1.4)**.
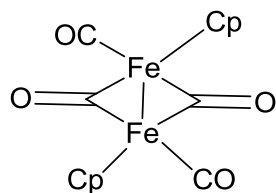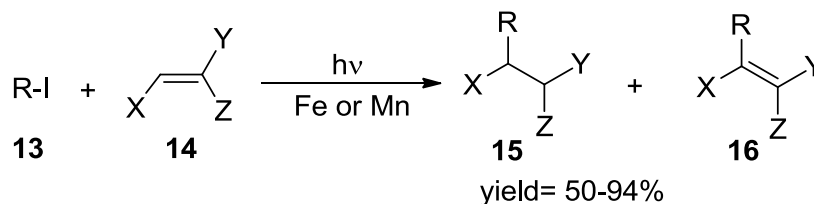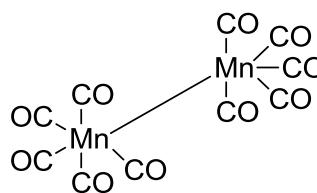
Scheme 1.4 The synthesis of saturated and unsaturated product.

It is interesting to note that all the above discussed methods for C-C bond formation not only involve the stoichiometric quantities of the corresponding metals but also require electrolysis, photochemical irradiation, or sonication methods to accomplish the desired coupling. Moreover, all the above mentioned reactions are radical mediated reactions and this makes the strategies more demanding. However, very few reports are available on reductive coupling of an alkyl halide with alkenes in the presence of catalytic amounts of the metal. Beletskaya's group[12] reported the condensation of organic bromides with vinyl compounds in the presence of nickel catalyst.

1.3.5 Reaction of alkyl bromide with alkene: Sustmann and coworkers[13] too exposed the similar types of nickel-catalyzed reactions **(Scheme 1.5)** where they solely reported reductive coupling of alkyl bromides **17** with a variety of electron withdrawing alkenes **18** and yielded the product **19** with 60-80% yield. The yields, once again were not quite high and they also reported an unavoidable employment of pyridine in excess.

$$R\text{-}Br \; + \; CH_2=CHR' \xrightarrow[\text{THF, Zn, pyridine}]{\text{NiCl}_2.6H_2O} RCH_2CH_2R'$$

17   **18**   **19**

yield= 60-80%

R= prim, sec., tert. alkyl, vinyl, phenyl
R'= -COOEt, -COCH$_3$, -CN
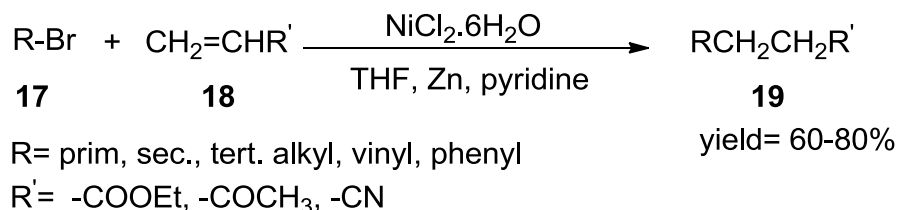
Scheme 1.5 Reductive coupling of alkyl bromide with various EW alkenes.

1.3.6 Reaction of α, β-unsaturated esters with alkyl iodides: Yoon *et al*. showed a polymer supported nickel-catalysed reductive coupling **(Scheme 1.6)** of alkyl iodides **20** with α, β-unsaturated esters **21**.[14] The catalyst used was a borohydride exchange resin Ni$_2$B-BER, in methanol solvent at room temperature. Although the yields of saturated ester **22** obtained were pretty good but the use of polymeric resin shackles the whole procedure. They also reported that not only secondary and tertiary bromides are readily reduced as primary bromide with comparable rate, but also 1-phenethyl bromide is coupled to 2,3-diphenylbutane (30%) beside the expected reduction to ethylbenzene (70%). This strongly recommended an involvement of radical intermediate.

20   **21**   **22**

yield= 68-95 %

R= prim, sec., tert. alkyl, cyclohexyl
R', R"= H, alkyl
R'''= methyl, ethyl
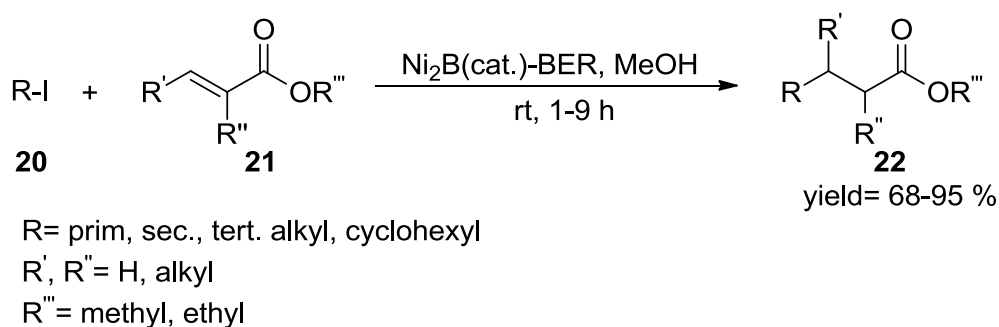
Scheme 1.6 Reductive coupling of alkyl iodide with α, β-unsaturated esters.

1.3.7 Homoallylation of aldehydes with 1,3-dienes: Masanari Kimura[15] reported for the first time that Ni-catalysts are able to promote the homoallylation of aldehydes **23** and **26** with a wide variety of 1,3-dienes **24** in the presence of triethylborane or diethylzinc to yield bishomoallyl alcohols **25** and **27** with excellent regio- and stereoselectivities **(Scheme 1.7)**.

Scheme 1.7 Homoallylation of aldehydes with 1,3-diene.

1.3.8 Synthesis of allylic amines: Qi-Lin Zhou *et al.*[16] reported the nickel-catalyzed reductive coupling reaction of aryl-substituted alkynes **28**, imines **29**, and Et_2Zn **30**, providing allylic amines **32** in high yields (up to 96%) and excellent chemoselectivities (RC/AC up to 42:1). They also accomplished an asymmetric version of this reaction by using chiral spiro phosphine ligands **31**, and high enantioselectivities (up to 94% ee) were achieved **(Scheme 1.8a)**. They initially conducted the nickel-catalyzed reductive coupling of 1-phenyl-1-propyne **33** with imines **34** by using Et_2Zn **30** as a reducing agent. Fortuitously, the *N*-tosyl protected imine **34** underwent the three-component coupling reaction smoothly in the presence of 10 mol % nickel catalyst formed in situ from $Ni(acac)_2$ and PPh_3. The expected reductive coupling product **35** was isolated along with the alkylative coupling product **36** and the direct Et_2Zn addition by-product **37** in a ratio of **(35/36/37)** 2:1:1 **(Scheme 1.8b)**. Other organometallic reagents such as Et_3B, Et_3Al, and $HSiEt_3$ were ineffective in this reaction. Replacement of the tosyl group with another protecting group such as phenyl, methyl, or $P(O)Ph_2$ was also unsuccessful for increasing the yield and chemoselectivity of the reaction. Both monodentate and bidentate phosphorus ligands can promote the coupling reaction; however, only the less-hindered and electron-rich ligand *n*-Bu_3P yielded the reductive coupling product in good yield (66%) and excellent chemoselectivity **(35/36/37)** 23:1:3. When the catalyst precursor $Ni(COD)_2$ was used the yield increased to 86%. Under the optimal conditions, the catalyst loading was reduced to 5 mol % and the ratio of the alkyne, imine, and Et_2Zn was lowered to 2:1:1. Imines with other sulfonyl protecting groups were also suitable substrates. Because the *N,N* dimethylsulfamoyl protecting group is easy to remove,[17] they chose imine **38** for further investigation. An isotope-labeling experiment between 1-phenyl-1-propyne **33**, imine **38** and Et_2Zn **30** showed that the transferred hydrogen was most likely from the ethyl group of Et_2Zn **(Scheme 1.8c)**. The studies for accurate mechanism are undergoing in this laboratory and will be reported in due course.

a)

28 **29** **30** **32** 94% ee

exclusive cis addition across alkyne

R^1= Ph, Et,

R^2= Me, Et, Ph

R^3= Ts,1,3-dimethyl-5-(methylsulfonyl)benzene, N,N dimethylmethanesulfonamide

R^4= Ph, o-MeOC$_6$H$_4$, o-MeC$_6$H$_4$, o-ClC$_6$H$_4$, m-MeC$_6$H$_4$, m-ClC$_6$H$_4$, p-MeOC$_6$H$_4$, p-MeC$_6$H$_4$, p-FC$_6$H$_4$, p-ClC$_6$H$_4$, p-CF$_3$C$_6$H$_4$, 3,4-Cl$_2$C$_6$H$_3$, 1-naphthyl, 2-naphthyl, n-Pr, i-Pr, c-C6H11,

Ligand **31**

b)

33 **34** **30** **35** **36** **37**

R^3 = Ts,1,3-dimethyl-5-(methylsulfonyl)benzene, N,N-dimethylmethanesulfonamide

Ni= Ni(acac)$_2$, Ni(COD)$_2$

c)

33 **38** **30** 100% **39**

Scheme 1.8 Reductive coupling (RC) of alkynes and imines.

1.3.9 Synthesis of Ketones: Hegui Gong *et al*.[18] reported Ni-catalyzed ketone **43** formation through mild reductive coupling of a diverse set of unactivated alkyl bromides and iodides **40** with particularly aryl acid anhydrides **41** (or acid **42** with Boc$_2$O additive) was successfully developed using zinc as the terminal reductant **(Scheme 1.9a)**. These conditions also allow direct coupling of alkyl iodides **44** with aryl acids **45** in the presence of ligand **46** and additives Boc$_2$O and MgCl$_2$ which finally yielded ketone **47** **(Scheme 1.9b)**.

a)

yield= 48-96%

R_{Alkyl}—X   +   [**41** anhydride $R-C(O)-O-C(O)-R$]

40

or

RCOOH + Boc$_2$O

42   yield= 30-83%

$\xrightarrow[\text{Zn}]{\text{Ni (Cat.)}}$

[**43** ketone $R-C(O)-R_{Alkyl}$]

43

R= alkyl and aryl

X= I, Br

Ni= Ni(COD)$_2$, Ni(acac)$_2$

Possible mechanism:

Ni^I/ Ni^{III} process for R_{Alkyl}-Br

L_n—Ni(COAr) $\xrightarrow{R_{Alkyl}\text{-Br}}$ ArOC—Ni(R$_{Alkyl}$)(L_n)

Ni (I)   Ni(III)

---

b)

R_{Alkyl}—I   +   ArCOOH

44   **45**

$\xrightarrow[\substack{Boc_2O\ (300\%) \\ MgCl_2\ (200\%)}]{\substack{Ni(COD)_2\ (10\%) \\ Ligand\ (15\%) \\ Zn\ (300\%)}}$

[**47** $R_{alkyl}-C(O)-Ar$]

47

yield= 30-83%

16 examples

[**46** phenanthroline ligand with R^1, R^2 substituents]

46

R^1=Ph, R^2=H

Ligand

Scheme 1.9 Reductive coupling (RC) of alkyl halides and aryl acid anhydride.

1.3.10 Palladium catalyzed corbonylation of olefins: Inomata and co-workers[19] revealed interesting palladium catalyzed mono- and bis(alkoxy carbonylation) of olefins **48** with carbon mono-oxide **49** in the presence of Cu(I) or Cu(II) chloride **(Scheme 1.10)**. Instead of high yield obtained by the Inomata reaction methodology there were some demerits associated in following the reaction procedure. The first demerit was the formation of mixture of products (**50, 51**) and the second was the requirement of carbon monooxide gas for carbonylation, making the procedure toxic and difficult to handle.

[olefin R-CH=CH$_2$] + CO $\xrightarrow[\text{CuCl}_2,\ \text{R'OH, THF}]{\text{PdCl}_2(\text{CH}_3\text{CN})_2}$ [**50** $R-CH(Me)-C(O)-OR'$] + [**51** $R-CH_2CH_2-C(O)-OR'$]

48   **49**   **50**   **51**

overall yield= 99%

R= CH$_3$(CH$_2$)$_7$, CH$_3$(CH$_2$)$_8$, CH$_3$(CH$_2$)$_9$, CH$_3$(CH$_2$)$_{11}$,

CH$_3$(CH$_2$)$_{15}$, Ph(CH$_2$)$_2$, PhOCH$_2$,TsCH$_2$,Ts(CH$_2$)$_2$

R'= Me, Et
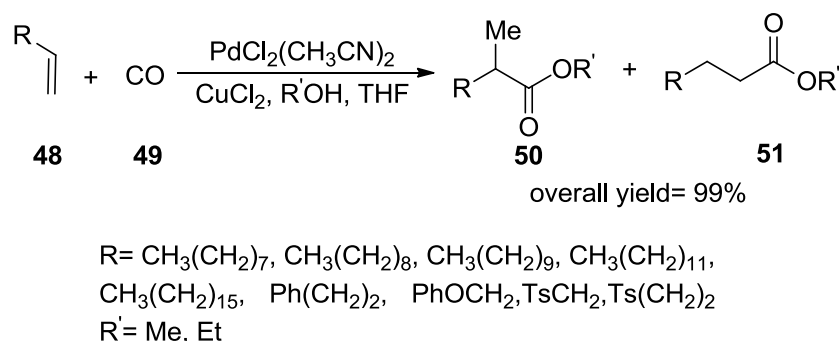
Scheme 1.10 Mono(alkoxycarbonylation) of terminal olefins.

1.4 Second Approach of Coupling Reaction

1.4.1 Cross coupling reaction: The second approach, presently a hot topic,[20] involves the cross coupling reaction for bringing about C-C bond formation. The usual strategy to synthesize such type of a

cross coupling product **54** through cross coupling reaction is to bring about the reaction of metal alkyls **52** with an alkyl electrophile **53** (halide, sulfonate, etc.) mediated by transition metal complexes of iron, nickel, palladium etc **(Scheme 1.11)**.

$$RM \ + \ M^{'}X \ \xrightarrow{\text{Fe/ Pd/ Ni}} \ RM^{'} \ + \ MX$$

52 **53** **54**
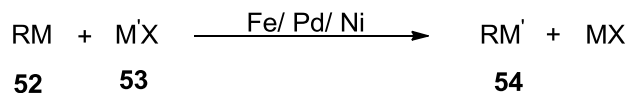
M= Zn, Zr, B, Hg, Si, Sn, Ge, Mg, Li, Al etc.
M$^{'}$= transition metal
R= alkyl, aryl groups
X= halide, sulfonate etc.

Scheme 1.11 Cross coupling reaction of metal alkyls and metal electrophiles.

The use of unactivated alkyl halides for the construction of C-C bonds catalyzed by transition metal complexes is very much challenging[21] because of the low reactivity of the unactivated alkyl halides toward transition metal complexes and the difficulty to overcome β-hydrogen elimination.

1.4.2 Cross-coupling reaction between alkyl electrophiles and organometallic nucleophiles: The well organized formation of C_{sp3}-C_{sp3} **57** from organic electrophiles **55** and mild nucleophiles **56**, compatible with a wide variety of functional groups, represents one of the subjects remaining to be solved in transition-metal-catalysed synthetic organometallic chemistry. The development of methods intended to accomplish the objective **(Scheme 1.12)** may almost complete the scope of metal-catalysed cross-coupling reactions.[22]

55 **56** **57**
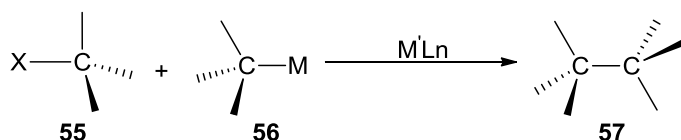
M = Li, Mg, Zn, Al, Sn, B, Si, etc.

M$^{'}$ = Ni, Pd, etc

X = halide, sulfonate, etc.

Scheme 1.12 A general metal-catalysed alkyl-alkyl cross-coupling reaction.

The mechanisms of the metal-catalyzed cross coupling reaction involves an oxidative-addition of an organic electrophile to a coordinatively unsaturated metal complex and form the intermediate species in the first step, followed by transmetalation from the nucleophile to the intermediate species and give di-organometal derivative. The coupled product obtained from a fast C-C reductive elimination generally

regenerates the active catalyst. The first step in case of alkyl halides or sulfonates is relatively slow and, in contrast, gives an alkyl metal complex and is suffered from β-hydride elimination which prevents the coupling process. For these reasons the coupling between sp^3-carbon atoms has not been developed as well as other C-C bond-forming reactions.

1.4.3 Suzuki cross coupling reaction: A few research groups have been fanatically concerned in such alkyl-alkyl cross-couplings reactions. Some of the foremost cross coupling reactions which have been recently reported by several researchers, involving in the construction of C_{sp3}-C_{sp3} bonds are as follows. Suzuki *et al.* revealed[23] a palladium catalyzed Suzuki cross-coupling reaction between primary alkyl iodide **58** and boron reagents **59**, in presence of base and bis(*tert*-butyl)methyl phosphine ligand as an additive and got the alkyl-alkyl cross coupling product **60 (Scheme 1.13)**.

$$R_{alkyl}\text{—I} \quad + \quad 9\text{-BBN-R}' \xrightarrow[\substack{\text{1.2 equiv NaOH} \\ \text{dioxane, 50 }^o\text{C}}]{\substack{\text{4\% Pd(PPh}_3)_4 \\ \text{16\% PtBu}_2\text{Me}}} R_{alkyl}\text{—R'}$$

58   **59**   **60**

Yield= 54-71%

R$'$= MeO$_2$C(CH$_2$)$_{10}$, C$_8$H$_{17}$, BnOCH$_2$CH$_2$CHMe, Me$_2$C=CH(CH$_2$)$_2$CHMe(CH$_2$)$_3$,
Me (CH$_2$)$_3$CH=CH, Ph
R$_{alkyl}$= Me, C$_6$H$_{13}$, t-Bu, NC(CH$_2$)$_3$
BBN= 9-Borabicyclo[3.3.1]nonane.
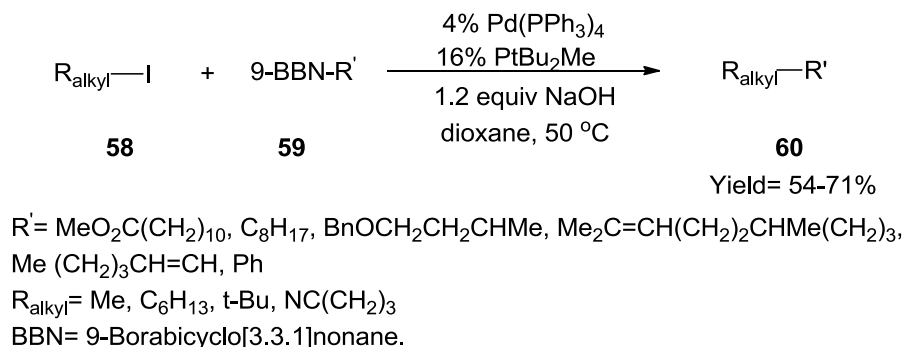
Scheme 1.13 Suzuki cross coupling reaction of alkyl halide with boron reagent.

1.4.4 Negishi cross coupling reaction: Fu and co-workers[24] once again reported the formation of C-C sigma bond through Negishi cross-coupling of primary alkyl chlorides, bromides and iodides with alkyl, alkenyl and arylzinc reagents in the presence of palladium complex. Benzyl heptyl ether **63 (Scheme 1.14)** was obtained by the treatment of benzyl 3-bromopropyl ether **61** with the zinc reagent **62** in the presence of Pd$_2$(dba)$_3$, tricyclopentyl phosphine ligand, and N-methylimidazole in THF-NMP cosolvent.

$$BnO\diagdown\diagup Br \quad + \quad n\text{-Bu}\text{—ZnBr} \xrightarrow[\substack{\text{2:1 THF:NMP} \\ \text{80 }^o\text{C, 14h}}]{\substack{\text{2\% Pd}_2\text{(dba)}_3 \\ \text{8\% ligand} \\ \text{1.2 NMI}}} BnO\diagdown\diagup n\text{-Bu}$$

61   **62**   **63**

yield= 70%
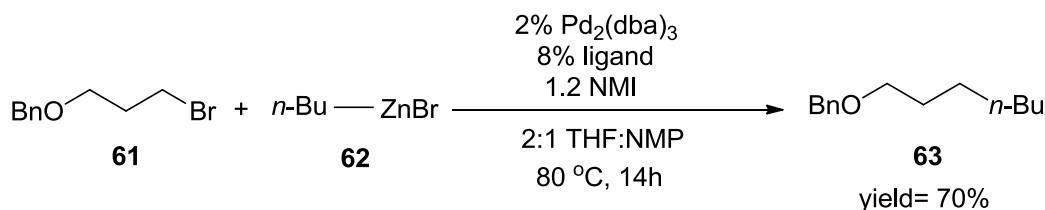
ligands: PCyp$_3$, PCy$_3$, P(i-Pr)$_3$, P(t-Bu)$_2$Me, P(t-Bu)$_3$, P(n-Bu)$_3$, PPh$_3$, P(o-tol)$_3$, P(2,4,6-trimethoxyphenyl)$_3$, P(2-furyl)$_3$, Cy2P(CH$_2$)$_2$PCy$_2$, 1,3-bis(mesityl)-4,5-dihydroimidazolium tetrafluoroborate, P(OPh)$_3$

Scheme 1.14 Negishi cross coupling reaction of benzyl 3-bromopropyl ether with the zinc reagent.

1.4.5 Kumada cross coupling reaction: Kambe and coworkers[25] reported the formation of C-C sigma bond and published a report which outlining the nickel catalyzed Kumada cross coupling of primary alkyl halides like alkyl chloride, bromides and tosylates with Grignard reagents. Here they used the 1,3-butadiene as an additive to avoid the β-hydride elimination. The treatment of bromoethyl cyclopropane **64** with *n*-octyl magnesium chloride **65** give nonylcyclopropane **66** in good yield (**Scheme 1.15**).

$$R\text{-}X \quad + \quad R'\text{-}MgX \xrightarrow[\text{THF, 0 }^{\circ}\text{C, 0.5 h}]{\substack{\text{NiCl}_2 \text{ (1 mol\%)} \\ \text{1,3-butadiene(10 mol\%)}}} R\text{-}R'$$

64   **65**   **66**
yield= 56-100%

R-X= $^{n}C_{10}H_{21}$-Br, $C_8H_8Br_2$, $PhCH_2CH_2OTs$, ^{n}Bu-OTs, Et-OTs, ^{n}Oct-Br, ^{n}Oct-C, C_4H_7Br
R'-MgX'= ^{n}Bu-MgCl, Et-MgBr, Ph-MgBr, C_3H_7-MgCl, nBu-MgCl, ^{n}Oct-Br
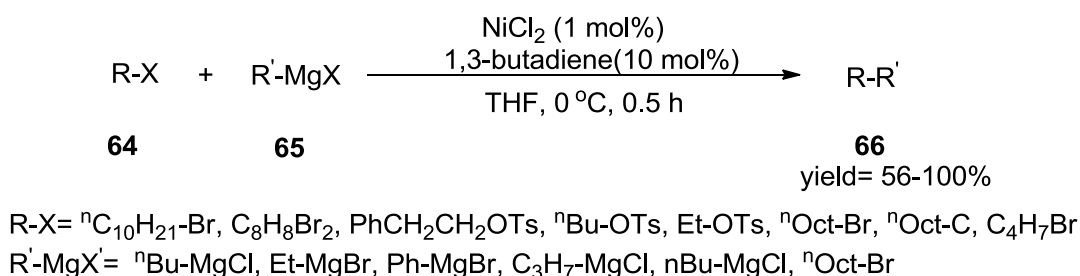
Scheme 1.15 Kumada cross coupling reaction of bromoethyl cyclopropane with *n*-octyl magnesium chloride.

1.4.6 Stille cross coupling reaction: The Stille cross-coupling reaction[26] is a very powerful method for the construction of new carbon-carbon bonds that has found application in disciplines ranging from natural-products synthesis (e.g., chloropeptin I[27] and apoptolidin[28]) to materials science (e.g., conducting polymers[29]). Unfortunately, the conditions that had previously been described for Negishi,[30] Suzuki,[31] and Hiyama[32] couplings of secondary alkyl halides were ineffective for the corresponding Stille reactions.

However, Gregory and his co-workers[33] again reported an tremendous exploitation of nickel catalysis to carry out a Stille cross-coupling of secondary alkyl halide **67** (bromides and iodides) with an assortment of tin reagents **68** to get C-C bond formation products **69 (Scheme 1.16)**.

$$\begin{array}{c}\text{Alkyl} \\ \text{Alkyl}\end{array}\!\!>\!\!X \quad + \quad Cl_3Sn\text{-}R \xrightarrow[\substack{\text{t-BuOH:i-BuOH} \\ \text{KOt-Bu, 60 }^{\circ}\text{C}}]{\substack{\text{10\% NiCl}_2 \\ \text{15\% 2,2'-bipyridine}}} \begin{array}{c}\text{Alkyl} \\ \text{Alkyl}\end{array}\!\!>\!\!R$$

67   **68**   **69**
R= aryl, alkenyl group,   Yield=55-72%
X= Br, I   10 examples
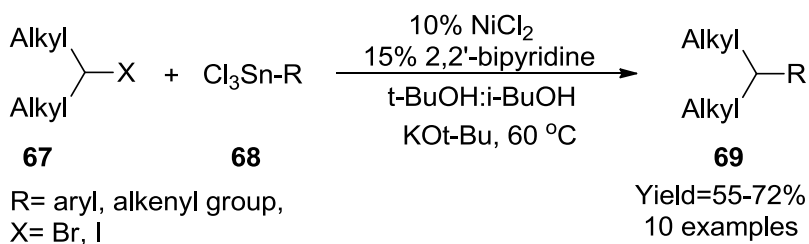
Scheme 1.16 Stille cross coupling of secondary alkyl halide with tin reagent.

1.4.7 Cross-coupling of aliphatic N-tosylaziridines with aliphatic organozinc reagents: Jamison *et al.* reported[34] on the first ligand (**72**) controlled, nickel-catalyzed cross-coupling of aliphatic N-tosylaziridines **70** with aliphatic organozinc **71** reagents (**Scheme 1.17**). The reaction protocol displays

complete regioselectivity for reaction at the less hindered C−N bond, and the products **73** are furnished in good to excellent yield for a broad selection of substrates. Moreover, they developed an air-stable nickel(II) chloride/ligand precatalyst that can be handled and stored outside a glovebox. In addition to increasing the activity of this catalyst system, this also greatly improves the practicality of this reaction, as the use of the very air-sensitive $Ni(cod)_2$ is avoided. Finally, mechanistic investigations, including deuterium-labeling studies, show that the reaction proceeds with overall inversion of configuration at the terminal position of the aziridine by way of aziridine ring opening by Ni (inversion), transmetalation (retention), and reductive elimination (retention).
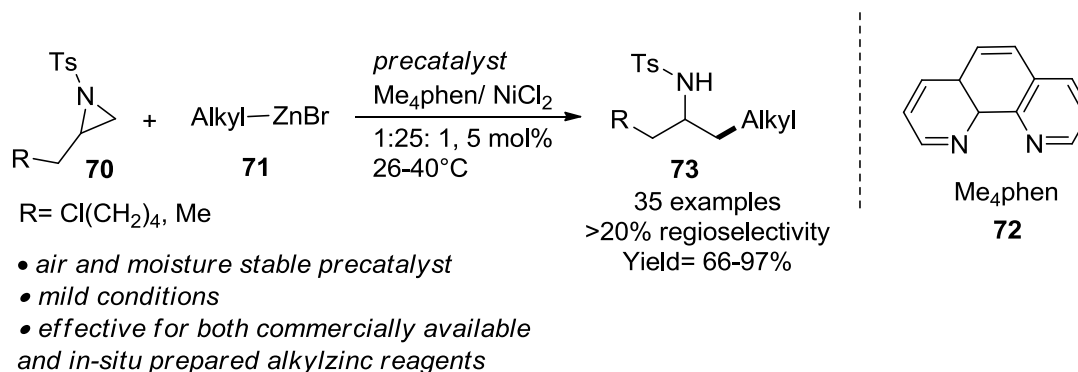
Scheme 1.17 Nickel-catalyzed cross-coupling of aliphatic N-tosylaziridines with aliphatic organozinc reagent.

1.4.8 Suzuki–Miyaura cross-coupling reactions: Diganta *et al.* reported a highly efficient green protocol for palladium acetate-catalysed ligand-free Suzuki–Miyaura[35] cross-coupling reactions in neat 'water extract of banana (WEB)' was developed **(Scheme 1.18)**. This method offers a mild, efficient and highly economical alternative to the existing protocols since the reaction proceeds in WEB at room temperature in air at very short reaction times (5–90 min) under 'ligand/external base/external promoter/organic medium' free conditions.

R^1= 4-OMe, 3-OMe. 4-Me, 4-Me, 4-Me, 4-NO_2, 4-CN, H, 4-CHO, 3-CHO, 2-CHO, 4-COMe
R^2= H, 4-OMe, 4-CF_3
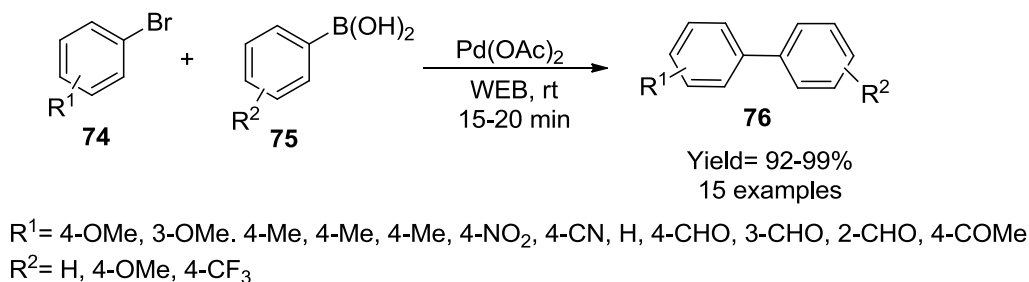
Scheme 1.18 Suzuki–Miyaura cross-coupling reactions in neat 'water extract of banana (WEB).

The **Scheme 1.18** shows the synthesis of Suzuki–Miyaura cross coupling product **76** by the coupling of aryl/ heteroaryl halide **74** with aryl boronic acid **75** in presence of palladium acetate catalyst at room temperature.

1.4.9 Stereospecific nickel-catalyzed cross-coupling reaction: Alkyl Grignard reagents that contain β-hydrogen atoms were used in a stereospecific[36] nickel-catalyzed cross-coupling reaction to form $C_{(sp3)}$-$C_{(sp3)}$ bonds **(Scheme 1.19)**. Aryl Grignard reagents were also utilized to synthesize 1, 1-diarylalkanes. Several compounds synthesized by this method exhibited selective inhibition of proliferation of MCF-7 breast cancer cells. Here the **scheme 1.19** shows the stereospecific synthesis of 1, 1-diarylalkane/1, 1-triarylalkane **79** by the coupling of benzylic ether **77** and alky/aryl Grignard reagent **78** in presence of Nickle catalyst.
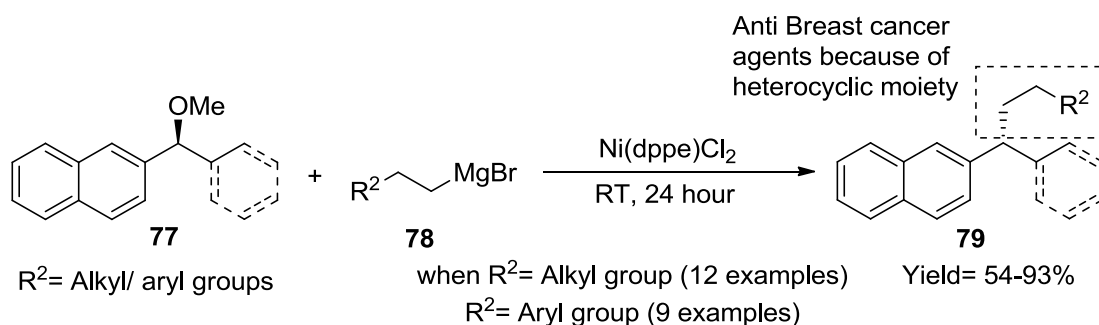
Scheme 1.19 Stereospecific nickel-catalyzed cross-coupling reactions of alkyl grignrd reagent and identification of anti breast cancer agents

From the literature, it is worth noting that till now very few reports are available on secondary alkyl halide where they have been used as the coupling partner. All the other reports have been mainly concerned with the use of primary alkyl halides as coupling partner only. Till now, no report has been published on tertiary alkyl groups as coupling partners.

1.5 Ring Opening Coupling Reaction

1.5.1 Nickel catalysed cyclisation of bicyclic alkenes with β-Iodo-(Z)-propenoates and o-Iodobenzoates

Oxabenzonorbornadienes and their aza- counterparts are long established as excellent substrates for coupling, coupling followed by ring opening, and various cyclisation reactions.[37] Although many ring opening reactions of oxabicyclic alkenes are known, unfortunately none of them describe the use of alkyl halides to accomplish the desired ring opening. In an effort to extend the recently developed strategy, there was an effort to explore the possibility of employing saturated alkyl halides to bring about the ring opening of oxabicyclic alkenes.

1.5.1.1 Reaction of oxabicyclic alkenes with arylic and vinylic halides: Cheng group reported[38] Palladium-catalyzed reductive couplings of organic halides with 7- heteroatom norbornadienes and developed new synthetic methods for substituted aryls and cis-1,2-dihydro-l-naphthyl alcohols and carbamates. This reaction involves the ring opening of bicyclic alkenes **80** with arylic and vinylic halides **81** to form mainly a ring opening product **82** and **83** (**Scheme 1.20**).
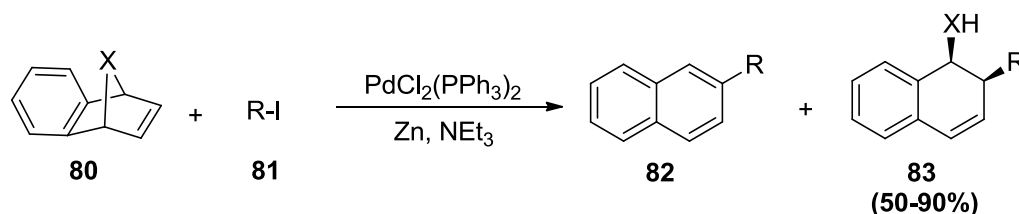
Case-1
X= NCOOMe
R= *p*-CH$_3$C$_6$H$_4$I, C$_6$H$_5$I, C$_6$H$_5$CH$_2$Br.
Case-2
X= O
R= *p*-CH$_3$C$_6$H$_4$I, *p*-CH$_3$OC$_6$H$_4$I, *m*-CH$_3$OC$_6$H$_4$I, *m*-CH$_3$C$_6$H$_4$I, C$_6$H$_5$I, *o*-CH$_3$C$_6$H$_4$I, *p*-OHC$_6$H$_4$I, *m*-ClC$_6$H$_4$I, *p*-CH$_3$COC$_6$H$_4$I, 1-iodonaphthalene, 2-iodothiophene, C$_6$H$_5$CH$_2$Br, *b*-bromostyrene, CH$_3$I

Scheme 1.20 Reductive coupling of organic halides with Norbornadienes.

1.5.1.2 Stereoselective ring opening reaction: Later, Chien-Hong Cheng and coworkers disclosed another similar report[39] wherein nickel (II) catalyst was used to bring about the highly stereoselective ring opening of 7-Oxa and Azanorbornenes with organic halides (**Scheme 1.21**). Nickel-catalyzed ring-opening reactions of 7-heteroatom norbornadienes and norbornenes with various organic halides to give products with multiple stereocenters were described. Treatment of 7-oxabenzonorbornadiene **84** and 7-carbomethoxy-7-azabenzonorbornadiene **85** with aryl iodides **86** in the presence of NiCl$_2$(PPh$_3$)$_2$ and Zn powder gave the corresponding ring-opening addition products *cis*-1,2-dihydro-2-aryl-1-naphthol **87** and methyl *N*-[*cis*-1,2-dihydro-2-aryl-1-naphthyl]-carbamate **88** completely stereoselectively in 40-99% yields (**Scheme 1.21a**). In most cases, addition reaction of aryl iodides **86** and **84** in the presence of NiCl$_2$(PPh$_3$)$_2$/Zn produces small amounts of(1S,2R)-2-phenyl-1,2-dihydronaphthalen-1-ol **89**, 1-naphthol **90** and 1,2-dihydro-1-naphthol **91**[40-41] (combined yields are less than 10%) as shown in **scheme 1.21b**. Compound **91** became a major product when the catalyst was changed from NiCl$_2$(PPh$_3$)$_2$ to NiCl$_2$(dppe). Addition of water (0.5 equiv.) increased the yield of 1,2-dihydro-1-naphthol to 44% yield ((**91:89**) 7:1). If MeOH was employed as solvent, product **91** was isolated in 81% yield.
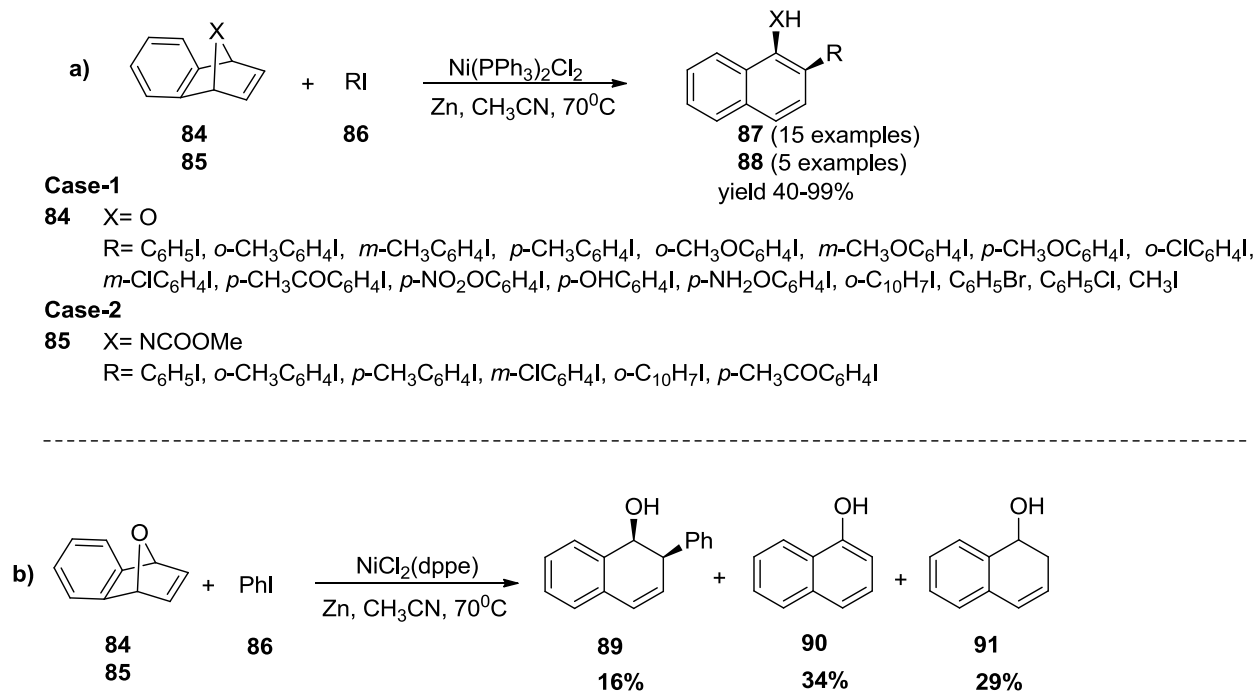
Scheme 1.21 Shows the ring opening of 7-Oxa and Azanorbornenes with organic halides .

1.5.1.3 Ring opening reactions of Oxabicyclic alkenes with terminal alkynes: Xue-Long Hou[42] and co-workers reported switch of addition and ring opening reactions of oxabicyclic alkenes **92** with terminal alkynes by sp^2-C-palladocycle **95** and sp^3-C-palladacycle **96** catalysis **(Scheme 1.22a)**. Palladacycles were found to be efficient catalysts for the reaction of oxabicyclic alkenes with terminal alkynes. A switch of reaction selectivity was realized using a palladacycle with a sp^2 or sp^3 C−Pd bond. Addition products **93** were afforded predominantly using a palladacycle with a sp^3 C−Pd bond, while ring-opening compounds **94** were the major products when palladacycles having a sp^2 C−Pd bond were used. DFT calculations revealed that the different trans-effects of the sp^2-C and sp^3-C donors in palladacycles are responsible for the switch in selectivity.

On the basis of the previous results,[43a-d] the reaction of 7-oxabenzonorbornadiene **97** with phenylacetylene **98** was tested in the presence of palladacycle **95** with an sp^2 C−Pd bond in 1,2-dichloroethane (DCE) at 50 °C **(Scheme 1.22b)**. The ring-opening product **99** was afforded in 84% yield accompanied by an 11% yield of addition product **100**. The substrate scope was investigated under the optimized conditions, and the reaction scheme is shown in as **Scheme 1.22c** where **101** and **102** give rise to **103** and **104.**

General scheme

R^1= H, OMe
R^2= H, OMe, Br
R^3= Ph, 4-Me-C$_6$H$_4$, 4-CF$_3$-C$_6$H$_4$, 2-Me-C$_6$H$_4$, 2-CF$_3$-C$_6$H$_4$, 6-MeO-naphthyl, SiMe$_3$, n-Bu,
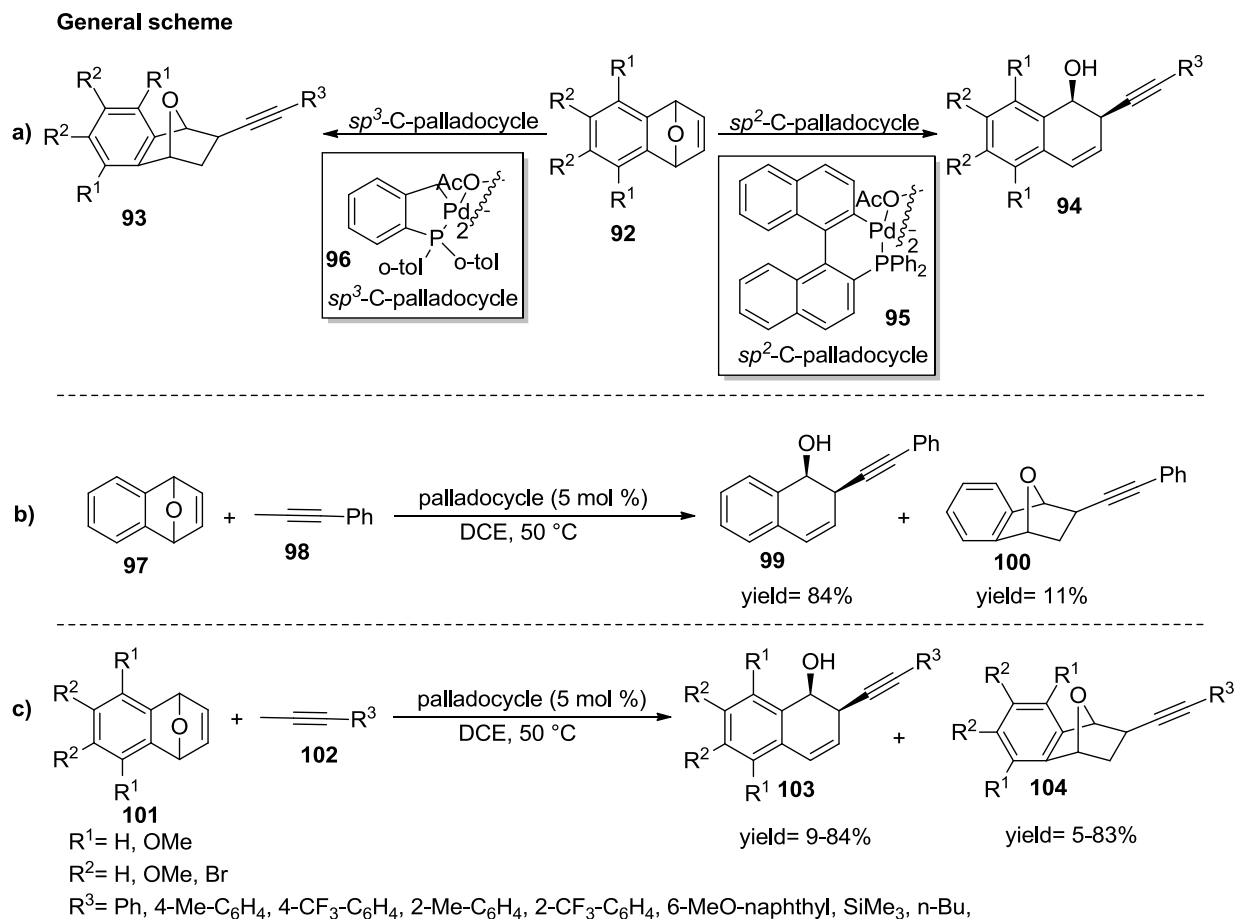
Scheme 1.22 Shows the switch of addition and ring opening reactions of Oxabicyclic alkenes with terminal alkynes by sp^2-C, P- and sp^3-C, Palladacycle catalysis.

To diversify and to enhance the utility of this reductive Heck reaction we planned to use oxabenzonorbornadienes as the alkene coupling partner. One of the reasons for doing so was that having already tested the veracity of our protocol with acrylates, which were electron-withdrawing alkenes, we wanted to try out another alkenic system, which was not conventionally electron-withdrawing. Oxabenzonorbornadienes and their aza counterparts are long established as excellent substrates for coupling, coupling followed by ring opening, and various cyclization reactions.[44] Although many ring-opening reactions of oxabicyclic alkenes are known, unfortunately none of them describe the use of saturated (sp^3) alkyl halides to accomplish the desired ring opening. The first such ring-opening report appeared in 1993, involving the ring opening of bicyclic alkenes with arylic and vinylic halides to form mainly fully aromatic ring-opening products.[45] Later, another report[46] appeared from the same lab wherein nickel catalyst was used to bring about the desired ring opening. In an effort to extend the reductive coupling strategy developed by Cheng group (described above), we wanted to explore the

possibility of employing saturated alkyl halides to bring about the ring opening of oxabicyclic alkenes.We, however, were more interested in using those substrates all of which contained β-hydrogens in their framework. Therefore, amplifying the scope of the reaction to substrates possessing β-hydrogen posed a challenge worth taking up. The results of the reaction between oxabenzonorbornadiene and saturated alkyl halides under nickel-catalyzed conditions have been discussed in chapter-2.

Section B: Heterocyclic molecules and their applications

1.6 A brief overview of heterocyclic molecules: A cyclic organic compound, in general termed as carbocyclic compound comprises a ring system containing all the carbon atoms in its skeleton. When at least one of the carbon atom in the carbocyclic ring is replaced by other atom (referred as heteroatom) then they are stated as heterocyclic compounds.[47-49]

The chemistry of heterocycles has great theoretical as well as practical importance. In fact, heterocyclic compounds filled more than half basket of the total chemical inventory of organic molecules. These structures form the basis for numerous pharmaceutical, agrochemical and biologically active compounds. Diverse compounds like alkaloids, antibiotics, essential amino acids, vitamins, haemoglobin, hormones and many synthetic drugs and dyes contains heterocyclic rings as core skeletons.[50] Though heterocyclic compounds with several heteroatoms are known in the literature, nitrogen is the most common which follows oxygen and sulfur among the others.[51-52] Nitrogen-containing heterocycles has importance in medical as well as organic chemistry because they constitute the main structure within a huge number of natural products and also because of their broad range of biological properties.[53] Particularly, condensed heterocycles act as synthetic building blocks and pharmacophores. Fused azaheterocycles comprise a family of biological agents with particularly interesting pharmacological properties related to planarity of the system and consequently to its DNA-chain intercalating ability, which make them suitable for anti-neoplastic and mutagenic applications.[54-57] Because of their useful applications in the biological field, synthesis of fused heterocycles has attracted the interest in modern drug discovery.[58-61]

Environmental considerations and simplicity of preparative procedure have bound organic chemists to look for greener synthetic choices and hence multicomponent reactions (MCRs) are now emerging as a responsible alternative tool in organic synthesis.[62] MCRs are also crucial in the design of new and bioactive small organic molecules[63a-h] as these procedures have distinctive green-chemistry[64] and atom-economy benefits.[65a-b]

Multicomponent reactions (MCRs) are one-pot reactions employing more than two starting materials, where most of the atoms of the starting materials are incorporated in the final products.[66] MCRs protocols are atom economic, for example, the majority if not all of the atoms of the starting materials are

incorporated in the product; they are efficient, for example, they efficiently yield the product since the product is formed in one step instead of multiple sequential steps; they are convergent, for example, several starting materials combine in one reaction to form the product; they exhibit a very high bond forming-index (BFI), for example, several non hydrogen atom bonds are formed in one synthetic transformation.[67]

Therefore MCRs are often a useful alternative to sequential multistep synthesis. Additionally, since MCRs are often highly compatible with a range of unprotected orthogonal functional groups, on a second level, the scaffold diversity of MCR can be greatly enhanced by the introduction of orthogonal functional groups into the primary MCR product and reacting them into subsequent transformations, e.g. ring formation reaction. This two layered strategy has been extremely useful in the past leading to a great manifold of scaffolds now routinely used in combinatorial and medicinal chemistry for drug discovery purpose.[68a-b]
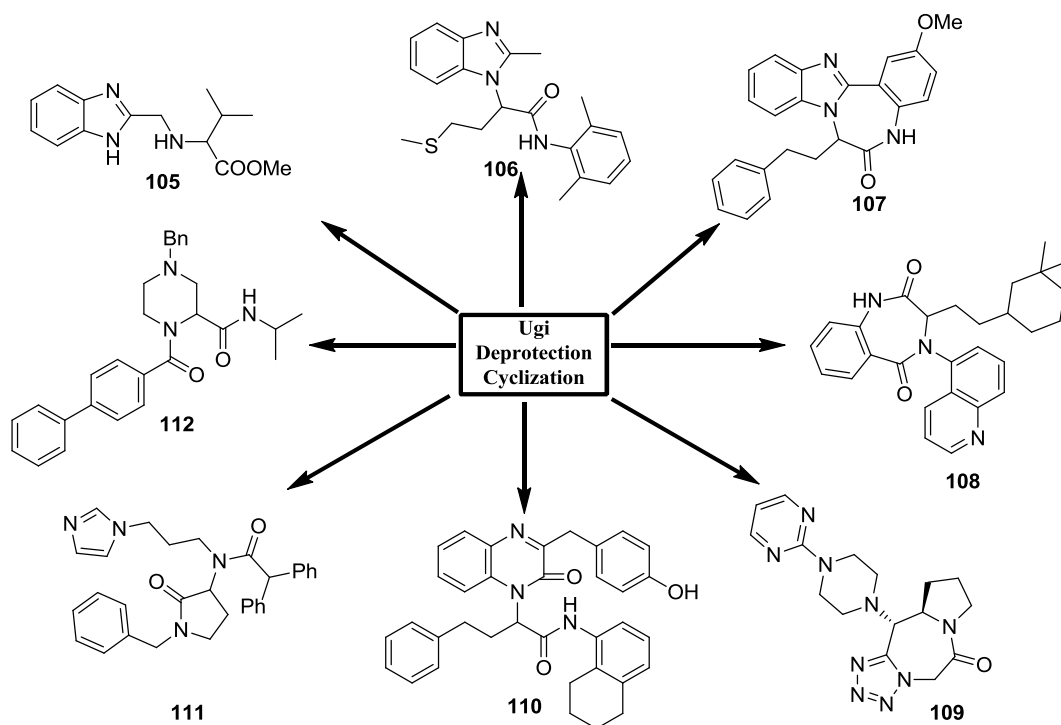
Scheme 1.23 UDC strategies allows for the great scaffold diversification of an initial Ugi reaction by using orthogonal protected bifunctional starting materials.

Thus, the initial MCR derived product can be considered as a synthetic hub to a vast diversity of novel cyclic or acyclic scaffolds by employing different secondary transformations. Typically, only 1-3 synthetic steps are needed to synthesize libraries of drug-like advanced compounds. A versatile example

of this strategy are the UDC- procedures (Ugi- Deprotection Cyclization) leading to a great scaffold diversity, e.g. benzimidazole (**105, 106, 107**), benzodiazepinedione (**108**), tetrazolodiazepinone (**109**), quinoxalinone (**110**), γ-lactams (**111**), and piperazines (**112**) (**Scheme 1.23**).[69a-n] The rapid and easy access to biologically relevant compounds by MCRs and the scaffold diversity of MCRs has been recognized by the synthetic community in industry and academia as a preferred method to design and discover biologically active compounds. The biological chemistry of MCRs however is very rich and provides great opportunities for drug hunters and researchers interested in small molecular weight compounds with biologically activity.

1.7 Pyranopyrazole as bioactive scaffold: As the section B of thesis chapter is mainly focused on chemistry of pyranopyrazole, diverse procedures reported for the synthesis of pyranopyrazole are briefly reviewed. Additionally, functionalization of these motifs has also been discussed systematically. Pyranopyrazoles are important class of biologically active heterocyclic compounds. They find applications as antibacterial,[70a-e] antifungal,[70a] antimicrobial,[71a-b] molluscicidal,[72] anti inflammatory,[73a-b] analgesic,[73b,74a-b] and biodegradable agrochemicals like insecticidal,[75] herbicidal agents[76] etc. Some substituted pyrano[2,3-c]pyrazoles have been found to be effective antiplatelet molecules[77a-b] which effect K^+ induced calcium dependent aortal contaction. Several pyrano[2,3-d]pyrazol-4-ones have demonstrated an affinity toward A1 and A2a adenosine receptors.[78a-b] Also 6-amino-5-cyano-dihydropyrano[2,3-c]pyrazoles have been identified as a screening hit for human Chk1 kinase inhibitors.[79]

1.8 Synthesis of Pyranopyrazole via two component reaction (2CR)

1.8.1 Synthesis of 4-aryl-4*H*-pyranopyrazoles: The first report of synthesis of dihydropyrano[2,3-c]pyrazoles was the reaction between 3-methyl phenylpyrazolin-5-one and tetracyanoethylene.[80] H. Otto and co-workers reported a base catalyzed two-component Michael type reaction between 4-arylidiene-1-phenyl-1*H*-pyrazol-5-one **113** and malononitrile **114** for the synthesis of various 4-aryl-4*H*-pyrano[2,3-c]pyrazoles **115** (**Scheme 1.24**).[81a-d]
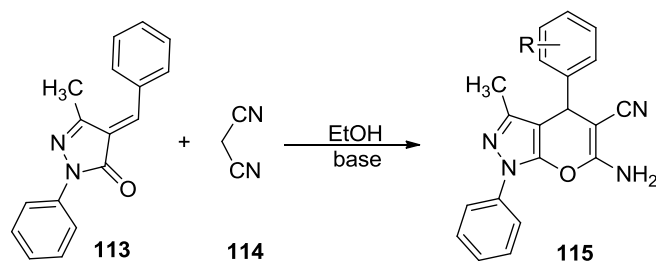
Scheme 1.24 Synthesis of 4-aryl-4*H*-pyrano[2,3-c]pyrazoles.

1.8.2 Synthesis of 4-alkyl and 4-aryl substituted Pyranopyrazole: Subsequently, 4-alkyl and 4-aryl-substituted pyranopyrazoles **118** were synthesized from reaction of 3-methyl-1*H*-pyrazol-5-one **116** with alkyl and arylidenemalononitrile **117 (Scheme 1.25)**.[82a-c]
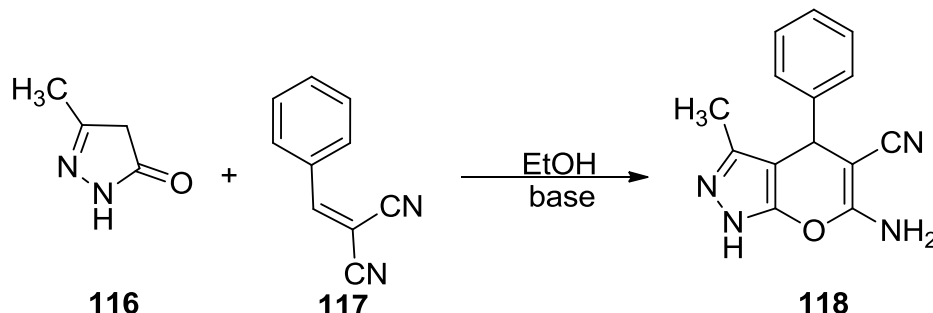
Scheme 1.25 Synthesis of 4-alkyl and 4-aryl substituted Pyranopyrazole.

1.8.3 Synthesis of Pyranopyrazole via CMUI: Y. Peng and co-workers have developed a two-component reaction involving pyran derivatives **120** and hydrazine hydrate **119** to obtain pyranopyrazoles **121** in water **(Scheme 1.26)**.[83] The reaction was promoted by a combination of microwave and ultrasonic irradiation (CMUI). The reported work had not only led to a practical synthetic method but also expand the usefulness of clean organic reactions in water.
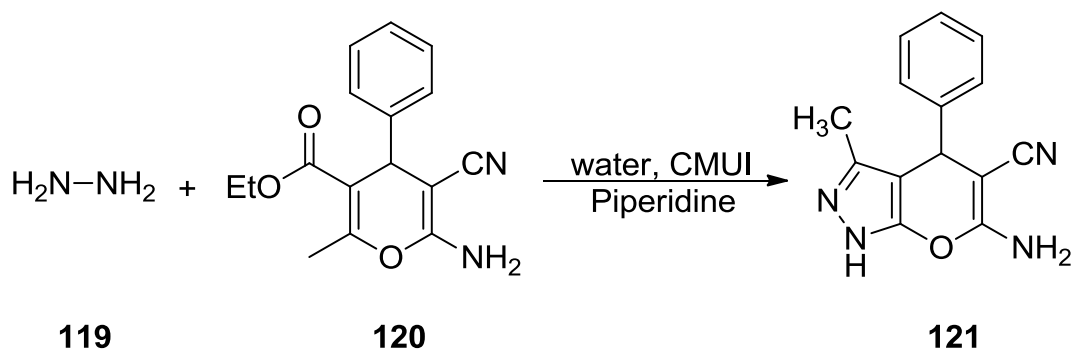
where CMUI= Combined Microwave Ultrasound Irradiation

Scheme 1.26 Synthesis of Pyranopyrazole through CMUI.

1.8.4 EDDA catalyzed synthesis of tetrahydroquinoline bearing Pyranopyrazole: Rameshwar Prasad Pandit and his colleagues[84] developed a new synthetic route to biologically interesting diverse tetrahydroquinolines **124** bearing pyranopyrazoles by reacting pyrazolones **122** and *N,N*-dialkylated aminobenzaldehydes **123** in the presence of EDDA **(Scheme 1.27)**. The key strategy underlying the methodology used was the domino Knoevenagel/heteroDiels–Alder reaction. This synthetic method provides a variety of novel tetrahydroquinolines in good yields.

Scheme 1.27 Shows the one-pot synthesis of tetrahydroquinoline derivatives bearing pyranopyrazole rings.

1.9 Synthesis of Pyranopyrazole via three component reaction (3CR)

1.9.1 Synthesis of Pyranopyrazole in ethanol: The most common and convenient approach toward diverse pyranopyrazoles is a base catalyzed three-component reaction[85a-d] (3CR) of pyrazol-5-one **116**, aldehydes **125**, and malononitrile **114**. Yu. A. Sharanin *et al*.[85a] have first developed this 3CR protocol for pyranopyrazole scaffolds **126** in ethanol using triethylamine as the catalyst **(Scheme 1.28)**. Later, S. Laufer and co-workers modified this 3CR protocol for combinatorial library of pyranopyrazole scaffolds.[85a-e]

Scheme 1.28 Synthesis of pyranopyrazole scaffolds by 3CR.

1.9.2 Synthesis of spiro pyranopyrazole: A. M. Shestopalov and co-workers reported the synthesis of spiro pyrazolopyran **129** via a three-component condensation between pyrazol-5-one **128,** N-methylpiperidone **127** and malononitrile **114** in absolute ethanol.[86a-b] However, this reaction occurred only on heating or when induced by electrochemical methods under an inert atmosphere **(Scheme 1.29)**.

Scheme 1.29 Shows the synthesis of spiro pyranopyrazole by electrochemical method.

1.9.3 Synthesis of spiro-oxindole via sequential one pot approach: Anshu Dandia *et al.*[87] developed a direct and efficient approach for the preparation of medicinally promising pyrazolopyridinyl spirooxindoles **133, 134** has been developed through a sequential one-pot, three-component reaction of easily available isatin **130**, a-cyanoacetic ester or malononitrile **132**, and 5-amino-3-methylpyrazole **131** catalyzed by sodium chloride in water **(Scheme 1.30)**. Desired products were obtained in high to excellent yields using a simple workup procedure. The product synthesized by using cyanoacetic ester showed high diastereoselectivity in which the stereochemistry of major diastereomer was confirmed by X-ray diffraction analysis.
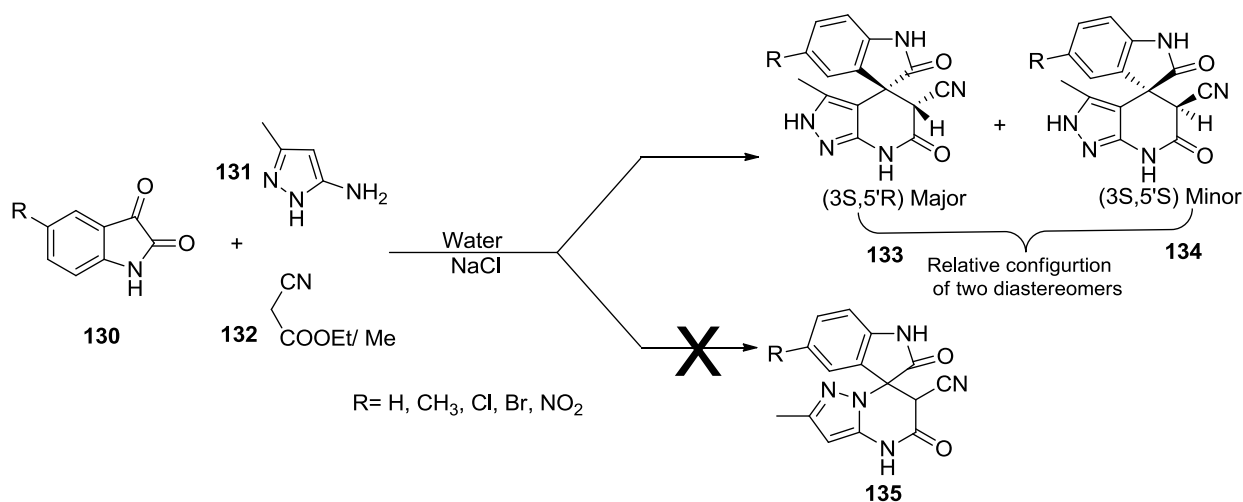
Scheme 1.30 Synthesis of spiro[indoline-3,4'-pyrazolo[3,4-*b*]pyridines].

The present green synthesis shows attractive characteristics such as the use of water as the reaction medium, one pot conditions, short reaction period, easy workup/purification, and reduced waste production, without use of any acid or metal promoters.

1.9.4 Synthesis of spiro-Pyranopyrazole annulated oxindole scaffolds: Combinatorial library of spiro pyranopyrazole annulated oxindole scaffolds **137** were synthesized by base catalyzed or elctrochemical 3CR between pyrazol-5-one **116**, cyclic ketones like istain **136** and malononitrile **114** in ethanol **(Scheme 1.31)**.[88a-d]
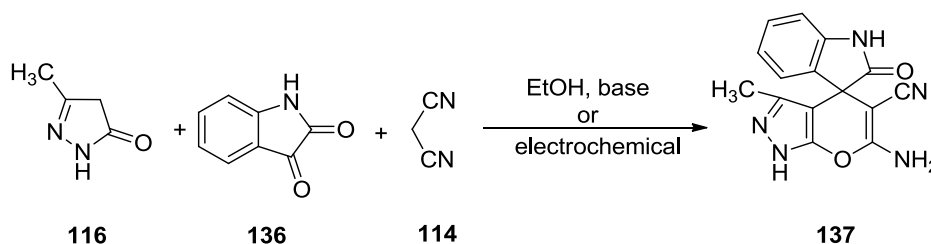
Scheme 1.31 Synthesis of spiro Pyranopyrazole annulated oxindole scaffolds.

1.9.5 Synthesis of 4-alkyl-6-amino-5-cyano-3-methyl(propyl,phenyl)-2*H*,4*H*-pyrano[2,3-*c*]pyrazoles: V. D. Dyachenko and co-workers[89] obtained 4-alkyl-6-amino-5-cyano-3-methyl(propyl, phenyl)-2*H*,4*H*-pyrano[2,3-*c*]pyrazoles **142** or **143** by reaction of 4-alkylmethylene-3-substituted 5-pyrazolones **138** with cyanothioacetamide **139** or malononitrile **114** in ethanol in the presence of morpholine.
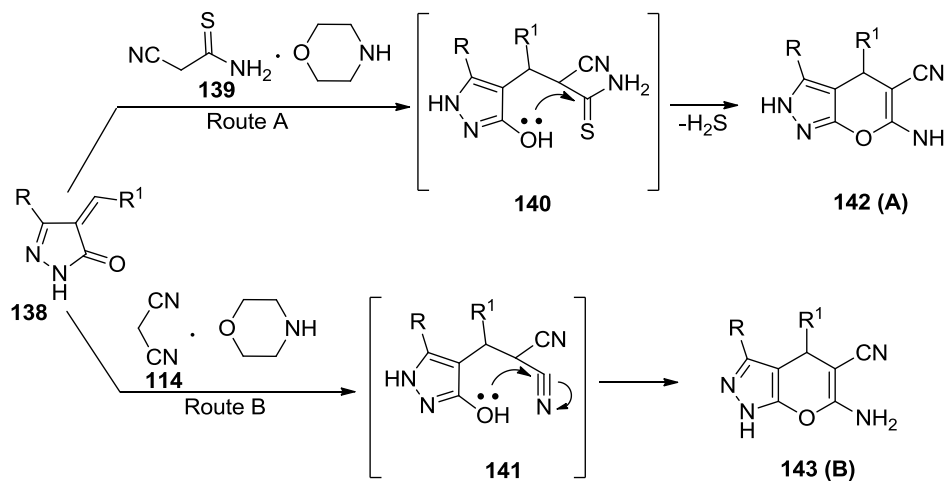
R = Ph, Me, Pr

R^1 = Me(CH$_2$)$_5$, Me$_2$CHCH$_2$, cyclohexyl, 2-butyl, 2-pentyl, Me(CH$_2$)$_8$, Ph(CH$_2$)$_2$, Me(CH$_2$)$_{10}$, Me$_2$CH, cyclohex

Scheme 1.32 Synthesis of 4-alkyl-6-amino-5-cyano-3-methyl(propyl, phenyl)-2H,4H-pyrano[2,3-c]pyrazoles.

Both routes probably include formation of the corresponding Michael adducts **140** and **141**, regioselectively undergoing ring closure under the reaction conditions to form the substituted pyrano[2,3-*c*]pyrazoles **142** and **143 (Scheme 1.32)**.

1.9.6 Microwave-assisted Knoevenagel–Hetero-Diels–Alder reaction: Radi *et al*. reported an organocatalyzed microwave-assisted Knoevenagel–Hetero-Diels–Alder reaction for the synthesis of 2,3-dihydropyran[2,3-*c*]pyrazoles **147** from pyrazol-2-one **144,** ethoxyethene **145** and aldehyde **146 (Scheme 1.33)**.[90] Using proline derivatives as catalyst in *t*-BuOH, the two diastereomers of the desired product were isolated in good yields with a 4:1 diastereomeric ratio.
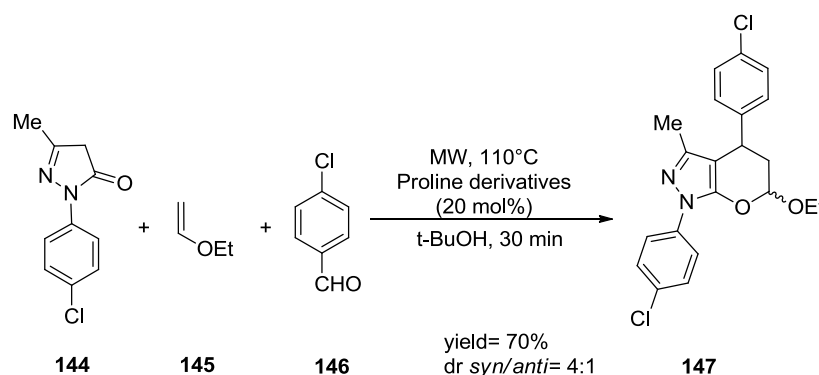
Scheme 1.33 Shows the synthesis of 2,3-dihydropyran[2,3-*c*]pyrazol.

1.9.7 Synthesis of dihydropyrano[c] chromenes from Friedländer reaction: Mehdi Khoobi *et al*.[91] proposed the novel hybrid derivatives of two known scaffolds; tetrahydroaminoquinoline and coumarin were synthesized and evaluated for both acetylcholinesterase(AChE) and butyrylcholinesterase (BuChE) activities. By means of an efficient nanocatalyst, the reaction time for the syntheses of the target compounds was reduced. Subsequently, Ellman's modified method was used to evaluate the enzyme inhibitory activity of the synthesized structures.

The synthesis of a novel series of Tacrine analogues **154** in a rather convenient way is described in this work. As outlined in **Scheme 1.34**, these compounds could be easily prepared by the AlCl$_3$ promoted Friedländer reaction[91] between the corresponding known dihydropyrano[*c*]chromenes **152** and cyclohexanone **153**. Several methods have been reported for the synthesis of dihydropyrano[*c*] chromenes **152**. Recently, the successful usage of magnetic nanocatalyst including (2-aminomethyl) phenol moiety on the surface of hydroxyapatite encapsulated maghemite γ-Fe$_2$O$_3$) in aqueous medium for the synthesis of 2-amino-5-oxo-4,5-dihydropyrano[3,2-*c*]chromene-3-carbonitriles has been reported. In refluxing water and in the presence of magnetic nanocatalyst **149**, the addition of 4-hydroxycoumarin **151** to the stirring mixture of various aldehydes, **148**, and malonitrile **114** yielded 7-substituted 2-amino-5-oxo-4,5-dihydropyrano[3,2-*c*]chromene-3-carbonitriles **152**. This 'onepot' reaction protocol proceeds through

formation of alkylidene or arylidenemalononitrile intermediate **150**. Treatment of pyranochromene **152**, with cyclohexanone **153**, in the presence of aluminum trichloride and in refluxing 1,2-dicholorethane as solvent, afforded the target molecules **154**. A notable feature of this procedure is the straightforward product isolation without formation of any side-products.

R= Methyl, Ethyl, *n*-Butyl, Phenyl, 3-Fluorophenyl, 4-Fluorophenyl, 2-Chlorophenyl, 3-Chlorophenyl, 4-Chlorophenyl, 2,4-Dichlorophenyl, 3-Nitrophenyl, 4-Methylphenyl, 4-Methoxyphenyl, 3,4-Dimethoxyphenyl, 3,4,5-Trimethoxyphenyl, Benzodioxole-5-yl, 4-Pyridyl, 2-Thienyl
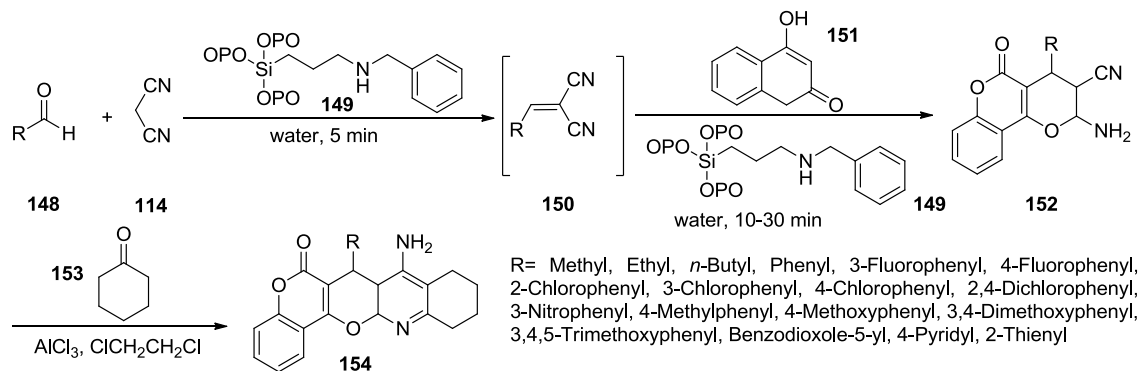
Scheme 1.34 Synthetic pathway of the target compounds 2-amino-5-oxo-4,5-dihydropyrano[3,2-*c*]chromene-3-carbonitriles and tacrine analogues.

1.9.8 Synthesis of Pyran derivatives in DES: Najmedin Azizi *et al*.[92] reported an ecofriendly one-pot multicomponent reaction of 1,3-dicarbonyl compounds **156**, aldehydes **155**, and malononitrile **114** was carried out in a different deep eutectic solvent (DES) based on choline chloride, to synthesize highly functionalized benzopyran and pyran derivatives **157** under catalyst-free conditions **(Scheme 1.35a)**.

ChCl= Choline chloride

R= C$_6$H$_5$, 4-OMe-C$_6$H$_4$, 4-Cl-C$_6$H$_4$, 3-NO$_2$C$_6$H$_4$, 4-OH-C$_6$H$_4$, 4-Me-C$_6$H$_4$, Furaldehyde, 4-F-C$_6$H$_4$, 4-NO$_2$-C$_6$H$_4$, 2,4-OMe-C$_6$H$_3$

1,3-dicarbonyl compounds (**179**)= Acetyl acetone, Ethyl acetoacetate, Methyl acetoacetate, Dimedone
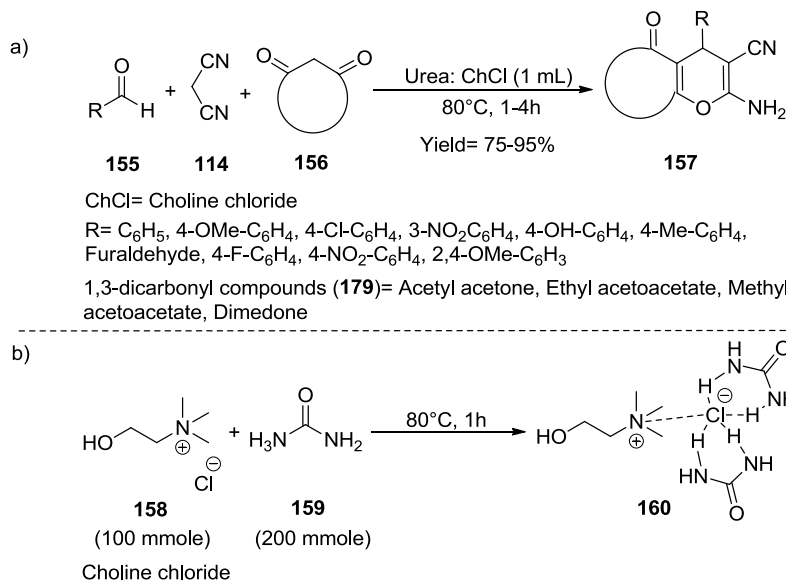
Scheme 1.35 Shows the (a) Green syntheses of pyran and benzopyran derivatives in DES and, (b) Deep eutectic solvent preparation (DES).

The results showed that urea: choline chloride based DES is the best solvent and is successfully applicable to a wide range of aldehydes, active methylene compounds with high yields (75–95%) and short reaction times (1–4 h). DES **160** forms by mixtures of quaternary ammonium salt **158** and a simple hydrogen bond donor (HDB) such as urea **159**, carboxylic acid, sugar and amide **(Scheme 1.35b)**. DESs exhibit some properties similar to ionic liquids such as non-volatility, biodegradability, low cost, thermal stability, and ready availability from bulk renewable resources without any further modification.[93–102]

1.10 Synthesis via four component reaction (4CR)

1.10.1 Synthesis and mechanism of 6-amino-5-cyano-3-methyl-4-aryl-2*H*,4*H*-dihydropyrano[2,3-*c*]pyrazoles: Vasuki and Kumaravel reported[103] an environmentally benign four-component reaction of hydrazine hydrate **119**, ethylacetoacetate **161**, aldehyde **162** and malononitrile **114** in aqueous medium at room temperature developed for the synthesis of 6-amino-5-cyano-3-methyl-4-aryl/heteroaryl-2*H*,4*H*-dihydropyrano[2,3-*c*]pyrazoles **163 (Scheme 1.36a)**. The formation of the product is proposed to involve the following tandem reactions: pyrazolone **116** formation by reaction between **119** and **161**, Knoevenagal condensation between **162** and **114** give **164**, Michael addition of **116** to **164**, followed by cyclization of **165** and tautomerization of **166** give the final product **163 (Scheme 1.36b)**.
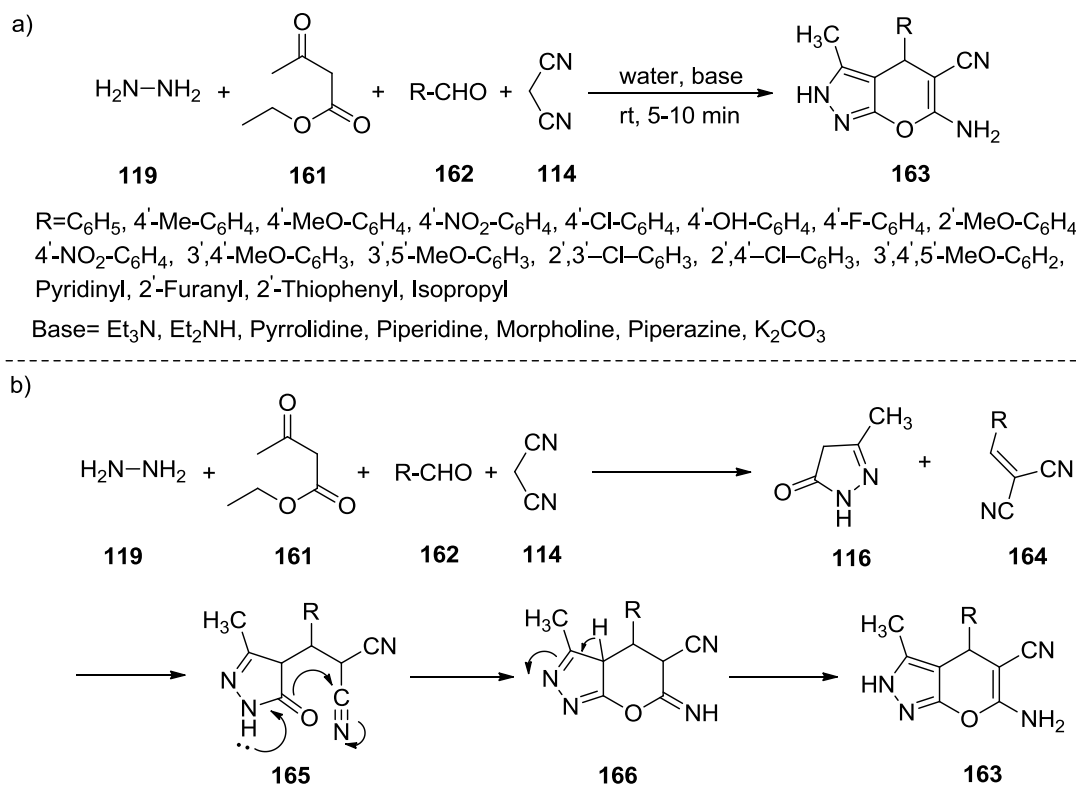
Scheme 1.36 Shows the (a) Synthesis of 6-amino-5-cyano-3-methyl-4-aryl/heteroaryl-2H,4H-dihydropyrano[2,3-c]pyrazoles (b) Mechanism of the reaction.

1.10.2 Imidazole catalyzed synthesis of Pyranopyrazole: Aisha Siddekha Aatika Nizam and M.A. Pasha[104] describe a one-pot four component synthesis of pyranopyroles **168** from aryl aldehydes **167**, ethyl acetoacetate **161**, malononitrile **114** and hydrazine hydrate **119** in the presence of catalytic amounts of an organocatalyst imidazole in water as medium **(Scheme 1.37)**. A plausible mechanism for the formation of imidazole catalyzed pyranopyrazoles has been envisaged. This method is rapid, simple, provides products in good yield, and is eco-friendly. In addition, based on the optimized geometry, the frequency and intensity of the vibrational bands of 6-amino-4-(4-methoxyphenyl)-5-cyano-3-methyl-1-phenyl-1,4-dihydropyrano[2,3-*c*]pyrazole were obtained by the density functional theory (DFT) calculations using 6-31G(d,p) basis set.
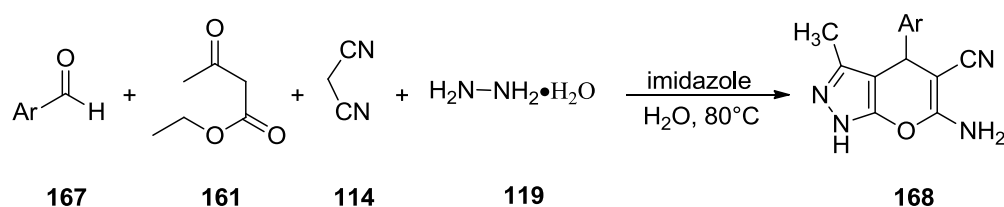
Ar= various aromatic aldehydes

Scheme 1.37 Synthesis of Pyranopyrazole from various substituted aromatic aldehydes.

1.10.3 L-proline catalyzed synthesis of Pyranopyrazole: Hormi Mecadon *et al*.[105] reported an efficient four-component synthesis of 6-amino-4-alkyl/aryl-3-methyl-2,4-dihydropyrano[2,3-*c*]pyrazole-5-carbonitriles **170** involving ethyl acetoacetate **161**, hydrazine hydrate **119**, malononitrile **114**, and various aldehydes **169** using L-proline (10 mol %) in water under mild reaction condition in excellent yields is established **(Scheme 1.38)**. A comparative study of L-proline with γ-alumina, basic alumina, and KF-alumina was also carried out. The generality and functional tolerance of this convergent and environmentally benign method is demonstrated.
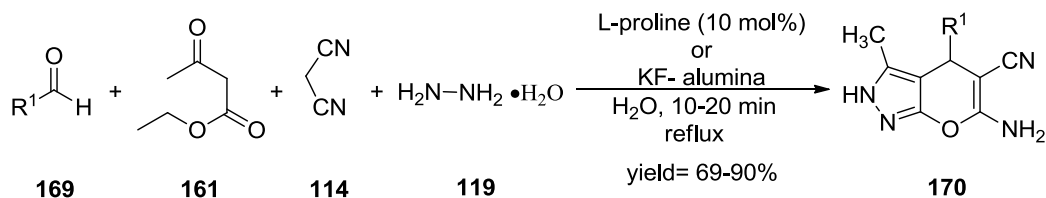
R^1=C$_6$H$_5$, 4-CH$_3$C$_6$H$_4$, 4-CH$_3$O$_6$H$_4$, 2-ClC$_6$H$_4$, 4-ClC$_6$H$_4$, 3-BrC$_6$H$_4$, 4-BrC$_6$H$_4$, 4-HOC$_6$H$_4$, 4-N(CH$_3$)$_2$C$_6$H$_4$, 2-NO$_2$C$_6$H$_4$, 3-NO$_2$C$_6$H$_4$, 4-NO$_2$C$_6$H$_4$, 3-CH$_3$O-4-HOC$_6$H$_3$, 3,4-(CH$_3$O)$_2$C$_6$H$_3$, 2,5-(CH$_3$O)$_2$C$_6$H$_3$, 3,4,5-(CH$_3$O)$_3$C$_6$H$_2$, 1-Naphthyl, 9-Anthranyl, Butyryl

Scheme 1.38 Synthesis of 6-amino-4-alkyl/aryl-3-methyl-2,4-dihydropyrano[2,3-*c*]pyrazole-5-carbonitriles.

1.10.4 Synthesis of Pyranopyrazole via non-catalytic approach: Santhosh Reddy Mandha *et al*.[106] envisaged an ecofriendly green approach for synthesis of substituted pyrano[2,3-*c*]pyrazoles (**173, 175**) via a multicomponent one pot approach from ethylacetoacetate, hydrazine hydrate, malononitrile and various substituted aldehydes in aqueous ethanol medium (1:1) at 100°C under totally non-catalytic conditions. The formation of **172** is believed to involve the Knoevenagel condensation of aldehyde **171** and malononitrile **114**. The intermediate **172** undergoes Michael addition with pyrazolin-5-one **116** (formed in situ from ethylacetoacetate and hydrazine hydrate) followed by an intra-molecular cyclization to give polyfunctionalized pyrano[2,3-*c*]pyrazoles **173** (**Scheme 1.39 route a**). In similar manner intermediate **172** react with **174** (formed in situ from ethylacetoacetate and phenylhydrazine) and finally give rise to **175** (**Scheme 1.39 route b**). The synthesized compounds were evaluated for their antibacterial, anti-inflammatory and cytotoxic activities.

Route a
R= 3-OH-Ph, 4-Br-Ph, 4-CH₃-Ph, 4-OH-Ph, C₆F₅, 3-pyridinyl, thien-2-yl, 4-C₁₁H₅Cl₃NO, 3-OC₆H₅-Ph, 3-C₁₁H₅Cl₃NO
Route b
R= Ph, 4-OH-Ph, 4-OCH₃-Ph, 4-NO₂-Ph, 3-OC₆H₅-Ph, 3-pyridinyl, 3-C₁₁H₅Cl₃NO
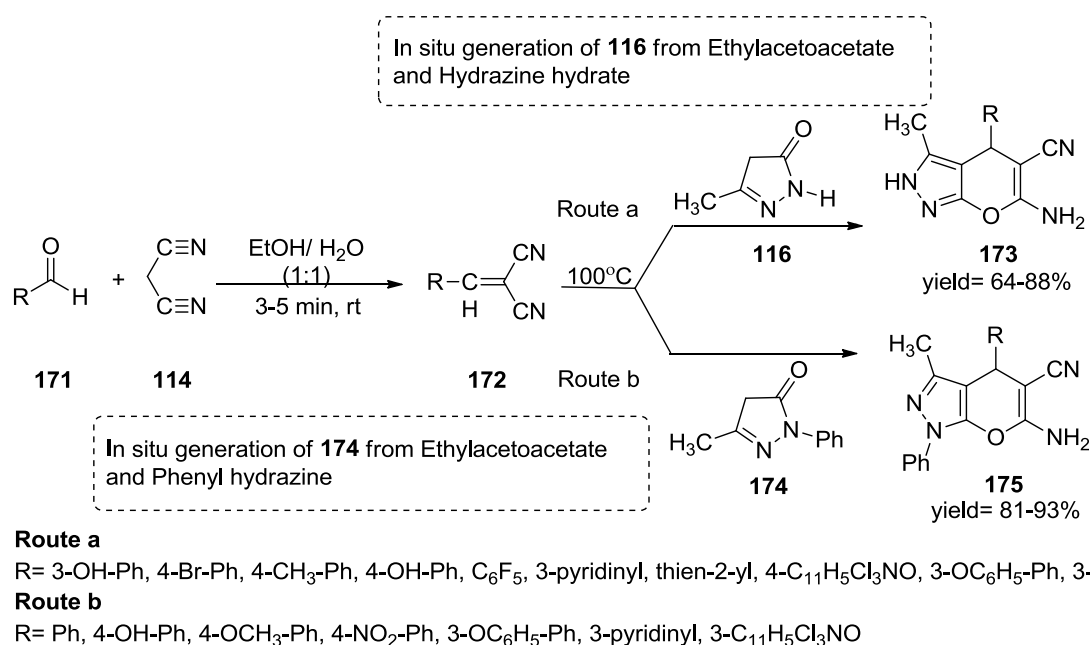
Scheme 1.39 Construction of various substituted pyrano[2,3-*c*]pyrazoles.

1.10.5 Ionic liquid catalyzed synthesis of Pyranopyrazole: Javed Ebrahimi *et al*.[107] reported a simple, green and efficient protocol for synthesis of dihydropyrano[2,3-*c*]pyrazole derivatives **177** is developed by a four component reaction of hydrazine hydrate **119**, ethyl acetoacetate **161**, malononitrile **114** and various benzaldehydes **176**, in the presence of 3-methyl-1-(4-sulphonic acid)butylimidazolium hydrogen sulphate [(CH₂)₄SO₃HMIM][HSO₄], an acidic ionic liquid and as a catalyst, under solvent-free conditions (**Scheme 1.40**]. The key advantages of this process are high yields, shorter reaction times, easy work-up, purification of products by non-chromatographic method and the reusability of the catalyst.

Scheme 1.40 [(CH$_2$)$_4$SO$_3$HMIM][HSO$_4$] catalysed synthesis of pyranopyrazole.

1.10.6 Barium hydroxide catalyzed synthesis of Pyranopyrazole: Sadeq Hamood Saleh Azzam[108] and M. A. Pasha reported Ba(OH)$_2$ catalyzed simple and efficient one-pot four-component reaction of Meldrums acid **179**, ethyl acetoacetate **161**, hydrazine hydrate **119**, and aromatic aldehydes **178** to give 3-methyl-4-aryl-4,5-dihydro-1*H*-pyrano[2,3-*c*]pyrazol-6-ones **180** in refluxing water is reported **(Scheme 1.41)**. The yields are high and the reactions go to completion in 1–2 h.

Ar= 3,4,5-(MeO)$_3$C$_6$H$_2$-, 4-MeOC$_6$H$_4$-, 3-MeOC$_6$H$_4$-, 2-ClC$_6$H$_4$-, 2-HOC$_6$H$_4$-, 4-FC$_6$H$_4$-, 3-NO$_2$C$_6$H$_4$-, HCHO, CH$_3$-, CH$_3$CH$_2$-, CH$_3$CH$_2$CH$_2$-

Scheme 1.41 Synthesis of 3-methyl-4-aryl-4,5-dihydro-1*H*-pyrano[2,3-*c*]pyrazol-6-ones.

1.10.7 Synthesis of bis-pyranopyrazole: A simple and efficient method was developed for the synthesis of multisubstituted bispyrano[2,3-*c*]pyrazole derivatives **(183a-f and 185a-f)** via one-pot reaction of β-keto esters **181**, hydrazine (or phenylhydrazine) **119 (184)**, terephthalaldehyde **182**, and malononitrile **114** in the presence of CeCl$_3$.7H$_2$O (10 mol%) as a catalyst **(Scheme 1.42)** by Keyume Ablajan *et al.*[109]. This method provides the products in good yields after a simple workup procedure without further purification.

(a)

181   **182**   **114**   **119**   **183a-f**
yield= 76%

(b)

181   **182**   **114**   **184**   **185a-f**
yield= 77%

220a= R^1= CH$_3$, R^2= CH$_3$ or C$_2$H$_5$ 222a= R^1= CH$_3$, R^2= CH$_3$ or C$_2$H$_5$
220b= R^1= C$_2$H$_5$, R^2= CH$_3$ or C$_2$H$_5$ 222b= R^1= C$_2$H$_5$, R^2= CH$_3$ or C$_2$H$_5$
220c= R^1= n-C$_3$H$_7$, R^2= CH$_3$ or C$_2$H$_5$ 222c= R^1= n-C$_3$H$_7$, R^2= CH$_3$ or C$_2$H$_5$
220d= R^1= iso-C$_3$H$_7$, R^2= CH$_3$ or C$_2$H$_5$ 222d= R^1= iso-C$_3$H$_7$, R^2= CH$_3$ or C$_2$H$_5$
220e= R^1= Ph, R^2= CH$_3$ or C$_2$H$_5$ 222e= R^1= Ph, R^2= CH$_3$ or C$_2$H$_5$
220f= R^1= CF$_3$, R^2= CH$_3$ or C$_2$H$_5$ 222f= R^1= CF$_3$, R^2= CH$_3$ or C$_2$H$_5$

Scheme 1.42 Four-component one-pot syntheses of multisubstituted bis-pyrano[2,3-*c*]pyrazoles.

1.10.8 Catalyst-free synthesis of novel spiro-pyranopyrazole derivatives: D. M. Pore[110] and his colleagues reported the catalyst-free multicomponent reaction (MCR) capable of affording a wide range of novel spiro-pyranopyrazole derivatives **188** from pyrazolone (in situ formed from acetylenic esters **187** with hydrazine hydrate **119)** at room temperature with isatin **186** and malononitrile **114 (Scheme 1.43)**. Catalyst- free conditions along with green solvent system make the process ecofriendly as well as economical. Simple reaction conditions and easy work-up procedure that resulted into simple isolation and purification of products by non-chromatographic methods, that is, by simple recrystallization from methanol as well as novelty are the significant advantages of the present protocol.

186   **114**   **119**   **187**   **188**
                                    R= Cl, I, OMe, Me   Yield= 82-91%
                                    R'= H, Me, CH$_2$CH$_3$
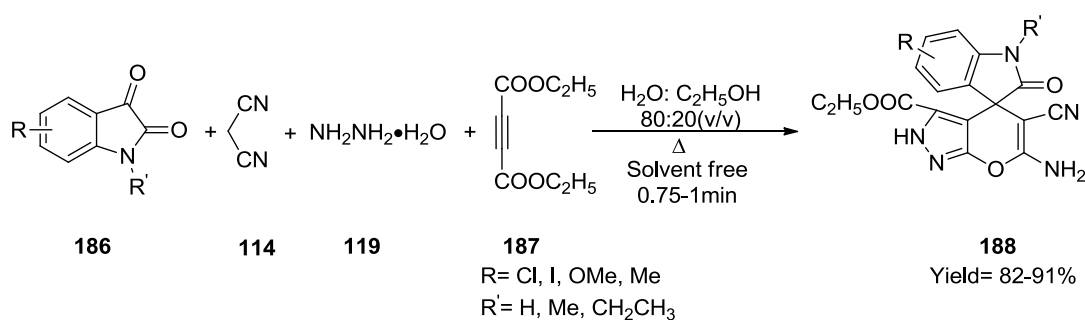
Scheme 1.43 An unprecedented catalyst-free, multicomponent synthesis of novel spiro pyrano[2,3-*c*]pyrazole derivatives.

1.10.9 Synthesis of spiro[indoline-3,4$^{'}$-pyrano[2,3-*c*]pyrazole]-3$^{'}$-carboxylate derivatives: Suman Pal and her colleagues[111] reported one pot four-component reaction for the efficient synthesis of

spiro[indoline-3,4'-pyrano[2,3-*c*]pyrazole]-3'-carboxylate derivatives **189**. A novel one pot protocol has been developed to synthesize various spiro-[indoline-3,4'-pyrano[2,3-*c*]pyrazole]-3'-carboxylate derivatives **(Scheme 1.44a)** from the four-component reaction of isatin **136**, malononitrile **114**, hydrazine derivatives **119** and dialkyl acetylenedicarboxylates **187**. In this process two C–C bonds, two C–N bonds and one C–O bond have formed in one pot. The notable features of this protocol are simple and environmentally benign reaction condition, easy isolation of products, applicable to a wide range of readily available starting materials and good yields.

On the basis of the above results a plausible reaction mechanism is shown in **Scheme 1.44b**. They believe that the initial step is formation of intermediate **190** by Knoevenagel condensation of isatin **136** and malononitrile **114**. The next step is the formation of pyrazolone **191** from the reaction of dialkyl acetylenedicarboxylate **187** and hydrazine hydrate **119**. Then intermediate **190** undergoes Michael addition to **191** in the presence of a base followed by enolization affording intermediate **192** which undergoes intramolecular cyclization to form **193**. In the final step **193** undergoes tautomerization and transforms into the desired product **189**.
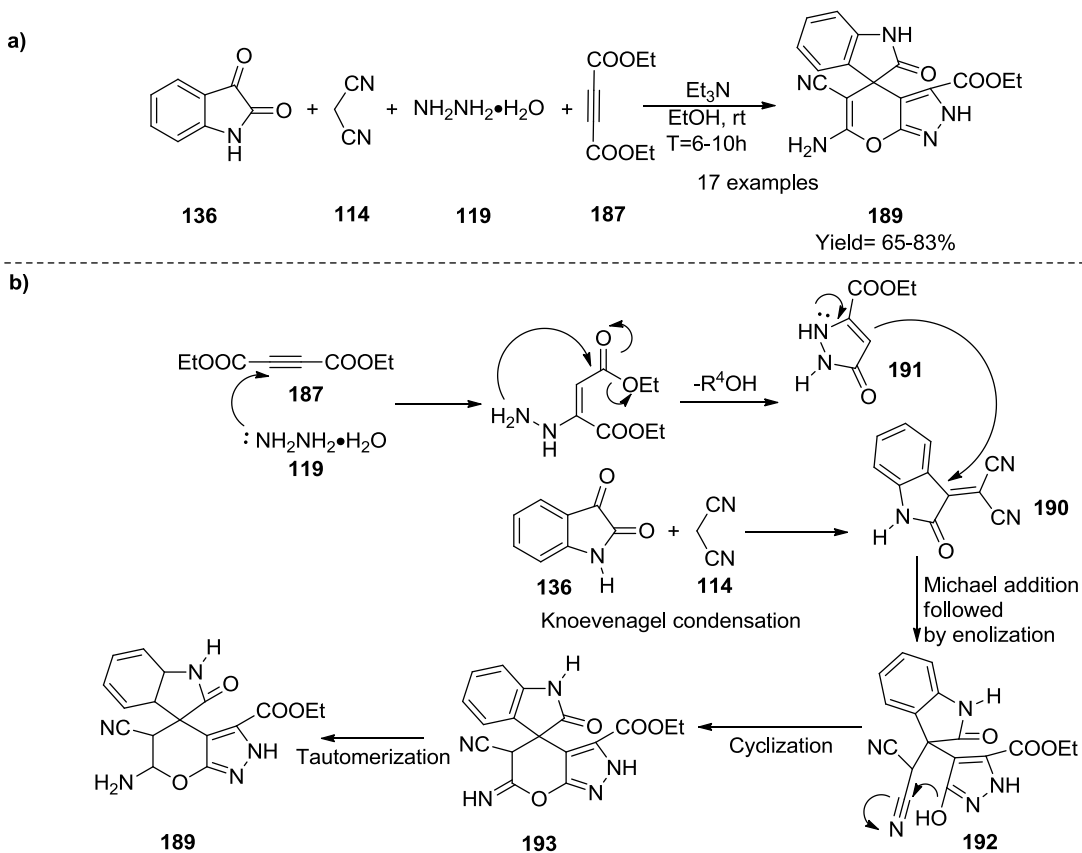
Scheme 1.44 Shows the (a) synthesis and (b) mechanism for the synthesis of [indoline-3,4'-pyrano[2,3-*c*]pyrazole]-3'-carboxylate derivatives.

1.10.10 Organocatalyst sodium benzoate catalyzed synthesis of Pyranopyrazole: Hamzeh Kiyani[112] and their colleagues reported an efficient, green, and facile four-component reaction for the preparation of pyrano[2,3-*c*]pyrazole derivatives **195** through the condensation reaction of aryl aldehydes **194**, ethyl acetoacetate **161**, malononitrile 1**14**, and hydrazine hydrate **119** or phenyl hydrazine **184** in the presence of commercially available organocatalyst sodium benzoate under aqueous condition is reported **(Scheme 1.45)**. The products are produced with high yields and in shorter reaction times.

R= H (10 examples)
R= Ph (7 examples)
Ar= C$_6$H$_5$, 4-NO$_2$C$_6$H$_4$, 3-NO$_2$C$_6$H$_4$, 2-NO$_2$C$_6$H$_4$,4-CH$_3$C$_6$H$_4$, 4-OCH$_3$C$_6$H$_4$, 4-(NMe)$_2$C$_6$H$_4$, 4-ClC$_6$H$_4$
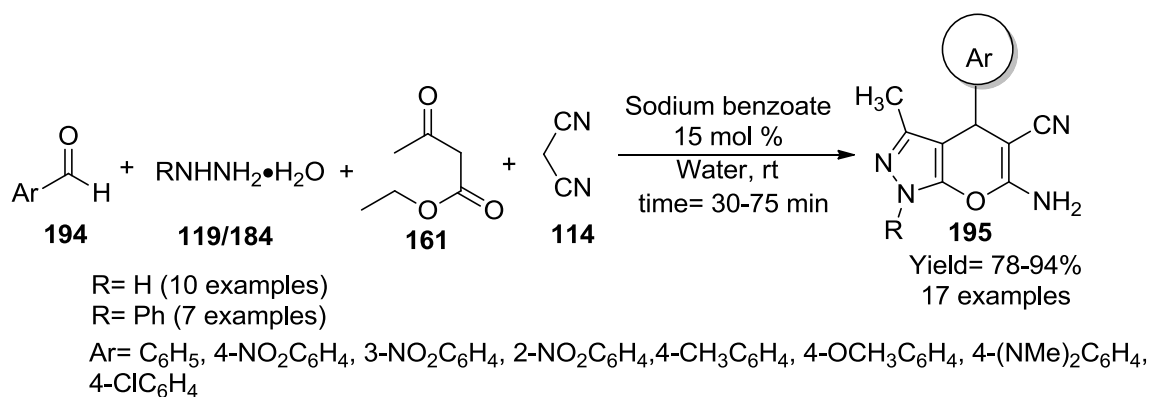
Scheme 1.45 Shows the synthesis of pyrano[2,3-*c*]pyrazole derivatives.

1.10.11 DMAP catalyzed synthesis of spiro-oxindole derivatives: Jun Feng *et al.*[113] developed an efficient and clean reaction process for the convenient and cheap synthesis of spirooxindole derivatives **(Scheme 1.46)** with one-pot reactions of isatins **136**, malononitrile **114** (or ethyl cyanoacetate **196**), and 5-pyrazolone derivatives **197** or **198**.

R^1= CH$_3$, C$_2$H$_5$, *n*-C$_3$H$_7$, *iso*-C$_3$H$_7$, Ph
R^2= CN, COOEt
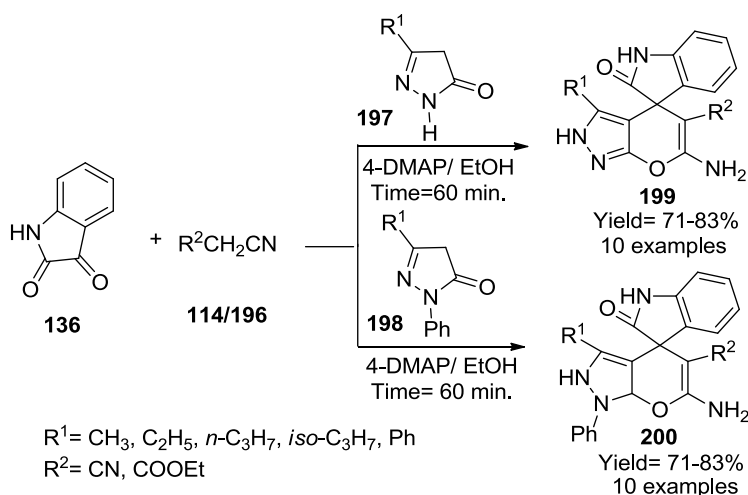
Scheme 1.46 Shows the synthesis of spirooxindole derivatives.

They also synthesized the compounds **199 (Scheme 1.46a)** and **200 (Scheme 1.46b)** by four component one pot reactions of isatins **136**, malononitrile **114** (or ethyl cyanoacetate **196**), hydrazine hydrate **119** (or

phenylhydrazine **184**), 1,3-dicarbonyl compounds **156/161** and compared the yield with three component one pot reaction. Both sets of reaction were conducted in EtOH in the presence of 4-DMAP catalyst. A series of spiro[indoline-3,4′-pyrano[2,3-*c*]pyrazole] derivatives **199** and **200** were quickly obtained in excellent yields by using the four-component one-pot reaction method.

1.10.12 DABCO catalyzed synthesis of pyrazolopyranopyrimidines: Majid M. Heravi[114] and their colleagues developed novel tricyclic fused pyrazolopyranopyrimidines **203** containing both biologically active pyranopyrazole and pyranopyrimidine templates and are synthesized by using a one-pot, four-component reaction involving ethyl acetoacetate **161**, hydrazine hydrate **119**, aldehydes **202**, and barbituric acid **201** catalyzed by DABCO in water **(Scheme 1.47)**. Pure target compounds are obtained in very good to excellent yields over short reaction times and with a straight forward work-up procedure.

Ar= C₆H₅, 2-MeOC₆H₄, 3O₂NC₆H₄, 4O₂NC₆H₄, 4MeC₆H₄, 4-ClC₆H₄
DABCO= 1,4-Diazabicyclo[2.2.2]octane
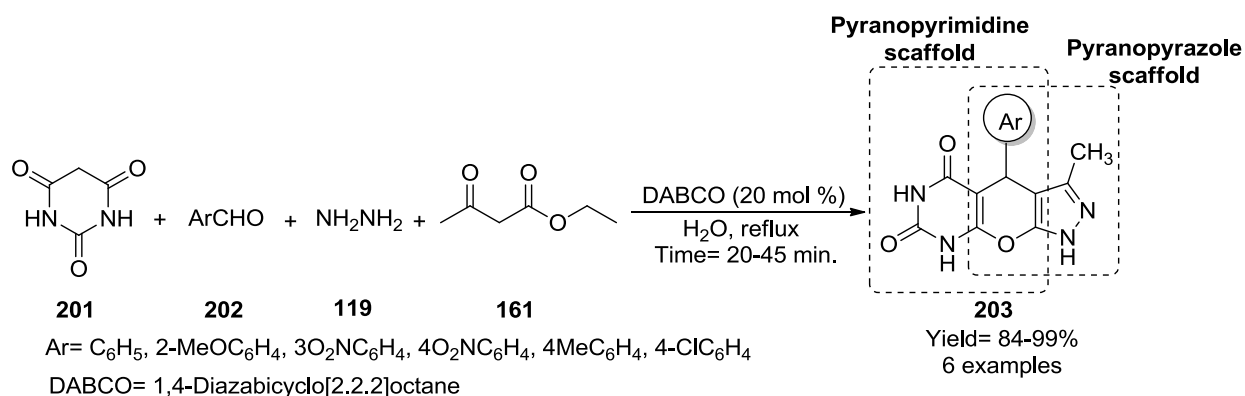
Scheme 1.47 Four-component synthesis of pyrazolopyranopyrimidines catalyzed by DABCO in water.

1.10.13 Synthesis of pyrano[4,3-*c*]pyrazoles: Ajay Kumar *et al.*[115] reported the synthesis of two series of compounds namely, 4-aryl/heteroaryl hydrazino-3-acetyl-6-methyl-2*H*-pyran-2-ones **206a-j** and pyrano[4,3-*c*]pyrazoles **208a-g**. The synthesis of **206a-j** is from 3-acetyl-4-chloro-6-methyl-2*H*-pyran-2-one **204** and various aryl/heteroaryl hydrazines **205 (Scheme 1.48a)**. Similarly they synthesis the 4-chloro-6-methyl-3-(1-(2-phenylhydrazono)ethyl)-2*H*-pyran-2-one **207** from **204** and **205** at different condition. Finally, pyrano[4,3-*c*]pyrazoles **208a-g** was synthesized by the reaction of **206a-g** and **207** via method A and B **(Scheme 1.48b).** Estimation of pharmacotherapeutic potential, possible molecular mechanism of action, toxic/side effects and interaction with drug-metabolizing enzymes were made for the synthesized compounds on the basis of prediction of activity spectra for substances (PASS) prediction results and their analysis by PharmaExpert software. COX inhibition predicted by PASS was confirmed by experimental evaluation and validated via docking studies. Out of all the compounds, compounds **206h**, **206j**, **208e**, **208g** exhibited good anti-inflammatory activity, whereas compounds **206b**, **206c**, **206h**,

206i, **206j**, **208b**, **208e**, **208g** showed excellent analgesic activity compared with standard drug Diclofenac sodium.

a)
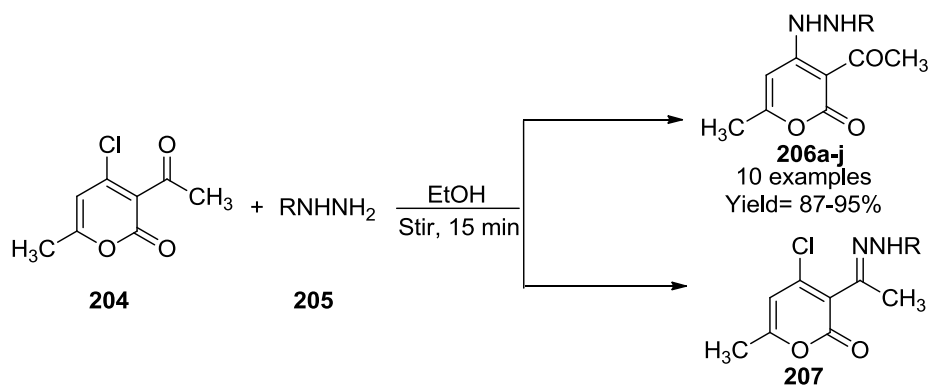
R= (a) C$_6$H$_5$; (b) 4-MeC$_6$H$_4$; (c) 4-ClC$_6$H$_4$; (d) 4-BrC$_6$H$_4$; (e) 4-MeOC$_6$H$_4$; (f) 4-NO$_2$C$_6$H$_4$; (g) 4-phenyl-2-thiazolyl; (h) 2-benzothiazolyl; (i) 4,6-dimethyl-2-pyrimidinyl (j) 4-methyl-2-quinolinyl

b)
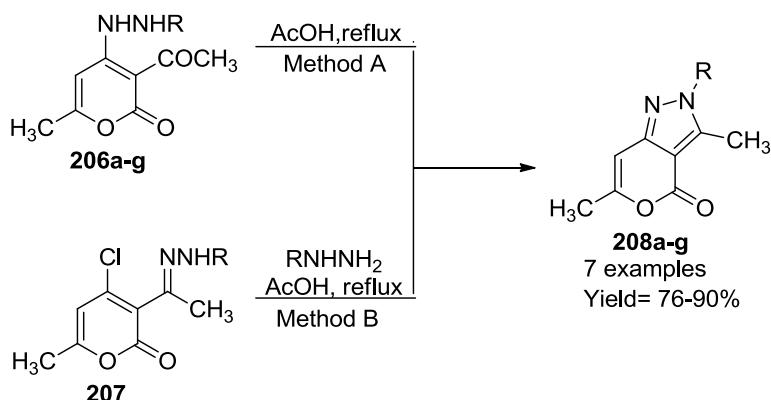
R = (a) C$_6$H$_5$; (b) 4-MeC$_6$H$_4$; (c) 4-ClC$_6$H$_4$ (d) 4-BrC$_6$H$_4$; (e) 4-MeOC$_6$H$_4$; (f) 4-NO$_2$C$_6$H$_4$; (g) 4-phenyl-2-thiazolyl

Scheme 1.48 Shows the synthesis of (a) 4-aryl/heteroaryl hydrazino-3-acetyl-6-methyl-2*H*-pyran-2-ones and (b) pyrano[4,3-*c*]pyrazoles.

1.10.14 Synthesis of pyrano[2,3-*c*]pyrazoles: Mahavir Parshad *et al.*[116] reported Iodine-mediated efficient synthesis of pyrano[2,3-*c*]pyrazoles and their antimicrobial activity. In this paper he synthesized, 1-phenyl-3-methyl-4-acetylpyrazol-5-one **210** from 1-phenyl-3-methylpyrazol-5-one **209** and used as starting material for the synthesis of *s-cis-(E)*-1-(5- hydroxy-3-methyl-1-phenyl-1*H*-pyrazol-4-yl)-3-aryl/hetarylprop-2-en-1-ones **212** in good yield (70–88 %) by condensation with aromatic aldehydes **211** (**Scheme 1.49a**). The *s-cis-(E)*-1-(5-hydroxy-3 methyl-1-phenyl-1*H*-pyrazol-4-yl)-3-arylprop-2-en-1-one **212** was heated in dimethyl sulfoxide at 110 °C in the presence of iodine that resulted in the formation of pyranopyrazole **213** rather than furanopyrazole **214 (Scheme 1.49b)**.
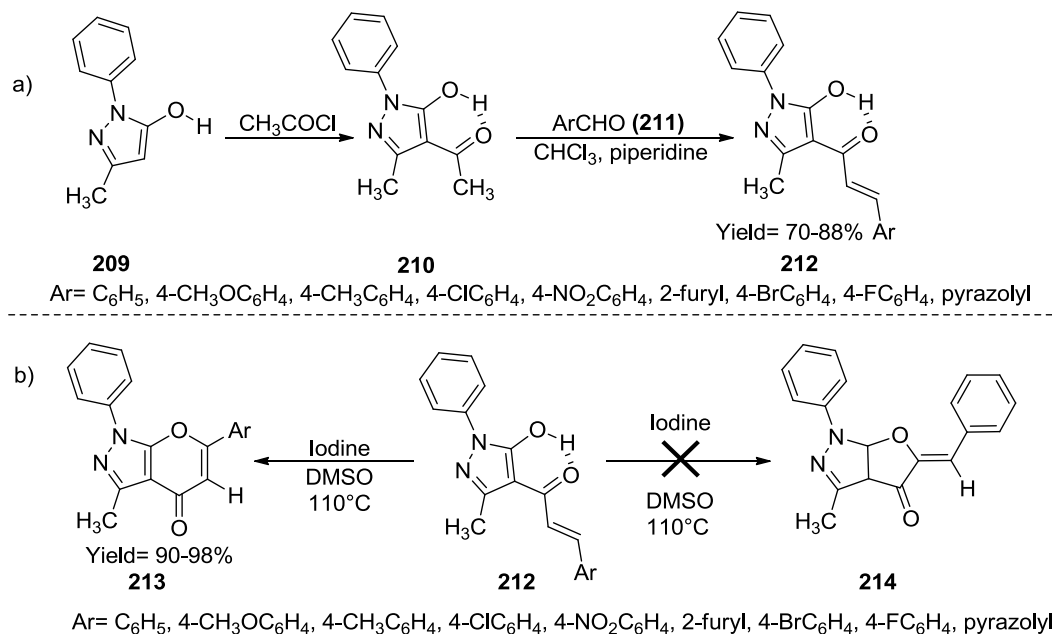
Scheme 1.49 Shows the synthesis of (a) *s-cis-(E)*-1-(5-hydroxy-3-methyl-1-phenyl-1*H*-pyrazol-4-yl)-3-arylprop-2-en-1-one and (b) pyranopyrazoles.

Section C: Drug designing and their molecular docking study

1.11 Introduction to Computer Aided Drug Design: Drug design or rational drug design, is the inventive method of finding new medications based on the information of the biological target. In the most basic sense, drug design involves design of small molecules that are complementary in shape and charge to the bimolecular target to which they interact and therefore will bind to it. In computational drug discovery we are using computational tools and softwares to simulate drug receptor interactions. In experimental based approach drugs were discovered through trial and error method. And also it was taking high R & D cost and also time consuming. Using computational drug discovery helps scientists to understand large insight to the drug receptor interactions. And also it helps to reduce the time and cost. There are two major types of drug design. The first is referred to as ligand-based drug design and the second, structure-based drug design.

1.11.1 Ligand-based design and screening: Computational approaches to drug design and screening can be either ligand- or target-based. If for a given therapeutic project, a set of active ligand molecules is known for the macromolecular target, but little or no structural information exists for the target, ligand-based computational methods can be employed. More specifically, quantitative structure activity relationship (QSAR) methods can be used, pharmacophore models developed, and shape searches performed based on the set of ligands. QSAR approaches involve the statistical analysis of a set of properties or descriptors for a series of biologically active molecules; the statistical model that is

developed is then used to predict the activity of additional compounds against the target. For example, the QSAR model can be used to predict which members of a series of proposed compounds are likely to be active and therefore should be synthesized and tested. As new compounds are assayed, the additional experimental data are used to refine the model. This general approach has been used in the pharmaceutical industry for many years to guide medicinal chemistry efforts. Typical small molecule descriptors include physicochemical properties such as molecular weight and clogP and hash codes based on the 2D structure of the ligands. Statistical approaches for determining the model may involve traditional least-squares optimization, neural networks, principal component analysis, etc. A pharmacophore model can also be derived from a set of known ligands for the target. Traditionally, a pharmacophore is the set of features common to a series of active molecules, where features can include acceptors, donors, ring centroids, hydrophobes, etc. A 3D pharmacophore specifies the spatial relationship between the groups or features, often defining distance ranges between groups, angles between groups or planes, and exclusion spheres. The programs like Phase, catalyst and UNITY can search large 2D or 3D molecular databases for additional molecules that possess the pharmacophore. Given just one active ligand known to bind to the target, a shape search can be performed, whereby 3D molecular databases are searched for other compounds that have the same shape. Knowledge of the bound conformation of the ligand is highly desirable and again can be obtained via NMR. If the bound ligand structure is not known experimentally, the lowest energy conformation of the small molecule in solution can be calculated and used for the shape search. With certain shape search methods some chemical matching can also be specified in addition to shape fit. 3D molecular databases can then be searched for other compounds that fit into that shape.

1.11.2 Target/structure-based drug design and screening: 'Structure-based' computational approaches require the 3D structure of the target. Typically, a high-resolution (< 2.5 Å) structure from X-ray crystallography or a suitably well-defined structure from NMR spectroscopy is used. It is also possible to design ligands for and screen against a homology model for which there is a high degree of confidence. In the structure-based drug design process, once a lead compound is identified, the 3D structure of the lead compound bound to target is solved. The structure of the ligand-target complex is examined and the interactions that the small molecule makes with the target are identified. At this point, computational methods play an important role in designing modifications to existing leads. The same computational methods can also be used for the design of entirely new compounds based on the 3D structure of the target alone. Given a lead compound, an iterative process of designing improvements to the existing lead, synthesizing and testing the designed compounds, and solving the 3D structure of each improved compound with the target begins. Many iterations of this cycle are carried out with the computational

chemist/molecular modeler working closely with medicinal chemists and biologists, until a highly potent compound or series of compounds has been developed. The best compounds then enter animal trials where efficacy, toxicity, and pharmacokinetic properties are studied. Efforts to identify toxic components or potential pharmacokinetic problems such as solubility, serum albumin binding, etc, during the design phase of the project are beginning to have an impact as the necessary computational tools are improved.

1.12 Present and future: Today, computer-aided drug design and screening methods impact the efforts of all pharmaceutical companies. As the computational technologies advance, the role they play in improving the efficiency of the drug discovery process will become increasingly important. In addition, as the body of structural information on potential therapeutic targets dramatically expands, which is expected to happen in the next few years, it will drive the development of the computational methodology. Greater automation, faster algorithms, and improved information management techniques will be required to handle the sheer volume of target-related information that will need to be processed. On a genomic scale, instead of looking at individual targets, families of related targets will be studied. The information available on ligand binding to these families will be vastly expanded. The job of the molecular modeler will be to effectively mine this data as well as translate the available structural information into a form directly usable by the bench chemist. This mission will ultimately cause a greater interface of bio- and chemoinformatics, leading to improved structural and functional genomics knowledge.

Before going in much detail about the drug designing process, it becomes very important to know about the cancer, wordwide distribution of cancer, their management and cancer targets so that a medicinal chemist can contribute in cure of cancer.

1.13 Cancer management by Inhibition

1.13.1 Cancer-the menace: Cancer is a group of diseases all corresponding to unregulated cell growth. In cancer, cells divide and grow unchecked, forming malignant tumors, and invade nearby parts of the body. It can spread also through the lymphatic system or the bloodstream. There are over 200 different known cancers that afflict humans.[117] Determining what causes cancer is complex. Many things are known to increase the risk of causing cancer, including tobacco used excessively, certain infections, radiation, lacking of physical activity, obesity, and environmental pollutants.[118] These can directly interfere with the genetic makeup of a person or combine with already present cellular genetic faults to trigger the disease.[119]

It is estimated that approximately 20,000 cancer deaths and 40,000 new cases of cancer each year in the U.S. are attributable to occupation.[120] Up to 10% of invasive cancers are related to radiation exposure,

including both ionizing radiation and non-ionizing ultraviolet radiation. Additionally, the vast majority of non-invasive cancers are non-melanoma skin cancers caused by non-ionizing ultraviolet radiation. Cancer can be detected in a number of ways, including the presence of certain signs and symptoms, screening tests, or medical imaging. Once a possible cancer is detected it is diagnosed by microscopic examination of a tissue sample.

1.13.2 Management of cancer: The treatment of cancer has undergone evolutionary changes as understanding of the underlying biological processes has increased. Tumor removal surgeries have been documented in ancient Egypt, hormone therapy was developed in 1896, and radiation therapy was developed in 1899. Chemotherapy, Immunotherapy, and newer targeted therapies are products of the 20th century. As new information about the biology of cancer emerges, treatments will be developed and modified to increase effectiveness, precision, survivability, and quality of life. There are many ways to manage cancer like surgery, radiation therapy, chemotherapy, immunotherapy and targeted therapy. All these cancer treatment techniques have some merits and demerits but our focus here is on target therapy and is discussed below in detail.

1.13.2.1 Targeted therapy: It became available in the late 1990s, has had a significant impact in the treatment of some types of cancer, and is currently a very active research area. This constitutes the use of agents specific for the deregulated proteins of cancer cells. Small molecule targeted therapy drugs are generally inhibitors of enzymatic domains on mutated, over-expressed, or otherwise critical proteins within the cancer cell. Prominent examples known in the market are the protein kinase inhibitors imatinib (Gleevec/Glivec) and gefitinib (Iressa). Monoclonal antibody therapy is another strategy in which the therapeutic agent is a cancer cell surface protein binding antibody. Examples include the anti-HER2/ neu antibody trastuzumab (Herceptin) used in breast cancer, and the anti-CD20 antibody rituximab, used in a variety of B-cell malignancies. Targeted therapy can also involve small peptides as "homing devices" which can bind to cell surface receptors or affected extracellular matrix surrounding the tumor. Radionuclides which are attached to these peptides eventually kill the cancer cell if the nuclide decays in the vicinity of the cell. Of these, our current interest lies in targeted therapy, in selective inhibition of the molecules promoting uncontrolled cell division. A lot of targeted enzymes have been approved, some waiting for approval as the **Figure 1.4**[121] indicates below. For study purposes, CDKs have been chosen for their targeting by commonly known drugs, and specifics which shall be elaborated later. The only problem with this 'smart drugs' approach is that it has not been successful yet due to factors like complexity of the process, incorrect target selection due to vast gene pool, poor efficacy and undesirable side effects, in spite of years of extensive preclinical and clinical testing.
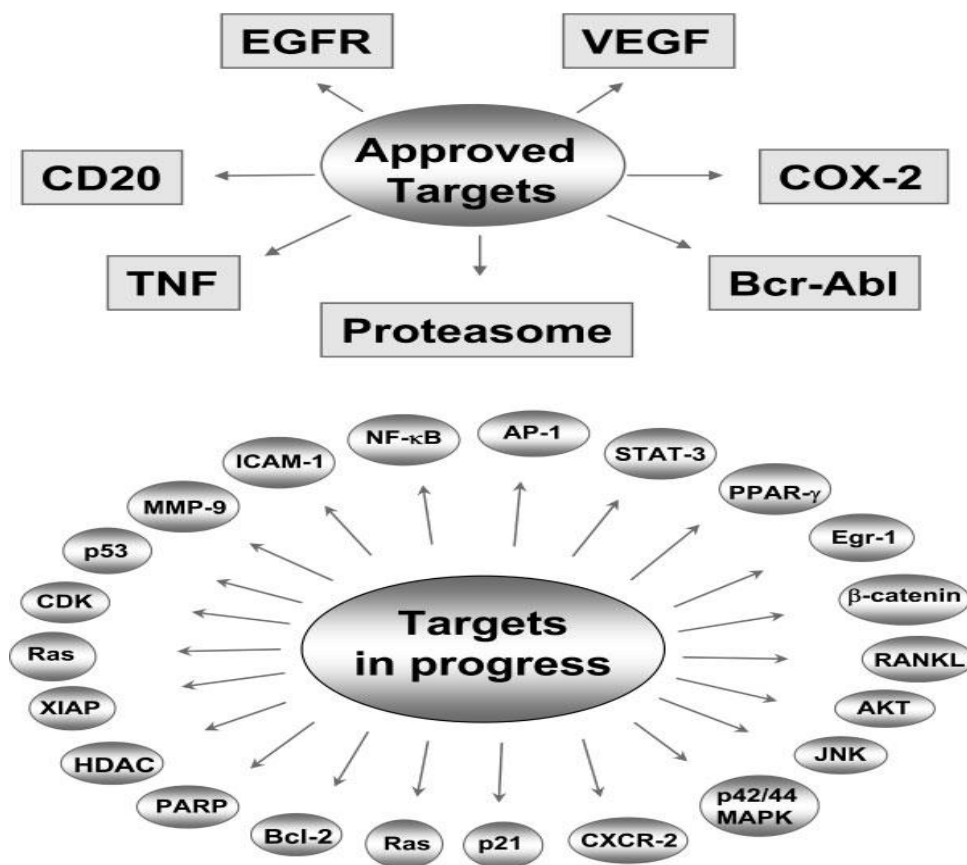
Figure 1.4 Target approved and under investigation for rational drug design.[121]

We shall be looking into this domain with a little more detail and see the approaches that people have used to design and synthesize the molecules that may as well be the solution to the long problem of using continual chemotherapy.

1.13.2.2 The Target-CDK: Our interest lies in this particular class of compounds, protein kinases, and so we need to answer the question of what their importance is. From the 1970s, research was focused on trying to discover the cellular factors which were leading to cancer, due to external factors. Focus was more on cellular signaling pathways, and it was found out that protein kinases[122] are a lot involved in this mechanism. However, lack of knowledge about these kinases, their number in the human body and structural complexity made it hard to immediately propose strategies for targeting. With time, various factors pointed out that several oncogenes were involved with protein kinases. Transformed cells contain more phosphoprotein than normal cells, and this imbalance is much more marked for phosphotyrosine than for phosphoserine or phosphothreonine. To reproduce, cells have to go through the cell cycle (**Figure 1.5**).[123] A non-replicating cell (said to be in G0) has no machinery to replicate DNA or separate its chromosomes, and once the decision is made to replicate, it first expresses genes which produce the

proteins which allow DNA to be duplicated, which is done in the G1phase of the cell cycle. (G stands for gap because it was originally thought cells were doing nothing at the gap times.) Then the DNA is reproduced during the (synthesis) S-phase. In the G2 phase, the S-phase proteins are demolished and the machinery to separate the chromosomes is built. Then in the final phase, the M-phase (mitosis), the chromosomes are separated and packed into two different nuclei, the cells are physically separated, the M-phase machinery is demolished, and the cells either stop reproducing (G0) or start another cell cycle (G1). Each of these phases of the cell cycle is marked by very heavy and distinctive bursts of phosphorylation, with a very highly regulated family of kinases, the so-called cyclin-dependent kinases (CDKs), playing a primary role.[122] Hence our interest lies with this class of protein kinases. We shall be describing them in details. They are also involved in regulating transcription, mRNA processing, and the differentiation of nerve cells.[124] They are present in all known eukaryotes, and their regulatory function in the cell cycle has been evolutionarily conserved. In fact, yeast cells can proliferate normally when their CDK gene has been replaced with the homologous human gene.[125]
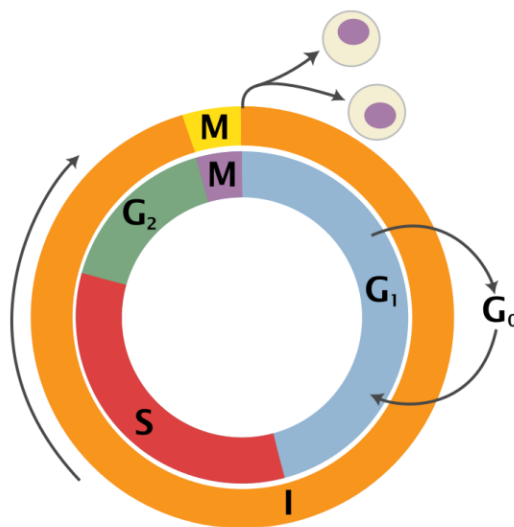
Figure 1.5 Schematic of the cell cycle. Outer ring: I= Interphase, M= Mitosis; Inner ring: M= Mitosis; G1= Gap Phase; S= Synthesis; G2= Gap Phase-2. The duration of mitosis in relation to the other phases has been exaggerated in this diagram.[123]

This means that novel drugs for treatment of chronic inflammation diseases such as arthritis and cystic fibrosis could be developed. Flavopiridol (Alvocidib) is the first CDK inhibitor to be tested in clinical trials after being identified in an anti-cancer agent screen in 1992. It competes for the ATP site of the CDKs.[126] More research is required, however, because disruption of the CDK-mediated pathway has potentially serious consequences; while CDK inhibitors seem promising, it has to be determined how

side-effects can be limited so that only target cells are affected. As such diseases are currently treated with glucocorticoids, which have often serious side-effects, even a minor success would be an improvement. Complications of developing a CDK drug include the fact that many CDKs are not involved in the cell cycle such as transcription, viral infection and neural physiology.[127]

The docking studies conducted later will involve a closer look at one of the proteins of the CDK Class (PDB ID: 1HCK and is shown in **Figure 1.6)**[128] and some of our compounds will be tested by means of virtual screening. Selected molecules will be docked using this program and the results will be compared with those obtained by well known general inhibitor drugs as a theoretical analysis, and later against some known CDK inhibitors.
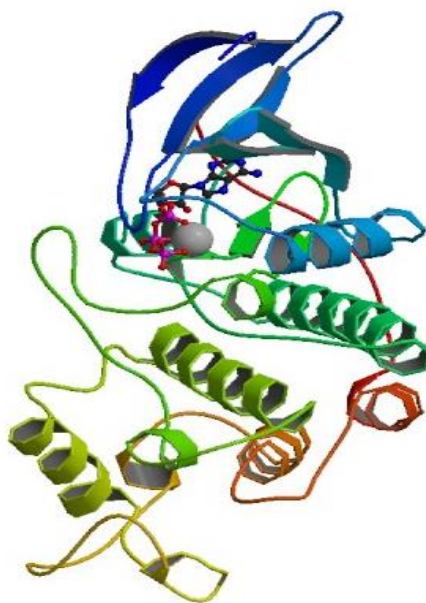
Figure 1.6 Shows the 3D view of 1HCK protein with ATP ligand.[128]

1.13.2.3 Designed Pyranopyrazole pharmacophore scaffold: This class of compounds has been chosen as the molecules to be docked in one of the CDK's of our choice, which will enable us to determine, after checking with some known drugs in the market, at least from a theoretical point of view, what could be selected for further scrutiny and further experimentation. It has been garnering a lot of attention from people (esp. synthetic chemists) due to its diverse bioactivity profile including anticancer, antimicrobial, anti-inflammatory and analgesic properties.[129] Also, discovering the inhibitory activity on CHK1 kinase, after pyranopyrazoles (or to be precise, dihydropyrano[2,3-*c*]pyrazole derivatives) were part of the enormous electronic database of compounds which was used in its entirety for docking studies on the ATP-binding site of CHK1,[130] and being part of an assay of small prioritized compounds, its impressive

results have prompted further research, experimentation and a number of strategized synthetic routes for this compound. The general structure of the compound is as such as shown in **Figure 1.7** below. Experiment suggests that its melting point increases from $131^{\circ}C$ onwards (varying R^2 from aliphatic chains to complex aromatic ones, depending on whether there are any contributions to hydrogen bonding or not).
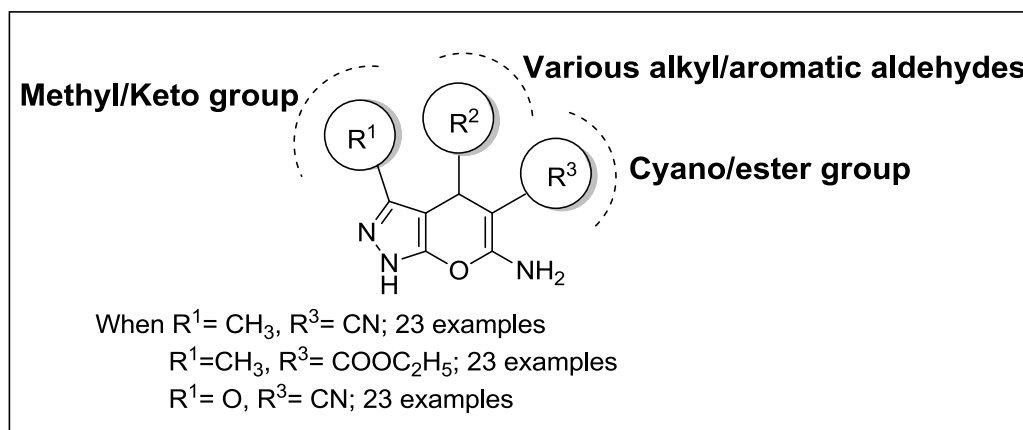
Figure 1.7 Designed pharmacophore of Pyranopyrazole scaffold.

These molecules are also being sought to be synthesized due to MCR strategies working out in case of them and hence, contributing heavily to atom economy and it is the ideal situation for creating large molecular libraries for bioactivity screening. The conservation of a large amount of reactants corresponding to success obtained in achieving a single product also hints that green synthesis can be attempted in the future with further experimental data on these compounds. Hence, we will be focusing on using these compounds for virtual screening on a CDK of our choice (within the basic rules of the docking software to be used). Finally we did the molecular dynamic study of the protein 1HCK to know about the stability of the protein and their flexible residues.

1.13.2.4 Designed Coumarin pharmacophore scaffold: Later on we extended our strategy for designed coumarin scaffolds **(Figure 1.8)** as CDK-2 inhibitors. Several researchers have proved the role of coumarins in the regulation of immune response, cell growth and differentiation.[131-132] The mechanism of action of anti-tumor drugs is basically to target the dividing cells that interrupt cell division. Coumarins are effectual not only for handling of cancer like renal cell carcinoma, malignant melanoma, leukemia[133-134], prostate cancer, and breast cancer[135-141], but also to treat the side effects caused by radiotherapy. In renal cell carcinoma[142] Coumarins have a cytotoxic mechanism and possess potential therapeutic function. Coumarin derivatives have also been found very effective anti-proliferative agents by regulating the release of cyclin D1[143-152] in case of leukemia, prostate, and breast cancer.

Several researchers have reported various anticancer coumarin based drugs eg. Genistein, Imperatorin,[153] Osthole,[154] Esculetin,[155-156] Fraxin,[157] Grandivittin,[158] Agasyllin,[158] Aegelinol benzoate,[158] Chartreusin[159] and Demethylchartreusin[159] etc. It has been established that coumarin and 7-hydroxycoumarin not only inhibit the cell growth of various types of cancer cell lines[160-162] but also used for the treatment of some human carcinomas.[163-166] There have been no adverse effects of coumarin reported in humans using doses upto 7 g daily, after two weeks of continued treatment.[167-168] The substitution patteren of various heterocyclic moieties influenced the biochemical, pharmacological, and therapeutic applications of simple coumarins. Our interest in anticancer drug discovery[169] motivated us to look up coumarins as potential CDK-2 inhibitor agents.

The designed pharmacophores not only focuses on designing of the coumarin molecules but also explores the effect of the substitution of OH group of the coumarin with various heterocyclic moieties at R^1, R^2, R^3 and R^4 position of the coumarins skeleton. All the designed analogues are shown in **Figure 1.8**. After docking them all, the best four molecules were selected and again docked by using GLIDE in Schrodinger for the authentication of the results. Furthermore, the molecular dynamics (MD) study was done for the best molecules selected from the studied positions R^1, R^2, R^3 and R^4.
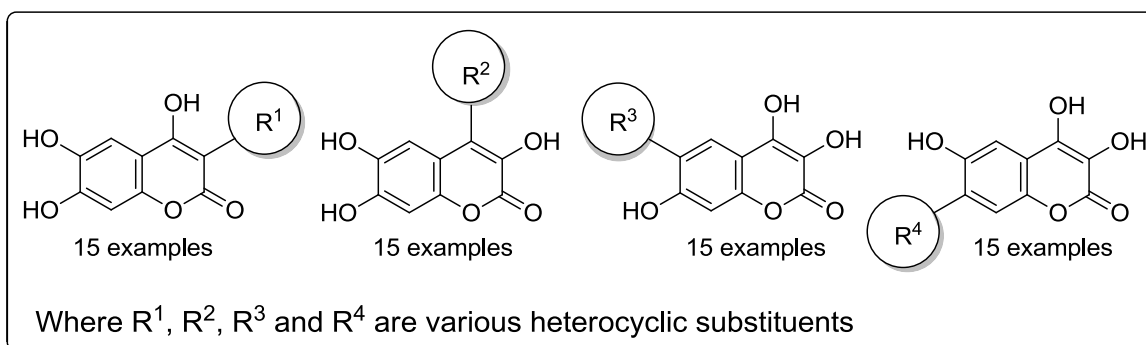
Figure 1.8 Designed pharmacophores of coumarin scaffold.

1.14 Molecular Docking: Molecular docking is a well established computational technique which predicts the interaction energy between two molecules. This technique mainly incorporates algorithms like molecular dynamics, Monte Carlo simulation, fragment based search methods which are mentioned in details in later part. Molecular docking studies are used to determine the interaction of two molecules and to find the best orientation of ligand which would form a complex with overall minimum energy. The small molecule, known as ligand usually fits within protein's cavity which is predicted by the search algorithm. These protein cavities become active when come in contact with any external compounds and are thus called as active sites. The results are analyzed by a statistical scoring function which converts interacting energy into numerical values called as the docking score; and also the interacting energy is

calculated. The primary criteria for evaluating docking strategies are docking accuracy, scoring accuracy, screening utility and speed.[170]

Docking accuracy reflects an algorithm's ability to discover a conformation (pose) and alignment of a ligand relative to a cognate protein that is close to that experimentally observed and to recognize the pose as correct. Scoring accuracy is the ability to correctly predict the rank order of binding affinities of ligands to a particular protein. Screening utility measures the ability of a docking algorithm to detect true ligands of a protein within a background of random ligands not thought to bind the protein. Speed denotes the time required for the completion of one successful docking process. The 3D pose of the bound ligand can be visualized using different visualizing tools like PyMOL, RasMol etc which could help in inference of the best fit of ligand. Predicting the mode of protein-ligand interaction can assume the active site of the protein molecule and further help in protein annotation. Moreover molecular docking has major application in drug discovery and designing.[171]

1.14.1 Different types of Interactions: Interactions between particles can be defined as a result of forces between the molecules contained by the particles. These forces are divided into four categories:

(A) Electrostatic forces: Forces with electrostatic origin due to the charges residing in the matter. The most common interactions are charge-charge, charge-dipole and dipole-dipole.

(B) Electrodynamics forces: The most widely known is the Van der Waals interactions.

(C) Steric forces: Steric forces are generated when atoms in different molecules come into very close contact with one another and start affecting the reactivity of each other. The resulting forces can affect chemical reactions and the free energy of a system.

(D) Solvent-related forces: These are forces generated due to chemical reactions between the solvent and the protein or ligand. Examples are hydrogen bonds (hydrophilic interactions) and hydrophobic interactions.

A common characteristic of all these forces is their electromagnetic nature. Other physical factors like conformational changes in the protein and the ligand are often necessary for successful docking.

1.14.2 Molecular docking sections: Molecular docking can be divided into two separate sections.

(1) Search algorithm- These algorithms determine all possible optimal conformations for a given complex (protein-protein, protein-ligand) in a environment i.e. the position and orientation of both molecules relative to each other. They can also calculate the energy of the resulting complex and of each individual interaction. The different types of algorithms that can be used for docking analysis are given below.

- Molecular dynamics
- Monte Carlo methods

- Genetic algorithms

- Fragment-based methods

- Point complementary methods

- Distance geometry methods

- Systematic searches

(2) Scoring function– These are mathematical methods used to predict the strength of the non-covalent interaction called as binding affinity, between two molecules after they have been docked. Scoring functions have also been developed to predict the strength of other types of intermolecular interactions, for example between two proteins or between protein and DNA or protein and drug. These configurations are evaluated using scoring functions to distinguish the experimental binding modes from all other modes explored through the searching algorithm. For example (calculating for the software AUTODOCK) the scoring potential is[172]:

$$V = W_{vdw} \sum_{i,j} \left(\frac{A_{ij}}{r_{ij}^{12}} - \frac{B_{ij}}{r_{ij}^{6}} \right) + W_{hbond} \sum_{i,j} E(t) \left(\frac{C_{ij}}{r_{ij}^{12}} - \frac{D_{ij}}{r_{ij}^{10}} \right) + W_{elec} \sum_{i,j} \frac{q_i q_j}{e(r_{ij}) r_{ij}} + W_{sol} \sum_{i,j} (S_i V_j + S_j V_i) e^{\frac{-r_{ij}^2}{2\sigma^2}}$$

The weighting constants W have been optimized to calibrate the empirical free energy based on a set of experimentally determined binding constants. The first term is a typical 6/12 potential for dispersion/ repulsion interactions. The parameters are based on the Amber force field. The second term is a directional H-bond term based on a 10/12 potential. The parameters C and D are assigned to give a maximal well depth of 5 k.cal/mol at 1.9 Å for hydrogen bonds with oxygen and nitrogen, and a well depth of 1 k.cal/mol at 2.5 Å for hydrogen bonds with sulfur. The function E(t) provides directionality based on the angle t from ideal H-bonding geometry. The third term is a screened coulomb potential for electrostatics. The final term is a desolvation potential based on the volume of atoms (V) that surround a given atom and shelter it from solvent, weighted by a solvation parameter (S) and an exponential term with distance-weighting factor σ = 3.5 Å.

1.14.3 Types of Docking: The following are majorly used type of docking are-

- **Lock and Key or Rigid Docking**– In rigid docking, both the internal geometry of the receptor and ligand is kept fixed during docking.

- **Induced fit or Flexible Docking**– In this model, the ligand is kept flexible and the energy for different conformations of the ligand fitting into the protein is calculated. Though more time consuming, this method can evaluate many different possible conformations which make it more reliable.

1.14.4 Major steps in molecular docking:

Step I– Building the Receptor: In this step the 3D structure of the receptor should be downloaded from PDB; and modified. Before modification, the Ramachandran Plot of the protein should be analyzed to see

if its maximum residues are in the acceptable region. Residues universally accepted are Glycine and Proline. Now, for corrections to unwanted residues, the editing and deleting can be done using the full versions of software like Discovery Studio and Schrodinger. This should include removal of the water molecules from the cavity, stabilizing charges, filling in the missing residues, generation the side chains etc according to the parameters available. After modification the receptor should be biological active and stable.

Step II– Identification of the Active Site: After the receptor is built, the active site within the receptor should be identified. The receptor may have many active sites but the one of the interest should be selected. Most of the water molecules and heteroatoms if present should be removed.

Step III– Ligand Preparation: Ligands can be obtained from various databases like ZINC, PubChem or can be created using tools like Chemsketch, Chemdraw.[173] Then the 3D structure of the compound should be energetically minimized using the tools available in the software (for example, in Chem3D, the MM2 tool section contains the 'Minimize Energy' function). While selecting the ligand, the LIPINSKY'S RULE OF 5 should be applied. The rule is important for drug development where a pharmacologically active lead structure is optimized stepwise for increased activity and selectivity, as well as drug-like properties, as described. For the selection of a ligand using LIPINSKY'S RULE the ligand should have to follow the following rules as mentioned below:

- Not more than 5 H bond donors.
- Molecular weight not more than 500 Dalton.
- Log P not over 5 for octanol water partition coefficient.
- Not more than 10 H bond acceptors.
- Log S value should be inbetween -6 to -3.

However, LIPINSKY's RULE is not absolute as many drugs often exhibit extreme potency and selective inhibition after violating some of them, like Lapatinib, and others.

Step IV- Docking: This is the last step, where the ligand is docked onto the receptor and the interactions are checked. The scoring function generates docking scores depending on which the ligand with the best fit is selected, and what parameters were entered in the first place. The software commonly used for docking are Schrodinger, AUTODOCK Tools, DOCK, iGemdock and Discovery Studio.

1.14.5 An Introduction to AUTODOCK: AUTODOCK is a suite of automated docking tools, created by the people of the Scripps Research Institute. It is designed to predict how small molecules, such as substrates or drug candidates, bind to a receptor of known 3D structure. Current distributions of AutoDock consist of two generations of software: AUTODOCK 4 and AUTODOCK VINA.[174]

(a) **AUTODOCK 4:** It actually consists of two main programs: autodock performs the docking of the ligand to a set of grids describing the target protein; autogrid pre-calculates these grids. In addition to using them for docking, the atomic affinity grids can be visualized. This can help, for example, to guide organic synthetic chemists design better binders.

(b) AUTODOCK VINA: It does not require choosing atom types and pre-calculating grid maps for them. Instead, it calculates the grids internally, for the atom types that are needed, and it does this virtually instantly.

The workers of Scripps Research Institute have also developed a graphical user interface called AutoDockTools, or ADT for short, which amongst other things helps to set up which bonds will treated as rotatable in the ligand and to analyze dockings. AUTODOCK has applications in:

- X-ray crystallography;
- Structure-based drug design;
- Lead optimization;
- Virtual screening(HTS);
- Combinatorial library design;
- Protein-protein docking;
- Chemical mechanism studies

It is very fast, provides high quality predictions of ligand conformations, and good correlations between predicted inhibition constants and experimental ones. AUTODOCK has also been shown to be useful in blind docking, where the location of the binding site is not known. Plus, AUTODOCK is free software and version 4 is distributed under the GNU General Public License and it's easy to obtain it. We shall be concentrating our efforts on AUTODOCK 4.2 only, from now on to avoid confusion with the AUTODOCK VINA Version.

1.14.6 Docking Procedure in AUTODOCK

Step 1: To start at the root of the problem, the enzyme to be considered must be selected carefully as we deal with the apoenzyme (protein body) of it and study its interactions. The files of these molecules are available at the Protein Data Bank in pdb format and will be downloaded and used for AUTODOCK. To start with the general information, the structural data of the proteins is available either from crystallographic studies or nuclear magnetic resonance, from which the crystal structure needs to be selected (for software compatibility) and the resolution of the structure must be less than 2.5 Å for producing accurate results. Its R-free value should be more than its observed R-value.

Step 2: The ligand information needs to be viewed, as the crystal structural data reveal ligands co-crystallized with the protein, hence if the already co-crystallized ligand structure is one that is structurally

similar to the ligands that need to be docked (also following Lipinsky's Rule of Five). The protein is then input into the AutoDock window for docking (**Figure 1.9**).
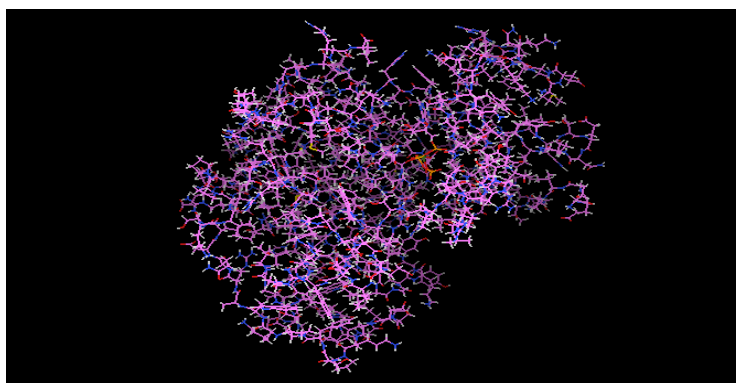
Figure 1.9 The protein input in the window of Autodock Tools.

Step 3: To prepare the protein for docking, we need to delete any residual water molecules related with it, remove the co-crystallized ligand (**Figure 1.10**), add polar Hydrogens and Gasteiger charges (as per the rules of AUTODOCK) and consider its torsional activity (**Figure 1.11**), whether any parts of the molecule are flexible or not. The reason for separating the molecule into flexible and rigid parts is that the amino acid acid residues belonging to the active site show definite rotation with respect to different interactions with variance in the ligands, in accordance with the Induced Fit Theory of enzymes. After merging the non-polar Hydrogens with the polar ones, we can proceed with the selection of the residues from the selected macromolecule. About two to three residues should be perfect for selection in AUTODOCK for flexible portion of the molecule. Those parts are cordoned off as the flexible section of the protein, and the rest as the rigid portion.
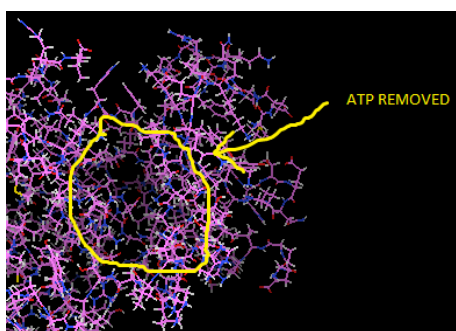
Figure 1.10 Protein section with ATP removed.
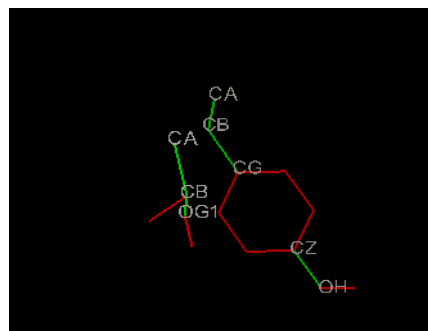
Figure 1.11 Residues in the protein with torsional activity.

Step 4: The ligand may have definitive torsional activity **(Figure 1.12)**, so that data must be input in the AUTODOCK software for later purpose. Firstly, its root of torsion can be auto-detected by the software or manually input, with its root expansion, then the ligand saved in the executable format of AUTODOCK, a pdbqt file (c.f pdb format, in the form of codes). The torsion detection has been based on the closest possible van der Waals and steric interactions.
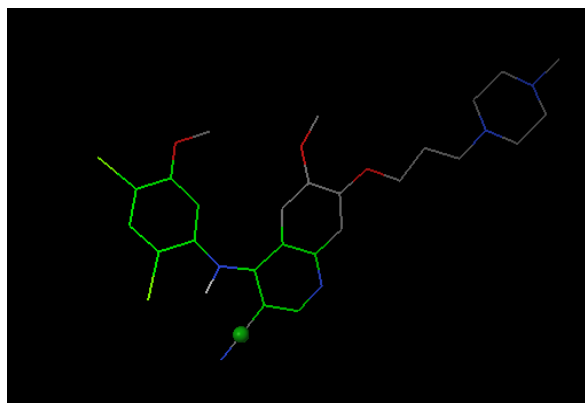
Figure 1.12 Input the ligand with auto detecting its center of torsion.
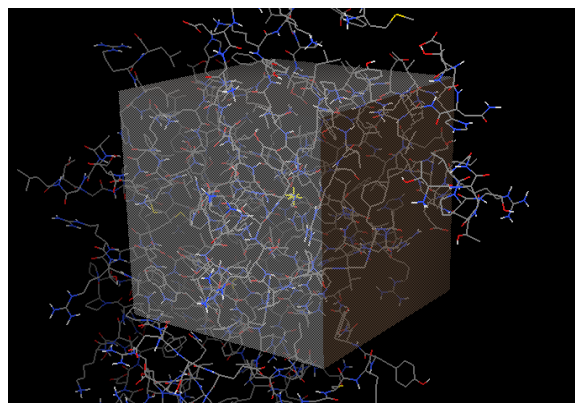
Figure 1.13 Creation and alignment of Grid box.

Step 5: The active sites of the particular protein must be isolated, as they will be used for creating the grid **(Figure 1.13)** for the center of activity with respect to the virtual interaction with the inhibitor ligand. The rigid section is generally used to create the grid box, with the active site being the center (the alignment is done after offsetting the grid box to proper coordinates). The grid map consists of a three-dimensional lattice of regularly spaced points, surrounding (either entirely or partly) and centered on some region of interest of the macromolecule under study. This could be a protein, enzyme, antibody, DNA, RNA or even a polymer or ionic crystal. Typical grid point spacing varies from 0.2 Å to 1.0 Å, and the default is 0.375 Å (roughly a quarter of the length of a carbon-carbon single bond). Each point within the grid map stores the potential energy of a 'probe' atom or functional group that is due to all the atoms in the macromolecule. The grid specifications can be handled with the help of the software, creating a grid parameter file, which is locked on and optimized with the help of the autogrid command, the output being a grid log file and then proper docking can be carried out without any interruptions. Generally while inputting the different types of atoms to consider, it is best to input as many as possible in the default window that chooses the basic atoms for mapping (for flexibility and for creating a universal grid parameter fie that will be able to handle a molecular library in terms of variance in terms of substituents in the ligands).

Step 6: To finally dock the molecule, the rigid and flexible residues are imported, along with the ligand, after finalizing the grid maps using autogrid4 executable/terminal. The docking search parameters are set to Genetic Algorithm (by default, as it is the most accurate search method as compared to the other two, Simulated Annealing and Local Search), where the most important parameter that is changed often, is the number of runs. The more the number of runs, the more the number of conformers, obtained in the final energy chart which can give a lot of details about the way in which the ligand oriented itself to fit into the active site. Finally, the output is saved as a docking parameter file (.dpf format) that may be of origin Lamarckian Genetic Algorithm, Genetic Algorithm, Simulated Annealing or Local Search (Lamarckian producing best results). Now the docking parameter file is called into the GUI window, with the external executable (A single command line is used in Terminal for Linux types, as mentioned earlier) and the docking results are written into a docking log file (.dlg format), generated automatically from the parameter file. The program running time is directly proportional to the number of runs input, ranging from 10 minutes for 3 runs to 1 hour 25 minutes for 20 runs (per file). The log file can be imported now, when analyzing the dockings, where the conformers are energetically grouped from best to worst, which can be played, giving a visual account of where the individual conformers bound and in which possible orientation.

Step 7: The docking results with analysis reveals interactional energies of the various conformations of the ligand within the active site of the protein body, and the one with minimum energy is chosen as the best result of the entire simulation. The root mean square expansion values are also chosen as the part of the energy calculations. The output parameters are saved as a docking log file (dlg format, obviously) where all the minimalistic interactional details are given, from the individual atoms, to entire sets of molecules. The dlg files can be analyzed for docking scores, and can be used to view the conformational interactions, and any individual conformer can be saved as a pdbqt file, along with the complex formed with the ligand from that particular conformation. Sometimes, in order to obtain a better graphical view, plugins like Rasmol and PyMOL or software like Discovery Studio Visualizer are used.

1.14.7 The Target: Human Cyclin Dependent Kinase 2: The molecular information of our target has been obtained from RCSB protein data bank. Further PDB data is shown in **Table 1.1**.

Table 1.1: PDB Data on Human Cyclin Dependent Kinase 2.[128]

PDB Entry	1HCK
Polymer	1
Classification	Protein Kinase (catalytic subunit)
Structure Weight (Da)	34508.29

Organism	Homo Sapiens
Gene Names	CDK2 CDKN2
Residues	298
Richest ATP Binding Site (Biological Codes, continuous)	GTYG (13-16)
Co-crystallized Ligand	Mg-ATP
Resolution	1.9 Å
R-Value	0.185
R-Free Value	0.272
Space Group	P 2_1 2_1 2_1
Unit Cell Lengths(a, b, c – in Å)	72.82, 72.66, 54.07
Unit Cell Angles (α, β, γ in degrees)	90, 90,90

1HCK has acceptable number of residues in the correct region as seen from its Ramachandran Plot **(Figure 1.14).** So, we can go ahead with the docking procedure. The structure of CDK-2 (PDB ID: 1HCK) protein with co-crystallized Mg-ATP ligand in 3D and 2D view are shown in **Figure 1.6** and **1.15** respectively.[128] The closer examination of 2D image (Taken from RCSB protein data bank) of the Mg-ATP ligand in the binding pocket of the protein give us the idea about the interaction shown by the co-crystallized ligand with the closer amino acids VAL18A, LEU134A, LYS129, LYS33A, THR14A, GLU81A, LEU83A, GLN131A, ASP86A and metal ion MG401A.

In **Figure 1.15** black dashed lines indicate hydrogen bonds, salt bridges, and metal interactions. Green solid line shows hydrophobic interactions. As can be expected from the relative hydrophilicity of the ATP molecule, most hydrogen bonds and salt bridges are formed with the phosphate moiety, while the adenine base and ribose are involved in only two hydrogen bonds each.

The hexacoordinate Mg^{2+} ion is bound to one oxygen from each phosphate with coordination bonds ranging in length from 1.82 to 2.29 Å. The coordination of all three phosphates of ATP by a single Mg^{2+} ion is very unusual and to our knowledge has never been observed before. The electron density for the Mg^{2+} ion is relatively weak which is reflected in the refinement of its occupancy to 0.6 with a B value of 32 Å.[175] Although the electron density in the presumed metal binding site is relatively weak for a Mg^{2+} atom, it was interpretated as Mg^{2+} because of the short coordination bonds (average 2.0 Å) to its ligands, octahedral coordination that is the preferred geometry for alkaline earth metal ions in complexes with oxygen donor groups.
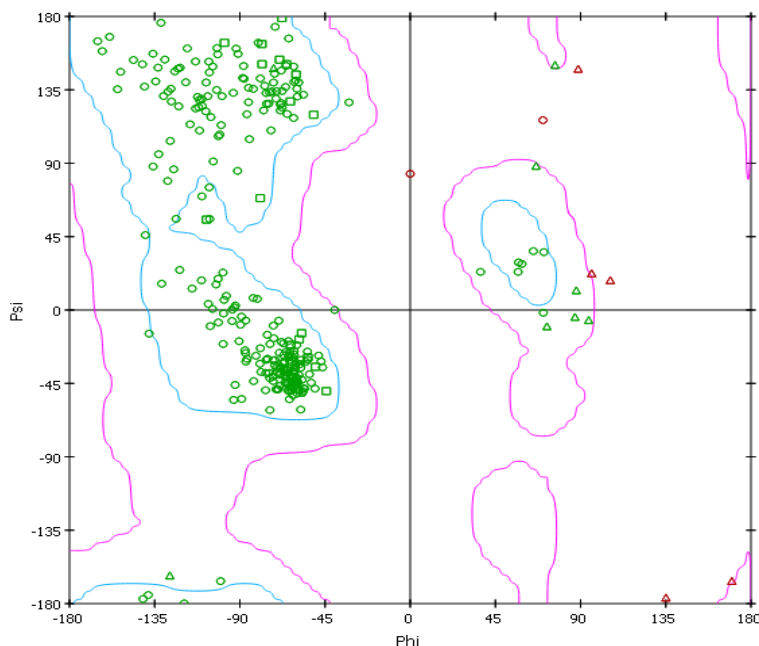
Figure 1.14 Ramachandran plot of the prepared protein 1HCK.
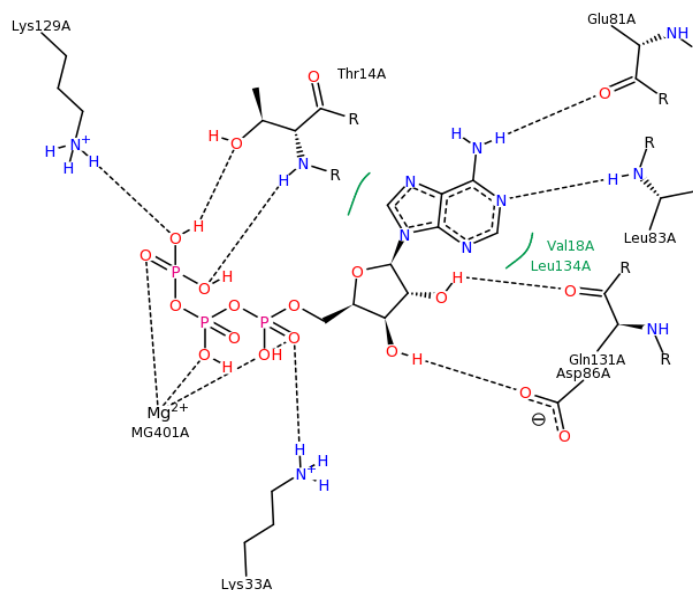
Figure 1.15 2D view of the Mg-ATP co-crystallized ligand inside the binding pocket of 1HCK.[128]

1.14.8 Docking on designed experimental and known drug molecules: From an academic interest point of view, some selected drugs were docked in the protein 1HCK, followed by the experimental molecules from the Pyrazolopyran class and designed coumarin derivatives after optimizing their 3D structures using the MM2 function of Chem3D Ultra 8.0 following the principles of competitive

inhibition of active ATP site of 1HCK. Though the docking has been restricted to AutoDock, a visual representation has required the use of Discovery Studio Client 3.5 (Visualier) from time to time. The docking was performed using AutoDock Tools Version 1.5.6 in a laptop with an i3 Core Processor, 2.3 GHz having 4GB RAM with a dedicated Graphics Card of 2GB. The docking was performed using THR14 (T) and TYR15 (Y) residues of the GTYG cluster of ATP binding sites (residues 13 to 16) as flexible ones, the Genetic Algorithm search set to 50 runs, which will generate 50 conformers, of which the best conformer has been chosen for every molecule (from an energetic perspective). The binding energies and the K_i (Inhibition Constants – here theoretical) values are the ones which will be compared with each other.

1.15 Drug-like properties: The properties which can distinguish drugs from other chemicals can be considered as drug like properties. Good pharmacokinetic[176] properties and toxicity profiles are necessary for any ligand to complete drug discovery process and to become successful drug. The crutial properties that should be considered for compounds with oral delivery (Lipinski's 'rule-of-five') includes molecular mass <500 daltons (Da), calculated octanol/water partition coefficient (ClogP) <5, number of hydrogen-bond donors <5, number of hydrogen-bond acceptors <10 and solubility property i.e log S value should be inbetween -6 to -3. These properties are then typically used to construct predictive ADME models and form the basis for what has been called property-based design. Molecular properties like molecular weight, ClogP, logS (solubility), number of hydrogen bond acceptors, number of hydrogen bond donors, drug likeness and toxicity risks like mutagenic, tumorigenic, irritant, effect on sexual reproduction and drug score were predicted for the designed analogs using online tools, OSIRIS property explorer and Molinspiration cheminformatics.

1.16 ADME study: Drug discovery and development are expensive and time-consuming processes. Recognition by the pharmaceutical industry that undesirable absorption, distribution, metabolism and excretion (ADME) properties of new drug candidates are the cause of many clinical phase drug development failures has resulted in a paradigm shift to identify such problems early in the drug discovery process. Thus, *in-vitro* approaches are now widely used to investigate the ADME properties of new chemical entities and, more recently, computational (*in-silico*) modelling has been investigated as a tool to optimise selection of the most suitable drug candidates for development. The objectives of *in-silico* modeling tools for predicting these properties to serve two key aims- first, at the design stage of new compounds and compound libraries so as to reduce the risk of late-stage attrition; and second, to optimize the screening and testing by looking at only the most promising compounds. The prediction of ADME and related properties are described below:

(A) Absorption: For a compound crossing a membrane by purely passive diffusion, a reasonable permeability estimate can be made using single molecular properties, such as log D or hydrogen-bonding capacity. The simplest *in-silico* models for estimating absorption are based on a single descriptor, such as log P or log D, or polar surface area, which is a descriptor of hydrogen-bonding potential. Different multivariate approaches, such as multiple linear regressions, partial least squares and artificial neural networks, have been used to develop quantitative structure–human-intestinal-absorption relationships.

(B) Bioavailability: Important properties for determining permeability seem to be the size of the molecule, as well as its capacity to make hydrogen bonds, its overall lipophilicity and possibly its shape and flexibility.

(C) Blood–brain barrier penetration: Drugs that act in the CNS need to cross the blood–brain barrier (BBB) to reach their molecular target. By contrast, for drugs with a peripheral target, little or no BBB penetration might be required in order to avoid CNS side effects. 'Rule-of-five'-like recommendations regarding the molecular parameters that contribute to the ability of molecules to cross the BBB have been made to aid BBB-penetration predictions; for example, molecules with a molecular mass of <450 Da or with PSA <100 Å are more likely to penetrate the BBB.

(D) Dermal and ocular penetration: The existing transdermal models are typically a function of the octanol/water partition coefficient and terms that have been associated with aqueous solubility, including hydrogen-bonding parameters, molecular weight and molecular flexibility. Commercial models for the prediction of solute-permeation rates through the skin are available, for example, the QikProp and DermWin programs.

(E) Metabolism: *In-silico* approaches to predicting metabolism can be divided into QSAR and three-dimensional- QSAR studies, protein and pharmacophore models and predictive databases. Some of the first-generation predictive-metabolism tools currently require considerable input from a computational chemist, whereas others can be used as rapid filters for the screening of virtual libraries, for example, to test for CYP3A4 liability. Perhaps the most intellectually satisfying molecular modeling studies are those based on the crystal structure of the metabolizing enzymes and several approaches that use databases to predict metabolism are available. Ultimately, such programs might be linked to computer-aided toxicity prediction on the basis of quantitative structure–toxicity relationships and expert systems for toxicity evaluation

1.17 *In-silico* prediction of toxicity issues: Toxicity is responsible for many compounds failing to reach the market and for the withdrawal of a significant number of compounds from the market once they have been approved. It has been estimated that ~20–40% of drug failures in investigational drug development can be attributed to toxicity concerns. The existing commercially available *in-silico* tools for forecasting

potential toxicity issues can be roughly classified into two groups. The first approach uses expert systems that derive models on the basis of abstracting and codifying knowledge from human experts and the scientific literature. The second approach relies primarily on the generation of descriptors of chemical structure and statistical analysis of the relationships between these descriptors and the toxicological end-point.

The primary emphasis of the current software packages is carcinogenicity and mutagenicity, although some packages do also include models and/or knowledge bases for other end-points, such as teratogenicity, irritation, sensitization, immunotoxicology and neurotoxicity. There is currently an unmet need for *in-silico* predictive toxicology software for other end-points important in drug development, such as QT prolongation hepatotoxicity and phospholipidosis. Molecular properties and toxicity risks were calculated by online tool OSIRIS property explorer and molinspiration cheminformatics. QikProp is a quick, accurate, easy-to-use absorption, distribution, metabolism, and excretion (ADME) prediction program present in the Schrödinger suite. QikProp predicts physically significant descriptors and pharmaceutically relevant properties of organic molecules, either individually or in batches. In addition to predicting molecular properties, QikProp provides ranges for comparing a particular molecule's properties with those of 95% of known drugs. QikProp also flags 30 types of reactive functional groups that may cause false positives in high-throughput screening (HTS) assays.

Section D: Corrosion inhibition study of the copper metal by designed inhibitors

1.18 Introduction of corrosion inhibitors

1.18.1 Corrosion is a natural process, which converts a refined metal to a more stable form, such as its oxide or hydroxide. It is the gradual destruction of materials (usually metals) by chemical reaction with their environment. Rusting, the formation of iron oxide is a well-known example of electrochemical corrosion. Many structural alloys corrode merely from exposure to moisture in air, but the process can be strongly affected by exposure to certain substances. Corrosion can be concentrated locally to form a pit or crack, or it can extend across a wide area more or less uniformly corroding the surface. Because corrosion is a diffusion-controlled process, it occurs on exposed surfaces. As a result, methods to reduce the activity of the exposed surface, such as passivation and chromate conversion, can increase a material's corrosion resistance. However, some corrosion mechanisms are less visible and less predictable.

1.18.2 Forms of Corrosion

The forms of corrosion described here use the terminology in use at NASA-KSC (Kennedy Space Centre).[177] There are other equally valid methods of classifying corrosion, and no universally accepted

terminology is in use. Keep in mind that a given situation may lead to several forms of corrosion on the same piece of material. Some different forms of corrosion **(Figure 1.16)** are described below:

1. Uniform Corrosion: This is also called general corrosion. The surface effect produced by most direct chemical attacks (e.g. as by an acid) is a uniform etching of the metal.

2. Galvanic Corrosion: Galvanic corrosion is an electrochemical action of two dissimilar metals in the presence of an electrolyte and an electron conductive path. It occurs when dissimilar metals are in contact.

3. Concentration Cell Corrosion: Concentration cell corrosion occurs when two or more areas of a metal surface are in contact with different concentrations of the same solution.

4. Pitting Corrosion: Pitting corrosion is localized corrosion that occurs at microscopic defects on a metal surface. The pits are often found underneath surface deposits caused by corrosion product accumulation.

5. Crevice Corrosion: Crevice or contact corrosion is the corrosion produced at the region of contact of metals with metals or metals with nonmetals. It may occur at washers, under barnacles, at sand grains, under applied protective films, and at pockets formed by threaded joints.

6. Filiform Corrosion: This type of corrosion occurs on painted or plated surfaces when moisture permeates the coating. Long branching filaments of corrosion product extend out from the original corrosion pit and cause degradation of the protective coating.

7. Intergranular Corrosion: Intergranular corrosion is an attack on or adjacent to the grain boundaries of a metal or alloy.

8. Stress Corrosion Cracking: Stress corrosion cracking (SCC) is caused by the simultaneous effects of tensile stress and a specific corrosive environment. Stresses may be due to applied loads, residual stresses from the manufacturing process, or a combination of both.

9. Corrosion Fatigue: Corrosion fatigue is a special case of stress corrosion caused by the combined effects of cyclic stress and corrosion. No metal is immune from some reduction of its resistance to cyclic stressing if the metal is in a corrosive environment.

10. Fretting Corrosion: The rapid corrosion that occurs at the interface between contacting, highly loaded metal surfaces when subjected to slight vibratory motions is known as fretting corrosion.

11. Erosion Corrosion: Erosion corrosion is the result of a combination of an aggressive chemical environment and high fluidsurface velocities.

12. Dealloying: Dealloying is a rare form of corrosion found in copper alloys, gray cast iron, and some other alloys. Dealloying occurs when the alloy loses the active component of the metal and retains the more corrosion resistant component in a porous "sponge" on the metal surface.

13. Hydrogen Damage: Hydrogen embrittlement is a problem with highstrength steels, titanium, and some other metals. Control is by eliminating hydrogen from the environment or by the use of resistant alloys.

14. Corrosion in Concrete: Concrete is a widely used structural material that is frequently reinforced with carbon steel reinforcing rods, post-tensioning cable or prestressing wires. The steel is necessary to maintain the strength of the structure, but it is subject to corrosion.

15. Microbial Corrosion: Microbial corrosion (also called microbiologically influenced corrosion or MIC) corrosion that is caused by the presence and activities of microbes. This corrosion can take many forms and can be controlled by biocides or by conventional corrosion control methods.
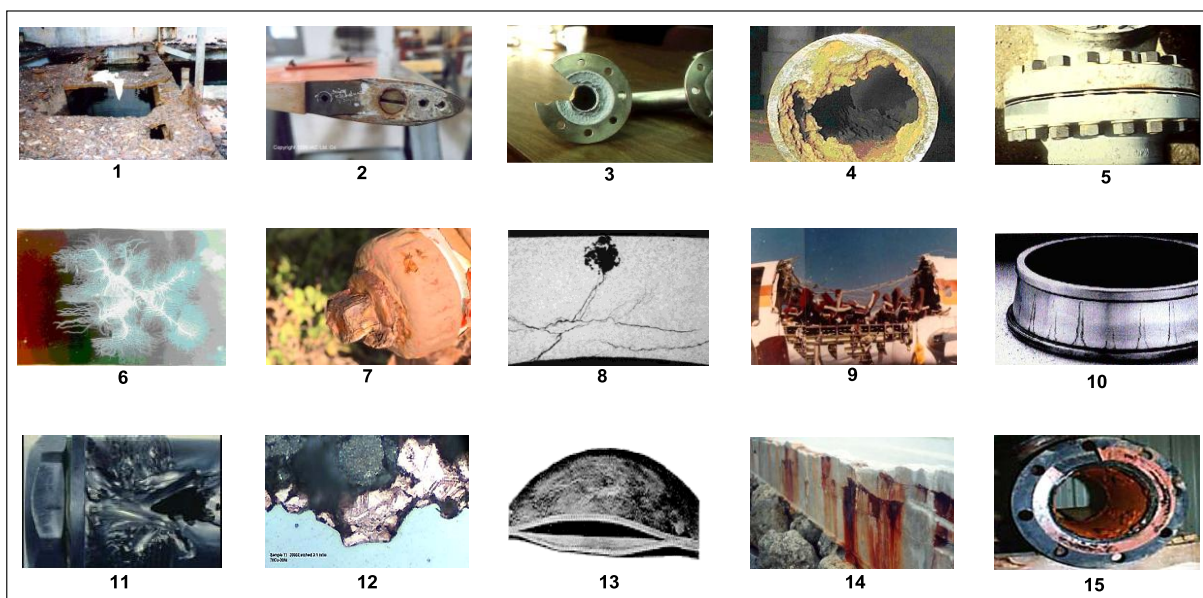
Figure 1.16 Shows the different forms of corrosion images.[177]

1.18.3 Consequences of Corrosion: The consequences of corrosion are many and varied and the effects of these on the safe, reliable and efficient operation of equipment or structures are often more serious than the simple loss of a mass of metal. Failures of various kinds and the need for expensive replacements may occur even though the amount of metal destroyed is quite small. Some of the major harmful effects of corrosion can be summarised as follows:

1. Reduction of metal thickness leading to loss of mechanical strength and structural failure or breakdown. When the metal is lost in localised zones so as to give a crack like structure, very considerable weakening may result from quite a small amount of metal loss.

2. Hazards or injuries to people arising from structural failure or breakdown (e.g. bridges, cars, aircraft).

3. Loss of time in availability of profile-making industrial equipment.

4. Reduced value of goods due to deterioration of appearance.

5. Contamination of fluids in vessels and pipes (e.g. beer goes cloudy when small quantities of heavy metals are released by corrosion).

6. Perforation of vessels and pipes allowing escape of their contents and possible harm to the surroundings. For example a leaky domestic radiator can cause expensive damage to carpets and decorations, while corrosive sea water may enter the boilers of a power station if the condenser tubes perforate.

7. Loss of technically important surface properties of a metallic component. These could include frictional and bearing properties, ease of fluid flow over a pipe surface, electrical conductivity of contacts, surface reflectivity or heat transfer across a surface.

8. Mechanical damage to valves, pumps, etc, or blockage of pipes by solid corrosion products.

9. Added complexity and expense of equipment which needs to be designed to withstand a certain amount of corrosion, and to allow corroded components to be conveniently replaced.

1.18.4 Corrosion Prevention: By retarding either the anodic or cathodic reactions the rate of corrosion can be reduced. This can be achieved in several ways:

1. Conditioning the Metal: This can be sub-divided into two main groups:

(a) Coating the metal, in order to interpose a corrosion resistant coating between metal and environment. The coating may consist of:

(i) Another metal, e.g. zinc or tin coatings on steel,

(ii) A protective coating derived from the metal itself, e.g. aluminium oxide on "anodised" aluminium,

(iii) Organic coatings, such as resins, plastics, paints, enamel, oils and greases.

(b) Alloying the metal to produce a more corrosion resistant alloy, e.g. stainless steel, in which ordinary steel is alloyed with chromium and nickel. Stainless steel is protected by an invisibly thin, naturally formed film of chromium sesquioxide Cr_2O_3.

2. Conditioning the Corrosive Environment

(a) Removal of Oxygen: The removal of oxygen could be achieved by the use of strong reducing agents e.g. sulphite. However, for open evaporative cooling systems this approach to corrosion prevention is not practical since fresh oxygen from the atmosphere will have continual access.

(b) Corrosion Inhibitors: A corrosion inhibitor is a chemical additive, which, when added to a corrosive aqueous environment, reduces the rate of metal wastage. It can function in one of the following ways-

(i) Anodic inhibitors: As the name implies an anodic inhibitor interferes with the anodic process.

$$Fe \longrightarrow Fe^{++} + 2e \qquad \text{Equation 1}$$
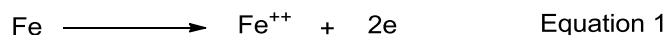
If an anodic inhibitor is not present at a concentration level sufficient to block off all the anodic sites, localised attack such as pitting corrosion can become a serious problem due to the oxidising nature of the inhibitor which raises the metal potential and encourages the anodic reaction **(equation 1)**. Anodic inhibitors are thus classified as "dangerous inhibitors". Other examples of anodic inhibitors include orthophosphate, nitrite, ferricyanide and silicates.

(ii) Cathodic inhibitors: The major cathodic reaction in cooling systems is the reduction of oxygen **(equation 2)**.

$$1/2 O_2 \ + \ H_2O \ + \ 2e \longrightarrow 2OH^- \qquad\qquad \text{Equation 2}$$
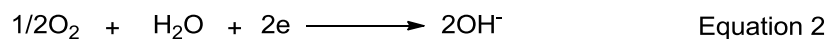
There are other cathodic reactions and additives that suppress these reactions called cathodic inhibitors. They function by reducing the available area for the cathodic reaction. This is often achieved by precipitating an insoluble species onto the cathodic sites. Zinc ions are used as cathodic inhibitors because of the precipitation of $Zn(OH)_2$ at cathodic sites as a consequence of the localised high pH. Cathodic inhibitors are classed as safe because they do not cause localised corrosion.

(iii) Adsorption type corrosion inhibitors: Many organic inhibitors work by an adsorption mechanism. The resultant film of chemisorbed inhibitor is then responsible for protection either by physically blocking the surface from the corrosion environment or by retarding the electrochemical processes. The main functional groups capable of forming chemisorbed bonds with metal surfaces are amino ($-NH_2$), carboxyl ($-COOH$), and phosphonate ($-PO_3H_2$) although other functional groups or atoms can form co-ordinate bonds with metal surfaces.

(iv) Mixed inhibitors: Because of the danger of pitting when using anodic inhibitors alone, it became common practice to incorporate a cathodic inhibitor into for mulated performance was obtained by a combination of inhibitors than from the sum of the individual performances. This observation is generally referred to a 'synergism' and demonstrates the synergistic action which exists between zinc and chromate ions.

3. Electrochemical Control: Since corrosion is an electrochemical process its progress may be studied by measuring the changes which occur in metal potential with time or with applied electrical currents. Conversely, the rate of corrosion reactions may be controlled by passing anodic or cathodic currents into the metal. If, for example, electrons are passed into the metal and reach the metal/electrolyte interface (a cathodic current) the anodic reaction will be stifled while the cathodic reaction rate increases. This process is called cathodic protection and can only be applied if there is a suitable conducting medium such as earth or water through which a current can flow to the metal to be protected. In most soils or natural waters corrosion of steel is prevented if the potential of the metal surface is lowered by 300 or 400

mV. Cathodic protection may be achieved by using a DC power supply (impressed current) or by obtaining electrons from the anodic dissolution of a metal low in the galvanic series such as aluminium, zinc or magnesium (sacrificial anodes). Similar protection is obtained when steel is coated with a layer of zinc. Even at scratches or cut edges where some bare metal is exposed the zinc is able to pass protective current through the thin layer of surface moisture. In certain chemical environments it is sometimes possible to achieve anodic protection, passing a current which takes electrons out of the metal and raises its potential. Initially this stimulates anodic corrosion, but in favourable circumstances this will be followed by the formation of a protective oxidised passive surface film.

1.19 Corrosion inhibitors study of Copper metal: The aim of this section was to study about the corrosion inhibitors for copper metal. Till now several researchers reported many inorganic, organic copper corrosion inhibitors but still there is need to develop the more stable, environmentally friendly, less costly corrosion inhibitors.

1.19.1 Corrosion inhibition by 2-Mercapto-1-methylimidazole: L. Larabi *et al.*[178] reported 2-Mercapto-1-methylimidazole **(Figure 1.17)** as corrosion inhibitor in hydrochloric acid for copper metal. The inhibition was investigated by dc polarization, ac impedance and weight loss techniques. Fukui indices, which are reactivity descriptors derived from density functional theory (DFT), was used to explain the great efficiency of this compound as corrosion inhibitor relatively to other imidazole derivatives.
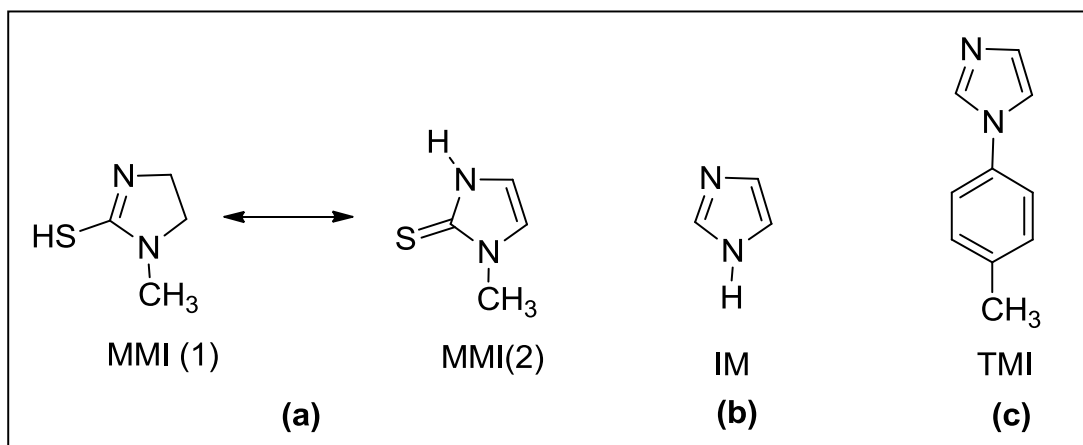
Figure 1.17 Shows the chemical structure of (a) MMI (b) IM and, (c) TMI.

1.19.2 Corrosion inhibition by MAP: The inhibiting effects of 2-mercapto-4-amino-5-nitroso-6-hydroxy pyrimidine (MAP, **Figure 1.18**) in 3.5% NaCl solutions at 25 °C on the copper metal was examined by K. F. Khaled.[179] Various techniques like weight loss, potentiodynamic polarization, electrochemical

impedance spectroscopy (EIS), and electrochemical frequency modulation (EFM) measurements were used to calculate the corrosion inhibition efficiency of MAP.
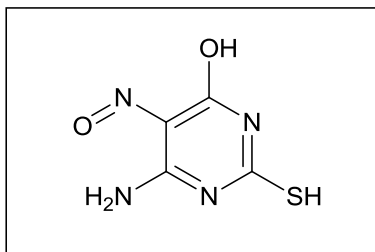
Figure 1.18 Shows the chemical structure of MAP.

1.19.3 Corrosion inhibition by ATA and AMTA: The corrosion behavior of unalloyed copper (99.999% Cu) in freely aerated 0.50M HCl solution and its corrosion inhibition by 3-amino-1, 2, 4-triazole (ATA, **Figure 1.19a**) and 3-amino-5-mercapto-1, 2, 4-triazole (AMTA, **Figure 1.19b**) at various concentarations were reported by El-Sayed and M. Sherif.[180] The analytical techniques like weight-loss, chronoamperometry (CA), potentiodynamic polarization (PDP), electrochemical impedance spectroscopy (EIS), and Raman spectroscopy were used to carry out the investigations. The inhibition of copper corrosion in the acid solution is achieved by strong adsorption of these organic molecules onto the copper surface and preventing the formation of cuprous chloride and oxy-chloride complex compounds.
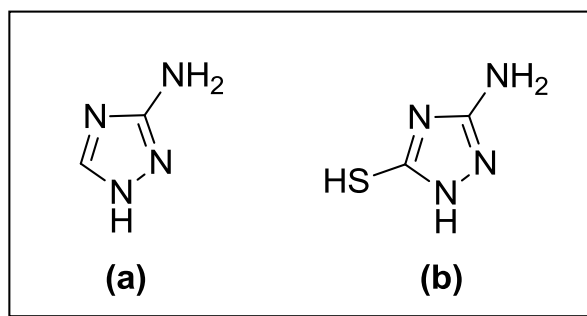
Figure 1.19 shows the chemical structures of (a) ATA and, (b) AMTA.

1.19.4 Corrosion inhibition by MBT and BTA: The cyclic voltammetry techniques (CV) and rotating disc electrode (RDE) technique was used by Hui Cang *et al*.[181] and reported the behaviour of pyrazole **(Figure 1.20a)** as corrosion inhibitor with their synergistic effect with benzotriazole **(BTA, Figure 1.20b)** or 2-mercaptobenzothiazole **(MBT, Figure 1.20c)** on the corrosion of copper in 0.05M $NaHCO_3$ solution.
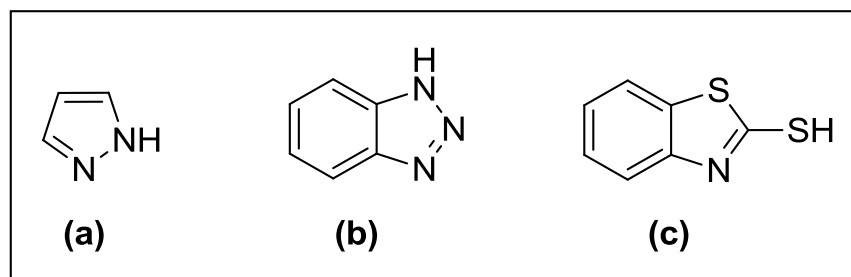
Figure 1.20 Shows the chemical structures of (a) Pyrazole (b) BTA and, (c) MBT.

They also reported the synergetic effect between pyrazole and BTA, but it was unconspicuous between pyrazole and MBT. Frumkin adsorption isotherm was obeyed by the adsorption of Pyrazole on copper surface.

1.19.5 Corrosion inhibition by ETDA: 5-Ethyl-1,3,4-thiadiazol-2-amine **(Figure 1.21)** was reported as corrosion inhibitor for copper metal by El-Sayed and M. Sherif[182] in neutral and acidic chloride solutions. The entire corrosion study was done by using a combination of electrochemical impedance spectroscopy (EIS) and weight-loss measurements; in addition to potentiodynamic polarization and chronoamperometry. The increase in polarization resistance of copper with increase in concentration of ETDA, decreases the corrosion current density and hence act as corrosion inhibitor. They recorded higher inhibition efficiency of ETDA for copper in NaCl solutions than HCl
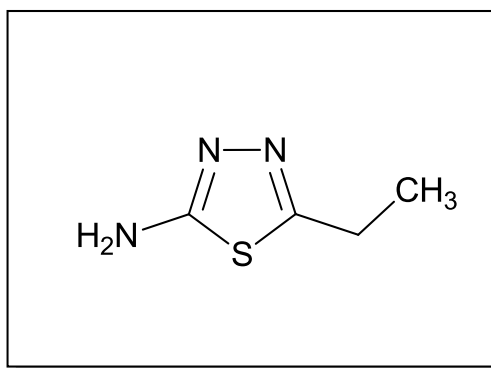
Figure 1.21 Shows the chemical structure of 5-Ethyl-1,3,4-thiadiazol-2-amine (ETDA).

1.19.6 Corrosion inhibition by pharmaceutical compounds: The inhibition effect of some pharmaceutical compounds **(Figure 1.22)** 6-Chloro-1,1-dioxo-3,4-dihydro- 2*H*-1,2,4 benzothiadiazine-7-sulfonamide (CDDBS), 1-((s)-3-mercapto-2-methyl propanoyl) pyrrolidine-2- carboxylic acid (MMPPC), and 3-(2-methoxy phenoxy) propane 1,2-diol (MPPD) in 2M HNO₃ at 30°C was investigated by Fouda *et al*.[183]
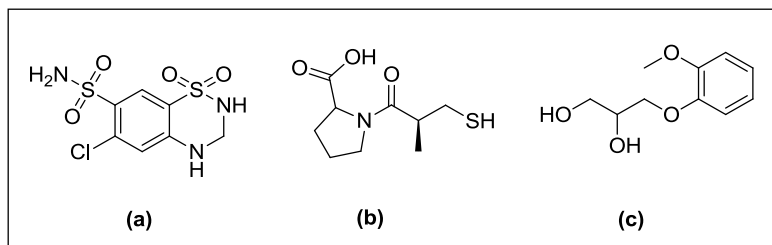
Figure 1.22 Shows the chemical structure of (a) CDDBS (b) MMPPC, and (c) MPPD.

They investigated the corrosion inhibition behaviour by using electrical frequency modulation (EFM) techniques, weight loss measurements, potentiodynamic polarization and electrochemical impedance spectroscopy (EIS). The Temkin's adsorption isotherm was followed by these compounds on copper surface. The relationships between the inhibition efficiency and some quantum chemical parameters have also been discussed.

1.19.7 Corrosion inhibition of CMA by BTA: The corrosion behaviour of a new type copper manganese-aluminium (CMA) alloy in artificial seawater was investigated by H. Gerengi *et al*.[184] They reported benzotriazole **(BTA, Figure 1.20b)** as corrosion inhibitor for CMA and investigated the detailed corrosion study using dynamic electrochemical impedance spectroscopy (DEIS), linear polarization resistance, and Tafel extrapolarization methods. The percent inhibition efficiency, IE (%), values obtained from the charge transfer resistance (Rct) values by DEIS method.

1.19.8 Corrosion inhibition by Benzotriazole, Salicylaldoxime and Cysteine: The comparative study of the active Benzotriazole **(Figure 1.20b)**, Salicylaldoxime **(Figure 1.23a)** and Cysteine **(Figure 1.23b)** as corrosion inhibitors were reported by Ian D. MacLeod and their coworkers.[185] They reported these inhibitors for the active chloride-based corrosion of Copper and Bronze artifacts. The aim of the study was to replace the widely used environmentally unfriendly benzotriazole with potential salicylaldoxime and cysteine inhibitors. Finally, they concluded that for most conservation applications salicylaldoxime behave as a pertinent and effective corrosion inhibitor on corroded copper and bronze, while cysteine presented the potential environmentally friendly replacemet for benzotriazole as corrosion inhibitor for metal artifacts.
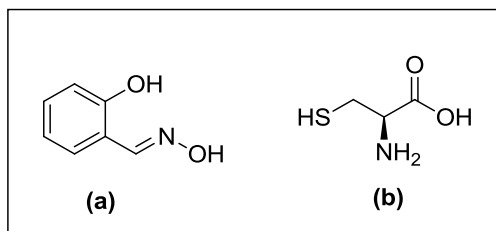
Figure 1.23 Shows the chemical structure of (a) Salicylaldoxime and (b) Cysteine.

1.19.9 Corrosion inhibition by amino acid Cysteine: Ana and co-worker[186] reported cysteine (**Figure 1.23b**) as corrosion inhibitor and their aim was to investigate a "green" non-toxic eco-friendly corrosion inhibitor for copper metal in an acidic solution of sodium sulphate. They used four basic methods such as optical microscopy, potentiodynamic measurements, chronoamperometric measurements, and open circuit potential measurements (OCP) in the investigation of corrosion inhibitor. The Langmuir adsorption isotherm was followed by the cysteine inhibitor and is chemisorbed on the surface of the metal.

1.19.10 Corrosion inhibition by various amino acids: The two well known gravimetric and potentiodynamic polarization methods were used by the Barouni group[187] in the investigation of various amino acids (**Figure 1.24**) such as: Acid aspartic (Asp), Acid Glutamic (Glu), Alanine (Ala), Asparagine (Asn), Glutamine (Gln), Leucine (Leu), Methionine (Met), and Threonine (The) as corrosion inhibitor for copper in 1M HNO_3 solution. The comparable results obtained by both the techniques show that Met behaves as the best inhibitor for the corrosion of copper in 1M HNO_3. Semi empirical (AM1 and MNDO) and ab-initio methods were used for correlation between inhibition efficiency and quantum chemical calculations
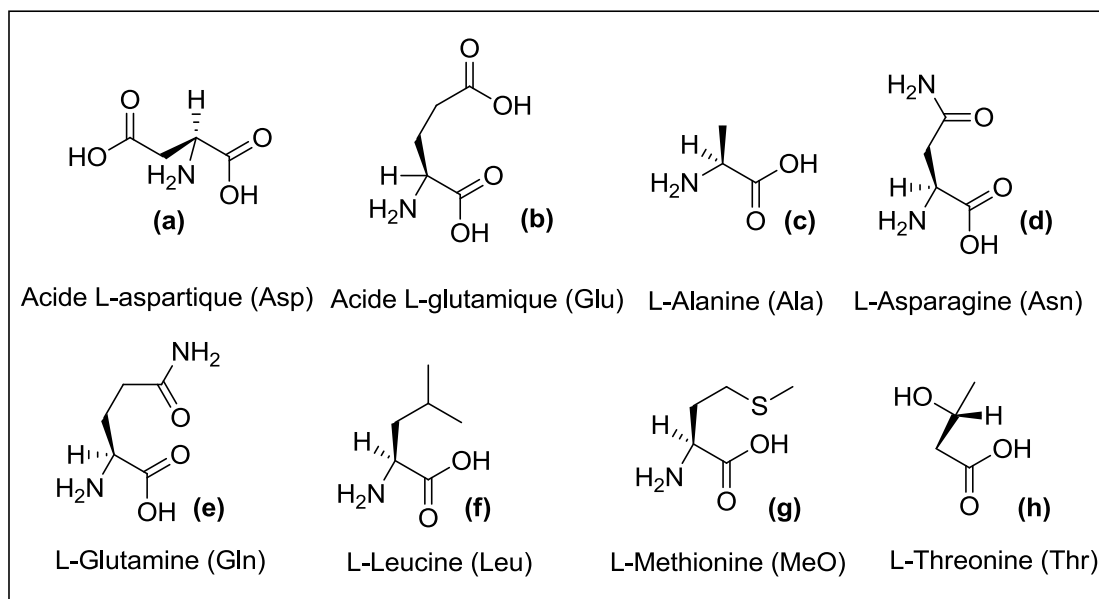
Figure 1.24 Shows the chemical structures of aminoacids tested (a) Aspartique (b) Glutamique (c) Alanine (d) Asparagine (e) Glutamine (f) Leucine (g) Methionine and, (h) Threonine.

1.19.11 Effect of Benzotriazole on corrosion inhibition under flow conditions: Parook and his colleagues[188] reported the benzotriazole (**Figure 1.20b**) as corrosion inhibitor in static environment for

copper metal. The proof for the protection of copper in dynamic flowing environment is inadequate. Therefore, they investigated the corrosion control of copper by using rotating cage in 3.5% NaCl solution in presence of benzotriazole. The flow test experiment was performed at different velocities 0.5–3.0 m/s (100– 700 rpm). Scanning electron microscopy, atomic force microscopy and contact angle measurements were used to examine the morphology of the copper surface. Adsorption of benzotriazole on copper surface in dynamic flowing environment follows the Langmuir adsorption isotherm.

1.20 Conclusions

The first chapter of the thesis is divided into four sections and each section gives the detailed overview of the various flovour of chemistry as:

(a) Reductive Heck type and cross coupling reactions.

(b) Biological significance and various synthetic methodologies for synthesis of Pyranopyrazole molecules by 2CR, 3CR and 4CR.

(c) Drug designing via molecular docking by using AutoDock tool 4.2 as well as Discovery Studio Viewer.

(d) Study of corrosion inhibitors for copper metal.

Although the lot of literature is available in all the four different areas discussed above but still there is gap in research discussed and somewhere thrust remain in researchers in search of new chemical entity. There is strong need to fill the gap in all the areas discussed above, that's why we tried our best to fill up the gap upto some level and discussed all these areas in detail with experimental proof in chapter-2, 3, 4, and 5 respectively.

1.21 References

[1] Grotjahn, D. B., *Comprehensive Organomatallic Chemistry.* 2nd ed.; Hegedus, Kidlington: **1995**; 703.

[2] Jia, C.; Kitamura, T.; Fujiwara, Y. *Acc. Chem. Res.* **2001**, *34*, 633.

[3] Marc, M.; Jie, L.; Lutz, A. *ACS Catal*. **2016**, *6*, 498.

[4] Heck, R. F. *Acc. Chem. Res.* **1979**, *12*, 146.

[5] Paul, M.; John, F. B.; David, K.; Ewan, K. G.; Jeremy, S. P.; Joseph, B. S. *Org. Process Res. Dev.* **2013,** *17*, 397.

[6] Sumino, S.; Fusano, A.; Fukuyama, T.; Ryu, I. *Acc. Chem. Res.* **2014**, *47*, 1563.

[7] Blanchard, P.; Kortbi, M. S.; Fourrey, J. L.; Malka, R. G. *Tetrahedron Lett.* **1992**, *33*, 3319.

[8] Blanchard, P.; Silva, D. A.; Kortbi, M. S.; Fourrey, J. L.; Malka, R. G. D. *J. Org. Chem.* **1993,** *58*, 6517.

[9] Sestelo, J. P.; Mascarenas, J. L.; Castedo, L.; Maurino, A. *J. Org. Chem.* **1993**, *58*, 118.

[10] Manchand, P. S.; Yiannikouros, G. P.; Belica, P. S.; Madan, P. *J. Org. Chem.* **1995**, *60*, 6574.

[11] Bernd, G.; Thoma, G. *Helv. Chim. Acta.* **1991**, *74,* 1135.

[12] Lebedev, S. A.; Lopatina, V. S.; Petrov, E. S.; Beletskaya, I. P. *J. Organomet. Chem.* **1988,** *344*, 253.

[13] Sustmann, R.; Hopp, P.; Holl, P. *Tetrahedron Lett*. **1989**, *30*, 689.

[14] Sim, T. B.; Choi, J.; Yoon, N. M. *Tetrahedron Lett.* **1996,** *37*, 3137.

[15] Masanari, K. *Org. Synth.* **2013,** *90*, 105.

[16] Chang, Y. Z.; Shou, F. Z.; Xin, L. W.; Lin, Q. Z. *J. Am. Chem. Soc.* **2010,** *132*, 10955.

[17] Jagt, R. B. C.; Toullec, P. Y.; Geerdink, D.; de-Vries, J. G.; Feringa, B. L.; Minnaard, A. J. *Angew. Chem. Int. Ed.* **2006**, *45*, 2789.

[18] Hongyu, Y.; Chenglong, Z.; Hengzhi, Y.; Kunhua, L.; Hegui, G. *Chem. Commun.* **2012,** *48*, 7034.

[19] Toda, S.; Miyamoto, M.; Kinoshita, H.; Inomata, K. *Bull. Chem. Soc. Jpn.* **1991,** *64*, 3600.

[20] Cárdenas D. J. *Angew. Chem. Int. Ed.* **2003**, *42*, 384.

[21] Luh, T. Y.; Leung, M. K.; Wong, K. T. *Chem. Rev.* **2000,** *100*, 3187.

[22] Negishi, E.; Liu, F. *Metal-catalyzed cross coupling reactions*. Diederich F., Stang P. J. Ed.; VCH, Weinheim: **1998,** 1.

[23] Ishiyama, T.; Abe, S.; Miyaura, N.; Suzuki, A. *Chem. Lett.* **1992,** *21*, 691.

[24] Jianrong, Z.; Gregory, C. F. *J. Am. Chem. Soc*. **2003,** *125*, 12527.

[25] Jun, T.; Hideyuki, W.; Aki, I.; Hitoshi, K.; Nobuaki, K. *J. Am. Chem. Soc.* **2002,** *124*, 4222.

[26] Espinet, P.; Echavarren, A. M. *Angew. Chem. Int. Ed.* **2004,** *43*, 4704.

[27] Deng, H.; Jung, J. K.; Liu, T.; Kuntz, K. W.; Snapper, M. L.; Hoveyda, A. H. *J. Am. Chem. Soc.* **2003,** *125*, 9032.

[28] Nicolaou, K. C.; Li, Y.; Sugita, K.; Monenschein, H.; Guntupalli, P.; Mitchell, H. J.; Fylaktakidou, K. C.; Vourloumis, D.; Giannakakou, P.; O'Brate, A. *J. Am. Chem. Soc.* **2003,** *125*, 15443.

[29] Yu, H.; Xu, B.; Swager, T. M. *J. Am. Chem. Soc.* **2003,** *125*, 1142.

[30] Zhou, J.; Fu, G. C. *J. Am. Chem. Soc.* **2003,** *125*, 14726.

[31] Zhou, J.; Fu, G. C. *J. Am. Chem. Soc.* **2004,** *126*, 1340.

[32] Powell, D. A.; Fu, G. C. J. *J. Am. Chem. Soc.* **2004,** *126*, 7788.

[33] David, A. P.; Toshihide, M.; Gregory C. F. *J. Am. Chem. Soc.* **2005,** *127*, 510.

[34] Kim, L. J.; Eric, A. S.; Timothy, F. J. *J. Am. Chem. Soc*. **2014,** *136*, 11145.

[35] Preeti, R. B.; Abdul A. A.; Bishwajit, S.; Barua, N. C.; Digant, S. *New J. Chem.* **2015,** *39*, 2440.

[36] Ivelina, M. Y.; George, A. J.; Charlotte, A. O.; Curtis, E. M.; Naomi, S. M.; Elizabeth R. J. *Angew. Chem. Int. Ed.* **2014,** *53*, 2422 .

[37] Arjona, O.; Dios, A.; Fernandez, P. R.; Plumet, J.; Viso, A. *J. Org. Chem.* **1994**, *59*, 3906.

[38] Duan, J. P.; Cheng, C. H. *Tetrahedron Lett.* **1993**, *34*, 4019.

[39] Feng, C. C.; Nandi, M.; Sambaiah, T.; Cheng, C. H. *J. Org. Chem.* **1999,** *64*, 3538.

[40] Brown, H. C.; Prasad, J. V. N. V. *J. Org. Chem.* **1985**, *50*, 3002.

[41] Jeffrey, A. M.; Jerina, D. M. *J. Am. Chem. Soc.* **1972**, *94*, 4048.

[42] Dong, L. M.; Chen, B.; Chang H. D.; Li, X. D.; Guang, C. G.; Xue, L. H. *Organometallics* **2013,** *32*, 4465.

[43] (a) Zhang, T. K.; Yuan, K.; Hou, X. L. *J. Organomet. Chem.* **2007,** *692*, 1912; (b) Zhang, T. K.; Mo, D. L.; Hou, X. L.; Dai, L. X. *Org. Lett.* **2008,** *10*, 3689; (c) Huang, X. J.; Mo, D. L.; Ding, C. H.; Hou, X. L. *Synlett* **2011, 7,** 943; (d) Ge, G. C.; Mo, D. L.; Ding, C. H.; Hou, X. L.; Dai, L. X. *Org. Lett.* **2012,** *22*, 5756.

[44] Rayabarapu, D. K.; Cheng, C. H. *Acc. Chem. Res.* **2007,** *40*, 971.

[45] Duan, J. P.; Cheng, C. H. *Tetrahedron Lett.* **1993,** *34*, 4019; (b) Duan, J. P.; Cheng, C. H. *Organometallics* **1995,** *14*, 1608.

[46] Feng, C. C.; Nandi, M.; Sambaiah, T.; Cheng, C. H. *J. Org. Chem.***1999,** *64*, 3538.

[47] Joule, J. A.; Mills, K., *Heterocyclic chemistry*. ed.; John Wiley & Sons: **2008**.

[48] Katritzky, A. R.; Rees, C. W.; Potts, K. T., *Comprehensive heterocyclic chemistry: the structure, reactions, synthesis and uses of heterocyclic compounds. ed.*; Pergamon Press Oxford, UK: **1984**; Vol. 4.

[49] Katritzky, A. R.; Ramsden, C. A.; Joule, J. A.; Zhdankin, V. V., *Handbook of heterocyclic chemistry. ed.*; Elsevier: **2010**.

[50] Pozharskii, A. F.; Soldatenkov, A. T.; Katritzky, A. R., *Heterocycles in life and society. An introduction to heterocyclic chemistry and biochemistry and the role of heterocycles in science, technology, medicine and agriculture*. ed.; John Wiley & Sons: **1997**.

[51] Gronowitz, S., *The chemistry of heterocyclic compounds, thiophene and its derivatives*. ed.; John Wiley & Sons: **2009**; Vol. 44.

[52] Evans, P. A.; Holmes, B. *Tetrahedron* **1991,** *47*, 9131.

[53] Preston, P. N., *The chemistry of heterocyclic compounds, benzimdazoles and cogeneric tricyclic compounds*. ed.; John Wiley & Sons: **2009**; Vol. 40.

[54] Hudson, B. P.; Barton, J. K. *J. Am. Chem. Soc.* **1998,** *120*, 6877.

[55] Fewell, S. W.; Woolford, J. L. *Mol. Cell. Biol.* **1999,** *19*, 826.

[56] Chan, H. L.; Liu, H. Q.; Tzeng, B. C.; You, Y. S.; Peng, S. M.; Yang, M.; Che, C. M. *Inorg. Chem.* **2002,** *41*, 3161.

[57] Bailly, C. *Curr. Med. Chem.* **2000,** *7*, 39.

[58] Álvarez-Corral, M.; Muñoz-Dorado, M.; Rodríguez-García, I. *Chem. Rev.* **2008,** *108*, 3174.

[59] Zeni, G.; Larock, R. C. *Chem. Rev.* **2004,** *104*, 2285.

[60] Zhu, J. *Eur. J. Org. Chem.* **2003,** *2003*, 1133.

[61] Zeni, G.; Larock, R. C. *Chem. Rev.* **2006,** *106*, 4644.

[62] Toure, B. B.; Hall, D. G. *Chem. Rev.* **2009,** *109*, 4439.

[63] (a) Dömling,A.; Wang, W.; Wang, K. *Chem. Rev.* **2012,** *112*, 3083; (b) Tejedor, D.; Garcia-Tellado, F. *Chem. Soc. Rev.* **2007,** *36*, 484; (c) Ugi, I. *Pure Appl. Chem.* **2001,** *73*, 187; (d) Liéby-Muller, F.; Simon, C.; Constantieux, T.; Rodriguez, J. *QSAR Comb. Sci.* **2006,** *25*, 432; (e) Simon, C.; Constantieux, T.; Rodriguez, J. *Euro. J. Org. Chem.* **2004,** *2004*, 4957; (f) Evdokimov, M. N.; Kireev, A. S.; Yakovenko, A. A.; Antipin, M. Y.; Magedov, I. V.; Kornienko, K. *J. Org. Chem.* **2007,** *72*, 3443; (g) Weber, L. *Drug Discov. Today* **2002,** *7*, 143; (h) Hulme, C.; Gore, V. *Curr. Med. Chem.* **2003,** 10, 51.

[64] Ciriminna, R.; Pagliaro, M. *Org. Process Res. Dev.* **2013,** *17*, 1479.

[65] (a) Trost, B. M. *Acc. Chem. Res.* **2002,** *35*, 695; (b) Leng, R. B.; Emonds, M. V. M.; Hamilton, C. T.; Ringer, J. W. *Org. Process Res. Dev.* **2012,** *16*, 415.

[66] Ugi, I.; Dömling, A.; Horl, W. *Endeavour* **1994,** *18*, 115.

[67] Tietze, L. F. *Chem. Rev.* **1996,** *96*, 115.

[68] (a) Dömling, A. *Chem. Rev.* **2006,** *106*, 17; (b) Wang, W.; Dömling, A. *J. Comb. Chem.* **2009,** *11*, 403.

[69] (a) Keating, T. A.; Armstrong, R. W. *J. Am. Chem. Soc.* **1996,** *118*, 2574; (b) Szardenings, A. K.; Burkoth, T. S.; Lu, H. H.; Tien, D. W.; Campbell, D. A. *Tetrahedron* **1997,** *53*, 6573; (c) Hulme, C.; Ma, L.; Cherrier, M. P.; Romano, J. J.; Morton, G.; Duquenne, C.; Salvino, J.; Labaudiniere, R. *Tetrahedron Lett.* **2000,** *41*, 1883; (d) Hulme, C.; Ma, L.; Romano, J.; Morrissette, M. *Tetrahedron Lett.* **1999,** *40*, 7925; (e) Golebiowski, A.; Klopfenstein, S. R.; Shao, X.; Chen, J. J.; Colson, A. O.; Grieb, A. L.; Russell, A. F. *Org. Lett.* **2000,** *2*, 2615; (f) Tempest, P.; Ma, V.; Thomas, S.; Hua, Z.; Kelly, M. G.; Hulme, C. *Tetrahedron Lett.* **2001,** *42*, 4959; (g) Nixey, T.; Tempest, P.; Hulme, C. *Tetrahedron Lett.* **2002,** *43*, 1637; (h) Faggi, C.; Marcaccini, S.; Pepino, R.; Cruz, P. M. *Synthesis* **2002,** *2002*, 2756; (i) Zhang, W.; Tempest, P. *Tetrahedron Lett.* **2004,** *45*, 6757; (j) Hulme, C.; Dietrich, J. *Molec. Divers.* **2009,** *13*, 195; (k) Tejedor, D.; Garcia, T. F. *Chem. Soc. Rev.* **2007,** *36*, 484; (l) Isambert, N.; Lavilla, R. *Chem. Eur. J.* **2008,** *14*, 8444; (m) Willy, B.; Mueller, T. J. J. *Arkivoc* **2008,** *2008*, 195; (n) Simon, C.; Constantieux, T.; Rodriguez, J. *Eur. J. Org. Chem.* **2004,** *2004*, 4957.

[70] (a) Hogale, M. B.; Pawar, B. N. J. *Indian Chem. Soc.* **1989**, *66*, 206; (b) Yu, S. M.; Kuo, S. C.; Huang, L. J.; Sun, S. S. M.; Huang, T. F.; Teng, C. M. *J. Pharm. Pharmacol.* **1992**, *44*, 667; (c) Catarzi, D.; Cecchi, L.; Colotta, V.; Filacchioni, G.; Martini, C.; Tacchi, P.; Lucacchini, A. *J. Med. Chem.* **1995**, *38*, 1330; (d) Colotta, V.; Catarzi, D.; Varano, F.; Melani, F.; Filacchioni, G.; Cecchi, L.; Trincavelli, L.; Martini, C.; Lucacchini, A. *II Farmaco* **1998**, *53*, 189; (e) Mityurina, K. V.; Kulikova, L. K.; Krasheninnikova, M. K.; Kharchenko, V. G. *Pharm. Chem. J.* **1981**, *15*, 861.

[71] (a) El-Tamany, E. S.; El-Shahed, F. A.; Mohamed, B. H. *J. Serb. Chem. Soc.* **1999**, *64*, 9; (b) Abdel-Rahman, A. H.; Keshk, E. M.; Hanna, M. A.; El-Bady, Sh. M. *Bioorg. Med. Chem.* **2004**, *12*, 2483.

[72] (a) Abdelrazek, F. M.; Metz, P.; Metwally, N. H.; El-Mahrouky, S. F. *Arch. Pharm – Pharm. Med. Chem.* **2006**, *339*, 456; (b) Abdelrazek, F. M.; Metz, P.; Kataeva, O.; Jaeger, A.; El-Mahrouky, S. F. *Arch. Pharm – Pharm. Med. Chem.* **2007**, *340*, 543.

[73] (a) Zaki, M. E. A.; Soliman, H. A.; Hiekal, O. A.; Rashad, A. E. *Z. Naturforsch.* **2006**, *61*, 1; (b) Kuo, S. C.; Huang, L. J.; Nakamura, H. *J. Med. Chem.* **1984,** *27*, 539.

[74] (a) Ueda, T.; Mase, H.; Oda, N.; Ito, I. *Chem. Pharm. Bull.* **1981**, *29*, 3522; (b) Vaid, R. K.; Dhindsa, G. S.; Kaushik, B.; Singh, S. P.; Dhawan, S. N. *Indian J. Chem., Sect B* **1986**, *25*, 569.

[75] Ismail, Z. H.; Aly, G. M.; El-Degwi, M. S.; Heiba, H. I.; Ghorab, M. M. Egypt. *J. Biotechnol.* **2003**, *13*, 73.

[76] Joshi, K. C.; Jain, R.; Arora, S. J. *J. Indian Chem. Soc.* **1988**, *65*, 277.

[77] (a) Yu, S. M.; Kuo, S. C.; Huang, L. J.; Sun, S. S. M.; Huang, T. F.; Teng, C. M. *J. Pharm. Pharmacol.* **1992**, *44*, 667; (b) Huang, L. J.; Hour, M. J.; Teng, C. M.; Kuo, S. C. *Chem. Pharm. Bull.* **1992**, *40*, 2547.

[78] (a) Catarzi, D.; Cecchi, L.; Colotta, V.; Filacchioni, G.; Martini, C.; Tacchi, P.; Lucacchini, A. *J. Med. Chem.* **1995**, *38*, 1330; (b) Colotta, V.; Catarzi, D.; Varano, F.; Melani, F.; Filacchioni, G.; Cecchi, L.; Trincavelli, L.; Martini, C.; Lucacchini, A. *Il Farmaco* **1998**, *53*, 189.

[79] Foloppe, N.; Fisher, L. M.; Howes, R.; Potter, A.; Robertson, A. G. S.; Surgenor, A. E. *Bioorg. Med. Chem.* **2006**, *14*, 4792.

[80] Junek, H.; Aigner, H. *Chem. Ber.* **1973,** *106*, 914.

[81] (a) Otto, H. H. *Arch. Pharm.* **1974**, *307*, 444; (b) Otto, H. H.; Schmelz, H. *Arch. Pharm. – Pharm. Med. Chem.* **1979**, *312*, 478; (c) Abdel-Latif, F. F. *Z. Naturforsch., B: Chem. Sci.* **1990**, *45*, 1675; (d) Dyachenko, V. D.; Rusanov, E. B. *Chem. Heterocycl. Compd.* **2004**, *40*, 231.

[82] (a) Sharanina, L. G.; Marshtupa, V. P.; Sharanin, Yu. A. *Khim. Geterotsikl Soedine.* **1980**, *10*, 1420; (b) Tacconi, G.; Gatti, G.; Desimoni, G. J. *J. Prakt. Chem.* **1980,** *322*, 831; (c) Rodinovskaya, L. A.; Gromova, A. V.; Shestopalov, A. M.; Nesterov, V. N. *Russ. Chem. Bull.* **2003,** *52*, 2207.

[83] Peng, Y.; Song, G.; Dou, R. *Green Chem.* **2006,** *8*, 573.

[84] Pandit, R. P.; Lee, Y. R. *Molec. Divers.* **2014,** *18*, 39.

[85] (a) Sharanin, Y. A.; Sharanina, L. G.; Puzanova, V. V. *J. Org. Chem. USSR.* **1983**, 2291; (b) Klokol, G. V.; Krivokolysko, S. G.; Dyachenko, V. D.; Litvinov, V. P. *Chem. Heterocycl. Compd.* **1999**, *35*, 1183; (c) Shestopalov, A. M.; Yakubov, A. P.; Tsyganov, D. V.; Emel'yanova, Y. M.; Nesterov, V. N. *Chem. Heterocycl. Compd.* **2002**, *38*, 1180; (d) Dyachenko, V. D.; Chernega, A. N. *Russ. J. Gen. Chem.* **2005**, *75*, 952; (e) Lehmann, F.; Holm, M.; Laufer, S. *J. Comb. Chem.* **2008,** *10*, 364.

[86] (a) Shestopalov, A. M.; Emeliyanova, Y. M.; Shestopalov, A. A.; Rodinovskaya, L. A.; Niazimbetova, Z. I.; Evans, D. H. *Org. Lett.* **2002**, *4*, 423; (b) Shestopalov, A. M.; Emeliyanova, Y. M.; Shestopalov, A. A.; Rodinovskaya, L. A.; Niazimbetova, Z. I.; Evans, D. H. *Tetrahedron* **2003**, *59*, 7491.

[87] Dandia, A.; Ashok, K. L.; Ruby S. *Tetrahedron Lett.* **2012**, *53*, 3012.

[88] (a) Hafez, E. A. A.; Galil, F. M. A.; Sherif, S. M.; Elnagdi, M. H. *J. Heterocycl. Chem.* **1986**, *23*, 1375; (b) Redkin, R. G.; Shemchuk, L. A.; Chernykh, V. P.; Shishkin, O. V.; Shishkina, S. V. *Tetrahedron* **2007**, *63*, 11444; (c) Litvinov, Y. M.; Mortikov, V. Y.; Shestopalov A. M. *J. Comb. Chem.* **2008**, *10*, 741; (d) Elinson, M. N.; Dorofeev, A. S.; Miloserdov, F. M.; Nikishin, G. I. *Molec. Divers.* **2009**, *13*, 47.

[89] Dyachenko, V. D.; Rusanov, E. B. *Chem. Heterocycl. Compd.* **2004,** 40, 231.

[90] Radi, M.; Bernardo, V.; Bechi, B.; Castagnolo, D.; Pagano, M.; Botta, M. *Tetrahedron Lett.* **2009**, *50*, 6572.

[91] Mehdi, K.; Masoumeh, A.; Alireza, M.; Amirhossein S.; Hamid, N.; Razavi, S. F.; Mehdi, G.; Alireza F.; Abbas, S. *Eur. J. Med. Chem.* **2013**, *68*, 291.

[92] Najmedin, A.; Dezfooli, S.; Khajeh, M.; Hashemi, M. M. *J. Mol. Liq.* **2013,** *186*, 76.

[93] Ramesh, S.; Shanti, R. *J. Mol. Liq.* **2012**, *166*, 40.

[94] Yue, C.; Fang, D.; Liu, L.; Yi, T. F. *J. Mol. Liq.* **2011,** *163*, 99.

[95] Wang, H.; Jing, Y.; Wang, X.; Yao, Y.; Jia, Y. *J. Mol. Liq.* **2012,** *170*, 20.

[96] Abbott, A. P.; Capper, G.; Davies, D. L.; Rasheed, R. K.; Tambyrajah, V. *Chem. Commun.* **2003,** *1*, 70.

[97] Abbott, A. P.; Barron, J.; Ryder, K.; Wilson, D. *Chem. Eur. J.* **2007,** *13*, 6495.

[98] Chen, Z.; Zhou, B.; Cai, H.; Zhu, W.; Zou, X. *Green Chem.* **2009,** *11*, 275.

[99] Chen, Z.; Zhu, W.; Zheng, Z.; Zou, X. J. *J. Fluorine Chem.* **2010,** *131*, 340.

[100] Zhang, Q.; De-Oliveira K. V.; Royer, S.; Jérôme, F. *Chem. Soc. Rev.* **2012,** *41*, 7108.

[101] Pawar, P. M.; Jarag, K. J.; Shankarling, G. S. *Green Chem.* **2011**, 13, 2130.

[102] Saha, M.; Pal, A. K. *ANP* **2012,** *1*, 61.

[103] Vasuki, G.; Kumaravel, K. *Tetrahedron Lett.* **2008,** *49*, 5636.

[104] Aisha, S.; Aatika, N.; Pasha, M. A. *Spectrochim. Acta, Part A* **2011,** 81, 431.

[105] Mecadon, H.; Rohman, R. M.; Laloo, B. M.; Kharkongor, I.; Myrboh, B. *Tetrahedron Lett.* **2011,** *52*, 3228.

[106] Santhosh, R. M.; Sravanthi, S.; Manjula, A.; Vittal, R. B.; Madhava, R. B.; Sridhar, B. *Bioorg. Med. Chem. Lett.* **2012,** *22*, 5272.

[107] Ebrahimi, J.; Mohammadi, A.; Pakjoo, V.; Bahramzad, E.; Habibi, A. *J. Chem. Sci.* **2012,** *124*, 1013.

[108] Azzam, S. H. S.; Pasha, M. A. *Tetrahedron Lett.* **2012,** *53*, 6834.

[109] Ablajan, K.; Wang, L. J.; Maimaiti, Z.; Lu, Y. T. *Monats. Chem.* **2014,** *145*, 491.

[110] Pore, D. M.; Patil, P. B.; Gaikwad, D. S.; Hegade, P. G.; Patil, J. D.; Undale. K. A. *Tetrahedron Lett.* **2013**, 54, 5876.

[111] Suman, P.; Md. Nasim, K.; Shaik, K.; Jahir, S. A.; Lokman, H. C. *Tetrahedron Lett.* **2013,** *54*, 5434.

[112] Kiyani, H.; Samimi, H. A.; Ghorbani, F.; Esmaieli. S. *Curr. Chem. Lett.* **2013,** *2*, 197.

[113] Feng, J.; Ablajan, K.; Sali, A. *Tetrahedron* **2014**, 70, 484.

[114] Majid, M. H.; Mousavizadeh, F.; Ghobadi, N.; Tajbakhsh, M. *Tetrahedron Lett.* **2014,** *55*, 1226.

[115] Kumar, A.; Lohan , P.; Aneja, D. K.; Gupta, G. K.; Kaushik, D.; Prakash, O. *Eur. J. Med. Chem.* **2012**, *50*, 81.

[116] Parshad, M.; Verma, V.; Kumar. D. *Monats. Chem.* **2014**, *145*, 1857.

[117] http://www.cancerresearchuk.org.

[118] Anand, P.; Kunnumakkara, A. B.; Sundaram, C.; Harikumar, K. B.; Lai, O. S.; Sung, B.; Aggarwal, B. B. *Pharm. Res.* **2008,** *25*, 2097.

[119] Kinzler, K. W.; Vogelstein, B. "Introduction". *The genetic basis of human cancer*. 2nd ed.; New York, Mc-Graw-Hill, Medical Pub. Division: **2002**; p. 5.

[120] http://www.cdc.gov/niosh/topics/cancer.

[121] Aggarwal, B. B.; Sethi, G.; Veera, B.; Sunil, K.; Shishodia, S. *J. Cell. Biochem.* **2007,** *102*, 580.

[122] Bridges.; Alexander, J. *Chem. Rev.* **2001,** *101*, 2541.

[123] www.google.co.in

[124] Morgan.; David, O. *The cell cycle: Principles of control.* 1st ed.; London, New Science Press: **2007**.

[125] Lee, Melanie.; Nurse, P. *Nature* **1987**, *327*, 31.

[126] Senderowicz, A. M. *Invest. New Drugs* **1999,** *17*, 313.

[127] Sausville, E. A. *Trends Mol. Med.* **2002,** *8*, S32.

[128] www.rcsb.org.

[129] Binani, M.; Bora, P. P.; Bez, G. *J. Chem.* **2013**, Article ID 920719, 8 pages.

[130] Foloppe, N.; Fisher, L. M.; Howes, R.; Potter, A.; Robertson, A. G. S.; Surgenor, A. E. *Bioorg. Med. Chem.* **2006,** *14*, 4792.

[131] Hoult, J. R.; Payá, M. *Gen. Pharmacol.* **1996,** *27*, 713.

[132] Vianna, D. R.; Hamerski, L.; Figueiro, F.; Bernardi, A.; Visentin, L. C. *Eur. J. Med. Chem.* **2012,** *57*, 268.

[133] Finn, G. J.; Kenealy, E.; Creaven, B. S.; Egan, D. A. *Cancer Lett.* **2002,** *183*, 61.

[134] Loprinzi, C. L.; Kugler, J. W.; Sloan, J. A.; Rooke, T. W.; Quella, S. K. *N. Eng. J. Med: Res. Rev.* **1999,** *340*, 346.

[135] Kostova, I. *Curr. Med. Chem. Anticancer Agents* **2005,** *5*, 2946.

[136] Murray, R. D. H.; Mendez, J.; Brown, S. A. *The natural coumarins: occurrence, chemistry and biochemistry*. Wiley, Newyork: **2010;** 1.

[137] Mironov, A.; Colanzi, A.; Polishchuk, R.; Beznoussenko, G.; Mironov, A.; Fusella, A.; Tullio, D. G.; Silletta, M.; Corda, D.; De-Matteis, M.; Luini, A. *Eur. J. Cell Biol.* **2004,** *83,* 263.

[138] Abdelmohsen, K.; Stuhlmann, D.; Daubrawa, F.; Klotz, L. *Arch. Biochem. Biophys.* **2005,** *434,* 241.

[139] Egan, D. A.; O'Kennedy, R.; Moran, E.; Thornes, R. D. *Drug Metab. Rev.* **1990,** *22,* 503.

[140] Ojala, T**.** Biological Screening of Plant Coumarins. PhD Thesis. Helsinki, Finland: University of Helsinki. **2001**.

[141] Grotz, K. A.; Wustenberg, P.; Kohnen, R.; Nawas, A. B.; Henneicke-von Zepelin, H. H.; Bockisch, A. *Br. J. Oral Maxillofac. Surg.* **2001,** *39*, 34.

[142] Carter, S. K.; Bakowski, M. T.; Hellman, K. *Chemotherapy of cancer*. 3rd ed.; New York, Wiley & Sons: **1989**.

[143] Finn, G. J.; Creaven, B. S.; Egan, D. A**.** *Cancer Lett.* **2004,** *205,* 69.

[144] Thornes, R. D.; Edlow, D. W.; Wood, S. *Johns Hopkins Med. J.* **1968,** *123*, 305.

[145] Finn, G. J.; Creaven, B. S.; Egan, D. A. *Melanoma Res.* **2001***, 11,* 461.

[146] Marshall, M. E.; Mendelsohn, L.; Butler, K.; Riley, L.; Cantrell, J.; Wiseman, C.; Taylor, R.; Macdonald, J. S. *J. Clin. Oncol.* **1987,** *5*, 862.

[147] Marshall, E. M.; Ryles, M.; Butler, K.; Weiss L**.** *J. Cancer Res. Clin. Oncol.* **1994,** *120*, 535.

[148] Myers, R. B.; Parker, M.; Grizzle, W. E. *J. Cancer Res. Clin. Oncol.* **1994,** *120,* S11.

[149] Wang, C. J.; Hsieh, Y. J.; Chu, C. Y.; Lin, Y. L.; Tseng, T. H. *Cancer Lett.* **2002,** *183*, 163.

[150] Orozco, J. F.; Lopez, G. J. S.; Nieto, R. A.; Velasco, V. M. A.; Molina, G. J. A.; Mendoza, P. N. *Lung Cancer* **2001,** *34*, 185.

[151] Musa, M. A.; Zhou, A.; Sadik O. A. *J. Med. Chem.* **2011,** *7,* 112.

[152] Chen, Y. L.; Lu, C. M.; Lee, S. J.; Kuo, D. H.; Chen, I. L.; Wang, T. C.; Tzeng, C. C. *Bioorg. Med. Chem.* **2005,** *13,* 5710.

[153] Portugal, J. *Curr. Med. Chem. Anti-Cancer Agents.* **2003,** *3,* 411.

[154] Yang, D.; Wang, G. T.; Tang, Q.; Ma, C. *Biosci., Biotechnol., Biochem.* **2010,** *74,* 1430.

[155] Yun, E. S.; Park, S. S.; Shin, H. C. *Toxicol. In Vitro* **2011,** *25,* 1335.

[156] Lee, C. R.; Shin, E. J.; Kim, H. C. *Lab. Anim. Res.* **2011,** *27,* 259.

[157] Whang, W. K.; Park, H. S.; Ham, I. *Exp. Mol. Med.* **2005,** *37,* 436.

[158] Rosselli, S.; Maggio, A. M.; Faraone, N. *Nat. Prod. Commun.* **2009,** *4,* 1701.

[159] Poole, S. K.; Poole, C. F. *Analyst* **1994,** *119,* 113.

[160] Marshall, M. E.; Kervin, K.; Benefield, C.; Umerani, A.; Albainy, J. S.; Zhao, Q.; Khazaeli, M. B. *J. Cancer Res. Clin. Oncol.* **1994,** *120*, S3.

[161] Myers, R. B.; Parker, M.; Grizzle, W. E. *J. Cancer Res. Clin. Oncol.* **1994,** *120*, S11.

[162] Kawaii, S.; Tomono, Y.; Ogawa, K.; Sugiura, M.; Yano, M.; Yoshizawa, Y. *Anticancer Res.* **2001,** *21,* 917.

[163] Thornes, R. D.; Daly, L.; Lynch, G.; Breslin, B.; Browne, H. Y.; Corrigan, T.; Daly, P.; Edwards, G.; Gaffney, E. *J. Cancer Res. Clin. Oncol.* **1994,** *120,* S32.

[164] Marshall, M. E.; Mohler, J. L.; Edmonds, K.; Williams, B.; Butler, K.; Ryles, M.; Weiss, L.; Urban, D.; Bueschen, A.; Markiewicz M. *J. Cancer Res. Clin. Oncol.* **1994,** *120*, S39.

[165] Mohler, J. L.; Williams, B. T.; Thompson, I. M.; Marshall, M. E. *J. Cancer Res. Clin. Oncol.* **1994,** *120,* S35.

[166] Angerer, E. V.; Kager, M.; Maucher, A. *J. Cancer Res. Clin. Oncol.* **1994,** *120*, S14.

[167] Lake, B. G. *Food Chem. Toxicol.* **1999,** *37,* 423.

[168] Marshall, M. E.; Butler, K.; Fried, A.; Phase, I. *Mol. Biother.* **1991,** *3*, 170.

[169] Sharma, A.; Shukla, P.; Pallavi, B.; Subhra, D.; Rajdeep, C. *Curr. Microwave Chem..* **2015,** *2,* 1.

[170] Ganguly, S.; Murugesan S. *Rasayan J. Chem.* **2008,** *1*, 251.

[171] Gareth T.; *Fundamental of medicinal chemistry;* Ch. 5.; John Wiley & Sons Ltd: **2000.**

[172] Garrett M. M.; David S. G.; Michael E. P.; William, L. L.; Ruth, H.; Stefano, F.; William, E. H.; Scott, H.; Rik, B.; Arthur, J. O.; *AutoDock Version 4.2, User Guide, Modification date: November* 05, 2012 08:37 D11/P11, AutoDock, AutoGrid, AutoDock Tools, Copyright © **1991-2009**.

[173] Paul, J. G.; Philip, M. D. *Curr. Opin. Struct. Biol.* **2000,** *10,* 401.

[174] autodock.scripps.edu.

[175] Blumer, K. J.; Johnson, G. L. *Trends Biochem. Sci.* **1994**, *19*, 236.

[176] Kumar, K. A.; Prathyusha, L.T.; Umamaheshwari, M.; Sivashanmugam, T.; Subhadradevi, V.; Jagannath, P.; Madeswaran, A.; Salesheir, F. J. *Chil. Chem. Soc.* **2012,** *57*, 1442.

[177] http://corrosion.ksc.nasa.gov.

[178] Larabi, L.; Benali, O.; Mekelleche , S. M.; Harek, Y. *Appl. Surf. Sci.* **2006,** *253*, 1371.

[179] Khaled, K. F. *Mat. Chem. Phys.* **2011,** *125*, 427.

[180] Sayed, E. M. S. *Int. J. Electrochem. Sci.* **2012,** *7*, 1884.

[181] Cang, H.; Wenyan, S.; Jinling, S.; Qi, X. *Int. J. Electrochem. Sci.* **2012,** *7*, 5626.

[182] Sayed, E. M. S. *Int. J. Electrochem. Sci.* **2012,** *7*, 2832

[183] Eldesokyl, A. M.; Hassan, H. M.; Fouda. A. S. *Int. J. Electrochem. Sci.* **2013,** *8*, 10376.

[184] Gerengi, H.; Slepski, P.; Bereket, G. *Mat. Corr.* **2012,** *63*, 9999.

[185] Ian, D.; Leod, M. *ESJ.* **2013,** *9*, 1857.

[186] Ana, T. S.; Marija, B. P.; Milan, B. R.; Snežana, M. M.; Milan, M. A. *Chem. Pap.* **2014,** *68*, 362.

[187] Barouni, K.; Kassale1, A.; Albourinel, A.; Jbara, O.; Hammouti, B.; Bazzi, L. *J. Mat. Environ. Sci.* **2014,** *5*, 456.

[188] Parook, F. K.; Vaithianathan, S.; Rupesh, K. B.; Srinivasan, M.; Rakesh C. B.; *Chem. Eng.* **2015,** *3*, 10.

Chapter II

Nickel Catalyzed Reductive Heck Coupling Reactions and Ring Opening of Oxabicyclic Alkenes

2.1 Introduction

Activation of C-H bonds is now much in vogue and transition metal mediated activations quite at the forefront of such research.[1a-b] The Heck reaction, though strictly not a C-H activation, has long been the beacon of alkenic C-H bond activation wherein vinylic or arylic halides react with alkenes in the presence of palladium catalyst to form coupled products[2a-g] **(Scheme 2.1)**. This reaction is one of the most powerful methods for the formation of C-C bonds. However, its major limitation is that one cannot use alkyl halides having hydrogen at the β-position to the halide atom, because such substrates suffer from β-hydride elimination problem.[3a-b] Therefore, if a strategy could be developed, which encompassed the successful use of sp^3 alkyl halides for such Heck couplings, it would go a long way in fulfilling the much sought after requirement of modern day transition-metal mediated synthesis.

R-X + ⫽R$_1$ ——Metat Cat.——▶ R⌇R$_1$ **Heck Coupling**

R-X + ⫽R$_1$ ——Metat Cat.——▶ R⌄R$_1$ **Reductive Heck Coupling**
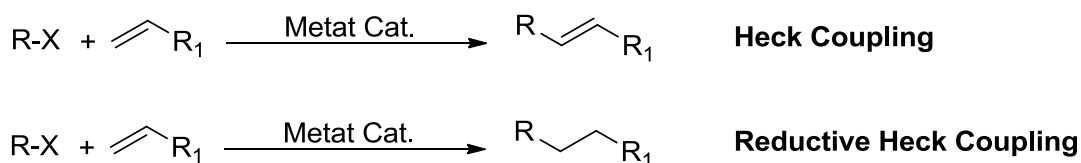
Scheme 2.1 The Heck and reductive Heck type reactions in the presence of metal catalyst.

Broadly, approaches to transition-metal mediated construction of C-C bonds can be subdivided into two main types. One of the approaches for bringing about C-C bond formation, presently a hot topic,[4a-k] involves the cross coupling reaction. The other approach involves stoichiometric[5a-e] or catalytic coupling of saturated alkyl halides with alkenes in the presence of transition metal complexes. Some researchers have reported methodologies, which outline the use of catalytic amounts of the metals to bring about the reductive coupling of an alkyl halide with alkenes.[6a-f] As regards reductive Heck type couplings, Amatore and others reported a related conjugate addition of aryl halides and triflates to activated olefins using cobalt catalyst.[7] Similarly, Shukla *et al*.[8] revealed a cobalt-catalyzed version of the reductive coupling of sp^3 alkyl halides with acrylates. Some other groups have also recently outlined nickel-catalyzed reductive couplings between: an alkyne and an epoxide;[9a] an aldehyde and an alkyne;[9b] dienes and aldehyde;[9c] enones and allenes;[9d] alkynes and imines;[9e] anhydrides and alkyl halides in the presence of Ni(COD)$_2$ catalyst.[9f] However, none of the reports have described a simple nickel-phosphine mediated reductive coupling of unactivated alkyl halides as most have used Ni(COD)$_2$ as the catalytic species along with some sort of an additive to bring about the desired coupling reaction. Furthermore, our reaction pathway appears to be the usual oxidative-addition driven rather than the complicated Ni^{II}/Ni^{III} route as envisaged by some of the previous reports. Nickel catalysis has its distinct advantages such as cheapness, availability, relative environment friendliness, and an unambiguous mechanistic pathway.[10] Additionally, saturated esters have been investigated for biodiesels, in food and pharmaceutical industries,

as emulsifying agents,[11a-b] etc. In our effort to find simple method to couple together a saturated alkyl halide and an electron withdrawing alkene, we decided to develop the simple Ni-catalyzed route to saturated esters.

2.2 Results and Discussion

At first we optimized the conditions for this reductive coupling reaction and **Table 2.1** demonstrates the effect of varying the catalyst and solvent on the overall reaction yield. In the absence of the nickel catalyst, i.e., with only zinc and solvent, there is no reaction at all and we recovered the starting bromo compound **(entry 1)**.

The use of nickel (II) species without any phosphine ligand, i.e., $Ni(acac)_2$ **(entry 14)** does not lead to formation of the product emphasizing the importance of phosphine ligands for this reductive coupling reaction. When bidentate phosphine containing nickel catalysts, e.g., $Ni(dppe)Br_2$ or $Ni(dppe)Cl_2$ are employed, there is some reaction but the yields are pretty low **(entries 2, 3)**. Comparing the activities of these bidentate ligands to others like $Ni(dppm)Br_2$, $Ni(dppm)Cl_2$ **(entries 4, 5)** it is clear that only dppe shows some activity, which may have an enhanced activity because of the bite angle of this particular ligand. Still, none of the bidentate phosphine ligands show any appreciable activity. The results obtained from monodentate phosphine ligands were, however, more encouraging. When $Ni(PPh_3)_2Br_2$ was employed, the yield was substantially enhanced to 66% **(entry 6)**. The best catalyst turned out to be $Ni(PPh_3)_2Cl_2$ giving **3k** in 82% yield **(entry 7)**. With the best catalyst in hand, we set out to examine the role of solvent. The use of tetrahydrofuran **(entry 9)** indicates some activity as the desired product is formed in 54% yield. However, using other solvents viz. toluene, DMF, dichlormethane, or ether, lead to much lower yields of 18, trace, 27, and 15%, respectively **(entries 10-13)**. Therefore, the solvent of choice is acetonitrile, which gives the best yield of **3k (entry 7)**.

Table 2.1: Effect of catalyst and solvent on the reductive coupling of saturated alkyl halides with acrylates.[a]
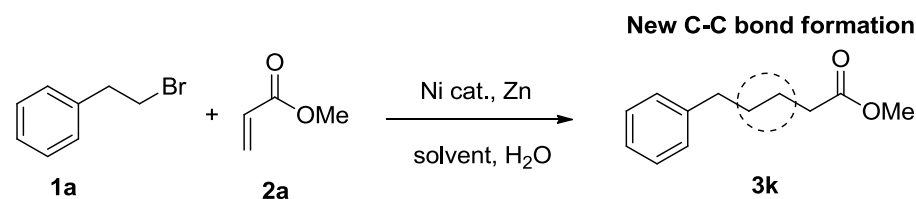
No.	Catalyst	Solvent	Yield (%)[b]
1	--	CH_3CN	0
2	$Ni(dppe)Br_2$	CH_3CN	17

3	Ni(dppe)Cl$_2$	CH$_3$CN	22
4	Ni(dppm)Br$_2$	CH$_3$CN	5
5	Ni(dppm)Cl$_2$	CH$_3$CN	10
6	Ni(PPh$_3$)$_2$Br$_2$	CH$_3$CN	66
7	Ni(PPh$_3$)$_2$Cl$_2$	CH$_3$CN	82
8	Ni(PPh$_3$)$_2$I$_2$	CH$_3$CN	55
9	Ni(PPh$_3$)$_2$Cl$_2$	THF	54
10	Ni(PPh$_3$)$_2$Cl$_2$	Toluene	18
11	Ni(PPh$_3$)$_2$Cl$_2$	DMF	Trace
12	Ni(PPh$_3$)$_2$Cl$_2$	DCM	27
13	Ni(PPh$_3$)$_2$Cl$_2$	Ether	15
14	Ni(acac)$_2$Br$_2$	CH$_3$CN	0

[a]Unless stated otherwise, all reactions were carried out with Ni-catalyst (0.1 mmol), Zn (2.5 mmol), (2-Bromoethyl)benzene **1a** (1.0 mmol), methyl acrylate **2a** (3.0 mmol), H$_2$O (1.0 mmol) and solvent (3.0 ml) at 80 $^\circ$C for 12 h under 1 atm N$_2$. [b]Yields were measured by ^{1}H NMR, using mesitylene as an internal standard.

2.2.1 Effect of varying of the amount of acrylate (2a) on the reaction

Since we were interested in knowing the most favorable condition for the reaction, we experimented with varying the amount of acrylate. It was quite interesting to note the impact of quantity of acrylate used on the reaction yield. Initially, we were tempted to take 1.2 equiv of the acrylate as compared to 1.0 equiv of the alkyl halide, for our reaction. But, the yields were found to be far below our expectations. So, we decided to change the amount of acrylate used at the beginning of the reaction, and we were pleasantly surprised to see that the increased concentration of the acrylate had a remarkable effect on reaction yields **(Table 2.2)**. When only 0.8 equiv of methyl acrylate is used, the yield is relatively low **(entry 1, Table 2.2)**. Progressively increasing the concentration of methyl acrylates, leads to corresponding increase in yield **(entries 2-4)**. However, after a certain optimum level of concentration has reached, there is no appreciable increase in the yield of **3k (entry 5)**. So, for all subsequent reactions, we used 3.0-3.5 equiv of the acrylate to get the best results.
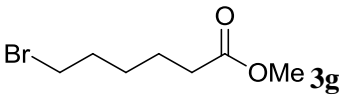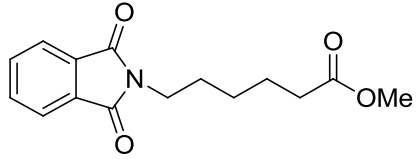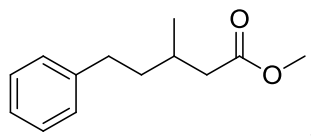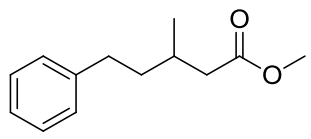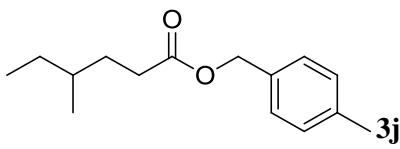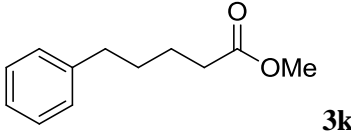
Table 2.2 Results of varying the quantity of methyl acrylate **(2a)** against 1.0 mmol of alkyl bromide **(1a)**.[a]

No.	Acrylate	Yield[b]
1	0.8	45
2	1.2	58
3	2.0	68
4	3.0	85
5	4.0	78

[a]Unless stated otherwise, all reactions were carried out with Ni-catalyst (0.10 mmol), Zn (2.50 mmol), (2-Bromoethyl)benzene **1a** (1.0 mmol), methyl acrylate **2a** (given amount), H_2O (1.0 mmol) and acetonitrile solvent (3.0 ml) at 80 $^\circ$C for 12 h under 1 atm N_2. [b]Yields were measured by ^1H NMR, using mesitylene as an internal standard.

2.2.2 Synthesis of saturated esters

A range of sp^3 alkyl bromides and iodides were treated with α, β- unsaturated esters in the presence of nickel catalyst to beget the saturated esters as shown in **Table 2.3**. Clearly, the strategy sustains a wide variety of esters including n-butyl acrylate, *tert*-butyl acrylate, and even substituted acrylates. The yields were reasonably good and one of the reasons for lower isolated yields was the inability of the products to appear clearly under the hand-held UV-lamp leading to loss of material during column chromatography. When 2'-bromoethylbenzene was treated with benzyl acrylate in the presence of [Ni(PPh$_3$)$_2$Cl$_2$] catalyst, acetonitrile solvent, and water as additive, at 80 °C, under inert conditions, the benzylic ester **(3a)** was obtained in 79% isolated yield. Similarly, the *tert*-butyl ester **(3b)** and the simple methyl ester **(3c)** derivatives were prepared in good yields by identical catalytic methods. Then, we tried the long chain decyl bromide to obtain the methyl tridecanoate **(3d)**, followed by the benzyl substituted long chain ester **(3e)** in modest yields. Likewise, the butyl 4,4-dimethylpentanoate **(3f)** and the bromo ester **(3g)** were obtained in reasonable yields. The heterocyclic dioxoindolinyl ester **(3h)** was also obtained albeit in moderate yield. Our methodology worked well even for the β-methyl substituted acrylate **(3i)**. The isobutyl halide too gave the desired ester by reacting with the tolyl acrylate **(3j)**. Finally, **3k** was obtained in good yield by treating 2'-bromoethylbenzene with methyl acrylate.

Table 2.3: Results of nickel-catalyzed reductive coupling of alkyl halides **(1)** with α, β-unsaturated esters **(2).**[a]

1a-i   **2a-e**   **3a-n**

1a: R = PhCH$_2$CH$_2$-,   X = Br
1b: R = PhCH$_2$CH$_2$CH$_2$-, X = Br
1c: R = CH$_3$(CH$_2$)$_9$-,   X = Br
1d: R = t-Butyl-,   X = Br
1e: R = BrCH$_2$CH$_2$CH$_2$-,   X = Br

2a: R^1 = Me, R^2 = R^3 = H
2b: R^1 = CH$_2$Ph, R^2 = R^3 = H
2c: R^1 = t-Butyl, R^2 = R^3 = H
2d: R^1 = n-Butyl, R^2 = R^3 = H
2e: R^1 = p-MeC$_6$H$_5$-, R^2 = R^3 = H
2f: R^1 = Me, R^2 = H, R^3 = Me

1f: R = N(CH$_2$)$_3$-, X = Br

1g: R = PhCH$_2$CH$_2$-,   X = I
1h: R = isobutyl-,   X = I

Entry	R-X (1)	Alkene (2)	Product (3)	Yield(%)[b]
1	1a 1g	2b	**3a**	79 85
2	1a 1g	2c	**3b**	75 74
3	1b	2a	**3c**	70
4	1c	2a	**3d**	72
5	1c	2b	**3e**	61
6	1d	2d	**3f**	77

7	**1e**	**2a**		66

Br~~~~~OMe **3g**

8	**1f**	**2a**		65

3h

	1g			80
9		**2f**		
	1a			78

3i

10	**1h**	**2e**		81

3j

11	**1a**	**2a**		82

3k

[a]Unless stated otherwise, all reactions were carried out with Ni-catalyst (0.10 mmol), Zn (2.50 mmol), Alkyl halide (**1**) (1.0 mmol), acrylate (**2**) (3.0 mmol), H_2O (1.0 mmol), CH_3CN (3.0 ml) at 80 $^\circ$C for 12 h under 1 atm N_2. [b]Isolated yields.

2.2.3 Mechanism

Based on the above results and known organometallic chemistry of nickel,[12] a plausible mechanism is proposed as depicted in **Scheme 2.2**. The catalytic reaction is likely initiated by the reduction of $NiCl_2(PPh_3)_2$ to Ni(0) in the presence of zinc powder. Then, oxidative- addition of alkyl bromide to Ni(0) occurs such that alkyl nickel(II) intermediate **(M1)** is generated. The coordination of double bond of the enone to the nickel center then takes place, forming the intermediate **M2**. Insertion of the coordinated double bond of acrylate to Ni-alkyl bond then occurs, giving rise to the saturated nickel intermediate **(M3)**. Then, either (a) transmetalation of the latter with the zinc bromide generated in the reaction forms zinc intermediate along with the regeneration of Ni(II), which is again reduced to Ni(0) active catalyst in presence of zinc powder, or (b) direct protonation of nickel intermediate leads to the formation of the final reductive coupling product **3**. In either case, protonation is supposedly the last step before the final formation of the product takes place. The protonation step was particularly crucial, as the addition of 1 equiv of water appeared to enhance the yield in all the cases.
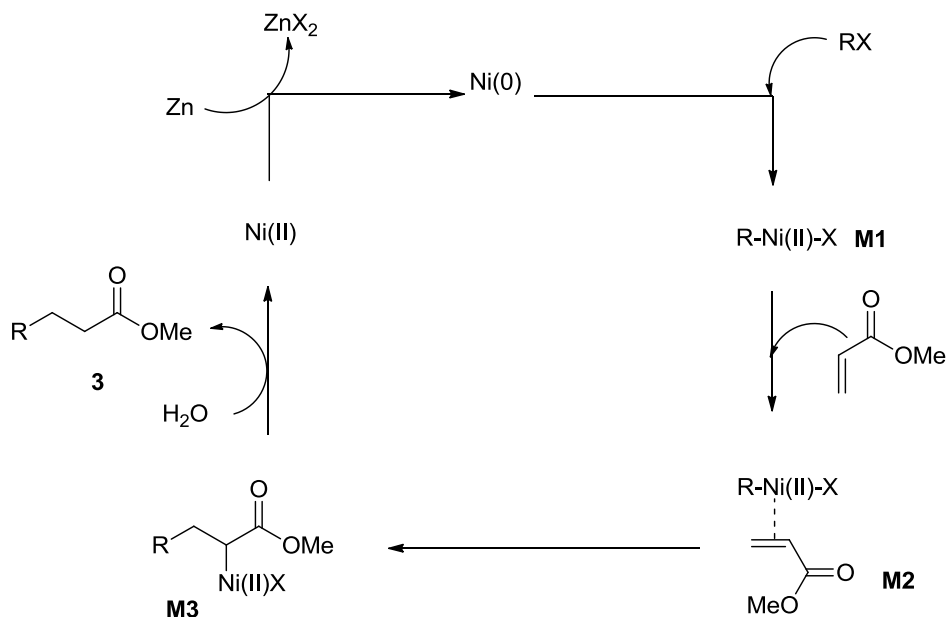
Scheme 2.2 Proposed mechanism of the reductive coupling of alkyl halides with electron-withdrawing alkenes in the presence of nickel catalyst.

The support for the final protonation step was provided by the deuterium labeling experiment we performed (**Figure 2.1**). The reaction of **1a** with **2a** in presence of the usual nickel catalyst and D_2O (1.0 mmol) afforded **3k**' with 70% deuterium at the α-carbon to the ester based on ^1H NMR. Thus, the relatively high percentage of deuterium in the product reinforces our proposed mechanism.
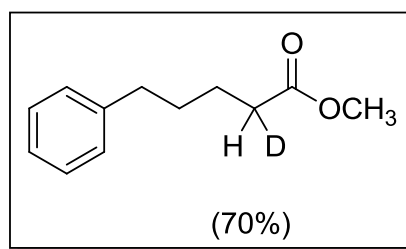
Figure 2.1 The formation of the deuterated product **3k**'.

2.2.4 Extension of the present reductive coupling to oxabicyclic alkene

To diversify and to enhance the utility of this reductive Heck reaction we planned to use oxabenzonorbornadienes as the alkene coupling partner. One of the reasons for doing so was that having already tested the veracity of our protocol with acrylates, which were electron-withdrawing alkenes, we wanted to try out another alkenic system, which was not conventionally electron-withdrawing. Oxabenzonorbornadienes and their aza-counterparts are long established as excellent substrates for coupling, coupling followed by ring opening, and various cyclization reactions.[13a-b] Although many ring-

opening reactions of oxabicyclic alkenes are known, unfortunately none of them describe the use of saturated (sp^3) alkyl halides to accomplish the desired ring opening. The first such ring-opening report appeared in 1993, involving the ring opening of bicyclic alkenes with arylic and vinylic halides to form mainly fully aromatic ring-opening products.[14a-b] Later, another report[15] appeared from the same lab wherein nickel catalyst was used to bring about the desired ring opening. In an effort to extend the reductive coupling strategy developed by us (described above), we wanted to explore the possibility of employing saturated alkyl halides to bring about the ring opening of oxabicyclic alkenes. We, however, were more interested in using those substrates all of which contained β-hydrogens in their framework. Therefore, amplifying the scope of the reaction to substrates possessing β-hydrogen posed a challenge worth taking up. The results of the reaction between oxabenzonorbornadiene and saturated alkyl halides under nickel-catalyzed conditions have been discussed herein. When oxabenzonorbornadiene (**4a**) was treated with 2'-iodoethylbenzene (**1a'**) in presence of NiBr$_2$(dppe) and Zn powder in acetonitrile solvent, the reaction seemed somewhat complicated as the proton NMR of the crude product showed more than expected peaks. After separation, the desired product **5a** was obtained in 25% yield along with 1, 2-dihydronaphthol (**6**) in 50% and 1-naphthol (**7**) in 10% yields, respectively (**Figure 2.2**).
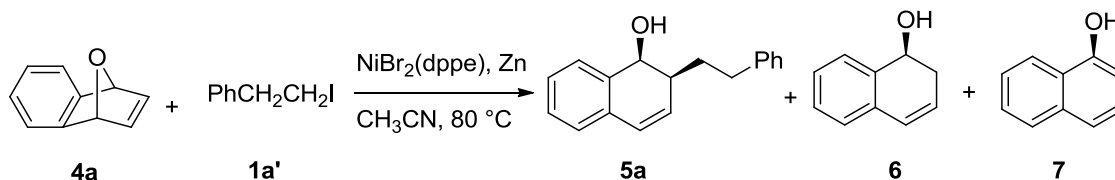
Figure 2.2 The usual products formed upon alkylative ring-opening reaction.

Such type of sometimes undesirable ring-opening products, i.e., dihydronaphthol (**6**) and naphthol (**7**) has also been reported during similar reactions as discussed earlier. Undaunted by such low yield, we set out to examine conducive reaction conditions so as to minimize the formation of naphthol type side products. To get a better idea of the conditions for this ring-opening reaction, the role of extra triphenylphosphine ligand was investigated by varying the quantity of extra PPh$_3$ added during the reaction and the results have been summarized briefly in **Table 2.4**. After experimenting with several reaction conditions, we found that the use of NiCl$_2$(PPh$_3$)$_2$ (0.1 mmol), extra PPh$_3$ (0.1 mmol), zinc powder (2.5 mmol) in THF solvent at 80°C afforded the desired product **5a** in 65% isolated yield. Thus, the amount of extra PPh$_3$ added was critical for the reaction as the addition of other phosphine ligands such as dppe or dppb (**not shown in Table 2.4**) proved rather detrimental. On the other hand, adding just 1 equiv of triphenylphosphine turned out to be ideal for the reaction. The formation of this product was somewhat intriguing due to the presence of β-hydrogen in the alkyl iodide starting material. Nevertheless, we were stimulated to test other such alkyl iodides, which possessed β- hydrogens in their framework. The results

of our study involving reaction of various oxabicyclic alkenes with saturated alkyl halides are summarized in **Table 2.5**.

Table 2.4: Results of varying the amount of phosphine ligand relative to 0.1 mmol of nickel(0) catalyst used in the reaction.
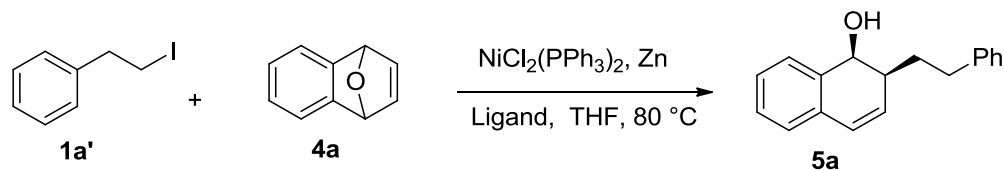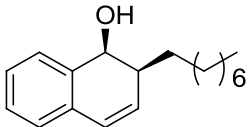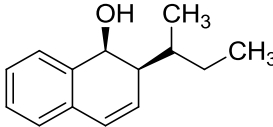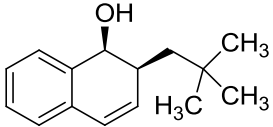
No.	Ligand	Amount[a]	Yield[b]
1	dppe	0.1	23
2	dppe	0.2	18
3	PPh$_3$	0.1	65
4	PPh$_3$	0.2	58
5	PPh$_3$	0.3	46
6	PPh$_3$	0.4	40

[a]Unless stated otherwise, all reactions were conducted as follows: oxabicyclic alkene (**4**) (2.0 mmol); alkyl halide (**1**) (1.0 mmol); NiCl$_2$(PPh$_3$)$_2$ (0.1 mmol); zinc powder (2.5 mmol), ligand (given amount); solvent (2.5 mL) at 80° C for 10h.[b]isolated yields.

Treatment of oxabenzonorbornadiene (2.0 mmol) with (2- iodoethyl)benzene (1.0 mmol) in the presence of NiCl$_2$(PPh$_3$)$_2$ (0.1 mmol), zinc metal powder (2.5 mmol) in THF solvent at 80 °C, resulted in the formation of 2(2-phenylethyl)-1,2-dihydronaphthol (**5a**) in 65% isolated yield (**entry 1, Table 2.5**).

Table 2.5: Results of ring-opening reaction of oxabenzonorbornadienes (**4**) with alkyl halides (**1**).[a]

No.	Alkyl halide(1)	Alkene(4)	Product	Yield(%)[b]
1	**1a′**	**4a**		**5a** (65)

2	**1l**	**4a**		**5b**	(68)
3	**1h** **1h′**	**4a**		**5c**	(54)
4	**1m′**	**4a**		**5d**	(50)
5	**1a**	**4a**		**5a**	15[c]
6	**1h**	**4a**		**5c**	12[c]
7	**1m**	**4a**		**5d**	10[c]

[a]Unless stated otherwise, all reactions were conducted as follows: oxabicyclic alkene (**4**) (2.0 mmol); alkyl halide (**1**) (1.0 mmol); $NiCl_2(PPh_3)_2$ (0.1 mmol); zinc powder (2.5 mmol), PPh_3 (0.1 mmol); solvent (2.5 mL) at 80° C for 10h; [b]isolated yields; [c]crude NMR yield.

When the same oxabenzonorbornadiene was treated with 1-iodooctane (**1l**), the anticipated coupling product **5b** was obtained in 68% yield (**entry 2**). The next substrate we used was a secondary alkyl iodide **1h**. We were delighted to find that when secondary isobutyl iodide (**1h′**) was employed, the expected product (**5c**) was formed (**entry 3**), although in a moderate yield of 54%. Incidentally, introduction of this secondary alkyl group (**1h**) had previously proved defiant under similar conditions vide Nakamura.[16] We were curious to know what happened when a hindered alkyl iodide was used. The relatively hindered neopentyl iodide (**1m′**) too went on to form the expected product (**5d**) in 50% of isolated yield (**entry 4**). When the corresponding saturated bromides, instead of the usual iodides were used, the yields were substantially reduced (**entries 5-7**) presumably due to the lower rates of oxidative-addition in the former (**Scheme 2.3**).

To get a better perspective on the role of catalyst, cobalt complexes were also examined but were found less effective. Among the cobalt catalysts scanned, e.g., $CoI_2(dppe)$, $CoCl_2(dppe)$, $CoCl_2(PPh_3)_2$, and $CoI_2(PPh_3)_2$, only the latter showed some promise (results not shown). Cobalt does not appear to be a good catalyst for the reaction. It would be pertinent to mention that all of the 1, 2-dihydronaphthol

products **(5)** were completely regio- and stereoselective as no other isomer was detected in the crude NMR spectra. The lower yields for these reactions were frustrating but not without reason. In all these cases, the inevitable ring opening of the oxabicyclic alkene to form **6** was the main impediment to the reaction, being formed in 30-40% yield in each case. Such ring opening, though common in reactions involving oxabenzonorbornadienes,[17a-b] was exacerbated by the rapid and unavoidable β-hydride elimination before the coupling step could effectively occur **(Scheme 2.4)**. The overall mechanism of this reaction appears the same as that reported earlier by Cheng lab.[15] However, the probable path to the formation of ring-opening product **6** is rationalized in **Scheme 2.4**.

1a: R = PhCH$_2$CH$_2$-,   X = Br
1a': R = PhCH$_2$CH$_2$-,   X = I
1h: R = CH$_3$(CH$_2$CH$_3$)CH-, X = Br
1h': R = CH$_3$(CH$_2$CH$_3$)CH-, X = I
1l: R = CH$_3$(CH$_2$)$_6$CH$_2$-,   X = I
1m: R = (CH$_3$)$_3$CCH$_2$-,   X = Br
1m':R = (CH$_3$)$_3$CCH$_2$-,   X = I

4: R^1 = R^2 = R^3 = R^4 = H
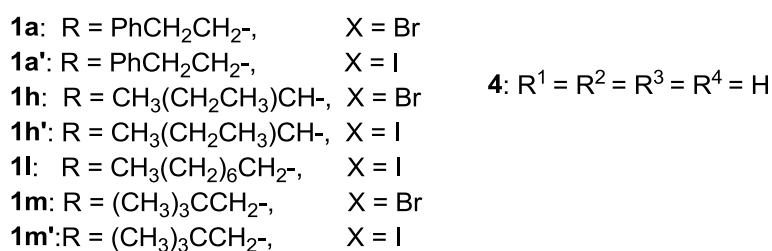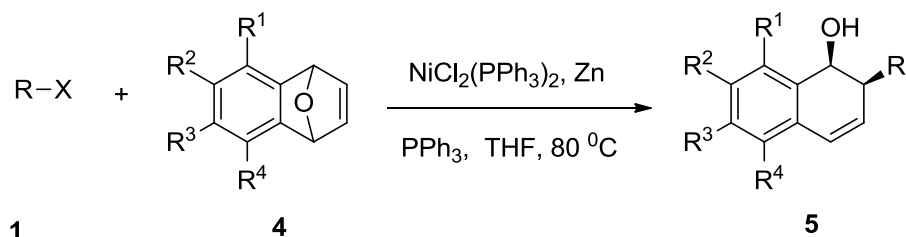
Scheme 2.3 Reaction of various oxabicyclic alkenes **(4)** with alkyl halides **(1)**.
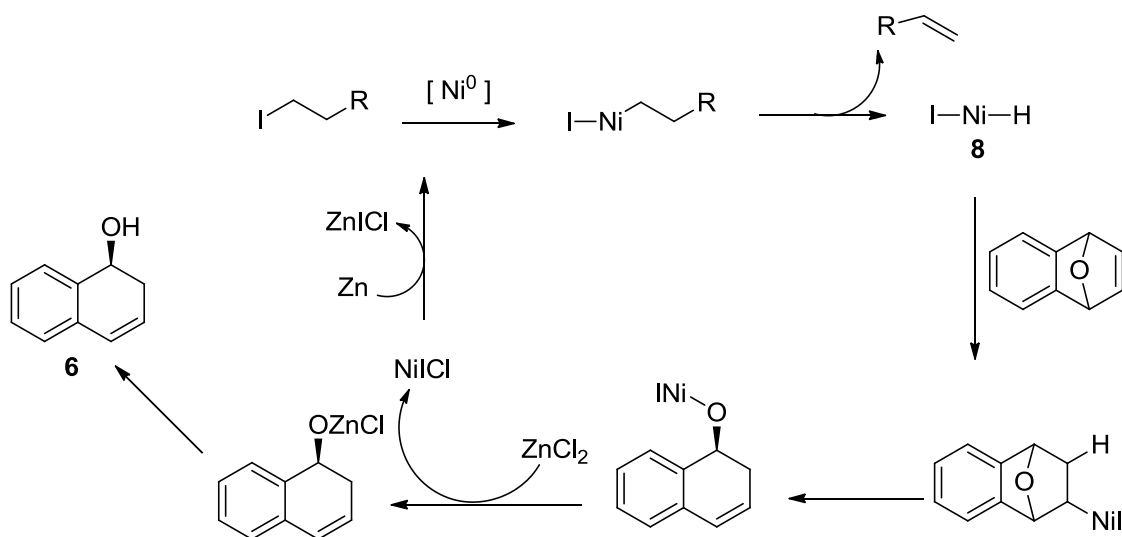
Scheme 2.4 Proposed pathway for the formation of product **6.**

The reaction starts with the usual oxidative-addition across the carbon-halogen bond. Immediate β-hydride elimination leading to the formation of nickel hydride species **8 (Scheme 2.4)**. In the next step, insertion of the oxabicyclic alkene takes place followed by β-oxy elimination and subsequent formation of the nickel alkoxide intermediate.[18] Transmetalation with zinc then forms zinc alkoxide, which eventually yields 1,2-dihydronaphthol **6**.

2.3 Conclusion

Thus, we have demonstrated a new nickel mediated reductive Heck type reaction whereby sp³ alkyl halides are reductively coupled with alkenes to give saturated esters. The strategy accommodates 1°, 2°, and 3° alkyl halides as also variously substituted acrylates. The versatility of this methodology was successfully extended to include oxabenzonorbornadiene type alkenes. The latter alkenes too coupled with the sp³ alkyl halides to give the corresponding alkylated bicyclic ring-opening products.

2.4 Experimental

2.4.1 Synthesis of benzyl acrylate (2b)

A two-neck, 250 mL capacity round bottom flask with a stir bar was taken and benzyl alcohol (solid, 1.2 g, 10.0 mmol) added to it. It was kept under vacuum for about 10 min and then flushed with nitrogen gas. Ether solvent was then added to the alcohol while stirring so as to dissolve the alcohol. Triethylamine (liquid, 1.4 mL, 10.2 mmol) was then added to the ether solution under nitrogen atmosphere. The resulting solution was allowed to stir for about half an hour. Acryloyl chloride (fuming liquid, 1.1 mL, 14.0 mmol) was added drop wise over a period of 20 min to the ether solution. Immediate pale precipitation occurred. The reaction mixture was allowed to stir for about 4 h. When TLC examination revealed the consumption of the starting alcohol, the flask was opened to air and allowed to stir. Brine solution was slowly added to the stirring mixture: the white precipitate slowly dissolved. After an ether work up, the organic layer was collected and dried over anhydrous $MgSO_4$, filtered, and concentrated. The desired benzyl acrylate **(2b)** was collected as colorless oil (yield 84%). An analogous procedure was used for the synthesis of all the acrylates.

2.4.2 Procedure for the reductive coupling of (2-bromoethyl) benzene 1a with methyl acrylate 2a

A sealed tube (20 mL) containing $NiCl_2(PPh_3)_2$ (0.1 mmol) and zinc powder (2.5 mmol) was evacuated and purged with nitrogen gas three times. Freshly distilled CH_3CN (2.5 mL), (2-bromoethyl) benzene **1a** (1.0 mmol), methyl acrylate **2a** (4.0 mmol) and H_2O (1.0 mmol) were added to the sealed tube via syringes. The reaction mixture was heated with stirring at 80 °C for 12 h and was then cooled, diluted with dichloromethane, and stirred in the air for 10 min. The mixture was filtered through a Celite and silica gel pad and washed with dichloromethane. The filtrate was concentrated and the residue was

purified on a silica gel column using hexane/ethyl acetate as eluant to afford the desired product **3a**. All the rest of the compounds of the **3** series were prepared similarly.

2.4.3 Procedure for the reductive coupling of 1a with oxabenzonorbornadiene[4]

The procedure was analogous to the one described above for the preparation of compounds of the **3** series. For ^{1}H and ^{13}C-NMR see the Appendices A-1.

Benzyl 5-phenylpentanoate (3a)

^{1}H NMR (400 MHz, CDCl$_3$): d 7.32 (m, 5H), 7.25 (m, 2H), 7.18 (m, 3H), 5.13 (s, 2H), 2.59 (t, 2H, J=6.4 Hz), 2.41 (t, 2H, J=6.4 Hz), 1.69 (m, 4H). ^{13}C NMR (100 MHz, CDCl$_3$): d 173.4, 142.1, 136.1, 128.5, 128.4, 128.3, 128.2, 128.2, 125.8, 66.1, 35.5, 34.1, 30.8, 24.6. HRMS calcd for C$_{18}$H$_{20}$O$_2$ 268.1463; found 268.1469.

tert-Butyl 5-phenylpentanoate (3b)

^{1}H NMR (400 MHz, CDCl$_3$): d 7.28 (d, 2H, J=7.2 Hz), 7.19 (t, 3H, J=7.2 Hz), 2.62 (t, 2H, J=6.4 Hz), 2.23 (t, 2H, J=6.4 Hz), 1.64 (m, 4H), 1.25 (s, 9H). ^{13}C NMR (100 MHz, CDCl$_3$): d 170.0, 142.3, 128.4, 128.3, 125.7, 80.0, 35.6, 35.4, 30.9, 28.1, 24.7. HRMS calcd for C$_{15}$H$_{22}$O$_2$ 234.1620; found 234.1621.

Methyl 6-phenylhexanoate (3c)

^{1}H NMR (400 MHz, CDCl$_3$): d 7.29 (d, 2H, J=7.2 Hz), 7.18 (t, 3H, J=7.2 Hz), 3.66 (s, 3H), 2.61 (t, 2H, J=8.0 Hz), 2.31 (t, 2H, J=8.0 Hz), 1.63 (m, 4H), 1.36 (p, 2H, J=8.0 Hz). ^{13}C NMR (100 MHz, CDCl$_3$): d 174.1, 142.4, 128.3, 128.2, 125.6, 51.4, 35.6, 33.9, 31.0, 28.7, 24.7. HRMS calcd for C$_{13}$H$_{18}$O$_2$ 206.1307; found 206.1311.

Methyl tridecanoate (3d)

^{1}H NMR (400 MHz, CDCl$_3$): d 3.65 (s, 3H), 2.28 (t, 2H, J=7.2 Hz), 1.26 (br s, 20H), 0.87 (t, 3H, J=7.2 Hz). ^{13}C NMR (100 MHz, CDCl$_3$): d 174.4, 70.9, 51.4, 34.1, 31.9, 29.6, 29.4, 29.3, 29.2, 29.1, 26.2, 24.9, 22.7, 14.1. HRMS calcd for C$_{14}$H$_{28}$O$_2$ 228.2089; found 228.2091.

Benzyl tridecanoate (3e)

^{1}H NMR (400 MHz, CDCl$_3$): d 7.33 (m, 5H), 5.12 (s, 3H), 2.35 (t, 2H, J=7.6 Hz), 1.64 (m, 4H), 1.25 (br s, 20H), 0.87 (t, 3H, J=7.2 Hz). ^{13}C NMR (100 MHz, CDCl$_3$): d 169.9, 142.5, 129.4, 128.5, 128.7, 66.1, 34.2, 31.9, 29.6, 29.5, 29.4, 29.3, 29.2, 26.5, 24.9, 24.5, 22.8, 14.2. HRMS calcd for C$_{20}$H$_{32}$O$_2$ 304.2402; found 304.2406.

n-Butyl 4,4-dimethylpentanoate (3f)

^{1}H NMR (400 MHz, CDCl$_3$): d 4.04 (t, 2H, J=6.5), 2.25 (t, 2H, J=6.2 Hz), 1.45-1.51 (m, 4H), 1.31-1.38 (m, 2H), 0.91 (t, 3H, J=7.2 Hz), 0.86 (s, 9H). ^{13}C NMR (100 MHz, CDCl$_3$): d 174.6, 64.2, 38.6, 30.7, 30.1, 30.0, 28.9 (3C), 19.1, 13.7. HRMS calcd for C$_{11}$H$_{26}$O$_2$ 186.1620; found 186.1622.

Methyl 6-bromohexanoate (3g)

^{1}H NMR (400 MHz, CDCl$_3$): d 3.65 (s, 3H), 3.39 (t, 2H, J=6.8 Hz), 2.31 (t, 2H, J=7.2 Hz), 1.84 (p, 2H, J=14.4 Hz), 1.62 (p, 2H, J=14.4 Hz), 1.44 (m, 2H). ^{13}C NMR (100 MHz, CDCl$_3$): d 173.1, 51.9, 33.7, 33.6, 32.4, 27.5, 24.1. HRMS calcd for C$_7$H$_{13}$BrO$_2$ 208.0099; found 208.0102.

Methyl 6-(1,3-dioxoisoindolin-2-yl)hexanoate (3h)

^{1}H NMR (400 MHz, CDCl$_3$): d 7.79 (m, 2H), 7.67 (m, 2H), 3.65 (t, 2H, J=7.6 Hz), 3.61 (s, 3H), 2.27 (t, 2H, J=7.2 Hz), 1.63 (m, 4H), 1.34 (m, 2H). ^{13}C NMR (100 MHz, CDCl$_3$): d 174.2, 168.6, 134.1, 132.3, 123.4, 51.7, 38.0, 34.0, 28.5, 26.5, 24.7. HRMS calcd for C$_{15}$H$_{17}$NO$_4$ 275.1158; found 275.1158.

Methyl 3-methyl-5-phenylpentanoate (3i)

^{1}H NMR (400 MHz, CDCl$_3$): d 7.23 (m, 2H), 7.15 (m, 3H), 3.67 (s, 1H), 2.59 (m, 2H), 2.34 (m, 1H), 2.17 (m, 1H), 1.58 (m, 2H), 1.02 (d, 3H, J=6.4 Hz). ^{13}C NMR (100 MHz, CDCl$_3$): d 173.5, 142.4, 132.0, 128.6, 125.7, 51.4, 41.5, 38.5, 33.3, 30.1, 19.6. HRMS calcd for C$_{13}$H$_{18}$O$_2$ 206.1307; found 206.1310.

4-Methylbenzyl 4-methylhexanoate (3j)

^{1}H NMR (400 MHz, CDCl$_3$): d 7.26 (d, 2H, J=8.0 Hz), 7.15 (d, 2H, J=8.0 Hz), 5.05 (s, 3H), 2.36 (s, 3H), 2.34 (m, 2H), 1.61 (m, 1H), 1.42 (m, 1H), 1.32 (m, 2H), 1.14 (m, 1H), 0.82 (m, 6H). ^{13}C NMR (100 MHz, CDCl$_3$): d 173.1, 138.0, 133.1, 129.2, 128.3, 128.1, 128.0, 66.3, 34.0, 32.1, 31.5, 29.1, 21.2, 18.8, 11.2. HRMS calcd for C$_{15}$H$_{22}$O$_2$ 234.1620; found 234.1622.

1,2-Dihydro-2-phenethylnaphthalen-1-ol (5a)

^{1}H NMR (400 MHz, CDCl$_3$): d 7.25 (m, 6H), 7.19 (m, 3H), 6.78 (d, 1H, J=7.0 Hz), 5.85 (m, 1H), 5.22 (s, 1H), 4.62 (d, 1H, J=4.0 Hz), 2.82 (m, 2H), 2.49 (m, 1H), 2.15 (m, 1H), 1.87 (m, 1H). HRMS calcd for C$_{18}$H$_8$O 250.1358; found 250.1360.

1,2-Dihydro-2-octylnaphthalen-1-ol (5b)

^{1}H NMR (400 MHz, CDCl$_3$): d 7.26 (d, 1H, J=8.0 Hz), 7.24 (m, 2H), 7.21 (d, 1H, J=8.0 Hz), 6.51 (m, 1H), 5.81 (m, 1H), 4.56 (d, 1H, J=4.4 Hz), 2.45 (m, 1H), 1.77 (m, 1H), 1.25 (br s, 12H), 0.88 (t, 3H, J=7.2 Hz). HRMS calcd for C$_{18}$H$_{26}$O 258.1984; found 258.1985.

2-sec-Butyl-1,2-dihydro-2-naphthalen-1-ol (5c)

^{1}H NMR (400 MHz, CDCl$_3$): d 7.28 (m, 3H), 7.23 (t, 1H, J=6.4 Hz), 6.61 (m, 1H), 5.96 (m, 1H), 4.64 (d, 1H, J=4.0 Hz), 2.19 (m, 1H), 1.79 (m, 1H), 1.32 (m, 2H), 1.18 (m, 3H), 1.01 (m, 3H). HRMS calcd for C$_{14}$H$_{18}$O 202.1358; found 202.1364.

1, 2-Dihydro-2-neopentylnaphthalen-1-ol (5d)

^{1}H NMR (400 MHz, CDCl$_3$): d 7.26 (m, 3H), 7.09 (d, 1H, J=7.2 Hz), 6.48 (m, 1H), 5.89 (m, 1H), 4.50 (t, 1H, J=6.0 Hz), 2.56 (m, 1H), 1.84 (m, 1H), 1.46 (m, 1H), 0.93 (s, 9H). HRMS calcd for C$_{15}$H$_{20}$O 216.1514; found 216.1515.

2.5 References

[1] (a) Mkhalid, I. A. I.; Barnard, J. H.; Marder, T. B.; Murphy, J. M.; Hartwig, J. F. *Chem. Rev.* **2010,** *110*, 890; (b) Shilov, A. E.; Shul'pin, G. B. *Chem. Rev.* **1997,** *97*, 2879.

[2] (a) Beletskaya, I. P.; Cheprakov, A. V. *Chem. Rev.* **2000,** *100*, 3009; (b) Ruan, J.; Xiao, J. *Acc. Chem. Res.* **2011,** *44*, 614; (c) Liu, C.; Tang, S.; Liu, D.; Yuan, J.; Zheng, L.; Meng, L.; Lei, A. *Angew. Chem. Int. Ed.* **2012,** *51*, 3638; (d) Liu, C.; Liu, D.; Zhang, W.; Zhou, L.; Lei, A. *Org. Lett.* **2013,** *15*, 6166; (e) Tang, S.; Liuz, C.; Lei, A. *Chem. Commun.* **2013,** *49*, 2442; (f) Liu, D.; Tang, S.; Yi, H.; Liu, C.; Qi, X.; Lan, Y.; Lei, A. *Chem. Euro. J.* **2014,** *20*, 15605; (g) Liu, D.; Liu, C.; Lei, A. *Pure Appl. Chem.* **2014,** *86*, 321.

[3] (a) Heck, R. F. *Org. React.* **1982,** *27*, 345; (b) Sumino, S.; Fusano, A.; Fukuyama, T.; Ryu, I. *Acc. Chem. Res.* **2014,** *47*, 1563.

[4] (a) Jana, R.; Pathak, T. P.; Sigman, M. S. *Chem. Rev.* **2011,** *111*, 1417; (b) Cardenas, D. J. *Angew. Chem. Int. Ed.* **2003,** *42*, 384; (c) Cardenas, D. J. *Angew. Chem. Int. Ed.* **1999,** *38*, 3018; (d) Luh, T. Y.; Leung, M.; Wong, K. T. *Chem. Rev.* **2000,** *100*, 3187; (e) Liu, C.; Zhang, H.; Shi, W.; Lei, A. *Chem. Rev.* **2011,** *111*, 1780; (f) Shi, W.; Liu, C.; Lei, A. *Chem. Soc. Rev.* **2011,** *40*, 2761; (g) Zhao, Y.; Wang, H.; Hou, X.; Hu, Y.; Lei, A.; Zhang, H.; Zhu, L. *J. Am. Chem. Soc.* **2006,** *128*, 15048; (h) Chen, M.; Zheng, X.; Li, W.; He, J.; Lei, A. *J. Am. Chem. Soc.* **2010,** *132*, 4101; (i) Liu, C.; Wang, J.; Meng, L.; Deng, Y.; Li, Y.; Lei, A. *Angew. Chem. Int. Ed.* **2011,** *50*, 5144; (j) He, C.; Guo, S.; Ke, J.; Hao, J.; Xu, H.; Chen, H.; Lei, A. *J. Am. Chem. Soc.* **2012,** *134*, 5766; (k) Zhang, H.; Shi, R.; Gan, P.; Liu, C.; Ding, A.; Wang, Q.; Lei, A. *Angew. Chem. Int. Ed.* **2012,** *51*, 5204.

[5] (a) Blanchard, P.; Da-Silva, A. D.; Fourrey, J. L.; Machado, A. S.; Malka, R. G. *Tetrahedron Lett.* **1992,** *33*, 8069; (b) Blanchard, P.; Kortbi, M. S.; Fourrey, J. L.; Malka, R. G. *Tetrahedron Lett* **1992,** *33*, 3319; (c) Maria, E. J.; Da-Silva, A. D.; Fourrey, J. L.; Machado, A.; Malka, R. G. *Tetrahedron Lett.* **1994,** *35*, 3301; (d) Manchand, P. S.; Yiannikouros, G. P.; Belica, P. S.; Madan, P. *J. Org. Chem.* **1995,** *60*, 6574; (e) Sestelo, J. P.; Mascarenas, J. P.; Castedo, L.; Mourino, A. *J. Org. Chem.* **1993,** *58*, 118.

[6] (a) Chang, H. T.; Jayanth, T. T.; Wang, C. C.; Cheng, C. H. *J. Am. Chem. Soc.* **2007,** *129*, 12032; (b) Sustmann, R.; Hopp, P.; Holl, P. *Tetrahedron Lett.* **1989,** *30*, 689; (c) Sim, T. B.; Choi, J.; Yoon, N. M. *Tetrahedron Lett.* **1996,** *37*, 3137; (d) Lebedev, S. A.; Lopatina, V. S.; Petrov, E. S.; Beletskaya, I. P. *J. Org. Chem.* **1988,** *344*, 253; (e) Gong, H.; Andrews, R. S.; Zuccarello, J. L.; Lee, S. J.; Gagne, M. R. *Org. Lett.* **2009,** *11*, 879; (f) Yin, H.; Wang, S.; Qian, Q.; Gong, H. *Org. Lett.* **2012,** *14*, 3352.

[7] Amatore, M.; Gosmini, C.; Perichon, J. *J. Org. Chem.* **2006,** *71*, 6130.

[8] Shukla, P.; Hsu, Y. C.; Cheng, C. H. *J. Org. Chem.* **2006,** *71*, 655.

[9] (a) Molinaro, C.; Montgomery, T. F. *J. Am. Chem. Soc.* **2003,** *125*, 8076; (b) Moslin, R. M.; Jamison, T. F. *Org. Lett.* **2006,** 8, 455; (c) Yang, Y.; Zhu, S. F.; Duan, H. F.; Zhou, C. Y.; Wang, L. X.; Zhou, X. L. *J. Am. Chem. Soc.* **2007,** *129*, 2248; (d) Li, W.; Chen, N.; Montgomery, J. *Angew. Chem. Int. Ed.* **2010,** *49*, 8712; (e) Zhou, C. Y.; Zhu, S. F.; Wang, L. X.; Zhou, X. L. *J. Am. Chem. Soc.* **2010,** *132*, 10955; (f) Zhao, C.; You, H.; Lin, K.; Gong, H. *Chem. Commun.* **2012,** *48*, 7034.

[10] Rosen, B. M.; Quasdorf, K.W.; Wilson, D. A.; Zhang, N. R.; Ana-Maria, G.; Neil, K. P. V. *Chem. Rev.* **2010,** *111*, 1346.

[11] (a) O'Neil, G. W.; Carmichael, C. A.; Goepfert, T. J.; Fulton, J. M.; Knothe, G.; Pui, L. L. C.; Lindell, S. R.; Mohammady, N. G. E.; Van Mooy, B. A. S.; Reddy, C. M. *Energy Fuels* **2012,** *26*, 2434; (b) Rogge, T. M.; Stevens, C. V.; Colpaert, A.; Levecke, B.; Booten, K. *Biomacromolecules* **2007,** *8*, 485.

[12] Huang, Y. C.; Majumdar, K. K. *J. Org. Chem.* **2002,** *67*, 1682.

[13] (a) Lautens, M.; Fagnou, K.; Hiebert, S. *Acc. Chem. Res.* **2003,** *36*, 48; (b) Rayabarapu, D. K.; Cheng, C. H. *Acc. Chem. Res.* **2007,** *40*, 971.

[14] (a) Duan, J. P.; Cheng, C. H. *Tetrahedron Lett.* **1993,** *34*, 4019; (b) Duan, J. P.; Cheng, C. H. *Organometallics* **1995,** *14*, 1608.

[15] Feng, C. C.; Nandi, M.; Sambaiah, T.; Cheng, C. H. *J. Org. Chem.* **1999,** *64*, 3538.

[16] Nakamura, M.; Matsuo, K.; Ito, S.; Nakamura, E. *J. Am. Chem. Soc.* **2004,** *126*, 3686.

[17] (a) Mo, D. L.; Chen, B.; Ding, C. H.; Dai, L. X.; Ge, G. C.; Hou, X. L. *Organometallics* **2013,** *32*, 4465; (b) Tsui, G. C.; Ninnemann, N. M.; Hosotani, A.; Lautens, M. *Org. Lett.* **2013,** *15*, 1064.

[18] Toda, S.; Miyamoto, M.; Kinoshita, H.; Inomata, K. *Bull. Chem. Soc. Jpn.* **1991,** *64*, 3600.

Chapter III

Introduction

Synthesis of Non-Spiro/Spiro Pyranopyrazole Heterocyclic Scaffolds via Different Synthetic Methodologies and their Various Biological and Pharmacological Activities

From the perspective of organic chemistry, synthesis of bioactive heterocyclic scaffolds with high molecular complexity, in minimum number of synthetic steps is an unending demand of chemistry Tandem reactions are one of the best alternative which fulfils the above discussed requirements.[1-2] The **Figure 3.1** shows the simple representation of the tandem process where product **D** could be synthesized in a single step as compared to conventional method where **D** could be synthesized via intermediate **C** also.
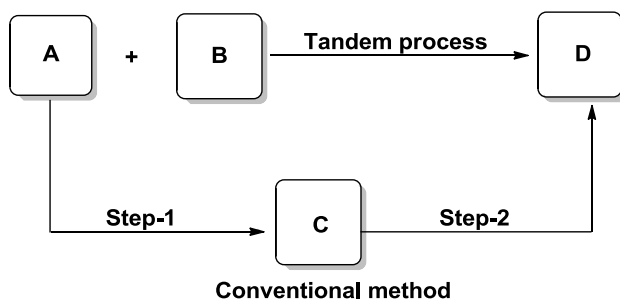
Figure 3.1 Shows the representation of Tandem process.

The major advantage of tandem reactions are that they

- build a large number of complexity in a target molecule in a single step
- evade separation of reaction intermediates and reduces the labor and time required for the given target molecule
- minimize the waste generation

This chapter describes the synthesis of pyranopyrazoles by various methodologies and their application in anticancer, antibacterial, antifungal, DNA binding, anti-oxidant and pharmacology study. Although many reports are available on the synthesis of these compounds, there is still paucity of studies pertaining to their studies on Hep3b liver toxicity cell line, calf thymus DNA binding, and antioxidant study on Wistar rats. So, our strategy was to plan, design, and synthesis of these molecules and then tests their biological activity in the hope of getting a drug lead.

Pyrazolopyridines were recognized as analgesic and anti-inflammatory agents.[3] Ueda *et al*.[4] thought that the introduction of a pyran ring instead of the pyridine ring might give pharmacologically better active compounds **(Figure 3.2)**. So, pyrano[2,3-*c*]pyrazoles were synthesized and tested for analgesic activity in mice. The analgesic activities **1, 2, 3** and **4** were examined in comparison with aminopyrine by oral administration to mice. The pharmacological result of compounds **1, 2** were almost the equal to that of aminopyrine (70% inhibition) and **3, 4** showed 50% inhibition.
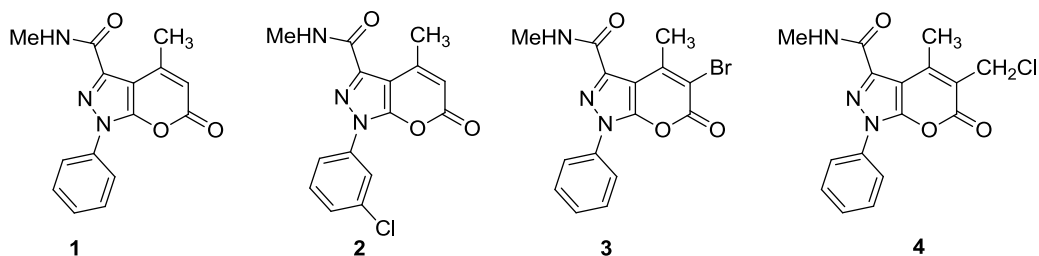
Figure 3.2 Shows the structures of pyrano[2,3-*c*]pyrazoles as analgesic agent.

Abidi *et al.*[5] synthesized a series of 6-amino-4-aryl-3-methyl-2,4-dihydropyrano[2,3-*c*]pyrazole-carbonitrile derivatives **(Figure 3.3)** and investigated the *in-vitro* cytotoxic activity of the synthesized compounds against cancer cell lines (SW48, A549, KB, HepG2) in comparison with anticancer drug doxorubicin, using MTT colorimetric assay. The synthesized compounds showed good and reasonable cytotoxicity compared with doxorubicin in some studied cell lines and the compounds **5, 6, 7** in KB cell line, **8** in A549 cell line, **8** in SW48 cell line showed the best results in close to the control drug.
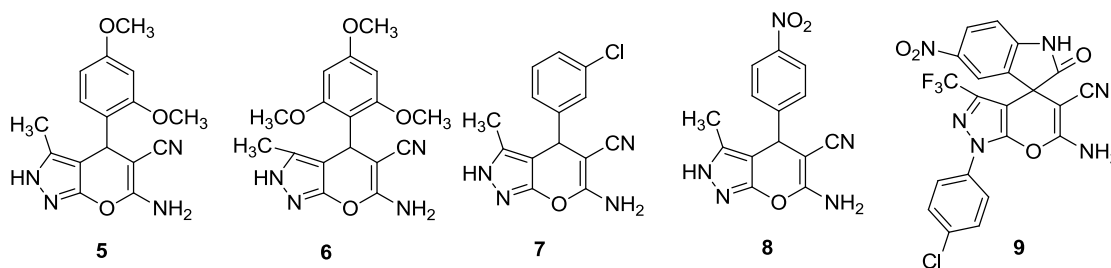
Figure 3.3 Shows the structures of 6-amino-4-aryl-3-methyl-2,4-dihydropyrano[2,3-*c*]pyrazole-carbonitrile as anticancer agent.

Later on 6-amino-5-cyno-3-trifluoromethylpyranopyrazole-4-spiro-oxindole derivatives were synthesized by Erugu *et al.*[6] and evaluated for *in-vitro* cytotoxicity against cell lines B16F10 (mouse mealanocarcinoma) and U937 (human histolytic lymphoma) by using MTT assay.[7] The potency of the compound **9** was best when nitro group was present in spiro- oxindole moiety and a chlorine atom in pyrazole moiety.

Huang *et al.*[8] reported a series of 1- and 2-arylmethyl-3,4-dimethylpyrano[2,3-*c*]pyrazol-6-one derivatives **(Figure 3.4)** and examined for their antiplatelet activities. Some of these compounds showed significant inhibitory activities. Among them, 1-phenylmethyl-3,4-dimethylpyrano[2,3-*c*]pyrazol-6(1*H*)-one **(10)** and 2-(2'-methoxyphenyl)methyl-3,4-dimethylpyrano[2,3-*c*]pyrazol-6(2*H*)-one **(11)** were the most effective. These inhibitors acted in a concentration-dependent manner. Later on Foloppe *et al.*[9] identified the compound 4-(6-amino-3-methyl-2,4-dihydropyrano[2,3-*c*]pyrazol-4-yl)benzene-1,2-diol **(12)** as a potential inhibitor of human Chk1 kinase.
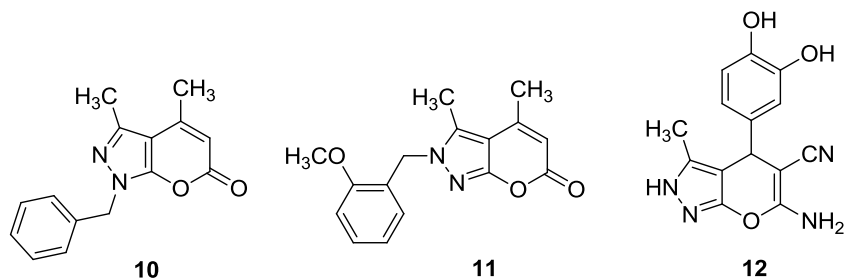
Figure 3.4 Shows the structures of arylmethyl-3,4-dimethylpyrano[2,3-*c*]pyrazol-6-one.

Ramtekkar *et al.*[10] reported the six hits out of 2499 pyranopyrazole derivatives through virtual screening against the ATP-binding site of Chk1 kinase using Glide 5.0 program.

Yu and their coworkers[11] demonstrated the *in-vivo* pharmacological effects **(Figure 3.5)** of 2-(4′methoxyphenylmethyl)-3,4-dimethylpyrano[2,3-*c*]pyrazol-6(2*H*)-one **(13)** and 2-(2′-thienylmethyl)-3,4-dimethylpyrano[2,3-*c*]pyrazol-6(2*H*)-one **(14)** on isolated thoracic aorta of rat.

Colotta *et al.*[12] synthesized a series of 1,4 dihydro-1-phenyl-3-methyl-6-(3-aminophenyl)-pyrano[2,3-*c*]pyrazol-4-one **15** and evaluated for bovine brain adenosine A_1 and A_{2A} receptor binding affinity, K_i value of 84 nM.
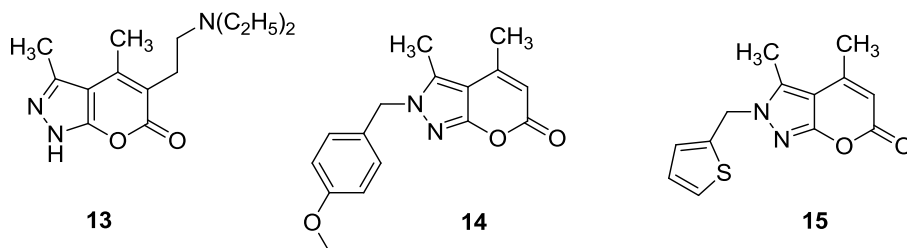
Figure 3.5 Shows the structure of pyrano[2,3-*c*]pyrazol-4-one as adenosine A_1 and A_{2A} receptor.

Mandour *et al.*[13] synthesized and comprehensively studied analgesic, anticonvulsant, and anti inflammatory activity of pyranopyrazole **(Figure 3.6)** scaffolds **(16a-g, 17a-g and 18a-g)**. Majority of the newly synthesized compounds possess potential antimicrobial activity against *E. coli and P. aeruginosa.*
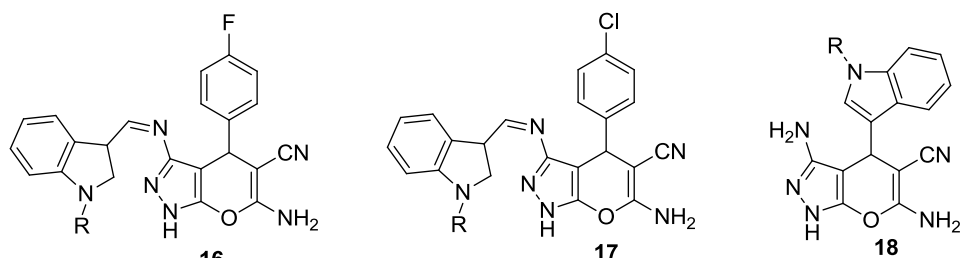
R = a: H, b: CH_2CH_3, c: COC_6H_5, d: COC_6H_4Cl-p, e: COC_6H_4Cl-o, f: $SO_2C_6H_5$, g: $SO_2C_6H_4Br$-p

Figure 3.6 Shows the pyranopyrazole scaffolds as analgesic, anticonvulsant, and anti inflammatory agent.

Kassem *et al.*[14] reported new fused pyranopyrazoles **(Figure 3.7)**, **19a-e** incorporated to 8-hydroxyquinoline through a sulfonyl bridge at position 5 and evaluated for antimicrobial activity by disc diffusion method, at different doses against a variety of pathogenic microorganisms, *E. coli, P. aeruginosa*, *S. aureus, B. cereus*, and one strain of fungi C. *albicans*.
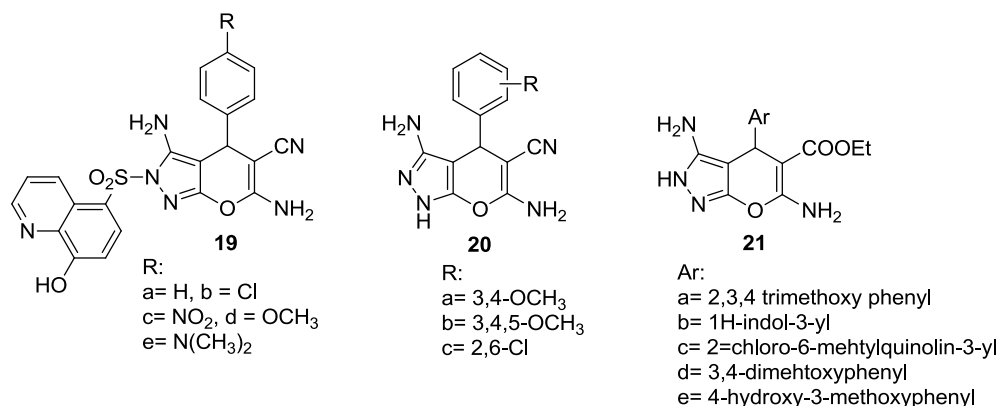
Figure 3.7 Shows the pyranopyrazoles scaffold as antibacterial and antimicrobial activity.

Katariya *et al.*[15] synthesized a series of pyrano[2,3-*c*]pyrazoles **(Figure 3.7)** compounds **20a-c** and tested their antifungal and antibacterial activity (MIC) in vitro by broth dilution method with two fungal strains A. *niger* and C. *albicans* and two bacterial strains *S. aurues* and *B. subtillitis*.

Amin *et al.*[16] synthesized a series of novel 6-amino-4-(aryl/heteroaryl)phenyl-3-methyl-2,4-dihydropyrano[2,3-*c*]pyrazole-5-carboxylate **(Figure 3.7)** derivatives (**21a-e**) and screened for their antibacterial and antifungal activity against *E. coli* and *A. niger.* and *S. aureus.*

Thus, as is clear from the foregoing discussion, many reports are available pertaining to the pyranopyrazoles as active antibacterial or ant-fungal agents, but only one report is available on their anticancer activity. This finding encouraged us to investigate further into their faster synthesis, and delve into their antioxidant, DNA binding, etc. activity. The sub-parts of this chapter give the details of the various eco-friendly synthetic methods of synthesis and the *in-vitro* and *in-vivo* biological activity testing of the synthesized pyranopyrazoles.

Chapter III

Part A

Fast Microwave Assisted Synthesis of Pyranopyrazole Derivatives as New Anticancer Agents

3.1 Introduction

Today, cancer is responsible for one in every eight deaths worldwide–more than HIV/AIDS, tuberculosis, and malaria combined[17] leading to increased research on small organic molecules that target cancer cells. 4*H*-Pyrans have been reported as the basic structural motifs for an array of useful compounds including natural products.[18] Similarly, pyrazoles have also been reported as useful starting materials for various bioactive small organic molecules.[19] Likewise, many reports are available concerning the applications of pyranopyrazoles as physiologically active compounds.[20-23] Pyrazole fused pyrans or pyranopyrazoles have been shown to possess various biological and pharmacological activities, such as antimicrobial[24-25], antiviral[26-27], sex pheromone[28], analgesic[29], and central nervous system active agents.[30] Some of these compounds are widely employed as cosmetics and pigments and as potential biodegradable agrochemicals[31], therefore, the planning, synthesis, and cytotoxic study of such compounds has attracted strong interest. To the best of our knowledge, there is only one report of a single pyrano[2,3-*c*] pyrazole derived pyranopyrazole compound as CHK-1 inhibitor antitumor agent.[32] Moreover, this report pertains to an *in-silico* evaluation of the said compound without any *in-vitro* experimental data. Keeping in mind the aforementioned biological applications, we embarked on a project to synthesize functionalized pyranopyrazoles as potential antitumor agents and the following paper describes the highlights of our preliminary synthetic and cytotoxicity results. The pyranopyrazoles were prepared and then evaluated for *in-vitro* anticancer activity against Hep3B cells.

Regarding the chemical synthesis of the pyranopyrazole pharmacophore, several reports are available in the literature. The first such reported synthesis described the reaction between 3-methyl-1 phenylpyrazolin-5-one and malonodinitrile.[33] A three-component reaction between N-methylpiperidone, pyrazoline-5-one, and malonodinitrile was reported by Shestopalov and co-workers[34-35] although the reaction required either heating or the use of electrochemical methods. Later, the same group reported a new four-component synthesis of pyranopyrazole.[36] Peng and co-workers[37] outlined an interesting variation by utilizing the environmentally benign technology of combined microwave and ultrasound irradiation. Vasuki *et al.* reported a fast four-component reaction in water.[38] Schlager and coworkers disclosed a very different multistep synthesis of pyranopyrazoles starting with 1–phenylpyrazole.[39] Recently, a few papers have been reported revealing the use of catalyst[40-41], nanoparticles[42], solvent-free method[43] or traditional refluxing conditions.[44-45] None of the groups however, reported a quick and exclusive microwave assisted (MWA) synthetic route to the pyranopyrazoles.

3.2 Results and Discussion

Now a days, the increased use of microwave in organic synthesis is considerably reducing the generation of hazardous waste and reaction times thereby contributing to the greening of modern organic

synthesis.[46-48] We, therefore, decided to develop the faster and relatively environmentally gentle MWA protocol for the synthesis of four-component condensation of malononitrile (**3**), ethyl acetoacetate (**1**), hydrazine hydrate (**2**), and various aldehydes (**4a1-4a14**). When starting with the synthesis of the desired pyranopyrazole pharmacophores (**5a1-5a14**) we first experimented with the previously mentioned two-step traditional method.[39] Herein, ethyl acetoacetate was mixed with hydrazine hydrate to yield 3-methylpyrazolone in the first step followed by condensation with malononitrile and aldehyde to yield the desired pyranopyrazoles in the second step.
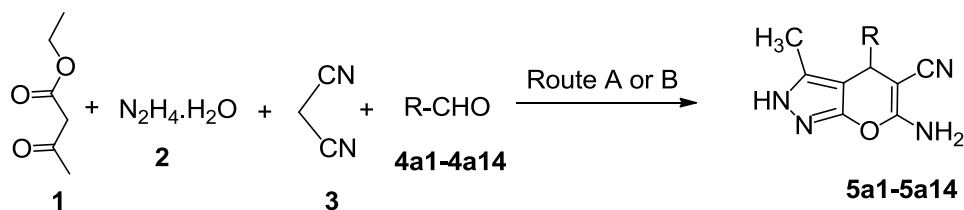
where R:

4a1= 3'-phenolic	4a8= 4'-chlorophenyl
4a2= 4'-bromophenyl	4a9= 2'-iodophenyl
4a3= 3'-bromophenyl	4a10= phenyl
4a4= 3'-nitrophenyl	4a11= *n*-butyl
4a5= 3'-thiophenyl	4a12= 4'-tolyl
4a6= 2'-pyrrolyl	4a13= 4'-pyridinyl
4a7= 3'-indolyl	4a14= 2'-fluorophenyl

Scheme 3.1 Traditional and MWA routes for the synthesis of pyranopyrazoles. Route A: Et_3N, EtOH, 1-2 h, rt, average yields 85%. Route B: MWA reaction, EtOH, Et_3N, 3-5 mins, average yields 81%.

The whole procedure took 5 to 6 hours and required two work-up stages. Therefore we decided to try out the faster one-step route where all the four components were sequentially added to give the desired compounds which took us about one to two hours reaction run times. Here again, though the reaction times were reduced it was not enough to lead to the sufficient greening of the overall synthetic technique. Hence, we finally experimented with the MWA synthetic strategy. To accomplish the MWA protocol, the aldehyde, malononitrile, and triethylamine were first mixed together in ethanol in the microwave apparatus followed by the addition of ethyl acetoacetate and hydrazine hydrate. Then the reaction mixture was placed in microwave and the reaction was completed within 3-5 minutes. The whole reaction usually took less than six minutes followed by a usual work up procedure. As shown in **Scheme 3.1**, it appeared that the overall yields were somewhat reduced for the MWA route. But then the slight loss of yields was more than compensated by the rapid reaction times. The various compounds prepared by this MWA method have been presented in **Table 3.1**.

The latter **Table 3.1** shows that our methodology works well for a variety of substituted aldehydes that were used as the starting materials: strongly and weakly electron-donating groups (**4a1, 4a11, 4a12**), mildly electron withdrawing groups (**4a2, 4a3, 4a8, 4a9, 4a14**), strongly electron withdrawing group (**4a4**), and heterocyclic compounds (**4a5, 4a6, 4a7, 4a13**). Also, the aldehydic moieties were selected such that these contained variously substituted heteroatomic substituent's at 1-, 2-, 3-, or 4- positions of the corresponding heterocycles or the benzene ring.

Table 3.1: MWA assisted synthesis of pyranopyrazoles via route A and route B.

No.	R (4a1-4a14)	Product	Route A (%)^a	Route A (T)^b	Route B (%)	Route B (T)	m. p. (°C)	Ref
1	3′-HO-C$_6$H$_4$ (**4a1**)	**5a1**	88	100	82	4	230-232	**32**
2	4′-Br-C$_6$H$_4$ (**4a2**)	**5a2**	82	130	80	3	177-178	**18**
3	3′-Br-C$_6$H$_4$ (**4a3**)	**5a3**	80	110	77	5	223-224	**29**
4	3′-NO$_2$-C$_6$H$_4$ (**4a4**)	**5a4**	86	140	81	5	191-192	**30**
5	3′-thiophenyl (**4a5**)	**5a5**	88	90	80	4	230-231	-
6	2′-pyrrolyl (**4a6**)	**5a6**	85	90	80	4	220-221	-
7	3′-indolyl (**4a7**)	**5a7**	81	110	79	5	210-212	-
8	4′-Cl-C$_6$H$_4$ (**4a8**)	**5a8**	77	130	70	3	175-176	**28**
9	2′-I-C$_6$H$_4$ (**4a9**)	**5a9**	80	140	75	5	250-251	-
10	C$_6$H$_5$ (**4a10**)	**5a10**	86	70	81	4	168-170	**28**
11	*n*-butyl (**4a11**)	**5a11**	82	120	83	5	238-240	**32**
12	4′-Me-C$_6$H$_4$ (**4a12**)	**5a12**	88	60	87	3	218-220	**30**
13	4′-pyridinyl (**4a13**)	**5a13**	94	100	85	4	228-230	**28**
14	2′-F-C$_6$H$_4$ (**4a14**)	**5a14**	90	110	87	5	267-268	-

^{a}isolated yields; ^{b}reaction time in minutes.

With the synthesized pyranopyrazole pharmacophores in hand, we selected the prepared compounds and tested them for *in-vitro* anticancer activity against the Hep3B hepatocellular carcinoma cell line as shown in **Figure 3.8**. The reason for testing them selectively for anticancer activity was that very few reports have appeared on the antineoplasmic activity of pyranopyrazole and that such a study would be the stepping stone for our undergoing anticancer project. The Hep3B cell line has been previously used by various scientists for evaluating the cytotoxicity of several systems.[49] When the designed pyranopyrazole

compounds were tested for the above-mentioned anti-tumor studies, we found that all of them were active showing sub-micromolar activity thus displaying better inhibition than the control (without drug).
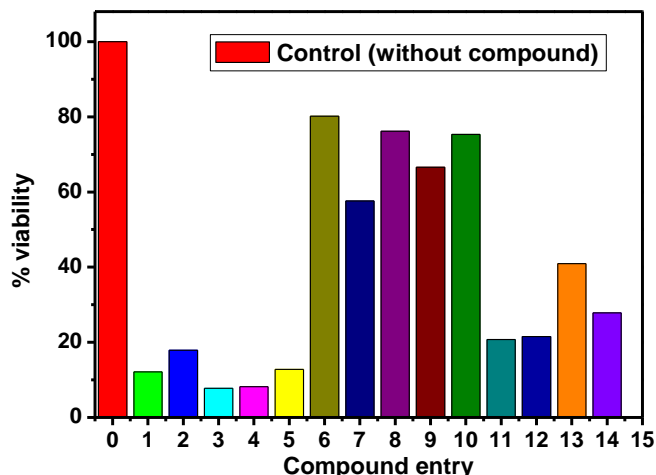
Figure 3.8 Plot of % viability of cells against each compound at 64 ug/ml.

3.2.1 Effect of drugs on cell viability of hepatocellular carcinoma cell line

Hep3B cells were treated with all the drugs each having six different concentrations for 24 hrs. The cell viability was determined using MTT assay. These compounds inhibited the cell viability of hep3B cell line in a dose-dependent manner **(Figure 3.9, 3.10 and 3.11)**.

	control	0.25ug/ml	1ug/ml	4ug/ml	16ug/ml	32ug/ml	64ug/ml
1	100	96.24309	97.01657	94.69613	69.61326	48.39779	12.1547
2	100	112.9282	107.8453	107.1823	44.64088	61.21547	17.90055
3	100	129.6133	121.326	99.8895	35.24862	8.176796	7.734807
4	100	109.3923	95.25862	105.6034	82.09945	49.28177	8.176796
5	100	100.663	103.8674	92.92818	40.33149	71.50685	12.81768
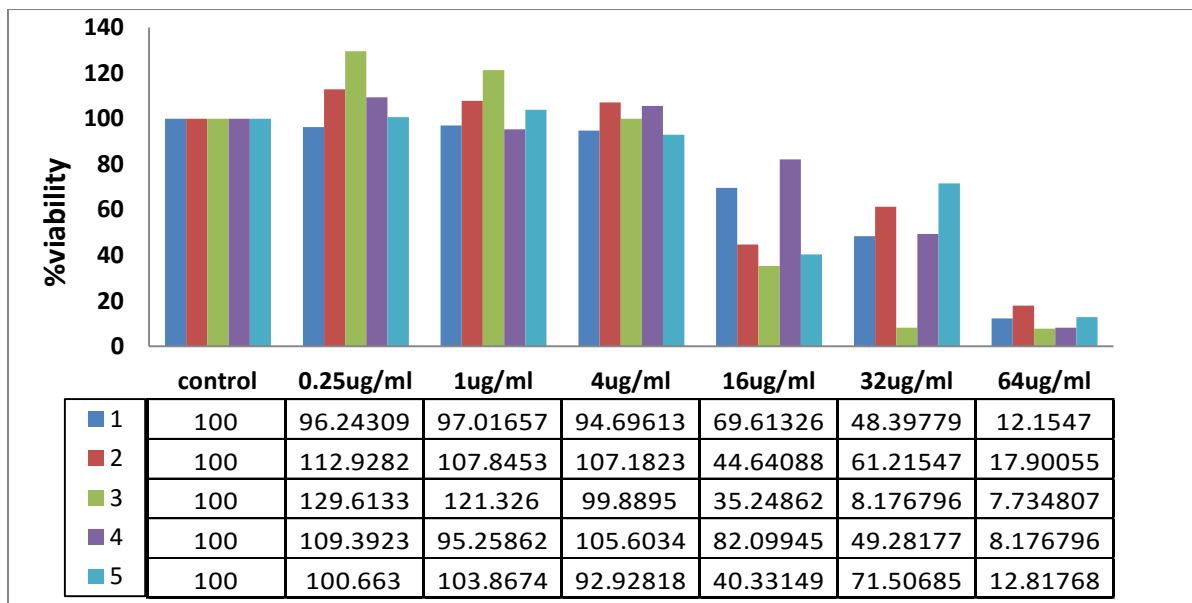
Figure 3.9 Graphical representation of % cell viability at various concentrations of drugs **(Product entry no. 1 – 5)**.

98

	control	0.5ug/ml	2ug/ml	8ug/ml	32ug/ml	64ug/ml	128ug/ml
6	100	98.41144	94.20175	95.23431	88.40349	80.14297	55.52025
7	100	94.99603	93.88403	91.02462	81.57268	57.58539	18.26847
8	100	95.07546	93.80461	93.88403	85.78237	76.17156	24.22558
9	100	96.50516	92.05719	98.64972	68.86418	66.56076	29.15012
10	100	89.59492	92.3749	93.16918	81.73153	75.29786	49.08658
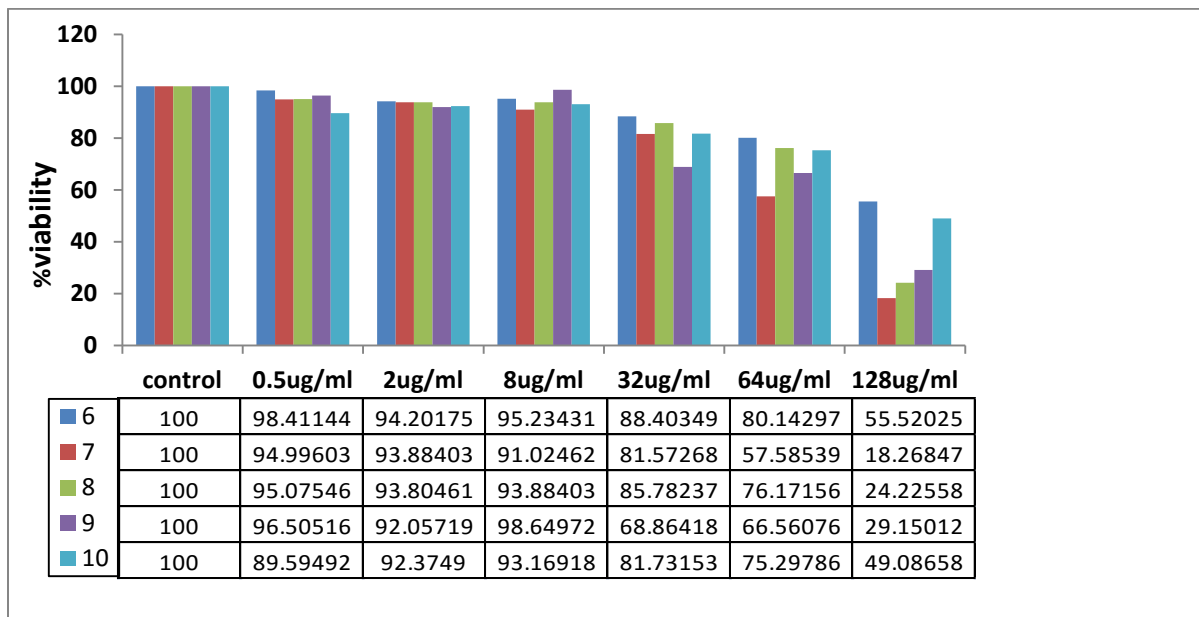
Figure 3.10 Graphical representation of % cell viability at various concentrations of drugs (**Product entry no. 6 – 10**).

	control	0.5ug/ml	2ug/ml	8ug/ml	32ug/ml	64ug/ml	128ug/ml
11	100	103.2086	109.7594	94.25134	33.28877	20.72193	15.24064
12	100	94.51872	119.7861	99.33155	37.96791	21.52406	18.31551
13	100	90.90909	89.17112	91.17647	60.96257	40.90909	18.71658
14	100	74.86631	57.08556	59.35829	51.47059	27.80749	19.38503
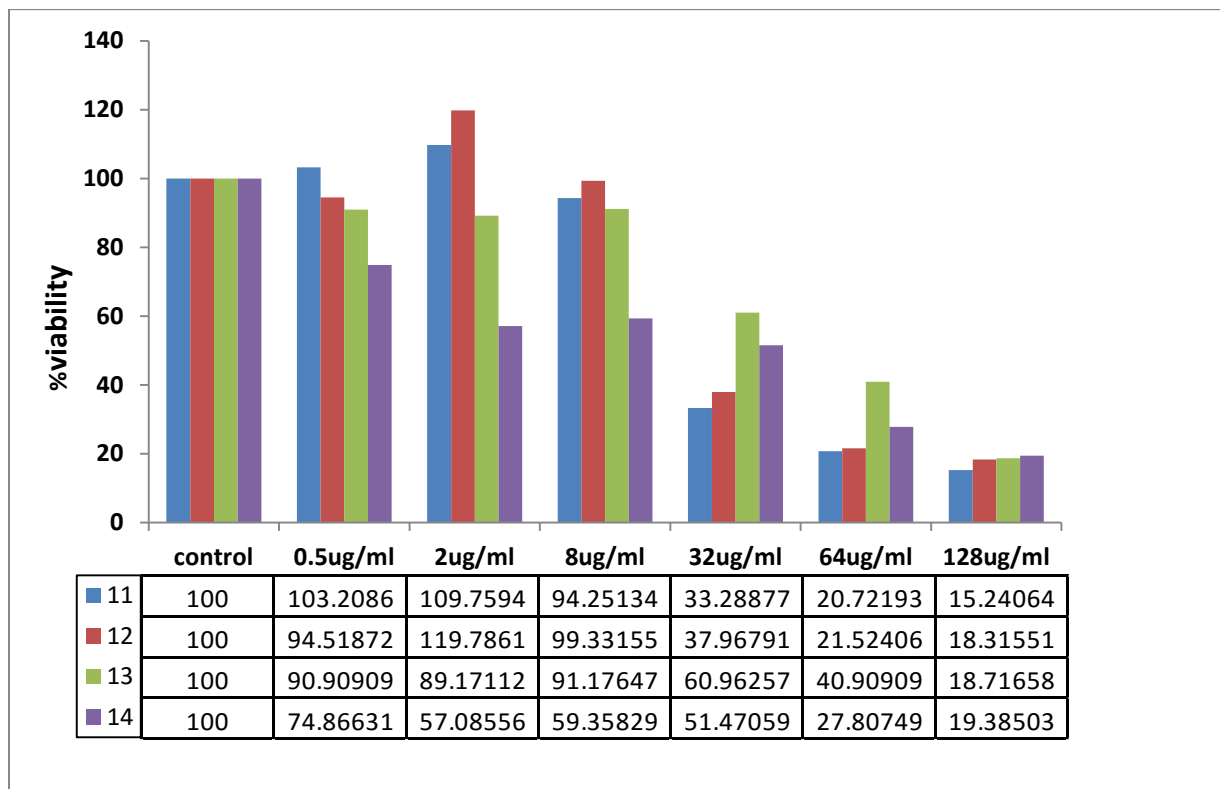
Figure 3.11 Graphical representation of % cell viability at various concentrations of drugs (**Product entry no. 11 – 14**).

IC50 values for all the compounds **(Table 3.2)** were found to be around **1** (5a1) - 32μg/ml, **2** (5a2) - 16μg/ml, **3** (5a3) between 4μg/ml to 16μg/ml , **4** (5a4) - 32μg/ml , **5** (5a5) - 16μg/ml to 32μg/ml, **6** (5a6) - 128μg/ml, **7** (5a7) - 64μg/ml, **8** (5a8) - in between 64μg/ml and 128μg/ml, **9** (5a9) in between 64g/ml to 128μg/ml, **10** (5a10) - 128μg/ml and similarly for compounds **11** (5a11) and **12** (5a12) between 8 and 32μg/ml, for **13** (5a13) between 32 to 64μg/ml, and for **14** (5a14)- 32μg/ml **(Figure 3.9, 3.10, and 3.11)**.

Table 3.2: Cytotoxicity results of first seven and next seven compounds.

No.[a]	IC_{50}[b]	No.[a]	IC_{50}[b]
1	32	8	64-128
2	16	9	64-128
3	4-16	10	128
4	32	11	8-32
5	16-32	12	8-32
6	128	13	32-64
7	64	14	32

[a]compound no.; [b]in μg/ml.

3.2.2 SAR (Structure-Activity Relationship) analysis

A rational analysis of the SAR (Structure-Activity Relationship) results of the first ten compounds reveals some interesting trends. The first five compounds **1** (5a1) to **5** (5a5) have an average IC50 value of 22.8 μg/ml while the next five have an average cytotoxicity of 102.4 μg/ml. Hence, it is evident that the first five compounds are relatively more potent. Now, observing the structures of the first five compounds (as depicted in **Table 3.1**), we find that all compounds except **2** (5a2) have heteroatom substituent's at the 3-position of the top-right sector **(Figure 3.12, circled)** of the pyranopyrazole skeleton. On the other hand, considering the structures of the last five compounds from **6** (5a6) to **10** (5a10), none of them possess heteroatom substituent's at the aforementioned 3-position of the pyranopyrazole except **7** (5a7) which again is the most active among the last five compounds. Therefore, it is quite clear that compounds having a heteroatom substituent at the 3-postion display better activity than those which bear either 1-, 2-, or 4- substituent. This leads to the rationale that the presence of heteroatom substituent's at or around the 3-position of the designed pyranopyrazole small molecules might play a critical role in enhancing the compounds anticancer activity under our experimental conditions.
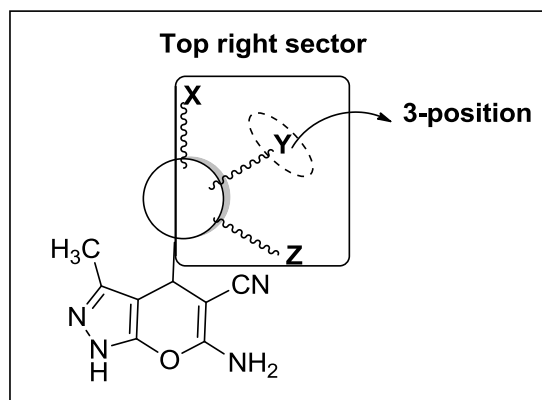
Figure 3.12 Pyranopyrazole pharmacophore scaffold.

Additional investigations related to this curious finding are required and further proof of concept experiments are currently being examined in our labs.

3.2.3 X-ray crystallographic study of the 6-amino-3-methyl-4-(*p*-tolyl)-1,4-dihydropyrano[2,3-*c*]pyrazole-5-carbonitrile (5a12 or entry no. 12 in Table 3.1)

3.2.3.1 Data collection, structure solution and refinement

Single crystal X-ray diffraction data of the title compound was collected on X' Calibur CCD area detector diffractometer, Oxford Diffraction using Mo *Ka* radiation (λ=0.7107 Å) at 293(2) K.[50] The crystal structure was solved by direct methods using SHELXS97[51] and refined by the full matrix least squares method using SHELXL97[52] present in the program suite WinGX.[53] All the non-hydrogen atoms are refined anisotropically and all the hydrogen atoms (except N1 H atoms) were geometrically fixed and allowed to ride on their parent C/N atoms with C-H= 0.93-0.98 Å and N-H distance of 0.86 Å. They were refined isotropically with Uiso (H)=1.2Ueq (C) or 1.5Ueq (C) for methyl H atoms. An ORTEP view of the molecule indicating atom numbering scheme (thermal ellipsoids drawn at 40% probability level) is shown in **Figure 3.13a** and the corresponding 2D structure of the crystallographic molecule is shown in **Figure 3.13b**. ORTEP diagram of the compound was generated using ORTEP32[54] and packing diagram was generated using PLATON21 software. Geometrical calculations were performed using PLATON[55] and PARST.[56] **Table 3.3** lists all crystallographic and refinement data. Intermolecular interactions are listed in **Table 3.4**. PIXEL calculations were performed in order to estimate the nature and energies associated with the intermolecular interactions which will enable us to explore the role of these interactions in the stabilization of the crystal lattice.

(a) (b)
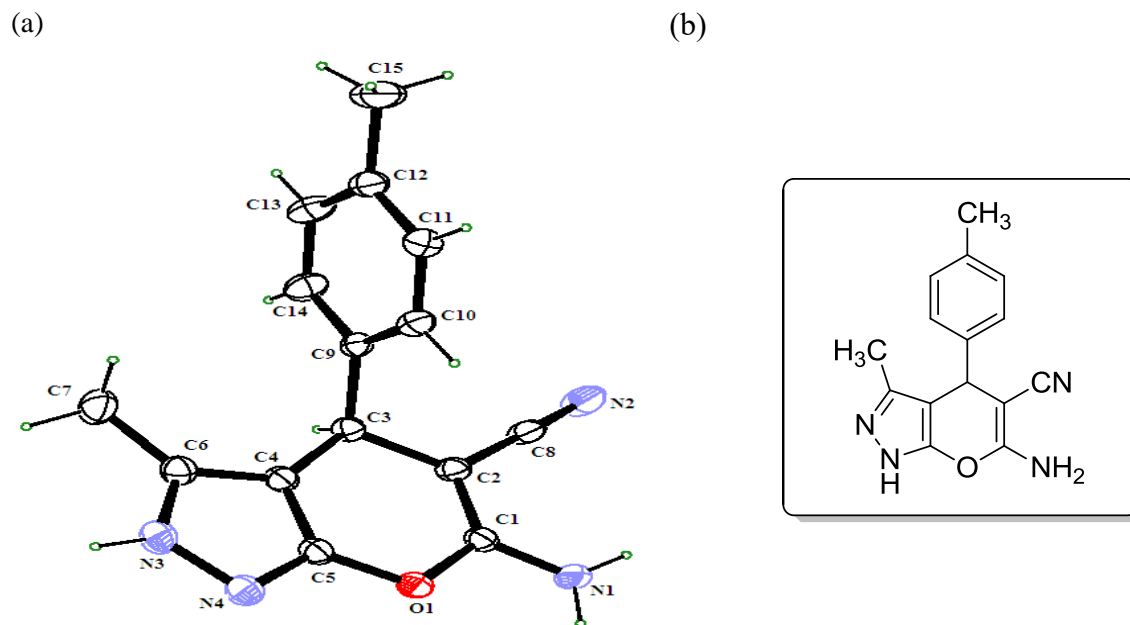
Figure 3.13 (a) ORTEP view of the molecule with displacement ellipsoids drawn at 40%. H atoms are shown as small spheres of arbitrary radii (b) 2D view of the molecule.

Table 3.3 Crystal and experimental data.

CCDC No	991567
Crystal description	Block
Crystal colour	White
Crystal size	0.3 x 0.2 x 0.2 mm
Empirical formula	$C_{15}H_{14}N_4O$
Formula weight	266.30
Radiation, Wavelength	Mo $K\alpha$, 0.71073 Å
Unit cell dimensions	$a =6.3757(4), b = 9.8950(8), c = 10.6311(9)$ Å,
	$\alpha = 78.519(7), \beta = 84.605(7), \gamma = 88.623(6)°$
Crystal system	Triclinic
Space group	P -1
Unit cell volume	654.35(9) Å^3
No. of molecules per unit cell, Z	2
Temperature	293(2)
Absorption coefficient	0.089 mm^{-1}
F(000)	280

Scan mode	ω scan
θ range for entire data collection	3.61 <θ< 26.00º
Range of indices	h= -7 to 6, k= -11 to 12, l= -13 to 12
Reflections collected/unique	4421/2561
Reflections observed (I > 2σ(I))	1831
R_{int}	0.0239
R_{sigma}	0.0470
Structure determination	Direct methods
Refinement	Full-matrix least-squares on F^2
No. of parameters refined	192
Final R	0.0467
wR(F^2)	0.1181
Weight	$1/[\sigma^2(F_o^2)+(0.069\ 8P)^2+0.0000P]$, where P=$[F_o^2+2F_c^2]$ / 3
Goodness-of-fit	1.032
$(\Delta/\sigma)_{max}$	0.001 (for tors H15A)
Final residual electron density	-0.229 <Δρ<0.239 Å^{-3}
Measurement	*X'calibur system – Oxford diffraction make, U.K.*
Software for structure solution	SHELXS97 (Sheldrick, 2008)
Software for refinement	SHELXL97 (Sheldrick, 2008)
Software for molecular plotting	ORTEP-3 (Farrugia, 2012) PLATON (Spek, 2009)
Software for geometrical calculation	PLATON (Spek, 2009) PARST (Nardelli, 1995)

Table 3.4 Intermolecular hydrogen bonding (e.s.d.`s in parentheses)

D–H…A	D–H (Å)	H…A (Å)	D…A (Å)	D–H…A (deg)	Symmetry code
N1-H1…N2	0.92(2)	2.32(2)	3.147(3)	174(1)	-x, -y+1, -z+1
N1-H2…N4	0.92(2)	2.33(2)	3.169(2)	171(2)	-x+1, -y+1, -z
C15-H15C ...N2	0.96	2.57	3.352(3)	139	-x-1, -y, -z+1

3.2.3.2 Theoretical calculations

To get a better understanding of the contribution of intermolecular interactions to the crystal packing, it is important to get a quantitative evaluation of these interactions. Calculation of the lattice energy not only offers a possible way for polymorph prediction but may also help to understand the supramolecular chemistry and self-assembly during the nucleation and crystal growth processes and helps to predict the

melting and solubility behavior of the compounds. The lattice energy of the title compound was calculated by PIXELC module in Couloumb-London- Pauli (CLP) computer program package (version 13.2.2012)23. The total lattice energy is partitioned into its coulombic, polarization, dispersion and repulsion contributions **(Table 3.5)**. In CLP, the coulombic terms are handled by Coulomb's law while the polarization terms are calculated in the linear dipole approximation, with the incoming electric field acting on local polarizabilities and generating a dipole with its associated dipole separation energy; dispersion terms are simulated in London's inverse sixth power approximation, involving ionization potentials and polarizabilities; repulsion is presented as a modulated function of wave function overlap All the stabilizing molecular pairs involved in crystal packing were selected from the mlc output file, which is generated after PIXEL energy calculations and were analyzed with their interaction energies. The symmetry operator and centroid–centroid distance along with coulombic, polarization, dispersion, repulsion and total interaction energies between the molecular pairs are presented in **Table 3.6**. The molecular pairs are arranged in decreasing order of their stabilization energies. The PIXEL method has been preferred for the quantification of intermolecular interactions, primarily because of the following reasons:

(1) It is computationally less demanding.[57]

(2) It allows partitioning of total interaction energy into corresponding coulombic,

polarization, dispersion, and repulsion contribution which facilitates a better understanding of the nature of intermolecular interactions contributing towards the crystal packing.[58]

(3) The energies obtained from PIXEL calculation are generally comparable with high level quantum mechanical calculations.[59-60]

Table 3.5 Lattice energy from CLP (in kcal mol^{-1}).

	E_{Cou}	E_{Pol}	E_{Disp}	E_{Rep}	E_{Tot}
Molecule 1	-22.90	-10.25	-38.26	30.64	-40.77

Table 3.6 PIXEL interaction energies (I.E. in kcal mol^{-1}) between molecular pairs related by a symmetry operation and the associated intermolecular interactions in the crystal.

Motif	Centroid distance (Å)	E_{Cou}	E_{Pol}	E_{Disp}	E_{Rep}	E_{Tot}	Symmetry	Important Interactions
1	9.438	-14.58	-5.38	-4.35	10.16	-14.15	$-x, 1 - y, 1 - z$	N1-H1….N2
2	6.542	-5.88	-5.45	-12.55	10.78	-13.10	$-x, -y, -z$	N3–H3A….Cg1 N3–H3A….C15 C7–H7C….C6

3	9.069	-11.38	-4.78	-5.19	8.72	-12.62	$1 - x, 1 - y, -z$	N1–H2….N4
								O1….O1
4	6.088	-1.67	-1.22	-12.59	7.72	-7.77	$-x, 1 - y, -z$	C14–H14….O1
								C3–H3….O1
5	7.276	-2.44	-1.07	-8.96	4.92	-7.52	$-x, -y, 1 - z$	C15–H15A….N1
								C11–H11….C10
6	6.376	-2.22	-1.15	-7.40	3.78	-7.03	$-1 + x, y, z$	C7–H7B….N4
7	8.907	-3.89	-1.91	-7.60	7.74	-5.66	$-1 - x, -y, 1 - z$	C15–H15B….N2

The compound 6-Amino-1,4-dihydro-3-methyl-4-phenylpyrano[2,3-*c*]pyrazole-5-carbonitrile, crystallizes in the triclinic crystal system with space group P-1. The molecule comprises of a pyrazole, pyran and a tolyl ring **(Figure 3.13)**. The bond distances in the title compound are within normal ranges[61] and comparable to the closely related structures.[62-63] The dihedral angle between the tolyl ring and the pyrazole ring is 86.46(5)° and between the tolyl and pyran ring is 84.07(5)°. The dihedral angle between the mean planes of the pyrazole and pyran ring is 2.39(6)° which confirms their coplanar character. All the rings are planar with a maximum deviation of 0.003(2) Å for the tolyl C11 atom, -0.002(2) Å for the pyrazole C5 atom and 0.022(2) Å for the pyran C3 atom. The carbonitrile group exhibits linearity, a feature commonly observed in carbonitrile compounds.[64]

Two N-H⋯N and one C-H⋯N intermolecular hydrogen bond interactions **(Figure 3.14)** are observed for maintaining the crystal packing, in which the N1-H1⋯N2 intermolecular interaction are observed to form $R^2_2(12)$ ring motifs[65] **(Figure 3.15)**. Details of intermolecular hydrogen bonds are given in **Table 3.4**.
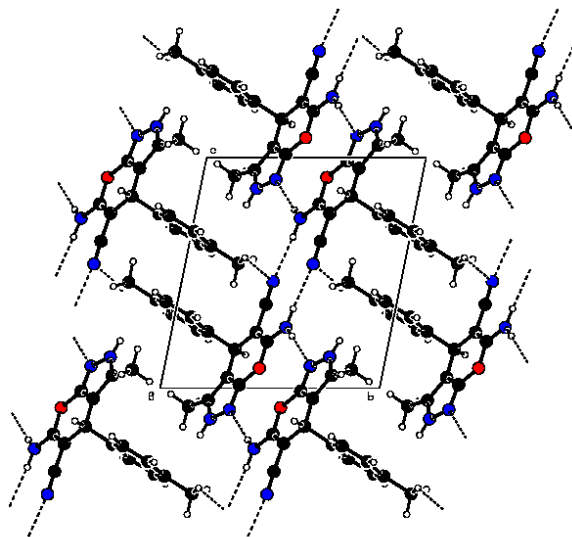
Figure 3.14 The crystal packing of the title compound viewed down the *a*-axis, showing intermolecular hydrogen bonding interactions as dashed lines.
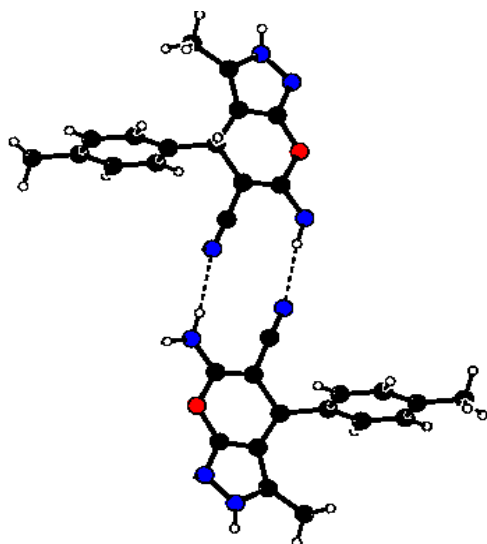
Figure 3.15 View of $R^2_2(12)$ ring motifs formed by N–H….N interaction between two molecules.

The lattice energy calculation for the title compound is given in **Table 3.5**. Molecular pairs of the title compound extracted from crystal structure along with their respective interaction energies are shown in **Figure 3.16**. The maximum stabilization to the crystal structure comes from N-H…N intermolecular interaction involving H1 with N2.
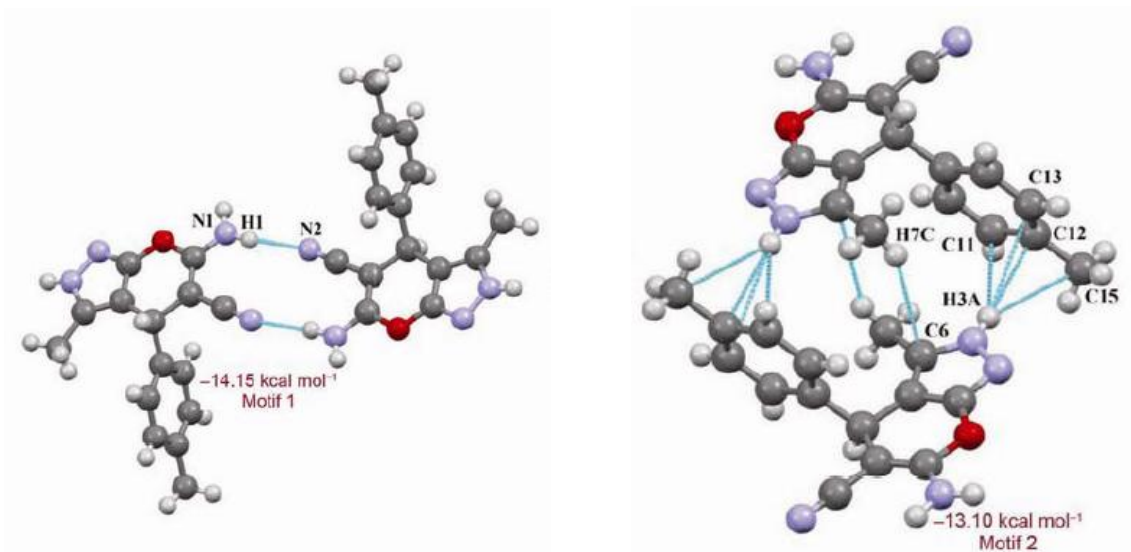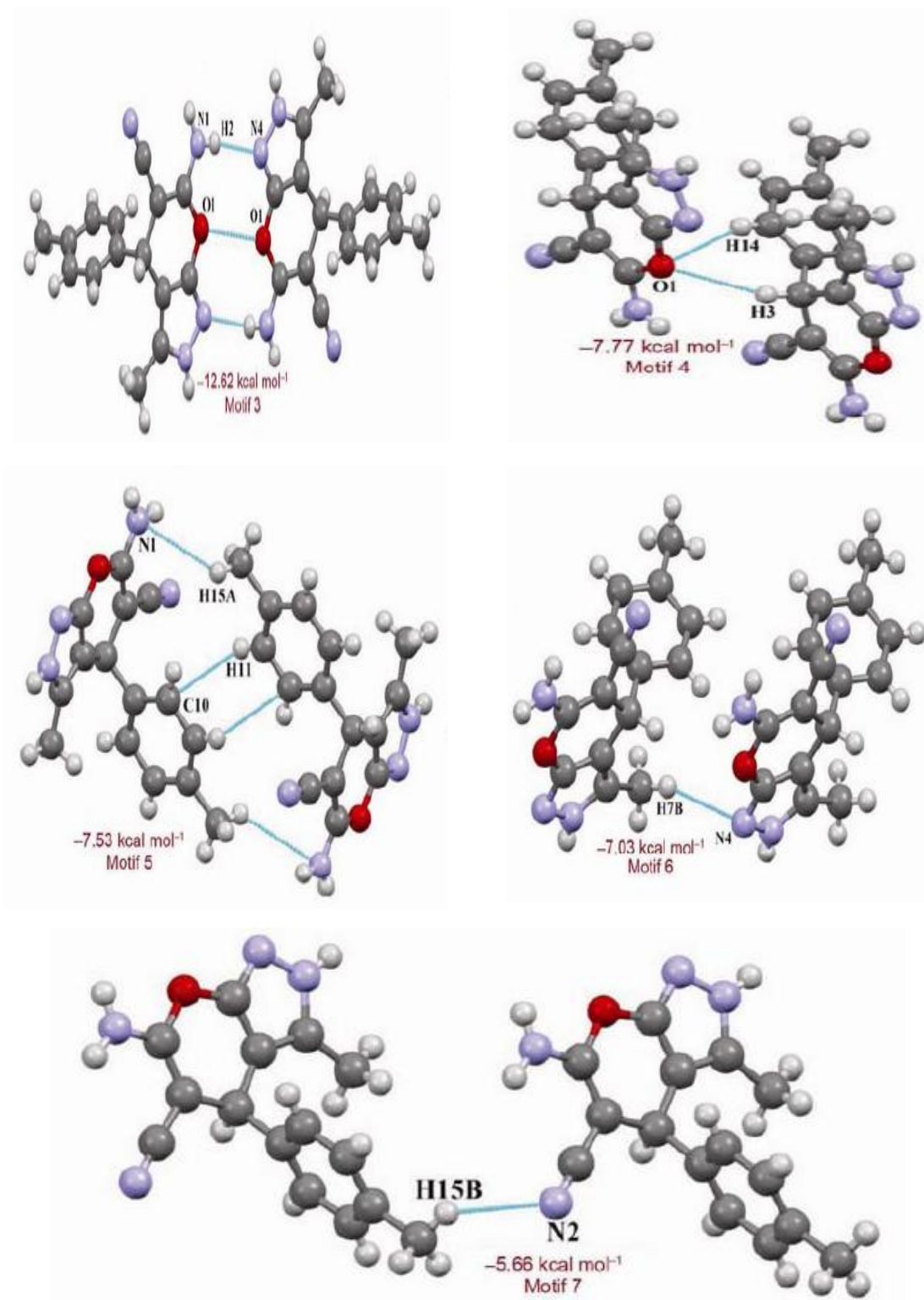
Figure 3.16 Molecular pairs (1–7) with their interaction energies.

The stabilization energy of this pair is -14.15 kcal mol^{-1} obtained using PIXEL and the interaction is mainly coulombic in nature. The next most stabilized pair shows the presence of bifurcated donor atom N3 involving H3A with Cg1 and C15, along with this interaction the molecular pair also shows the presence of C-H…C interaction (involving H7C with C6) and hence form dimer. The stabilization energy of this pair is -13.10 kcal mol^{-1}. Molecular pair 3 shows the presence of N-H…N interaction (involving H2 with N4) and O1…O1 interaction resulting in a stabilization energy of -12.62 kcal mol^{-1}. Another molecular pair (Motif 4) shows the presence of bifurcated acceptor atom O1 with H3 and H14 having interaction energy of -7.77 kcal mol^{-1} with major contribution from dispersion component. The next most stabilized molecular pair involves C-H…N and C-H…C hydrogen bonding involving H15A interacting with N1 and H11 interacting with C10, respectively with an interaction energy of -7.53 kcal mol^{-1} and the stabilization mainly comes from dispersion component. Molecular pair 6 and 7 shows the presence of C-H…N interaction involving H7B with N4 and H15B with N2 having interacting energies of -7.03 kcal Mol^{-1} and -5.66 kcal mol^{-1}, respectively providing additional stabilization to the crystal packing. The combined nature of these interactions is mainly dispersive in nature.

3.3 Conclusions

In this part of chapter-3, we have outlined the initial findings of the design, synthesis, anticancer activity, and a brief SAR evaluation of a series of compounds having pyranopyrazole pharmacophore. The synthesis involved an unprecedented rapid, environment friendly, and MWA strategy. The synthesized compounds were tested for anticancer cytotoxic activity against Hep3B cells and all were found to be potent and showed reasonably good IC50 values as shown in **Table 3.2**. A quick SAR of the resulting compounds revealed that the presence of heteroatom substituent's at the 3- position of the top right part of the pyranopyrazole might be significant in anticancer studies. Further research based on these preliminary studies is going on in our labs. Crystallographic analysis of 6-amino-3-methyl-4-(*p*-tolyl)-1,4-dihydropyrano[2,3-*c*]pyrazole-5-carbonitrile and energy calculations show the presence of different key structural motifs which aid in the stabilization of crystal packing. Analysis of different structural motifs shows that weak intermolecular interactions are also the major contributors that stabilize the crystal packing in addition to strong interactions. This demonstrates that the calculation of lattice energies is a useful approach to assess the stability of molecular crystals in which dispersion type interactions make up an essential part of the intermolecular interactions.

3.4 Experimental

3.4.1 General methods of synthesis

Two-step method: Typical reaction procedure for the synthesis of pyranopyrazoles at room temperature on magnetic stirrer (two-step): Ethyl acetoacetate (1.0 equiv, 2.0 mmol, 0.25 ml) was taken in a round bottom flask and mixed with ethanol (3 ml) with dropwise addition of hydrazine hydrate (1.0 equiv, 2.0 mmol, 0.10 ml). The mixture was stirred for about 1 hour at 60°C. The solid obtained was filtered, washed with distilled water and cold methanol, and then recrystallized from ethanol. In another round bottom flask, the required aldehyde (1.1 equiv) and malononitrile (1.1 equiv, 2.2 mmol, 0.12 ml) were taken and mixed with 4 ml of ethanol followed by drop wise addition of triethylamine (1.5 equiv, 3.0 mmol, 0.42 ml). The mixture was allowed to stir for about 3-4 hours(while being monitored by TLC) at room temperature, filtered and washed with water, and then with a mixture of ethyl acetate : hexane (20 : 80). The final pyranopyrazole compound obtained was eventually recrystallized from ethanol.

Method A (one-step): the aldehyde (1.1 equiv), malononitrile (1.1 equiv, 2.2 mmol, 0.12 ml), and triethylamine (1.5 equiv, 3.0 mmol, 0.42 ml) were added successively to about 4ml of ethanol kept in a round bottom flask at ambient temperature. The mixture was allowed to stir vigorously for a few minutes. Ethyl acetoacetate (1.0 equiv, 2.0 mmol, 0.25 ml) and hydrazine hydrate (1.0 equiv, 2.0 mmol, 0.10 ml) were added to the reaction mixture and the contents of the flask were stirred for about one hour. The solid thus precipitated was subjected to a similar work up as in the two-step method described above.

Method B (MWA synthesis): The microwave instrument used for the MWA synthesis experiments was CEM Discover BenchMate Reactor. All the reactions were performed in 10 mL pressure vials at 80–100 Watt power at 60°C under high stirring mode. The reactants were added in the microwave apparatus in a similar fashion as in method B and stirred for 3-5 minutes. After the reaction, the contents of the flask were filtered, and analogous work up, purification, and recrystallization was done.

3.4.2 Materials and method for biological activity

For determining the *in-vitro* cytotoxicity, Hep3B cells (procured from NCCS Pune) growing in log phase were briefly seeded at a density of 2000 cells per well in a 96 well plate and incubated for 24 hours with 5% CO_2 at 37°C. The cells were treated with different drugs (namely compounds entry no. **1-10**) at concentrations of 0.25µg/mL, 1µg/ml, 4µg/ml, 16µg/ml, 32µg/ml and 64µg/ml diluted with DMSO (SDFCL, cat no- 20323 L05) for 24 hours with respective controls. Following drug treatment, 20ul MTT/PBS (MTT: Sigma, cat no-M5655) (Stock concentration 5mg/ml) PBS (Invitrogen, cat no-21300-025) was added and incubated for 4hours. The formazan crystals thus formed were solubilized using DMSO and readings were obtained at 495nm using an enzyme-linked immune-sorbent assay (ELISA) micro-plate reader (Start-fax 2100). Percentage of viable cells was calculated using formula:

Viability (%) = (mean absorbance value of drug treated cells) / (mean absorbance value of control) *100

3.4.3 Characterization of compounds not reported in the literature

Our data for the previously reported compounds was found to be identical and the corresponding references have been included in the **Table 3.1**. (For ^{1}H and ^{13}C-NMR spectra see Appendices A-1).

6-amino-3-methyl-4-(thiophen-3-yl)-1,4-dihydropyrano[2,3-c]pyrazole-5-carbonitrile (5a5)

Light creamy yellow solid, ^{1}HNMR (400 MHz, d6- DMSO) δ: 12.10 (s, 1H), 7.28 (1H), 7.26 (2H), 6.83 (2H), 4.73 (s, 1H), 1.86 (s, 3H). ^{13}CNMR (100 MHz, d6-DMSO) δ: 160.7, 154.5, 145.0, 135.5, 126.6, 125.9, 120.7, 120.7, 96.8, 78.5, 57.0, 31.3, 9.6. HRMS calcd for $C_{12}H_{10}N_4OS$ 258.058, found 258.057.

6-amino-3-methyl-4-(1H-pyrrol-2-yl)-1,4-dihydropyrano[2,3-c]pyrazole-5-carbonitrile (5a6)

Very light creamy yellow solid, ^{1}HNMR (400 MHz, d6- DMSO) δ: 12.05 (s, 1H), 10.51 (1H), 6.56-6.73 (3H), 5.84 (2H), 4.64 (s, 1H), 1.84 (s, 3H). ^{13}CNMR (100 MHz, d6-DMSO) δ: 160.7, 154.7, 135.6, 133.2, 120.8, 116.8, 106.6, 105.1, 96.7, 78.6, 56.9, 29.5, 9.4. HRMS calcd for $C_{12}H_{11}N_5O$ 241.096, found 241.098.

6-amino-4-(1H-indol-3-yl)-3-methyl-1,4-dihydropyrano[2,3-c]pyrazole-5-carbonitrile (5a7)

White solid, ^{1}HNMR (400 MHz, d6-DMSO) δ: 12.01 (s, 1H), 10.86 (1H), 6.84-7.36 (5H), 6.75 (2H), 4.85 (s, 1H), 1.77 (s, 3H). ^{13}CNMR (100 MHz, d6-DMSO) δ: 160.5, 154.9, 136.8, 135.4, 125.5, 121.0, 120.7, 118.1, 116.7, 11.4, 78.6, 58.1, 28.2, 9.6. HRMS calcd for $C_{16}H_{13}N_5O$ 291.112, found 291.111.

6-amino-4-(2-iodophenyl)-3-methyl-1,4-dihydropyrano[2,3-c]pyrazole-5-carbonitrile (5a9)

Very light yellow solid, ^{1}HNMR (400 MHz, d6-DMSO) δ: 12.15 (s, 1H), 7.01-7.35 (multiplet, 4H), 6.75 (2H), 4.96 (s, 1H), 1.76 (s, 3H). ^{13}CNMR (100 MHz, d6-DMSO) δ: 160.9, 154.7, 135.4, 128.6, 120.0, 78.4, 56.3, 18.3, 9.9. HRMS calcd for $C_{14}H_{11}N_4O$ 377.998, found 377.996.

6-amino-4-(2-fluorophenyl)-3-methyl-1,4-dihydropyrano[2,3-c]pyrazole-5-carbonitrile (5a14)

Dirty white solid, ^{1}HNMR (400 MHz, d6-DMSO) δ: 12.13 (s, 1H), 6.94 (2H), 7.24 (m, 4H), 4.87 (s, 1H), 1.81 (s, 3H). ^{13}CNMR (100 MHz, d6-DMSO) δ: 161.3, 154.9, 135.2, 129.7, 128.5, 124.5, 115.4, 99.5, 96.5, 78.8, 55.6, 29.8, 9.4. HRMS calcd for $C_{14}H_{11}FN_4O$ 270.092, found 270.095.

Chapter III

Part B

Novel Spiro/Non-Spiro Pyranopyrazoles: Ecofriendly Synthesis, *in-vitro* Anticancer Activity, DNA Binding and Molecular Docking Study

3.5 Introduction

Cancer is one of the highly deadly diseases of worldwide importance and is one of the leading causes of death globally.[66] The mortality to incidence ratio is one of the highest for hepatocellular carcinoma cases. Cirrhosis (scarring of the liver) is the most common cause of liver cancer,[67] and it may be caused by alcohol abuse, hepatitis B or C virus infection, autoimmune diseases of the liver, hemochromatosis (iron overload in the body), or chronic inflammation of the liver.

Among the available chemical scaffolds, most of the heterocycles containing Nitrogen have always attracted immense interest in cancer research because of their widespread presence as part of the skeletal backbone of many therapeutic agents. For instance, several researchers reported pyrazole fused heterocycles including pyrazolo[1,5-*a*]pyrimidine,[68] pyrazolo[4,3-*d*]pyrimidin-7-one,[69] pyrazolo[3,4-*d*]pyrimidine,[70-72] pyrazolo[1,5-*a*]pyridine[73] and pyrazolo[3,4-*b*]pyrrolo[3,4-*d*]pyridine[74] etc. Similarly, substituted pyrano[2,3-*c*]pyrazoles are also much sought after because of their various potential applications in pharmaceutical field. They possess a wide range of biological activities like anticancer,[75-76] anti-inflammatory,[76] antimicrobial,[77-78] human Chk1 kinase[79] and also as biodegradable agrochemicals.[79]

Regarding the synthesis of pyranopyrazoles, several researchers reported multistep protocols[80-81] and multi-component reaction[82] (MCR) protocols etc. Thus, literature survey reveals a variety of three and four component MCR's for the construction of different pyranopyrazoles. In this part of thesis, we report synthesis of non-spiro (**5a-j, scheme 3.2, Table 3.7**) and spiro (**9a-h and 13a-c, scheme 3.3 and 3.4, Table 3.8**) substituted pyranopyrazole scaffolds through MCR in one step by one pot approach. Although the conventional synthetic methodologies have a broad scope but the major disadvantage associated is the generation of copious amount of waste as side product. In this aspect, in modern drug discovery, the MCRs have evolved as a precious tool because of their inherent atom economy, structural multiplicity of the products, and efficiency when compared to conventional multistep syntheses. Following the synthesis, the preliminary biological evaluation of all the synthesized molecules through **scheme 3.2, 3.3,** and **3.4** as shown in **Table 3.7** and **3.8** has been done *in-vitro* on Hep3B hepatocellular carcinoma cell line. The best five molecules, from each **Table 3.7** and **3.8** which showed significant IC_{50} values were selected and tested for calf thymus DNA binding study by UV-visible spectroscopy by taking the OD in presence and absence of drug molecule with DNA. This type of study was imperative to get an insight into the possible mechanism of the anticancer study. Finally, the most potent compound (**5h**) was docked with CDK-2 kinase to get a clearer picture of the binding mode of the ligand. To the best of our knowledge, this study is first of its kind in-depth combined investigation comprising synthesis, *in-vitro* exploration, and *in-silico* docking of pyranopyrazoles.

3.6 Chemistry of non-spiro and spiro pyranopyrazole moieties

3.6.1 Chemistry of non-spiro pyranopyrazole compounds

To accomplish the aim of identifying new physiologically active compounds, several researchers reported the synthesis of substituted 6-amino-4*H*-pyrazolo[3,4-*b*]pyrans. Junek *et al.*[79] were the first group to represent this class of compounds which was obtained from the reaction of 3-methyl-1-phenylpyrazolin-5-one with tetracyanoethylene. Various other groups[83-85] synthesized varieties of 6-amino-5-cyano-4-aryl-4*H*-pyrazolo[3,4-*b*]pyrans by condensation of 4-arylidenepyrazolin-5-ones with malononitrile or by arylidenemalononitriles with 3-methylpyrazolin-5-ones. Sharanin and co-workers[84] developed the simple approach towards the synthesis of 6-amino-5-cyano-4-aryl-4*H*-pyrazolo[3,4-*b*]pyrans by condensation of aromatic aldehydes, malononitrile, and substituted pyrazolin-5-ones in ethanol medium using triethylamine as a catalyst.

In the present paper, all the non-spiro compounds **(5a-j)** were synthesized by successive addition of the four components ethylacetoacetate, hydrazine hydrate, malononitrile, and the aldehyde to give the desired compounds **(scheme 3.2, route A, Table 3.7)** within 2-3 hour. Although the reaction yields were reasonable, the methodology was not adequate to lead to the satisfactory greening of the overall synthetic technique. Hence, we eventually experimented with the microwave assisted (MWA) synthetic strategy. To accomplish the MWA protocol **(scheme 3.2, route B, Table 3.7)**, we mixed the aldehyde, malononitrile, and triethylamine in ethanol in the microwave apparatus followed by the addition of ethyl acetoacetate and hydrazine hydrate. Finally, the reaction mixture was kept in the microwave apparatus and the reaction was accomplished within 3-5 minutes. The overall reaction took less than 6 minutes for completion. From **Table 3.7**, it is observed that the general yield of the MWA protocol and the traditional protocol was comparable and the slight loss of yield for the MWA methodology was more than compensated by the rapid reaction times. The reduction in reaction time and cleaner reactions leading to comparable yields are the two main advantages of the microwave assisted synthesis over the conventional method. In addition, the use of microwave irradiation not only minimizes the formation of unwanted by products but also reduces the need for organic solvents; sometimes even leading to solvent free reactions. In a previous paper, we reported that some pyrazole-fused heterocyclic compounds could be synthesized by microwave irradiation strategy.[86] These results encouraged us to adopt microwave irradiation for the synthesis of pyrazole derivatives with structural diversity. The comparison of the percentage yield and the reaction completion time for both conventional as well as microwave assisted synthesis is shown in **Table 3.7** and the corresponding graphs are shown in **Figure 3.17** and **3.18** respectively.

(a)

Where R= 2'-Furanyl; 2'-thiophenyl; 2'-pyridinyl; 2'-HO-C$_6$H$_4$; 4'-HO-C$_6$H$_4$; 4'-O$_2$N-C$_6$H$_4$; 4'-F-C$_6$H$_4$; 4'-(N,N-dimethylamino)-C$_6$H$_4$; 3',4'-di-MeO-C$_6$H$_3$

(b)

Where R= 3-OH-C$_6$H$_4$

N-Phenyl substituted non-spiro pyranopyrazole
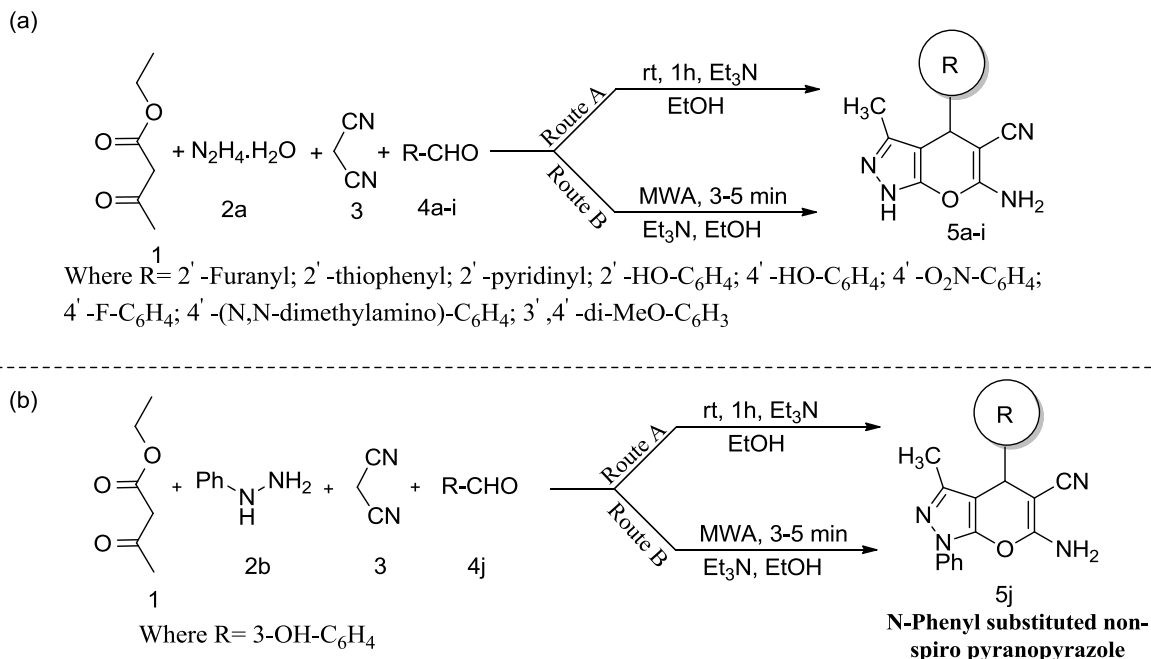
Scheme 3.2 Synthesis of non-spiro pyranopyrazole via (a) conventional method and (b) Microwave assisted synthesis.

Table 3.7: Synthesized pyranopyrazoles (non-spiro), yields, time, and references.

No.	Aldehyde (R =)	Product	Route A[a] (%)[c]	(T)[d]	Route B[b] (%)	(T)	Observed m.p. (°C)	Ref
1	2′-Furanyl (**4a**)	(**5a**)	92	130	82	5	240-244	**87**
2	2′-thiophenyl (**4b**)	(**5b**)	93	100	90	5	187-189	**88**
3	2′-pyridinyl (**4c**)	(**5c**)	85	150	76	3	245-247	**91**
4	2′-HO-C$_6$H$_4$ (**4d**)	(**5d**)	91	70	81	4	213-215	**87**
5	4′-HO-C$_6$H$_4$ (**4e**)	(**5e**)	84	120	78	4	223-226	**87**
6	4′-O$_2$N-C$_6$H$_4$ (**4f**)	(**5f**)	77	110	73	5	195-196	**89**
7	4′-F-C$_6$H$_4$ (**4g**)	(**5g**)	83	100	80	3	244-246	**87**
8	4′-(N,N-dimethylamino)-C$_6$H$_4$ (**4h**)	(**5h**)	90	120	83	3	232-234	**87**
9	3′,4′-*di*-MeO-C$_6$H$_3$ (**4i**)	(**5i**)	78	120	85	2	194-195	**89**
10	3-OH-C$_6$H$_4$ (**4j**)	(**5j**)	84	120	82	2	169-170	**90**

[a]one-step traditional heating; [b]one-step MWA synthesis; [c]isolated yields; [d]time in minutes.
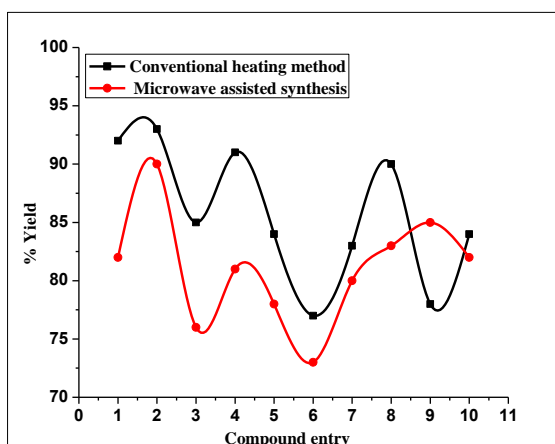
Figure 3.17 Shows the plot of compound entry vs % yield.
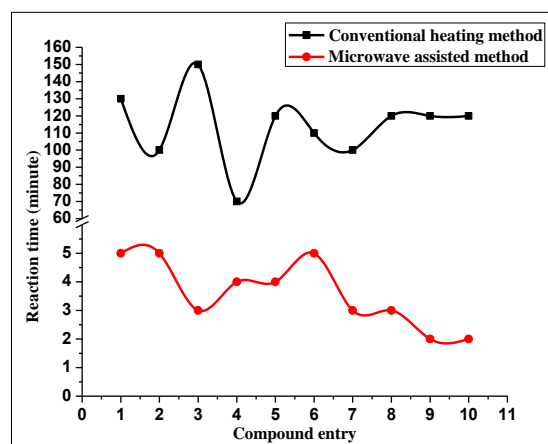
Figure 3.18 Shows the plot of compound entry vs % reaction time.

3.6.2 Chemistry of spiro-pyranopyrazole compounds

Similar to the non-spiro derivatives, all the novel spiro-pyranopyrazole compounds (**9a-h and 13a-c, scheme 3.3 and 3.4**) were synthesized by conventional method as well as through the reflux method. Although, the procedure is the same for both the methods the difference lies in the time of completion of the reactions. All the spiro compounds were prepared by mixing of the analogous three components wherein substituted ketones (**8a-h and 12a-c, scheme 3.3 and 3.4**) were used in place of aromatic aldehydes as shown in **Table 3.8**. Anatoliy *et al.*[92] reported the synthesis of substituted 6-amino-5-cyanospiro-4-(piperidine-4')-2*H*,4*H*-dihydropyrazolopyrans, **9d** from the base-catalyzed reaction of substituted piperidin-4-ones (**8d, scheme 3.3, in Table 3.8**), pyrazol-5-ones (**6**), and malononitrile (**7**) in ethanol at 20 °C. In our case, we found that there was no need of triethylamine as a catalyst in synthesis of **9d** as shown in **Table 3.8** because the presence of alkyl substituent at nitrogen atom of the piperidinone increases its basicity high enough to make the process autocatalytic. However, it was observed during the experiment that a base catalyst, such as triethylamine is necessary for all other reactions (**preparation of 9a-h and 13a-c, Table 3.8**). The structures of all the spiro compounds that were prepared were confirmed by the usual method and by comparison with the known structures of 6-amino-5-cyanospiro-4-(piperidine-4')-2*H*,4*H*-dihydropyrazolopyrans such as **9d** which have been determined by available IR and NMR data in literature. According to Anatoliy *et al.*[92] the compound **9d** exists in the tautomeric form **9d(A)** as opposed to **9d(B)** as shown in **Figure 3.19** which was corroborated in our findings as well.
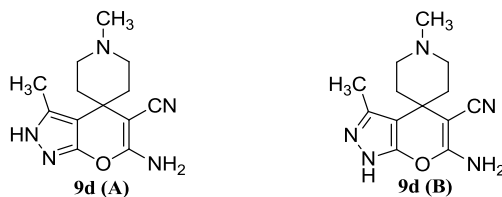
Figure 3.19 The tautomeric forms of the spiro-pyranopyrazole scaffold **9d**.
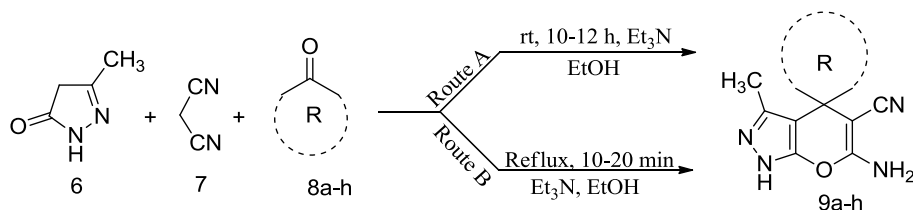
Where 8a-h= Isatin, 5-Chloro-isatin, 5-Bromo-isatin, N-methyl-piperidine, 1,4-Cyclohexane dione, 1-Benzyl-4-piperidone, Acetophenone, 4-OH-acetophenone

Scheme 3.3 Synthesis of nitrile substituted spiro pyranopyrazole compounds: (a) without heating (room temperature) and (b) under reflux.

We observed that for the synthesis of spiro compounds **(9a-h and 13a-c)**, reflux method (80-100°C) is much better than the room temperature method in terms of the yields. This is because of the better yield obtained and the lesser time taken by the reaction through the refluxing protocol **(route B)** as shown in **scheme 3.3** and **3.4**. The comparison of percentage yield and the reaction completion time for both refluxing as well as the room temperature methods (20-25 °C) is shown in **Table 3.8** and the corresponding graphs are shown in **Figure 3.20** and **3.21** respectively. In **Table 3.8**, the first eight compounds from **9a-h** were synthesized by **scheme 3.3** and the last three compounds **13a-c** were synthesized by **scheme 3.4**. Interestingly, a close observation of **scheme 3.3** (-CN substituent at the 5′ position of the pyran ring) and **scheme 3.4** (-COOC$_2$H$_5$ substituent at the 5′ position of the pyran ring) reveals that there is not much difference in the yield or time of the reaction after substitution of the ester group in place of nitrile group **(scheme 3.4)** at 5th position in the pyran ring.
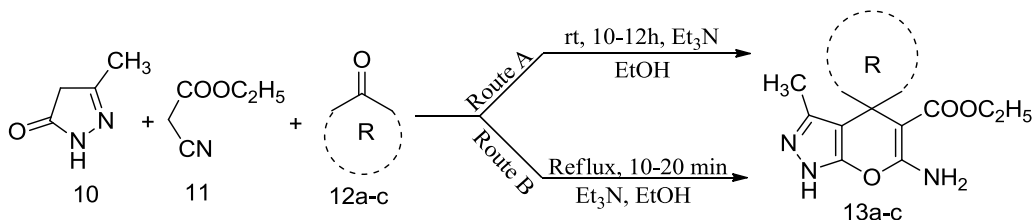
Where 12a-c= Isatin, 5-Chloro-isatin, 5-Bromo-isatin,

Scheme 3.4 Synthesis of ester substituted spiro pyranopyrazole derivatives: (a) without heating (room temperature) and (b) under reflux.

Table 3.8: Synthesized substituted spiro-pyranopyrazoles.

No	Ketones (R =)	Compd.	Route A[a] (%)[c]	(T)[d]	Route B[b] (%)	(T)	Observed m.p. (°C)	Ref
1	Isatin **(8a)**	**(9a)**	60	600	70	10	272-274	**93**
2	5-Cl-isatin **(8b)**	**(9b)**	70	600	85	12	270-272	**94**
3	5-Br-isatin **(8c)**	**(9c)**	75	480	82	10	290-291	-
4	N-methyl-piperidione **(8d)**	**(9d)**	72	660	80	15	160-162	**95**
5	1,4-Cyclohexanedi-one **(8e)**	**(9e)**	60	1200	70	20	158-160	-
6	1-Benzyl-4-piperidone **(8f)**	**(9f)**	65	720	78	20	188-190	-
7	Acetophenone **(8g)**	**(9g)**	77	600	85	10	212-213	**96**
8	4-OH-acetophenone **(8h)**	**(9h)**	78	720	90	10	111-112	-
9	Isatin **(12a)**	**(13a)**	80	600	85	10	279-280	**94**
10	5-Cl-isatin **(12b)**	**(13b)**	65	600	75	12	269-270	**94**
11	5-Br-Isatin **(12c)**	**(13c)**	80	720	90	10	265-267	-

[a] one-step room temperature; [b] one-step reflux; [c] isolated yields; [d] time in minutes.
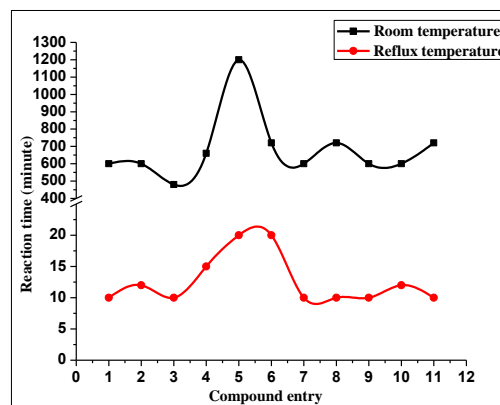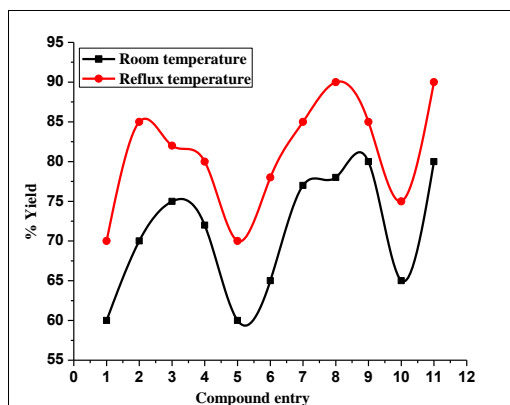
Figure 3.20 Shows the plot of compound entr vs % yield for spiro-molecules.

Figure 3.21 Shows the plot of compound entry vs % reaction time for spiro-molecules.

3.7 Anticancer activity on Hep3B cell line

3.7.1 Cell line and culture medium: Human hepatocellular carcinoma cell line, Hep3B were obtained from NCCS, Pune, India, cultured in a humidified incubator set at 37°C, 5% CO_2, in minimal essential medium (MEM; Hi media, # 41500-067) supplemented with 10% fetal bovine serum (FBS; Invitrogen, #26140-079) and 100U/mL penicillin, 100μg/mL streptomycin (Invitrogen, # 10378-016). Cells were

typically grown to 60–70% confluence, rinsed in phosphate-buffered saline (PBS), detached by treating with trypsin (0.05% trypsin) for 2 min and placed into fresh medium prior to treatments.

3.7.2 Determination of *in-vitro* cell cytotoxicity by *MTT assay*: For determining the *in-vitro* cytotoxicity, Hep3B cells were seeded at a density of 4000 cells per well in 96 well plates and incubated overnight at optimum culture conditions. The drug stocks at different dilutions were prepared in 100μl volume of DMSO (0.2%; SDFCL, # 2032). A DMSO control was also performed. For each compound, five dilutions were prepared and measurements were performed in triplicates. Following treatment for 24h, 20μl of MTT (Stock concentration 5 mg/ml; Sigma, #M5655) dissolved in 1 X PBS was added to each well at a final concentration of 1mg/mL and incubated for 4h. After 4 h, media was aspirated from all wells. Formazan crystals formed due to presence of live cells were solubilized in 150 μL DMSO. Readings were obtained at 495 nm with a differential filter of 630 nm using an enzyme-linked immune-sorbent assay (ELISA) micro-plate reader (Start-fax 2100, Awareness Tech. Ltd). The concentration required for 50% inhibition of viability (IC_{50}) was determined graphically. Percentage of viable cells was calculated using the formula:

Viability (%) = (mean absorbance value of drug treated cells) / (mean absorbance value of control) *100

3.8 Calf Thymus DNA binding study by OD method

3.8.1. Materials and methods for DNA intercalation study: DNA intercalation studies were performed using UV-Visible spectroscopy with calf thymus DNA (CT-DNA, Calbiochem). Stock solution of CT-DNA was prepared by dissolving it in Tris-EDTA (TE) buffer solution and the concentration of dissolved DNA was determined by Nanodrop (Simply Nano, GE Healthcare Life Sciences) at 260 nm. Purity of DNA was checked by monitoring the ratio of the absorbance at 260 nm to 280 nm. The spiro and non-spiro compounds at IC_{50} concentration, obtained from cell cytotoxicity assay were used for DNA interaction study. Briefly, each compound was mixed separately with different concentrations of CT-DNA prepared by serial dilution. The absorption spectra of only DNA at different dilutions and DNA in mixture with different drug concentrations were measured through nanodrop at 260 nm. The readings were taken either just after mixing the drug and DNA (0h) or after 3h of incubation at 37°C. TE and TE with individual compound were set as blank while measuring the optical density of DNA and DNA plus compounds respectively.

3.9 Results and Discussion

3.9.1 Anticancer activity of non-spiro pyranopyrazole scaffolds: With the synthesized non-spiro pyranopyrazole pharmacophores in hand, we selected all the prepared compounds and tested them for *in-vitro* anticancer activity against the Hep3B hepatocellular carcinoma cell line and the results are shown in

Figure 3.22 and **3.23**. The reason for testing them selectively for anticancer activity was that very few reports had appeared on the antineoplasmic activity of pyranopyrazoles; we did a preliminary cytotoxic study and found promising results. Thus encouraged, we decided to test the DNA binding of these synthesized compounds to get some insight into the mechanism of their antineoplasmic activity. The Hep3B cell line has been previously used by various scientists for evaluating the cytotoxicity of several systems.[97]
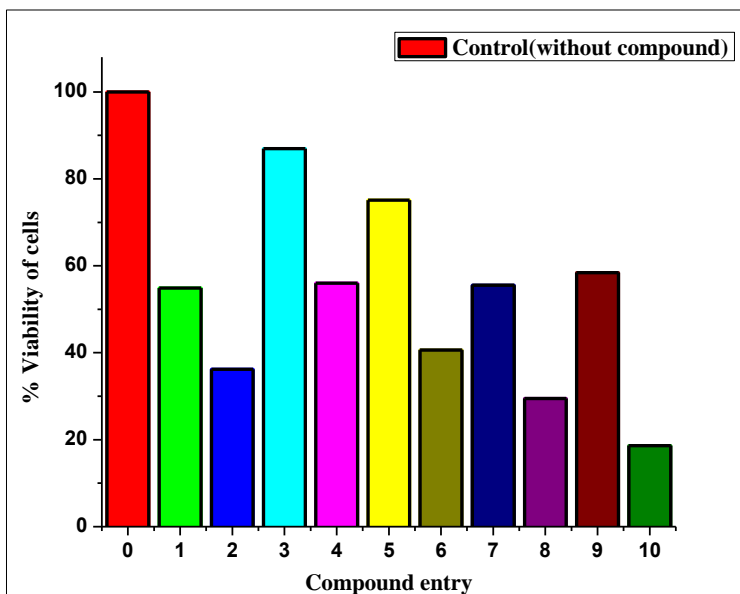
Figure 3.22 Shows the plot of compound entry vs % viability of cells at 64 µg/ml.
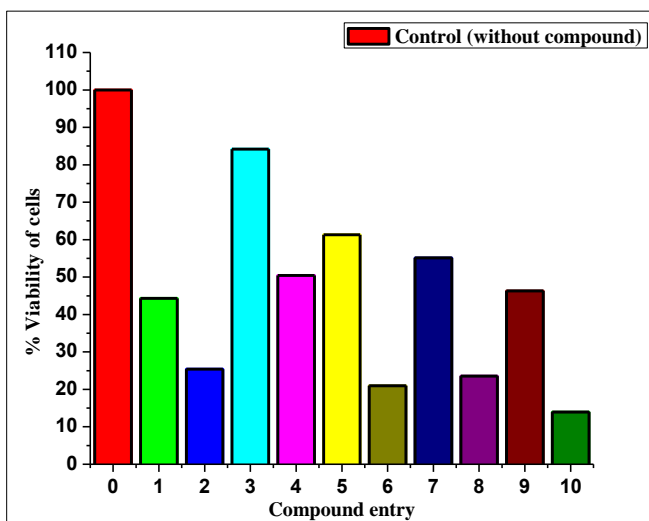
Figure 3.23 Shows the plot of compound entry vs % viability of cells at 128 µg/ml.

118

The IC$_{50}$ values of all the synthesized non-spiro compounds are shown in **Table 3.9**. Although the values obtained are significant but a closer observation shows that compound entry no. 8 (**5h**) and 10 (**5j**) as shown in **Table 3.9** are the best molecules showing the IC$_{50}$ value of 8μm. The molecules which show the significant IC$_{50}$ values are in the order as: **5j≈5h>5b>5f>5a≈5g> 5d≈5e≈5i>5c** and is represented by the corresponding compound entries as **10≈8>2>6>1≈7>4≈5≈9>3** as shown in **Table 3.9**. The overall activity and the graphical representation of % cell viability at various concentrations are shown in **Figure 3.24**.
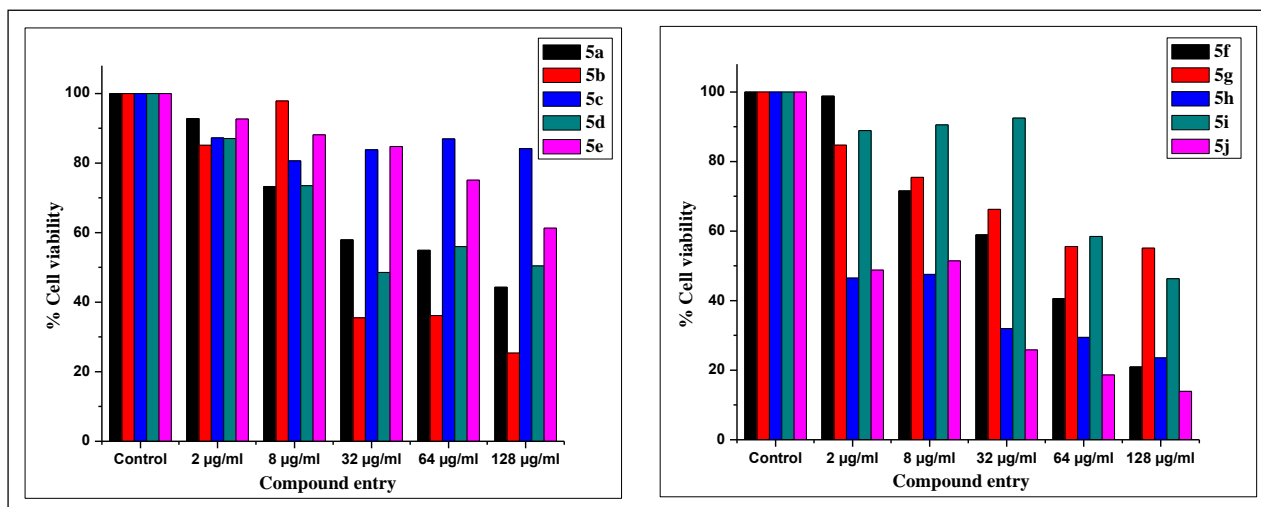
Figure 3.24 Shows the graphical representation of % cell viability at various concentrations of drugs.

Table 3.9: Cytotoxicity results of first five and next five (non-spiro) compounds.

No.[a]	IC$_{50}$[b]	No.	IC$_{50}$
1	64	6	32
2	8-32	7	64
3	>>128	8	8
4	128	9	128
5	128	10	8

[a]compound no.; [b]in μg/ml.

3.9.2 Anticancer activity of spiro pyranopyrazole scaffolds

The *in-vitro* anticancer activity of all the synthesized spiro compounds were tested against Hep3B cell line and the results obtained at 64 μg/ml and 128 μg/ml are shown in **Figure 3.25** and **3.26** respectively. The spiro compounds show more cytotoxic effect at 128 μg/ml as shown in **Figure 3.26**. A closer look of the **Figure 3.25** and **3.26** shows that for compound entry no. 10 (**13b**) the cytotoxic activity is not reliable at 128 μg/ml because the compound **13b** increases the number of cancer cells (Hep3B cells) by labor of

division at this concentration but at 64µg/ml the compound **13b** shows the significant activity. The calculated IC_{50} values of all the spiro compounds are shown in **Table 3.10**.
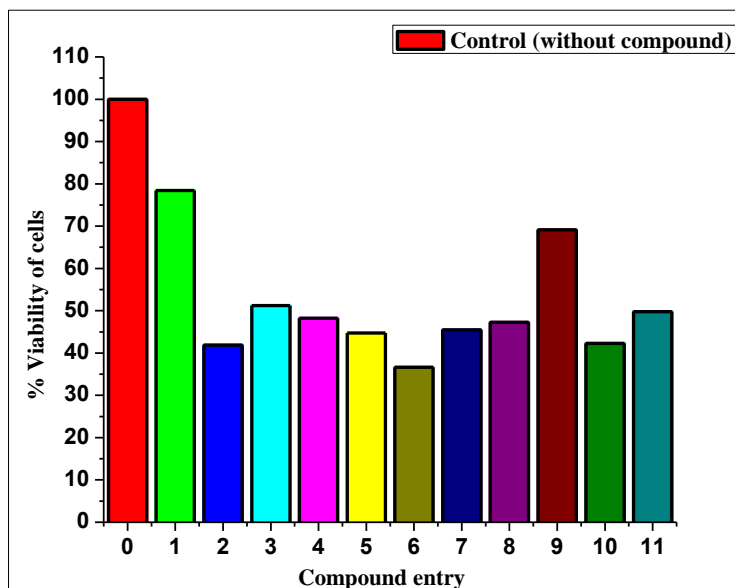
Figure 3.25 Shows the plot of compound entry vs % viability of cells at 64 µg/ml.
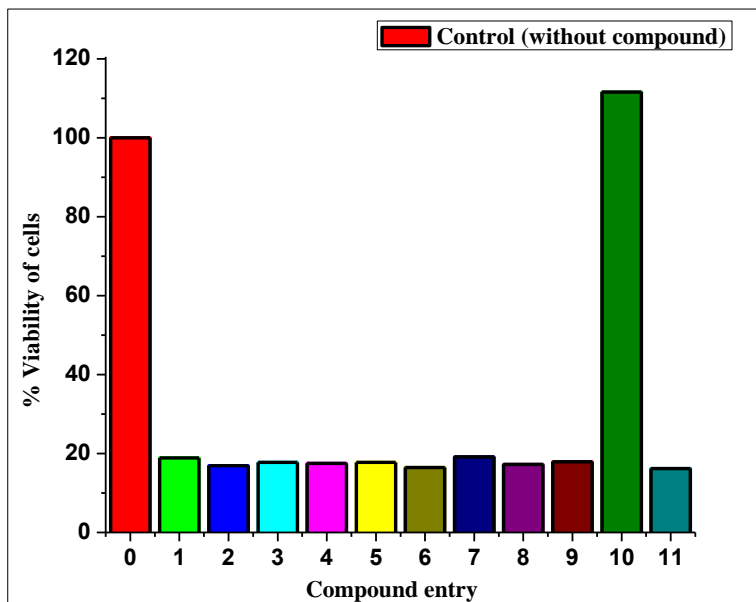
Figure 3.26 Shows the plot of compound entry vs % viability of cells at 128 µg/ml.
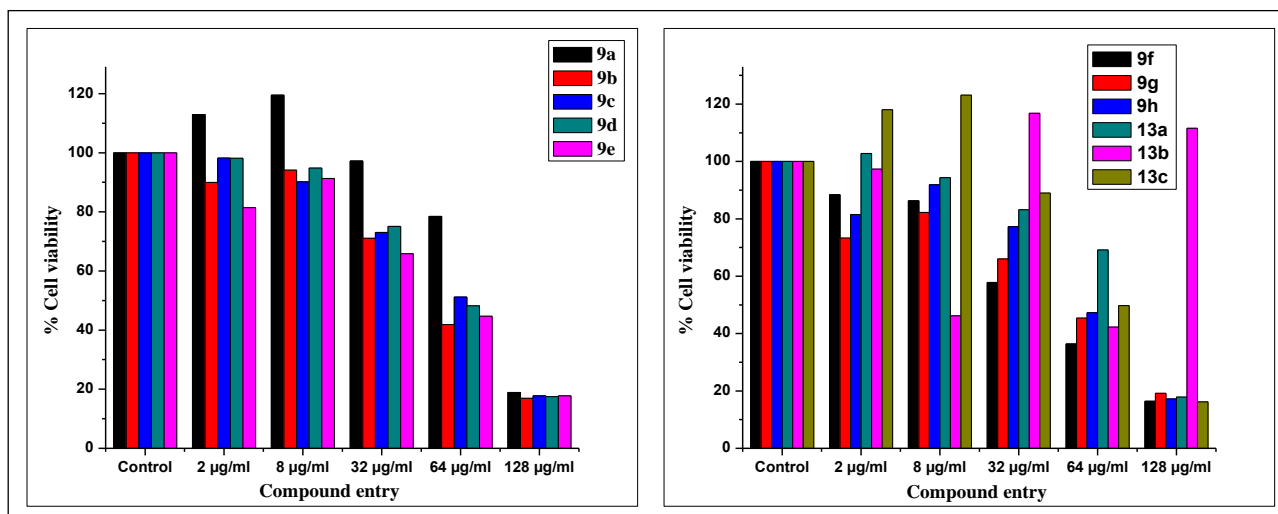
Figure 3.27 Shows the graphical representation of % cell viability at various concentrations of drugs.

All the compounds show significant anticancer activity except compound entry no. 1 (**9a**) and 9 (**13a**) showing IC_{50} values in the range of 64-128 μm. A closer observation of **Table 3.10** shows that the -CN substituted compounds **(synthesized by scheme 3.3, entry no. 1-8, 9a-h)** and $COOC_2H_5$ **(synthesized by scheme 3.4, entry no. 9-11, 13a-c)** substituted compounds show comparable anticancer activity. Some -CN substituted compounds like **9b**, **9e,** and **9f** (entry no. 2, 5, 6) show much better IC_{50} values than all other in -CN substituted spiro series as well as $COOC_2H_5$ substituted spiro series. The overall activities of all the spiro compounds at various concentrations are shown in **Figure 3.27**.

Table 3.10: Cytotoxicity results of first six and next five (spiro) compounds.

No.[a]	IC_{50}[b]	No.[a]	IC_{50}[b]
1	64-128	7	32-64
2	32-64	8	64
3	64	9	64-128
4	64	10	64
5	32-64	11	64
6	32		

[a]compound no.; [b]in μg/ml.

3.9.3 DNA binding studies

3.9.3.1 DNA binding study of Calf Thymus DNA (CT-DNA) by the best five non-spiro pyranopyrazole scaffolds

The two strands of DNA are bound together mainly by stacking interactions, hydrogen bonds and hydrophobic effect between the complementary bases. The bonds limit the resonance of the aromatic ring and hence the absorbance of UV light is limited; when the DNA double helix is treated with agents that disrupt the interactive force holding the double helical structure, the absorbance increases. These two spectral features[98] of DNA are known as hypochromic and hyperchromic effect respectively which provides information about the conformational and structural changes in DNA. Here, out of ten non-spiro pyranopyrazole compounds tested against Hep3b cell line, the best five molecules **5a**, **5f**, **5g**, **5h**, and **5j** were selected and tested for DNA binding study of CT- DNA by Nanodrop at 260 nm and all the results obtained at 0 hour and after 3 hour are shown in **Table 3.11** and the corresponding graphs are shown in **Figure 3.28** and **3.29** respectively. At 0 (zero) hour, we observed that after addition of compounds **5a**, **5f**, **5g**, **5h**, and **5j** at different concentrations there was no significant difference in OD values. However, after 3 hour the OD value of DNA with compound shows a trend towards an increase in absorption or a hyperchromic shift which can be taken as a confirmation of drug binding with the CT-DNA molecule. The hyperchromic effect can be putatively attributed to several effects like, a damage of the DNA by the drug molecule resulting in unfolding or unzipping of the secondary structure or the double helix resulting in increased absorbance. The results were more prominent at lower concentrations of the DNA when incubated for 3 hours with DNA. Therefore, the results certainly confirm that these compounds have the potential to interact with DNA altering their spectral properties and simultaneously exert a cytotoxic effect to cancer cells.

Table 3.11: DNA binding study of CT DNA by non-spiro pyranopyrazole molecules.

| S. No | DNA conc.µ g/ml | Readings at 0 hour TE + Drug (Blank) | | | | | | Readings after 3hour TE + Drug (Blank) | | | | | |
| | | OD values from nano drop exp. | | | | | | OD values from nano drop exp. | | | | | |
		DNA	5a	5f	5g	5h	5j	DNA	5a	5f	5g	5h	5j
1	1.30	26.25	22.38	24.7	24.98	24.64	23.55	26.75	27.63	26.15	26.24	26.09	24.94
2	0.655	13.25	11.48	15.97	13.26	13.6	18.56	14.2	18.97	15.48	15.67	16.29	16.83
3	0.338	7.33	5.34	10.65	18.22	7.08	8.31	6.53	8.14	9.68	7.54	9.36	8.64
4	0.167	3.58	1.27	4.39	12.71	3.9	4.32	3.18	4.18	4.9	4.67	7.72	4.48
5	0.089	1.98	1.67	7.66	11.47	3.31	1.76	1.45	5.19	7.56	2.31	7.09	1.71
6	0.046	0.99	2.46	3.26	18.34	4.72	1.01	0.87	2.28	3.18	4.99	4.59	0.84
7	0.024	0.68	1.24	1.18	5.84	0.76	0.58	0.24	1.49	2.26	1.26	0.8	0.63
8	0.010	0.24	0.86	0.78	5.51	0.14	0.28	0.13	0.47	1.31	1.95	0.04	0.58
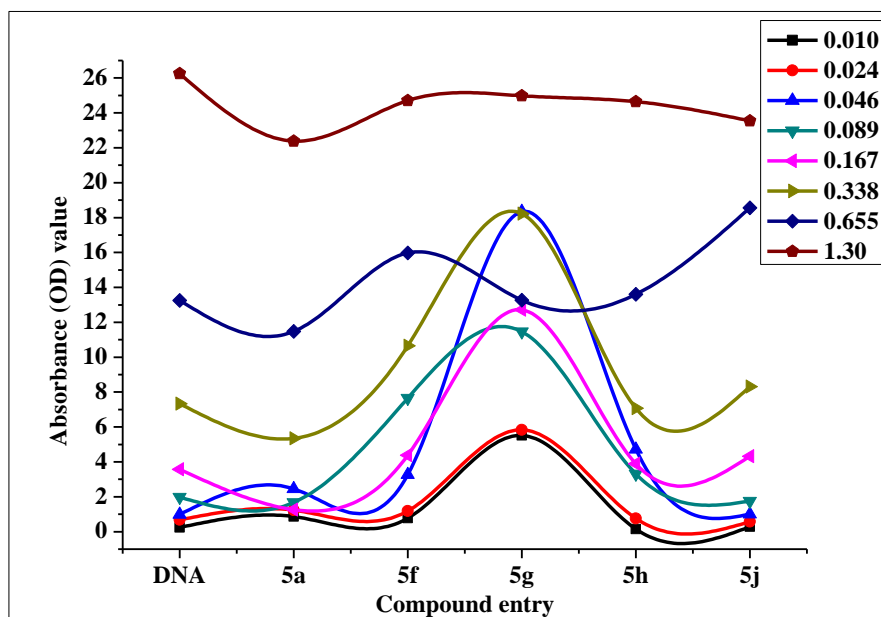
Figure 3.28 Absorption spectra of DNA in the absence and in the presence of increasing amounts of non-spiro-pyrazolopyran compounds at 0 hour.
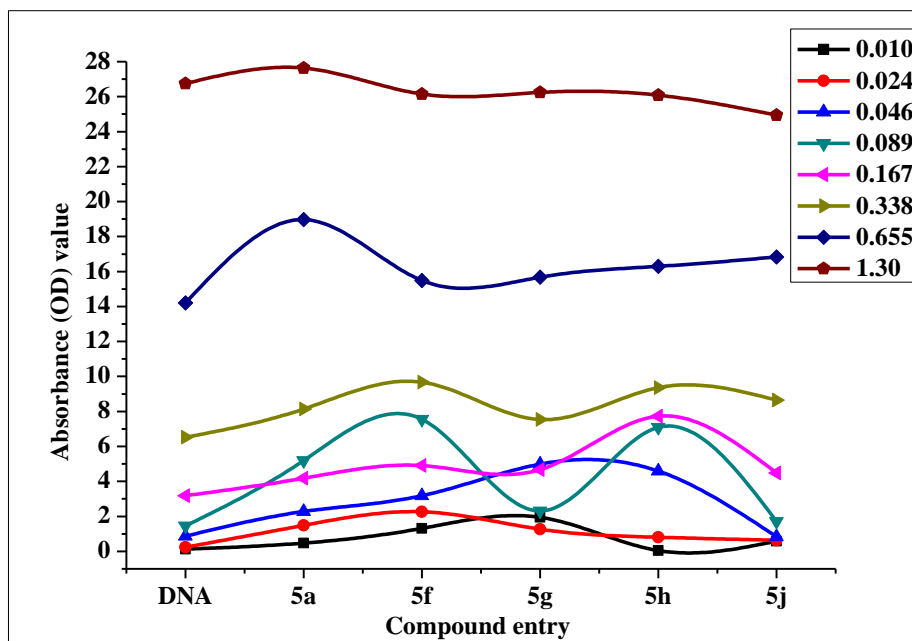
Figure 3.29 Absorption spectra of DNA in the absence and in the presence of increasing amounts of non-spiro-pyrazolopyran compounds after 3 hour.

3.9.3.2 DNA binding study of Calf Thymus DNA by the best five spiro pyranopyrazole scaffolds

Based on the principle of different type of interactions of compounds with DNA described above, out of the eleven spiro molecules tested against Hep3B cell line, the best five molecules were selected for DNA binding study. The absorption spectra of only DNA at different dilutions and in mixture with different drug concentrations was measured as described before. The results obtained are presented in **Table 3.12**. No significant difference in OD values after immediate addition of the drug and even after incubating the spiro compounds for 3 hours with DNA was observed. The change in OD values were not as significant compared to incubation of non-spiro compounds with DNA. This does suggest that spiro and non-spiro compounds probably have different mechanism induction of cytotoxicity; where majority of non-spiro compounds showed interaction with DNA resulting in a hyperchromic effect, similar observations were not obtained with spiro compounds.

Table 3.12: DNA binding study of CT-DNA by spiro-pyranopyrazole molecules.

		Readings at 0 hour TE+Drug (Blank)						Readings after 3 hour TE+Drug (Blank)					
No	DNA conc.µg/ml	OD values from nano drop exp. at 260 nm						OD values from nano drop exp. at 260 nm					
		DNA	9c	9d	9g	9h	13c	DNA	9c	9d	9g	9h	13c
1	1.000	21.37	19.7	21.69	19.82	22.94	19.93	20.89	20.80	22.25	21.30	23.16	20.09
2	0.561	11.22	11.48	12.25	11.07	13.57	11.37	11.82	11.76	11.90	11.31	13.91	11.67
3	0.291	5.8	5.39	5.41	5.64	5.54	6.24	5.91	5.96	5.49	5.51	5.81	6.71
4	0.143	2.8	2.1	2.86	2.75	2.66	3.04	2.74	2.86	2.78	2.83	2.82	3.42
5	0.073	1.38	1.84	1.36	0.94	1.24	1.29	1.23	2.18	1.37	0.89	1.43	1.46
6	0.037	0.67	0.31	0.64	0.8	0.61	0.11	0.54	0.62	0.71	0.82	0.70	0.17
7	0.018	0.32	0.11	0.32	0.3	0.2	0.16	0.33	0.19	0.28	0.46	0.28	0.21
8	0.008	0.16	0.02	0.19	0.004	0.03	0.03	0.13	0.05	0.18	0.03	0.20	0.02

The absorbance graph at 0 (zero) and 3 hour of the best selected spiro compounds at various concentration are shown in **Figure 3.30** and **3.31** respectively. The comparison of absorbance values for non-spiro and spiro pyranopyrazole compounds at concentration of 1.30 and 1 µg/ml at 0 (zero) hour and after 3 hour are shown in **Figure 3.32**. From the analysis of bar graph **(Figure 3.32)** we can say that the non-spiro compounds have higher intensity and are showing hyperchromic shift after 3 hour. On the other hand spiro compounds also showed hyperchromic shift after adding of drug but it is very less intense and prominent in case of spiro molecules as compared to non-spiro one.
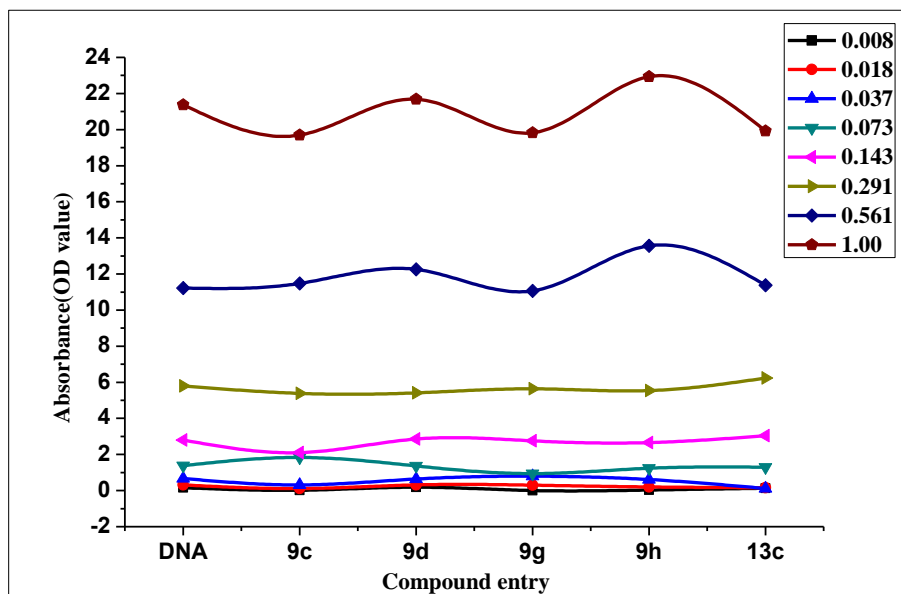
Figure 3.30 Shows the absorbance spectra of DNA in the absence and in the presence of spiro Pyranopyrazole at 0 hour.
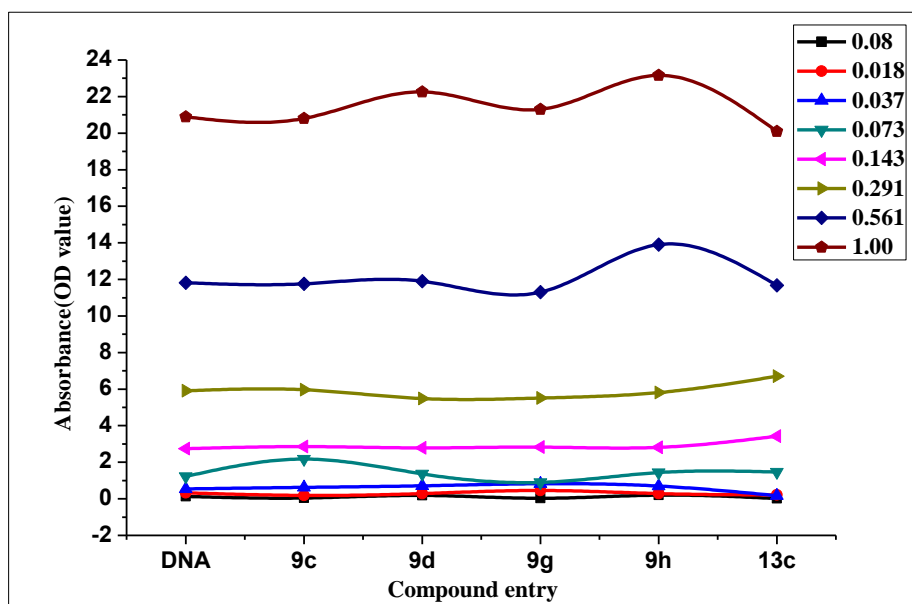
Figure 3.31 Shows the absorbance spectra of DNA in the absence and in the presence of spiro Pyranopyrazole after 3 hour.
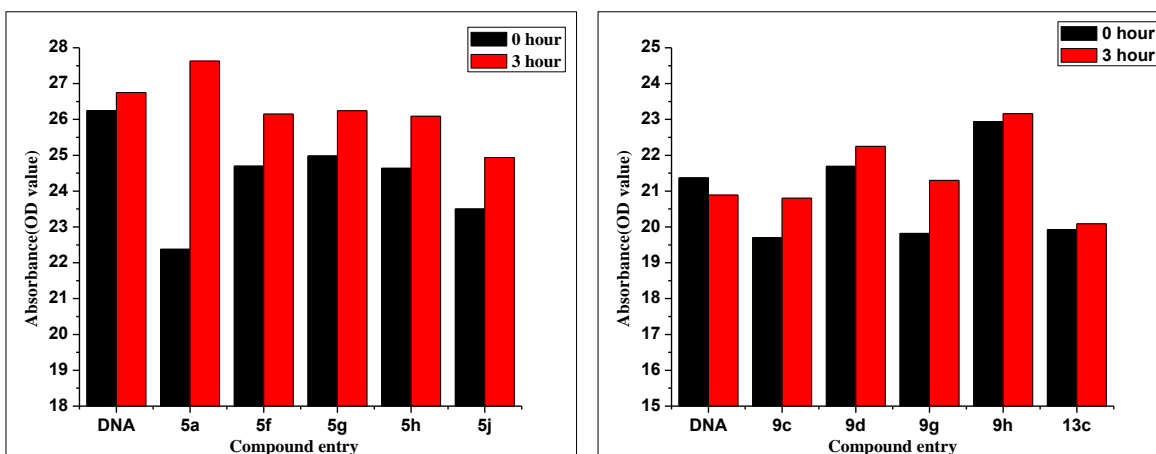
Figure 3.32 (Left)**:** the absorbance spectra of DNA in the absence and presence of non-spiro Pyranopyrazole compounds at 1.30 μg/ml; (right): absorbance spectra of DNA in the absence and presence of spiro pyranopyrazole compounds at 1.00 μg/ml.

3.10 Molecular Docking of the non-spiro molecule 5h

3.10.1 Software required

Molecular modeling software Auto Dock 4.2 installed on a PC with 2.3GHz processor, 4GB RAM with a dedicated Graphics Card of 2GB with windows XP SP2 as the operating system was used for the entire docking study.

3.10.2 Receptor used for docking

CDK-2 (Cyclin Dependent Kinase) enzyme co-crystallized with Mg-ATP ligand (PDB ID: 1HCK) is used as target receptor.

3.10.3 Experimental procedure of molecular docking

Among the reasons why CDK-2 was chosen as the target protein was that Foloppe *et al.*[99] had previously reported the pyranopyrazole scaffold as a potentialCDK-2 inhibitor in a virtual screening study. Thus, the molecular docking study was done on target protein CDK-2 which was downloaded from RCSB protein data bank. THR14 (T) and TYR15 (Y) residues of the GTYG cluster of ATP binding sites (residues 13 to 16) were used as flexible ones. Later on, the refinement of the target protein was done by removal of water molecules, adding polar hydrogens and kollmann charges. The grid was centered on the active site of the protein and a grid spacing of 0.375 Å and $60 \times 60 \times 60$ number of points was used for the docking study. The separate grid maps were generated by the auto grid program for all types of atom of the ligand structure and one for the electrostatic interaction. The energy minimized conformations of the synthesized ligand **5h** was obtained by using PRODRG online server (http://davapc1.bioch.dundee.ac.uk/prodrg/). The calculation of Gasteiger- Huckel charges for the energy minimized conformation of ligand **5h** was

done and saved in default format of Autodock. For 50 runs, around 50 possible binding confirmations were generated by Autodock using LGA search. A maximum number of 2.5×10^5 energy evaluations and 2.7×10^4 generations has been done by default protocol with initial population of 150 randomly placed individuals. A mutation rate of 0.02 and a crossover rate of 0.8 were used.

3.10.3.1 Validation of docking

Standard drug Flavopiridol is used for calibration and validation of docking process. Subsequently, the hydrogen-bonding **(Figure 3.33)** and van der Waals interaction **(Figure 3.34)** of the standard drug (CDK-2 inhibitor) with the receptor protein was also determined for validation.
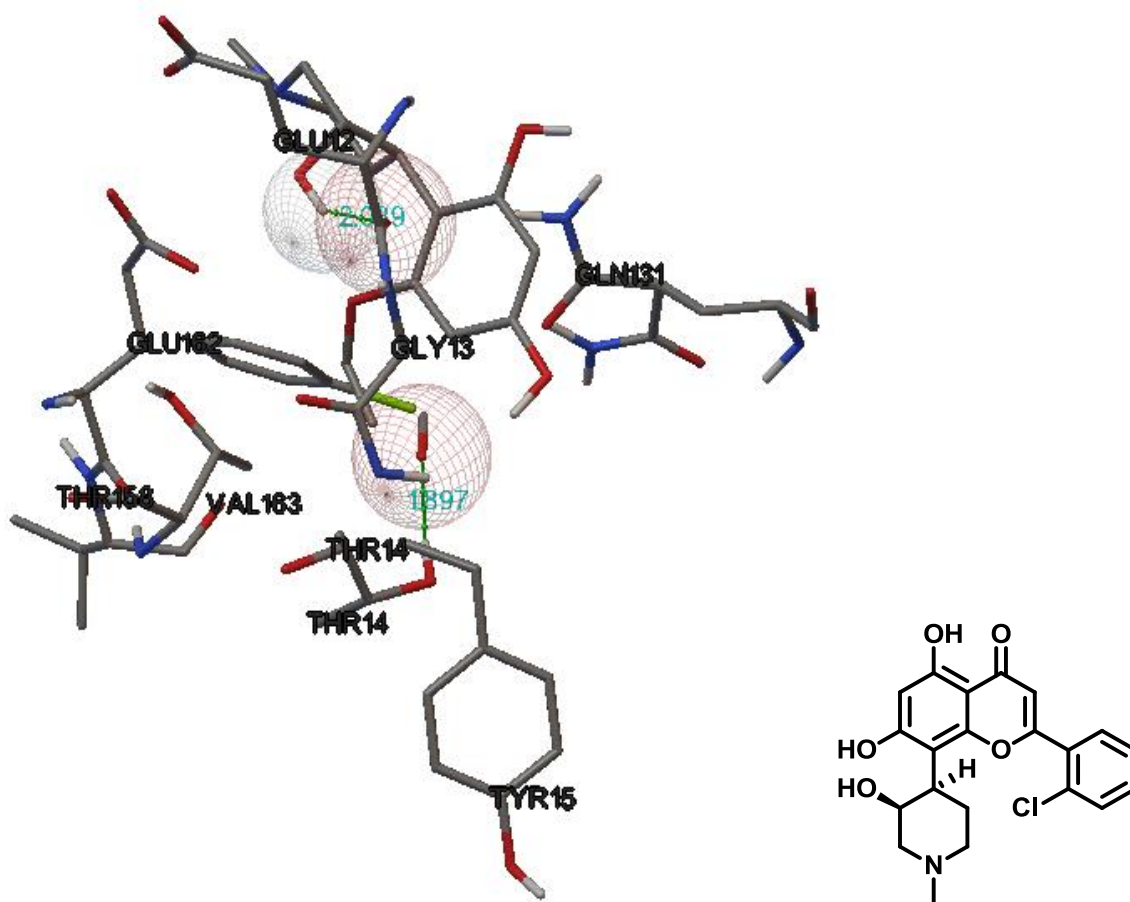
Figure 3.33 H-bonding interaction of standard drug Flavopiridol with CDK-2 and the structure of Flavopiridol.
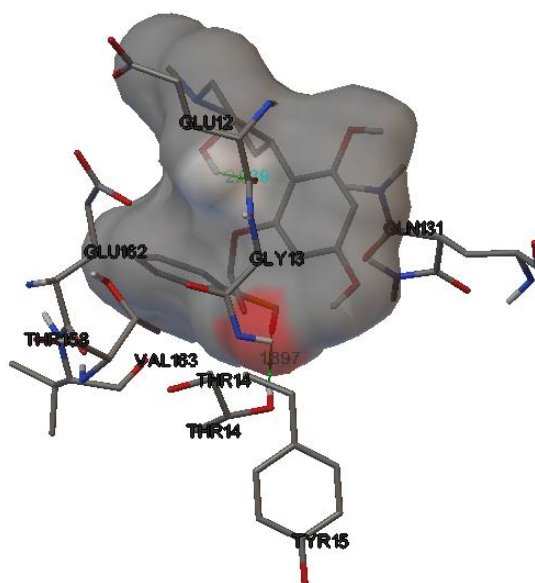
Figure 3.34 Showing the van der Walls interaction of standard drug Flavopiridol with CDK-2.

3.11 Hydrogen bonding interaction

Hydrophilic body (–NH) in pyrazolon ring and cyano group (–CN) attached with pyran ring behave as hydrogen bond donor and hydrogen bond acceptor respectively in the designed analog **5h** and are responsible for hydrogen bonding interaction with hydrophilic amino acids GLY-13 and GLU-12 (**Figure 3.35**) of target protein.
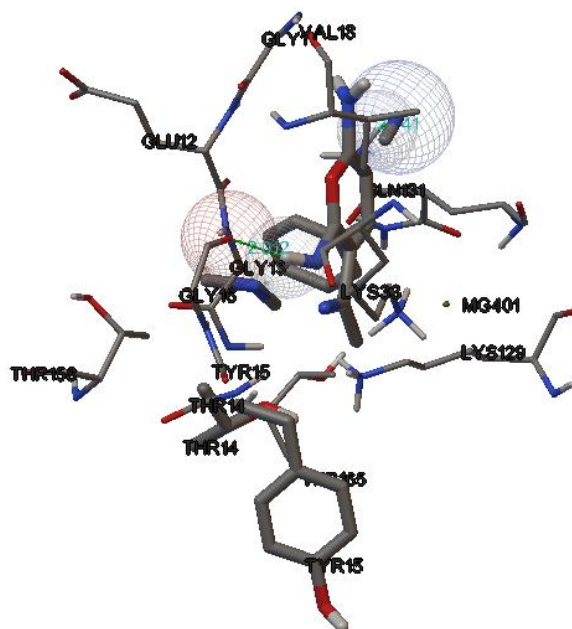
Figure 3.35 Showing the H-bonding interaction of non-spiro pyranopyrazole **5h** with CDK-2.

GLY-13 and GLU-12 are active site amino acid residues that are mainly involved in hydrogen bond interaction with designed analogs and might be responsible for CDK-2 inhibition activity as depicted. Docking studies revealed that, cyano (–CN) and –NH of designed ligands act as hydrogen bond acceptor and hydrogen bond donor, respectively, in the ligand-receptor interactions.

3.12 Van der Waals interaction

Van der Waals interaction plays a major role in the determination of binding free energy of ligand-receptor complex. Amino acids GLU12, GLY13, TYR15, GLY16, VAL18, LYS33, LYS129, and GLN131 of target receptor are indeed responsible for van der Waals interaction **(Figure 3.36)** with ligands **5h (Table 3.7)** to form stable receptor-ligand complex. van der Waals interaction exhibited by prototype compound **5h** with target protein and amino acid residues present within the van der Waals radius are shown in **Figure 3.36**. In addition, another docking parameter, namely, predicted inhibitory constant (K_i) was also determined. The inhibitory constant is a measure of compound's inhibitory potency of a biological or biochemical function. Inhibitory constant is exponential to the binding free energy of receptor ligand complex. The synthesized analog **5h** showed significant inhibitory constant values of 60.68 nM against CDK-2 enzyme with that of standard Flavopiridol (129.29 nM). The synthesized analogue **5h** not only showed a huge increase in the binding energy (-9.85 kcal/mol) *vis-à-vis* Flavopiridol but also in line with the theoretical values obtained for the calibration of other well-known CDK inhibitors like kenpaullone (-10.68 kcal/mol), indirubin (-11.20 kcal/mol) and olomoucine (-8.90 kcal/mol).
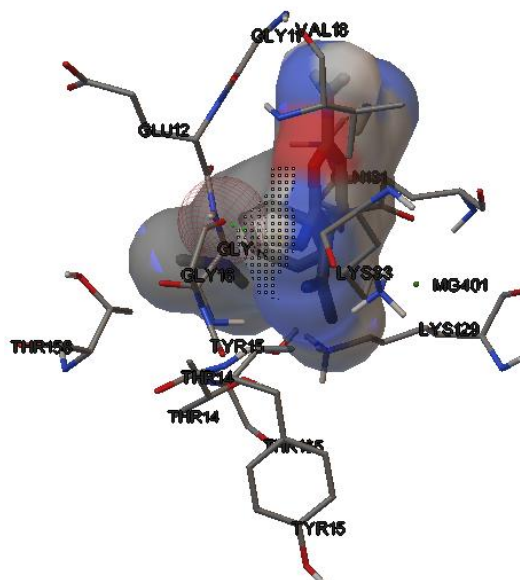
Figure 3.36 Showing the van der Walls interaction of non-spiro pyranopyrazole **5h** with CDK-2.

3.13 Conclusions

Two series of pyranopyrazole compounds (spiro and non-spiro substituted) were synthesized by environmental friendly MCR methodology. The synthesized molecules were tested for their cytotoxicity on Hepatocellular carcinoma Hep-3B cell line and it was found that many compounds, especially the non-spiro ones, inhibited the growth of cancer cells in dosage dependent manner. To get an insight into the mechanism of antineoplasmic activity, their DNA intercalation study was performed by UV-visible spectroscopy which showed that the non-spiro molecules do interact with DNA. The latter result also correlates to their relatively better *in-vitro* activity. Finally, the molecule with best IC_{50} value was selected and docked against CDK-2 protein. The docking results conferred with the overall experimental findings that there is significant binding interaction with the vital amino acid residues which may be contributing to their cytotoxic activity.

3.14 Experimental

3.14.1 General procedure for synthesis of non-spiro pyranopyrazole[86]

Scheme 3.2 (Route A): Here although the synthesized non-spiro molecules are different from Part A of Chapter-3 but we follow the same procedure in the synthesis of these molecules as discussed in Part A of Chapter-3.

Scheme 3.2 (Route B): (MWA synthesis): For MWA synthesis also we follow the same procedure as discussed in Part A of Chapter-3.

3.14.2 General procedure for synthesis of spiro-pyranopyrazole

Scheme 3.3 (Route A): A solution of the corresponding ketone (10.0 mmol), malononitrile (10.0 mmol), pyrazol-5 one (10.0 mmol), and 0.5 mL of triethylamine (no Et_3N in the synthesis of **9d**) was also added in absolute ethanol (25 mL) and stirred for 10-12 h at room temperature. The precipitate that formed was filtered off, washed with ethanol and hexane, and recrystallized from ethanol.

Scheme 3.3 (Route B): A solution of the corresponding ketone (10.0 mmol), malononitrile (10.0 mmol), pyrazol-5-one (10.0 mmol), and 0.5 mL of triethylamine (no Et_3N in the synthesis of **9d**) in absolute ethanol (25 mL) was refluxed (80-100°C) for 10-20 min. The precipitate that formed was filtered off, washed with ethanol and hexane, and recrystallized from ethanol.

Scheme 3.4 (Route A): A solution of the corresponding ketone (10.0 mmol), ethylcyanoacetate (10.0 mmol), pyrazol-5 one (10.0 mmol), and 0.5 mL of triethylamine was added in absolute ethanol (25 mL) and stirred for 10-12 h at room temperature. The precipitate that formed was filtered off, washed with ethanol and hexane, and recrystallized from ethanol.

Scheme 3.4 (Route B): A solution of the corresponding ketone (10.0 mmol), ethylcyanoacetate (10.0 mmol), pyrazol-5-one (10.0 mmol), and 0.5 mL of triethylamine in absolute ethanol (25 mL) was refluxed for 10-20 min. The precipitate that formed was filtered off, washed with ethanol and hexane, and recrystallized from ethanol.

3.14.3 Characterization data: For ^{1}H and ^{13}C-NMR spectra see Appendices A-1.

6'-amino-5-bromo-3'-methyl-2-oxo-1'H-spiro[indoline-3,4'-pyrano[2,3-c]pyrazole]-5'-carbonitrile (9c): Brown solid. ^{1}HNMR (400MHz, d$_6$-DMSO) δ: 12.31 (s, 1H), 10.73 (1H), 6.81-7.40 (3H), 2.46 (2H), 1.53 (s, 3H). ^{13}CNMR (400MHz, d$_6$-DMSO) δ: 178.41, 162.62, 155.52, 141.05, 135.59, 134.54, 131.69, 127.45, 118.74, 114.57, 112.02, 95.17, 54.93, 47.83, 9.77.

6'-amino-1,3'-dimethyl-1'H-spiro[piperidine-4,4'-pyrano[2,3-c]pyrazole]-5'-carbonitrile(9d): White solid. ^{1}H NMR (400MHz, d$_6$-DMSO) δ: 11.97 (s, 1H, NH); 6.49 (s, 2H, NH$_2$); 2.81 (m, 2H); 2.62 (m, 2H); 2.26 (s, 6H); 2.10 (m, 2H); 1.77 (m, 2H). ^{13}CNMR (400MHz, d$_6$-DMSO) δ: 172, 161.1, 139.1, 135.2, 130.2, 128.20, 68.10, 54.35, 33.35, 33.17.

6'-amino-3'-methyl-4-oxo-1'H-spiro[cyclohexane-1,4'-pyrano[2,3-c]pyrazole]-5'-carbonitrile (9 e): Dark yellow solid. ^{1}H NMR (400MHz, d$_6$-DMSO) δ: 12.62 (s, 1H, NH); 5.11 (s, 2H, NH$_2$); 2.81 (m, 2H); 2.62 (m, 2H);; 2.10 (m, 2H); 1.77 (m, 2H); 1.93 (s, 3H). ^{13}CNMR (400MHz, d$_6$-DMSO) δ: 140.98, 130.40, 127.54, 102.75, 40.57, 39.95, 12.06.

6'-amino-1-benzyl-3'-methyl-1'H-spiro[piperidine-4,4'-pyrano[2,3-c]pyrazole]-5'-carbonitrile (9f): Yellow solid. ^{1}HNMR (400MHz, d$_6$-DMSO) δ: 12.17 (s, 1H), 10.51 (1H), 6.72-7.25 (3H), 3.64 (2H), 0.72 (s, 3H), 1.56 (t, 3H), 2.45 (q, 2H). ^{13}CNMR (400MHz, d$_6$-DMSO) δ: 129.28, 128.54, 119.9, 62.45, 53.28, 50.15, 40.56, 29.17, 12.21.

Ethyl 6'-amino-6-bromo-3'-methyl-3-oxo-1'H-spiro[indoline-2,4'-pyrano[2,3-c]pyrazole]-5'-carboxylate (13c): White solid. ^{1}HNMR (400MHz, d$_6$-DMSO) δ: 12.17 (s, 1H), 10.51 (1H), 6.72-7.25 (3H), 3.64 (2H), 0.72 (s, 3H), 1.56 (t, 3H), 2.45 (q, 2H). ^{13}CNMR (400MHz, d$_6$-DMSO) δ: 179.72, 163.39, 154.76, 141.75, 130.16, 130.59, 125.97, 113.74, 111.19, 96.86, 73.97, 59.27, 47.70, 39.93, 13.64, 9.45

Chapter III

Part C

Novel Grinding Method for the Synthesis of Pyranopyrazole and their Evaluation as Antimicrobial and *in-vitro/in-vivo* Anti-oxidant Agents

3.15 Introduction

Environmental considerations and simplicity of preparative procedure have bound organic chemists to look for greener synthetic choices and hence multi-component reactions (MCRs) are now emerging as a responsible alternative tool in organic synthesis.[100] MCRs are also crucial in the design of new and bioactive small organic molecules[101a-i] as these procedures have distinctive green-chemistry[102a-d] and atom-economy benefits.[103a-b] With the emergence of drug-resistant pathogens, there has been increasing research towards the discovery of new small organic molecules that target these pathogens.[104a-b] Moreover, there has been a more than 40 year gap between the discovery of new small molecule antibiotics: fluoroquinolones (in 1962) and the oxazolidinone linezolid (in 2000).[105] Hence, the search for better and resilient antimicrobials continues. Similarly, fungal-infections have been unremittingly increasing especially in immunity-deficient patients such as those suffering from AIDS, cancer, etc.[106a-b] Fluconazole, itraconazole, and ketoconazole are some of the azole containing compounds that have been well established as first line of defense against fungal infections.

Our efforts to prepare pyrazole and pyran based heterocyclic compounds as potential bioactive molecules, led us to the synthesis of pyranopyrazoles, i.e. pyran fused pyrazoles. 4*H*-Pyrans have been reported as the basic structural pharmacophores for a range of useful compounds such as natural products[107a-b], other biologically and pharmacologically active compounds[108a-d], agrochemicals[109], etc. Therefore, the synthesis of such compounds has generated strong scientific interest. Similarly, pyrazoles have also been reported as excellent starting materials for various bioactive small organic molecules.[110a-b] Pyranopyrazoles have also been described as physiologically active compounds having applications such as antimicrobial[111], antiviral[112], sex pheromone[113], etc. Therefore, the designing and synthesis of such heterocyclic fused-core compounds continues to draw scientific curiosity.

Regarding the chemical synthesis of the pyranopyrazole pharmacophore, several reports are available in the literature. The first reported synthesis related to the reaction between 3-methyl-1-phenylpyrazolin-5-one and tetracyanoethylene.[114] Subsequently, other groups reported related syntheses of a series of 6-amino-5-cyano-4-aryl-*4H*-pyrazolo[3,4-*b*]pyrans.[115a-b] A useful three-component reaction between *N*-methylpiperidone, pyrazolin-5-one and malonodinitrile was reported by Shestopalov and co-workers.[116a-b] Subsequently, the same group described a new four-component MCR assisted synthesis of pyranopyrazoles.[117] Peng and co-workers[118] outlined an interesting variation of the MCR strategy by utilizing the environmentally safe technology of combined microwave and ultrasound irradiation. Vasuki *et al*. reported a fast four-component reaction in water.[119] Schlager and co-workers disclosed an altered multistep synthesis of pyranopyrazoles starting with 1-phenylpyrazole.[120] Recently, a few papers have revealed the use of catalyst[121a-b], nanoparticles[122], or traditional refluxing conditions.[123a-b] A three-

component proline-catalysed grinding method was disclosed by Guo and co-workers[124] followed by a similar DBU-catalysed report by Bhavanarushi *et al*.[125] However, none of the groups reported an exclusive four component, solvent-free grinding method assisted synthesis. In the same vein, while many reports are available regarding the applications of pyranopyrazoles but the full extent of their antimicrobial potential has not been explored given the fact that the search for multidrug resistant antimicrobials is the need of the hour. Furthermore, we wanted a novel and quick green route to the synthesis of these interesting pharmacophores, which encouraged us to take up their detailed synthesis and evaluation.

3.16 Results and Discussion

In this part of the thesis we report an efficient, eco-friendly, and solvent-free four-component reaction protocol for the synthesis of pyranopyrazole derivatives by grinding method. To the best of our knowledge, this is the first report of four component grinding synthesis of pyranopyrazoles. The prepared compounds were subsequently tested for their *in-vitro* antibacterial and antifungal activities. Initially, we followed the reported two-step grinding methodology where in the first step 3-methyl-1*H*-pyrazol-5(4*H*)-one was synthesized by grinding together ethyl acetoacetate and hydrazine hydrate in a mortar with pestle. In the next step, the resulting pyrazolon was collected without further purification and subjected to additional grinding by adding the aldehyde, malononitrile, and triethylamine as base for 5 min as shown in **Scheme 3.5**.
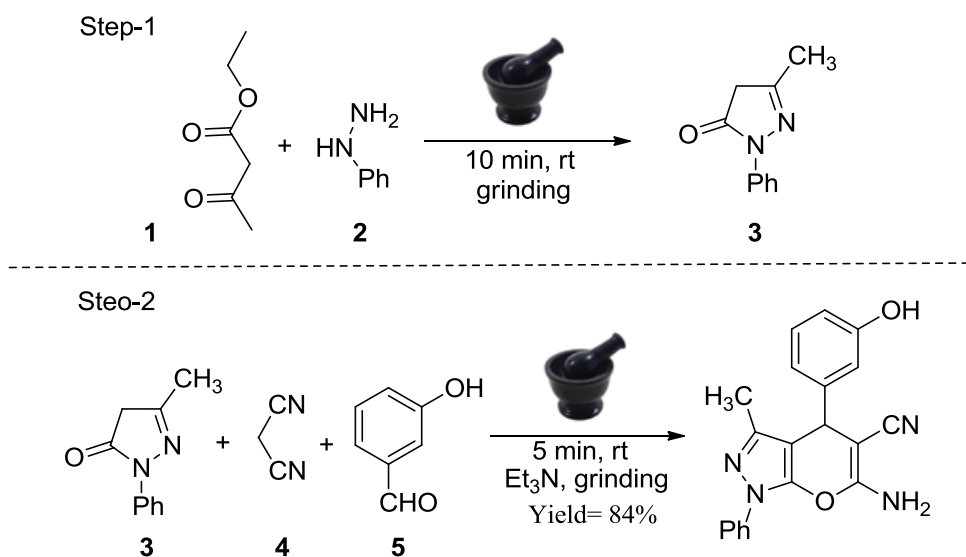
6c18 (entry no. 18 in Table 3.13 and 3.14)

Scheme 3.5 Route A, two-step strategy for the synthesis of *N*-phenyl substituted pyranopyrazole **6c18.**

The reaction was continuously monitored by TLC. But, when we tested **6c18 (entry no. 18, Table 3.14)** against the *E. coli* bacterial strain and then against *F. oxyparum* fungal strain, it was found to be inactive. The latter SAR (Structure-Activity Relationship) result coupled with the observation that the whole synthetic procedure took two steps, prompted us to look for: i) a modified pharmacophore and ii) a simpler swifter synthetic procedure. Hence, instead of going for the tedious two-step synthetic protocol we investigated the faster one-step route. In the swifter one-step protocol, all the four components viz. ethyl acetoacetate, hydrazine hydrate, aldehyde, malononitrile, and triethylamine were collected in a mortar and ground thoroughly using the pestle **(Scheme 3.6)**. Thus, by employing the one-step grinding assisted protocol the whole reaction sequence was over in 5 to 8 minutes. To get a better comparative idea, all the subsequent pyranopyrazoles were prepared by both the routes: route A (two-step grinding) and route B (one-step grinding), an appraisal of which is shown in **Table 3.13**.
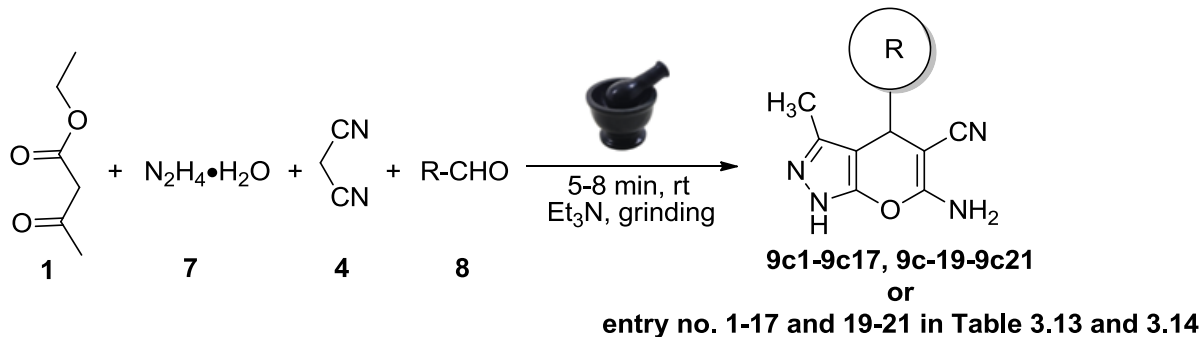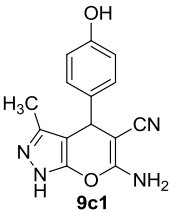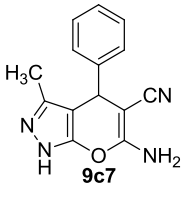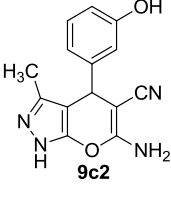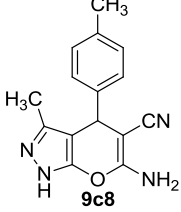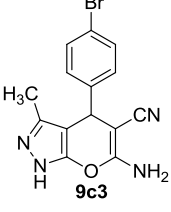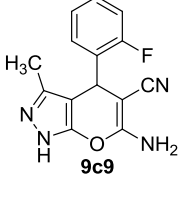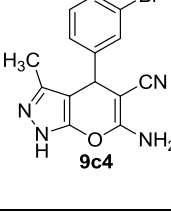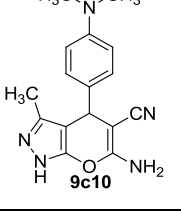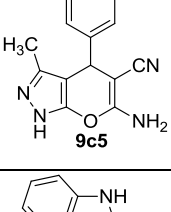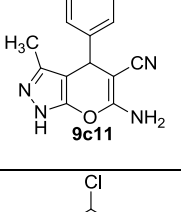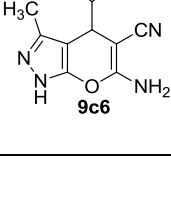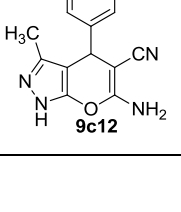
Scheme 3.6 Route B, one-step grinding protocols for synthesizing pyranopyrazoles.
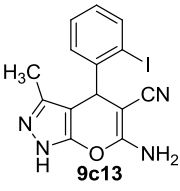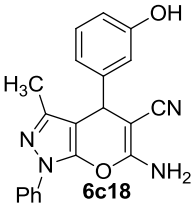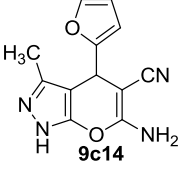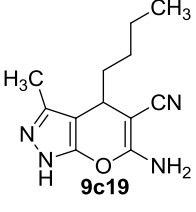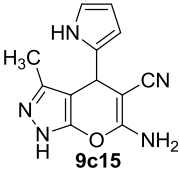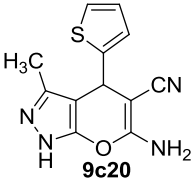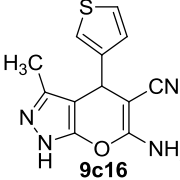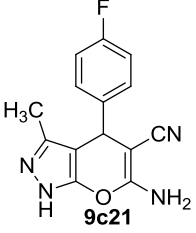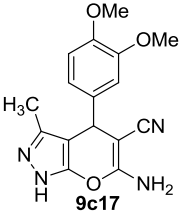
Table 3.13 presents all the pyranopyrazole compounds that were prepared for antimicrobial activity. The compounds were synthesized by both route A and route B, and their reaction timings and the respective isolated yields have been detailed in **Table 3.13**. A look at the table brings out the clear conclusion that the one-step scheme gave comparatively better yields to the two-step scheme with the additional benefit of significantly reduced reaction run times. A range of variously substituted aldehydic compounds were selected for synthesis. As shown in **Table 3.13**, the strongly electron-donating OH-substituted compound **9c2 (entry no. 2)** that mimicked **6c18 (entry no. 18)**, was prepared followed by its 4-hydroxy analogue **9c1 (entry no. 1)**. Similarly, mildly electron-withdrawing group **(9c3, 9c4, 9c9, 9c12, 9c13** or **entry no. 3, 4, 9, 12, 13)**, strongly electron-withdrawing **(9c5** or **entry no. 5)**, heterocyclic **(9c6, 9c11, 9c14, 9c15, 9c16, 9c20** or **entry no. 6, 11, 14, 15, 16, 20)**, and some compounds having non-polar moieties **(9c7, 9c8, 9c19** or **entry no. 7, 8, 19)** were also inducted into the pyranopyrazole core and tested consequently for antibacterial and antifungal activity.

Table 3.13: Characterization of the synthesized pyranopyrazoles by route A and B.

No.	Structure	% yield[a] (time)[b]		Mp (°C)	Ref[c]	No.	Structure	% yield[a] (time)[b]		Mp (°C)	Ref[c]
		A[d]	B[e]					A[d]	B[e]		
1	9c1	84 (15)	85 (5)	223-225	**119**	7	9c7	90 (18)	90 (8)	169-170	**119**
2	9c2	85 (20)	88 (5)	230-232	-	8	9c8	85 (20)	90 (6)	220-221	**119**
3	9c3	80 (22)	82 (5)	177-178	**113**	9	9c9	70 (19)	74 (6)	267-268	-
4	9c4	79 (18)	81 (6)	223-224	**118**	10	9c10	85 (18)	90 (5)	232-234	**121a-b**
5	9c5	85 (24)	82 (7)	191-192	**119**	11	9c11	92 (15)	92 (6)	228-230	**108**
6	9c6	87 (15)	91 (5)	210-211	-	12	9c12	79 (25)	80 (8)	175-176	**113**

13		75 (18)	80 (8)	250-252	-	18		85 (15)	84 (5)	169-170	**121a-b**
14		90 (15)	82 (5)	240-242	**114**	19		72 (25)	70 (10)	239-240	**112**
15		89 (16)	85 (5)	220-222	-	20		87 (20)	85 (7)	240-241	**114**
16		76 (20)	79 (6)	230-231	-	21		78 (18)	80 (6)	244-246	**110a-b**
17		89 (23)	89 (7)	194-195	**110**						

[a]isolated yields; [b]time in minutes; [c]end-of-text reference; [d]Route A; [e]Route B.

The SAR analysis of the microbial activity results shown in **Table 3.14** and their graphical illustration as depicted in **Figure 3.38** and **Figure 3.39** brings out the following facts. Considering only the antibacterial activity first, it is found that compound **9c4 (entry no. 4)** bearing the *m*-Br substituent is the solitary compound that is mildly active against all the three strains. In fact, most of the pyranopyrazoles are only slightly active against the Gram-negative strains while only analogue **9c4 (entry no. 4)** showed activity against Gram-positive strains. Significantly, none of the compounds is active against *S. aureus*, the Gram-positive bacterial strain. At least a couple of inferences are unequivocal. Comparing the activities of

136

analogs **9c2** (bearing N-H, entry no. 2) and **6c18** (bearing N-Ph, entry no. 18), it becomes obvious that the presence of N-H bearing HBD (Hydrogen-Bond Donor) ability as opposed to the presence of N-Ph in the pyrazole moiety increases the activity. Furthermore, analogues **9c2 (entry no. 2)** and **9c6 (entry no. 6)** bearing HBD capacity are the most potent among all the compounds. Although it may be too early to generalize, nevertheless based on the preliminary activity data available in **Table 3.14**, the SAR reveals that the presence of HBD capable group at the 3-position **(Figure 3.37)** of the top right sector of the pharmacophore might be crucial for improved activity against Gram-negative bacterial strains. Similarly, looking at the antifungal activity data in isolation, it is found that in general, the synthesized pyranopyrazoles are relatively more active against tested fungal strains than the tested bacterial strains. A total of eleven compounds are active against fungal strains. Also, the fact emerges that among the compounds active against fungi there seems discrimination on the basis of position or nature of the attached groups. Now, considering the overall of the activity results, it can be safely concluded that the compounds that are active against bacteria inactive against the fungal strains and vice versa. In other words, the tested compounds show complementary activity. Interestingly, comparing our antifungal results with a previous report,[111] our compounds returned better activity. Of course, this inference requires further investigation before a generalization can be made.

Table 3.14: Antibacterial and antifungal activities of the synthesized pyranopyrazole.

No.	Prod. code	Bacterial strains						Fungal strains					
		E. coli		S. aureus		Pseudomonas Putida		F. oxysporum		F. gramillarium		F. monalliforme	
		inhib zone[a]	MIC[b]	inhib zone	MIC	inhib zone	MIC	inhib zone	MIC	inhib zone	MIC	inhib zone	MIC
1	**9c1**	13	128	-	-	-	-	-	-	-	-	-	-
2	**9c2**	18	64	-	-	16	64	-	-	-	-	-	-
3	**9c3**	14	128	-	-	-	-	-	-	-	-	-	-
4	**9c4**	12	128	13	>128	14	>128	-	-	-	-	-	-
5	**9c5**	12	128	-	-	14	>128	-	-	-	-	-	-
6	**9c6**	18	64	-	-	14	128	14	64	15	64	14	64
7	**9c7**	14	128	-	-	-	-	14	64	14	64	15	64
8	**9c8**	15	128	-	-	-	-	14	64	15	64	15	64
9	**9c9**	15	128	-	-	-	-	15	128	15	128	-	-

10	**9c10**	12	128	-	-	12	>128	14	>64	-	-	16	64
11	**9c11**	0	-	-	-	-	-	-	-	-	-	-	-
12	**9c12**	0	-	-	-	-	-	16	64	14	64	14	64
13	**9c13**	0	-	-	-	-	-	14	64	14	>64	14	>64
14	**9c14**	0	-	-	-	-	-	16	>64	16	>64	16	>64
15	**9c15**	0	-	-	-	-	-	16	64	16	64	18	64
16	**9c16**	0	-	-	-	-	-	16	128	16	128	18	>64
17	**9c17**	0	-	-	-	-	-	14	>64	14	>64	16	>64
18	**6c18**	0	-	14	>128	15	>128	-	-	-	-	-	-
19	**9c19**	0	-	-	-	-	-	-	-	-	-	-	-
20	**9c20**	0	-	-	-	-	-	-	-	-	-	-	-
21	**9c21**	0	-	-	-	-	-	-	-	-	-	-	-
22[c]	-	22	16	22	16	22	16	-	-	-	-	-	-
23[d]	-	-	-	-	-	-	-	20	30	18	30	20	30

[a]zone of inhibition in mm; [b]Minimum Inhibitory Concentration assay in µg/mL; [c]control: Chloramphenicol (used for antibacterial assay only); [d]control: Amphotericin-B (used for antifungal assay only).
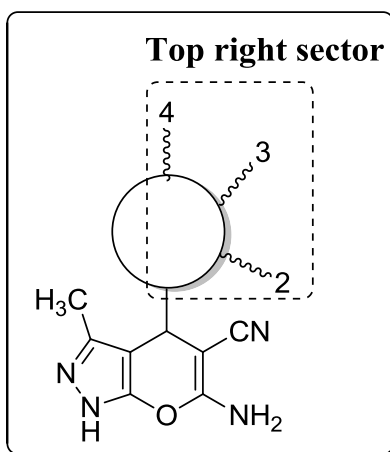
Figure 3.37 Depicting the top right sector (dotted) where the 3-position is found crucial for antibacterial activity.
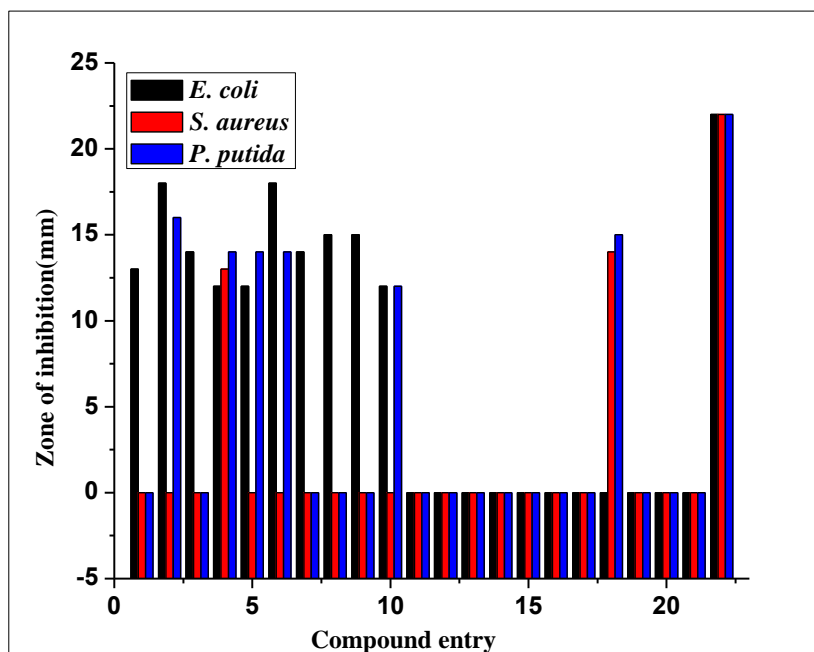
Figure 3.38 Shows Zone of Inhibition vs Compound entry for *E. coli, S. aureus, Pseudomonas putida.*
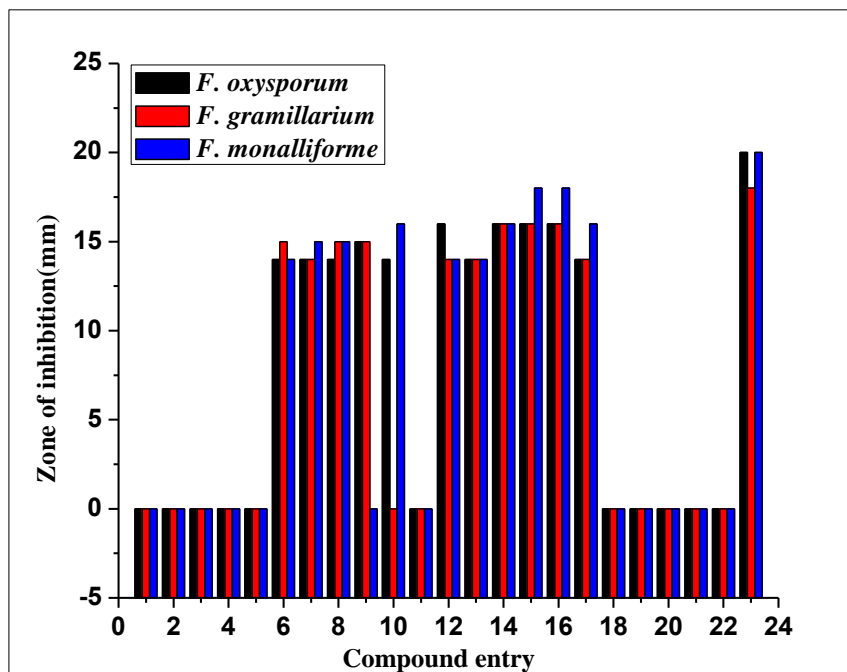
Figure 3.39 Zone of Inhibition vs Compound entry for *F. oxysporum, F. gramillarium, F. monalliforme.*

3.17 Anti-oxidant study of the selected Pyranopyrazole

Alzheimer's disease (AD) is the most common neurodegenerative disorder, and its incidence increases with age.[126] AD is characterized by the presence of extracellular deposits of amyloid beta (Aβ) caused by an abnormal processing of amyloid-beta precursor protein (APP), intracellular neurofibrillary tangles (NFT) composed of aggregated hyperphosphorylated tau proteins in brain. These features are accompanied by mitochondrial dysfunction and alterations in neuronal synapses.[126] The exact molecular and pathophysiological mechanisms of AD are still elusive. Although most studies have suggested that the Aβ peptide (amyloid cascade hypothesis) may initiate and/or contribute to the pathogenesis of AD, the mechanisms through which it causes neuronal loss, and tau abnormalities still remain poorly understood. Reactive oxygen species (ROS) and reactive nitrogen species (RNS), contribute to the pathogenesis of numerous human degenerative diseases[127] and have been implicated in the pathogenesis of neurodegenerative disorders including AD and Parkinson's disease, among others.[128] Brain tissue is particularly susceptible to oxidative damage. It is very rich in easily oxidizable polyunsaturated fatty acids and transition metal, such as iron and ascorbate, which are key players in oxidation and facilitate the formation of oxygen free radicals. Moreover, it is also characterized by a low content of antioxidant defence systems.[129]

Intracerebroventricular (ICV) administration of streptozotocin (STZ) in rats is commonly employed to study experimental sporadic dementia of Alzheimer's type. STZ has been reported to produce behavioral, neurochemical, biochemical and histopathological changes similar to aging brain.[130-132] The present study was designed to investigate the effect of pyranopyrazole compounds against streptozotocin induced oxidative stress in rats.

The researchers from all over the world tried to explore the heterocyclic compounds of the medium size ring[133-134] from last two-three decades[135] because of their characteristic property in the medicinal chemistry.[136] The fused heterocyclic compounds become the main research focus in the recent years because of their pharmacological importance and among them pyranopyrazole class has drawn the attention world-wide. In pyranopyrazole six membered pyran ring fused with the five membered pyrazole ring and its nucleus is a versatile source of biologically important molecule. The fused heterocycle pyranopyrazole have the four possible isomers- pyrano[2,3-*c*]pyrazole, pyrano[3,2-*c*]pyrazole, pyrano[4,3-*c*]pyrazole, pyrano[3,4-*c*]pyrazole. Out of four possible isomers pyrano[2,3-*c*] pyrazoles have been explored the most because of their pharmacological importance and their role in the field of medicinal chemistry. Herein, the best seven anticancer compounds **(Figure 3.40)** we selected from the **Part A of Chapter-3**[137] and finally all the compounds were tested for their *in-vitro/in-vivo* oxidative stress study. All the seven selected compounds have given different compound codes **(AK-16, 18, 20, 26,**

28, 50, 62) here to avoid the confusion. All the selected pyranopyrazole scaffolds with AK series and their previous code as given in part A of Chapter-3 are listed below in **Figure 3.40**.
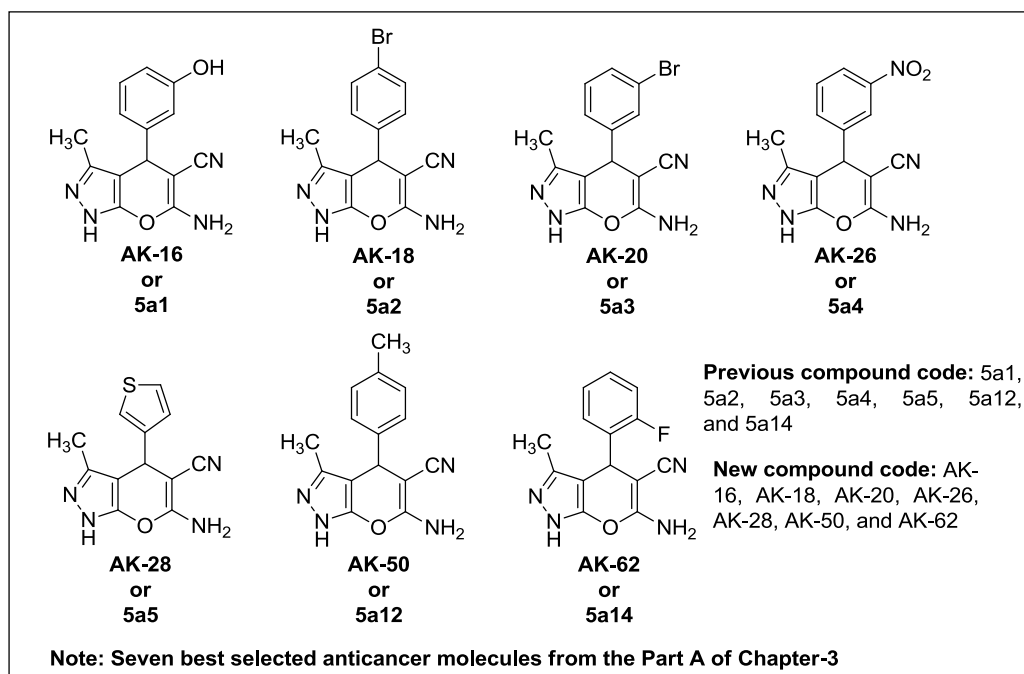
Figure 3.40 Shows the seven best selected pyranopyrazole anticancer molecules.

3.18 Pharmacological evaluation

3.18.1 *In-vitro* oxidative stress assay: Nitric oxide scavenging activity was estimated using Griess IlIosvoy reaction.[138] Briefly, sodium nitroprusside is known to decompose in aqueous solution at physiological pH (7.2) producing Nitric oxide (NO). Under aerobic conditions, NO reacts with oxygen to produce stable products (nitrate and nitrite). The quantities of which can be determined using Griess reagent. Scavengers of nitric oxide compete with oxygen leading to reduced production of nitrite ions.[139] For this experiment, sodium nitroprusside (5 mM) in phosphate buffered saline was mixed with all samples (0.25 mg/ml) prepared using methanol. Ascorbic acid and blank dilutions were prepared in a similar manner. Solutions were incubated at 25ºC for 2 hours. Thereafter, 1.5 ml of Griess reagent (1% sulphanilamide, 0.1 % N-(1-naphthyl) ethylenediamine dihydrochloride and 3% phosphoric acid) was added to each test tube. The absorbance was measured, immediately, at 546 nm and percentage scavenging activity **(Figure 3.41)** was calculated using following equation:

$$\text{Inhibition (\%)} = (A_0 - A_1 / A_0) \times 100$$

Where A_0 is the absorbance of control and A_1 is the absorbance of test.
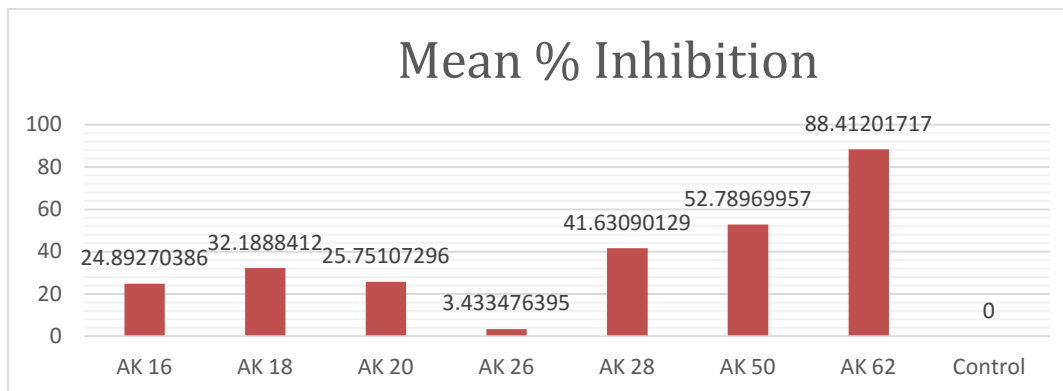
Figure 3.41 Shows the compound entry vs mean % inhibition of oxidative stress.

3.18.2 *In-vivo* oxidative stress activity: Based upon their in-vitro antioxidant activity, we screen two best compounds for evaluation of their *in-vivo* antioxidant property. For *in-vivo* study, we divided the animals into 4 groups,

Group 1: Sham control, (served as double vehicle control), received citrate buffer ICV in a volume of 5 µl in each ventricle on day 1 as a vehicle for STZ and 30 % v/v DMSO in normal saline (i.p), as a vehicle for **AK-50** and **AK-62** for 7 days.

Group 2: Rats were infused with ICV-STZ (3 mg/kg) dissolved in citrate buffer in a volume of 5 µl in each ventricle on day 1.

Group 3 and 4: Rats received **AK-50** (0.1 mg/kg i.p.) and **AK-62** (0.1 mg/kg i.p.) after the STZ administration starting from day 1 and continued once daily for a period of 7 days.

The doses were selected based upon the action of these drugs on spontaneous locomotor activity as evaluated using actophotometer. We administer various doses (0.1-1 mg/kg i.p.) of **AK-50** and **AK-62** to small number of animals and observed any change in locomotor activity. Higher doses of these compounds resulted in toxicity in animals. Based upon the locomotor activity as well as *in-vivo* toxicity we selected the doses. To induce central oxidative stress we administered the male Wistar rats with intracerebroventricular streptozotocin (3 mg/kg) bilaterally using following coordinates: 0.8 mm posterior to bregma; 1.5 mm lateral to sagittal suture; 3.6 mm ventral from the surface of the brain (Paxinos and Watson 1986).[140] After this, the animals were treated with **AK-62** and **AK-50** (0.1mg/kg i.p.) once daily for 7 days. At the end of treatment phase, we sacrifice the animals and their brains were removed. The brains were then homogenized with ice cold 0.1 M phosphate buffer (pH 7.4) in a volume 10 times (w/v). The homogenate was centrifuged at 12,000 g for 15 min (4 °C) and aliquots of supernatant were separated and used for biochemical estimations. The experimental procedures on animals were in compliance with the Institutional Animal Ethics Committee of BITS, Pilani, Rajasthan (India).

3.18.3 Estimation of Malondialdehyde (MDA): The quantitative measurement of MDA[141], an end product of lipid peroxidation, in brain homogenate was performed according to the method of Wills 1996. The amount of MDA **(Figure 3.42)** was measured after its reaction with thiobarbituric acid at 532 nm using spectrophotometer (Shimadzu, UV-1700).
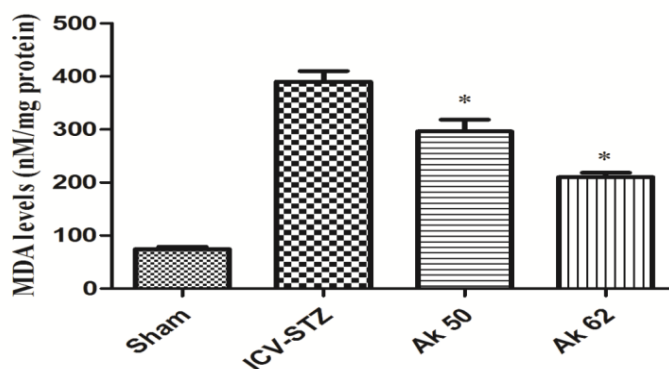
Values are expressed as mean ± SEM. ($^*P$ <0.05 vs ICV-STZ).

Figure 3.42 Shows the estimation of malondialdehyde.

3.18.4 Estimation of Reduced glutathione (GSH): Reduced glutathione is an established indicator of the oxidative stress.[142] Its amount in brain was estimated **(Figure 3.43)** according to the usual method described by Ellman in 1959. 1 ml supernatant was precipitated with 1 ml of 4% sulfosalicylic acid and cold digested at 4 °C for 1 h. The samples were centrifuged at 1200g for 15 min. To 1 ml of the supernatant, 2.7 ml of phosphate buffer (0.1 M, pH 8) and 0.2 ml of 5,5′-dithiobis-(2-nitrobenzoic acid) (DTNB) were added. The yellow color that developed was measured immediately at 412 nm using a spectrophotometer.
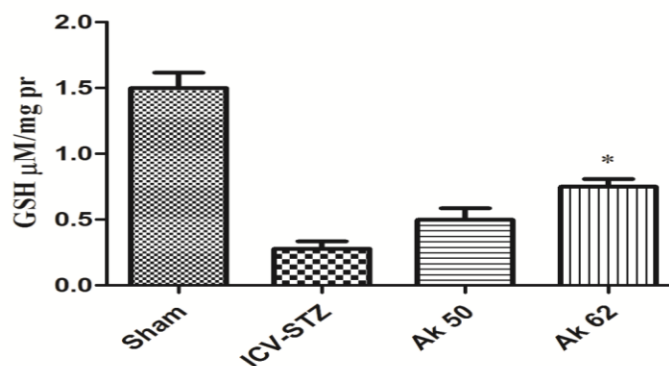
Values are expressed as mean ± SEM. ($^*P$ <0.05 vs ICV-STZ).

Figure 3.43 Shows the estimation of reduced glutathione.

3.18.5 Results and discussion of Pharmacological study

In the present study, all the compounds **(AK-16, 18, 20, 26, 28, 50 and 62)** were tested for their antioxidant properties using nitric oxide radical scavenging assay. The percentage of inhibition was calculated and it was observed that free radicals were scavenged by the test compounds at 0.25 mg/ml concentration. The maximum and minimum percentage of inhibition was shown by **AK-62** (88.4%) and **AK-26** (3.43%), respectively. The level of MDA, an end product of lipid peroxidation was found to be significantly higher in STZ treated animals as compared to sham group. However, treatment with both **AK-50** and **AK-62** significantly attenuated MDA levels as compared to ICV-STZ treated animals. Moreover, the level of endogenous antioxidant, reduced glutathione, was found to be reduced in ICV-STZ treated animals. However, treatment with **AK-62** significantly restored the level of GSH.

In this study, it is evident that the compounds from AK-series possess effective antioxidant activities. *In-vitro* antioxidant activity of this series of compounds was investigated in the present study by nitric oxide scavenging assay and hydrogen peroxide radical scavenging activity.

In nitric oxide scavenging assay, the radicals generated from sodium nitroprusside in aqueous solution at physiological pH interact with oxygen to produce nitrite ions which is estimated with Griess reagent.[139] This method has proved the antioxidant potential of the compound **(AK-50 and AK-62)** in comparison with the reference antioxidant, ascorbic acid. Moreover, in the hydrogen peroxide radical scavenging activity assay, we found significant antioxidant activity for **AK-62** against the standard, ascorbic acid. Based upon these results, it was assumed that these compounds could prove to be beneficial in conditions with elevated oxidative stress, such as AD. However, the major concern was related to their ability to cross the blood brain barrier (BBB). To induce AD like oxidative stress condition in brain, we administered STZ bilaterally in ICV region of rat brain. ICV-STZ administration results in significant elevation in MDA levels as well as reduction in reduced glutathione (GSH). Similar elevation in oxidative stress markers after STZ administration has been reported previously.[132, 143-144]

During the *in-vivo* studies, we found a significant increase in oxidative stress marker, MDA and a significant reduction in antioxidant enzyme, GSH level as a result of STZ treatment. These results are consistent with earlier reports.[143-144] However, treatment with **AK-62** and **AK-50** attenuated the MDA levels and restored the level of GSH, suggesting the antioxidant potential of these compounds. Thus based upon these observations, it could be suggested that these compounds hold significant antioxidant potential. However more future studies are warranted to prove their efficacy and molecular mechanisms involved in *in-vivo* conditions.

3.19 Conclusions

In conclusion, we have developed a novel, benign, and fast four-component, one-pot, solvent-free grinding based MCR strategy for obtaining a variety of useful pyranopyrazole compounds. The three-component and the four-component protocols were fully investigated and their relative reaction yields and reaction timings well contrasted. The analogues were designed and chosen for synthesis based on the initial activity of compound **6c18 (Table 3.13, entry no. 18).** The synthesized compounds were tested against a Gram-positive and two Gram-negative bacterial strains and three different fungi and many of the molecules were found to be active against the fungal assays. Two of the synthesized compounds **9c2 (entry no. 2)** and **9c6** (**entry no. 6**) turned out to be more potent against Gram-negative bacteria than the others **(Table 3.14)**. The results of these observation and the subsequent SAR pointed to the significant conclusion that the presence of H-bond donors at the 3-postion of the top right sector of the heterocyclic moiety of the pyranopyrazole pharmacophore may play a crucial role in enhancing the antimicrobial activity. Interestingly, compounds active against bacteria were generally inactive against fungi and vice versa. Further investigations as proof of concept of our findings are currently being established in our lab as the ultimate aim of such a study is to design compounds against multidrug resistant microbes.

The seven best anticancer molecules were selected from the Part A of Chapter-3 and were tested for *in-vitro* antioxidant stress study by Nitric oxide radical scavenging assay. Finally the best two molecules **(AK-50 and AK-62)** having excellent *in-vitro* antioxidant activity were selected and tested for *in-vivo* antioxidant study on rat brain. The antioxidant potential **AK-50** and **AK-62** were confirmed by administration of these compounds in rat brain, attenuated the MDA levels and restored the level of GSH.

3.20 Experimental

3.20.1 Synthesis procedure of Pyranopyrazole by grinding methodology

Route A (Two-step, three component grinding protocol): ethyl acetoacetate (2.53 mL, 20.0 mmol) and hydrazine hydrate (0.98 mL, 20.0 mmol) were ground together in a mortar with pestle for 5 min without adding any solvent or catalyst. 3-Methyl-1*H*-pyrazol-5(4*H*)-one so formed was collected and then grinded again by adding the 3-hydroxybenzaldehyde (2.68 g, 22.0 mmol), malononitrile (1.10 mL, 20.0 mmol) and triethylamine (5.55 mL, 40.0 mmol) as base for further 10 min. The weight of the product **9c1** (entry no. 1 in Table 3.13) obtained was 4.50 g (84% yield).

Route B (one-step, four component grinding protocol): All the four reactants were added together followed by triethylamine in the same proportion as in route A in the mortar and ground with the pestle for 5 min. The reaction was continuously monitored by TLC. After the reaction, the contents of the flask were diluted with dichloromethane (5 mL), filtered, and subjected to column chromatography to get 4.56 g (85% yield) of the pure compound **9c1** (entry no. 1 in Table 3.13).

3.20.2 Materials & Methodology for antibacterial assay:[145] All the synthesized compounds were evaluated for their *in-vitro* antibacterial activity against two Gram-negative bacterial strains: *E. coli* and *Pseudomonas putida* and one Gram-positive bacteria *Staphylococcus aureus* and their activities were compared with a commercially available broad spectrum antibiotic Chloramphenicol. For the experimental work, 20 mL of autoclaved Mueller-Hinton (Himedia, India) agar medium was poured into glass petri plates and the agar plates were swabbed with 100 μL inocula of each test organism (106 cfu/mL). After the adsorption, well size of 6 mm diameter was made by the sterile metallic borer and the solution of working compound (128 μg/mL) was poured into the wells. The plates were incubated at 37 °C for 18-24 h. DMSO was used as a negative control. MIC assay (Minimum Inhibitory Concentration assay) was performed to determine the lowest concentrations of compound necessary to inhibit the visible growth of microorganisms. MIC values were evaluated for all the compounds using broth microdilution method. Assay was carried out for the compounds at 16, 32, 64, 128 μg/mL concentrations. A set of tubes containing Mueller-Hinton broth medium with different concentrations of compound were prepared. The tubes were inoculated with bacterial cultures (106 cfu/mL) and incubated on a rotary shaker (180 rpm) at 37 °C for 18-24 h under dark conditions. MIC value was defined as lowest concentrations of compound that prevented the visible growth of the bacteria after the incubation period. Chloramphenicol was used as a positive control at a concentration of 16 μg/mL.

3.20.3 Materials & Methodology for antifungal assay:[146] Antifungal activities of chemically synthesized compounds were determined by agar well diffusion method at a varying concentration for all the compounds. For the experimental work, Potato dextrose broth (PDB, Himedia, India) was freshly prepared and autoclaved at 121 °C at 15 psi for 15 min. After cooling to room temperature a loopful of fungal mycelium was inoculated into freshly prepared PDB broth for 4-5 days at 28 °C. After the proper growth, 100 μL of this inoculum was uniformly spread on the Potato dextrose agar plate. Following the adsorption of inoculum, well size of 9 mm diameter was prepared by the sterile metallic borer and compound solution was added in respective wells. Plates were incubated at 28 °C for 4 days under dark conditions. Mean diameter of inhibition zone was measured to determine the antifungal activity. The experiment was performed in triplicates. MIC assay of all the compounds was performed at 16.0, 32.0, 64.0, 128.0 μg/mL concentrations. Tubes containing 10 mL of sterilized czapeks dox broth medium was inoculated with 100 μL of freshly grown culture. Appropriate amount of compound was added to achieve the desired concentrations. The tubes were incubated at 28 °C for 4 days under dark conditions and carefully observed for the presence of turbidity.

3.20.4 Characterization data: (For ^{1}H and ^{13}C-NMR spectra see Appendices A-1).

6-amino-4-(3-hydroxyphenyl)-3-methyl-1,4-dihydropyranopyrazole-5-carbonitrile (9c2 or entry no. 2): Off-white solid. ^{1}H NMR (400 MHz, DMSO-d_6) δ: 11.97 (s, 1H), 9.17 (1H), 8.12-7.05 (2H), 7.06 (m, 4H), 4.45 (s, 1H), 1.84 (s, 3H). ^{13}C NMR (100 MHz, DMSO-d_6) δ: 160.6, 157.2, 145.3, 135.5, 128.8, 118.1, 114.2, 113.8, 78.5, 78.4, 78.2, 77.8, 58.2, 9.7. HRMS calcd for $C_{14}H_{12}N_4O_2$ 268.096, found 268.099.

6-amino-4-(1H-indol-3-yl)-3-methyl-1,4-dihydropyranopyrazole-5-carbonitrile (9c6 or entry no. 6): white solid. ^{1}H NMR (400 MHz, DMSO-d_6) δ: 12.01 (s, 1H), 10.86 (1H), 6.84-7.36 (5H), 6.75 (2H), 4.85 (s, 1H), 1.77 (s, 3H). ^{13}C NMR (100 MHz, DMSO-d_6) δ: 160.5, 154.9, 136.8, 135.5, 125.5, 121.0, 120.7, 118.1, 116.7, 11.5, 78.7, 58.1, 28.2, 9.6. HRMS calcd for $C_{16}H_{13}N_5O$ 291.112, found 291.111.

6-amino-4-(2-fluorophenyl)-3-methyl-1,4-dihydropyranopyrazole-5-carbonitrile (9c9 or entry no. 9): Dirty white solid. ^{1}H NMR (400 MHz, DMSO-d_6) δ: 12.13 (s, 1H), 6.94 (2H), 7.24 (m, 4H), 4.87 (s, 1H), 1.81 (s, 3H). ^{13}C NMR (100 MHz, DMSO-d_6) δ: 161.3, 154.9, 135.2, 129.7, 128.5, 124.5, 115.4, 99.5, 96.5, 78.8, 55.6, 29.8, 9.4. HRMS calcd for $C_{14}H_{11}FN_4O$ 270.092, found 270.095.

6-amino-4-(2-iodophenyl)-3-methyl-1,4-dihydropyranopyrazole-5-carbonitrile (9c13 or entry no. 13): Off-white solid. ^{1}H NMR (400 MHz, DMSO-d_6) δ: 12.15 (s, 1H), 7.01-7.35 (multiplet, 4H), 6.75 (2H), 4.96 (s, 1H), 1.76 (s, 3H). ^{13}C NMR (100 MHz, DMSO-d_6) δ: 160.9, 154.8, 135.4, 128.6, 120.0, 78.4, 56.3, 18.3, 9.9. HRMS calcd for $C_{14}H_{11}IN_4O$ 377.998, found 377.996.

6-amino-3-methyl-4-(1H-pyrrol-2-yl)-1,4-dihydropyranopyrazole-5-carbonitrile (9c15 or entry no. 15): Light creamy yellow solid. ^{1}H NMR (400 MHz, DMSO-d_6) δ: 12.05 (s, 1H), 10.51 (1H), 6.56-6.73 (3H), 5.84 (2H), 4.64 (s, 1H), 1.84 (s, 3H). ^{13}C NMR (100 MHz, DMSO-d_6) δ: 160.68, 154.66, 135.61, 133.22, 120.85, 116.87, 106.67, 105.10, 96.71, 78.60, 56.94, 29.56, 9.44. HRMS calcd for $C_{12}H_{11}N_5O$ 241.096, found 241.098.

6-amino-3-methyl-4-(thiophen-3-yl)-1,4-dihydropyranopyrazole-5-carbonitrile (9c16 or entry no. 16): Pale solid. ^{1}H NMR (400 MHz, DMSO-d_6) δ: 12.10 (s, 1H), 7.28 (1H), 7.26 (2H), 6.83 (2H), 4.73 (s, 1H), 1.86 (s, 3H). ^{13}C NMR (100 MHz, DMSO-d_6) δ: 160.70, 154.59, 145, 135.50, 126.62, 125.95, 120.72, 96.89, 78.53, 57.07, 31.34, 9.62. HRMS calcd for $C_{12}H_{10}N_4OS$ 258.058, found 258.057.

3.21 References

[1] Winkler, J. D. *Chem. Rev.* **1996**, *96*, 167.

[2] Liu, Y.; Wan, J. P. *Org. Biomol. Chem.* **2011**, *9*, 6873.

[3] Denzel, T.; Hoehn, H. US. Patent 3903096 *Chem. Abstr.* **1975**, *83*, 2026257.

[4] Ueda, T.; Mase, H.; Oda, N.; Ito, I. *Chem. Pharm. Bull.* **1981**, *29*, 3522.

[5] Adibi, H.; Hosseinzadeh, L.; Farhadi, S.; Ahmadi, F. *J. Rep. Pharma. Sci.* **2013**, *2*, 116.

[6] Erugu, Y.; Sangepu, B.; Varre, K.; Pamanji, R.; Bomma, Y.; Janapala, V. R.; Srinivasarao, V.; Tigulla, P.; Jetti, V. R. *World J. Pharma. Sci.* **2014**, *3*, 1895.

[7] Mosmann, T. *J. Immunol Methods* **1983**, *65*, 55.

[8] Huang, L. J.; Hour, M. J.; Teng, C. M.; Kuo, S. C. *Chem. Pharm. Bull.* **1992**, *40*, 2547.

[9] Foloppe, N.; Fisher, L. M.; Howes, R.; Potter, A.; Robertson, A. G.; Surgenor, A. E. *Bioorg. Med. Chem.* **2006**, 14, 4792.

[10] Ramtekkar, R.; Kumarvel, K.; Vasuki, G.; Sekar, K.; Krishna, R.; *Letts. Drug Des. Discov.* **2009**, *6*, 579.

[11] Yu, S. M.; Kuo, S. C.; Huang, L. J.; Sun, S. M.; Huang, T. F.; Teng, C. M. *J. Pharm. Pharmacol.* **1992**, *44*, 667.

[12] Colotta, V.; Catarzi, D.; Varano, F.; Melani, F.; Filacchioni, G.; Cecchi, L.; Trincavelli, L.; Martini, C.; Lucacchini, A. *Il Farmaco.* **1998**, *53*, 189.

[13] Mandour, A. H.; Sawy, E. R; Ebaid, S. M. *Acta Pharm.* **2012**, *62*, 15.

[14] Kassem, E. M.; Sawy, E. E. R.; Alla, A. H. I,; Mandour, A. H.; Abdel, M. D.; Safty, E. M. M. *Egypt. Pharm. J.* **2012**, *11*, 116.

[15] Katariya, L. K.; Kharadi, G. J. *IJPRS* **2014**, 3, 627.

[16] Amin, B. N.; Parikh, A. R.; Parikh, H.; Gudaparthi, V. *J. Pharm. Res.* **2014**, 3, 51.

Part A References

[17] American Cancer Society. Cancer Facts & Figures. Atlanta: American Cancer Society; **2014**.

[18] Henrikson, J. C.; Ellis, T. K.; King, J. B.; Cichewicz, R. H. *J. Nat. Prod.* **2011**, *74*, 1959.

[19] Polshettiwar, V.; Varma, R. S. *Tetrahedron Lett.* **2008**, *49*, 397.

[20] Junek, H.; Aigner, H. *Chem. Ber.* **1973**, *106*, 914.

[21] Tacconi, G.; Gatti, G.; Desimoni, G. *J. Prakt. Chem.* **1980,** *322*, 831.

[22] Sharanina, L. G.; Marshtupa, V. P.; Sharanin, Yu. A. *Khim. Geterotsikl. Soedin.* **1980**, *10*, 1420.

[23] Sharanin, Yu. A.; Sharanina, L. G., Puzanova, V. V. *Zh. Org. Khim.* **1983**, *19*, 2609.

[24] Thumar, N. J.; Patel, M. P. *Arkivoc.* **2009**, *13*, 363.

[25] Khafagy, M. M.; Wahab, A. A. H.; Eid, F. A.; Agrody, E. A. M. *Farmaco.* **2002**, *57*, 715.

[26] Smith, P. W.; Sollis, S. L.; Howes, P. D.; Cherry, P. C.; Starkey, I. D.; Cobley, K. N.; Weston, H.; Scicinski, J.; Merritt, A.; Whittington, A.; Wyatt, P.; Taylor, N.; Green, D.; Bethell, R.; Madar, S.; Fenton, R. J.; Morley, P. J.; Pateman, T.; Beresford, A. *J. Med. Chem.* **1998**, *41*, 787.

[27] Martinez, A. G.; Marco, L. J. *Bioorg. Med. Chem. Lett.* **1997**, *7*, 3165.

[28] Bianchi, G.; Tava, A. *Agric. Biol. Chem.* **1987**, *51*, 2001.

[29] Srivalli, T.; Satish, K.; Suthakaran, R. *Int. J. Innov. Pharm. Res.* **2011**, *2*, 172.

[30] Eiden, F.; Denk, F. *Arch. Pharm.* **1991**, *324*, 353.

[31] Hafez, E. A. A.; Elnagdi, M. H.; Elagamey, A. G. A.; Ei-Taweel, F. M. A. A. *Heterocycles*. **1987**, *26*, 903.

[32] Foloppe, N.; Fisher, L. M.; Howes, R.; Potter, A.; Robertson, A. G. S.; Surgenor A. E. *Bioorg. Med. Chem.* **2006**, *14*, 4792.

[33] Junek, H.; Aigner, H. *Chem. Ber.* **1973**, *106*, 914.

[34] Shestopalov, A. M.; Emeliyanova, Y. M.; Shestopalov, A. A.; Rodinovskaya, L. A.; Niazimbetova, Z. I.; Evans, D. H. *Tetrahedron,* **2003**, *59*, 7491.

[35] Shestopalov, A. M.; Emeliyanova, Y. M.; Rodinovskaya, L. A.; Niazimbetova, Z. I.; Evans, D. H. *Org. Lett.* **2002**, *4*, 423.

[36] Litvinov, Y. M.; Shestopalov, A. A.; Rodinovskaya, L. A.; Shestopalov, A. M. *J. Comb. Chem.* **2009**, *11*, 914.

[37] Peng, Y.; Song, G.; Dou, R. *Green Chem.* **2006**, *8*, 573.

[38] Vasuki, G.; Kumaravel, K. *Tetrahedron Lett.* **2008**, *49*, 5636.

[39] Schlager, T.; Schepmann, D.; Lehmkuhl, K.; Holenz, J.; Vela, J. M.; Buschmann, H.; Wünsch, B. *J. Med. Chem.* **2011**, *54*, 6704.

[40] Kiyani, H.; Samimi, H.; Ghorbani, F.; Esmaieli, S. *Curr. Chem. Lett.* **2013**, *2*, 197.

[41] Mecadon, H.; Rohman, M. R.; Kharbangar, I.; Kharkongor, I.; Rajbangshi, M.; Myrboh, B. *Tetrahedron Lett.* **2011**, *52*, 3228.

[42] Aleem, M. A. E.; Remaily, A. A. E. *Tetrahedron,* **2014**, *70*, 2971.

[43] Bhavanarushi, S.; Kanakaiah, V.; Yakaiah, E.; Saddanapu, V.; Addlagatta, A.; Rani, J. V. *Med. Chem. Res.* **2013**, *22*, 2446.

[44] Matar, A. H. M.; Khalil, K. D.; Adam, A. Y.; Elnagdi, M. H. *Molecules.* **2010**, *15*, 6619.

[45] Mandha, S. R.; Siliveri, S.; Alla, M.; Bommena, V. R.; Bommineni, M. R.; Balasubramanian, S. *Bioorg. Med. Chem. Lett.* **2012**, *22*, 5272.

[46] Tierney, J. P.; Lidstrom, P. *Microwave assisted organic synthesis: blackwell publishing. oxford,* UK: **2005**.

[47] Polshettiwar, V.; Varma, R. S. *Acc. Chem. Res* **2008**, *41*, 629.

[48] Roberts, B. A.; Straus, C. A. *Acc. Chem. Res* **2005**, *38*, 653.

[49] Knasmuller, S.; Sundermann, M. V.; Kevekordes, S.; Darroudi, F.; Huber, W. W.; Hoelzl, C.; Majer, B. *J. Toxicol.* **2004**, *198*, 315.

[50] Oxford Diffraction.; *Crys Alis PRO*. Oxford Diffraction Ltd, Yarnton, England: **2010**.

[51] Sheldrick, G. M. *Acta Crystallogr.* **2008,** *A64*, 112.

[52] Dömling, A.; Wang, W.; Wang, K. *Chem. Rev.* **2012,** *112*, 3083.

[53] Farrugia, L. J. *J. Appl. Crystallogr.* **1999,** *32***,** 837.

[54] Farrugia, L. J. *J. Appl. Crystallogr.* **2012,** *45*, 849.

[55] Spek, A. L. *Acta Crystallogr.* **2009,** *D65*, 148.

[56] Nardelli, M. *J. Appl. Crystallogr.* **1995,** *28*, 659.

[57] Gavezzotti, A. *N. J. Chem.* **2011,** *35***,** 1360.

[58] Dunitz, J, D.; Gavezzotti, A. *Cryst. Growth Des.* **2012,** *12,* 5873.

[59] Dunitz, J. D.; Gavezzotti, A. *Chem. Soc. Rev.* **2005,** *38*, 2622.

[60] Maschio, L.; Civalleri, B.; Ugliengo, P.; Gavezzotti, A. *J. Phys Chem. A* **2011,** *115*, 11179.

[61] Allen, F. H.; Kennard, O.; Watson, D. G.; Brammer, L.; Orpen, A. G.; Taylor, R. *J. Chem. Soc. Perkin Trans.* **1987,** *2,* S1.

[62] Low, J. N.; Cobo, J.; Portilla, J.; Quiroga, J.; Glidewell, C. *Acta Crystallogr.* **2004,** *E60*, 1034.

[63] Sharma, N.; Brahmachari, G.; Banerjee, B.; Kant, R.; Gupta, V. K. *Acta Crystallogr.* **2014,** *E70*, 875.

[64] Mohamed, S. K.; Akkurt, M.; Tahir, M. N.; Abdelhamida, A. A.; Allahverdiyevd, M. A. *Acta Crystallogr.* **2012,** *E68*, 1414.

[65] Bernstein, J.; Davis, R. E.; Shimoni, L.; Chang, N. L. *Angew. Chem. Int. Ed. Engl.* **1995,** *34*, 1555.

Part B References

[66] http://www.who.int/mediacentre/factsheets/fs297/en/ accessed January 15, **2015**.

[67] http://www.liverfoundation.org/abouttheliver/info/cirrhosis/ accessed February 17, **2016**.

[68] Kim, I.; Song, J. H.; Park, C. M.; Jeong, J. W.; Kim, H. R.; Ha, J. R.; Hyun, Y. L.; Cho, Y. S.; Kang, N. S.; Jeon, D. J. *Bioorg. Med. Chem. Lett.* **2010,** *20*, 922.

[69] Devegowda, V. N.; Kim, J. H.; Han, K. C.; Yang, E. G.; Choo, H.; Pae, A. N.; Nam, G.; Choi, K. I. *Bioorg. Med. Chem. Lett.* **2010,** *20*, 1630.

[70] Bakavoli, M.; Bagherzadeh, G.; Vaseghifar, M.; Shiri, A.; Pordel, M.; Mashreghi, M.; Pordeli, P.; Araghi, M. *Eur. J. Med. Chem.* **2010,** *45*, 647.

[71] Ghorab, M. M.; Ragab, F. A.; Alqasoumi, S. I.; Alafeefy, A. M.; Aboulmagd, S. A. *Eur. J. Med. Chem.* **2010,** *45*, 171.

[72] Gilbert, A. M.; Nowak, P.; Brooijmans, N.; Bursavich, M. G.; Dehnhardt, C.; Santos, E. D.; Feldberg, L. R.; Hollander, I.; Kim, S.; Lombardi, S.; Park, K. J.; Venkatesan, A. M.; Mallon, R. *Bioorg. Med. Chem. Lett.* **2010,** *20*, 636.

[73] Mousseau, J. J.; Fortier, A.; Charette, A. B. *Org. Lett.* **2010,** *12*, 516.

[74] Nascimento, J. N. M.; Mendes, T. C. F.; Leal, D. M.; Corrêa, C. M. N.; Sudo, R. T.; Zapata, S. G.; Barreiro, E. J.; Fraga, C. A. M. *Bioorg. Med. Chem. Lett.* **2010,** *20*, 74.

[75] Wang, J. L.; Liu, D.; Zheng, Z. J.; Shan, S.; Han, X.; Srinivasula, S. M.; Croce, C. M.; Alnemri, E. S.; Huang, Z. *Proc. Natl. Acad. Sci. U.S.A.* **2009,** *97*, 7124.

[76] Zaki, M. E. A.; Morsy, E. M.; Abdul, M. *Heterocycl. Commun.* **2004,** *10*, 97.

[77] Mazaahir, K.; Shilpi, S.; Khalilur, R. K.; Sharanjit, S. T. *Bioorg. Med. Chem. Lett.* **2005,** *15*, 4295.

[78] *Sharma, A.; Pallavi, B.; Jha, P. N.; Singh, R.P.;* Shukla, P. *Heterocycles* **2015**, *91*, 1615.

[79] Junek, H.; Aigner, H. *Chem. Ber.* **1973,** *106*, 914.

[80] Arabanian, A.; Mohammadnejad, M.; Balalaie, S.; Gross, J. H. *Bioorg. Med. Chem. Lett.* **2009,** *19*, 887.

[81] Rashinkar, G.; Salunkhe, R. *J. Mol. Catal. A: Chem.* **2010,** *316*, 146.

[82] Sharma, A.; Shukla, P.; Sumati, A.; Rajni, K. *Bull. Mat. Sci.* **2015,** *38*, 1119.

[83] Tacconi, G.; Gatti, G.; Desimoni, G. *J. Prakt. Chem.* **1980,** *322*, 831.

[84] Sharanina, L. G.; Marshtupa, V. P.; Sharanin, Yu. A. *Khim. Geterotsikl. Soedin.* **1980,** *10*, 1420.

[85] Sharanin, Y. A.; Sharanina, L. G., Puzanova, V. V. *Zh. Org. Khim.* **1983,** *19*, 2609.

[86] Sharma, A.; Chowdhury, R.; Dash, S.; Pallavi, B.; Shukla, P. *Curr. Microwave Chem.* **2015,** *2*, 1.

[87] Pawar, P. B.; Jadhav, S. D; Patil, B. M.; Shejwal, R. V.; Patil, S. *Arch. Appl. Sci. Res.* **2014,** *6*, 150.

[88] Mecadon, H.; Rohman, M. R.; Kharbangar, I.; Laloo, B. M.; Kharkongor, I.; Rajbangshi, M.; Myrboh B. *Tetrahedron Lett.* **2011,** *52*, 3228.

[89] Vasuki, G.; Kumaravel, K. *Tetrahedron Lett.* **2008,** *49*, 5636.

[90] For recent reports: (a) Kiyani, H.; Samimi, H.; Ghorbani, F.; Esmaieli, S. *Curr. Chem. Lett.* **2013,** *2*, 197.

[91] Fathy, M. A.; Nadia H. M.; AFINIDAD LXV Noviembre-Diciembre **2008,** 538.

[92] Anatoliy, M. S.; Yuliya, M. E.; Aleksandr, A. S.; Lyudmila, A. R.; Zukhra, I. N.; Dennis, H. E. *Org. Lett.* **2002,** *4*, 423.

[93] Santhosh, R. M.; Sravanthi, S.; Manjula, A.; Vittal, R. B.; Madhava, R. B.; Sridhar, B. *Bioorg. Med. Chem. Letts.* **2012,** *22*, 5272.

[94] Manouchehr, M.; Roghayeh, H. N.; Farhad, S.; Khalil, T.; Mehdi, R. *Med. Chem. Res.* **2015,** *24*, 1916.

[95] Anatoliy, M. S.; Yuliya, M. E.; Aleksandr, A. S.; Lyudmila, A. R.; Zukhra, I. N.; Dennis, H. E. *Tetrahedron* **2003,** *59*, 7491.

[96] Manisha, B.; Pranjal, P. B.; Ghanashyam, B.; Hassan, A. *ACS Sustainable Chem. Eng.* **2013,** *1*, 440.

[97] Knasmuller, S.; Sundermann, M. V.; Kevekordes, S.; Darroudi, F.; Huber, W. W.; Hoelzl, C.; Bichler, J.; Majer, B. J. *Toxicol.* **2004,** *198*, 315.

[98] Li, Q. S.; Yang, P.; Wang, H. F.; Guo, M. L. *J. Inorg. Biochem.* **1996,** *64*, 181.

[99] Foloppe, N.; Fisher, L. M.; Howes, R.; Potter, A.; Robertson, A. G. S.; Surgenor, A. E. *Bioorg. Med. Chem.* **2006,** *14*, 4792.

Part C References

[100] Toure, B. B.; Hall, D. G. *Chem. Rev.* **2009,** *109*, 4439.

[101] (a) Dömling, A.; Wang, W.; Wang, K. *Chem. Rev.* **2012,** *112*, 3083; (b) Zhu, J.; Bienayme, H.; *In multicomponent reactions*. ed.; by Zhu. J.; Bienayme, H.; Wiley-VCH Verlag GmbH & Co, KGaA, Weinheim: **2005;** (c) Tejedor, T.; Garcia, T. F. *Chem. Soc. Rev.* **2007,** *36*, 484; (d) Ugi, I. *Pure Appl. Chem.* **2001,** *73*, 187; (e) Liéby, F.; Simon, C.; Constantieux, T.; Rodriguez, J. *QSAR Comb. Sci.* **2006,** *25*, 432; (f) Simon, C.; Constantieux, T.; Rodriguez, J. *Eur. J. Org. Chem.* **2004,** *2004*, 4957; (g) Evdokimov, N. M.; Kireev, A. S.; Yakovenko, A. A.; Antipin, M. Y.; Magedov, I. V.; Kornienko, A. *J. Org. Chem.* **2007,** *72*, 3443; (h) Weber, L.; *Drug Discov. Today* **2002,** *7*, 143; (i) Hulme, C.; Gore, V.; *Curr. Med. Chem.* **2003,** 10, 51.

[102] (a) Anastas, P. T.; Warner, J. C. *Green chemistry: Theory and practice.* Oxford University Press, Oxford, UK: **1998**; (b) Anastas, P. T.; Williamson, T. *Green chemistry, frontiers in benign chemical synthesis and process.* Oxford University Press, Oxford, UK: **1998**; (c) Ciriminna, R.; Pagliaro, M. *Org. Process Res. Dev.* **2013,** *17*, 1479; (d) Winterton, N. *Chemistry for sustainable technologies: a foundation.* Royal Society of Chemistry, Cambridge, UK: **2011**.

[103] (a) Trost, B. M. *Acc. Chem. Res.* **2002,** *35*, 695; (b) Leng, R. B.; Emonds, M. V. M.; Hamilton, C. T.; Ringer, J. W. *Org. Proc. Res. Dev.* **2012,** *16*, 415.

[104] (a) Cohen, M. L.; *Nature*, **2000,** *406*, 762; (b) Edman, J. D. Emerging vectorborne diseases and their control: new discoveries in agrochemicals. *ACS Symposium Series*: **2004**; Vol. 892.

[105] Walsh, C. *Nat. Rev. Microbiol.* **2003,** *1*, 65.

[106] (a) Richardsn, M. D. *J. Antimicrob. Chemother.* **1991,** *28*, 1; (b) Ablordeppey, S. Y.; Fan, P.; Ablordeppey, J. H.; Mardenborough, L. *Curr. Med. Chem.* **1999,** *6*, 1151.

[107] (a) Henrikson, J. C.; Ellis, T. K.; King, J. B.; Cichewicz, R. H. *J. Nat. Prod.* **2011,** *74*, 1959; (b) Hatakeyama, S.; Ochi, N.; Numata, H.; Takano, S. *J. Chem. Soc., Chem. Commun.* **1988,** *17*, 1202.

[108] (a) Martínez, G. A.; Friedländer, M. J. *Bioorg. Med. Chem. Lett.* **1997,** *7*, 3165; (b) Skommer, J.; Wlodkowic, D.; Mättö, M.; Eray, M.; Pelkonen, J. *J. Leukemia Res.* **2006,** *30*, 322; (c) Anderson, D. R.; Hegde, S.; Reinhard, E.; Gomez, L.; Vernier, W. F.; Lee, L.; Liu, S.; Sambandam, A.; Snider, P. A.; Masih, L. *Bioorg. Med. Chem. Lett.* **2005,** *15*, 1587; (d) Wang, J. L.; Liu, D.; Zhang, Z. J.; Shan, S.; Han, X.; Srinivasula, S. M.; Croce, C. M.; Alnemri, E. S.; Huang, Z. *Proc. Natl. Acad. Sci. U.S.A.* **2000,** *97*, 7124.

[109] Hafez, E. A. A.; Elnagdi, M. H.; Elagamey, A.; Ei-Taweel, F. M. A. A. *Heterocycles*, **1987,** *26*, 903.

[110] (a) Fustero, S.; Sánchez, R. M.; Barrio, P.; Simón, F. A. *Chem. Rev.* **2011,** *111*, 6984; (b) Polshettiwar, V.; Varma, R. S. *Tetrahedron Lett.* **2008,** *49*, 397.

[111] Thumar, N. J.; Patel, M. P. *Arkivoc* **2009,** *xiii*, 363.

[112] Smith, P. W.; Sollis, S. L.; Howes, P. D.; Cherry, P. C.; Starkey, I. D.; Cobley, K. N.; Weston, H.; Scicinski, J.; Merritt, A.; Whittington, A.; Wyatt, P.; Taylor, N.; Green, D.; Bethell, R.; Madar, S.; Fenton, R. J.; Morley, P. J.; Pateman, T.; Beresford, A. *J. Med. Chem.* **1998,** *41*, 787.

[113] Bianchi, G.; Tava, A. *Agric. Biol. Chem.* **1987,** *51*, 2001.

[114] Junek, H.; Aigner, H. *Chem. Ber.* **1973,** *106*, 914.

[115] (a) Wamhoff, H.; Kroth, E.; Strauch, C. *Synthesis* **1993,** 1129; (b) Tacconi, G.; Gatti, G.; Desimoni, G.; Messori, V. *J. Prakt. Chem.* **1980,** *322*, 831.

[116] (a) Shestopalov, A. M.; Emeliyanova, Y. M. Shestopalov, A. A.; Rodinovskaya, L. A.; Niazimbetova, Z. I.; Evans, D. H. *Tetrahedron*, **2003,** *59*, 7491; (b) Shestopalov, A. M.; Emeliyanova, Y. M.; Shestopalov, A. A.; Rodinovskaya, L. A.; Niazimbetova, Z. I.; Evans, D. H.; *Org. Lett.* **2002,** *4*, 423.

[117] Litvinov, Y. M.; Shestopalov, A. A.; Rodinovskaya, L. A.; Shestopalov, A. M. *J. Comb. Chem.* **2009,** *11*, 914.

[118] Peng, Y.; Song, G.; Dou, R. *Green Chem.* **2006,** *8*, 573.

[119] Vasuki, G.; Kumaravel, K. *Tetrahedron Lett.* **2008,** *49*, 5636.

[120] Schläger, T.; Schepmann, D.; Lehmkuhl, K.; Holenz, J.; Vela, J. M.; Buschmann, H.; Wünsch, B. *J. Med. Chem.* **2011,** *54*, 6704.

[121] (a) Kiyani, H.; Samimi, H.; Ghorbani, F.; Esmaieli, S.; *Curr. Chem. Lett.* **2013,** *2*, 197; (b) Mecadon, H.; Rohman, M. R.; Kharbangar, I.; Laloo B. M.; Kharkongor, I.; Rajbangshi, M.; Myrboh, B. *Tetrahedron Lett.* **2011,** *52*, 3228.

[122] Aleen, E. M. A.; Remaily, E. A. A.; *Tetrahedron*, **2014,** *70*, 2971.

[123] (a) Matar, A. H. M.; Khalil, K. D.; Adam, A. Y.; Elnagdi, M. H. *Molecules.* **2010,** *15*, 6619; (b) Mandha, S. R.; Siliveri, S.; Alla, M.; Bommena, V. R.; Bommineni, M. R.; Balasubramanian, S. *Bioorg. Med. Chem. Lett.* **2012,** 22, 5272.

[124] Guo, S. B.; Wang, S. X.; Li, J. T. *Synth. Commun.* **2007,** *37*, 2111.

[125] Bhavanarushi, S.; Kanakaiah, V.; Yakaiah, E.; Saddanapu, V.; Addlagatta, A.; Vatsala, R. J. *Med. Chem. Res.* **2013,** *22*, 2446.

[126] Mattson, M. P. *Nature* **2004**, *430*, 631.

[127] Jung, H. A.; Min, B. S.; Yokozawa, T.; Lee, J. H.; Kim, Y. S.; Choi, J. S. *Biol. Pharm. Bull.* **2009,** *32*, 1433.

[128] Reynolds, A.; Laurie, C.; Mosley, R. L.; Gendelman, H. E. *Int. Rev. Neurobiol.* **2007,** *82*, 297.

[129] Floyd, R. A. *Proc. Soc. Exp. Biol. Med.* **1999,** *222*, 236.

[130] Salkovic, P. M.; Hoyer, S. *J. Neural. Transm.* **2007,** *72*, 217.

[131] Ishrat, T.; Hoda, M. N.; Khan, M. B.; Yousuf, S.; Ahmad, M.; Khan, M. M. *Eur. Neuropsychopharmacol.* **2009,** *21*, 1.

[132] Deshmukh, R.; Sharma, V.; Mehan, S.; Sharma, N.; Bedi, K. L. *Eur. J. Pharmacol.* **2009,** *620*, 49.

[133] Elnagdi, M. H.; Elmoghayar, M. R. H.; Elgemeie,G. E. H. *Adv. Heterocycl. Chem.* **1987**, *41*, 319.

[134] Elnagdi, M. H.; Elmoghayar, M. R. H.; Sadek, K. U. *Adv. Heterocycl. Chem* **1990**, *48*, 223.

[135] Jug, K.; Oricine, D.C.; Katritzky, A. R. *Chem. Rev.* **2001**, *101*, 1421.

[136] Pozharskii, A. F.; Sodatemkov, A. T.; Kartritzky, A. R. *Heterocycle in life and society.* 1st ed.; Wiely: **1997**; 301.

[137] Sharma, A.; Pallavi, B.; Subhra, D.; Rajdeep, C.; Shukla, P. *Curr Micro. Chem*. **2015,** *2*, 1.

[138] Garrat, D. C. *The quantitative analysis of drugs. Chapman and Hall Ltd*., Japan: **1964;** *3*, 456.

[139] Asirvatham, R.; Christina, A. J.; Murali, A. *Adv. Pharm. Bull.* **2013,** *3*, 115.

[140] Paxinos, G.; Watson, C. *The rat brain in stereotaxic coordinates*. 2nd ed.; Academic Press, San Diego: **1986.**

[141] Wills, E. D.; *Biochem. J.* **1966,** *99*, 667.

[142] Mytilineou, C.; Kramer, B. C.; Yabut, J. A. *Parkinsonism Relat. Disord. **2002**, 8,* 385.

[143] Rai, S.; Kamat, P. K.; Nath, C.; Shukla, R. *Neuroimmunol.* **2012,** *254*, 1.

[144] Khan, M. B, Khan, M. M.; Khan, A.; Ahmed, M. E.; Ishrat, T.; Tabassum, R.; Vaibhav, K. *Neurochem. Int.* **2012,** *61*, 1081.

[145] Andrews, J. M.; *J. Antimicrob. Chemother.* **2001,** *48*, 5.

[146] Jorgensen, J.; Crawford, S.; McElmeel, M.; Fiebelkorn, K. *J. Clinic. Microbiol.* **2004,** *42*, 1800.

Chapter IV

Introduction

Designing, Molecular Docking, and Molecular Dynamics Study of CDK-2 Inhibitors as Anticancer Agents

This chapter describes the designing of the potent pharmacophore, molecular docking, molecular dynamics and pharmacokinetic study of the designed molecules. The computational study of the molecules describes the theoretical understanding of the designed pharmacophore and their interaction with the active site of the protein so that a medicinal chemist can synthesize molecules in the lab with proper planning and can get the lead drug molecule. The docking of all the designed molecules has been done by AutoDock tool 1.5.6 and their molecular view was seen by Discovery Studio Client 3.5 and Glide. Whether, the protein was stable **(Chapter-4, Part-A)** for docking or not was confirmed by molecular dynamics study by using Groningen 1.5.0 software.
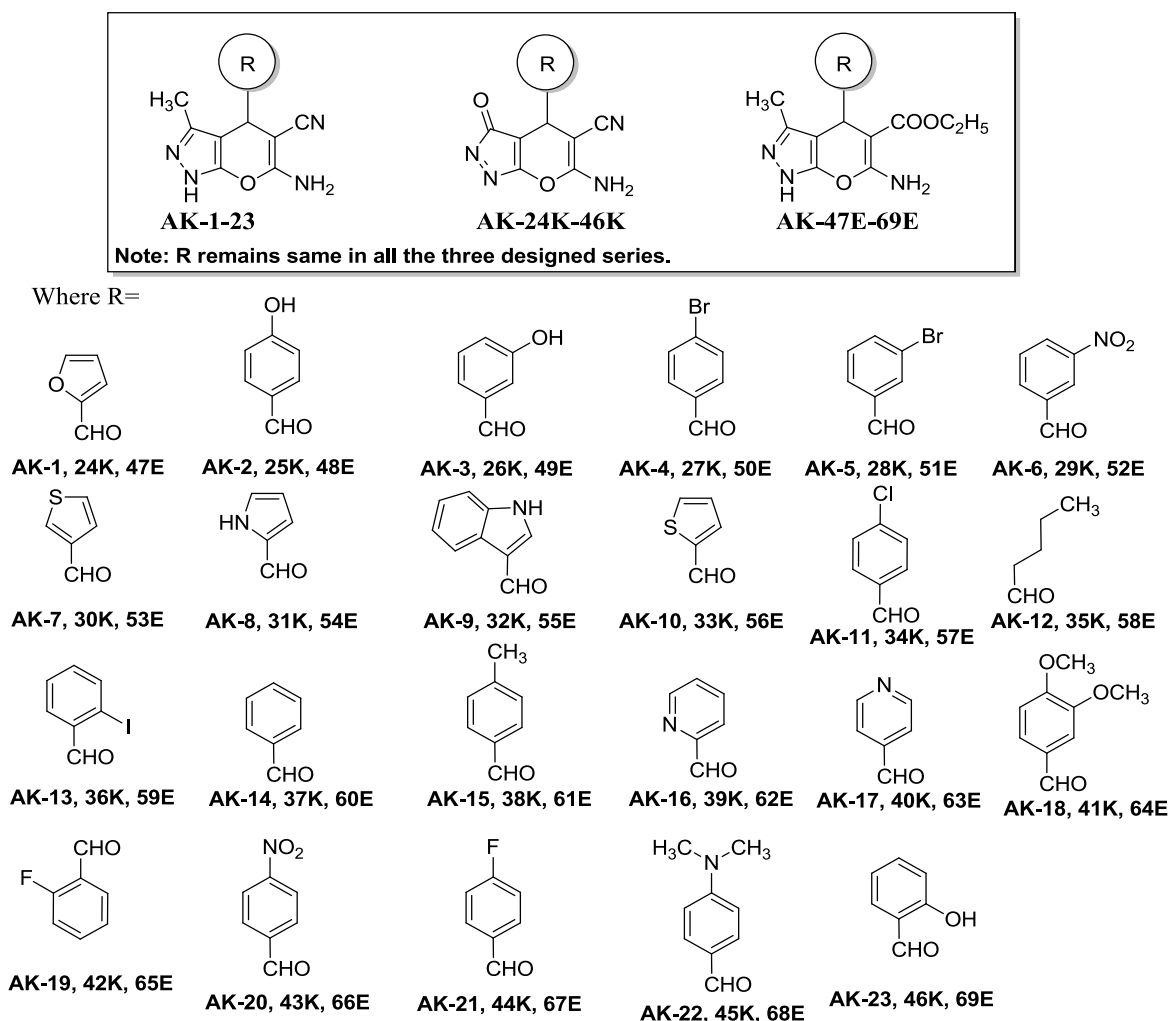
Figure 4.1 Shows the designed pyranopyrazole scaffolds as CDK-2 inhibitor.

Later on, to find out that up to what time the designed ligand is stable inside the binding pocket of the protein, molecular dynamics study was done **(Chapter-4, Part-B)**. All 131 designed molecules i.e. 69

pyranopyrazole **(Figure 4.1)** and 62 coumarin derivatives **(Figure 4.2)** not only showed good binding energy (K.cal/mol^{-1}) score but also give excellent inhibitory constant (K$_i$) value.

Later on, we checked and calculated the pharmacokinetic properties also for all the 131 molecules, for improvement in the designing of the drug molecules and to understand the consequences of the different functional groups present in the molecule. The detailed study of all the designed pyranopyrazoles and coumarin scaffolds is discussed in **part-A** and **part B** of **chapter 4** respectively.
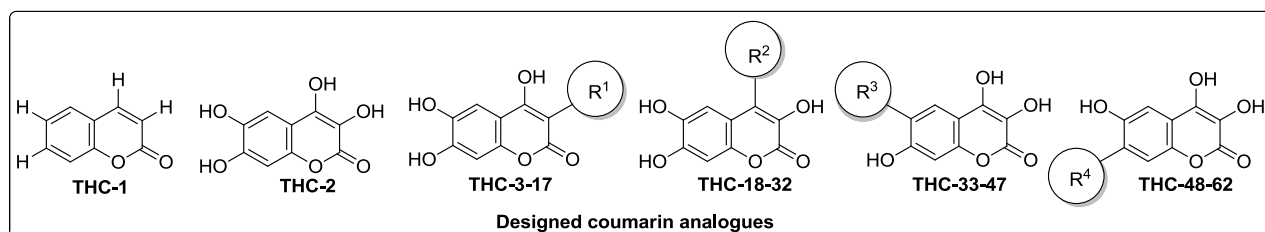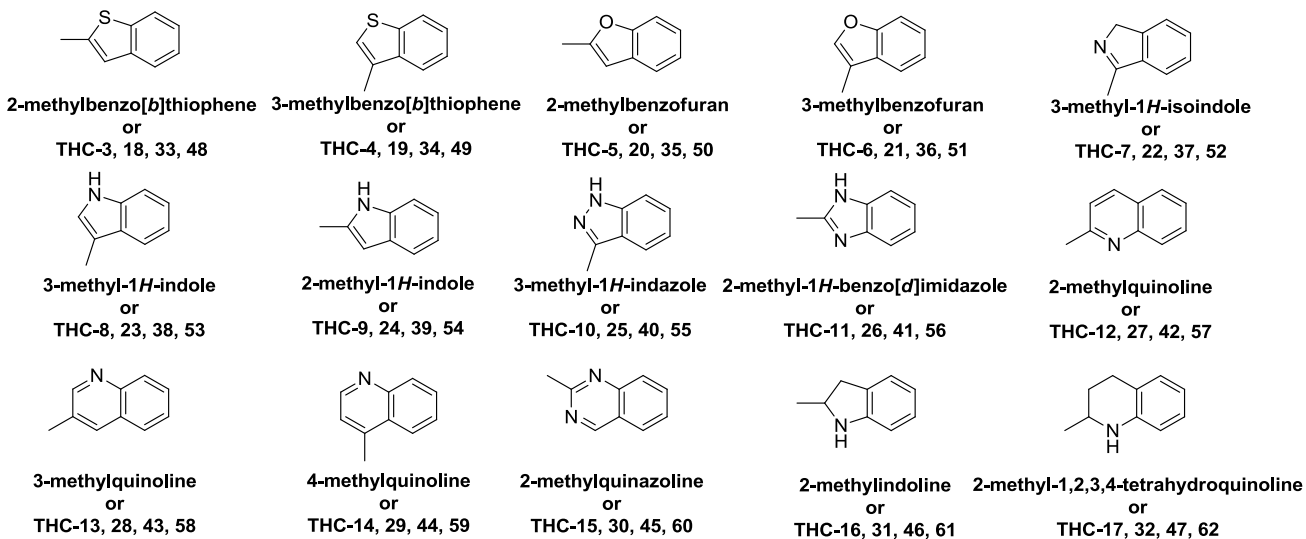
Figure 4.2 Shows the designed coumarin scaffolds as CDK-2 inhibitor.

Chapter IV

Part-A

de-novo Design, and *in-silico* Studies of Novel Pyranopyrazole Derivatives as Inhibitors of Cyclin Dependent Kinase-2 (PDB ID: 1HCK)

4.1 Introduction

Cancer is a group of diseases all corresponding to unregulated cell growth. In cancer, cells divide and grow unchecked, forming malignant tumors and invade nearby parts of the body. Today, cancer is responsible for one in every eight deaths worldwide – more than HIV/AIDS, tuberculosis and malaria combined; and about 1,665,540 new cancer cases[1] are expected to be diagnosed in 2014 in the USA alone. Hence, the search for small molecule anticancer therapeutics remains relevant. Protein kinases are important drug targets for immunologic, oncogenic, metabolic and other disorders. The development of selective protein kinase inhibitors is widely considered a promising approach to drug development. The common strategy, which has led to the development of drugs such as Glivec and Iressa, is to target the ATP binding site.[2-3] Other approaches include substrate mimicking inhibitors[4-9] bi-substrate analogs that target both the ATP and acceptor binding sites[10] like Src homology 2 domain.[11] The cyclin-dependent kinases (CDKs) are a family of serine-threonine protein kinases which control the process of cell cycle progression in multiplying eukaryotic cells.[12-16] The activity of CDKs is dependent upon the presence of cyclin partners whose levels are regulated to ensure that the phases of the cell cycle proceed in the precise order. Aberrant CDK control and consequent damage of cell cycle checkpoint function have been directly associated with the molecular pathology of cancer.[17] These CDK related events are among the most common genetic changes found in human cancers and clinically, they are often responsible for a poor prognosis. In view of the strong link between CDKs and the molecular pathology of cancer, CDKs are being studied as possible targets for therapeutic medication.[18-20] The recognition of the importance of CDKs to the process of cell division has inspired an interest in them as potential targets for diseases such as cancer, psoriasis and restenosis[20-22] as well as for the prevention of chemotherapy-linked side effects such as alopecia.[23]

A number of small-molecule inhibitors of CDKs have been identified[24-30] and are described in recent reviews.[18, 31-34] Flavopiridol is the first CDK inhibitor to advance into clinical trials and is being evaluated as an anticancer agent.[35-37] In addition, peptide inhibitors of CDK2 were recently shown to preferentially induce transformed cells to undergo (apoptosis) relative to untransformed cells.[38] X-ray crystallographic analysis of a substantial number of CDK2/inhibitor complexes has expounded the diverse binding modes of different inhibitors in atomic detail.[39] Several types of CDK inhibitors have so far been designated: staurosporine, UCN-01,[40] flavopiridol (L86 8275),[41] butyrolactone-I,[42] other purine derivatives,[31, 43-45] indirubin,[46] paullones,[47] and others.[48-50] Furthermore, a novel series of anilinopyrazoles[51] has been designed based on the X-ray crystal structure analysis. Most compounds from this series not only showed sub-nanomolar IC_{50} values for CDK2, but also reveal almost 1000-fold selectivity to other kinases including CDK1. Two closely related classes of oxindole-based

compounds,[52] 1*H*-indole-2,3-dione-3-phenylhydrazones and 3-(anilinomethylene)-1,3-dihydro-2*H*-indol-2-ones were shown to potently inhibit CDK2. Similarly, small molecule CDK inhibitors, including the purine analog olomoucine have antimitotic activity and have been shown to inhibit cancer cells.[44, 53] MDL 106,327DA was identified through database mining using olomoucine as the lead structure and found to inhibit CDK-2/cyclin E with an IC_{50} value of 50 nM which was then steadily modified to find the optimum inhibitory activity for CDK-2/cyclin E. Identification of *N*-(4-Piperidinyl)-4-(2,6-dichlorobenzoylamino)-1*H*-pyrazole-3-carboxamide (AT75195), a new CDK inhibitor using structure based drug design was reported by Paul group.[54] AT75195, is currently being evaluated in clinical trials for the treatment of human cancers. Gray *et al.*[55] revealed the preparation of O^6-cyclohexylmethylguanine derivatives bearing substituted aryl groups[56-61] as CDK-2 inhibitors. Afterwards, evaluation of the effects of purine C-8 substitution within a series of CDK1/2-selective O^6-cyclohexylmethylguanine derivatives revealed that, potency decreases initially with increasing size of the alkyl substituent.[62] Subsequent structural analysis showed why these compounds adopt unusual binding modes. A convenient route for the synthesis of 2-arylamino-4-cyclohexylmethyl-5-nitrosopyrimidine[63] CDK inhibitors was developed to prepare a small series of compounds and the results were consistent with the known binding mode of NU6027 within the ATP-binding site of CDK2. Quantitative structure activity relationship (QSAR) and docking methods are two commonly used computational methods in structure-based drug design (SBDD). QSAR studies establish a statistical connection between the biological activity of compounds and a set of molecular descriptors obtained from their structures. In docking studies, different search algorithms (simulated annealing, genetic algorithm) are used along with scoring functions (molecular mechanic) to study the binding interactions of the ligands with target protein.[64]

Pyrazole fused pyrans (pyrazolopyrans) are well-established group of heterocyclic molecules possessing wide applications having a comprehensive spectrum of biological and pharmacological activities such as antimicrobial[65], antiviral[66], mutagenicity[67], sex pheromone[68], antitumour[69], cancer therapy[70], analgesic[71], antitumor[72] and central nervous system related activity. Some of these compounds are broadly employed as cosmetics and pigments as well as potential biodegradable agrochemicals.[73] 4*H*-pyrans have been reported as the basic structural motifs for a gamut of useful compounds such as natural products and drug precursors. Similarly, pyrazoles have also been reported as excellent starting materials for the synthesis of various bioactive small organic molecules.[74] Therefore, design and docking study of such pyrazole fused pyran compounds has stimulated strong scientific interest.

In the war against cancer, inhibition of enzymes that would have otherwise resulted in the promotion of uncontrolled cytokinesis is one of the targets for further research. Among the various enzymes that can be

used as targets, protein kinases have been listed as potential targets due to their involvement in cell signaling pathways. Hence, their inhibition and successful targeting could ensure pioneering research work, which would help in reducing the use of chemotherapy and prolong the lives of millions of people. It has been found out that, repetitions of certain oncogenic expressions were being caused by protein kinases. Our focus is on inhibition of one of the protein 1HCK of the CDK-2 (Cyclin Dependent Kinases) class, as they are intrinsically involved in the cell cycle regulation.[75-77]

Selected molecules of the pyrazolopyran class which is being investigated for its bioactivity were docked and the results are compared with standard CDK-2 inhibitor of our choice. Complications of developing a CDK inhibitor include the fact that, many CDKs are not involved in the cell cycle such as transcription, viral infection and neural physiology.[78]

Softwares required

Molecular modeling software Auto Dock 4.2 installed on a PC with 2.3 GHz processor, 4GB RAM with a dedicated Graphics Card of 2GB with windows XP SP2 as the operating system was used for the entire docking study. Discovery studio client 3.5 (visualizer) was used to get Ramachandran plot of the refined protein (PDB ID: 1HCK).

Receptors used for docking

CDK-2 (Cyclin dependent kinase) enzyme co-crystallized with Mg-ATP ligand (PDB ID: 1HCK) is used as target receptor. Standard drug olomoucine is used for calibration and validation of docking process.

4.2 Experimental

4.2.1 Molecular docking studies

Docking is an approach to rational drug design that seeks to predict the structure and binding free energy of ligand-receptor complex. It not only gives an idea about how the ligand is going to bind with the receptor but also up to what extent conformational changes can be brought in the receptor structure upon binding with ligand. The docking studies for all the 69 designed analogues were performed using molecular modeling software autodock 4.2. The docking study was performed using THR14 (T) and TYR15 (Y) residues of the GTYG cluster of ATP binding sites (residues 13 to 16) as flexible ones. Target protein, Cyclin dependent kinase-2 enzyme [PDB ID: 1HCK] was taken from the RCSB protein data bank and Ramachandran plot[79] of prepared protein 1HCK **(Figure 4.3)** was obtained from Discovery Studio viewer. In the apoenzyme structure, almost all residue conformations fall in energetically favored regions of the Ramachandran plot, and in the ATP-enzyme complex. Target protein was further refined by removal of water molecules, adding polar hydrogens and kollmann charges. For the docking study, a grid spacing of 0.375 Å and $60 \times 60 \times 60$ number of points was used. The grid was centered on the active

site. The auto grid program generated separate grid maps for all atom types of the ligand structures and one for electrostatic interactions.
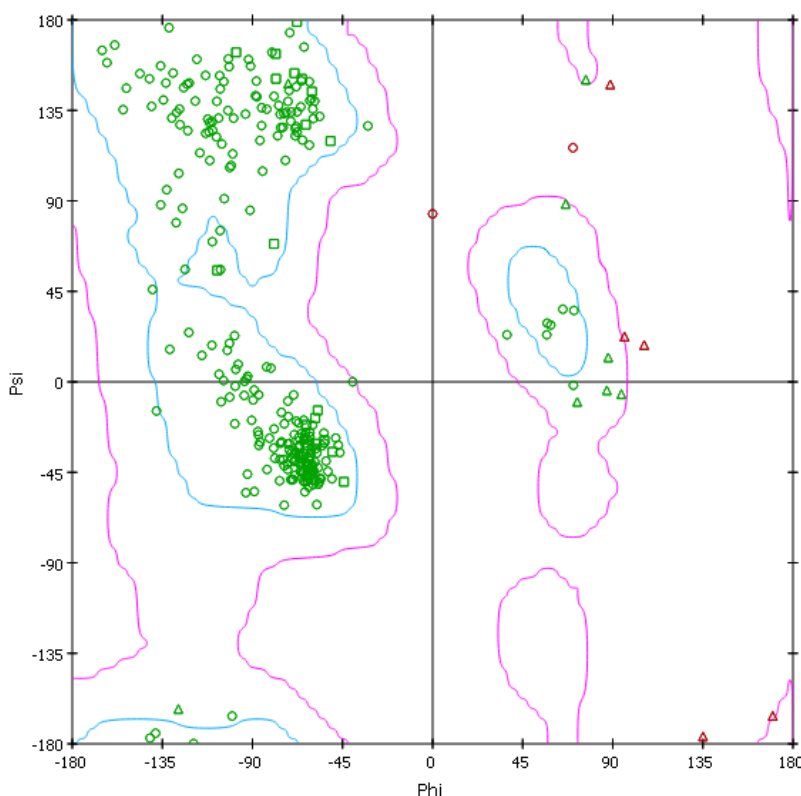
Figure 4.3 Ramachandran plot of the prepared protein 1HCK obtained by Discovery Studio Viewer.

PRODRG online server (http://davapc1.bioch.dundee.ac.uk/prodrg/) was used to generate the energy minimized conformations of the designed ligands in pdb format. Energy minimized conformation of ligands was subjected to calculation of Gasteiger–Huckel charges and saved in default format of Autodock. Autodock generated 50 possible binding conformations i.e., 50 runs for each docking using LGA search. Default protocol was applied with initial population of 150 randomly placed individuals, a maximum number of 2.5×10^5 energy evaluations and 2.7×10^4 generations. A mutation rate of 0.02 and a crossover rate of 0.8 were used.

4.2.2 Validation of docking

Target receptor CDK-2 (PDB ID: 1HCK) co-crystallized with Mg-ATP was used for docking study. Co-crystallized ATP was extracted and docked back into the active site of receptor to validate the docking calculations. It was evident that, the docked pose of the re-docked ATP was almost superimposed with that of the co-crystallized ligand with acceptable root mean square deviation of 0.835 Å **(Figure 4.4)**. Subsequently, the Mg-ATP hydrogen-bonding **(Figure 4.5)** and Van der Waals interaction **(Figure 4.6)** with the receptor protein was also determined for validation.
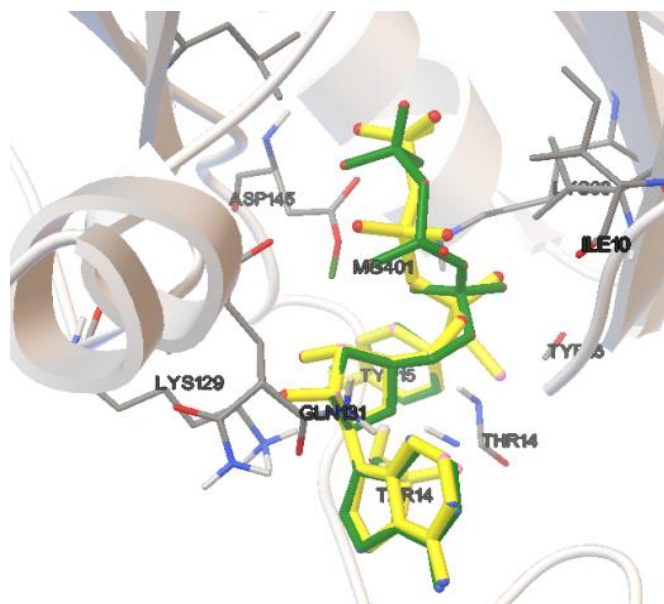
Figure 4.4 Redocked mode of ATP (green) superimposed with the co-crystallized Mg-ATP in the binding pocket of CDK-2 (PDB ID: 1HCK). ATP is shown as stick model and the amino acid residues interacting with the co-crystallized Mg-ATP are shown as line model.
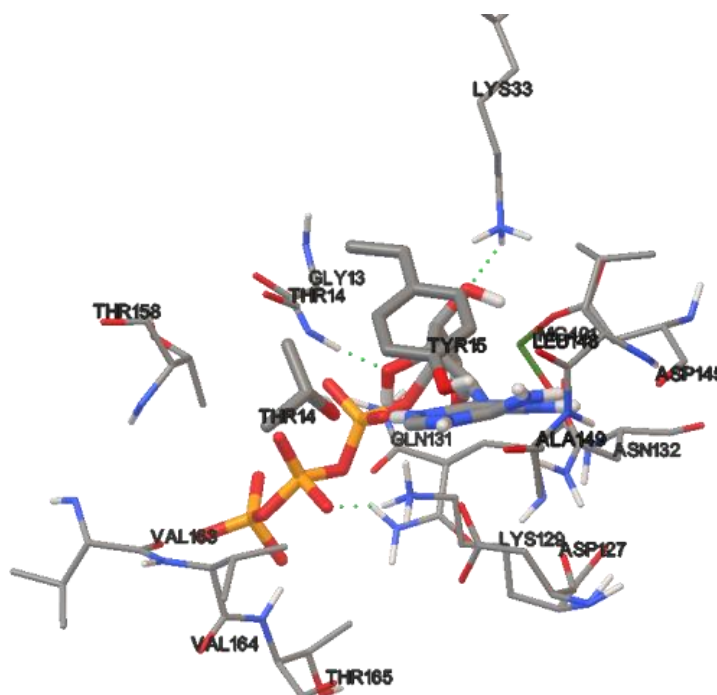
Figure 4.5 Hydrogen bonding interaction of ATP with CDK-2 (PDB ID: 1HCK) with various amino acid residues LYS-129, LYS-33 and THR-14 of the receptor.
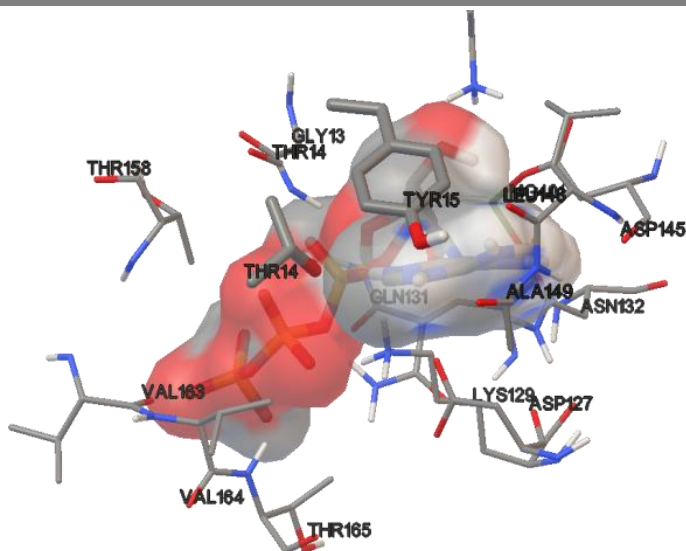
Figure 4.6 Van der Waals interaction of ATP with CDK-2 (PDB ID: 1HCK) with various amino acid residues of the receptor.

Then, the standard drug (olomoucine) was subjected to docking study in order to check the reliability and reproducibility of the docking parameters used for the study. Hydrogen bonding and van der Waals interaction exhibited by the standard drug olomoucine with the active site amino acid residues of 1HCK protein was shown in **Figure 4.7** and **Figure 4.8** respectively.
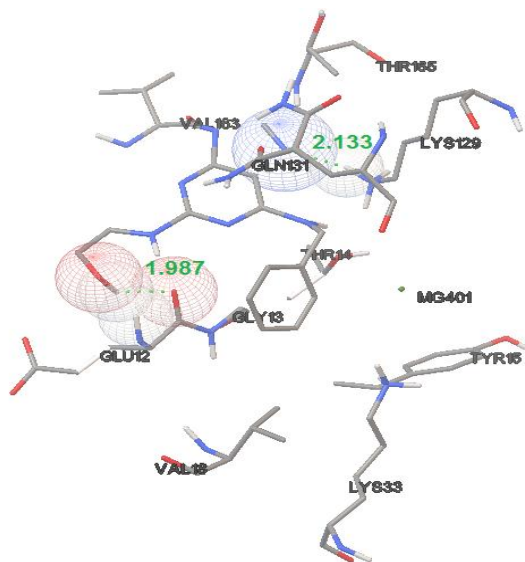
Figure 4.7 Binding mode of standard drug olomoucine in the ATP pocket of CDK-2 (PDB ID: 1HCK). Hydrogen bond interactions (2.133 Å) with LYS 129 and GLU 12 (1.987 Å) amino acid residues of CDK-2 (PDB ID: 1HCK), respectively, are shown as dotted lines. Rest of the protein is suppressed for clarification purposes.
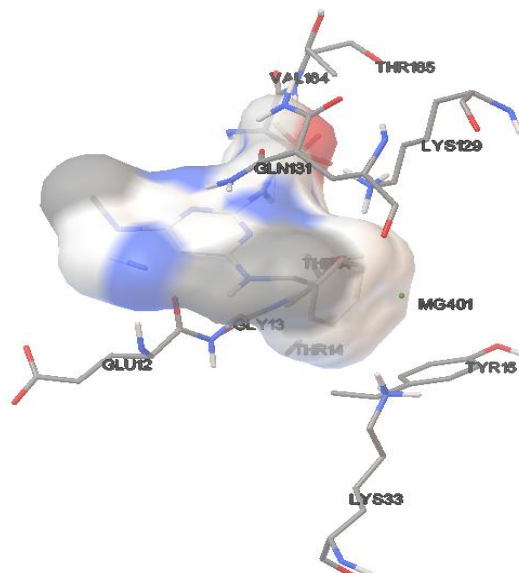
Figure 4.8 Van der Waals interaction of standard drug olomoucine with various amino acid residues of the receptor.

4.2.3 Molecular Dynamic Study

The accuracy and validity of the docking procedure was further verified by a Molecular Dynamic study performed as described below:

GROningen Machine for Chemical Simulations V4.6.1 (GROMACS) computational package[80] was used to carry out the Molecular dynamics (MD). Prior to energy minimization, protein was placed in the center of a cubic box having sides of 1.5 nm and was solvated in Space Point Charge216 (SPC216) water model and approximately 28,000 water molecules were present in the system. The whole system was neutralized by adding Cl⁻ ions. All bonding and non-bonding interactions were determined by using GROMOS96 43a1 force field.[81] Steepest-descent followed by conjugate gradient algorithms were used for energy minimization of the target protein (PDB ID: 1HCK). The system was simulated at room temperature 300 K, 1 bar pressure. The temperature and pressure of the system was regulated by Berendsen weak coupling method. The long-range electrostatics[82] were handled using the particle Mesh Ewald (PME) method with default parameter (distance for the Van der Waals and Coulomb cutoff were 12 Å and 1.2 Å spacing for the fast Fourier transform grid). Finally, MD simulations for protein were carried out for 2 ns. During the production simulation no constraints were applied to the protein.

4.2.4 Molecular parameters

Good pharmacokinetic properties and toxicity profiles are essential for any ligand to complete drug discovery process and to become successful drug[83] candidate. Hence, in the present study, Lipinski rule of five parameters and toxicity properties were predicted for the designed compounds using molinspiration cheminformatics (http://www.molinspiration.com) and OSIRIS property explorer

(http://www.organic-chemistry.org/prog/peo) respectively. Lipinski's rule of five is used to demonstrate the pharmacokinetic properties such as absorption, distribution, metabolism and excretion by their molecular properties like ClogP ($\leq$5), molecular weight ($\leq$500), number of hydrogen bond acceptors ($\leq$5) and number of hydrogen bond donors ($\leq$10). Molecules violating more than one of these rules may have problem with bioavailability.[84-85] Absorption and distribution properties of a molecule greatly depend on its aqueous solubility. In the present study, we also reported predicted aqueous solubility of the designed analogs. The values given here are logarithm value of aqueous solubility (logS) measured in mol/lit. More than 90% of the marketed drugs have the estimated log S value in between -6 and -3. Drug likeness is a qualitative concept used in drug design for how ''drug-like'' a substance is with respect to factors like bioavailability.[86] There are many approaches which assess a compounds drug-likeness based upon topological descriptors, fingerprints of MDL structure keys or other properties like ClogP, molecular weight and toxicity profile. The drug-likeness is calculated by using following equation as-

$$d = \frac{\sum v_i}{\sqrt{n}}$$

where $\sum v_i$ is the summming up score values of the fragments, and n is the number of fragments in the molecule under investigation.

Around 80% of the marketed drugs have positive drug-likeness value (http://www.organic-chemistry.org/prog/peo). A positive value states that, the molecule contains predominantly fragments which are frequently present in commercial drugs. Toxicity risks like mutagenicity, tumorigenicity, irritancy and the effect on sexual reproduction were predicted for the designed analogs and are reported. Toxicity risk alerts are an indication of that particular compound that may be harmful concerning the risk category specified. However, risk alerts are not fully reliable for compounds toxicity. It is an *in-silico* prediction of compounds toxicity based on sub-structures present in the compound and their toxicity. The drug score (ds) is a handy value and is useful to judge the compound's overall potential to qualify as drug. Drug score of a molecule mainly depends on the druglikeness, ClogP, logS, molecular weight and toxicity risks of the molecule. It is calculated from the following formula:

$$ds = \pi \left(\frac{1}{2} + \frac{1}{2} si \right).\pi ti$$

ds = drug score, si = contribution directly calculated from ClogP, logS, molecular weight and drug likeness, ti = contribution directly calculated from toxicity risks.

4.3 Results and discussion

The docking studies of the designed analogs and standard drug olomoucine **(Figure 4.9)** were performed using molecular modeling software autodock 4.2. In the present study, two docking parameters such as binding free energy (K.cal/mole) and predicted inhibitory constant (Ki) values for all three series (I, II and III) were determined and are showed in **Table 4.1, 4.2,** and **4.3** respectively. Binding free energy of the individual compound was calculated using the following formula:

$$Binding\ Energy = [(1) + (2) + (3) - (4)]$$

where 1 denotes final intermolecular energy [van der Waals energy + hydrogen bonds + desolvation energy + electrostatic energy (K.cal/mol)], 2 denotes final total internal energy [internal energy of ligand + internal energy of receptor (K.cal/mol)], 3 denotes torsional free energy (K.cal/mol) and 4 denotes unbound system's energy (K.cal/mol).

In docking studies, binding free energy value is indirectly proportional to enzyme inhibitory activity. In the present study, our designed analogs showed binding free energy values in the range of -12.31 to -9.07 for series-I, -12.15 to -9.90 for series-II and -11.27 to -8.89 for series-III. Among the designed analogs, AK-6, AK-16, AK-26, AK-30, AK-60, AK-64 from series-I **(Table: 4.1)** and AK-6K, AK-20K, AK-42K, AK-50K, AK-64K, AK-72K from series-II **(Table: 4.2)** and AK-16E, AK-26E, AK-32E, AK-48E, AK-50E, AK-60E from series-III **(Table: 4.3)** showed significant binding free energy values of -10.66, -10.71, -12.31, -10.51, -10.70, -12.08 for series-I **(Table: 4.1)** and -11.76, -11.63, -12.10, -11.65, -12.13, -12.15 for series-II **(Table: 4.2)** and -10.78, -10.99, -10.93, -10.72, -10.73, -11.27 kcal/mol for series-III **(Table: 4.3)** respectively against CDK-2 receptor with that of standard drug olomoucine (-8.90 kcal/mol). The overlay view of these analogs is showed in **Figure 4.12**, **4.14** and **4.19** for series-I, II, and III respectively. Closer observation of receptor-ligand complex reveals that, like other standard CDK-2 inhibitors, the designed analogs also adopt the same conformation in the ATP active site of CDK-2. A brief Structure-Activity-Relationship (SAR) is quite unequivocal. Comparing the B.E values of the three series **(Tables- 4.1, 4.2, and 4.3)**, series-II with the ketone group on the pyrazole turns out as the best. This implies that, the presence of HBD at the top-left part of the pyrazole moiety is crucial for enhanced activity. Secondly, compounds bearing nitro-substituent's (AK-26, 64; AK-26K, 64-K; and AK-26E, 64-E) consistently exhibit good B.E profiles. Thirdly, Iodo and n-butyl substituent's turned out to be the worst in terms of their binding energies. Hydrogen bonding and van der Waals interactions were observed between ligands and amino acids of the receptor protein. These interactions play an important role in the determination of binding free energy and stability of receptor-ligand complex.

4.3.1 Hydrogen bonding interaction

Hydrophilic body (–NH) in pyrazolone and oxygen (-O-) in pyran ring behave as hydrogen bond donor and hydrogen bond acceptor respectively in the designed analog AK-26 and are responsible for hydrogen bonding interaction with hydrophilic amino acids GLU-162 (**Figure 4.10**) and LYS-129 (**Figure 4.11**) of target protein in series-I. Overlay stereo view of best designed analogues of six molecules of series-I AK-6 (white), AK-16 (red), AK-26 (yellow), AK-30 (green), AK-60 (pink) and AK-64 (blue) in the inhibitory binding pocket of 1HCK has been shown in **Figure 4.12**. Similarly, keto group (-C=O) on pyrazolone moiety and oxygen from the pyran ring showed hydrogen bonding interaction with GLU-131 and LYS-33 (**Figure 4.13**) respectively in series-II analog AK-72K. Overlay stereo view of best designed analogues of six molecules of series-II AK-6K (green), AK-20K (red), AK-42K (yellow), AK-50K (white), AK-64K (blue) and AK-72K (pink) in the inhibitory binding pocket of 1HCK has been shown in **Figure 4.14**. In series-III, hydrophilic body (*m*-OCH$_3$) of analog AK-60E showed hydrogen bonding interaction with both ASN-132 (**Figure 4.15**) as well as THR-14 (**Figure 4.16**) and -NH and -O- showed interaction with LYS-33 (**Figure 4.17**) and LYS-129 (**Figure 4.18**) respectively. Overlay stereo view of best designed six analogues of series-III AK-16E (red), AK-26E (yellow), AK-32E (green), AK-48E (pink), AK-50E (blue), AK-60E (white) in the inhibitory binding pocket of 1HCK has been shown in **Figure 4.19**. Among these, GLU-162, GLU-131, LYS-129, LYS-33, ASN-132 and THR-14 are active site amino acid residues that are mainly involved in hydrogen bond interaction with designed analogs and might be responsible for CDK-2 (PDB ID: 1HCK) inhibition activity as depicted in **Figure 4.19**. Docking studies revealed that, carbonyl oxygen and -NH of designed ligands act as hydrogen bond acceptor and hydrogen bond donor, respectively, in the ligand-receptor interactions.
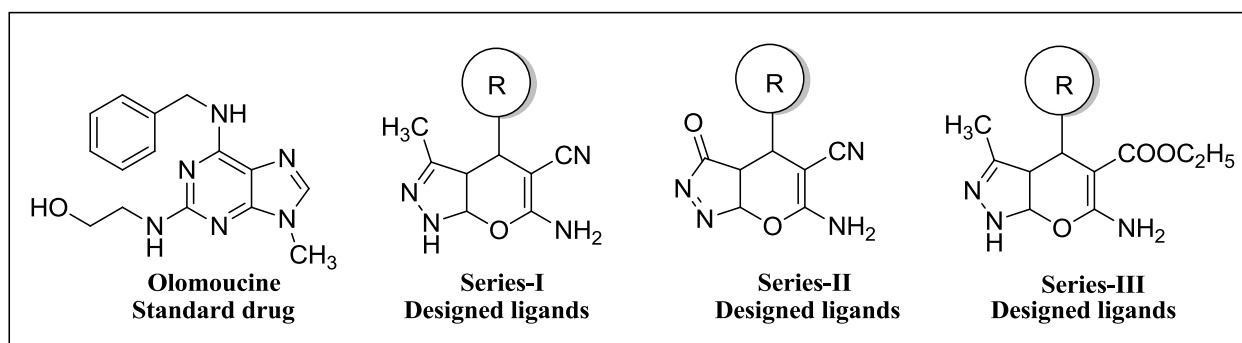
Figure 4.9 Structure of standard drug and the designed ligands.
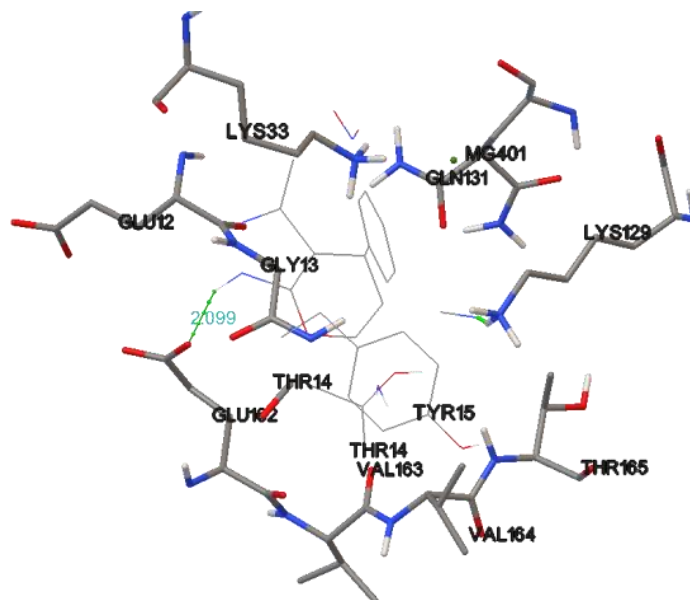
Figure 4.10 Hydrogen bonding interaction of AK-26 with GLU-162 of 1HCK. Ligand is shown as ball and sticks, receptor amino acids as lines and hydrogen bond interaction as dotted lines. Rest of the protein is suppressed for clarification purposes.
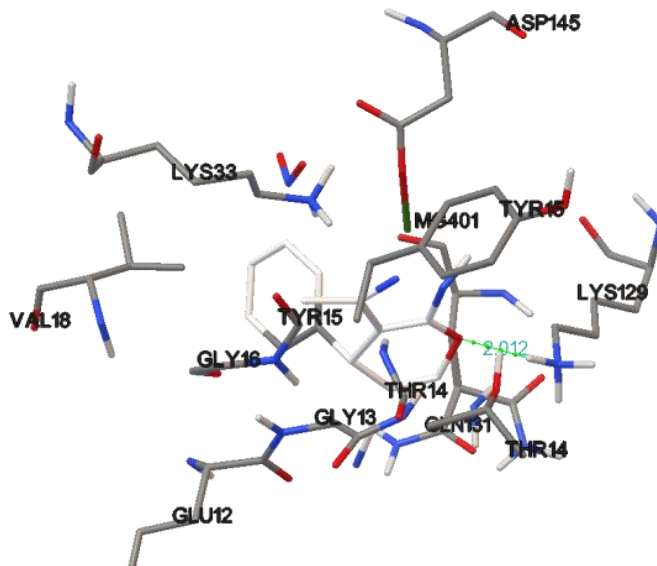
Figure 4.11 Hydrogen bonding interaction of AK-26 with LYS-129 of 1HCK. Ligand is shown as ball and sticks, receptor amino acids as lines and hydrogen bond interaction as dotted lines. Rest of the protein is suppressed for clarification purposes

166

Table 4.1: Docking result of the designed analogs of series-I.

S. No.	Comp[a]	R	B.E.[b]	K_i[c]
1	Olomoucine	-	-8.90	299.67
2	AK-6	2-furanyl	-10.66	15.25
3	AK-14	4-OH-C_6H_4	-9.71	76.28
4	AK-16	3-OH-C_6H_4	-10.71	14
5	AK-18	4-Br-C_6H_4	-9.80	65.45
6	AK-20	3-Br-C_6H_4	-9.85	60.40
7	AK-26	3-NO_2-C_6H_4	-12.31	0.944
8	AK-28	3-thiophenyl	-9.30	152.40
9	AK-30	2-pyrrolyl	-10.51	19.79
10	AK-32	3-indolyl	-10.44	22.38
11	AK-34	2-thiophenyl	-9.75	70.83
12	AK-42	4-Cl-C_6H_4	-9.55	99.53
13	AK-44	*n*-butyl	-9.18	185.34
14	AK-46	2-I-C_6H_4	-9.53	102.61
15	AK-48	C_6H_5	-10.33	26.70
16	AK-50	4-CH_3-C_6H_4	-9.80	65.84
17	AK-54	2-pyridinyl	-10.42	23.14
18	AK-56	4-pyridinyl	-10.17	35.21
19	AK-60	3,4-di-$OCH_3C_6H_3$	-10.70	14.32
20	AK-62	2-F-C_6H_4	-9.07	222.92
21	AK-64	4-NO_2-C_6H_4	-12.08	1.40
22	AK-72	4-F-C_6H_4	-9.26	162.03
23	AK-74	4-(N,N-dimethylamino)-C_6H_4	-9.85	60.68
24	AK-76	2-OH-C_6H_4	-10.24	31.45

[a]compound; [b]Binding Energy in K.cal/mole; [c]Inhibition constant in nM.
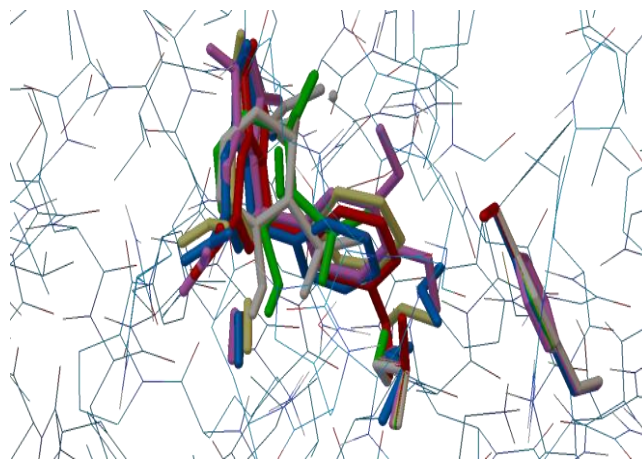
Figure 4.12 Overlay stereo view of series-I AK-6 (white), AK-16 (red), AK-26 (yellow), AK-30 (green), AK-60 (pink), AK-64 (blue) in the inhibitory binding pocket of 1HCK.

Table 4.2: Docking result of the designed analogs of series-II.

S. No.	Comp[a]	R	B.E.[b]	K_i[c]
1	AK-6K	2-furanyl	-11.76	2.40
2	AK-14K	4-OH-C_6H_4	-10.75	13.15
3	AK-16K	3-OH-C_6H_4	-10.37	25.24
4	AK-18K	4-Br-C_6H_4	-11.59	3.20
5	AK-20K	3-Br-C_6H_4	-11.63	2.98
6	AK-26K	3-NO_2-C_6H_4	-11.51	3.63
7	AK-28K	3-thiophenyl	-10.54	18.79
8	AK-30K	2-pyrrolyl	-10.92	9.84
9	AK-32K	3-indolyl	-11.26	5.58
10	AK-34K	2-thiophenyl	-10.66	15.35
11	AK-42K	4-Cl-C_6H_4	-12.10	1.35
12	AK-44K	*n*-butyl	-10.22	32.28
13	AK-46K	2-I-C_6H_4	-9.90	54.97
14	AK-48K	C_6H_5	-11.09	7.40
15	AK-50K	4-CH_3-C_6H_4	-11.65	2.91
16	AK-54K	2-pyridinyl	-11.38	4.55
17	AK-56K	4-pyridinyl	-10.94	9.59
18	AK-60K	3,4-di-$OCH_3C_6H_3$	-11.02	8.33
19	AK-62K	2-F-C_6H_4	-10.64	15.76
20	AK-64K	4-NO_2-C_6H_4	-12.13	1.28
21	AK-72K	4-F-C_6H_4	-12.15	1.24
22	AK-74K	4-(N,N-dimethylamino)-C_6H_4	-11.26	5.59
23	AK-76K	2-OH-C_6H_4	-10.53	19.18

[a]compound; [b]Binding Energy in K.cal/mole; [c]Inhibition constant in nM.
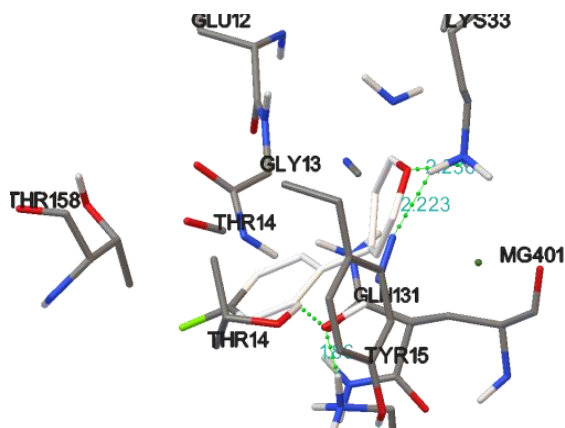
Figure 4.13 Hydrogen bonding interaction of AK-72K with GLU-131 and LYS-33 of 1HCK.
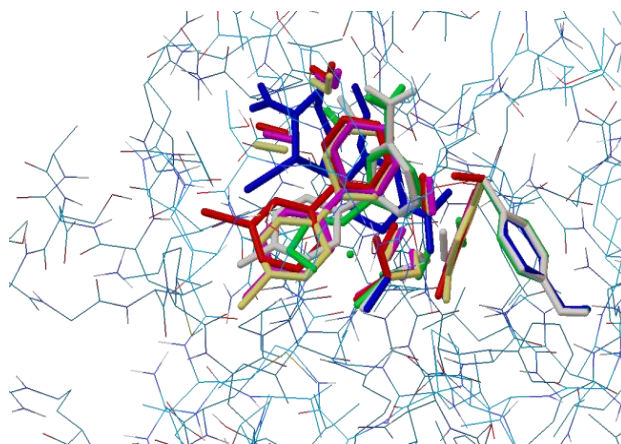
Figure 4.14 Overlay stereo view of series-II AK-6K (green), AK-20K (red), AK-42K (yellow), AK-50K (white), AK-64K (blue), AK-72K (pink), in the inhibitory binding pocket of 1HCK.

Table 4.3: Docking result of the designed analogs of series-III.

S. No.	Comp[a]	R	B.E.[b]	K_i[c]
1	AK-6E	2-furanyl	-9.90	55.16
2	AK-14E	$4\text{-OH-C}_6\text{H}_4$	-10.13	37.25
3	AK-16E	$3\text{-OH-C}_6\text{H}_4$	-10.78	12.58
4	AK-18E	$4\text{-Br-C}_6\text{H}_4$	-8.89	303.07
5	AK-20E	$3\text{-Br-C}_6\text{H}_4$	-9.83	61.80
6	AK-26E	$3\text{-NO}_2\text{-C}_6\text{H}_4$	-10.99	8.72
7	AK-28E	3-thiophenyl	-9.02	246.52
8	AK-30E	2-pyrrolyl	-8.81	350.31
9	AK-32E	3-indolyl	-10.93	9.65
10	AK-34E	2-thiophenyl	-9.04	234.83
11	AK-42E	$4\text{-Cl-C}_6\text{H}_4$	-10.24	31.12
12	AK-44E	*n*-butyl	-9.62	88.66
13	AK-46E	$2\text{-I-C}_6\text{H}_4$	-10.04	43.95
14	AK-48E	C_6H_5	-10.72	13.79
15	AK-50E	$4\text{-CH}_3\text{-C}_6\text{H}_4$	-10.73	13.75
16	AK-54E	2-pyridinyl	-10.24	31.21
17	AK-56E	4-pyridinyl	-10.46	21.57
18	AK-60E	$3,4\text{-di-OCH}_3\text{C}_6\text{H}_3$	-11.27	5.51
19	AK-62E	$2\text{-F-C}_6\text{H}_4$	-9.85	60.20
20	AK-64E	$4\text{-NO}_2\text{-C}_6\text{H}_4$	-10.21	32.61
21	AK-72E	$4\text{-F-C}_6\text{H}_4$	-9.24	169.54
22	AK-74E	$4\text{-(N,N-dimethylamino)-C}_6\text{H}_4$	-9.24	168.21
23	AK-76E	$2\text{-OH-C}_6\text{H}_4$	-10.60	17.06

[a]compound; [b]Binding Energy in K.cal/mole; [c]Inhibition constant in nM.
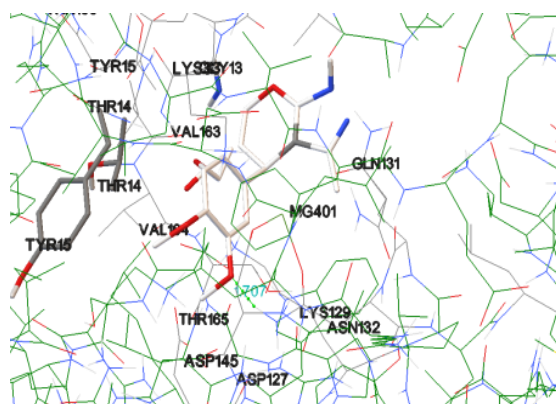
Figure 4.15 Hydrogen bonding interaction of AK-60E with ASN-132 in the binding pocket of 1HCK.
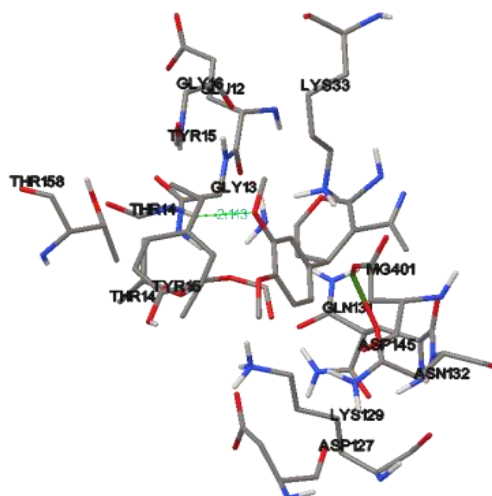
Figure 4.16 Hydrogen bonding interaction of AK-60E with THR-14 in the binding pocket of 1HCK.
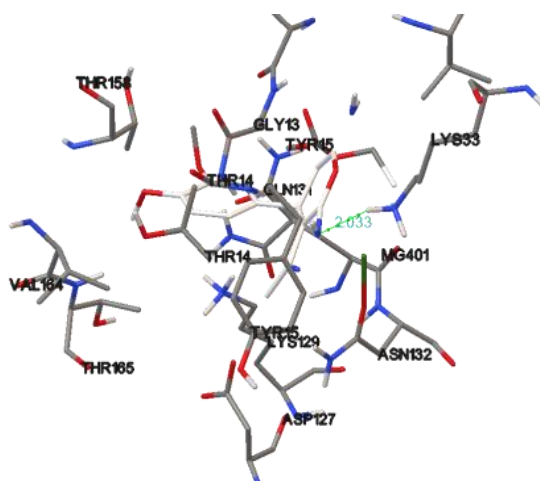
Figure 4.17 Hydrogen bonding interaction of AK-60E with LYS-33 in the binding pocket of 1HCK.
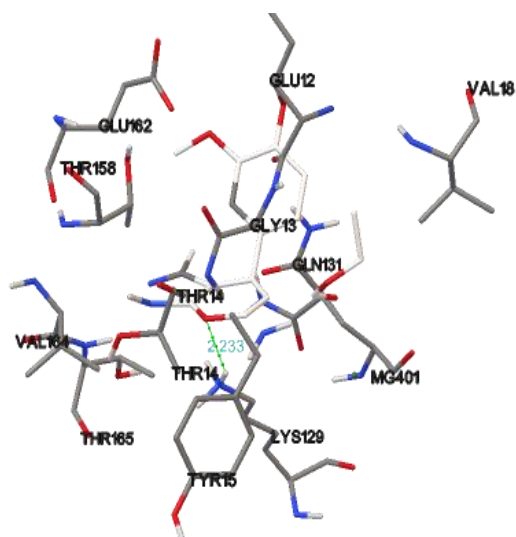
Figure 4.18 Hydrogen bonding interaction of AK-60E with LYS-129 in the inhibitory binding pocket of 1HCK protein.
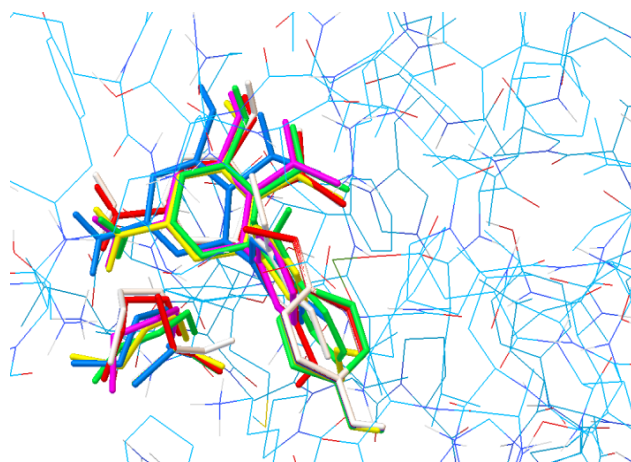
Figure 4.19 Overlay stereo view of series-III AK-16E (red), AK-26E (yellow), AK-32E (green), AK-48E (pink), AK-50E (blue), AK-60E (white) in the inhibitory binding pocket of 1HCK.

4.3.2 Van der Waals interaction

Van der Waals interaction plays a major role in the determination of binding free energy of ligand-receptor complex. Amino acids GLY11, GLY13, GLY16, GLU12, VAL18, THR14, TYR-15, LYS-33, GLN131, LYS129, ILE10 and MG401 (Mg^{2+}) of target receptor are responsible for van der Waals interaction **(Figure 4.20)** with ligands AK-26 in series-I **(Table: 4.1)** indeed to form stable receptor-ligand complex. Similarly, GLY11, GLU12, GLY13, GLY16, THR14, TYR15, THR158, LYS33, LYS129 amino acids and MG401 (Mg^{2+}) with ligand AK-72K in series-II **(Table: 4.2, Figure 4.21)** and amino acids GLU12, GLY13, LYS33, THR14, THR158, TYR15, ASP127, ASP145, ASN132 and

MG401 (Mg^{2+}) with ligand AK-60E in series-III **(Table: 4.3, Figure 4.22)** are responsible for van der walls interaction. Van der Waals interaction exhibited by prototype compound AK-26, AK-72K and AK-60E with target protein and amino acid residues present within the van der Waals radius are shown in **Figure 20**, **21** and **22** respectively. In addition, another docking parameter, namely, predicted inhibitory constant (K_i) was also determined. The inhibitory constant is a measure of compound's inhibitory potency of a biological or biochemical function. Inhibitory constant is exponential to the binding free energy of receptor ligand complex. In the present study, our designed analogs showed inhibitory constant values in the range of 0.944 to 222.92 nM for series-I, 1.24 to 54.97 nM for series-II and 5.51 to 350.31 nM for series-III compounds. Among the designed 69 analogs from all three series, AK-6, AK-16, AK-26, AK-30, AK-60, AK-64, AK-6K, AK-20K, AK-42K, AK-50K, AK-64K, AK-72K, AK-16E, AK-26E, AK-32E, AK-48E, AK-50E and AK-60E showed significant inhibitory constant values of 15.25, 14.00, 0.94, 19.79, 14.32, 1.40, 2.40, 2.98, 1.35, 2.91, 1.28, 1.24, 12.58, 8.72, 9.65, 13.79, 13.75 and 5.51nM respectively against CDK-2 enzyme (PDB ID: 1HCK) with that of standard olomoucine (299.67 nM). After keen observation of docking results, it was found that, different substitutions on the designed pyrazolopyran pharmacophore greatly affected the stability of receptor-ligand complex and inhibitory constant values. After analyzing all the three series of the designed analogs, it was observed that, the series-I trend suggests a combination of H-bonding, electronic and steric interaction plays a major role; hence only few compounds showed increased energy values. It also predicted the positional disturbances greatly, when comparing the substituent's like phenyl and tolyl groups as well as *o*-, *m*- and *p*- positioning around aromatic substituent's, even for the pyridine nuclei, on position 2- and 4. Best docking score in series-I **(Table: 4.1)** is of AK-26 analogue. The series-II analogues showed a huge increase in the binding energy of all the compounds, in line with the theoretical values obtained for the calibration of well-known CDK inhibitors like flavopiridol (-9.40 kcal/mol), kenpaullone (-10.68 kcal/mol), indirubin (-11.20 kcal/mol) and olomoucine (-8.90 kcal/mol) etc. This showed that, replacement of the methyl group **(series-I, Table: 4.1)** on the pyrazolon moiety with a keto group **(series-II, Table: 4.2)** has served a double purpose: removal of steric hindrance in some cases and a huge increase in stability due to the electronic effects of the keto group. This series need to be scrutinized further as preliminary screening of these compounds down to a sizable chunk has not been possible. Best docking score in series-II **(Table: 4.2)** is of AK-72K analog. Finally the series-III **(Table: 4.3)** showed binding energy data similar to the series-I **(Table: 4.1)**, but less due to further steric disturbances and electronic repulsions created by the introduction of larger ester group instead of the cyanide group. Best Docking Score in series-III **(Table: 4.3)** is of AK-60E analog.
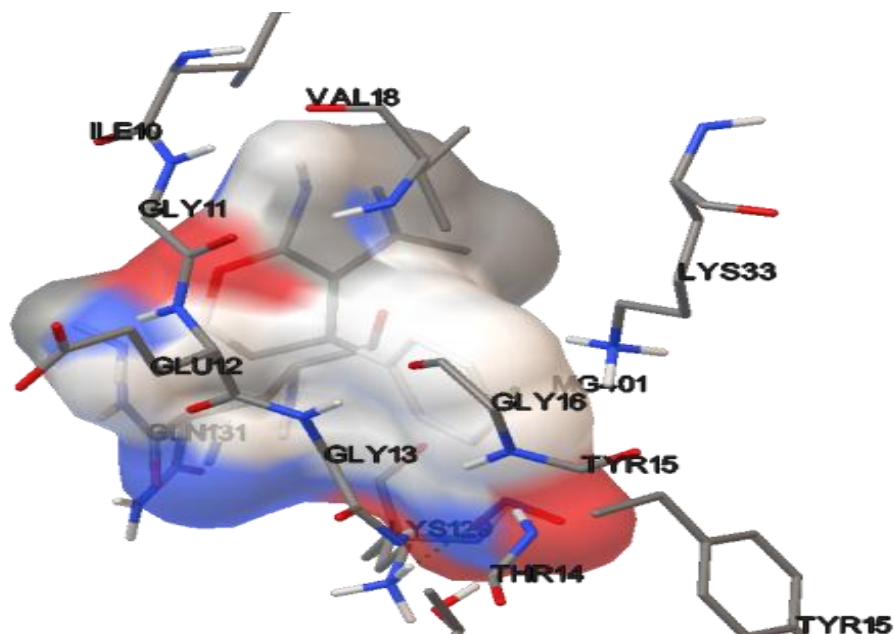
Figure 4.20 Van der Waals interaction of AK-26 with various amino acid residues in the inhibitory binding pocket of 1HCK.
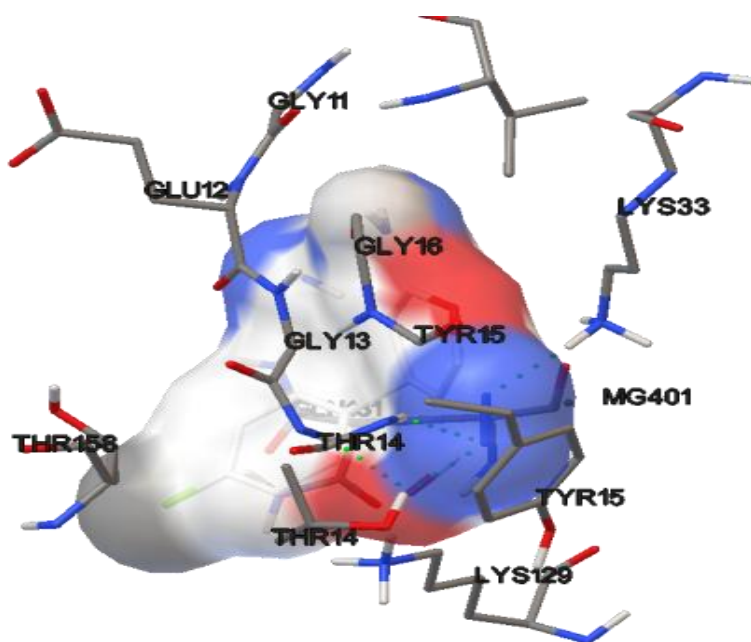
Figure 4.21 Van der Waals interaction of AK-72K with various amino acid residues in the inhibitory binding pocket of 1HCK.
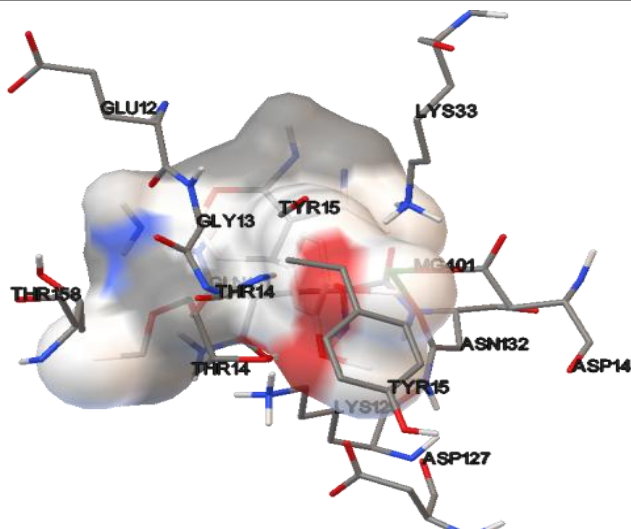
Figure 4.22 Van der Waals interaction of AK-60E with various amino acid residues in the inhibitory binding pocket of 1HCK.

In order to get a better perspective of our docking protocol, we decided to re-add the water molecules that have been removed at the starting of the docking procedure. From all the designed 69 analogues, the compound AK-26 with highest score from first series and the molecule having lowest score from third series (AK-30E) were docked without deleting water and the results have been summarized in **Table 4.4**.

Table 4.4: Docking results of analogues AK-26 and AK-30E with and without water.

S. No.	Compound code	Mol.wt.	Without water		With water
			B.E.(K.cal/mol)	K_i (nM)	B.E.(K.cal/mol)
1	AK-26	297	-12.31	0.944	+118.99
2	AK-30E	288	-8.81	350.31	+152.08

Thus, retaining of water molecules in the protein results in positive binding energy value implying that, the compound will not be stable inside the pocket of protein or, in other words, the compound does not show the desired favorable interaction.

4.3.3 Molecular dynamics simulations

Analysis of the RMSD graph for target protein **(Figure 4.23)**, revealed that, the protein reached an equilibrium condition within 500 ps of simulation and the backbone RMSD varied between 2 and 2.5 Å during the simulation.

Result suggesting that, protein is more stabilized throughout the simulation. The potential energy **(Figure 4.24)** of the protein was found to be -1.16403e+06 kJ mol^{-1}.
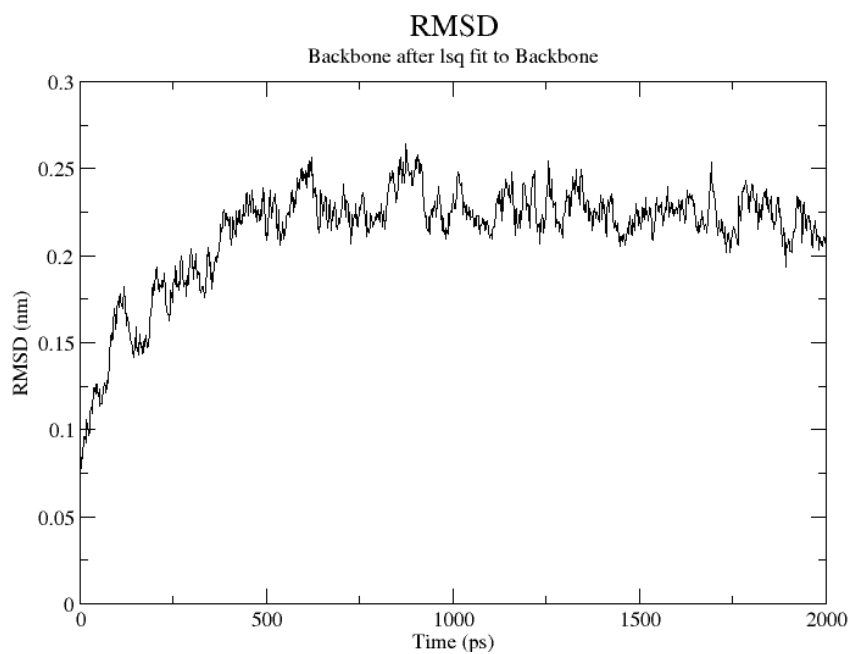
Figure 4.23 Showing the RMSD graph of the target protein 1HCK.
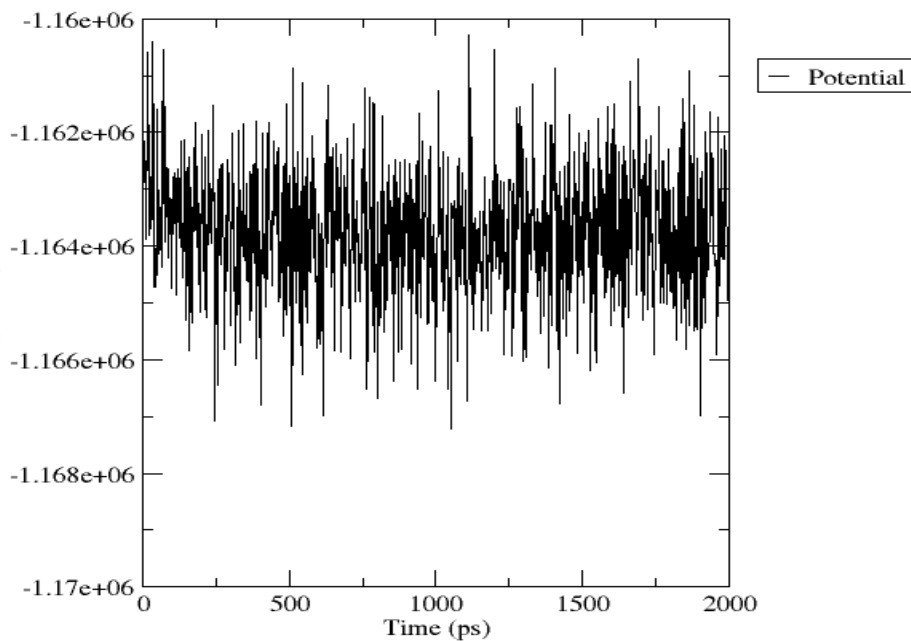
Figure 4.24 Showing the potential energy graph of the target protein 1HCK.

4.3.4 Molecular parameters

Molecular properties like molecular weight, ClogP, logS (solubility), number of hydrogen bond acceptors, number of hydrogen bond donors, drug likeness and toxicity risks like mutagenic, tumorigenic, irritant, effect on sexual reproduction and drug score were predicted for the designed analogs using online tools, OSIRIS property explorer (http://www.organic-chemistry.org/prog/peo/) and molinspiration cheminformatics (http://www.molinspiration.com/). Predicted molecular properties of the designed analogs are reported in **Table 4.5**. Among the 69 designed analogs in three series (23 molecule in each series), five molecules AK-18K, AK-20K, AK-32K, AK-42K, and AK-46K were violated 2 times (No. of HBA and solubility) from Lipinski rule of five. Only single violation from Lipinski rule of five is accepted; any molecule violating more than once from Lipinski rule of five parameters may have problems in bioavailability.[84-85] Some of the designed molecules such as AK-6K, AK-16K, AK-18K, AK-20K, AK-26K, AK-28K, AK-30, AK-32, AK-34K, AK-42K, AK-44K, AK-46K, AK-48K, AK-50K, AK-54K, AK-56K, AK-60K, AK-62K, AK-64K, AK-72K, AK-74K and AK-76K showed predicted active risk of producing mutagenicity and tumorigenicity. The analogs AK-14K and AK-60K exhibited predicted active risk of producing mutagenicity, reproductive effects and high risk of tumorigenicity. The analogs AK-14 and AK-60 showed predicted active risk (i.e. compounds showing any one effect with single positive sign) and high risk (i.e. compounds showing any one effect with double positive sign) of producing reproductive effects respectively. The analogs AK-74 and AK-74E exhibited predicted high risk of tumorigenicity only. However, risk alerts for the designed analogs may not be fully reliable and in order to avoid risk of taking unsafe compounds, we screened off AK-14, AK-60, AK-74, AK-6K, AK-14K, AK-16K, AK-18K, AK-20K, AK-26K, AK-28K, AK-30K, AK-32K, AK-34K, AK-42K, AK-44K, AK-46K, AK-48K, AK-50K, AK-54K, AK-56K, AK-60K, AK-62K, AK-64K, AK-72K, AK-74K, AK-76K and AK-74E molecules for further study. It should be noted that, the calculations of toxicity are not analyzed in detail as these results are merely preliminary druggability predictions. Further comprehensive studies are currently underway in our labs.

Table 4.5: Predicted molecular parameters of the designed analogs.

S. No	Comp. Code	MW	CLogP	No. of HBA	No. of HBD	Solub.	Drug likeness Score	MUT	TUM	IRR	REP	Drug Score
1	AK-6	242	0.21	6	3	-4.11	-2.3	-	-	-	-	0.45
2	*AK-14*	268	0.68	6	4	-4.14	-1.61	-	-	-	+	0.38
3	AK-16	268	0.68	6	4	-4.14	-2.16	-	-	-	-	0.45
4	AK-18	331	1.75	5	3	-5.26	-3.65	-	-	-	-	0.34

5	AK-20	331	1.75	5	3	-5.26	-5.64	-	-	-	-	0.33
6	AK-26	297	0.1	8	3	-4.89	-7.54	-	-	-	-	0.37
7	AK-28	258	0.81	5	3	-4.33	-2.04	-	-	-	-	0.45
8	AK-30	241	-0.2	6	4	-3.48	-1.72	-	-	-	-	0.51
9	AK-32	291	1.06	6	4	-4.96	-1.32	-	-	-	-	0.44
10	AK-34	258	0.89	5	3	-4.44	-0.59	-	-	-	-	0.54
11	AK-42	286	1.63	5	3	-5.17	-0.56	-	-	-	-	0.47
12	AK-44	232	2.12	5	3	-4.46	-7.69	-	-	-	-	0.39
13	AK-46	378	1.46	5	3	-5.45	-1.97	-	-	-	-	0.35
14	AK-48	252	1.02	5	3	-4.43	-1.71	-	-	-	-	0.46
15	AK-50	266	1.37	5	3	-4.78	-3.32	-	-	-	-	0.39
16	AK-54	253	0.08	6	3	-3.66	-1.71	-	-	-	-	0.5
17	AK-56	253	0.02	6	3	-3.64	-2.57	-	-	-	-	0.47
18	AK-60	312	0.88	7	3	-4.47	-0.02	-	-	-	++	0.46
19	AK-62	270	1.13	5	3	-4.74	-3.66	-	-	-	-	0.38
20	AK-64	297	0.1	8	3	-4.89	-12.06	-	-	-	-	0.37
21	AK-72	260	1.13	5	3	-4.74	-2.32	-	-	-	-	0.41
22	AK-74	295	0.92	6	3	-4.47	-2.89	-	++	-	-	0.25
23	AK-76	268	0.68	6	4	-4.14	-2.36	-	-	-	-	0.45
24	AK-6K	242	-0.12	7	2	-5.21	-9.0	+	++	-	-	0.17
25	AK-14K	268	0.34	7	3	-5.24	-8.27	+	++	-	+	0.13
26	AK-16K	268	0.34	7	3	-5.24	-8.85	+	++	-	-	0.17
27	AK-18K	331	1.42	6	2	-6.37	-10.34	+	++	-	-	0.13
28	AK-20K	331	1.42	6	2	-6.37	-12.34	+	++	-	-	0.13
29	AK-26K	297	-0.23	9	2	-5.99	-14.24	+	++	-	-	0.15
30	AK-28K	258	0.47	6	2	-5.43	-8.73	+	++	-	-	0.16
31	AK-30K	241	-0.53	7	3	-4.58	-8.65	+	++	-	-	0.19
32	AK-32K	291	0.73	7	3	-6.06	-8.0	+	++	-	-	0.14
33	AK-34K	258	0.56	6	2	-5.54	-7.26	+	++	-	-	0.16
34	AK-42K	286	1.3	6	2	-6.27	-7.23	+	++	-	-	0.14
35	AK-44K	232	0.58	6	2	-5.27	-14.4	+	++	-	-	0.17
36	AK-46K	378	1.13	6	2	-6.55	-8.66	+	++	-	-	0.13
37	AK-48K	252	0.69	6	2	-5.53	-8.4	+	++	-	-	0.16
38	AK-50K	266	1.03	6	2	-5.88	-10.0	+	++	-	-	0.15
39	AK-54K	253	-0.26	7	2	-4.76	-8.39	+	++	-	-	0.18
40	AK-56K	253	-0.31	7	2	-4.74	-9.27	+	++	-	-	0.18
41	AK-60K	312	0.55	8	2	-5.57	-6.69	+	++	-	+	0.12
42	AK-62K	270	0.79	6	2	-5.85	-10.34	+	++	-	-	0.15
43	AK-64K	297	-0.23	9	2	-5.99	-18.74	+	++	-	-	0.15

44	*AK-72K*	270	0.79	6	2	-5.85	-8.99	+	++	-	-	0.15
45	*AK-74K*	295	0.59	7	2	-5.57	-9.57	+	++	-	-	0.16
46	*AK-76K*	268	0.34	7	3	-5.24	-9.06	+	++	-	-	0.17
47	AK-6E	289	0.53	7	3	-3.87	-0.99	-	-	-	-	0.53
48	AK-14E	315	0.99	7	4	-3.89	-0.26	-	-	-	-	0.59
49	AK-16E	315	0.99	7	4	-3.89	-0.78	-	-	-	-	0.54
50	AK-18E	378	2.06	6	3	-5.02	-2.3	-	-	-	-	0.36
51	AK-20E	378	2.06	6	3	-5.02	-4.27	-	-	-	-	0.34
52	AK-26E	344	0.42	9	3	-4.65	-6.09	-	-	-	-	0.37
53	AK-28E	305	1.12	6	3	-4.09	-0.68	-	-	-	-	0.54
54	AK-30E	288	0.11	7	4	-3.23	-0.4	-	-	-	-	0.62
55	AK-32E	338	1.38	7	4	-4.71	-0.02	-	-	-	-	0.54
56	AK-34E	305	1.2	6	3	-4.2	0.66	-	-	-	-	0.66
57	AK-42E	333	1.94	6	3	-4.92	0.62	-	-	-	-	0.58
58	AK-44E	279	2.44	6	3	-4.22	-6.28	-	-	-	-	0.39
59	AK-46E	425	1.77	6	3	-5.2	-0.62	-	-	-	-	0.41
60	AK-48E	299	1.34	6	3	-4.19	-0.41	-	-	-	-	0.56
61	AK-50E	313	1.68	6	3	-4.53	-1.95	-	-	-	-	0.42
62	AK-54E	300	0.39	7	3	-3.42	-0.43	-	-	-	-	0.61
63	AK-56E	300	0.34	7	3	-3.39	-1.16	-	-	-	-	0.54
64	AK-60E	359	1.2	8	3	-4.22	1.28	-	-	-	-	0.68
65	AK-62E	317	1.44	6	3	-4.5	-2.28	-	-	-	-	0.42
66	AK-64E	344	0.42	9	3	-4.65	-10.66	-	-	-	-	0.37
67	AK-72E	317	1.44	6	3	-4.5	-1.1	-	-	-	-	0.48
68	*AK-74E*	342	1.23	7	3	-4.22	-1.52	-	++	-	-	0.28
69	AK-76E	315	0.99	7	4	-3.89	-0.95	-	-	-	-	0.53

Compounds violating more than one time from Lipinski rule of 5 and compounds exhibited predicted toxicity are in Italics

HBA hydrogen bond acceptor, *HBD* hydrogen bond donor, *MUT* mutagenic, *TUM O* tumorigenic, *IRRI* irritant, *REP* reproductive effective, ''+'' active risk, ''++'' High risk ''–'' non-active risk.

4.4 Conclusions

In the present study, we have designed 69 novel pyrazolopyran analogs as CDK-2 inhibitors based on pharmacophore requirements. Docking study of the designed analogs was performed using molecular modeling software Autodock 4.2. Activity comparison showed that, **AK-26** (having 3-nitro substituent), **AK-72K** (having 4-flouro substituent) and **AK-60E** (having 3,4-dimethoxy substituent) are the significant analogs showed better binding free energy and predicted inhibitory constant values as compare to standard drug olomoucine. Similarly, among the three significant compounds in all the three series, it turns out that, AK-26 is by far the best analogue overall. Lipinski rule of five parameter and toxicity

parameters of the designed analogs were predicted using OSIRIS property explorer and molinspiration cheminformatics online tools. Among the designed analogs, AK-6, AK-16, AK-26, AK-30, AK-60, AK-64 from series-I **(Table- 4.1)**, AK-6K, AK-20K, AK-42K, AK-50K, AK-64K, AK-72K from series-II **(Table- 4.2)** and AK-16E, AK-26E, AK-32E, AK-48E, AK-50E, AK-60E from series-III **(Table- 4.3)** showed significant binding free energy and predicted inhibitory constant values as compared to standard drug olomoucine. Even though compounds like AK-60 from series-I **(Table: 4.1)**, AK-42K, AK-64K, AK-72K from series-II **(Table: 4.2)** and AK-76E from series-III **(Table: 4.3)** showed significant binding free energy and predicted inhibitory constant values, they have been screened off for next level of study because of their predicted poor pharmacokinetic and toxicity profile. From this study, it was concluded that, hydrogen bond donor and hydrogen bond acceptor groups in pharmacophore are very much important to form stable receptor-ligand complex as well as for better inhibitory potency. GROningen Machine for Chemical Simulations V4.6.1 (GROMACS) computational package was used to carry out the Molecular dynamics (MD) study and was used to validate the docking procedure.

Chapter IV

Part-B

de-novo Design, Molecular Dynamics, and *in-silico* Studies of Coumarin Derivatives as Inhibitors of Cyclin Dependent Kinase-2 (PDB ID: 1HCK)

4.5 Introduction

For past three decades, computer-aided drug discovery/design[87] methods have played a major role in the development of therapeutically significant small molecules and have also been helpful in toxicity prediction and optimization of several physiological properties including anticancer activity. These methods are broadly classified as either structure-based or ligand-based methods. Structure-based methods are in principle analogous to high-throughput screening in both target and ligand and the structure information is overbearing. Structure-based approaches may include ligand docking, pharmacophore, and ligand design methods. Additionally, cancer cells are known to display deregulations in multiple signaling pathways, leading to uncontrolled cell proliferation and acquired anti-apoptosis properties.[88]

Protein kinases are a large family of enzymes that are essential for the regulation of many diverse cell functions through phosphorylation of other enzymes and structural proteins.[89] In recent years, numerous biochemical and structural studies have contributed enormously to our increased understanding of the former's role in signal transduction[90-93] and cell cycle regulation.[94-96] This has led to better understanding of cancer mechanism. For example, crystal structures of several serine/threonine protein kinases, including cyclic-AMP dependent protein kinase (cAPK)[97], mitogen-activated protein kinase (MAPK)[98], twitchin kinase[99], casein kinase 1 (CK1)[100], phosphorylase kinase (PhK)[101], and cyclin-dependent kinase 2 (CDK2)[102], revealed, with the help of structural studies done on them, a common two-domain core structure with enzyme-specific variations.[103] Thus, cell cycle progression is regulated by a series of sequential events that include the activation and subsequent inactivation of cyclin dependent kinases and cyclins. CDKs form active heterodimeric complexes by binding to their regulatory subunits, cyclins. Eleven members of the CDK family are reported so far, and each member of the family has a specific function in cell-cycle regulation. Several Cdks, mainly Cdk2, Cdk4, and Cdk6, work cooperatively to drive cells from G1 phase into S phase. Furthermore, kinases can be blocked by small molecules and recently, mitotic kinases such as CDKs[104-105], Polo-like-kinases[106-107], and Aurora kinases[108] have been studied as potential targets for cancer therapy with fewer side effects than traditional cytotoxic drugs. Among protein kinases, CDK2 appears to play a central role in cell cycle regulation, and efforts are underway to develop specific inhibitors of CDKs as potential antimitogenic drugs.[109-111]

The detailed structural analysis of CDK2 can provide valuable information for the design of new ligands that can bind in the ATP binding pocket and inhibit CDK2 activity.[112-115] Thus, we concentrated our efforts towards developing small-molecule inhibitors that inhibit CDKs. Most of the currently available molecules target the ATP-binding site of these enzymes.[116-118] Such an approach might create serious

problems as catalytic residues are well conserved across eukaryotic protein kinases. However, compounds such as Flavopiridol, Olomoucine, and Butyrolactone-1 that exhibit greater specificity for CDKs have shown promise. In the present study our focus is to develop the coumarin molecules as CDK-2 inhibitors because of various biological properties possessed by the coumarin pharmacophore.

Coumarins are a group of compounds belonging to the benzopyran family isolated from plant product Tonka bean, *coumarou* in 1820 **(Figure 4.25)**.[119]

(A) α-Benzopyran   (B) γ-Benzopyran
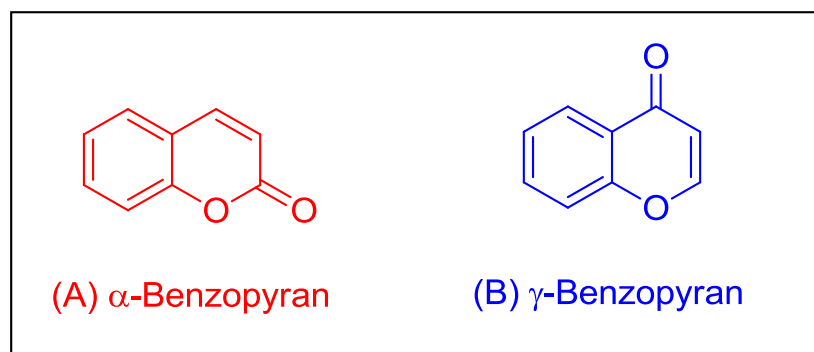
Figure 4.25 The chemical structures of benzopyrone subclasses, with the basic coumarin structure (benzo-α-pyrone) [A], and flavonoid (benzo-γ-pyrone [B]).

Benzopyrones are subdivided into benzo-α-pyrones and benzo-γ-pyrones of which coumarins and flavonoids are prime members of benzo-α-pyrones and benzo- γ-pyrones class respectively. Dietary exposure to benzopyrones is quite significant, as these compounds are found in vegetables, fruits, seeds, nuts, coffee, tea, and wine. It is estimated that the average western diet contains approximately 1g/day of mixed benzopyrones. It is, therefore, quite logical to see why extensive research into their pharmacological and therapeutic properties is underway over many years. Researchers have also proved the selective cytotoxicity of coumarins for tumor cells and also the effect of coumarins in the regulation of immune response, cell growth, and differentiation.[120-121] The mechanism of action of anti-tumor drugs is basically to target the dividing cells that interrupt cell division. Although new techniques like chemotherapy and radiotherapy provide best results for the treatment for cancer but these trigger various side effects. Coumarins are effective not only for treatment of cancers like malignant melanoma, renal cell carcinoma, leukemia[122-123], prostate cancer, and breast cancer[124-130], but also to treat the side effects caused by radiotherapy. The relapse of melanoma diagnosis has been minimized by the use of 4-hydroxy coumarin along with warfarin to maintain therapy and to inhibit the tumor spread.[131] Coumarins have an established cytotoxic mechanism and possess potential therapeutic function in renal cell carcinoma.[132] In case of leukemia, prostate, and breast cancer, cyclin D1 is released in amounts more than normal levels

and coumarin derivatives have also been found very effective anti-proliferative agents by regulating the release of cyclin D1.[133-142]

Several researchers have reported various anticancer coumarin based drugs e.g. Genistein, Imperatorin,[143] Osthole,[144] Esculetin,[145-146] Fraxin,[147] Grandivittin,[148] Agasyllin,[148] Aegelinol benzoate,[148] Chartreusin,[149] and Demethylchartreusin[150] etc. It has been established that some coumarin compounds, including coumarin and 7-hydroxycoumarin, inhibit the cell growth of various types of cancer cell lines.[150-152] Many accounts have appeared pertaining to the use of coumarin, or its metabolite 7-hydroxycoumarin, for the treatment of some human carcinomas.[153-156] No adverse effects of coumarins have been reported in humans using doses up to 7 g daily, after two weeks of continued treatment.[157-158]

The biochemical, pharmacological, and therapeutic applications of simple coumarins could be influenced by their substitution pattern. The main focus of the present paper is to design and develop effective coumarin derivatives for CDK-2 inhibitors. Our interest in anticancer drug discovery[159] motivated us to look up coumarins as potential CDK-2 inhibitor agents. The present paper not only focuses on designing of the coumarin molecules but also explores the effect of the substitution of OH group of the coumarin with various heterocyclic moieties at R^1, R^2, R^3, and R^4 position i.e. 3-, 4-, 6-, and 7- positions respectively of the coumarin skeleton. The general structures of all the designed analogues are shown in **Figure 4.26**. After docking them all, the best four molecules were selected and again docked by using GLIDE in Schrodinger for the authentication of the results. Furthermore, the molecular dynamics (MD) study was done for the best molecules selected from the studied positions 3-, 4-, 6- and 7-.
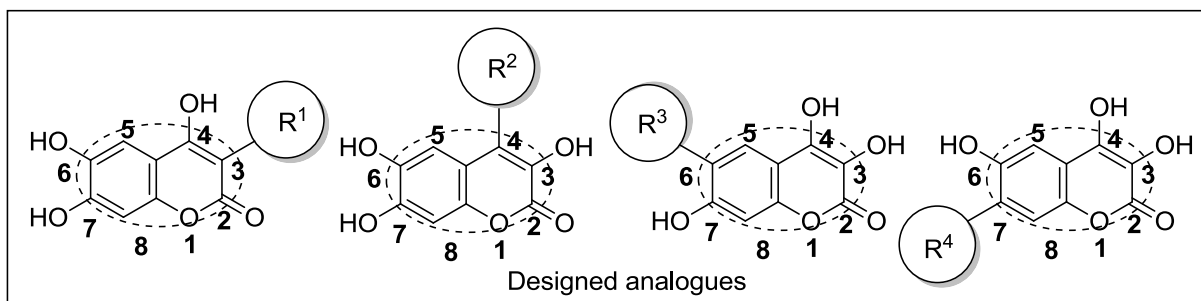
Figure 4.26 The designed coumarin analogues.

Softwares required

Molecular modeling software Auto Dock 4.2 downloaded from www.scripps.edu was used for the entire docking study. The best four molecules from each site after substitution R^1, R^2, R^3, R^4 were docked on GLIDE/Schrodinger software and their molecular dynamic and simulation study was done by using GROMACS 5.0.4 molecular dynamics package software for 10 ns.

Receptors used for docking

CDK-2 enzyme co-crystallized with Mg-ATP ligand was used as target receptor. Standard drug olomoucine and Deschloroflavopiridol were used for calibration and validation of the docking.

4.6 Experimental

4.6.1 Molecular parameter

Toxicity profile and good pharmacokinetic properties are very decisive for any ligand to complete drug discovery process and to become a successful drug.[160] Hence, in the present paper, Lipinsky's rule of five parameters and toxicity properties of the designed coumarin ligands were predicted by molinspiration cheminformatics (http://www.molinspiration.com/) and OSIRIS property explorer (http://www.organic-chemistry.org/prog/peo/) respectively. The activity and selectivity increases by stepwise optimization of the pharmacological lead structure and their drug like physicochemical properties during drug discovery are confirmed by Lipinski's rule of five. However, the rule does not predict if a compound is pharmacologically active. The pharmacokinetic properties like adsorption, distribution, metabolism, and excretion were calculated by molecular properties like ClogP (≤5), molecular weight (≤500), number of hydrogen bond acceptors (≤5), and number of hydrogen bond donors (≤10). All calculated molecular properties of the compounds follow strictly the Lipinski's rule of five. If the designed molecule violates the Lipinski's rule more than once then there occurs the problem of bioavailability.[161-162] The aqueous solubility plays vital role in adsorption and distribution study of the designed scaffolds and here we calculated the predicted aqueous solubility in terms of log S (logarithm value of aqueous solubility) measured in mol/L. For approximately 90% of the marketed drugs the estimated logS values lie between -6 and -3. Druglikeness is a qualitative concept and is estimated from the molecular structure of the designed molecules before the substance is even synthesized and tested. Druglikeness does not evaluate the actual specific effect of the drug (biological activity) but can estimate the druglikeness of any designed molecule. Several factors like topological descriptors, fingerprint of MDL structure keys or some other properties like ClogP, molecular weight, and toxicity profile play important role in evaluating the druglikeness of the designed molecules. The druglikeness is calculated by using the equation given below:

$$d = \frac{\sum v_i}{\sqrt{n}}$$

Where $\sum v_i$ is the summming up score values of the fragments, and n is the number of fragments in the molecule under investigation.

In the present paper, the toxicity risks like mutagenicity, tumorigenicity, irritancy, and the effect on sexual reproduction were predicted for all the designed analogs as shown in the **Table 4.6**. *In-silico*

prediction of compound toxicity is important because it may arise due to its own substructure and sometimes the evaluation of this type of risk is designated as toxicity risk. It is an indication that a particular compound may be harmful concerning the risk category specified. It is important to keep in mind that all the risk alerts are not fully reliable for compound toxicity. The overall potential of the designed compounds to qualify as drug molecule depends upon the drug score (ds) value and the drug score value depends upon several factors like druglikeness, ClogP, logS, molecular weight, and toxicity risk of the molecule. The drug score value is calculated from the following formula:

$$ds = \pi \left(\frac{1}{2} + \frac{1}{2} \text{si} \right) . \pi \text{ti}$$

$$s = \frac{1}{1 + e^{ap+b}}$$

where ds = drug score, si = contribution directly calculated from ClogP, logS, molecular weight and drug likeness, ti = contribution directly calculated from toxicity risks and the values 1.0, 0.8, and 0.6 for no risk, medium risk, and high risk respectively. The drug likeness (pi) is calculated from the spline curve where the parameter a and b are (1, -5), (1, 5), (0.012, -6), and (1, 0) for ClogP, logS, molecular weight, and druglikeness, respectively.

4.6.2 Molecular docking studies

Docking is an approach to rational drug design and very helpful in predicting the structure and binding free energy of ligand-receptor complex. It gives us the information on how the ligand molecule is going to bind with the receptor and what amino acid residues may be involved in providing flexibility to it. The molecular modeling software autodock 4.2 has been used for the docking of all designed 62 coumarin molecules. The best four molecules were later docked by using Schrodinger to refine the results and to perform the molecular dynamic study of the best molecules inside the pocket of the protein. The docking was performed using THR14 (T) and TYR15 (Y) residues of the GTYG cluster of ATP binding sites (residues 13 to 16) as flexible ones. The target protein, cyclin dependent kinase-2 enzyme, was downloaded from RCSB protein data bank. Target protein preparation was done by removal of water molecules, by adding polar hydrogens and kollmann charges. A grid spacing of 0.375 Å and $60 \times 60 \times 60$ number of points was used for the docking study of all the designed coumarin molecules. The grid was centered on the active site. The auto grid program generated separate grid maps for all atom types of the ligand structures and one for electrostatic interactions. The PRODRG online server (http://davapc1.bioch.dundee.ac.uk/prodrg/) was used to minimize the conformational energy of the designed ligands in pdb format. The Gasteiger-Huckel charges have been calculated for the energy minimized confirmations and saved in the default format of the Autodock. Autodock generated 50 possible binding conformations i.e., 50 runs for each docking using LGA search. Default protocol was

applied with initial population of 150 randomly placed individuals, a maximum number of 2.5×10^5 energy evaluations and 2.7×10^4 generations. A mutation rate of 0.02 and a crossover rate of 0.8 were used.

4.6.3 Validation of docking

Prior to docking, validation of docking is very important. The validation of docking was done by extracting out the co-crystallized ATP of the target protein CDK-2 and then docked back into the active site of the receptor. It was evident that the docked pose of the re-docked ATP was almost superimposed with that of the co-crystallized ligand with acceptable root mean square deviation of 0.85 Å **(Figure 4.27)**. Subsequently, the Mg-ATP hydrogen-bonding (pink dotted line) and hydrophobic interaction (green dotted line) with the receptor protein was also determined for validation and are shown in **Figure 4.28**. The reproducibility and the reliability of the docking parameters have been done by the docking of the standard drug (olomoucine and deschloroflavopiridol). Hydrogen bonding and hydrophobic interaction of the standard drug with the active site amino acid residues of 1HCK protein is shown in **Figure 4.29** (Deschloroflavopiridol) and **Figure 4.30** (Olomoucine) respectively.
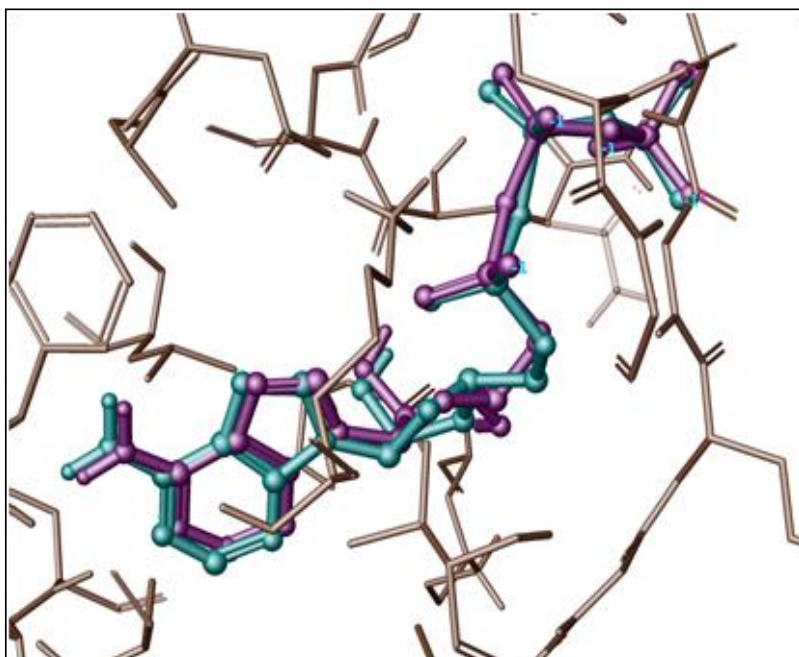
Figure 4.27 Redocked mode of ATP (green) superimposed with the co-crystallized Mg-ATP in the binding pocket of CDK-2 (PDB ID: 1HCK). ATP is shown as stick model and the amino acid residues interacting with the co-crystallized Mg-ATP are shown as line model.
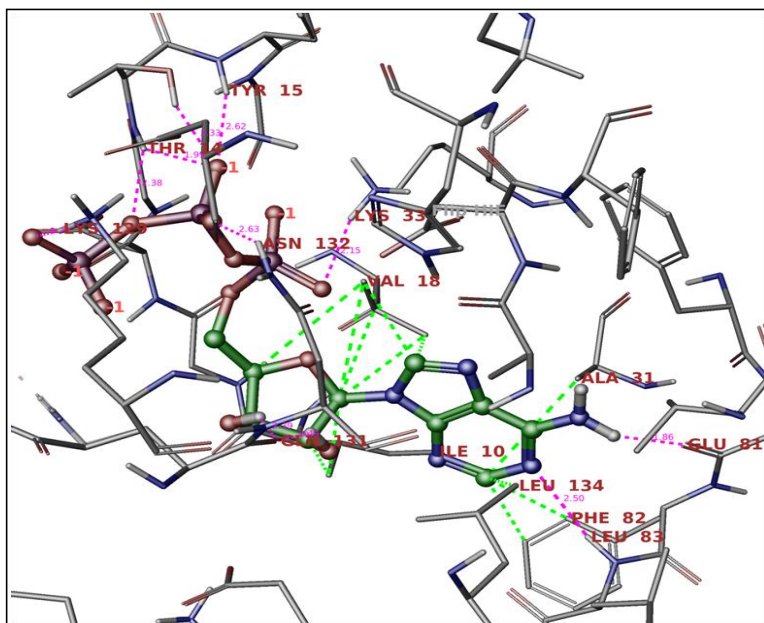
Figure 4.28 Hydrogen bonding interaction (Pink dotted lines) and hydrophobic interaction (green dotted line) of ATP with CDK-2 (PDB ID: 1HCK) with various amino acid.
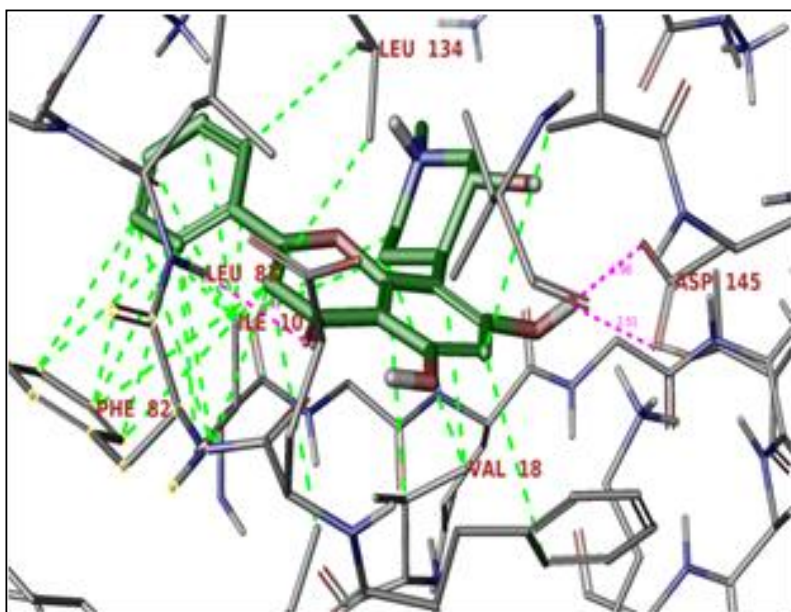
Figure 4.29 Overlay docked view of Deschloroflavopiridol at the ATP binding site of 1HCK, showing the hydrogen and hydrophobic interactions by the pink and green dotted lines respectively.

186
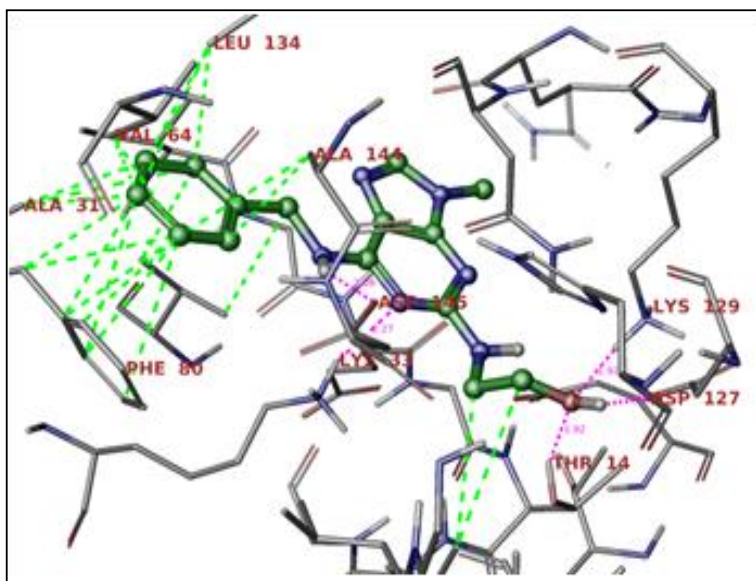
Figure 4.30 Overlay docked view of Olomoucine at the ATP binding site of 1HCK, showing the hydrogen and hydrophobic interactions by the pink and green dotted liners respectively.

4.7 Results and discussion

The molecular modeling software autodock 4.2 was used for the docking study of the designed analogs. Later on, the best four molecules and the standard drugs deschloroflavopiridol and olomoucine **(Figure 4.29 and 4.30)** were docked by using Glide/Schrodinger software in order to identify the enzyme inhibitory potential of the designed coumarin analogues against CDK-2. The docking parameters such as binding free energy (K.cal/mol) and predicted inhibitory constant (Ki) for all 62 designed analogs were determined and are shown in **Table 4.6**.Binding energy for each compound has been calculated by using the following formula:

$$\text{Binding Energy} = [(A) + (B) + (C) - (D)]$$

where A denotes the intermolecular energy, which is sum of the [van der Waals energy + hydrogen bonds + desolvation energy + electrostatic energy (kcal/mol)], B denotes final total internal energy [internal energy of ligand + internal energy of receptor (kcal/mol)], C denotes torsional free energy (kcal/mol), and D denotes unbound system's energy (kcal/mol).In docking studies binding free energy and enzyme inhibitory activity are inversely proportional to each other as:

$$\text{B.E.} = \frac{1}{K_i}$$

Compounds showing high binding energy (negative) have lower enzyme inhibitory constant and vice versa.

In the present study, our designed analogs showed binding free energy values in the range of: 12.07 to -8.06 when we vary the position 3- **(Table 4.6, entry 3-17)**; -11.87 to -8.02 when variation is made at position 4- (**Table 4.6, entry 18-32**); -12.72 to -10.06 when variation is done at position 6- **(Table 4.6, entry 33-47)**, and -12.50 to -8.35 when variation is done at position 7- **(Table 4.6, entry 48-62)** of the designed coumarin molecule with different heterocyclic moieties. Among the designed 62 analogs, THC-14, THC-15, THC-41, THC-42, THC-43, THC-47, THC-53, THC-58, and THC-59 **(Table 4.6)** showed significant binding free energy values of -12.00, -12.07, -12.10, -12.68, -12.72, -12.13, -12.01, -12.38, and -12.50 kcal/mol respectively against CDK-2 receptor with that of standard drug Deschloroflavopiridol (-8.87 kcal/mol) and olomoucine (-6.08 kcal/mol). The binding energy in decreasing order exhibits the following trend for the designed ligands: THC-43>THC-42>THC-59>THC-58>THC-47>THC-41>THC-15>THC-53>THC-14. From the binding energy trend we infer that THC-43 is the most potent molecule in CDK-2 inhibition. Closer observation of receptor-ligand complex reveals that, the designed analogs adopt the same conformation in the ATP active site of CDK-2 as do other standard CDK-2 inhibitors. Hydrogen bonding and hydrophobic interactions were observed between ligands and amino acids of the receptor protein. These interactions play an important role in the determination of binding free energy and stability of receptor-ligand complex.

4.7.1 Structure-Activity-Relationship (SAR)

A brief SAR **(Figure 4.31)** is quite unambiguous. Comparing the binding energy values of the designed coumarin analogs we found that when we vary the 6th position i.e. R^3 fragment as compared to R^1, R^2, and R^4, the B.E (K.cal/mol) increases and most of the molecules like THC-41, THC-42, THC-43, and THC-47 have excellent binding free energy and inhibitory constant value. Although in some molecules, when we vary the 7th position i.e. R^4 of the coumarin molecule, significant binding free energy and inhibitory constant values are exhibited, e.g. THC-53, THC-58, and THC-59. But still closer observation reveals that the 6th position of the coumarin analogs is the best position where a desired substitution may lead to enhanced inhibitory activity of protein CDK-2. Thus overall, significant binding energy and inhibitory constant values are in the order as $R^3 > R^4 > R^1 > R^2$ (i.e. position 6 > 7 > 3 > 4). Hence, some SAR inferences are unequivocal: (a) substitution by a heterocycle at the 6th position invariably leads to excellent binding; (b) a similar substitution at the 7th position also leads to good binding ability. The reason behind better activity of the 6th and 7th position substituted coumarin molecule may be because of the reduced steric hindrance caused by the substituted heterocyclic molecules at these positions. (c) Another interesting observation: when quinolinyl, quinazolinyl, indazolyl, and indolyl type moieties are present as substituents, then we get better score irrespective of the position (i.e. whether the substitution

occurs at R^1, R^2, R^3, and R^4) of the coumarin molecule; but still the 6th position remains the best with respect to all other positions.
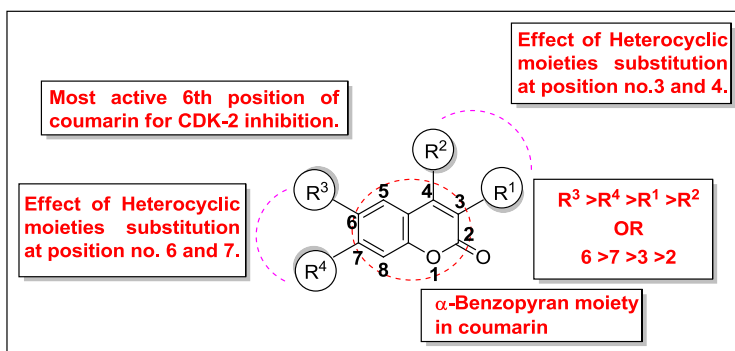
Figure 4.31 Shows the brief SAR analysis of the designed analog.

The substitution of the benzothiophenyl fragment in coumarin molecule shows lower binding energy at all the positions of the coumarin molecule and is one of the exceptional case predicted during observation of **Table 4.6**.

Table 4.6: Docking results of the designed analogs.

No.	Comp code	R^1	R^2	R^3	R^4	B.E.	K_i
1	THC-1	H	H	H	H	-9.21	177.54nM
2	THC-2	OH	OH	OH	OH	-9.36	138.01nM
3	THC-3	3-(benzo[b]thiophen-2-yl)	OH	OH	OH	-8.06	1.23uM
4	THC-4	3-(benzo[b]thiophen-3-yl	OH	OH	OH	-11.74	2.49nM
5	THC-5	3-(benzofuran-2-yl)	OH	OH	OH	-11.90	1.90nM
6	THC-6	3-(benzofuran-3-yl)	OH	OH	OH	-10.15	36.11nM
7	THC-7	3-(1H-isoindol-3-yl)	OH	OH	OH	-11.04	8.05nM
8	THC-8	3-(1H-indol-3-yl)	OH	OH	OH	-10.51	19.94nM
9	THC-9	3-(1H-indol-2-yl)	OH	OH	OH	-10.29	28.81nM
10	THC-10	3-(1H-indazol-3-yl)	OH	OH	OH	-11.24	5.79nM

11	THC-11	3-(1H-benzo[d]imidazol-2-yl)	OH	OH	OH	-11.81	2.19nM
12	THC-12	3-(quinolin-2-yl)	OH	OH	OH	-10.42	23.07nM
13	THC-13	3-(quinolin-3-yl)	OH	OH	OH	-11.05	7.96nM
14	THC-14	3-(quinolin-4-yl)	OH	OH	OH	-12.00	1.59nM
15	THC-15	3-(quinazolin-2-yl)	OH	OH	OH	-12.07	1.41nM
16	THC-16	3-(indolin-2-yl)	OH	OH	OH	-10.86	11.04nM
17	THC-17	3-(1,2,3,4-tetrahydroquinolin-2-yl)	OH	OH	OH	-10.48	20.79nM
18	THC-18	OH	4-(benzo[b]thiophen-2-yl)	OH	OH	-8.80	352.65nM
19	THC-19	OH	4-(benzo[b]thiophen-3-yl)	OH	OH	-8.02	1.33uM
20	THC-20	OH	4-(isobenzofuran-1-yl)	OH	OH	-9.44	121.30nM
21	THC-21	OH	4-(benzofuran-3-yl)	OH	OH	-8.54	549.10nM
22	THC-22	OH	4-(1H-isoindol-3-yl)	OH	OH	-10.05	43.06nM
23	THC-23	OH	4-(1H-indol-3-yl)	OH	OH	-10.71	14.19nM
24	THC-24	OH	4-(1H-indol-2-yl)	OH	OH	-10.81	11.94nM
25	THC-25	OH	4-(1H-indazol-3-yl)	OH	OH	-11.08	7.51nM
26	THC-26	OH	4-(1H-benzo[d]imidazol-2-yl)	OH	OH	-11.73	2.52nM
27	THC-27	OH	4-(quinolin-2-yl)	OH	OH	-10.97	9.04nM
28	THC-28	OH	4-(quinolin-3-yl)	OH	OH	-11.87	2.00nM
29	THC-29	OH	4-(quinolin-4-yl)	OH	OH	-10.05	43.16nM
30	THC-30	OH	4-(quinazolin-2-yl)	OH	OH	-10.49	20.34nM
31	THC-31	OH	4-(indolin-2-yl)	OH	OH	-8.97	264.61nM
32	THC-32	OH	4-(1,2,3,4-tetrahydroquinolin-2-yl)	OH	OH	-11.16	6.59nM
33	THC-33	OH	OH	6-(benzo[b]thiophen-2-yl)	OH	-11.32	5.05nM
34	THC-34	OH	OH	6-(benzo[b]thiophen-	OH	-10.39	24.22nM

				3-yl)			
35	THC-35	OH	OH	6-(benzofuran-2-yl)	OH	-10.83	11.53nM
36	THC-36	OH	OH	6-(benzofuran-3-yl)	OH	-11.09	7.37nM
37	THC-37	OH	OH	6-(1H-isoindol-3-yl)	OH	-10.06	42.23nM
38	THC-38	OH	OH	6-(1H-indol-3-yl)	OH	-11.13	6.92nM
39	THC-39	OH	OH	6-(1H-indol-2-yl)	OH	-11.91	1.87nM
40	THC-40	OH	OH	6-(1H-indazol-3-yl)	OH	-11.70	2.65nM
41	THC-41	OH	OH	6-(1H-benzo[d]imidazol-2-yl)	OH	-12.10	1.35nM
42	THC-42	OH	OH	6-(quinolin-2-yl)	OH	-12.68	507.78pM
43	THC-43	OH	OH	6-(quinolin-3-yl)	OH	-12.72	478.16pM
44	THC-44	OH	OH	6-(quinolin-4-yl)	OH	-10.71	14.22nM
45	THC-45	OH	OH	6-(quinazolin-2-yl)	OH	-11.96	1.71nM
46	THC-46	OH	OH	6-(indolin-2-yl)	OH	-11.45	4.08nM
47	THC-47	OH	OH	6-(1,2,3,4-tetrahydroquinolin-2-yl)	OH	-12.13	1.28nM
48	THC-48	OH	OH	OH	7-(benzo[b]thiophen-2-yl)	-9.31	149.34nM
49	THC-49	OH	OH	OH	7-(benzo[b]thiophen-3-yl)	-10.34	26.29nM
50	THC-50	OH	OH	OH	7-(benzofuran-2-yl)	-10.88	10.63nM
51	THC-51	OH	OH	OH	7-(benzofuran-3-yl)	-8.35	759.88nM
52	THC-52	OH	OH	OH	7-(1H-isoindol-3-yl)-	-11.18	6.33nM
53	THC-53	OH	OH	OH	7-(1H-indol-3-yl)-	-12.01	1.57nM
54	THC-54	OH	OH	OH	7-(1H-indol-2-yl)	-9.85	60.71nM
55	THC-55	OH	OH	OH	7-(1H-indazol-3-yl)	-11.24	5.78nM

56	THC-56	OH	OH	OH	7-(1H-benzo[d]imidazol-2-yl)	-11.39	4.45nM
57	THC-57	OH	OH	OH	7-(quinolin-2-yl)	-10.42	23.07nM
58	THC-58	OH	OH	OH	7-(quinolin-3-yl)	-12.38	843.83pM
59	THC-59	OH	OH	OH	7-(quinolin-4-yl)	-12.50	687.04pM
60	THC-60	OH	OH	OH	7-(quinazolin-2-yl)	-11.50	3.73nM
61	THC-61	OH	OH	OH	7-(indolin-2-yl)	-11.28	5.38nM
62	THC-62	OH	OH	OH	7-(1,2,3,4-tetrahydroquinolin-2-yl)	-11.40	4.37nM

Finally, after analysis of all the results of **Table 4.6**, we were curious to find out the stability of the best compound from each studied position of the coumarin molecule inside the binding pocket of the protein molecule through molecular dynamics and simulation study. So, we chose four best molecules from each position of the coumarin molecule i.e. THC-15, THC-28, THC-43, and THC-59 and docked the molecules using SCHRODINGER Maestro software for comparison with autodock score and for a better reproducibility of the results. The hydrogen bonding and hydrophobic interaction in 2D and 3D view for all the four selected molecules are shown in **Figure 4.32** and **4.33** respectively. The GLIDE score and Autodock score comparison of binding energy and inhibitory constant values are shown in **Table 4.7**.

Table 4.7: Docking score comparison of best four molecules from each position of the coumarin molecule by Autodock and GLIDE.

S.No.	Comp. code	Autodock score		Glide	
		B.E. (K.cal/mol)	K_i	Glide Score (K.cal/mol)	Glide Emodel
1	THC-15	-12.07	1.41 nM	-9.21	-56.23
2	THC-28	-11.87	2.00 nM	-8.97	-65.38
3	THC-43	-12.72	478.16 pM	-7.66	-58.01
4	THC-59	-12.50	687.04 pM	-9.06	-64.41

The ATP binding site of the protein kinases are the most common targets for the design of small molecule inhibitors. It is very difficult to develop selective kinase inhibitors because of the similarities between

kinase domains. However, the development of small structural differences between the ATP binding site of closely homologous kinases has been used effectively to present specificity of inhibition.

4.7.2 Hydrogen bonding interaction

In **Figure 4.32a**, the 2D view of THC-15 **(entry 3-17, Table 4.6)** shows that all the atoms responsible for H-bonding behave as H-bond acceptors. Here the OH group present at 3rd position was substituted by quinolin-2-yl. The hydrophilic oxygen of the OH group at 4th position of coumarin forms hydrogen bonds with the adjacent LYS33 amino acid. The 6th and 7th position of coumarin in THC-15 shows hydrogen bonding interaction with the THR14 and LYS129 respectively whereas hydroxyl group of the 6th and 7th position behaves as H-bond acceptor and the corresponding amino acids as H-bond donors. LYS129 shows the H-bonding with both the substituted hydroxyl group at 6th and 7th position of the coumarin molecule. The corresponding 3D view of the designed ligand THC-15 interaction with bond distances to the receptor amino acids are shown in **Figure 4.33a**.

Similarly, the **Figure 4.32b** and **4.33b** show the interaction of the best selected molecule **(entry 18-32, Table 4.6)** THC-28 with the various amino acids in 2D and 3D views respectively. Here, the hydroxyl group present at 4th position of designed ligand was substituted by quinolin-3-yl moiety. A close observation of 2D view of **Figure 4.32b** shows that almost all the heteroatom's of the designed ligand behave as H-bond donors. Here, the H (Hydrogen) of the substituted -OH group at 3rd position of coumarin forms H-bond with ASP145. The H (Hydrogen) of the -OH group substituted at 6th and 7th position of coumarin shows H-bonding with LEU83. Also, LEU83 appears to form bifurcated H-bond with both the H atom of the OH group present at 6th and 7th position of coumarin molecule.

Figure 4.32c and **4.33c** show the 2D and 3D views of the various interactions of the designed ligand THC-43 **(best selected ligand from entry 33-47, Table 4.6)**. All the heteroatom's responsible for H-bonding behave as H-bond acceptors. The 6th position of the designed ligand THC-43 was substituted with quinolin-3-yl group. Oxygen of the keto group which behaves as a H-bond acceptor forms H-bond with LYS129. The Hydroxyl group present at the 3rd position of the designed ligand forms bifurcated H-bond i.e. one with LYS129 and the other one with THR14. The Oxygen atom of the OH group present at the 4th position of the designed ligand forms H-bond with LYS33.

Similarly, the **Figure 4.32d** and **4.33d** show the interaction in 2D and 3D views of the designed ligand THC-59 **(entry 48-62, Table 4.6)** where the OH group of 7th position was substituted by quinolin-4-yl moiety as shown in **Table 4.6**. Here, all the H-bond forming atoms of the ligand behave as H-bond donors. The OH group present at 3rd and 6th position of the designed ligand forms H-bond with GLU12 and ASP86 respectively. The corresponding 3D view with bond distance is shown in **Figure 4.33d**.

Overall, we can say that the Hydroxyl groups present in the designed ligands are responsible for the H-bonding interaction inside the active site of the protein CDK2.
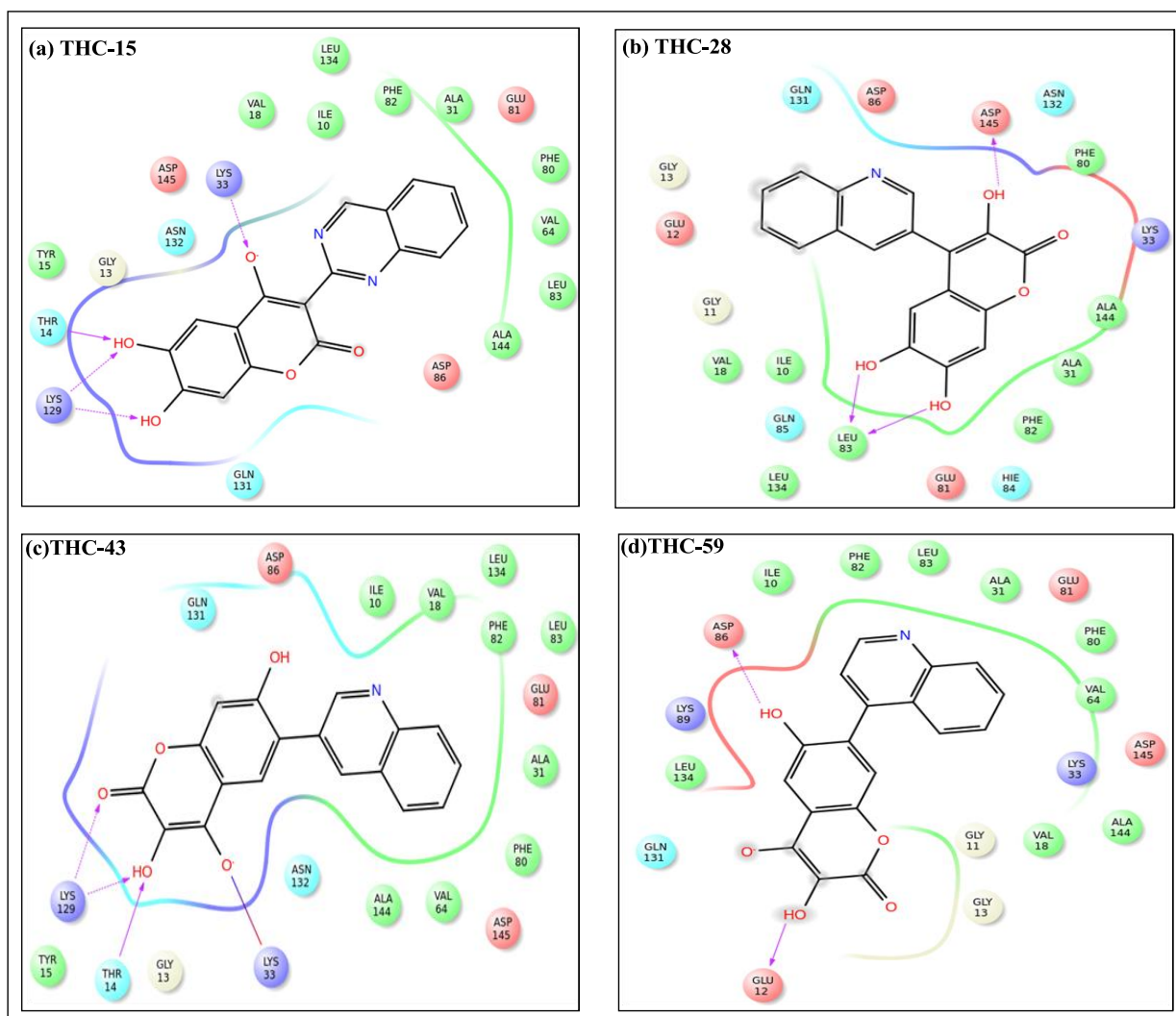
Figure 4.32 Shows the 2D view of the ligand-protein amino acids interaction as-(a) THC-15 (b) THC-28 (c) THC-43 and (d) THC-59.

4.7.3 Hydrophobic interaction

Although the hydrophobic interactions are weak interaction like H-bonding interactions but play very important role in the stability of the molecule inside the active site of the protein. According to Davis,[163] most of the marketed drugs consist of around 16 types of hydrophobic atoms, with three to four acceptor and two to three donor atom. These hydrophobic interactions not only play very important role in drug designing but are also very cooperative in increasing the binding affinity among the target drug and receptor protein.

Several researchers reported the link of hydrophobic interaction with the binding affinity and drug efficacy and later on optimized such interactions by their incorporation at the site of H-bonding.[164] Even though the approach is not so proficient in the designing of drug molecules but sometimes the presence of water molecule makes the hydrophobic region quiet valuable.[163-164]

The binding affinity of the drug molecule with the target receptor can be increased by engineering the target or the drug or the interface between the drug and target receptor. The probability of the biological activity of the drug lead increases by increasing the number of hydrophobic atoms in the active core of drug-target interface.

All the green circled amino acids like VAL-18, ILE-10, LEU-134, PHE-82, ALA-31, PHE-80, VAL-64, LEU-83, ALA-144, and TYR-15 show hydrophobic interaction with THC-15 (**Figure 4.32a**); PHE-80, ALA-144, ALA-31, PHE-82, LEU-83, LEU-134, ILE-10, and VAL-18 show hydrophobic interaction with THC-28 (**Figure 4.32b**); ILE-10, VAL-18, LEU-134, PHE-82, LEU-83, ALA-31, PHE-80, VAL-64, ALA-144, and TYR-15 show hydrophobic interaction with THC-43 (**Figure 4.32c**) while ILE-10, PHE-82, LEU-83, ALA-31, PHE-80, VAL-64, VAL-18, ALA-144, and LEU-134 show hydrophobic interaction with THC-59 (**Figure 4.32d**). The corresponding 3D images with hydrophobic interactions of designed ligand THC-15, THC-28, THC-43, and THC-59 are shown in **Figure 4.33a**, **4.33b**, **4.33c**, and **4.33d** respectively. All the hydrophobic interactions are shown by green dotted lines in **Figure 4.33**.

4.7.4 Electrostatic interaction

In **Figure 4.32a**, the most common amino acids which show the electrostatic interaction with the designed ligand THC-15 are ASP-145, ASN-132, THR-14, GLN-131, GLU-81, and ASP-86. THC-28 designed ligand shows electrostatic interaction with GLU-12, ASP-86, ASP-145, GLU-81, GLU-12, GLN-131, ASN-132, and GLN-85 amino acids as shown in **Figure 4.32b**. The amino acids responsible for ionic electrostatic interaction with the designed ligand THC-43 are THR-14, GLN-131, ASN-132, ASP-86, GLU-81, and ASP-145 amino acids as shown in **Figure 4.32c**. The designed ligand THC-59 shows the electrostatic interaction with ASP-86, GLU-81, ASP-145, GLU-12, and GLN-131 amino acids as shown in **Figure 4.32d**.

All the amino acids which show electrostatic interaction are circled in red and dark blue color. The corresponding electrostatic interactions of all the designed ligand THC-15, THC-28, THC-43, and THC-59 in 3D view with green dotted lines are shown in **Figure 4.33a**, **4.33b**, **4.33c**, and **4.33d** respectively.
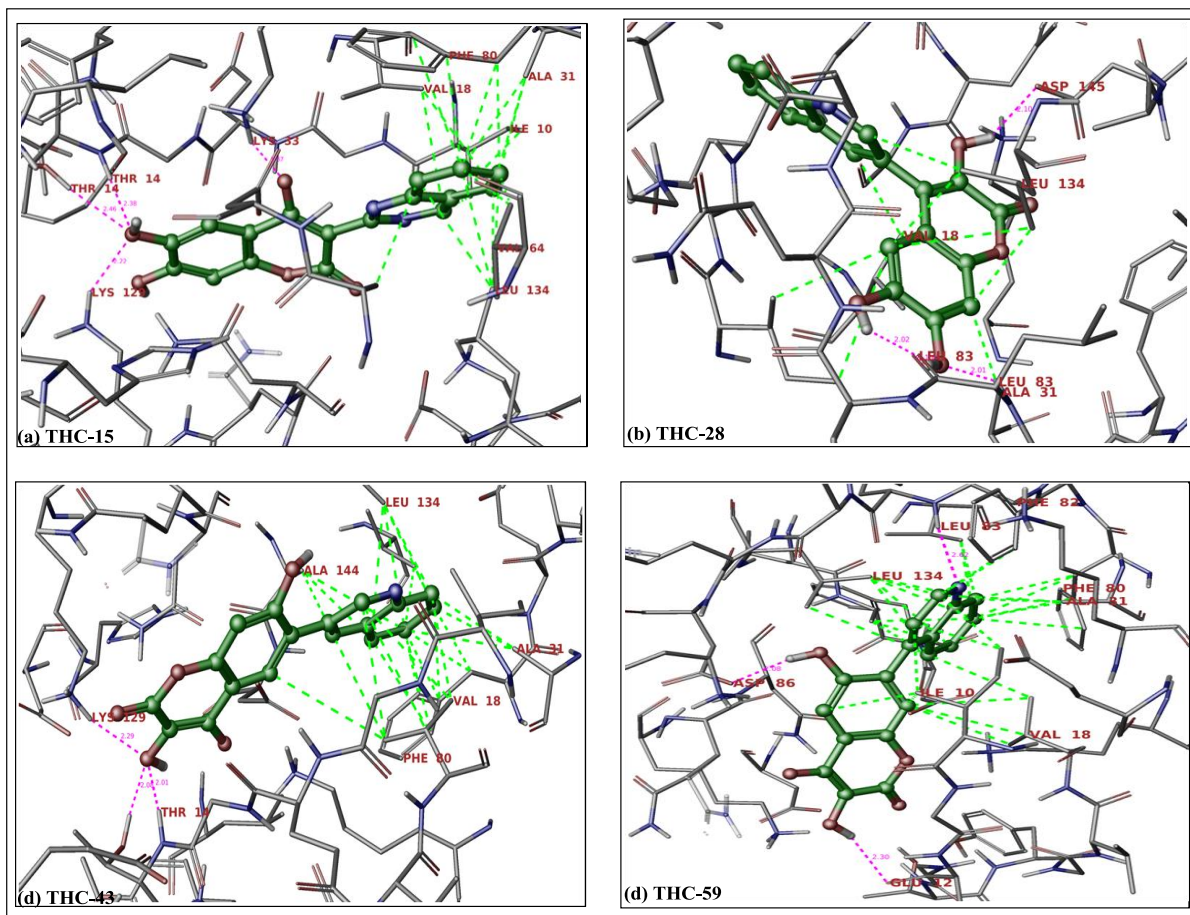
Figure 4.33 Shows the Hydrogen bonding interaction and Hydrophobic interaction of ligand (THC-15, THC-28, THC-43, and THC-59) with 1HCK protein. Ligand is shown as ball and sticks, receptor amino acids as lines and hydrogen bond interaction as pink dotted lines and Hydrophobic interaction as green dotted lines. Rest of the protein is suppressed for clarification purposes.

4.7.5 Molecular parameters

All the molecular properties of the designed analogs were predicted by using online tools, OSIRIS property explorer and molinspiration cheminformatics (http://www.molinspiration.com/). Predicted molecular properties of the designed analogs are reported in **Table 4.8**.All the 60 molecules **(entry 3 to 62 in Table 4.6)** were designed by heterocyclic molecular substitution at 3rd, 4th, 6th, and 7th position of the Tetrahydroxy coumarin (THC-2) molecule shown by entry 2 in **Table 4.6**. All the designed coumarin analogs follow the Lipinski's rule of five. There is no violation of the Lipinski's rule observed from **Table 4.8.** Some of the designed analogs like THC-18, THC-19, THC-20, THC-21, THC-22, THC-23, THC-24, THC-25, THC-26, THC-27, THC-28, THC-29, THC-30, THC-31, THC-32, THC-33, THC-34, THC-35, THC-36, THC-38, THC-39, THC-49, THC-51, and THC-53 showed high risk (++) of reproductive effect.

Only two molecules THC-54 and THC-56 showed predicted high risk (++) and active risk (+) of producing mutagenicity. THC-14 showed active risk (+) of tumorigenicity. The high risk (++) of mutagenicity, tumorigenicity, and reproductive effect is shown by THC-1. However, risk alerts for the designed analogs may not be fully consistent and in order to evade risk of taking hazardous compounds, we screened off THC-1, THC-14, THC-18, THC-19, THC-20, THC-21, THC-22, THC-23, THC-24, THC-25, THC-26, THC-27, THC-28, THC-29, THC-30, THC-31, THC-32, THC-33, THC-34, THC-35, THC-36, THC-38, THC-39, THC-49, THC-51, THC-53, THC-54, and THC-56 molecules for further study. It should be noted that these results are merely preliminary druggability predictions and the calculations of toxicity are not analysed in detail. A close analysis of **Table 4.8** predicted that entry nos. 3-17, 18-32, 33-47, and 48-62 represents the designed analogs when we vary the heterocyclic moieties at position no. 3, 4, 6, and 7 respectively. In general, modification at the 4-position of coumarins appears to give rise to high risk (++) of reproductive effect predicted in these molecules. The substitution at position 3- shows no side effect except THC-14 which shows the active risk of tumorigenicity. The substitution at 6th position shows the high binding affinity with the CDK-2 protein but some molecules showed high risk of reproductive effect also e.g. THC-33, THC-34, THC-35, THC-36, THC-37, THC-39, and THC-40. Similarly, substitution at position 7 also shows no side effect except very few molecules which do show some side effects e.g. THC-49, THC-51, THC-53, and THC-56. The side effect decreasing order trend observed from **Table 4.8** is $R^2 > R^3 > R^4 > R^1$ (3 > 4 > 7 > 6). The detailed comprehensive studies of the designed molecules are currently underway in our labs.

Table 4.8: Predicted molecular parameters of the designed analogs.

S.No.	Compd code	M.wt.	C log P	HBA	HBD	Solub.	Drug likeness	MUT	TUMO	IRRI	REP	Drug score
1	*THC-1*	146.14	1.5	2	0	-2.37	-1.83	++	++	-	++	0.12
2	THC-2	210.14	-0.08	6	4	-1.24	-1.87	-	-	-	-	0.55
3	THC-3	326.32	2.6	5	3	-3.62	0.76	-	-	-	-	0.69
4	THC-4	326.32	2.52	5	3	-3.51	-0.15	-	-	-	-	0.6
5	THC-5	310.26	2.18	6	3	-3.45	0.21	-	-	-	-	0.66
6	THC-6	310.26	2.13	6	3	-3.43	-0.28	-	-	-	-	0.61
7	THC-7	309.27	1.2	6	3	-3.04	0.22	-	-	-	-	0.69
8	THC-8	309.27	1.72	6	4	-2.79	0.72	-	-	-	-	0.74

9	THC-9	309.27	1.77	6	4	-2.82	1.1	-	-	-	-	0.78
10	THC-10	310.26	0.94	7	4	-2.37	1.56	-	-	-	-	0.83
11	THC-11	310.26	1.17	7	4	-1.76	0.4	-	-	-	-	0.74
12	THC-12	321.28	2.05	6	3	-3.0	-1.07	-	-	-	-	0.55
13	THC-13	321.28	2.0	6	3	-2.97	-1.07	-	-	-	-	0.55
14	*THC-14*	321.28	2.0	6	3	-2.97	-1.07	-	+	-	-	0.44
15	THC-15	322.27	1.32	7	3	-2.05	-1.07	-	-	-	-	0.57
16	THC-16	311.29	1.84	6	4	-2.96	2.35	-	-	-	-	0.83
17	THC-17	325.32	2.19	6	4	-3.23	1.36	-	-	-	-	0.76
18	*THC-18*	326.32	2.73	5	3	-4.26	0.59	-	-	-	++	0.37
19	*THC-19*	326.32	2.64	5	3	-4.15	-0.33	-	-	-	++	0.33
20	*THC-20*	310.26	2.31	6	3	-4.1	0.05	-	-	-	++	0.36
21	*THC-21*	310.26	2.26	6	3	-4.07	-0.43	-	-	-	++	0.33
22	*THC-22*	309.27	0.72	6	3	-3.05	0.05	-	-	-	++	0.4
23	*THC-23*	309.27	1.84	6	4	-3.44	0.54	-	-	-	++	0.42
24	*THC-24*	309.27	1.9	6	4	-3.46	0.92	-	-	-	++	0.44
25	*THC-25*	310.26	1.07	7	4	-3.01	1.37	-	-	-	++	0.48
26	*THC-26*	310.26	1.29	7	4	-2.41	0.22	-	-	-	++	0.42
27	*THC-27*	321.28	2.17	6	3	-3.64	-1.26	-	-	-	++	0.3
28	*THC-28*	321.28	2.12	6	3	-3.62	-1.26	-	-	-	++	0.3
29	*THC-29*	321.28	2.12	6	3	-3.62	-1.26	-	-	-	++	0.3
30	*THC-30*	322.27	1.45	7	3	-2.7	-1.26	-	-	-	++	0.33
31	*THC-31*	311.29	1.37	6	4	-2.97	2.03	-	-	-	++	0.5
32	*THC-32*	325.32	1.71	6	4	-3.24	1.05	-	-	-	++	0.45
33	*THC-33*	326.32	3.01	5	3	-4.88	0.26	-	-	-	++	0.32
34	*THC-34*	326.32	2.77	5	3	-4.86	-0.74	-	-	-	++	0.27
35	*THC-35*	310.26	2.47	6	3	-4.48	-0.28	-	-	-	++	0.32
36	*THC-36*	310.26	2.38	6	3	-4.78	-0.84	-	-	-	++	0.28

37	THC-37	309.27	1.27	6	3	-3.93	-0.34	-	-	-	-	0.58
38	*THC-38*	309.27	1.97	6	4	-4.15	0.15	-	-	-	++	0.37
39	*THC-39*	309.27	2.06	6	4	-3.84	0.59	-	-	-	++	0.4
40	THC-40	310.26	1.23	7	4	-3.09	0.98	-	-	-	-	0.75
41	THC-41	310.26	1.51	7	4	-3.89	-0.12	-	-	-	-	0.6
42	THC-42	321.28	2.34	6	3	-4.02	-1.64	-	-	-	-	0.46
43	THC-43	321.28	2.24	6	3	-4.33	-1.64	-	-	-	-	0.44
44	THC-44	321.28	2.24	6	3	-4.33	-1.64	-	-	-	-	0.44
45	THC-45	322.27	1.67	7	3	-4.18	-1.64	-	-	-	-	0.46
46	THC-46	311.29	1.85	6	4	-3.46	1.53	-	-	-	-	0.77
47	THC-47	325.32	2.2	6	4	-3.72	0.56	-	-	-	-	0.66
48	THC-48	326.32	3.01	5	3	-4.88	0.26	-	-	-	-	0.53
49	*THC-49*	326.32	2.77	5	3	-4.86	-0.74	-	-	-	++	0.27
50	THC-50	310.26	2.47	6	3	-4.47	-0.28	-	-	-	-	0.53
51	*THC-51*	310.26	2.38	6	3	-4.78	-0.84	-	-	-	++	0.28
52	THC-52	309.27	1.27	6	3	-3.93	-0.34	-	-	-	-	0.58
53	*THC-53*	309.27	1.97	6	4	-4.15	0.15	-	-	-	++	0.37
54	*THC-54*	309.27	2.06	6	4	-3.84	0.59	++	-	-	-	0.4
55	THC-55	310.26	1.23	7	4	-3.09	0.98	-	-	-	-	0.75
56	*THC-56*	310.26	1.51	7	4	-3.89	-0.12	+	-	-	-	0.48
57	THC-57	321.28	2.34	6	3	-4.02	-1.64	-	-	-	-	0.46
58	THC-58	321.28	2.24	6	3	-4.33	-1.64	-	-	-	-	0.44
59	THC-59	321.28	2.24	6	3	-4.33	-1.64	-	-	-	-	0.44
60	THC-60	322.27	1.67	7	3	-4.18	-1.64	-	-	-	-	0.46
61	THC-61	311.29	1.85	6	4	-3.46	1.53	-	-	-	-	0.77
62	THC-62	325.32	2.2	6	4	-3.72	0.56	-	-	-	-	0.66

Note: Compounds violating more than one time from Lipinski rule of 5 and compounds exhibited predicted toxicity are in Italics. *HBA* hydrogen bond acceptor, *HBD* hydrogen bond donor, *MUT* mutagenic, *TUMO* tumorigenic, *IRRI* irritant, *REP* reproductive effective, ''+'' active risk, ''++'' High risk ''−'' non-active risk.

4.8 Molecular Dynamics Simulations

4.8.1 Method of Molecular Dynamic Simulations

THC15-CDK2 complex was simulated with GROMACS 5.0.4 molecular dynamics package to assess the stability. Gromos43a2 force field was used do define the atom types. Ligand parameters were obtained from PRODRG (http://davapc1.bioch.dundee.ac.uk/cgi-bin/prodrg) server. THC15-CDK2 complex was placed in a cubic box filled with SPC water molecules and the system was neutralized by the addition of required number of Na^+ and Cl^- ions. Then the system was minimized with steepest descent algorithm. Energy minimized system was equilibrated at 300 K for 150 ps followed by equilibration at 1 atm pressure for 150 ps. Production dynamics was carried for 10 ns and the trajectories were analyzed with the available programs within the GROMACS package with default parameters.

4.8.2 Results of Molecular Dynamic Simulations

Top scored THC analog along with CDK2 was simulated for 10 ns with GROMACS 5.0.4 to study the behavior of the THC15-CDK2complex. Initial energy of the complex was -8.35257×10^5 kJ/mol which was stable throughout the simulation with minor variations of $\pm 3.330 \times 10^3$ kJ/mol. Energy plot of the complex shows that the overall energy minima is well maintained in the course of the simulation period **(Figure 4.34A)**. Root mean square deviation shows that the maximum deviation **(Figure 4.34B)** of the protein is 3.32 Å in respect to the initial protein backbone, which means that all the ensembles of the protein-ligand complex conformations were within a deviation of 3.32 Å. Average RMSD value for the last 2 ns is 2.75Å and at the end of the simulation was 3.06 Å. Throughout the simulation, average, maximum, and minimum root mean square deviations of the ligand THC-15was 0.9, 1.71, and 0.29 Å, respectively **(Figure 4.34C)**. Generally validation of docking was done by redocking the ligand present in the crystal structure. The deviation cut off for the docked ligand to its original crystallized orientation is maximum 2 Å. In this aspect, lower RMSD value shows the stable interaction of the ligand inside the binding site of the CDK2.

Next, atomic fluctuations of the amino acid residues were calculated with respect to the initial equilibrated structure with Root Mean Square Fluctuation (RMSF) graph **(Figure 4.34D)**. RMSF will help to find the local changes in the structure during the molecular dynamics simulation. Typically, amino acids present in the C- and N-terminal regions of the protein are more flexible than others. Alpha helix and beta strands are more rigid than the unstructured part of the protein. Sharp peaks in the RMSF plot indicate that the residues are fluctuating more during simulation. A total of 294 amino acids were there in the protein; 58% of the amino acids (173amino acids) were fluctuating between 1-2 Å and 3.4% (10 amino acids) of the residues are fluctuating between 3-4 Å and are present in the loop portions of the

CDK2. Lys298 and Arg297 residues are showing maximum fluctuations of 4-5 Å, which are present in the C-terminal of the protein.
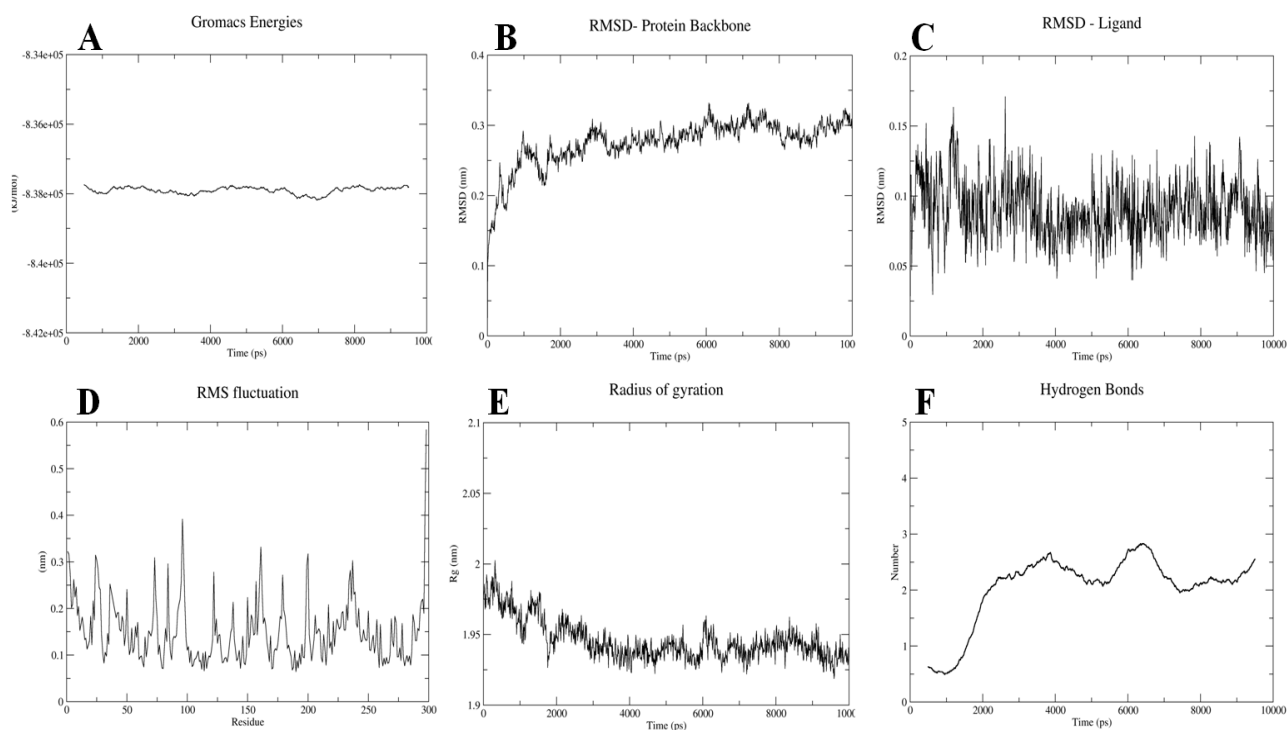
Figure 4.34 Molecular dynamic simulation of THC15-CKD2 complex for 10 ns. (A) Potential energy of the complex, (B) RMSD of the protein backbone, (C) RMSD of the ligand, (D) RMSF of the amino acid residues, (E) radius of gyration of complex and (F) Average number of H-bonds of the complex.

Radius of gyration (Rg) value is a measure of the compactness of a protein which was calculated as a RMS distance between the centre of gravity and end of the protein. In other words Rg is a measure assessing the stability of the folded protein. Radius of gyration of the initial starting structure was 1.97399 nm and the value decreased to 1.93452 nm at the end of 10 ns and MD simulation showing the THC15-CDK2 complex was stable and well folded **(Figure 4.34E)**. During the MD simulation an average of 2-3 H-bonds were observed between the THC15 and CDK2 **(Figure 4.34F)**. Overall, MD simulation suggests that THC15 forms stable interaction with the target CDK2.

4.9 Conclusions

The coumarins are of great value due to their therapeutic property. Their physiological, anti-tumor, and bacteriostatic activity marks coumarins as novel pharmacophores for therapeutic applications. Several studies have established multiple potential roles of coumarins which include disease spread and prevention, growth modulation, antioxidant and anti-tumor effects, etc. In the present study, we have

designed 62 novel coumarin analogs as CDK-2 inhibitors based on pharmacophore requirements. Docking study of the designed analogs was performed using molecular modeling software Autodock 4.2. Thereafter, the best four molecules were selected and docked again by using GLIDE on Schrodinger Maestro software for better authentication of the results. Activity comparison showed that THC-15 (3-substituted), THC-28 (4-substituted), THC-43 (6-substituted), and THC-59 (7-substituted) are the significant analogs showing better binding free energy and predicted inhibitory constant values as compared to standard drug Deschloroflavopiridol (-8.87) and Olomoucine (-6.08) as shown in **Figure 4.29** and **4.30** respectively. Similarly, among the all significant designed analogs, it turns out that THC-43 is by far the best analogue overall. OSIRIS property explorer and molinspiration cheminformatics online tools were used to predict Lipinski rule of five parameter and toxicity parameters of the designed analogs. Among the designed analogs, THC-4, THC-5, THC-11, THC-14, THC-15 (all 3-substituted), THC-25, THC-26, THC-27, THC-28, THC-32 (all 4-substituted), THC-41, THC-42, THC-43, THC-45, THC-47 (all 6-substituted), THC-53, THC-58, THC-59, THC-60, and THC-62 (all 7-substituted) showed significant binding free energy and predicted inhibitory constant values as compared to standard drug Deschloroflavopiridol and Olomoucine. Even though compounds like THC-1, THC-14, THC-18, THC-19, THC-20, THC-21, THC-22, THC-23, THC-24, THC-25, THC-26, THC-27, THC-28, THC-29, THC-30, THC-31, THC-32, THC-33, THC-34, THC-35, THC-36, THC-38, THC-39, THC-49, THC-51, THC-53, THC-54, and THC-56 showed significant binding free energy and predicted inhibitory constant values, they have been screened off for next level of study because of their predicted poor pharmacokinetic and toxicity profile. From this study, it was concluded that hydrogen bond donor and hydrogen bond acceptor groups in pharmacophore are very much important to form stable receptor-ligand complex as well as for better inhibitory potency. The molecular dynamics and simulation study was further done on selected analogs to find out the stability of the molecules inside the binding pocket of the CDK-2.

4.10 References

Part- A

[1] http://www.cancer.org. Accessed 6 Feb, **2015**.

[2] Traxler, P.; Fabbro, D.; Ruetz, S.; Buchdunger, E.; Cowan, J. S.; Fendrich, G.; Liebetanz, J.; Mestan, J.; O'Reilly, T.; Chaudhuri, B.; Fretz, H.; Zimmermann, J.; Meyer, T.; Caravatti, G.; Furet, P.; Manley, P. *Pharmacol. Ther.* **2002,** *93*, 79.

[3] Engh, R. A.; Bossemeyer, D. *Pharmacol. Ther.* **2002,** *93*, 99.

[4] Blum, G.; Gaziz, A.; Levitzki, A. *Biochem.* **2000,** *39*, 15705.

[5] Lou, Q.; Leftwich, M. E.; McKay, R. T.; Salmon, S. E.; Rychetsky, L.; Lam, K. S. *Cancer Res.* **1997,** *57*, 1877.

[6] Alfaro, L. J.; Yuan, W.; Phan, B. C.; Kamath, J.; Lou, Q.; Lam, K. S.; Hruby, V. J. *J. Med. Chem.* **1998,** *41*, 2252.

[7] Ramdas, L.; Obeyesekere, N. U.; Sun, G.; McMurray, J. S.; Budde, R. J. *J. Pept. Res.* **1999,** 53, 569.

[8] Eichholtz, T.; Bont, D. B.; Widt, J.; Liskamp, R. M.; Ploegh, H. L. *J. Biol. Chem.* **1993,** *268*, 1982.

[9] Yakymovych, I.; Engstrom, U.; Grimsby, S.; Heldin, C. H.; Souchelnytskyi, S. *Biochem.* **2002,** *41*, 11000.

[10] Parang, K.; Cole, P. A. *Pharmacol. Ther.* **2002,** *93*, 145.

[11] Sawyer, T. K.; Bohacek, R. S.; Dalgarno, D. C.; Eyermann, C. J.; Kawahata, N.; Metcalf, C. A.; 3rd Shakespeare, W. C.; Sundaramoorthi, R.; Wang, Y.; Yang, M. G. *Mini Rev. Med. Chem.* **2002,** *2*, 475.

[12] Pines, J. *Biochem. J.* **1995,** *308*, 697.

[13] Chevalier, S.; Blow, J. J. *Curr. Opin. Cell Biol.* **1996,** *8*, 815.

[14] Nurse, P.; Masui, Y.; Hartwell, L. *Nature Med.* **1998,** *4*, 1103.

[15] Sherr, C. J. *Science* **1996,** *274*, 1672.

[16] Morgan, D. O. *Nature* **1995,** *374*, 131.

[17] Hall, M.; Peters, G. *Adv. Cancer Res.* **1996,** *68*, 67.

[18] Gray, N.; Detivaud, L.; Doerig, D.; Meijer, L. *Curr. Med. Chem.* **1999,** *6*, 859.

[19] Walker, D. H. *Curr. Top Microbiol. Immunol.* **1998,** *227*, 149.

[20] Garrett, M. D.; Fattaey, A. *Curr. Opin. Genet. Dev.* **1999,** *9*, 104.

[21] Meijer, L.; Leclerc, S.; Leost, M. *Pharmacol. Ther.* **1999,** *82*, 279.

[22] Webster, K. R. *Expert. Opin. Invest. Drugs.* **1998,** *7*, 865.

[23] Davis, S. T.; Benson, B. G.; Bramson, H. N.; Chapman, D. E.; Dickerson, S. H.; Dold, K. M.; Eberwein, D. J.; Edelstein, M.; Frye, S. V.; Gampe, J. R. T.; Griffin, R. J.; Harris, P. A.; Hassell, A. M.; Holmes, W. D.; Hunter, R. N.; Knick, V. B.; Lackey, K.; Lovejoy, B.; Luzzio, M. J.; Murray, D.; Parker, P.; Rocque, W. J.; Shewchuk, L.; Veal, J. M.; Walker, D. H.; Kuyper, L. F. *Science* **2001,** *291*, 134.

[24] Barvian, M.; Boschelli, D. H.; Cossrow, J.; Dobrusin, E.; Fattaey, A.; Fritsch, A.; Fry, D.; Harvey, P.; Keller, P.; Garrett, M.; La, F.; Leopold, W.; Namara, M. D.; Quin, M.; Trumpp, K. S.; Toogood, P.; Wu, Z.; Zhang, E. *J. Med. Chem.* **2000,** *43*, 4606.

[25] Gussio, R.; Zaharevitz, D. W.; Grath, M. C. F.; Pattabiraman, N.; Kellogg, G. E.; Schultz, C.; Link, A.; Kunick, C.; Leost, M.; Meijer, L.; Sausville, E. A. *Anticancer Drug Des.* **2000,** *15*, 53.

[26] Gray, N. S.; Wodicka, L.; Thunnissen, A. M.; Norman, T. C.; Kwon, S.; Espinoza, F. H.; Morgan, D. O.; Barnes, G.; Clerc, L. S.; Meijer, L.; Kim, S. H.; Lockhart, D. J.; Schultz, P. G. *Science* **1998,** *281*, 533.

[27] Brooks, E. E, Gray, N. S.; Joly, A.; Kerwar, S. S.; Lum, R.; Mackman, R. L.; Norman, T. C.; Rosete, J.; Rowe, M.; Schow, S. R.; Schultz, P. G.; Wang, X.; Wick, M. M.; Shiffman, D. *J. Biol. Chem.* **1997,** *272*, 29207.

[28] Buquet, F. C.; Lallemand, F.; Montagne, M. N.; Mester, J. *Anticancer Drugs* **1997,** *8*, 623.

[29] Legraverand, M.; Ludwig, O.; Bisagni, E.; Leclerc, S.; Meijer, L. *Bioorg. Med. Chem. Lett.* **1998,** *8*, 793.

[30] Shu, L.; Joshua, K. B.; Lindsay, O. K.; Padmavathy, N. P.; Campbell, M. *ACS Chem. Bio.* **2010,** *5*, 1169.

[31] Sielecki, T. M.; Boylan, J. F.; Benfield, P. A.; Trainor, G. L. *J. Med. Chem.* **2000,** *43*, 1.

[32] Noble, M. E. M.; Endicott, J. A. *Pharmacol. Ther.* **1999,** *82*, 269.

[33] Adams, J. L.; Lee, D. *Curr. Opin. Drug Discuss. Dev.* **1999,** *2*, 96.

[34] Marcos, M.; Paolo, P.; Mariano, B. James, R. B. *Trends Pharmacol. Sci.* **2008**, *29*, 16.

[35] Senderowicz, A. M.; Headlee, D.; Stinson, S. F.; Lush, R. M.; Kalil, N.; Villalba, L.; Hill, K.; Steinberg, S. M.; Figg, W. D.; Tompkins, A.; Arbuck, S. G.; Sausville, E. A. *J. Clin. Oncol.* **1998,** *16*, 2986.

[36] Sedlacek, H. H.; Czech, J.; Naik, R.; Kaur, G.; Worland, P.; Losiewicz, M.; Parker, B.; Carlson, B.; Smith, A.; Senderowicz, A., Sausville, E. *Int. J. Oncol.* **1996,** *9*, 1143.

[37] Chaudhuri, B.; Fretz, H.; Muller, L.; Schoepfer, J.; Seeber, E.; Meijer, L.; Lozach, O.; Vangrevelinghe, E.; Furet, P. *J. Med. Chem.* **2002,** *45*, 1741.

[38] Chen, Y. N. P.; Sharma, S. K.; Ramsey, T. M.; Jiang, L.; Martin, M. S.; Baker, K.; Adams, P. D.; Bair, K. W.; Kaelin, W. G. *Proc. Natl. Acad. Sci. U.S.A.* **1999**, *96*, 4325.

[39] Fischer, P. M.; Endicott, J.; Meijer, L. *Prog. Cell Cycle Res.* **2003,** *5*, 235.

[40] Pindur, U.; Kim, Y. S.; Mehrabani, F. *Curr. Med. Chem.* **1999,** *6*, 29.

[41] Losiewicz, M. D.; Carlson, B. A.; Kaur, G.; Sausville, E. A.; Worland, P. J. *Biochem. Biophys. Res. Commun.* **1994,** *201*, 589.

[42] Brana, M. F.; Garcia, M. L.; Lopez, B.; Pascual, T. B.; Ramos, A.; Pozuelo, J. M.; Dominguez, M. T. *Org. Biomol. Chem.* **2004,** *2*, 1864.

[43] Vesely, J.; Havlicek, L.; Strnad, M.; Blow, J. J.; Donella, D. A.; Pinna, L.; Letham, D. S.; Kato, J.; Detivaud, L.; Leclerc, S. *Eur. J. Biochem.* **1994,** *224*, 771.

[44] Azevedo, W. F.; Leclerc, S.; Meijer, L.; Havlicek, L.; Strnad, M.; Kim, S. H. *Eur. J. Biochem.* **1997,** *243*, 518.

[45] Legraverend, M.; Ludwig, O.; Bisagni, E.; Leclerc, S.; Meijer, L.; Giocanti, N.; Sadri, R.; Favaudon, V. *Bioorg. Med. Chem.* **1999,** *7*, 1281.

[46] Hoessel, R.; Leclerc, S.; Endicott, J. A.; Nobel, M. E.; Lawrie, A.; Tunnah, P.; Leost, M.; Damiens, E.; Marie, D.; Marko, D.; Niederberger, E.; Tang, W.; Eisenbrand, G.; Meijer, L. *Nature Cell Biol.* **1999,** *1*, 60.

[47] Zaharevitz, D. W.; Gussio, R.; Leost, M.; Senderowicz, A. M.; Lahusen, T.; Kunick, C.; Meijer, L.; Sausville, E. A. *Cancer Res.* **1999,** *59*, 2566.

[48] Kent, L. L.; Campbell, H. N. E.; Lau, T.; Wu, J. C.; Thompson, S. A.; Nori, M. *Biochem. Biophys. Res. Commun.* **1999,** *260*, 768.

[49] Gray, N.; Detivaud, L.; Doerig, C.; Meijer, L. *Curr. Med. Chem.* **1999,** *6*, 859.

[50] Imbach, P.; Capraro, H. G.; Furet, P.; Mett, H.; Meyer, T.; Zimmermann, J. *Bioorg. Med. Chem. Lett.* **1999,** *9*, 91.

[51] Tang, J.; Lisa, M.; Hideyuki, S.; Masaichi, H.; Yoshiaki, W.; Naohiko, N. *Bioorg. Med. Chem. Lett.* **2003,** *13*, 2985.

[52] Bramson, H. N.; Corona, J.; Stephen, T. D.; Scott, H. D.; Mark, E.; Stephen, V. F.; Robert, T.; Gampe, J. R.; Phil, A. H.; Hassell, A.; William, D. H.; Robert, N. H.; Karen, E. L.; Brett, L.; Michael, J.; Luzzio, V. M.; Warren, J. R.; David, R.; Lisa, S.; James, M. V.; Duncan, H. W.; Lee, F. K. *J. Med. Chem.* **2001**, *44*, 4339.

[53] Vesely, J.; Havlicek, L.; Strnad, M.; Blow J. J.; Donella, D. A.; Letham, D. S.; Kato, J.; Detivaud, L.; Leclerc, S. *Eur. J. Biochem.* **1994,** *224*, 771.

[54] Paul, G. W.; Andrew, J. W.; Valerio, B.; John, A. B.; Maria, G. C.; David, M. C.; Deborah, J.; Lindsay, A.; Devine, T. R. E.; Ruth, E. F.; Lewis, E. J.; Rachel, L.; Menamin, M. E. F. N.; Michael, A. O. B.; Marc, O. R.; Matthias, R.; Gordon, S.; Matt, S. S.; Gary, T.; Margaret, T. W.; Alison, J. A. W. *J. Med. Chem.* **2008,** *51*,4986.

[55] Gray, N. S.; Wodicka, L.; Thunnissen, A. M.; Norman, T. C.; Kwon, S.; Espinoza, F. H.; Morgan, D. O.; Barnes, G.; Clerc, L. S.; Meijer, L.; Kim, S. H.; Lockhart, D. J.; Schultz, P. G. *Science* **1998,** *281,* 533.

[56] Dreyer, M. K.; Borcherding, D. R.; Dumont, J. A.; Peet, N. P.; Tsay, J. T.; Wright, P. S.; Bitonti, A. J.; Shen, J.; Kim, S. H. *J. Med. Chem.* **2001,** *44*, 524.

[57] Beattie, J. F.; Breault, G. A.; Ellston, R. P.; Green, S.; Jewsbury, P. J.; Midgley, C. J.; Naven, R. T.; Minshull, C. A.; Pauptit, R. A.; Tucker, J. A.; Pease, J. E. *Bioorg. Med. Chem. Lett.* **2003,** *13*, 2955.

[58] Breault, G. A.; Ellston, R. P.; Green, S.; James, S. R.; Jewsbury, P. J.; Midgley, C. J.; Pauptit, R. A.; Minshull, C. A.; Tucker, J. A.; Pease, J. E. *Bioorg. Med. Chem. Lett.* **2003,** *13*, 2961.

[59] Thomas, H. D.; Wang, L. Z.; Roche, C.; Bentley, J.; Cheng, Y.; Hardcastle, I. R.; Golding, B. T.; Griffin, R. J.; Curtin, N. J.; Newell, D. R. *Eur. J. Cancer* **2011,** *47*, 2052.

[60] Fabbro, D.; Ruetz, S.; Buchdunger, E.; Cowan, J. S.; Fendrich, G.; Liebetanz, J.; Mestan, J.; O'Reilly, T.; Traxler, P.; Chaudhuri, B.; Fretz, H.; Zimmermann, J.; Meyer, T.; Caravatti, G.; Furet, P.; Manley, P. *Pharmacol. Ther.* **2002,** *93*, 79.

[61] Schlosser, M.; Michel, D. *Tetrahedron* **1996,** *52*, 99.

[62] Benoit, C.; David, J. P.; Elizabeth, A.; Allyson, J. C.; Celine, C.; Aude, E.; Jane, A. E.; Bernard, T. G.; Karen, H.; Ian, R. H.; Philip, J. J.; David, R. N.; Martin, E. M. N.; Celine, R.; Lan, Z. W.; Roger, J. G. *J. Med. Chem.* **2014,** *57*, 56.

[63] Kerry, L. S.; Johanne, B.; Thomas, F. B.; Hilary, C. A.; Cheng, Y.; Nicola, J. C.; Jane, A. E.; Bernard, T. G.; Ian, R. H.; Philip, J.; Veronique, M.; David, R. N.; Martin, E. M. N.; Rachel, J. P.; David, J. P.; Lan, Z. W.; Roger, J. G. *Bioorg. Med. Chem. Lett.* **2003,** *13*, 3079.

[64] Masanda, V. H.; Patila, K. N.; Jawarkarb, R. D.; Haddac, T. B.; Youssoufi, M. H.; Alafeefy, A. A. *J. Comput. Method Mol. Des.* **2011,** *1*, 39.

[65] Khafagy, M. M.; Wahas, E. A. H. F. A.; Eid, F. A.; Agrody, E. A. M. *Farmaco* **2002,** *57*, 715.

[66] (a) Smith, W. P.; Sollis, L. S.; Howes, D. P.; Cherry, C. P.; Starkey, D. I.; Cobley, N. K.; Weston, H.; Scicinski, J.; Merritt, A.; Whittington, A.; Wyatt, P.; Taylor, N.; Green, D.; Bethell, R.; Madar, S.; Fenton, R. J.; Morley, P. J.; Pateman, T.; Beresford, A. *J. Med. Chem.* **1998,** *41*, 787; (b) Martinez, A. G.; Marco, L. J. *Bioorg. Med. Chem. Lett.* **1997,** *7*, 3165.

[67] Hiramoto, K.; Nasuhara, A.; Michiloshi, K.; Kato, T.; Kikugawa, K. *Mutat. Res.* **1997,** *395*, 47.

[68] Bianchi, G.; Tava, A. *Agric. Biol. Chem.* **1987,** *51*, 2001.

[69] Mohr, S. J.; Chirigos, M. A.; Fuhrman, F. S.; Pryor, J. W. *Cancer Res.* **1975,** *35*, 3750.

[70] Skommer, J.; Wlodkowic, D.; Matto, M.; Eray, M.; Pelkonen, J. *Leukemia Res.* **2006,** *30*, 322.

[71] Srivalli, T.; Satish, K.; Suthakaran, R. *Int. J. Innov. Pharm. Res.* **2011,** *2*, 172.

[72] Foloppe, N.; Fisher, L. M.; Howes. R.; Potter, A.; Robertson, A. G. S.; Surgenor, A. E. *Bioorg. Med. Chem.* **2006,** *48*, 4792.

[73] Hafez, E. A. A.; Elnagdi, M. H.; Elagamey, A. G. A.; Taweel, E. F. M. A. A. *Heterocycles* **1987,** *26*, 903.

[74] Polshettiwar, V.; Rajender, S. V. *Tetrahedron Lett.* **2008,** *49*, 397.

[75] Norbury, C.; Nurse, P. *Annu. Rev. Biochem.* **1992,** *6*, 441.

[76] Nigg, E. A. *Curr. Opin. Cell. Biol.* **1993,** *5*, 187.

[77] Morgan, D. O. *Nature* **1995,** *374*, 131.

[78] Sausville, E. A. *Trends Mol. Med.* **2002,** *8*, S32.

[79] Ramachandran, G. N.; Sasisekharan, V. *Adv. Protein Chem.* **1968,** *23*, 283.

[80] Spoel, D.; Lindahl, E.; Hess, B.; Groenhof, G.; Mark, A. E.; Berendsen, H. J. *J. Comput. Chem.* **2005,** *26*, 1701.

[81] Scott, W. R. P.; Hunenberger, P. H.; Tironi, I. G.; Mark, A. E.; Billeter, S. R.; Fennen, J.; Torda, A. E.; Huber, T.; Kruger, P.; Gunsteren, V. W. F. *J. Phys. Chem. A* **1999,** *103*, 3596.

[82] Abraham, M. J.; Gready, J. E. *J. Comput. Chem.* **2011,** *32*, 2031.

[83] Kumar, K. A.; Prathyusha, L. T.; Umamaheshwari, M.; Sivashanmugam, T.; Subhadradevi, V.; Jagannath, P.; Madeswaran, A,; Salesheir, F, *J. Chil. Chem. Soc.* **2012,** *57*, 1442.

[84] Daisy, P.; Suveena, S.; Rajalakshmi, M.; Lilly, V. *Der. Pharm. Chem.* **2011,** *3*, 51.

[85] Hou, T.; Wang, J.; Zhang, W.; Xu, X. *J. Chem. Inf. Model.* **2007,** *47*, 460.

[86] Vistoli, G.; Pedretti, A.; Testa, B. *Drug Discov. Today* **2008,** *13,* 285.

Part-B

[87] Gregory, S.; Sandeep, K. K.; Jens, M.; Edward, W. L. *Pharmacol. Rev.* **2014,** *66*, 334.

[88] Meier, P.; Finch, A.; Evan, G. *Nature* **2000,** *407*, 796.

[89] Hanks, S. K.; Quinn, A. M.; Hunter, T. *Science* **1988,** *241*, 42.

[90] Blumer, K. J.; Johnson, G. L. *Trends Biochem. Sci.* **1994,** *19*, 236.

[91] Davis, R. J. *Trends Biochem. Sci.* **1994,** *19*, 470.

[92] Marshall, C. J. *Cell* **1995,** *80*, 179.

[93] Schultz, J.; Ferguson, B.; Sprague, G. F. *Curr. Opin. Genet. Dev.* **1995,** *5*, 31.

[94] Norbury, C.; Nurse, P. *Annu. Rev. Biochem.* **1992,** *61*, 441.

[95] Nigg, E. A. *Curr. Opin. Cell Biol.* **1993,** *5*, 187.

[96] Morgan, D. O. *Nature* **1995,** *374*, 131.

[97] Knighton, D. R.; Zheng, J.; Eyck, T. L. F.; Ashford, V. A.; Xuong, N. H.; Taylor, S. S.; Sowadski, J. M. *Science* **1991,** *253*, 407.

[98] Zhang, F.; Strand, A.; Robbins, D.; Cobb, M. H.; Goldsmith, E. J. *Nature* **1994,** *367*, 704.

[99] Hu, S. H.; Parker, M. W.; Lei, J. Y.; Wilce, M. C. J.; Benian, G. M.; Kemp, B. E. *Nature* **1994,** *369,* 581.

[100] Xu, R. M.; Carmel, G.; Sweet, R. M.; Kuret, J.; Cheng, X. *EMBO J.* **1995,** *14*, 1015.

[101] Owen, D. J.; Noble, M. E.; Garman, E, F.; Papageorgiou, A. C.; Johnson, L. N. *Structure* **1995,** *3*, 467.

[102] Bondt, D. H. L.; Rosenblatt, J.; Jancarik, J.; Jones, H. D.; Morgan, D. O.; Kim, S. H. *Nature* **1993,** *363*, 595.

[103] Taylor, S. S.; Radzio, A. E. *Structure* **1994,** *2*, 345.

[104] Vassilev, L. T.; Tovar, C.; Chen, S.; Knezevic, D.; Zhao, X.; Sun, H. *Proc. Natl. Acad. Sci. USA.* **2006,** *103*, 10660.

[105] Malumbres, M.; Pevarello, P.; Barbacid, M.; Bischoff, J. R. *Trends Pharmacol. Sci.* **2008,** *29*, 16.

[106] Johnson, E. F.; Stewart, K. D.; Woods, K. W.; Giranda, V. L.; Luo, Y. *Biochem.* **2007,** *46*, 9551.

[107] Gleixner, K. V.; Ferenc, V.; Peter, B.; Gruze, A.; Meyer, R. A.; Hadzijusufovic, E. *Cancer Res.* **2010,** *70*, 1513.

[108] Harrington, E. A.; Bebbington, D.; Moore, J.; Rasmussen, R. K.; Adeogun, A. A. O.; Nakayama, T. *Nat. Med.* **2004,** *10*, 262.

[109] Kitagawa, M.; Okabe, T.; Ogino, H.; Matsumoto, H.; Suzuki, T. I.; Kokubo, T.; Higashi, H.; Saitoh, S.; Taya, Y.; Yasuda, H.; Ohba, Y.; Nishimura, S.; Tanaka, N.; Okuyama, A. *Oncogene* **1993,** *8*, 2425.

[110] Losiewicz, M. D.; Carlson, B. A.; Kaur, G.; Sausville, E. A.; Worland, P. J. *Biochem. Biophys. Res. Commun.* **1994,** *201*, 589.

[111] Vesely, J.; Havlicek, L.; Strnad, M.; Blow, J. J.; Donella, D. A.; Pinna, L.; Letham, D. S.; Kato, J. Y.; Detivaud, L.; Leclerc, S.; Meijer, L. *Eur. J. Biochem.* **1994,** *224*, 771.

[112] Hochegger, H.; Takeda, S.; Hunt, T. *Nat. Rev. Mol. Cell Biol.* **2008,** *9*, 910.

[113] Jayalakshmi, S.; Nagaraju, A.; Nagarajan, P. *AAPS J.* **2006,** *8*, E204.

[114] Murray, A. W. *Cell* **2004,** *116*, 221.

[115] Fischer, P. M.; Endicott, J.; Meijer, L. *Prog. Cell Cycle Res.* **2003,** *5*, 235.

[116] Dai, Y.; Grant, S. *Curr. Opin. Pharmacol.* **2003,** *3*, 362.

[117] Harper, J. W.; Adams, P. D. *Chem. Rev.* **2001,** *101*, 2511.

[118] Ekholm, S. V.; Reed, S. I. *Curr. Opin. Cell Biol.* **2000,** *12*, 676.

[119] Lacy, A.; O'Kennedy, R. *Curr. Pharm. Des.* **2004,** *10*, 3797.

[120] Hoult, J. R.; Payá, M. *Gen. Pharmacol.* **1996,** *27*, 713.

[121] Vianna, D. R.; Hamerski, L.; Figueiro, F.; Bernardi, A.; Visentin, L. C. *Eur. J. Med. Chem.* **2012,** *57*, 268.

[122] Finn, G. J.; Kenealy, E.; Creaven, B. S.; Egan, D. A. *Cancer Lett.* **2002,** *183*, 61.

[123] Loprinzi, C. L.; Kugler, J. W.; Sloan, J. A.; Rooke, T. W.; Quella, S. K. *N. Engl. J. Med.* **1999,** *340*, 346.

[124] Kostova, I. *Curr. Med. Chem. Anticancer Agents* **2005,** *5*, 29.

[125] Murray, R. D. H.; Mendez, J.; Brown, S. A. *The Natural Coumarins: occurrence, chemistry and biochemistry*. Wiley, Newyork: **2010**; 1.

[126] Mironov, A.; Colanzi, A.; Polishchuk, R.; Beznoussenko, G.; Mironov, A.; Fusella, A.; Tullio, D. G.; Silletta M.; Corda, D.; Matteis, D. M.; Luini, A. *Eur. J. Cell Biol.* **2004,** *83*, 263.

[127] Abdelmohsen, K.; Stuhlmann, D.; Daubrawa, F.; Klotz, L. *Arch. Biochem. Biophys.* **2005,** *434*, 241.

[128] Egan, D. A.; O'Kennedy, R.; Moran, E.; Thornes, R. D. *Drug Met. Rev.* **1990,** *22*, 503.

[129] Ojala, T. *Biological screening of plant coumarins*. PhD Thesis, University of Helsinki, Finland: **2001**; 95.

[130] Grotz, K. A.; Wustenberg, P.; Kohnen, R.; Nawas, A. B.; Zepelin, H. V. H. H.; Bockisch, A. *Br. J. Oral Maxillofac. Surg.* **2001,** *39*, 34.

[131] Holbrook , A. M.; Pereira, J. A.; Labiris, R.; Donald, M. H.; Douketis, J. D.; Crowther, M.; Wells, P. S. *Arch. Intern. Med.* **2005,** *165*, 1095.

[132] Carter, S. K.; Bakowski, M. T.; Hellman, K. *Chemotherapy of cancer*, 3rd ed.; Wiley & Sons, New York: **1989**.

[133] Finn, G. J.; Creaven, B. S.; Egan, D. A. *Cancer Lett.* **2004,** *205*, 69.

[134] Thornes, R. D.; Edlow, D. W.; Wood, S. *Johns Hopkins Med. J.* **1968,** *123*, 305.

[135] Finn, G. J.; Creaven, B. S.; Egan, D. A. *Melanoma Res.* **2001,** *11*, 461.

[136] Marshall, M. E.; Mendelsohn, L.; Butler, K.; Riley, L.; Cantrell, J.; Wiseman, C.; Taylor, R.; Macdonald, J. S. *J. Clin. Oncol.* **1987,** *5*, 862.

[137] Marshall, E. M.; Ryles, M.; Butler, K.; Weiss, L. *J. Cancer Res. Clin. Oncol.* **1994,** *120*, 535.

[138] Myers, R. B.; Parker, M.; Grizzle, W. E. *J. Cancer Res. Clin. Oncol.* **1994,** *120*, S11.

[139] Wang, C. J.; Hsieh, Y. J.; Chu, C. Y.; Lin, Y. L.; Tseng, T. H. *Cancer Letts.* **2002,** *183*, 163.

[140] Jimenz, O. F.; Lopez, G. J. S.; Nieto, R. A.; Velasco, V. M. A.; Molina, G. J. A.; Mendoza, P. N. *Lung Cancer* **2001,** *34*, 185.

[141] Musa, M. A.; Zhou, A.; Sadik, O. A. *J. Med. Chem.* **2011,** *7*, 112.

[142] Chen, Y. L.; Lu, C. M.; Lee, S. J.; Kuo, D. H.; Chen, I. L.; Wang, T. C.; Tzeng, C. C. *Bioorg. Med. Chem.* **2005,** *13*, 5710.

[143] Portugal, J. *Curr. Med. Chem.* Anticancer Agents **2003,** *3*, 411.

[144] Yang, D.; Wang, G. T.; Tang, Q.; Ma, C. *Biosci. Biotechnol. Biochem.* **2010,** *74*, 1430.

[145] Yun, E. S.; Park, S. S.; Shin, H. C. *Toxicol. In Vitro* **2011,** *25*, 1335.

[146] Lee, C. R.; Shin, E. J.; Kim, H. C. *Lab. Anim. Res.* **2011,** *27*, 259.

[147] Whang, W. K.; Park, H. S.; Ham, I. *Exp. Mol. Med.* **2005,** *37*, 436.

[148] Rosselli, S.; Maggio, A. M.; Faraone, N. *Nat. Prod. Comm.* **2009,** *4*, 1701.

[149] Poole, S. K.; Poole, C. F. *Analyst* **1994,** *119*, 113.

[150] Marshall, M. E.; Kervin, K.; Benefield, C.; Umerani, A.; Albainy, J. S.; Zhao, Q.; Khazaeli, M. B. *J. Cancer Res. Clin. Oncol.* **1994,** *120*, S3.

[151] Myers, R. B.; Parker, M.; Grizzle, W. E. *J. Cancer Res. Clin. Oncol.* **1994,** *120*, S11.

[152] Kawaii, S.; Tomono, Y.; Ogawa, K.; Sugiura, M.; Yano, M.; Yoshizawa, Y. *Anticancer Res.* **2001,** *21*, 917.

[153] Thornes, R. D.; Daly, L.; Lynch, G.; Breslin, B.; Browne, H.; Browne, H. Y.; Corrigan, T.; Daly, P.; Edwards G.; Gaffney, E. *J. Cancer Res. Clin. Oncol.* **1994,** *120*, S32.

[154] Marshall, M. E.; Mohler, J. L.; Edmonds, K.; Williams, B.; Butler, K.; Ryles, M.; Weiss, L.; Urban, D.; Bueschen, A.; Markiewicz, M. *J. Cancer Res. Clin. Oncol.* **1994,** *120*, S39.

[155] Mohler, J. L.; Williams, B. T.; Thompson, I. M.; Marshall. M. E. *J. Cancer Res. Clin. Oncol.* **1994,** *120*, S35.

[156] Angerer, E. V.; Kager, M.; Maucher, A. *J. Cancer Res. Clin. Oncol.* **1994,** *120*, S14.

[157] Lake, B. G. *Food Chem. Toxicol.* **1999,** *37*, 423.

[158] Marshall. M. E.; Butler, K.; Fried, A. *Mol. Biother.* **1991,** *3*, 170.

[159] Sharma, A.; Shukla, P.; Pallavi, B.; Subhra, D.; Rajdeep, C. *Curr. Microwave Chem.* **2015,** *2*, 1.

[160] Kumar, K. A.; Prathyusha, L. T.; Umamaheshwari, M.; Sivashanmugam, T.; Subhadradevi, V.; Jagannath, P.; Madeswaran, A.; Salesheir, F. *J. Chil. Chem. Soc.* **2012,** *57*, 1442.

[161] Daisy, P.; Suveena, S.; Rajalakshmi, M.; Lilly, V. *Der. Pharm. Chem.* **2011,** *3*, 51.

[162] Hou, T.; Wang, J.; Zhang, W.; Xu, X. *J. Chem. Inf. Model.* **2007,** *47*, 460.

[163] Davis, A. M.; Teague, S. *Angew. Chem. Int. Ed.* **1999,** *38*, 736.

[164] Qian, S. B.; Waldron, L.; Choudhary, N.; Klevit, R. E. Chazin, W. J. *J. Biol. Chem.* **2009,** *284*, 26797.

Chapter V

Physical Investigations and Theoretical Studies of Some Selected Substituted Pyranopyrazoles Adsorption on Mild Copper Metal in Acid Solution

5.1 Introduction: The use of inhibitors has been reported to offer protection for metals and alloys in most environments and therefore, over the years, this has been subject of interest in corrosion science and engineering research.[1-3] Heterocyclic molecules having N, O, and S heteroatom's possess tremendous potential as corrosion inhibitors for mild steel in acid solution.[4-7] Pyranopyrazoles (ppz), a family of N- and O-heterocyclic's, have been reported as basic structural motifs for a gamut of useful compounds such as natural products and drug precursors.[8] Furthermore, pyrazole fused pyrans are well established group of heterocyclic molecules possessing wide applications such as analgesic, CHK-1 inhibitor, antitumor agents and used as an important scaffold in pharmaceuticals and agrochemicals.[9] The inhibitive properties of these molecules make their assessment very important for industrial as well as academic researchers to develop environment friendly benign corrosion inhibitors.

The preference for these corrosion inhibitors is because of the presence of heteroatom's (N, O)[10-13] and better π electron conjugation, enhancing an improved coordination and adsorption property. These heterocyclic molecules not only follow some known adsorption isotherm but also behave as adsorptive centers on the surface of metal and inhibit the growth of corrosive agents by creating a barrier between the metal surface and corrosive agents.

The stability of the inhibitor film on the metal surface depends upon several physicochemical properties of the molecules and are related to many characteristic features such as occurrence of certain functional groups, presence of electron density on the heteroatom's (donor atom), aromaticity, steric effect, nature of medium causing corrosion, presence of charge on surface of metal, structure of the designed inhibitor scaffold, and the interaction between[14] the p and d orbital's of inhibitor and metal surface respectively. All the above mentioned features found in drug molecules that's why these days researchers focused on drug molecules as corrosion inhibitors for metallic surface. The huge literature is available on the drug molecules where several researchers reported them as corrosion inhibitors in acidic medium[15-18]. Hence the designing and synthesis of organic inhibitors[19] become an active research area in the development of new corrosion inhibitors for metallic surface.

Now a days, various theoretical and experimental techniques have been developed and the density functional theory (DFT) method based quantum chemical calculations have become high-tech theoretical technique because it gives accurate basic imperative parameters and detailed structural properties of the chemical inhibitors.[20] Quraishi *et al*.[18, 21–23] have recently studied various substituted heterocyclic compounds, in acidic solution, as corrosion inhibitors for mild steel. Formerly, some reports on pyrazole were revealed as these compounds behave as corrosion inhibitors for aluminium and copper metal in HCl solution. However, as per our knowledge, till now no reports are available regarding detailed study on pyranopyrazoles as corrosion inhibitors for mild Cu. Some chemical and synthetic corrosion inhibitors

that have reportedly shown to exhibit good corrosion resistance are not prepared in a green chemistry fashion and may not be eco-friendly thus creating undesirable environmental threat.[24-27]

Therefore, efforts toward identifying any potential eco-friendly and less expensive corrosion inhibitors remain relevant and progressive. Cu metal is very useful for several industrial and manufacturing industries and the study of its corrosion inhibition is of great importance. The present study was done to scrutinize five pyranopyrazoles as corrosion inhibitors for mild Cu metal in 1 M HCl solution. The molecular design and synthesis of corrosion inhibitors scaffold is based on pyranopyrazoles which contain a primary amine, a secondary amine, and a cyanide functional group with nitrogen and oxygen heteroatom in the core of the ppz skeleton and which also possess several π-bonds and efficiently inhibit the corrosion of mild Cu in acidic medium. Additionally, the presence of delocalized electrons increases the pyranopyrazole scaffold inhibition activity. The structure of the designed novel selected organic pyranopyrazole (PPZ) corrosion inhibitor is shown in **Figure 5.1**. The rationale for designing the selected ppz compounds was to choose a N-heterocyclic, S-heterocyclic, simple aromatic, slightly polar, and more polar substituted moieties.

5.2 Experimental:

5.2.1 Synthesized inhibitors: The pyranopyrazole (PPZ) inhibitors[28-30] were prepared by one-step protocol according to **scheme 3.1** and **3.2** already discussed in **Part A** and **B** of **Chapter-3** and are shown in **Figure 5.1**.
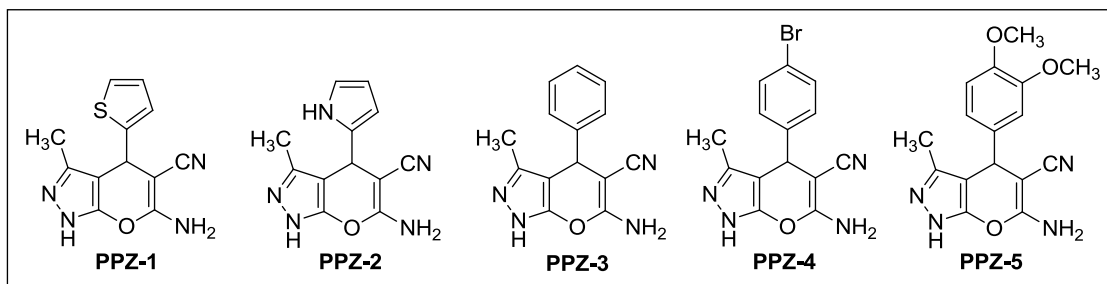

Figure 5.1 Shows the five selected Pyranopyrazole (PPZ) scaffolds as corrosion inhibitors.

5.2.2 Theoretical study: All the reported computations were performed using Q-CHEM 4.1 software. The geometry-optimizations and the single-point computations were all performed at B3LYP/TZ (2d,p) level of theory. Frequency jobs were run to ensure that the optimized geometries are indeed local minima. The computed parameters, namely, E_{HOMO}, E_{LUMO}, ΔE ($E_{LUMO} - E_{HOMO}$), dipole moment, and Mulliken and Lowdin charges on heteroatom's have been reported in **Table 5.1**.

5.2.3 Surface characterization: For SEM and EDX analysis NOVA NANO SEM 450 BRUCHER instrument was used. The chemical composition of the corrosion product was evaluated by EDX detector.

For SEM imaging the sample was prepared by using mild Cu specimens of size 2×2 (length $\times$ breadth) cm having thickness 1.9 mm. All the designed Cu strips were dipped in the absence and presence of optimal concentration (600 mg L^{-1}) of PPZs for three hours in acidic medium. Subsequently, the mild copper strips were removed for washing and degreased with acetone.

5.2.4 XRD (X-Ray Diffraction) study: All the organic material deposited samples were tested by Rigaku Miniflex X-Ray Diffractometer, with 2θ from 10-100° with scan rate of 3° per minute. The mild copper specimen of size 2×2 (length $\times$ breadth) cm having thickness of 1.9 mm was cleaned with acetone and methanol before immersing it into 1 M HCl solution in the presence of PPZ for 3 hours. Subsequently, the copper specimens were removed from the solution of HCl and washed with acetone and absolute ethanol.

2.2.5 Electrochemical measurements: A conventional three electrode cell was used to carry out the electrochemical experiments with a CHI604e electrochemical instrument. Glassy carbon electrode (GCE), platinum wire, and Ag-AgCl were used as working electrode, counter electrode, and reference electrode, respectively. To clean GCE surface, GCE was polished with 1 micron and 0.05 micron alumina before use. All the experiments were done in 1M HCl solution after dipping of mild copper strips for 30 minutes and in absence and presence of diverse inhibitors. The electrode was allowed to corrode freely and its open circuit potential (OCP) was recorded with 0.1 sec and 200 sec for sample interval and run time, respectively.

5.2.6 Impedance measurement: Measurement of impedance of a sample as a function of frequency of applied electric field is termed as impedance spectroscopy (IS). The electrochemical impedance study was performed by using HIOKI 3522-50 LCR HiTESTER instrument with sweeping frequency from 100 KHz to 1 mHz. All the experiments were done in 1M HCl after dipping of mild copper strips, having dimension 10×35 (breadth $\times$ height) mm with 5 mm separation, in 1M HCl solution with and without different inhibitors with various concentrations.

5.2.7 Conductivity study: The mild copper specimens of size 6×6 (length $\times$ breadth) cm having thickness 1.9 mm, were cut by using sheet cutting machine and later on washed and degreased with distilled water, acetone, and ethanol respectively. Thereafter, all the specimens were dried at room temperature before dipping into the 1M HCl solution. Subsequently, the copper specimens were dipped for 12 hours in 1M HCl solution in the absence and then in the presence of the required optimal concentration (500 mg L^{-1}) of PPZs. Conductivity study was done by four probe method at 23 °C and 9 points were traced for each specimen for better reproducibility of the results. Finally, the mean value/average value was taken for further analysis.

5.2.8 Mechanical property via tensile testing: The mild copper specimen of size 62×10 (length $\times$ breadth) mm having average thickness 1.9 mm, of strip shape were cut by using sheet cutting machine.

Horizontal and vertical shaper was used to give shape to the gauge length (GL), gauge width (GW), and width (W) of the specimen. Finally, Buffing and Finishing was done for smoothening, shining, and for removing the extra edges of the mild copper specimen before dipping into the inhibitor solution. Then, the Cu specimens were immersed in 1M HCl solution for 12 hour in the absence and presence of optimal concentration (500 mg L^{-1}) of PPZs. Finally, deposited copper strips were removed from the solution, dried, and subjected to tensile testing. All the tensile testing experiments were carried out at 33 °C by using DYNAMIC UNIVERSAL TEST MACHINE of 100 KN (Kilo Newton) capacity having ITW hydraulic top and lower wedge grip pressure 210 bar, of model number AC0511T3. All the specimens were tested and stretched with the rate of 0.5 mm/min.

5.3 Results and Discussion

5.3.1 Computational investigations: The optimized ground state geometries of PPZ-1, PPZ-2, PPZ-3, PPZ-4, and PPZ-5 are presented in **Figure 5.2**.
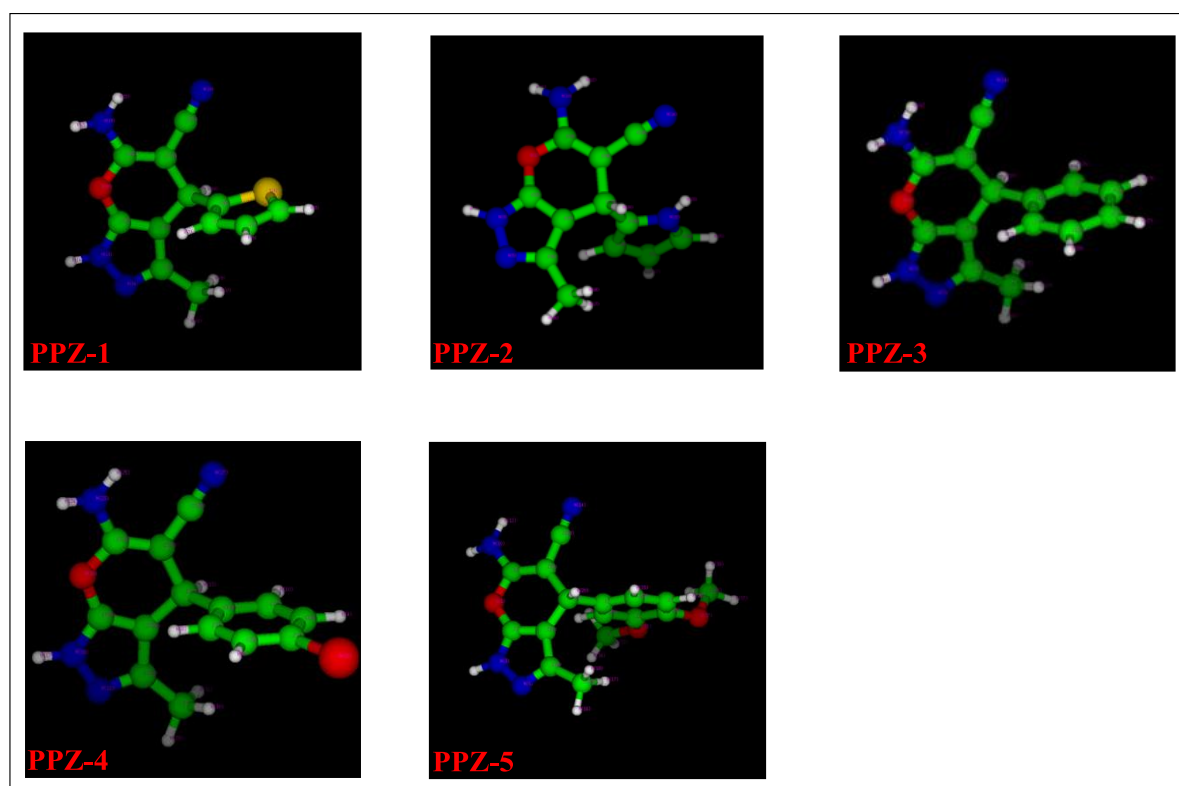

Figure 5.2 Shows the optimized structures of PPZs.

Figure 5.3 presents the HOMO and LUMO iso-density surfaces of all the molecules. For PPZ-3, the electron density in HOMO is majorly concentrated on pyranopyrazole fragment, whereas in LUMO, it gets delocalized over the entire molecule. While the HOMO shows strong pi-type bonding interactions

across the joint of the 6- and 5- membered rings of pyranopyrazole fragment and along the O—NH$_2$—CN region, the LUMO is characterized by pi-type anti-bonding interactions in this region. Both HOMO and LUMO, exhibit strong anti-bonding interactions between *meta*-N and N-H of the five-membered ring with a remarkable difference of bonding-interaction in HOMO between *meta*-N and the carbon bonded to the methyl group, as opposed to LUMO. In short, HOMO to LUMO electronic transition involves charge-transfer to the benzene ring substituted on the 6-membered ring of pyranopyrazole fragment of PPZ-3. The bonding patterns in PPZ-4 are very similar except for the presence of the weak election density on the bromine. The HOMOs of PPZ-2 and PPZ-5 differ from PPZ-3 and PPZ-4 in that the electron density is significantly concentrated on the substituting ring rather than the pyranopyrazole fragment. In PPZ-1, the electron-density is fairly delocalized in both HOMO and LUMO, with slightly more bonding interactions in LUMO across substituent and 6-membered ring as compared to HOMO. To summarize, the HOMO to LUMO excitation results in substituent to pyranopyrazole charge transfer in PPZ-1(weak), PPZ-2, and PPZ-5 (strong), while in case of PPZ-3 and PPZ-4, strong charge transfer from pyranopyrazole to the substituent is observed.
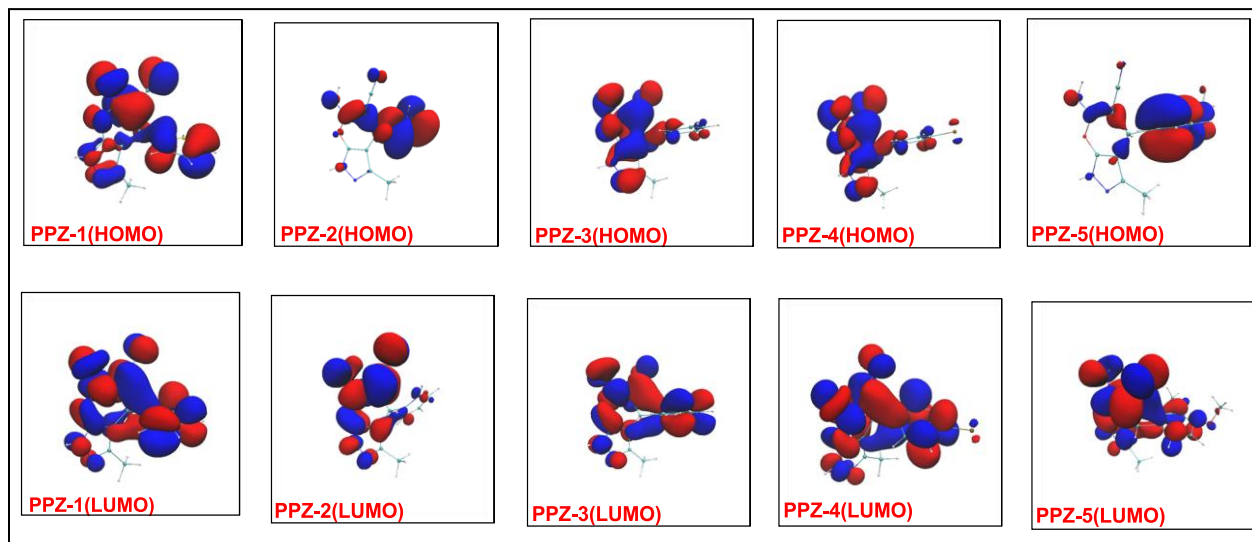

Figure 5.3 Frontier molecular orbital density distributions of PPZs.

The largest HOMO-LUMO (11.8 eV) corresponds to PPZ-3 and the smallest HOMO-LUMO gap (11.2 eV) corresponds to PPZ-2. The difference between these gaps is only 0.6 eV and smaller than the typical error-bar of a DFT method. Therefore, HOMO-LUMO gap may give only semi-qualitative insight about behavior of the molecules.

The largest HOMO-LUMO gap (11.8 eV) of PPZ-3 **(see Table: 5.1)** indicates its low inhibition efficiency. However, polarity of molecules plays crucial role in deciding the inhibition efficiency. The low inhibition efficiency of PPZ-3 is also supported by its moderately small dipole moment of 3.7 D. On

the other hand, the still smaller dipole moment (3.2 D) of PPZ-2 does not favor inhibition in spite of the smallest HOMO-LUMO gap of 11.2 eV. The high polarity of PPZ-4 and PPZ-5 characterized by largest dipole moment value of 5.2 D promotes inhibition and the moderate HOMO-LUMO gap of 11.5 eV favors it further. On the other hand, PPZ-1, which has almost the same HOMO-LUMO gap is slightly less prone to inhibition due to relatively lower dipole moment of 4.4 D. In all the molecules, the amino nitrogen sites are prone to electrophilic addition/substitution or electron-donation due to their high charge-density predicted by both Mulliken and Lowdin population analyses.

**Table 5.1.** Shows the quantum chemical parameters.

Inhibitors	Atom	Mulkins Charges	Lowdin Population	HOMO Energy (eV)	HOMO-LUMO GAP (eV)	Dipole Moment (Debye)
PPZ-1	1 S	0.2106	0.2109	-8.5988	11.4832	4.3570
	13 N	-0.2217	-0.2220			
	15 O	-0.5055	-0.5056			
	16 N	-0.2939	-0.2938			
	20 N	-0.5419	-0.5419			
	24 N	-0.0461	-0.0459			
PPZ-2	1 O	-0.5074	-0.5075	-7.9457	11.2111	3.2224
	3 N	-0.2225	-0.2224			
	5 N	-0.2939	-0.2938			
	10 N	-0.5419	-0.5420			
	14 N	-0.0547	-0.0548			
	22 N	-0.3728	-0.3729			
PPZ-3	1 O	-0.5063	-0.5064			
	3 N	-0.2229	-0.2228			
	5 N	-0.2947	-0.2946	-8.8437	11.8370	3.7097
	10 N	-0.5428	-0.5429			
	14 N	-0.0490	-0.0488			
PPZ-4	1 Br	-0.0015	-0.0013			
	16 N	-0.2211	-0.2210			
	18 O	-0.5051	-0.5052			
	19 N	-0.2932	-0.2928	-8.9798	11.5104	5.1476
	23 N	-0.5405	-0.5405			
	27 N	-0.0452	-0.0450			
PPZ-5	1 O	-0.5056	-0.5056			
	3 N	-0.2230	-0.2233			
	5 N	-0.2968	-0.2969			
	10 N	-0.5435	-0.5434	-8.3539	11.5104	5.1575
	14 N	-0.0488	-0.0488			
	27 O	-0.4636	-0.4637			
	32 O	-0.4364	-0.4363			

Thus, one can qualitatively predict PPZ-4 and PPZ-5 to have highest inhibition efficiency with amino nitrogen of PPZ-5 to be the most prone to electrophilic addition-substitution not only due to the high charge density at nitrogen, but also due to substituent → pyranopyrazole charge transfer. PPZ-1 will have

slightly less inhibition efficiency as compared to that of PPZ-4 and PPZ-5, but slightly more than that of PPZ-2. Thus, PPZ-3 seems to be least prone to inhibition.

5.3.2 Surface investigations

5.3.2.1 Scanning Electron Microscopy (SEM) Analysis: To know the morphology of the Cu surface after the deposition of all PPZ compounds, SEM study was performed. All the micrographs (**Figure 5.4a−f)** were taken after 3 hour of dipping of copper metal in 1 MHCl solution in absence and presence of the required optimal concentration (600 mg L^{-1}) of PPZ inhibitors. **Figure 5.4a** shows the micrograph of pure copper metal surface and one can very easily observe scratches on the metal surface. **Figure 5.4b-f** represents the morphologies of the copper metal specimens deposited with different PPZ material. A closer observation shows that less damage occurred on copper metal specimens with deposited PPZ material in acidic medium. This clearly implies that the PPZ inhibitors can shield mild copper metal surface successfully in 1M HCl solution because of the barrier created by these inhibitor molecule between the metal surface and the solution environment. In the presence of PPZ-2, the morphology of the copper metal surface looks very even and seems less corroded which may be because of strong adsorption of this inhibitor on the copper metal surface **(Figure 5.4c)**. Interestingly, similar phenomena were also confirmed from the aforementioned theoretical study.
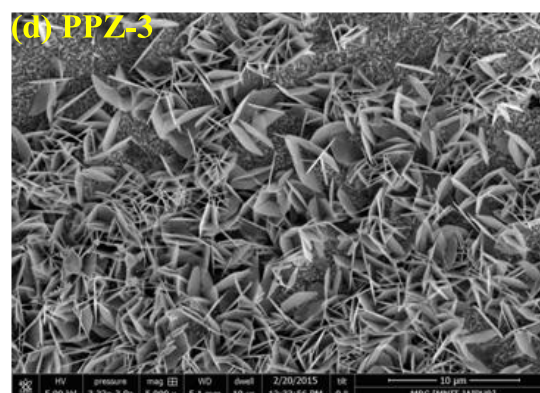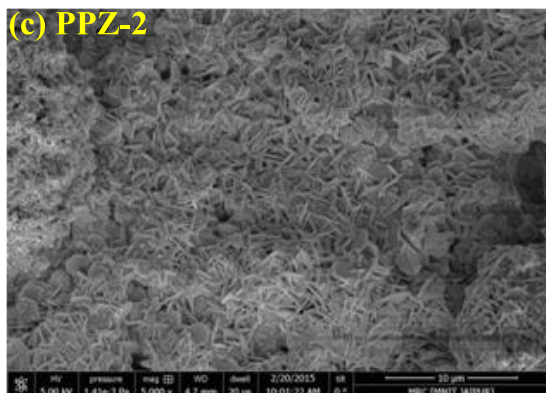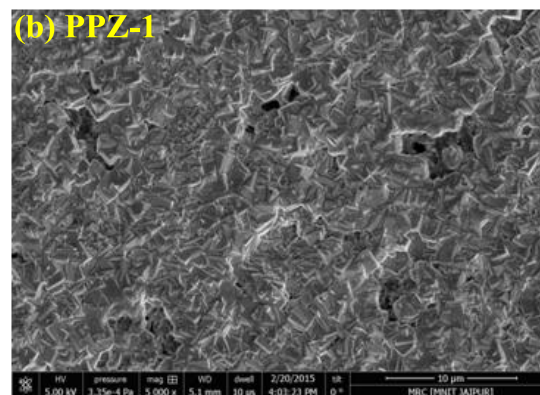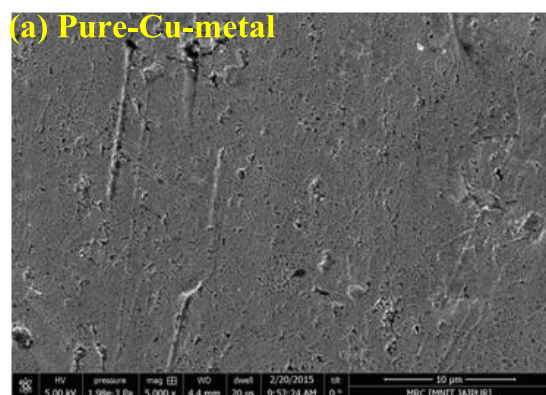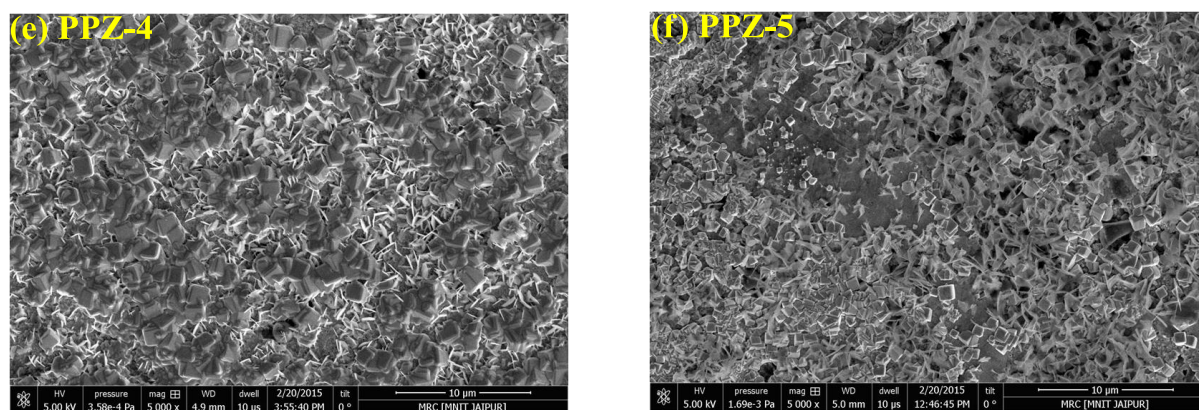
Figure 5.4 The SEM micrographs of mild copper surface: (a) Pure-Cu-metal, (b) PPZ-1, (c) PPZ-2, (d) PPZ-3, (e) PPZ-4, and (f) PPZ-5.

5.3.2.2 EDS Analysis: EDS (Energy Dispersive Spectroscopy) analysis was performed to know the presence of heteroatom's (C, N, and O) and metal ions which were employed in the reaction mixture. The presence of elements on copper metal surface without and with deposition of PPZ material was confirmed by spectra obtained from EDS coupled with SEM instrument. The atomic contents of various elements present on the copper metal surface in percentage are shown in **Table 5.2**, while the peak corresponding to particular elements are shown in EDS spectra as depicted in **Figure 5.5**. The EDS spectra of pure-Cu-metal specimen show only the characteristic copper element peak **(Figure 5.5a)**. However, the copper metal samples treated with inhibitors **(Figure 5.5b-f)** in 1 M HCl solutions show additional peaks of N, O, and C which confirm the adsorption of inhibitors on metal surface. The presence of Cl peaks is presumably due to HCl. The spectral investigation of **Figure 5.5b−f** shows that the percentage content of Cu significantly suppressed relative to the pure mild copper specimen because of deposition of the PPZ compounds on the metal surface. Thus, EDS analysis further confirmed the formation of protective film on mild copper surface.

Table 5.2 Percentage atomic contents of copper metal plate without and with deposition of inhibitor obtained from EDS spectra.

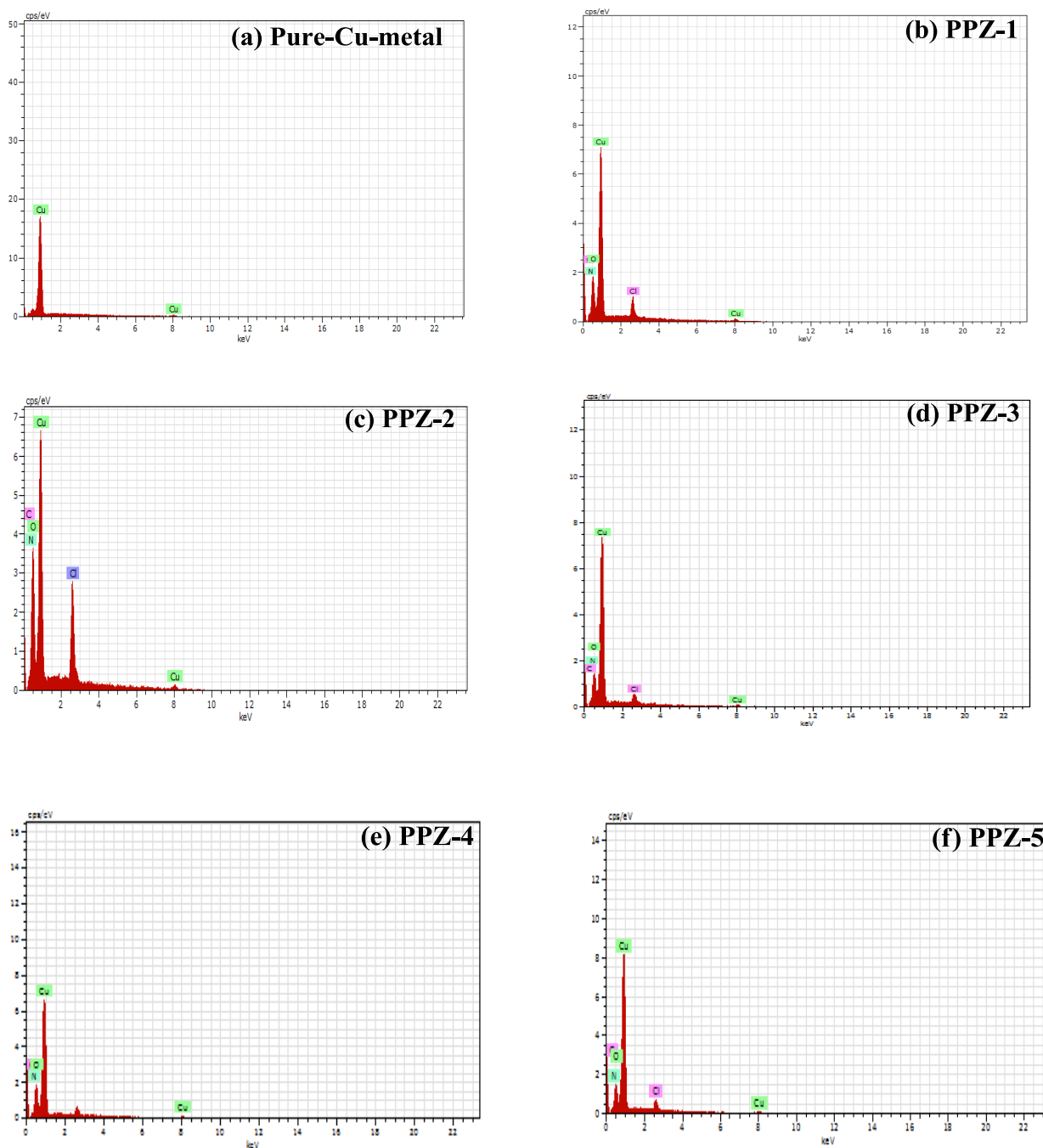| Sr. No.	Inhibitors	Cu	C	O	N	Cl
1	Pure-Cu-metal	100.00	-	-	-	-
2	PPZ-1	69.54	1.80	15.08	7.49	6.09
3	PPZ-2	50.90	1.69	24.07	9.70	13.64
4	PPZ-3	77.16	1.00	12.09	6.47	3.28
5	PPZ-4	76.77	1.16	15.38	6.69	-
6	PPZ-5	78.01	1.34	10.99	5.73	3.93

Figure 5.5 EDS of mild Copper surfaces: (a) Pure-Cu-metal, (b) PPZ-1, (c) PPZ-2, (d) PPZ-3, (e) PPZ-4, and (f) PPZ-5.

5.3.2.3 XRD Analysis: The presence of PPZ material on Cu surface was confirmed by SEM and EDS analysis. To authenticate our result, XRD analysis was also performed on Cu surface before and after deposition of PPZ material. XRD is one of the important techniques in finding out the deposition of

material on the metal surface as shown in **Figure 5.6**. XRD spectra of pure copper metal surface gives very fine high intensity peak at 2θ = 43, 50, and 74 for (111), (200), and (220) planes of Cu, respectively. The same 2θ values are present when organic PPZ materials were deposited on Cu metal surface but with decrease in intensity. This decrease is due to the deposition of the PPZ material on the mild copper surface which creates a barrier between the copper metal and the external solution environment. In the XRD spectra of Cu/PPZ-1, PPZ-3, and PPZ-5 samples, the presence of other peaks confirms the sample is more crystalline. XRD spectra of all the specimens before and after deposition of PPZ materials are shown in **Figure 5.6**.
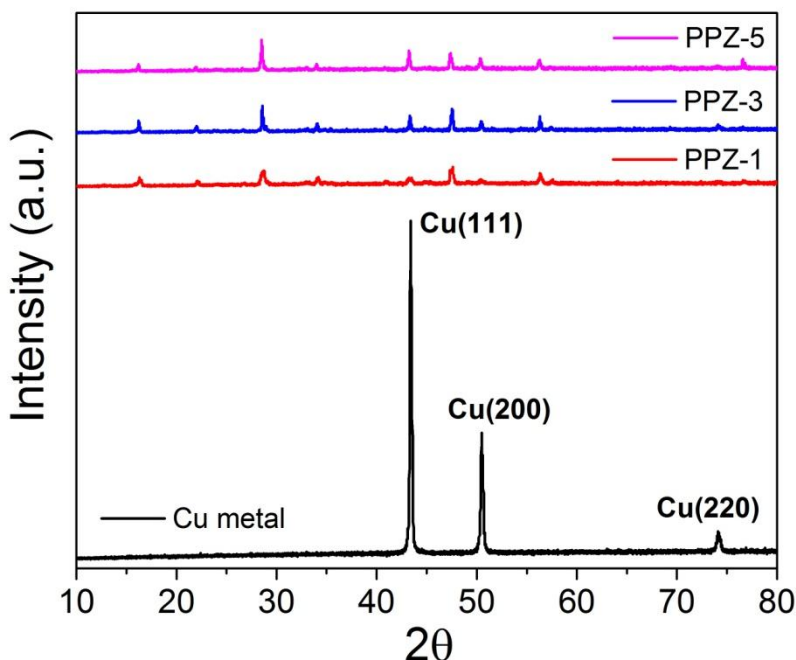

Figure 5.6 Shows the XRD spectra of Pure Cu metal and the metal with deposition of PPZ-1, PPZ-3 and PPZ-5.

5.3.3 Electrochemical measurements

5.3.3.1 Open circuit potential (OCP): The open circuit potential "sometime called corrosion potential or equilibrium potential" is the potential of the working electrode with respect to the reference electrode at which there is no current or potential is being applied to the cell. The measurements of the OCP based experiments are referred as potentiometric experiments. It is necessary to sustain the steadiness of the OCP before carrying out potentiodynamic polarization and EIS. The OCP of the working electrode vs. time not only plays the decisive role in explaining the corrosion domain but also plays a significant role in determining the threshold concentrations of inhibitors. The deviation of the OCP of the glassy carbon electrode with time in the absence and presence of 2.0 mg of PPZs samples in 1M HCl solution is shown

in **Figure 5.7**. A close observations of **Figure 5.7** show that there is no change in the features of the E-t curve with the adding of PPZs (2.0 mg) to 1M HCl solution.
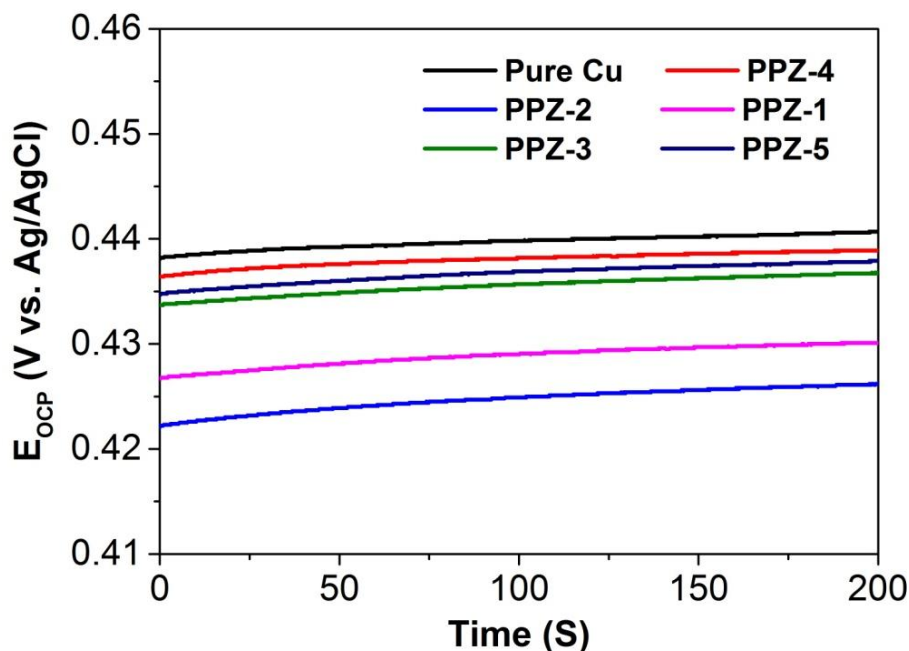

Figure 5.7 OCP vs time curves at 308 K for copper metal in 1M HCl solution in absence and presence of different concentrations of PPZs.

5.3.3.2 Impedance study: AC Technique: Electrochemical impedance was performed with sweeping frequency from 100 KHz to 1 mHz. More clear evidence is consider from Cole-Cole or Nyquist plot i.e. Z'' vs Z′ plots. In impedance spectroscopy |Z''| vs |Z′| plot gives information about the charge transfer from sample to electrolyte.

EIS plays important role in study of system response against the small change in amplitude of the ac signal. The examination of system response gives the useful information about the reaction taking place in corrosive medium, interface and its structure The impedance response not only change with the PPZs inhibitor but also increases with increases with increase in concentration of inhibitor molecule PPZs. **Figure 5.8a-f** shows the impedance plots (Nyquist plots) of the mild copper metal at 308 K in 1M HCl with nil **(Figure 5.8a)** and different concentrations of PPZs **(Figure 5.8b-f)**. The diameter of the semicircle of Nyquist plot increases with the increase in PPZ concentration **(Figure 5.8)** which confirms that corrosion is generally a progression of charge transfer.[31] Moreover, it was found that larger diameter semicircles **(Figure 5.8b-f)** were obtained in the presence of PPZ inhibitors than without PPZs **(Figure 5.8a)**. It should be noticed that depression and deviation in the large semicircles of the Nyquist plots, frequently referred to as the heterogeneity in the solid surface and current density,[32] is because of-
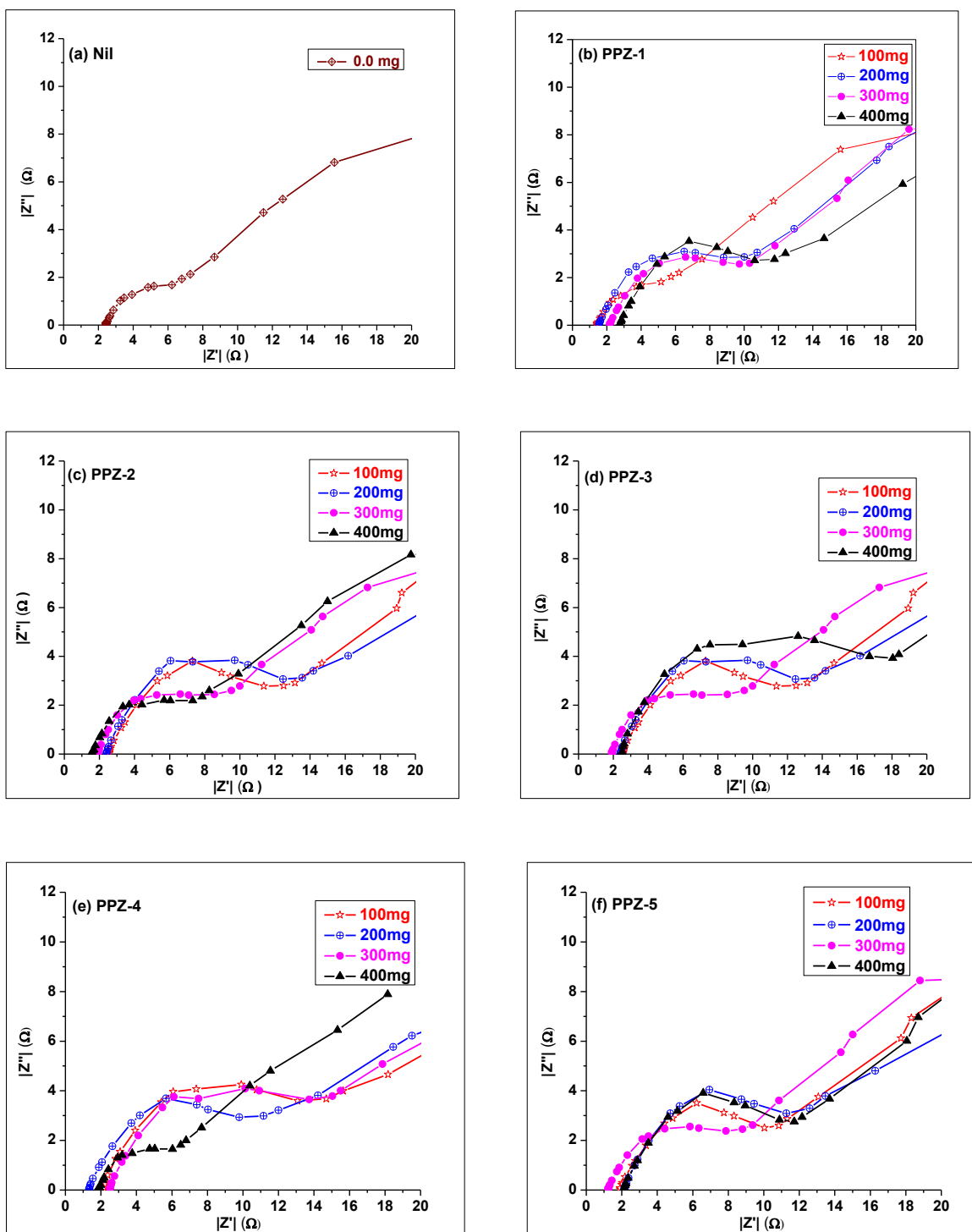
Figure 5.8 The Nyquist plots for mild Cu metal was carried out with frequency from 100 KHz to 1 mHz in 1 M HCl as: (a) without PPZ and (b-f) with various concentrations of PPZ inhibitors at 307 K.

-roughness in surface, presence of impurities, grain boundaries, dislocations, and adsorption of inhibitors.[33] The overall combined Nyquist or cole-cole plot of |z'| vs |z"| are shown in **Figure 5.9a**.

Figure 5.8b-f shows capacitive loop with single semicircle and inductive loop with extremely small semicircle in the higher and lower frequency range respectively. Generally, the charge transfer process or electrical double layer capacitor (C_{dl}) is associated with the high frequency (HF) capacitive loop while the adsorption-desorption and adsorption relaxation process (covered the reaction surface) of inhibitor molecules on the surface of electrode is associated with the inductive loop.[34-36]

This indicates that increases in the concentration of the inhibitor molecule increases the resistance of copper metal surface against corrosion in chloride solutions.[37] On the other hand, we can say that at lower frequency, the inductive behavior may be because of several reasons like: (i) The layer stabilization by products of corrosion reaction on the surface of electrode (ii) inhibitor molecules with their reactive products and (iii) dissolution of the metal surface.[38] In case of nonideal frequency response, distributed capacitance is used to analyze the electrochemical system (mild Copper/1 M HCl) and is confirmed by the deformation in the semicircle whose center falls below the real axis. The **Figure 5.9b** represents the equivalent circuit model obtained from the EIS data.

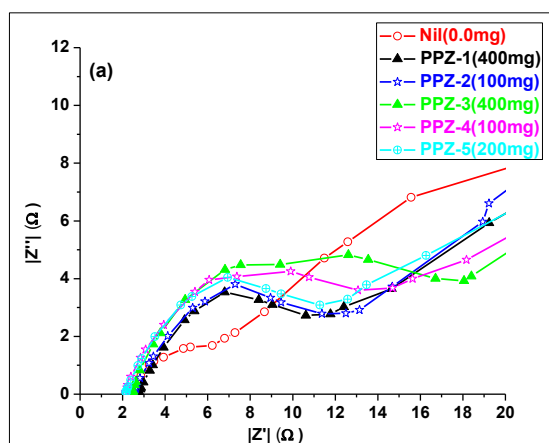**Figure 5.9 (a)** Nyquist plots of |z'| vs |z"| of best PPZs inhibitors having excellent inhibition efficiency (*η%*) at particular concentration for mild copper metal surface in 1 M HCl solution.

Where R1 = R_s
R2 = R_{ct}
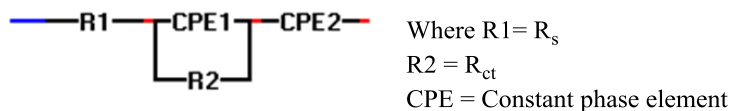CPE = Constant phase element

Figure 5.9 (b) Shows the equivalent circuit model of mild copper metal in 1M HCl solution with different concentrations of inhibitors to fit the EIS data.

The parameters of the equivalent circuit model as shown in **Figure 5.9b** can be defined by standard convention as; CPE represents the constant phase element, R_{ct} the charge transfer resistance, and R_S material resistance (Rs). CPE is generally behave as a double layer capacitor rather than pure capacitor and is substituted in the circuit to fit the semicircle more precisely. The relation of Z_{CPE}, of a CPE with admittance, Y_{CPE} and angular frequency, ω are expressed as[39]

$$Z_{CPE} = (1/Y_0)[(j\omega)_n]^{-1}$$

$$\omega = 2\pi f_{max}$$

$$j = -1^{1/2}$$

where Y_0 is the amplitude in $\mu F\ cm^{-2}$, f_{max} is the maximum frequency of AC, and n represents the phase shift, of the heterogeneity of the mild copper surface. **Figure 5.10a-f** represents the experimentally generated Z′ vs f Bode phase plots for all the tested PPZs material at various concentrations.
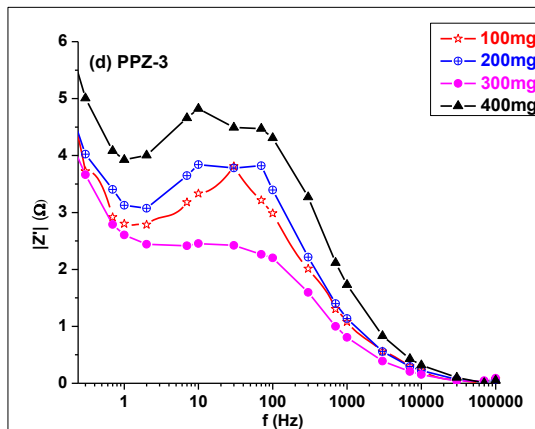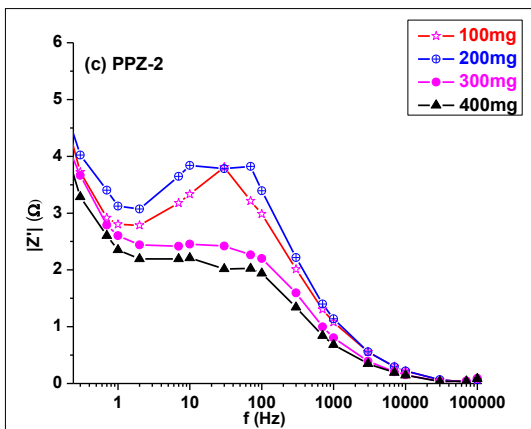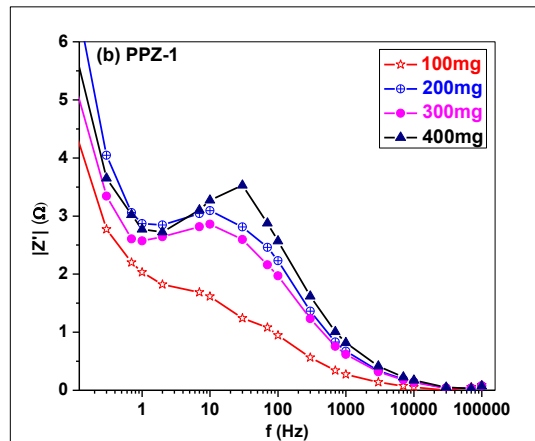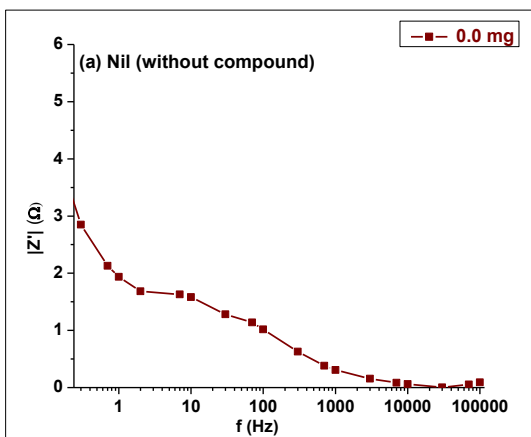
Figure 5.10 Shows the experimentally generated EIS plots of Z′ vs f : (a) without PPZ (b) with PPZ-1 (c) PPZ-2 (d) PPZ-3 (e) PPZ-4 and (f) PPZ-5.

The calculated results obtained after impedance measurements are shown in **Table 5.3**. From **Table 5.3** it is noted that the R_S value is smaller than R_{ct} value in all the ca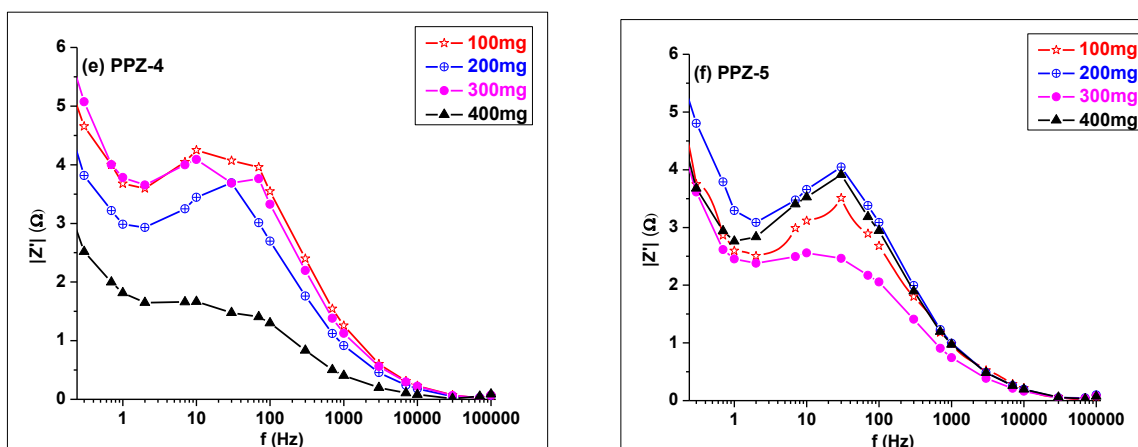ses i.e. in the absence and presence of inhibitors. The related inhibitor efficiency (η %) was calculated by putting the charge transfer resistance R_{ct} value and is evaluated using the following:

$$\eta\% = \left(1 - \frac{R_{ct}^0}{R_{ct}^i}\right) \times 100$$

Where R_{ct}^i and R_{ct}^0 represent the charge transfer resistance with and without PPZ inhibitor respectively. The increase in the concentration of PPZ inhibitor increases the R_{ct}^i value and reach utmost at optimal concentration of 400mg L^{-1} in case of PPZ-1, PPZ-3 and PPZ-4 inhibitors. Alternatively, in case of PPZ-2 and PPZ-5 the trend was not systematic and the careful observation of the **Table 5.3** reveals that the R_{ct} value approach maximum at 100 mg and 200 mg in PPZ-2 and PPZ-4 respectively.

The most prominent outcome and the maximum R_{ct} value obtained were **18.8212** and **19.9528** Ω for **PPZ-3** and **PPZ-4** at 400 and 100 mg L^{-1} respectively. The change in R_{ct} value is because of the continuous removal of water molecules from the surface of electrode by PPZ inhibitors and ultimately it leads to decreased attack of corrosive agent (HCl solution) on the metal surface.[40] However, the increase in R_{ct} value not only increases the inhibitor molecules adsorption on the surface of metal but also increases the thickness of insulated barrier layer.[41] Later on Helmholtz proved the same R_{ct} concept through the Helmholtz model.[42]

Table 5.3 Shows the Impedance parameters for the corrosion of mild copper metal and the inhibition efficiencies of PPZs inhibitors on the mild copper metal surface at different concentrations at 308K.

S.No.	Inhibitors	$C_{inh}(mg/L)$	R_S (Ω)	R_{ct}(Ω)	θ	η%
1	Blank	0.0	2.4556	10.3734	-	-
2	PPZ-1	100	1.4220	10.6114	0.02	2.24
		200	1.6079	13.0284	0.20	20.37
		300	2.2342	13.192	0.21	21.36
		400	2.7883	13.5904	0.23	23.67
3	PPZ-2	100	2.5735	14.6234	0.29	29.06
		200	2.4078	12.1092	0.14	14.33
		300	1.9274	13.2068	0.21	21.45
		400	1.5504	12.0874	0.14	14.18
4	PPZ-3	100	2.5735	14.6234	0.29	29.06
		200	2.4033	12.1092	0.14	14.33
		300	1.9274	13.2068	0.21	21.45
		400	2.5048	18.8212	0.44	44.88
5	PPZ-4	100	2.1428	19.9528	0.48	48.01
		200	1.3538	11.3362	0.08	8.49
		300	2.5098	12.22	0.15	15.11
		400	1.9052	12.0676	0.14	14.04
6	PPZ-5	100	1.9297	12.4462	0.16	16.65
		200	2.1444	13.8796	0.25	25.26
		300	1.2363	11.6836	0.11	11.21
		400	2.1760	13.1696	0.21	21.23

5.3.4 Conductivity and sheet resistivity measurements by four probe method: Four-point probe **(Figure 5.11)** characterization is a standard method for studying the electrical properties of solids and thin films.[43] To obtain the expected surface sensitivity and spatial resolution, the probe spacing in four-point probe technique has to be reduced to microscale. Therefore, microscopic four-point probes (M4PPs) need to be combined with some microscopy techniques. In the past few years, two types of M4PPs systems have been developed which are monolithic micro-four-point probe and four-point scanning tunneling microscopy probe approaches.[43] The four point probe consists of four equally spaced tungsten metal tips with finite radius and to minimize the sample damage during probing, each tip is supported by the spring on the end so that the probe tips which one is the part of auto-mechanical stage can travel up and down during measurements. A high impedance current source is used to supply current through the outer probes and a voltmeter measures the voltage across the inner two probes to determine the sample resistivity. The inner probe draws no current because of the high impedance voltmeter in the circuit. Therefore, the

unwanted voltage drop (IR drop) at point B and point C occur because of contact resistance between probes and the sample is eliminated from the potential measurements.

The electric field is generated by the current carried through the outer probes in the sample. In **Figure 5.12**, the electric field lines are drawn solid and the equipotential lines are drawn broken. The inner two probes measure the potential difference between point B and C. Probe life and sample surface damage are the other two main challenges for microscopic four-point probe technique. To deal with such problems, we can use flexible cantilevers as the probe and keep a certain angle between the probe and the sample surface.
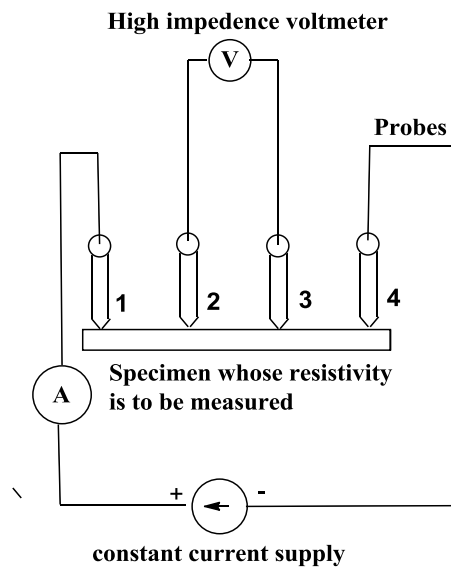

Figure 5.11 Four probe method of measurement of resistivity.
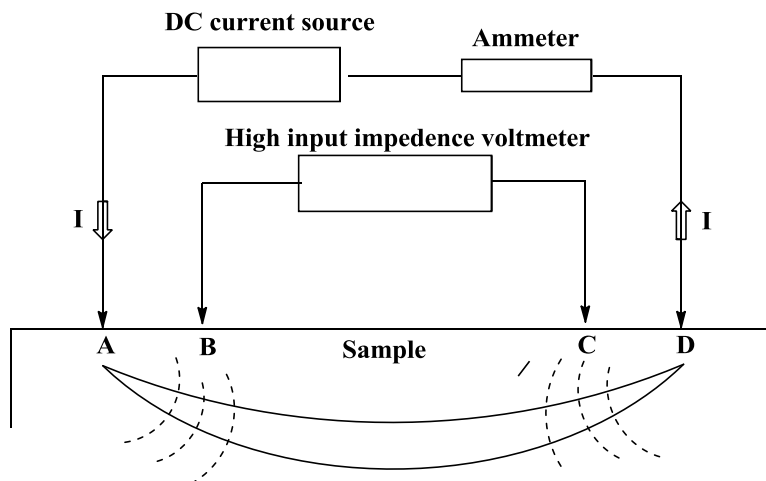

Figure 5.12 Shows the electric field and equipotential lines.

All the mild copper samples having specification of $60 \times 60 \times 0.2$ mm (length $\times$ breadth $\times$ thickness) were kept on the quad map testing machine for conductivity and resistivity. By using four probe method 9 points were traced **(Figure 5.13)** from the sample of wafer lot 1, wafer shape square type, wafer size 60 mm with edge exclusion 10 mm. All the samples were tested in CEERI (Central Electronics Research Institute, Pilani, India) and the results obtained of the tested samples are given below in **Table 5.4**. From **Table 5.3**, the result analysis shows that all the synthesized PPZs material increases the resistivity and resistance of the mild copper plate after deposition. Out of five PPZs, PPZ-2, PPZ-4, and PPZ-5 show the highest resistivity and resistance value and the contour plot obtained during testing is shown in **Figure 5.13**. The increase in resistance after deposition of PPZs material on the mild copper metal surface provides the supporting information for corrosion inhibitor.

Table 5.4 Showing the electrical property of the mild copper sheet with and without deposition of PPZs.

| No.	Inhibitor	Concent-ration of PPZ (mg/L)	Thickness ($\Box M$)	Resistance Rs(Ohm/sq)	Resistivity Res(Ohm cm)	Voltage (mVOhm/sq)	Current (I) (mA)	V/I
1	Pure-Cu-metal	0.0	1900	0.000126	0.000021	0.126	1000	0.000028
2	Pure-Cu-metal in 1M HCl	0.0	1900	2.49877E+11	4.10997E+10	249.877	1E-09	5.51362E+10
3	Pure-Cu-metal in methanol	0.0	1900	0.000095	0.000016	0.095	1000	0.0000021
4	PPZ-1	1250	1900	868898.1875	142915.9375	86.88981875	0.0001	191725.09375
5	PPZ-2	1250	1900	5.14464E+10	8.46188E+9	51.4464	1E-09	1.13518E+10
6	PPZ-3	1250	1900	128066.484375	21064.308594	128.0664716	0.00099999999	28258.269531
7	PPZ-4	1250	1900	5.29076E+11	8.70222E+10	529.076	1E-09	1.16742E+11
8	PPZ-5	1250	1900	9.67097E+10	1.59068E+10	96.7097	1E-09	2.13393E+10
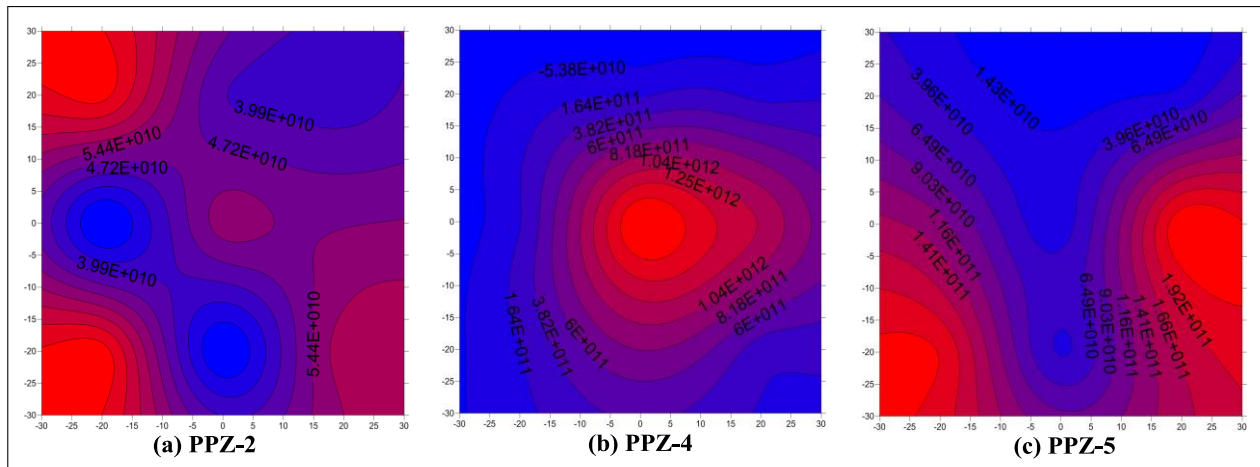
Figure 5.13 Shows the resistivity at various points on the mild copper metal plate: (a) PPZ-2, (b) PPZ-4 and (c) PPZ-5.

5.3.5 Mechanical property measurements: Tensile testing is one of the most widely used methods for measuring mechanical properties of materials and it has been used to measure Young's modulus, ultimate tensile strength, and other mechanical properties of mild copper metal strips. Measurement of the mechanical properties is a challenging task because the properties depend on the specimen preparation, specimen shape, and testing conditions (e.g., temperature and strain rate). Some standards, including the American Society for Testing and Materials (ASTM) standards, were established for tensile testing of different engineering materials. However, there are no existing standards for tensile testing of mild copper metal strips after deposition of PPZs inhibitor. Thus, it is difficult to compare tensile testing results when the specimen with deposition of different PPZs. The most common specimen shapes that have been used for tensile testing are rectangular (strip) and dumbbell shapes. But here we compare the mechanical properties of strip shape specimens without and after deposition of the PPZs material. The strip specimens have three control parameters: gauge length (GL), width (W), and thickness (T). Here R (radius of fillet) and D (Distance between the grip area which is equal to Gauge length (in strip space specimens), are not the interested one as interested in dumbbell shape specimen. All the characteristic property of the prepared mild copper strips are shown in **Table 5.5**. The present paper focuses on the deposition of PPZs inhibitors on the mild copper strips **(Figure 5.14)** and comparison of their mechanical property. All the tensile testing has been done by DYNAMIC UNIVERSAL TEST MACHINE of 100 KN (Kilo Newton) capacity having ITW hydraulic top and lower wedge grip pressure 210 bar, of model number AC0511T3 at 33°C. All the specimens were tested and stretched with the rate of 0.5 mm/min. All the analysed results are summarized in **Table 5.6** and the images obtained during mechanical testing of the samples are shown in **Figure 5.15**.
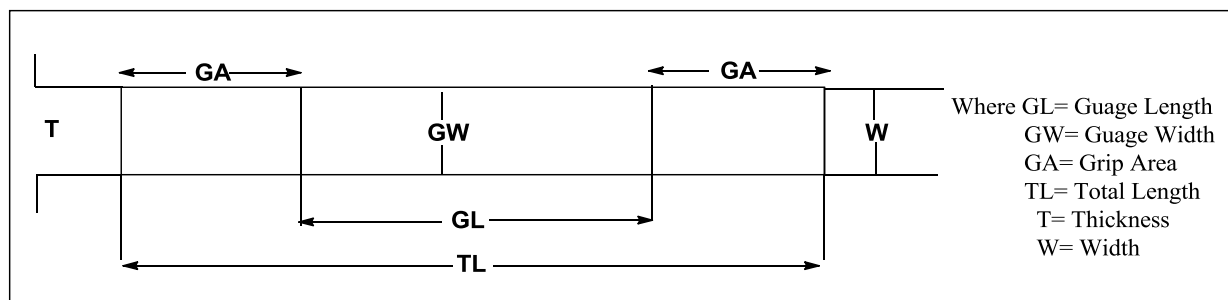
228

Figure 5.14 Strip shape tensile test specimen.

Table 5.5. Finite element analysis tensile testing specimen information.

S.No.	Inhibitor	Shape	Thickness (mm)	GL (mm)	GW (mm)	W (mm)	GA (mm)	R (mm)	D (mm)	TL (mm)
1	Pure Cu metal	Strip	1.80	20	10.5	10.5	21.8	NA	20	63.6
2	PPZ-1	Strip	1.81	20	9.37	9.37	21.8	NA	20	63.6
3	PPZ-2	Strip	1.83	20	9.82	9.82	21.8	NA	20	63.6
4	PPZ-3	Strip	1.82	20	9.89	9.89	21.8	NA	20	63.6
5	PPZ-4	Strip	1.81	20	9.79	9.79	21.8	NA	20	63.6
6	PPZ-5	Strip	1.86	20	9.93	9.93	21.8	NA	20	63.6

Table 5.6 Mechanical property of the tensile testing specimens.

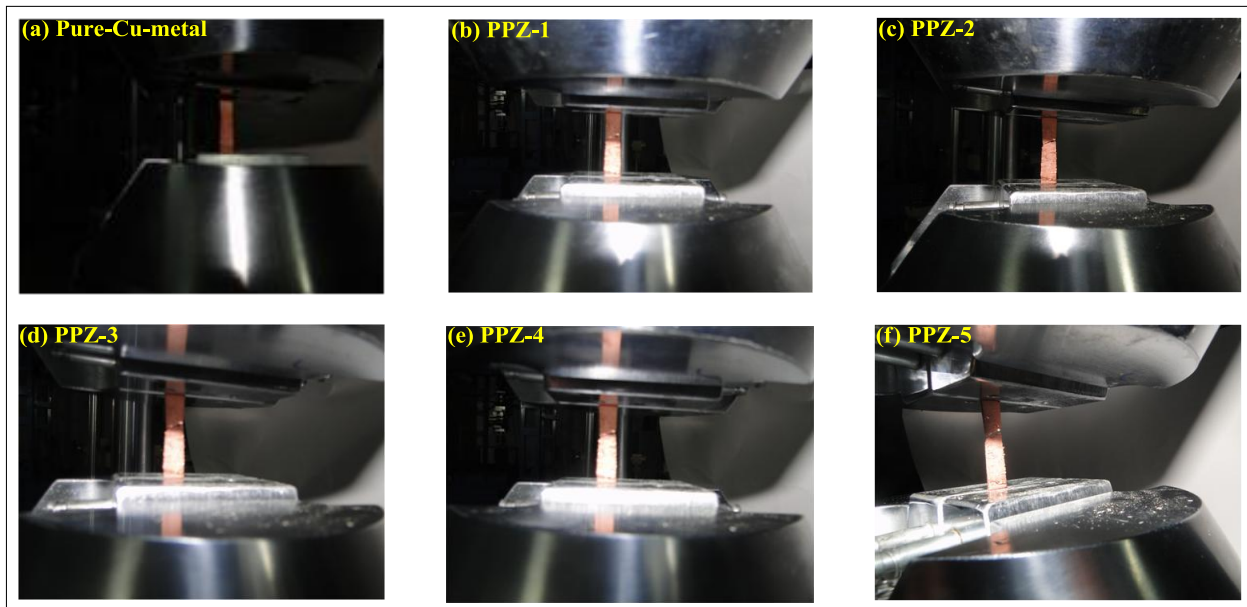| S.No.	Inhibitor	Shape	Peak Stress (MPa)	Yield Strain (%)	Young modulus (GPa)	Yield load (kN)	Peak load (kN)
1	Pure Cu metal	Strip	209.532	0.59	20.198	1.718	4.058
2	PPZ-1	Strip	207.091	0.618	21.047	1.588	3.512
3	PPZ-2	Strip	191.433	0.633	17.695	1.435	3.44
4	PPZ-3	Strip	189.995	0.724	12.622	1.379	3.42
5	PPZ-4	Strip	189.45	0.574	18.845	1.401	3.357
6	PPZ-5	Strip	203.197	0.606	24.745	1.87	3.753

Figure 5.15 Shows the images of test samples: (a) Pure-Cu-metal, (b) PPZ-1, (c) PPZ-2, (c) PPZ-3, (d) PPZ-4 and PPZ-5.

From **Table 5.6**, we can observe that the strain on the metal increases after deposition of PPZs material on the mild copper strips. The strain is almost comparable in PPZ-1, PPZ-2, and PPZ-5. PPZ-3 shows the highest strain while PPZ-4 shows the lowest strain value. The comparison of the strain (%) vs stress (MPa), true strain (mm) vs true stress (MPa), load (kN) vs displacement (mm) and specimen entry vs-

Figure 5.16 Shows the strain (%) vs Stress (MPa) graph of: (a) Pure Cu-metal, (b) PPZ-1, (c) PPZ-2, (d) PPZ-3, (e) PPZ-4 and (f) PPZ-5.
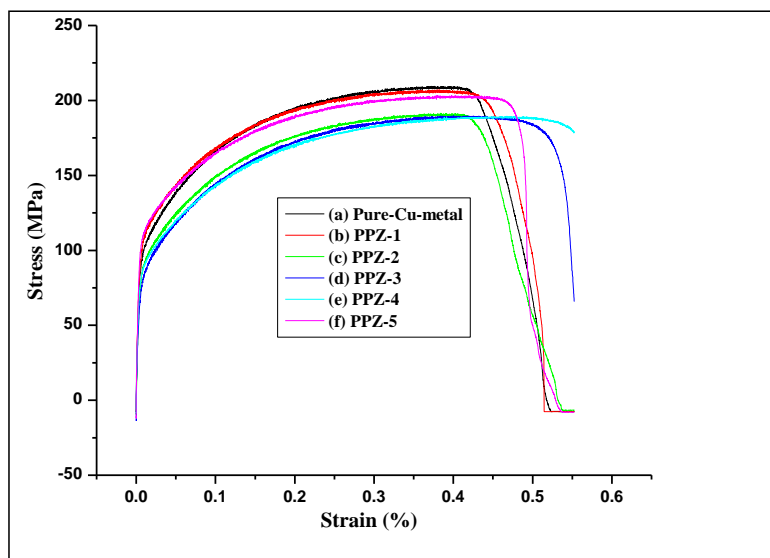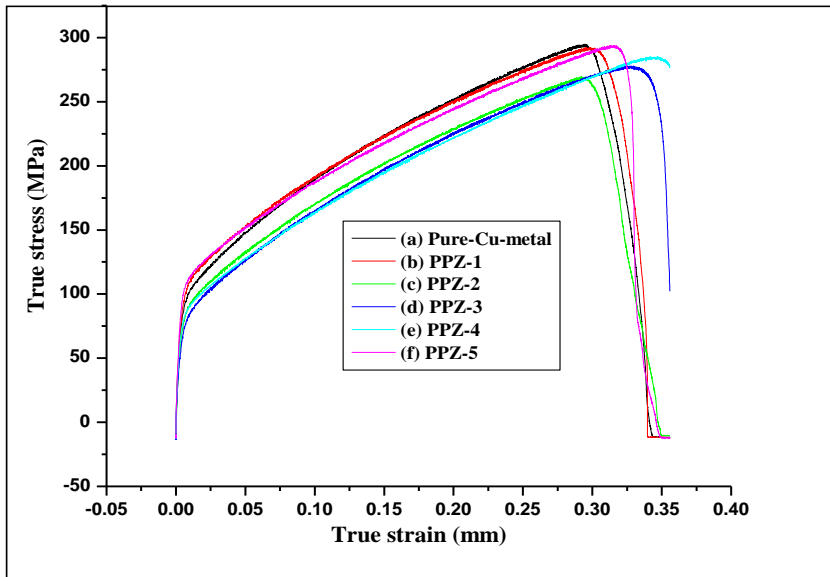
Figure 5.17 Shows the true strain (mm) vs true stress (MPa) graph of: (a) Pure-Cu-metal, (b) PPZ-1, (c) PPZ-2, (d) PPZ-3, (e) PPZ-4 and (f) PPZ-5.
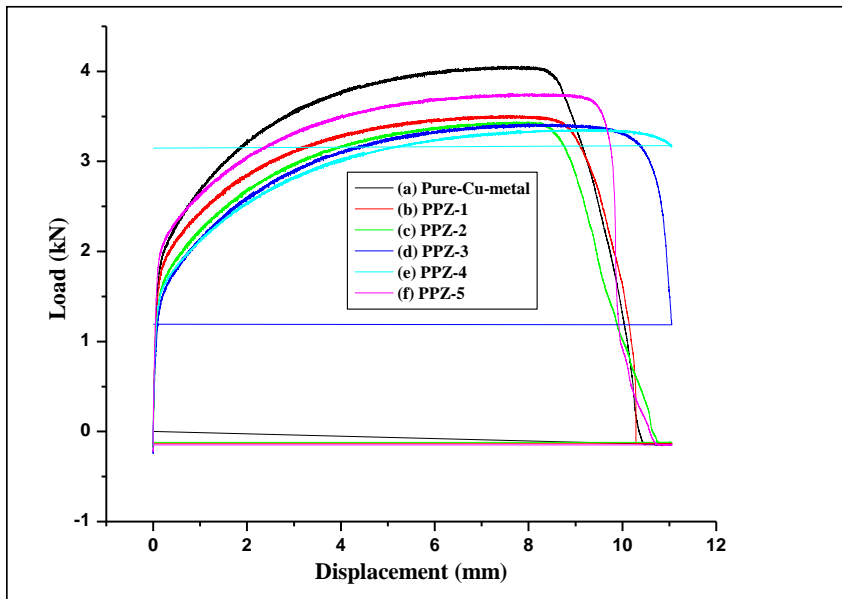

Figure 5.18 Shows the load (kN) vs displacement (mm) graph of: (a) Pure- Cu-metal, (b) PPZ-1, (c) PPZ-2, (d) PPZ-3, (e) PPZ-4 and (f) PPZ-5.
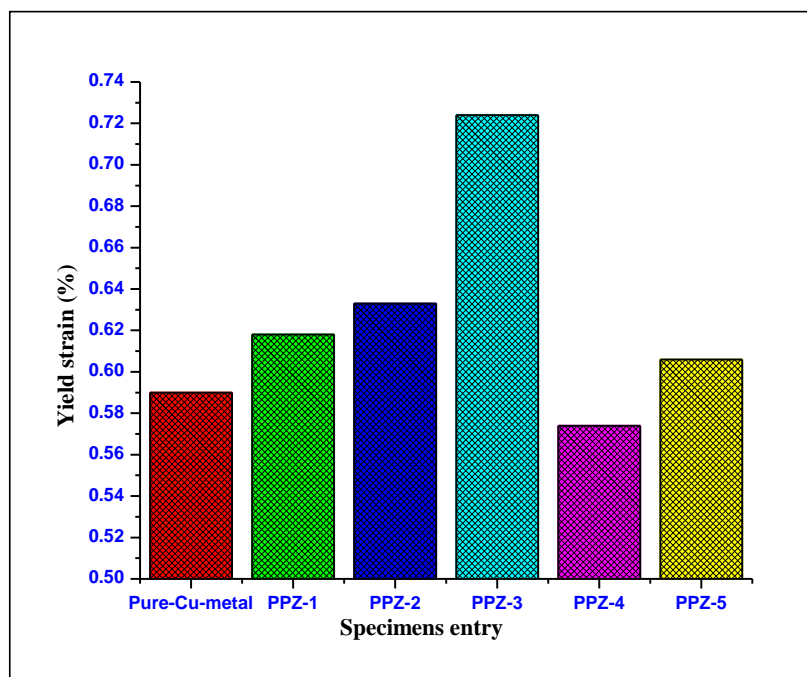
Figure 5.19 shows the specimen entry vs yield strain graph of: (a) Pure- Cu-metal, (b) PPZ-1, (c) PPZ-2, (d) PPZ-3, (e) PPZ-4 and (f) PPZ-5.

-yield strains are shown in **Figure 5.16, 5.17, 5.18,** and **5.19** respectively. After analysis of the results we can say that PPZs type organic material would not only be the promising material as corrosion inhibitor but also helpful in improving the strength of the mild copper.

5.3.6 Adsorption and Inhibition Mechanism

Corrosion is the process of returning of a metal to its natural state, i.e., the ores from which it was originally obtained. Metals corrode because they move to a thermodynamically stable state and the process also involves oxidation of the metal. The adsorption mechanism depends upon the structure of inhibitor molecule and the charge on the metal surface. The electric field generated in-between the metal/electrolyte interface is the main cause of the generation of charge on the metal surface.

In a solution of HCl, copper metal plate is positively charged and there occurs adsorption of PPZs inhibitor at the metal/acid solution interface. The adsorption on metal/acid solution interface occurs via three processes as discussed below: **(a) Chemisorption**: It occurs between the empty d-orbital of copper metal surface and lone pair of electrons present on the heteroatom of PPZ inhibitor. **(b) Physisorption**: It is the electrostatic interaction between the Cl^- ion of HCl solution and the protonated PPZ inhibitor on metal/acid solution boundary. **(c) Retrodonation**: It is reverse of chemisorption where the filled d-orbitals of copper metal surface interact with the empty orbitals present on the PPZ inhibitor molecules.

Usually, these inhibitor molecules retard the corrosion process via forming metal-inhibitor complex in-between the metal/acid solution interface and show remarkable corrosion inhibition efficiency up-to optimal concentrations by covering metal surface with inhibitor molecules.

Notably, the chemistry behind the adsorption of PPZ corrosion inhibitor is very interesting and can be roughly explained as follows. At first, the neutral PPZ molecules become protonated in aqueous HCl solution. Thereafter, these protonated PPZ molecules interact with the copper metal surface for electron. Initially, the protonated PPZs inhibitor molecules compete with H^+ ions for electron present on the metal surface but after liberating hydrogen gas, the PPZ inhibitor molecule return to its neutral state. In this neutral state, the lone pairs of electron present on the heteroatom (N, O, S) of PPZ inhibitors interact with the empty d-orbital of the copper metal surface and favor chemisorption. Finally, the accumulated electrons on copper metal surface make it more negative and this negative charge is relieved by reterodonation i.e. the electrons are transferred from the filled d-orbital of metal surface to empty antibonding π^* orbital of PPZ inhibitor molecules. Experimental as well as theoretical data obtained expose that $\eta\%$ (inhibition efficiency) for the five PPZs inhibitor molecules are in the order of PPZ-2 > PPZ-1 > PPZ-4≈PPZ-5> PPZ-3 in terms of the HOMO-LUMO energy gap. In other words, ΔE and $\eta\%$ follow the order: PPZ-5 > PPZ-4 > PPZ-1 > PPZ-3 > PPZ-2 in terms of dipole moment. The presence of extra heteroatom present in the pyrazole ring and the existence of two methoxy groups at 3rd and 4th position in phenyl moiety of PPZ-2 and PPZ-5 respectively make the inhibitor molecules excellent for corrosion inhibition of copper metal. PPZ-3 behaves as a weak corrosion inhibitor for copper metal surface because of absence of ring-activating group.

5.4 Conclusions

(i) To the best of our knowledge, this is the first time report that five selected PPZs acts as very good corrosion inhibitors for mild copper metal in 1M HCl solution, and that the extent of inhibition efficiency was dependent on the concentration of the inhibitors.

(ii) Polarization curves proved that PPZs behaves as mixed type inhibitors. The impressive performance of the inhibitors has been confirmed from Nyquist plots. EIS plots indicated that the increase in R_{ct} (charge transfer resistance) value and decrease in C_{dl} (double layer capacitance) value with increase in concentration of PPZs is because of adsorption of PPZ inhibitor molecules on the surface of metal.

(iii) SEM, EDS, and XRD spectra results supported the formation of a film on the mild copper surface.

(iv) Quantum chemical calculations corroborate the inhibition efficiencies obtained from experimental results.

(v) Among the five inhibitors, the performance of PPZ-2 and PPZ-5 is superior to that of other PPZs due to its high electron density, which favors its adsorption on the metal surface.

(vi) The sheet resistivity study of the PPZ material on copper metal gives the fabulous result and the analysis of the data shows that the PPZ material deposition on copper metal surface increases the resistivity of the copper metal plates and make it less conductive which again supports the corrosion study. PPZ-2, PPZ-4, and PPZ-5 show the highest value of resistance and resistivity as compared to other PPZs.

(vii) The deposition of PPZ material on mild copper strips increases the tensile strain of the copper strips which could be future promising material not only as corrosion inhibitor but also in improving the strength of copper metal of various vehicle tools and equipments. Among all the PPZs discussed in the paper, PPZ-3 deposition shows the higher strain as compared to others.

5.5 References

[1] Musa, A. Y.; Jalgham, R. T. T.; Mohamad, A. B. *Corros. Sci.* **2012,** *56*, 176.

[2] Ozkir, D.; Kayakirilmaz, K.; Bayol, E.; Gurten, A. A.; Kandemirli, F. *Corros. Sci.* **2012,** *56*, 143.

[3] Kumar, S. L. A.; Gopiraman, M.; Kumar, S. M.; Sreekanth, A. *Ind. Eng. Chem. Res.* **2011,** *50*, 7824.

[4] Tao, Z.; Zhang, S.; Li, W.; Hou, B. *Ind. Eng. Chem. Res.* **2010,** *49*, 2593.

[5] Hmamou, D. B.; Salghi, R.; Zarrouk, A.; Hammouti, B.; Deyab, A. S. S.; Bazzi, L.; Zarrok, H.; Chakir, A.; Bammou, L. *Int. J. Electrochem. Sci.* **2012,** *7*, 2361.

[6] Sangeetha, M.; Rajendran, S.; Muthumegala, T. S.; Krishnaveni, A. *Z. Materijala.* **2011***, 52*, 3.

[7] Saji, V. S. *Recent Patents Corr. Sci.* **2010,** *2*, 6.

[8] Srivalli T.; Satish K.; Suthakaran R. *Int. J. Innov. Pharma. Res.* **2011,** *2*, 172.

[9] Vasuki, G.; Kumaravel, K. *Tetrahedron Lett.* **2008,** *49*, 5636.

[10] Benabdellah, M.; Touzani, R.; Aouniti, A.; Dafali, A.; Kadiri, E. S.; Hammouti, B.; Benkaddour, M. *Mater. Chem. Phys.* **2007,** *105*, 373.

[11] Fiala, A.; Chibani, A.; Darchen, A.; Boulkamh, A.; Djebbar, K. *Appl. Surf. Sci.* **2007,** *253*, 9347.

[12] Shafei, E. A. A.; Maksoud, A. E. S. A.; Fouda, A. S. *Corros. Sci.* **2004,** *46*, 579.

[13] Abdallah, M. *Corros. Sci.* **2002,** *44*, 717.

[14] Machnikova, E.; Whitmire, K. H.; Hackerman, N. *Electrochim. Acta.* **2008,** *53*, 6024.

[15] Shukla, S. K.; Quraishi, M. A. *Corros. Sci.* **2009,** *51*, 1007.

[16] Shukla, S. K.; Singh, A. K.; Ahamad, I.; Quraishi, M. A. *Mater. Lett.* **2009,** *63*, 819.

[17] Singh, A.K.; Quraishi, M. A. *Corros. Sci.* **2010,** *52*, 152.

[18] Ahamad, I.; Quraishi, M. A. *Corros. Sci.* **2010,** *52*, 651.

[19] Quraishi, M. A.; Sardar, R.; Mater. R. *Mater. Chem. Phys.* **2002,** *78*, 425.

[20] Obot, I. B.; Egbedi, O. N. O.; Eseola, A. O. *Ind. Eng. Chem. Res.* **2011,** *50*, 2098**.**

[21] Ahamad, I.; Prasad, R.; Quraishi, M. A. *Corros. Sci.* **2010,** *52*, 1472.

[22] Singh, A. K.; Quraishi, M. A. *Mater. Chem. Phys.* **2010,** *123*, 666.

[23] Yadav, D. K.; Maiti, B.; Quraishi, M. A. *Corros. Sci.* **2010,** *52*, 3586.

[24] Meligi, E. A. A. *Recent Patents Corr. Sci.* **2010,** *2*, 22.

[25] Halambek, J.; Berkovic, K.; Vorkapic, F. J. *Corros. Sci.* **2010,** *52*, 3978.

[26] Umoren, S. A.; Obot, I. B.; Ebenso, E. E.; Okafor, P. C.; Ogbode, O.; Oguzie, E. E. *Anti-Corros. Methods Mater.* **2006,** *53*, 277.

[27] Umoren, S. A.; Obot, I. B.; Ebenso, E. E.; Okafor, P. C. *Portugaliae Electrochem. Acta.* **2008,** *26*, 267.

[28] Sharma, A.; Shukla, P.; Pallavi, B.; Chowdhury, R.; Dash, S. *Curr. Microwave Chem.* **2015,** *2*, 1.

[29] Guadalupe, H. J.; Ochoa, G. E.; Rivas, M. P. J.; Cruz, J.; Pandiyan, T. A. *J. Electroanal. Chem.* **2011,** *655*, 164.

[30] Li, X.; Deng, S.; Fu, H. *Prog. Org. Coat.* **2010,** *67*, 420.

[31] Tan, K. W.; Kassim, M. J. *Corros. Sci.* **2011,** *53*, 569.

[32] Bouklah, M.; Hammouti, B.; Lagrenee, M.; Bentiss, F. *Corros. Sci.* **2006**, *48*, 2831.

[33] Okafor, P. C.; Liu, C. B.; Zhu, Y. J.; Zheng, Y. G. *Ind. Eng. Chem. Res.* **2011,** *50*, 7273.

[34] Tao, Z.; Zhang, S.; Li, W.; Hou, B. *Corros. Sci.* **2009**, *51*, 2588.

[35] Popova, A.; Sokolova, E.; Raicheva, S.; Christov, M. *Corros. Sci.* **2003**, *45*, 33.

[36] Sorkhabi, A. H.; Jeddi, G. N.; Hashemzadeh, F.; Jahani, H. *Electrochim. Acta.* **2006**, *51*, 3848.

[37] Sayed, E. S. M. *Int. J. Electrochem. Sci.* **2012**, *7*, 2832.

[38] Khaled, K. F. *Electrochim. Acta.* **2010,** *55*, 5375.

[39] Jeyaprabha, C.; Sathiyanarayanan, S.; Venkatachari, G.; *Appl. Surf. Sci.* **2006**, *253*, 432.

[40] Yadav, D. K.; Quraishi, M. A.; Maiti, B. *Corros. Sci.* **2012**, *55*, 254.

[41] Khaled, K. F.; Qahtani, A. M. M. *Mater. Chem. Phys.* **2009**, *113*, 150.

[42] Ahamad, I.; Prasad, R.; Quraishi, M. A. *J. Solid State Electrochem.* **2010**, *14,* 2095.

[43] Li, J.; Wang, Y.; Ba, D. C. *Phys. Procedia.* **2012,** *32*, 347.

Chapter VI

Conclusions and Future Scope

Summary

6.1 General conclusions

The current thesis entitled "**Nickel Catalyzed Coupling Reactions and Studies on Pyranopyrazole Heterocyclic Molecules.**" deals with the synthesis of transition metal catalysed Heck type coupling of alkyl halides with alkene, synthesis of pyranopyrazole and their various biological, computational study, and corrosion inhibition of copper metal application.

Moreover, modern upsurge in synthetic field, transition metal catalyzed C−H bond activation and functionalization has turned out as a most powerful tool for the construction of C−C bond without the necessity of pre-activation of substrates. These transition metal catalysts offer the C−C bond formations with high efficiencies, high functional group tolerance and excellent regioselectivities.

In recent years, the major concern in medicinal chemistry is to access the potent organic molecule structures in a reduced number of synthetic steps from the simple and readily available starting materials. In this perspective, a method has been developed for non-spiro/spiro pyranopyrazole scaffolds via multi-bond forming protocols such as multi-component reactions and one-pot sequential reactions for the development of multistep synthesis in a single step.

In the present work, all the non-spiro pyranopyrazole scaffolds were synthesized via three component and four component reaction approach in ethanol medium by conventional, microwave assisted (MWA), and grinding methodology. A four-component reaction developed between components in ethanol at room temperature is a superior protocol for building a combinatorial library of pyranopyrazole scaffold in terms of increase in the dimensionality of the MCR, effectiveness, and eco-friendliness. The thesis also gives the idea about the synthesis of spiro pyranopyrazole in ethanol medium at room temperature and heating method. Ethanol as reaction medium is found to significantly influence the path of the reaction for non-spiro/spiro pyranopyrazole scaffolds by facilitating formation and stabilization of charged/polarized intermediates, besides serving as green reaction medium.

The non-spiro pyranopyrazole molecules show various applications like anticancer, antimicrobial, antifungal, anti-oxidative stress, CDK-2 inhibitors, and corrosion inhibition of copper metal. The spiro-pyranopyrazole shows anticancer and CT-DNA binding activity.

6.2 Specific conclusions

The thesis entitled "**Nickel Catalyzed Coupling Reactions and Studies on Pyranopyrazole Heterocyclic Molecules**" is divided in five chapters. A brief overview of these chapters is discussed below.

The first chapter of thesis describes a concise literature overview of transition metal catalysed C-C bond formation via reductive coupling of various alkyl halides with acrylates and oxabenzonorbornadiene. The

chapter also shows the detailed literature overview of pyranopyrazole synthesis by two component, three component and four component reaction by various synthesis methodologies. The detailed study of the drug designing and molecular docking has been discussed here step wise to counter the menace of cancer by inhibiting the CDK-2 kinase protein by Autodock tool 1.5.6. The designed and synthesized corrosion inhibitors of copper metal by the various researchers, till now has been discussed in detail.

The second chapter of the thesis commences with significance of nickel (II or 0) catalysed reactions for the synthesis of miscellaneous reductive coupled molecules. Thus, here we demonstrated the synthesis of saturated esters by reductive coupling of sp^3 alkyl halide with alkenes in presence of nickel (II or 0) catalyst. The $1^°$, $2^°$, and $3^°$ alkyl halides and variously substituted acrylates has been accommodated by this strategy. The flexibility of this methodology was effectively extended to include oxabenzonorbornadiene type alkenes and too coupled with the sp^3 alkyl halides to give the corresponding alkylated bicyclic ring-opening products.

The third chapter of the thesis begins with brief history of pyranopyrazole molecules and their various biological and pharmacological activities along with some classical examples. This chapter is primarily divided into three parts and each one is discussed below:

Part A: In this part a series of non-spiro pyranopyrazole scaffolds were synthesized by traditional and unreported rapid- four component microwave approach. Later on the molecules were tested *in-vitro* for anticancer activity against the hep3b cell line. A close SAR analysis reveals that heteroatom substituents at a 3-position of the pharmacophore is responsible for the activity of the synthesized scaffolds. Crystallographic analysis of 6-amino-1,4-dihydro-3-methyl-4-phenylpyrano[2,3-*c*]pyrazole-5-carbonitrile was done by X-ray diffraction method and energy associated with structural motif was calculated by using PIXEL software.

Part B: Eco-friendly MCR methodology is used to synthesize non-spiro and spiro pyranopyrazole molecules. The anticancer activities of all the compounds were tested against hep3b cancer cell line. It was found that most of the synthesized compound, especially the non-spiro scaffolds inhibit the growth of cancer cells in dosage dependent manner. Later on the best five molecules from each series were selected and their CT-DNA binding study was done by UV-visible spectroscopy which showed that the non-spiro molecules do interact with DNA. Finally, the best non-spiro molecule with best IC_{50} value was selected and docked against CDK-2 protein. The docking result of non-spiro molecule showed significant binding interaction with the amino acid residues which may be contributing to their cytotoxic activity.

Part C: In this chapter a novel solvent free four-component synthesis of pyranopyrazole heterocycles by grinding methodology is discussed. The reaction completed in very short reaction time with good yield at room temperature. The *in-vitro* antibacterial and antifungal activity against three different strains were

checked for all the synthesized compounds. A closer SAR analysis gives the idea that the tested compounds are more active against antifungal strains. Later on, the seven best anticancer compounds from Part A and B of Chapter-3 were selected and evaluated further for their *in-vitro* and *in-vivo* oxidative stress activities assay. The significant *in-vitro* as well as *in-vivo* antioxidant properties were possessed by **AK-50** and **AK-62** non-spiro pyranopyrazoles.

The fourth chapter describes about the designing, molecular docking, molecular dynamics, and pharmacokinetic study of pyranopyrazole and coumarin derivatives. The chapter is divided into two parts.

Part A: All the 69 designed pyranopyrazole molecules "CDK-2 inhibitors" were docked by using molecular modeling software Autodock 4.2. AK-26, AK-72K, and AK-60E showed the noteworthy binding free energy and predicted inhibitory constant values as compared to standard drug olomoucine. OSIRIS property explorer and molinspiration cheminformatics online tools were used to find out Lipinski rule of five parameters and toxicity parameters of all the designed ligands. GROMACS V4.6.1 computational package was used to carry out the Molecular dynamics (MD) study and was used to authenticate the docking procedure.

Part B: The novel 62 coumarin pharmacophores were designed as CDK-2 inhibitors and docking study of all the molecules was performed using molecular modeling software Autodock 4.2. Thereafter, the best four molecules from four different series (one from each series) having best docking score were docked again by using GLIDE on Schrodinger. THC-15, THC-28, THC-43, and THC-59 pharmacophore showed the noteworthy binding free energy and predicted inhibitory constant values as compared to standard drug Deschloroflavopiridol (-8.87) and Olomoucine (-6.08). Lipinski rule of five parameter and toxicity parameters of the designed analogs were predicted by OSIRIS property explorer and molinspiration cheminformatics online tools. The molecular dynamics and simulation study was further done on the selected best analog THC-15 to find out the stability of the molecules inside the binding pocket of the CDK-2 up to 10 ns with GROMACS 5.0.4 to study the behavior of the THC15-CDK2complex.

The fifth chapter describes about the corrosion inhibition of mild copper metal in 1M HCl solution by using PPZs organomaterial. The scope of inhibition effectiveness was dependent on the concentration of the inhibitors. In most of the cases the Nyquist plot semicircle increase with increase in concentration of the inhibitors which confirms the increase of impedance. EIS plots indicated that R_{ct} values increase and C_{dl} values decrease with increasing inhibitor concentration. Later on the sheet resistivity study confirms the high resistance created by material. The tensile strain of the copper strips increases with the deposition of the PPZ material. The inhibition efficiencies obtained from experimental results were substantiated by the Quantum chemical calculations. The high electron density of the PPZ-2 and PPZ-5 favors its

adsorption on metal surface and make them the best inhibitors than all other PPZs discussed in the chapter.

6.3 Future scope of the research work

Transition metal catalyzed reductive Heck type coupling of alkyl halides with alkene delivers C−C bonds, is undoubtedly a precious tool for the construction of miscellaneous molecular frameworks. Last decade has witnessed an astonishing bunch of publications with this concept and a high abundant of synthetic libraries have been achieved using this strategy. As it is evident from the introduction and literature review that although traditional organic chemistry synthesis approaches are well established nevertheless some major drawbacks still remain in their practical execution e.g., harsh conditions, use of strong acidic or alkaline media, higher temperatures or pressures. Therefore, there is a strong need for the use of milder reaction conditions. As it is clear from the background provided in the introduction, most of the reported carbon-carbon bond forming reactions are either stoichiometric or low yielding, or require the use of cross-coupling strategies, or need Grignard reagents as additives. Also, majority of these couplings are radical mediated ones and therefore, a usual oxidative-addition driven reductive coupling in which both the coupling partners contain sp^3 carbons, is still elusive. Furthermore, employing transition-metal catalysts not only reduces the reaction times and simplifies the procedures, but also propels some unusual and normally difficult reactions to proceed under relatively mild conditions. The use of Nickel complexes has not been fully explored and considering their advantages over the Palladium catalysis, there is a need to bridge this gap and exploit a simpler transition-metal mediated route to organic synthesis.

As many natural products in addition to pharmacologically active molecules contain fused heterocyclic compounds as their central frameworks, synthesis of these molecules by means of hybrid methodologies is a potential alternative to traditional linear syntheses. The thesis mainly focused on chemistry of pyranopyrazole drug skeletons and these fused structures have been synthesized while utilizing tandem reactions and multicomponent protocols. As the synthesized molecules are the key structures of wide range of drugs, the developed procedures can be tuned further to access the drugs in a reduced number of steps or probably in a single step. These procedures have wide scope and can be employed for the synthesis of a diverse range of either bioactive heterocyclic molecules or to access new heterocyclic libraries for biological screenings. The synthetic methodologies and novel fused heterocyclic compounds provided in the thesis will be a fine and adoptable example for the systematic construction of fused heterocycles for biological screenings. Furthermore, the application of pyranopyrazole derivatives as anticancer agents needs to be further examined, as these small molecules derived from these pharmacophores could be potential drugs. Although there have been reports pertaining to the use of pyranopyrazole derivatives as bioactive molecules, the full potential of these versatile small molecule
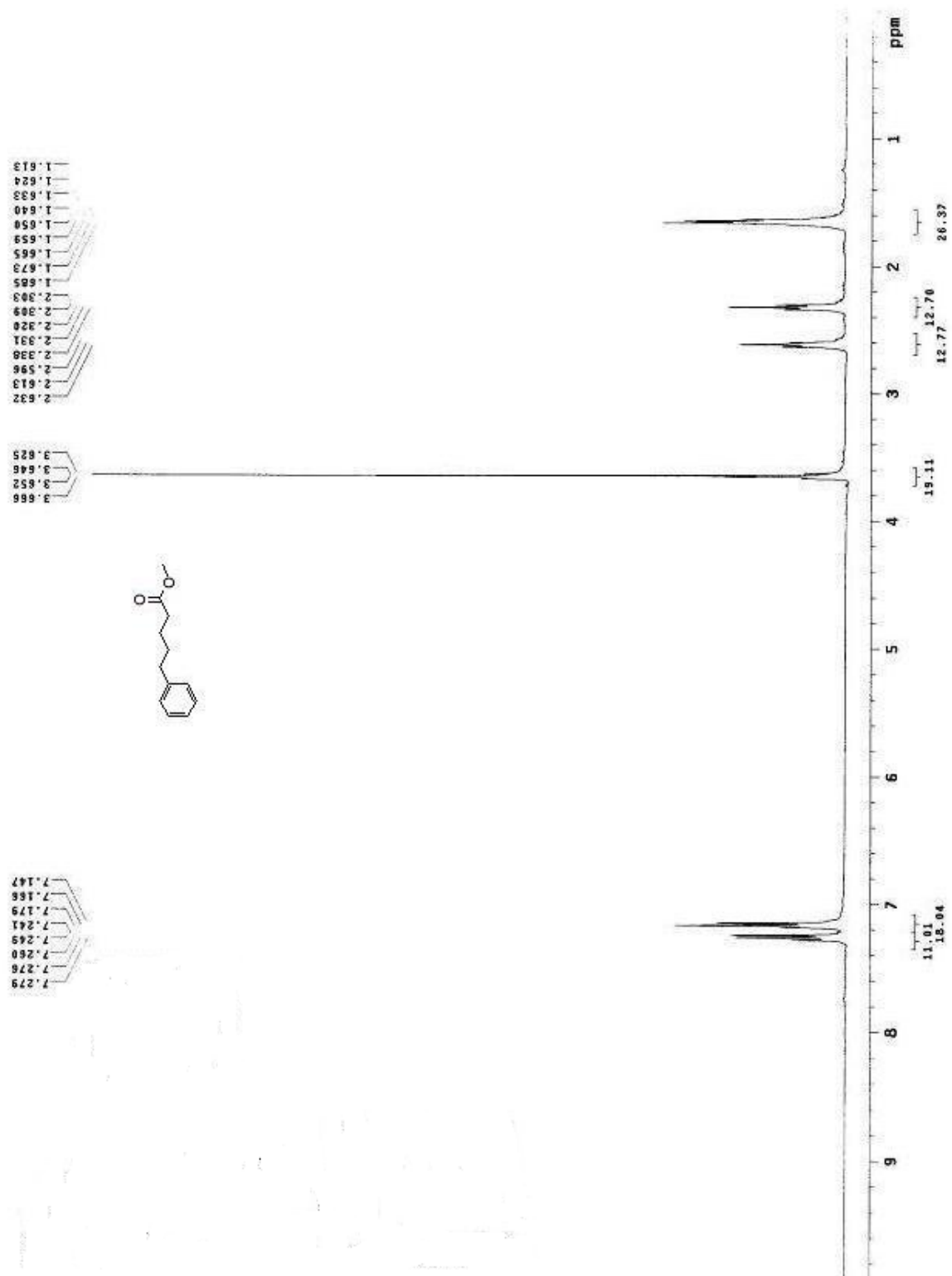
inhibitors have yet to be realized. Thus, a multicomponent reaction (MCR) is a green approach towards the synthesis of various heterocyclic compounds and for a researcher there is lot of scope to change the reaction condition, to change the catalyst or to modify the catalyst or even to develop various novel multicomponent reactions.

There are many kinase inhibitors in the clinic, mainly as anticancer strategies but still the development of kinase inhibitors has proved to be very difficult because of complex structure of kinase family proteins. So there is huge scope for the researchers to develop the structure based specific drug molecules as kinase inhibitors.
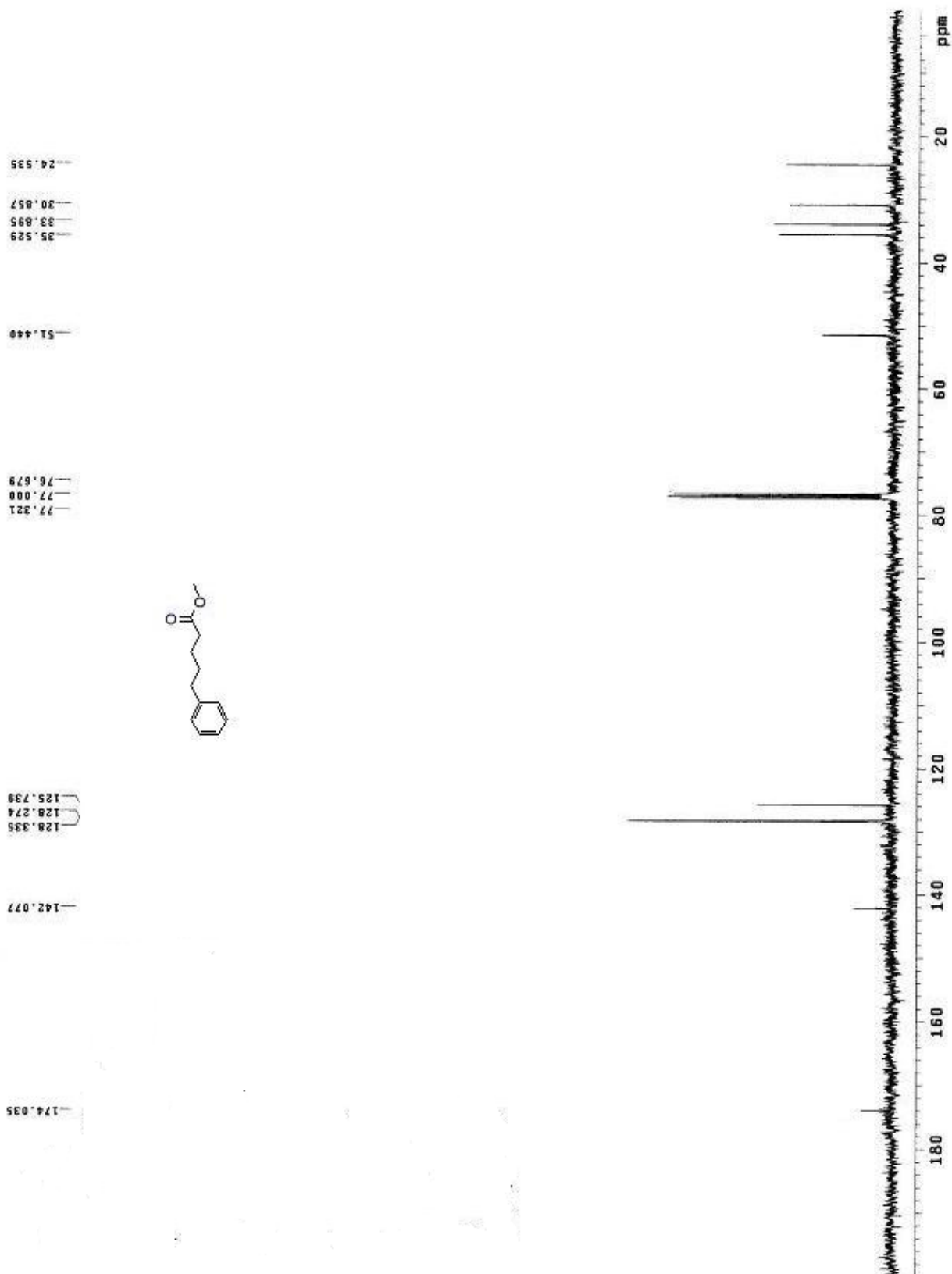
Till now several researchers developed the organic and inorganic inhibitor for copper metal but still there are thrust among researchers to develop stable inhibitor which can inhibit the corrosion of the metal. It is a challenge worth taking up for the research community to develop less toxic, stable, environmental friendly corrosion inhibitors at minimum cost.
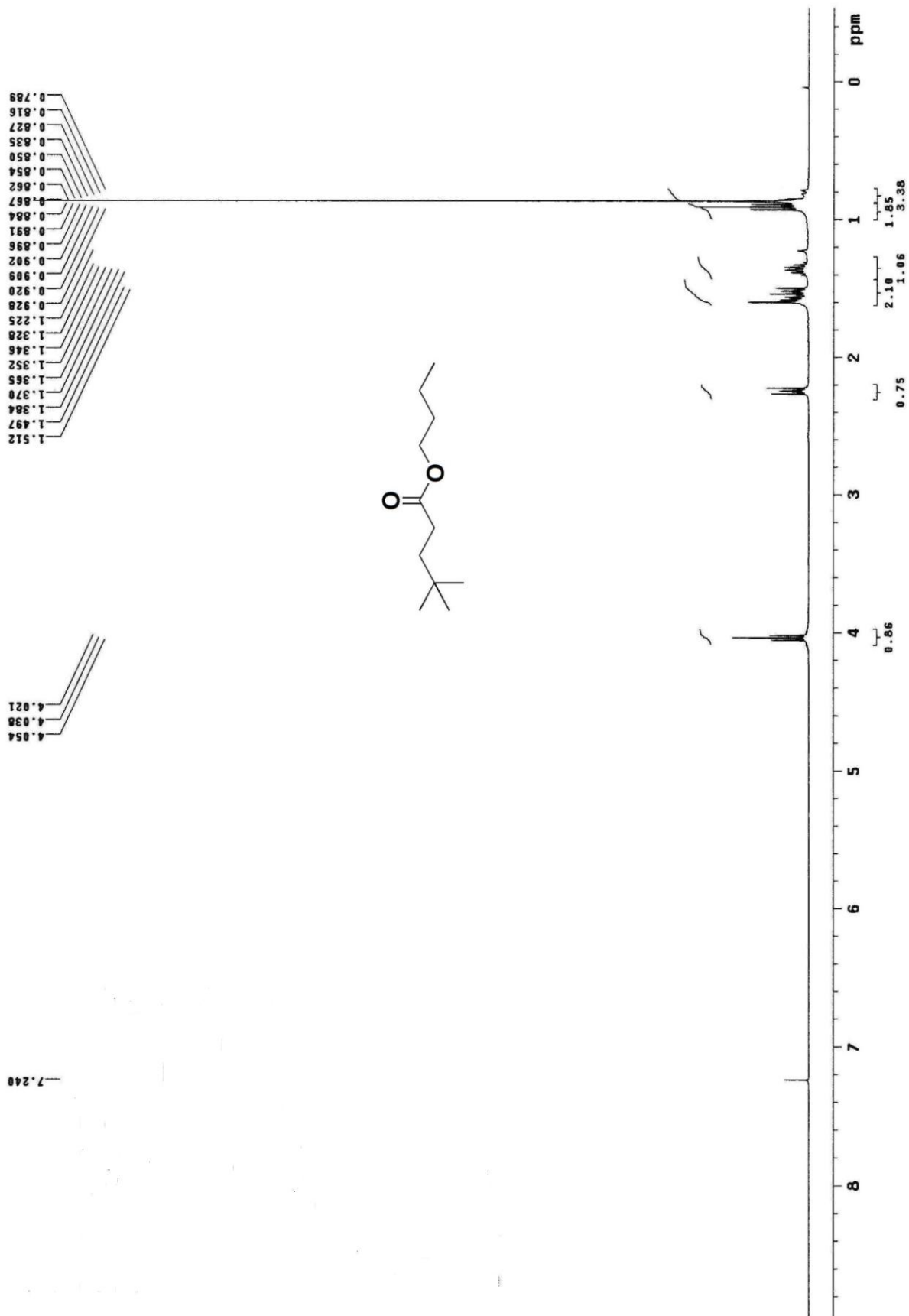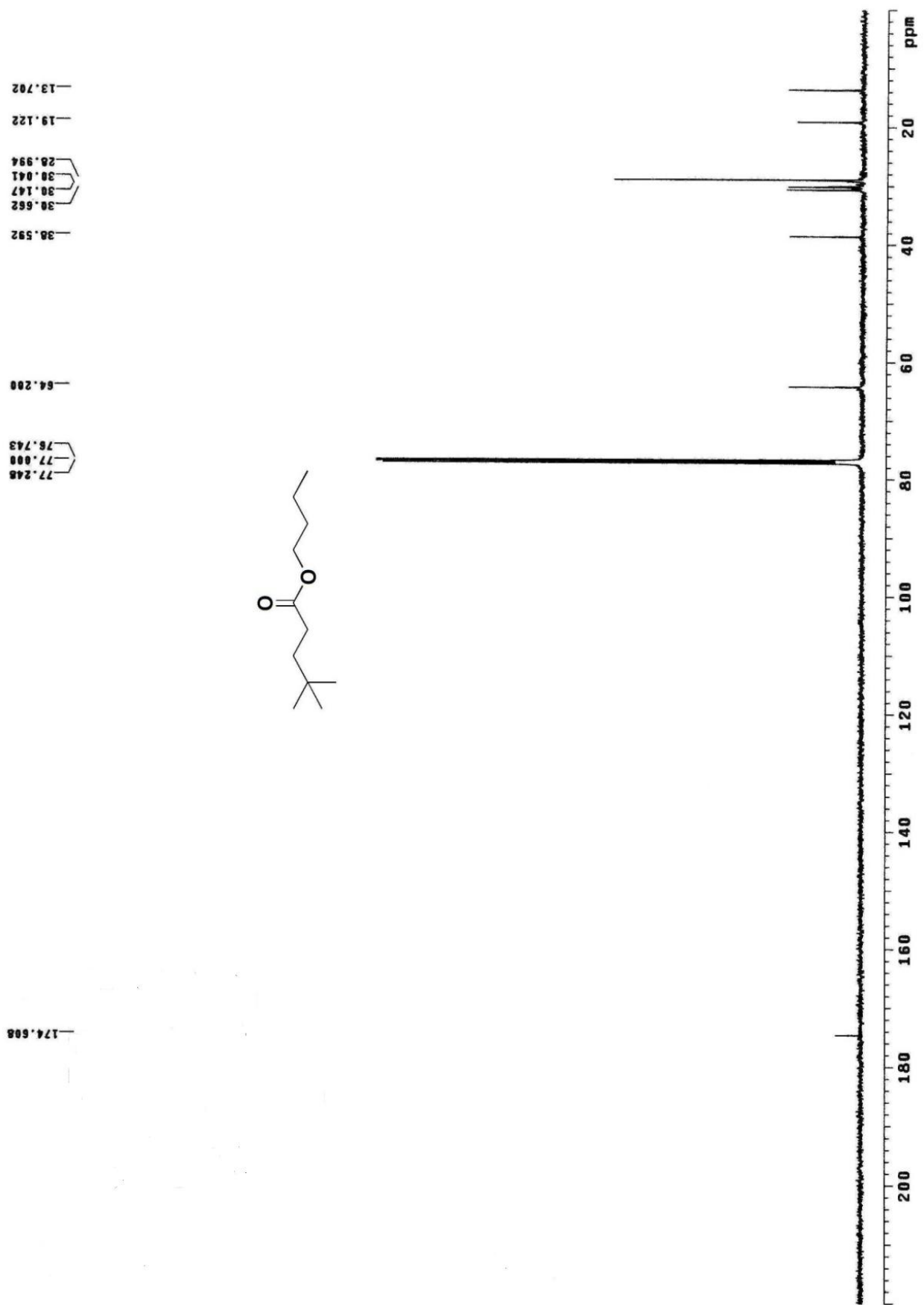
Appendices

Chapter-2

^{1}H-NMR spectra of 3k in Table 2.3

24.535
30.857
33.895
35.529
51.440
76.679
77.000
77.321
125.738
128.274
128.395
142.077
174.035

¹³C-NMR Spectra of compound 3k in Table 2.3

0.789
0.816
0.827
0.835
0.850
0.854
0.862
0.867
0.884
0.891
0.896
0.902
0.909
0.920
0.928
1.225
1.328
1.346
1.352
1.365
1.370
1.384
1.497
1.512

4.021
4.038
4.054

7.240

1.85
3.38
1.06
2.10
0.75
0.86

ppm

¹H-NMR spectra of 3f in Table 2.3

13.702
19.122
28.994
30.041
30.147
30.662
38.592

64.200

76.743
77.000
77.248

174.608

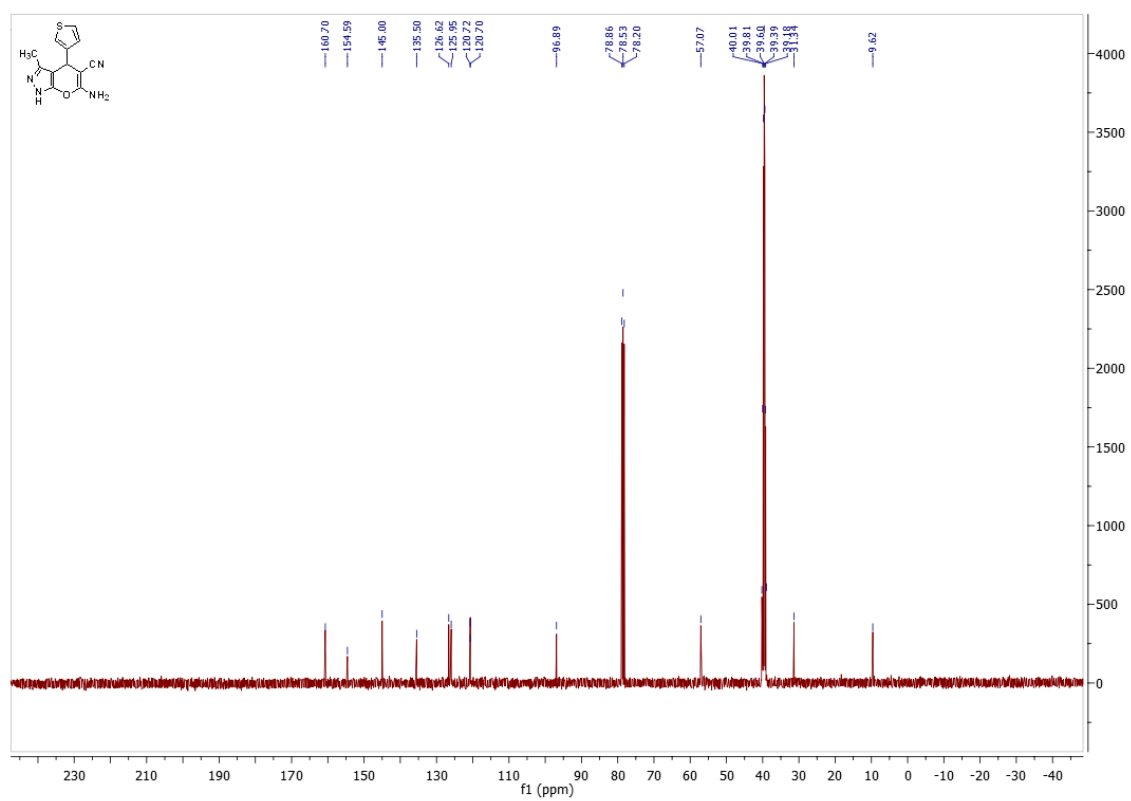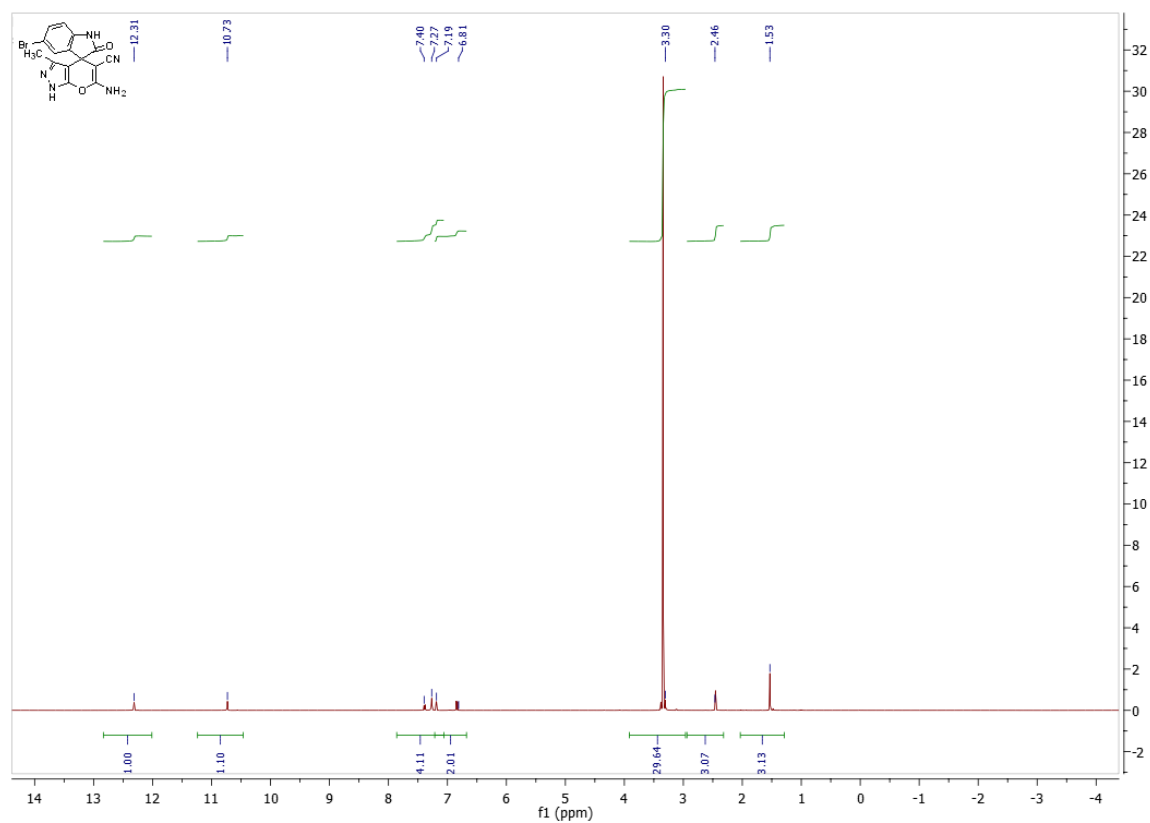**¹³C-NMR Spectra of compound 3f in Table 2.3**
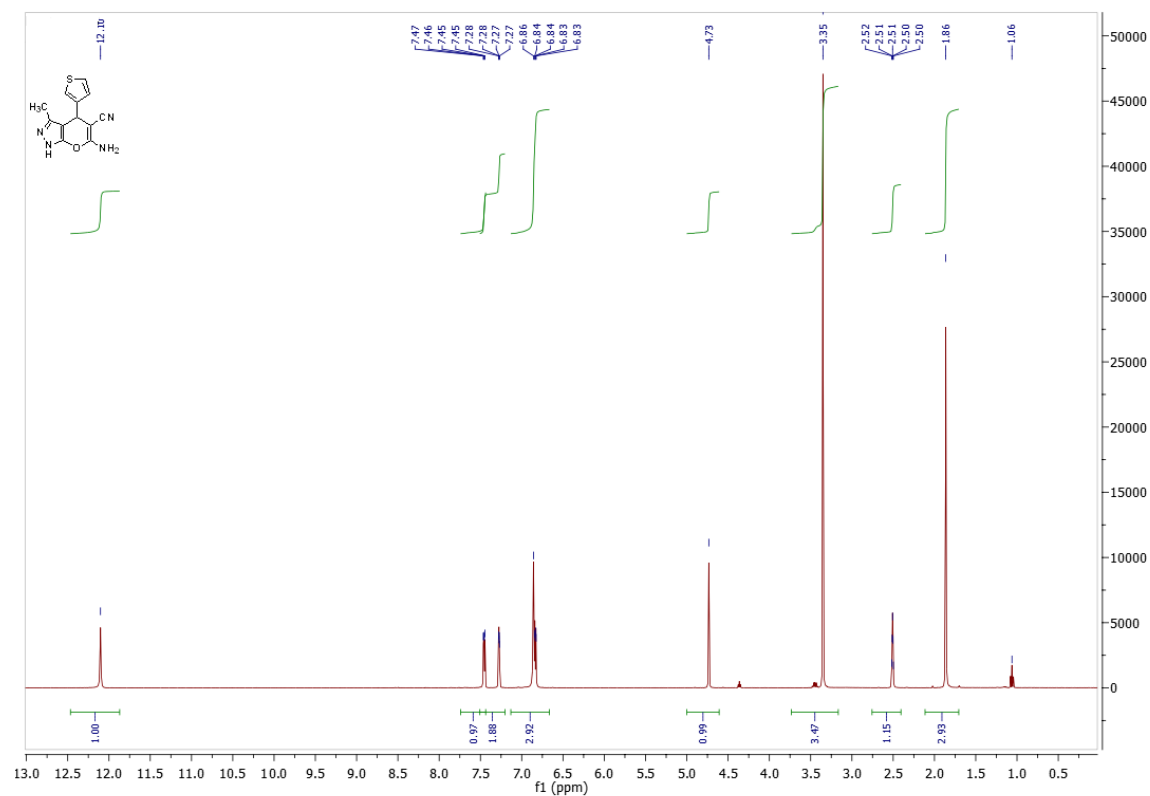
¹H-NMR spectra of compound 5a5 (entry no. 5) in Table 3.1

¹³C-NMR spectra of compound 5a5 (entry no. 5) in Table 3.1

^{1}H-NMR spectra of compound 9c (entry no. 3) in Table 3.8
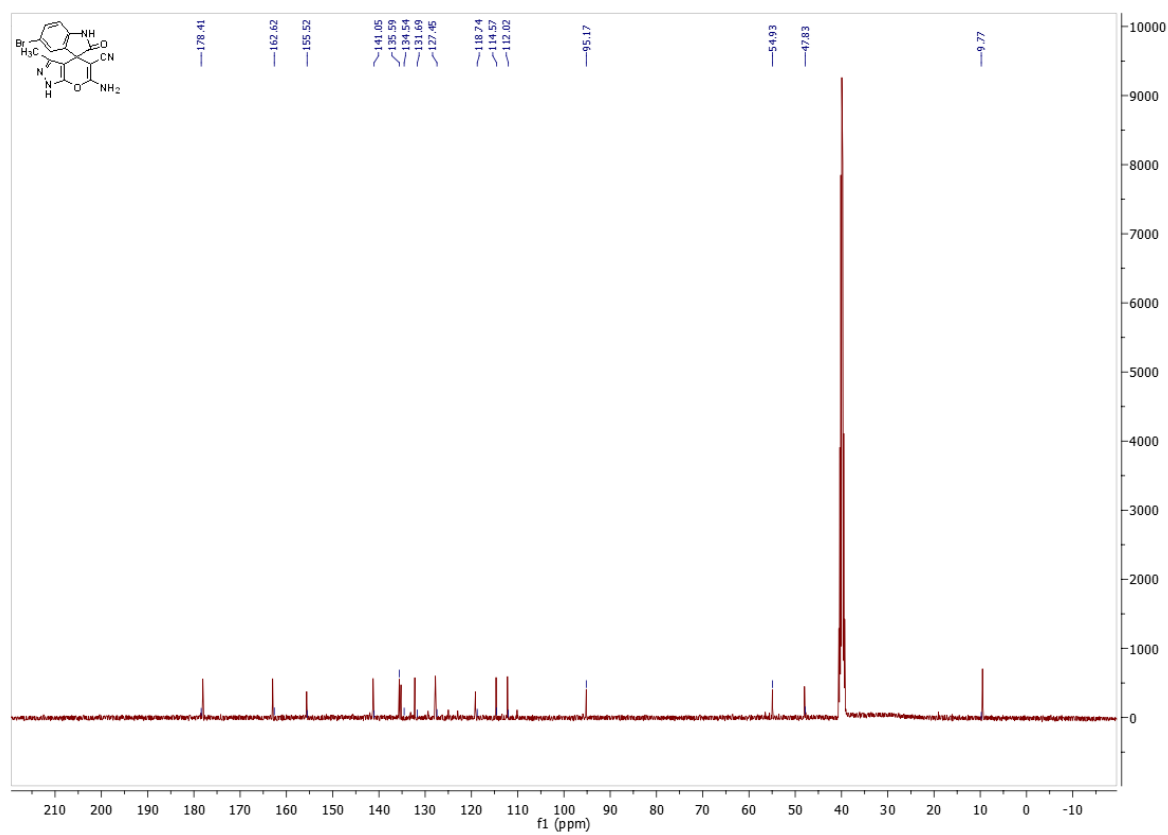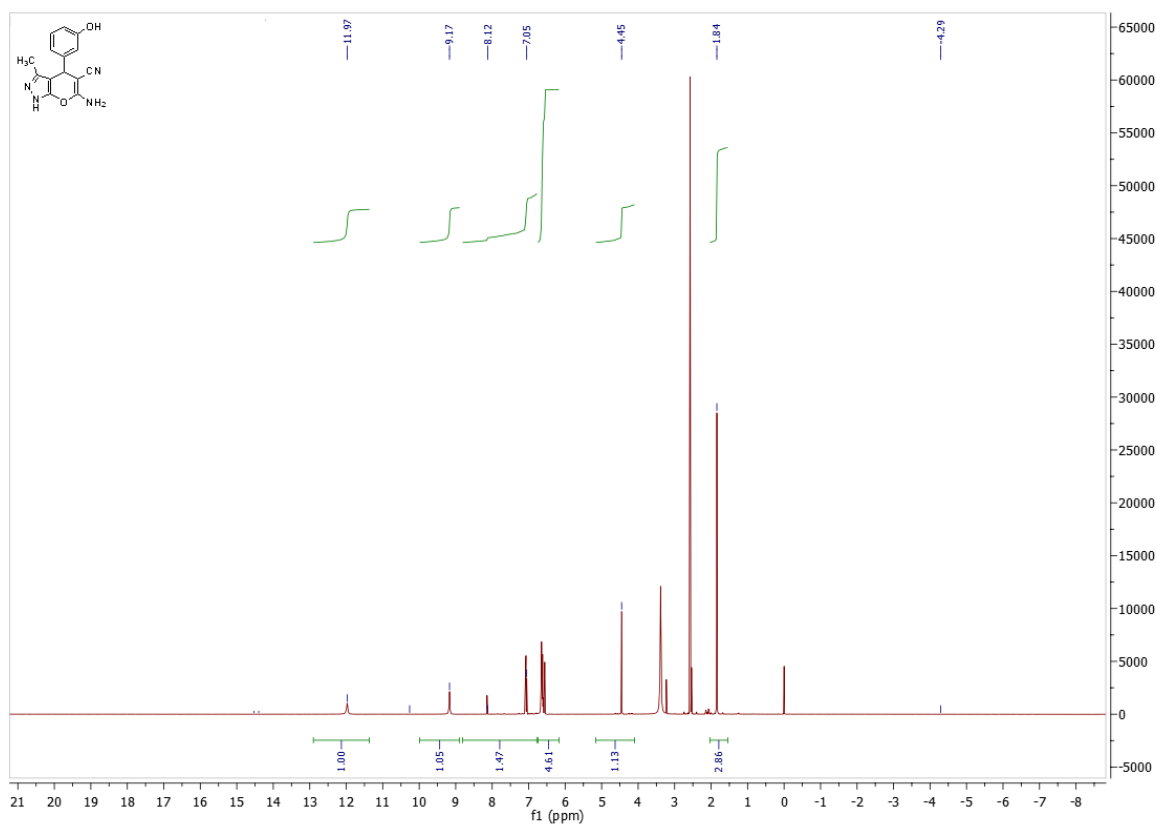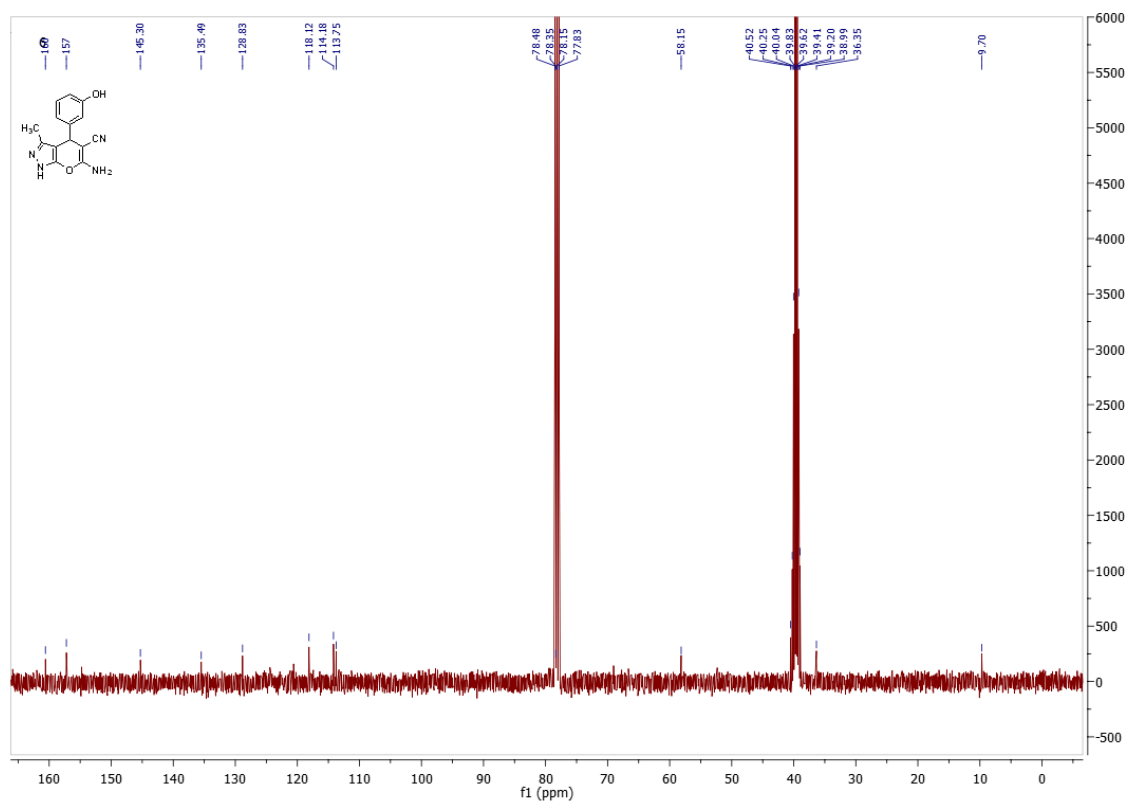

^{13}C-NMR spectra of compound 9c (entry no. 3) in Table 3.8

Chapter-3(Part-C)

¹H-NMR spectra of compound 9c2 (entry no. 2) in Table 3.13

¹³C-NMR spectra of compound 9c2 (entry no. 2) in Table 3.13

1. **Ashok Sharma**, Badvel Pallavi, Chien Hong Cheng, Paritosh Shukla. Nickel-catalyzed reductive Heck type coupling of saturated alkyl halides with acrylates and oxabenzonorbornadiene. *Tetrahedron* **2015**, *71(15)*, 2260-2266.

2. **Ashok Sharma**, Rajdeep Chowdhury, Subhra Dash, Badvel Pallavi and Paritosh Shukla. Fast microwave assisted synthesis of Pyranopyrazole derivatives as new anticancer agents. *Current Microwave Chemistry,* **2015**, *2(1)*, 1-6.

3. **Ashok Sharma**, Paritosh Shukla, Sumati Anthal, and Rajni Kant. Synthesis of functionalized Pyrazolopyran derivatives: comparison of two-step vs one-step vs microwave assisted protocol and X-ray crystallographic analysis of 6-Amino-1,4-dihydro-3-methyl-4-phenylpyrano[2,3-c]pyrazole-5-carbonitrile. *Bulletin of Material Science*, **2015**, *38(5)*, 1119-1127.

4. **Ashok Sharma**, Badvel Pallavi, Rajnish Prakash Singh, Prabhat Nath Jha, and Paritosh Shukla. Novel grinding synthesis of Pyranopyrazole analogues and their evaluation as antimicrobial agents. *Heterocycles*, **2015**, *91*, 1615-1627.

5. **Ashok Sharma**, Leena Fageria, Rajdeep Chowdhury, Paritosh Shukla. Novel Spiro/non-Spiro Pyranopyrazoles: eco-Friendly Synthesis, in-vitro Anticancer Activity, DNA binding, and Molecular Docking Study. **2016** (Communicated).

6. **Ashok Sharma**, Sourabh Sharma, Rajeev Taliyan, Paritosh Shukla. Design and Synthesis of novel pyrano[2,3-*c*]pyrazoles and their Pharmacological evaluation as antioxidant agents. **2016** (Communicated).

7. **Ashok Sharma**, Dinesh Kumar, Prashant Uday Manohar, Surojit Pande, Anshuman Dalvi, Paritosh Shukla Synthesis, Physical Investigations, and Theoretical Approach of Substituted Pyranopyrazoles: Adsorption on Mild Copper Metal in Acid Solution. **2016** (Communicated)

8. **Ashok Sharma**, Riddhidev Banerjee, Ashok Penta, S. Murugesan, Paritosh Shukla. *De-novo* designing and *in-silico* studies of novel pyrazolopyran pharmacophores as inhibitors of cyclin dependent kinase-2. **2016** (Communicated).

9. **Ashok Sharma**, Riddhidev Banerjee, Mariasoosai Ramya Chandar Charles, Mohane Selvaraj Coumar, Subhash Chander, S. Murugesan, Paritosh Shukla. *De-novo* Design, Molecular Dynamics, and *in-silico* Studies of Coumarin Derivatives as Inhibitors of Cyclin Dependent Kinase-2. **2016** (Communicated).

10. A. N. Singh, A. Singhal, R. Gupta, **Ashok Sharma**, Paritosh Shukla. A novel approach for the removal of Nitrate ion from underground water by using *solanum tuberosum* gel method. **2016** (Communicated).

11. Chetan Aditya, **Ashok Sharma**, Paritosh Shukla. On-water system" A review on simple organic reactions and their kinetic study by Marcus and Beattie model approach. **2016** (Communicated).

12. **Ashok Sharma**, Dinesh Kumar, Prashant Uday Manohar, Surojit Pande, Paritosh Shukla Synthesis, Physical Investigations, and Theoretical Approach of Substituted Pyranopyrazoles: Adsorption on Mild Aluminium Metal in Acid Solution. **2016** (Under progress)

13. **Ashok Sharma**, Riddhidev Banerjee, Mariasoosai Ramya, Chandar Charles, Mohane Selvaraj Coumar, Subhash Chander, S. Murugesan, Paritosh Shukla. *De-novo* Design, Molecular Dynamics, and *in-silico* Studies of PPZs Derivatives as Inhibitors of Aurora A,: Cyclin Dependent Kinase-2. **2016** (Under progress).

14. **Ashok Sharma**, Dinesh Kumar, Prashant Uday Manohar, Paritosh Shukla. A detailed theoretical study of pyrano[2,3-*c*]pyrazoles molecules by Q-Chem. **2016** (Under Progress).

15. **Ashok Sharma**, Paritosh Shukla. A review on synthesis of Pyranopyrazole via various methodology and their biological applications. **2016** (Under Progress).

16. **Ashok Sharma**, Paritosh Shukla. A review on study of corrosion inhibitors for mild copper and aluminium metal. **2016** (Under Progress).

(A) Oral presentations

1. Delivered oral talk on Design, Synthesis and Preliminary SAR of Pyranopyrazole derivatives as Novel Anticancer agent on **Research Scholar Day** in Physics Department of **BITS Pilani**, Pilani campus Rajasthan.

(B) Poster presentations

1. <u>Ashok Sharma</u>, Paritosh Shukla. Presented poster in Symposium on Recent Trend in Chemical Sciences in BITS Pilani Rajasthan on **25th March 2012**.

2. <u>Ashok Sharma</u>, Paritosh Shukla. Presented poster in 2nd UK-India Med. Chem. Congress on Medicinal chemistry in Indian Institute of Chemical Technology (IICT) Hyderabad, India; **22-23 March 2013**.

3. <u>Ashok Sharma</u>, Paritosh Shukla. Presented poster in Medicinal Chemistry Conference in Indian Institute of Technology (IIT) Madras, India; **25-26 October 2013**.

4. <u>Ashok Sharma.</u> Attended 8th CRSI-RSC joint Symposium on Medicinal chemistry in Indian Institute of Technology (IIT) Bombay, India on **6th February 2014**.

5. <u>Ashok Sharma</u>, Paritosh Shukla. Presented poster in 16th CRSI-RSC Joint Symposium on Medicinal chemistry in Indian Institute of Technology (IIT) Bombay, India; **7-9th February 2014**.

6. <u>Ashok Sharma</u>, Paritosh Shukla. Presented poster in Indo-US Conference on Molecular Modeling and Informatics in Drug Design (M^2ID^2) in National Institute of Pharmaceutical Education and Research, Mohali (NIPER), India; **3-6 November 2014**.

7. <u>Ashok Sharma</u>, Paritosh Shukla. Presented poster in National Conference in Nano and Functional Material (NFM-2014) in BITS Pilani, India; **7-8 November 2014**.

8. <u>Ashok Sharma</u>, Paritosh Shukla. Presented poster in National Workshop on Analytical Instrumentation in Chemical Engineering (WAICE-2015) in BITS Pilani, India; **27-28 February 2015**.

9. <u>Ashok Sharma</u>, Paritosh Shukla. Presented poster on Research Scholar Day in the Physics Department of BITS Pilani, Pilani Campus on **15th March 2015**.

10. <u>Ashok Sharma</u>, Paritosh Shukla. Presented poster in International Conference on "Nascent Developments in Chemical Sciences" in BITS Pilani, India; **16-18 October 2015**.

11. <u>Ashok Sharma</u>, Paritosh Shukla. Presented poster in International Conference on "Emerging Technologies : Micro to Nano 2015" in Manipal University Rajasthan, India; **24-25 October 2015**.

12. <u>Ashok Sharma</u>, Paritosh Shukla. Presented poster in International Conference on "Recent Developments in Medical Biotechnology and Structure Based Drug Designing [RDMBSBDD-2015]" on **December 6-7, 2015** in Indian Institute of Technology Guwahati, India.

13. <u>**Ashok Sharma**</u>, Badvel Pallavi, Leena Fageria, Rajdeep Chowdhary, Subhash Chander, S. Murugesan, Paritosh Shukla. Presented poster in National Conference on "Organic Chemistry in Sustainable Development: Recent Advances and Future " in BITS-Pilani, Rajasthan, India; **29-30 August 2016**.

(C) Workshops

1. Attended National Workshop on LATEX and MATLAB for Beginners (NWLMB-2014) in BITS Pilani, India; **24-28 December 2014**.

2. Attended National Workshop on Analytical Instrumentation in Chemical Engineering (WAICE-2015) in BITS Pilani, India; **27-28 February 2015**.

3. Attended the Q-Chem User Workshop at BITS-Pilani, Pilani Campus, Rajasthan, India on **19th October 2015**.

4. Attended Seminar & Workshop on Liquid Chromatography Tandem Mass Spectrometry in BITS Pilani, India; **23-24 August 2016**.

5. Attended Workshop on IPR, Patent, and Copy Right in BITS-Pilani, Rajasthan on **23 August 2016.**

(D) List of Awards and Honor in Ph.D Tenure

1. Got the **3rd prize** for best poster presentation in Symposium On Recent Trend in Chemical Sciences in BITS Pilani Rajasthan on **25th March 2012.**

2. Got **1st prize** for best poster presentation in National Workshop on Analytical Instrumentation in Chemical Engineering (WAICE-2015) in BITS Pilani, India; **27-28 February 2015.**

3. Got **2nd** best poster presentation award in IIT Guwahati in International Conference on "Recent Developments in Medical Biotechnology and Structure Based Drug Designing [RDMBSBDD-2015]" on **December 6-7, 2015.**

4. Honored by BITS Pilani in BITSCAN magazine of **2016** for getting award in IIT Guwahati on **December 6-7, 2015**.

Ashok Sharma obtained his graduation degree in Medical Science from Kurukshetra University Kurukshetra, Haryana, India during 2005-08. Later on, he obtained his masters degree in chemistry from Thapar University Patiala, Punjab, India during 2008-10. During his M.Sc period he completed one project on Biodiesel in summer term under Professor Satnam Singh and the second project on Zirconium phosphoborate for M.Sc. thesis under Professor Susheel Mittal and Professor Rajiv Mehta. In August 2010, he joined Department of Chemistry, BITS Pilani for PhD program under the guidance of Dr. Paritosh Shukla with the financial assistance from the institute. During his PhD tenure he was actively involved in the synthesis of Nickel catalyzed coupling reactions, medicinally important pyranopyrazole molecules and their various biological and pharmacological properties, detailed computational study of the designed CDK-2 inhibitors, and in the development of corrosion inhibitors for copper and aluminium metal. He has published four research articles in peer reviewed international journals and presented papers in thirteen national/international conferences/symposiums. He also attended four technical workshops during his PhD tenure on analytical instrumentation, Q-Chem, LATEX & MATLAB, and Liquid Chromatography Tandem Mass Spectrometry . He got three best poster presentation awards for research presented in conferences as well as honored by BITS Pilani University by publishing his name in BITSCAN magazine in 2016.

His research interest lies in the transition metal catalyzed organic reactions, development of new methods for the synthesis of bioactive heterocyclic motifs and the construction of novel fused heterocyclic libraries using various methodologies, designing and synthesis of small molecular weight pharmacophores which can control stem cell fate in each step of the cell cycle, design and synthesis of novel anti-HIV inhibitors, targeted against Tat protein. Computational study of the molecules by docking and molecular dynamics, and synthesis of organic/inorganic material having various applications.

Dr. Paritosh Shukla is Assistant Professor of Chemistry at the Birla Institute of Technology and Science, Pilani (BITS-Pilani). He obtained his PhD degree in 2005 from Department of Chemistry, National Tsing Hua University (NTHU), Hsinchu, Taiwan, under the guidance of Professor Chien Hong Cheng. During his doctoral studies Dr. Paritosh Shukla worked on the development of appropriate synthetic methodologies for Nickel and Cobalt catalyzed organic reactions. He was postdoctoral fellow at School of Chemical Sciences, Academia Sinica, Taipei, Taiwan, from January 2006 to July 2007, where he worked on synthesis and characterization of organic materials. His second stint as postdoctoral fellow was in National Health Research Institutes (NHRI), Jhunan, Taiwan, from August 2007 till February 2010, where he worked in the field of medicinal chemistry. He joined the Department of Chemistry, Birla Institute of Technology and Science, Pilani, India as Assistant Professor in March, 2010. Since then, he has been involved in teaching M.Sc., B.E., and PhD students. His current research areas include transition metal mediated organic synthesis; preparation and characterization of heterocyclic compounds; applications of the synthesized compounds in biology and materials science; drug discovery via design of new chemical entities, etc. He currently has two PhD students working with him. He has completed one UGC funded Major Research Project as a PI and presently is co-PI in another project titled "Waste, Water, and Energy" collaborating with Prof Raj Kumar Gupta of the Physics department, BITS-Pilani.